UNIVERSIDAD NACIONAL AUTÓNOMA DE MÉXICO

FACULTAD DE INGENIERÍA

SIMULACIÓN DINÁMICA DE UN MOTOR DE RELUCTANCIA ACCIONADO POR CONMUTACIÓN (MRAC) DE BAJO CONSUMO DE ENERGÍA ELÉCTRICA

T E S I S

QUE PARA OBTENER EL TÍTULO DE:

INGENIERO ELÉCTRICO-ELECTRÓNICO

P R E S E N T A

JORGE ALBERTO ROSAS FLORES

DIRECTOR DE TESIS: ING. ARTURO MORALES COLLANTES

México, D.F. 2003

CONTENIDO.

Tabla de contenido i
Índice de Figuras v
Índice de Tablas vii
Nomenclatura viii
Motivos e inquietudes para el desarrollo de este tema 1
Prefacio 2
Introducción 4
Objetivo 6
Hipótesis 7

CAPITULO 1
ANTECEDENTES (MOTORES ELÉCTRICOS) 8

1.1 Motores eléctricos. 8
1.2 Los motores eléctricos en la historia. 9
1.3. Tipo de corriente de alimentación para los motores eléctricos 12
1.3.1 Fundamentos de corriente alterna. 12
1.3.2 Fundamentos de corriente continua 14
1.4 Clasificación y funcionamiento de los motores eléctricos 15
1.5 Usos de los motores eléctricos. 22

CAPITULO 2
LOS MRAC (PROPIEDADES) 24

2.1 Principios de operación de los MRAC 24
2.2 Funcionamiento de los MRAC. 26
2.3 Características de los MRAC. 28
2.3.1 Características par-velocidad 28
2.3.2 Fuente conmutada de alimentación. 29
2.3.3 Geometría de los MRAC. 31

2.4 Sección estructural de los MRAC. 32
2.4.1 Devanados del estator. 32
2.4.2 Laminación del rotor. 33
2.4.3 Entrehierro. 34
2.4.4 Balanceo del rotor. 35
2.5 Control de los MRAC 37
3.7 ¿Que ofrecen los MRAC? 38
2.6.1 Ventajas. 38
2.6.2 Desventajas. 40
2.7 Avances tecnológicos en los motores de reluctancia. 40

CAPITULO 3
MODELO MATEMÁTICO DE LOS MRAC. 43

3.1 ¿Porqué el uso de un modelo matemático? 44
3.1.1 Requisitos de un modelo matemático. 45
3.2 Modelo matemático general de los MRAC. 46
3.2.1 Ecuaciones electromagnéticas. 46
3.2.2 Ecuación general de par. 47
3.2.3.- Simplificación de la ecuación de par. 52
3.3 Modelo utilizado para la simulación. 52
3.3.1 Modelo simplificado del MRAC. 52

CAPITULO 4
SIMULACION DEL MRAC 55

4.1 Simulación de motores eléctricos. 56
4.1.1 Definición de simulación. 56
4.1.2 El porque de la simulación. 56
4.1.3 Componentes de una simulación por computadora. 57
4.1.4 Diseño de la simulación por computadora. 58
4.1.5 Ventajas y desventajas de la simulación. 59
4.2 Revisión bibliográfica de simulación en los MRAC. 59

4.3 Simulador utilizado en este trabajo (Matlab - Simulink). 60
4.3.1 Matlab. 61
4.3.2 Simulink. 62
4.4 Simulación en Matlab – Simulink 63
4.4.1 Programación en Matlab 64
4.4.2 Simulación basada en Simulink. 65

CAPITULO 5
RESULTADOS DE SIMULACION. 66

5.1 Parámetros del MRAC 67
5.2 Listados para la simulación en Matlab 67
5.2.1 Listado para el programa de inicio. 67
5.2.2 Listado para el programa de conmutación. 69
5.2.3 Listado para el programa de inductancia. 70
5.2.4 Listado para el programa de par 72
5.3. Simulación en Simulink 73
5.4 Resultados de simulación. 75
5.4.1 Inductancia. 76
5.4.2 Tensión de alimentación. 78
5.4.3 Corriente. 79
5.4.4 Par. 82
5.4.5 Velocidad. 84
5.5 Caracterización del MRAC. 86
5.5.1 Obtención de la potencia del MRAC 86
5.6 Pequeño momento de inercia. (gran respuesta dinámica) 87
5.7 El motor de reluctancia mejor aprovechamiento para bajas revoluciones. 89
5.8 Consumo de energía. 90
5.9 Costos en los motores eléctricos. 93
5.9.1 Estimación de manufactura. 94

CONCLUSIONES Y RECOMENDACIONES. 96

BIBLIOGRAFÍA. 99

APENDICE I 101
APENDICE II 109

ÍNDICE DE FIGURAS

FIGURA 1.1 Fundamento de un generador de corriente alterna

FIGURA 1.2 Vista de un generador de corriente continua

FIGURA 1.3 Vista de un pequeño motor de corriente continua.

FIGURA 1.4 Vista de un motor síncrono.

FIGURA 1.5 Vista de un motor tipo jaula de ardilla

FIGURA 1.6 Vista de un MRAC.

FIGURA 2.1 Corte transversal de un MRAC.

FIGURA 2.2 Curva par-velocidad de los MRAC

FIGURA 2.3 Conmutador electrónico para un MRAC 3ϕ

FIGURA 2.4 Geometría de los MRAC

FIGURA 2.5 Devanados de los MRAC

FIGURA 2.6 Rotor de un MRAC

FIGURA 2.7 Programa “demo” de estudio de ruido en los MRAC

FIGURA 2.8 Modelo utilizado para el estudio de ruido en los MRAC.

FIGURA 2.9 Polos del rotor de un MRAC.

FIGURA 2.10 Estructura de un MRAC con 6 polos en el estator y 4 polos en el rotor

FIGURA 3.1 Interpretación gráfica de la energía de campo magnético

FIGURA 3.2 Interpretación gráfica de la co-energía de campo magnético.

FIGURA 3.3 Inductancia de cada fase de un MRAC 6/4

FIGURA 3.4 Arcos de rotor y estator de un MRAC 6/4

FIGURA 5.1 Esquema de simulación en Simulink

FIGURA 5.2 Esquema detallado del esquema de simulación en Simulink

FIGURA 5.3 Inductancia de fase

FIGURA 5.4 Acercamiento de la gráfica 5.3

FIGURA 5.5 Inductancia en los MRAC

FIGURA 5.6 Voltaje de alimentación del MRAC

FIGURA 5.7 Corriente de fase del MRAC.

FIGURA 5.8 Acercamiento de la gráfica 5.7

FIGURA 5.9 Par obtenido del MRAC

FIGURA 5.10 Acercamiento de la curva 5.9

FIGURA 5.11 Velocidad del MRAC.

FIGURA 5.12 Acercamiento de la figura 5.11

FIGURA 5.13 Representación gráfica de los momentos de inercia

FIGURA 5.14 Máximo par motor permitido en régimen permanente, referido respecto al momento de inercia

FIGURA 5.15 Comparación gráfica de corriente eléctrica entre motores

ÍNDICE DE TABLAS

TABLA No 1 Usos de los motores eléctricos en la industria

TABLA No 2 Caracterización del motor de reluctancia simulado

TABLA No 3 Comparación de momentos de inercia de distintos motores eléctricos de proporciones semejantes

TABLA No 4 Corriente eléctrica a plena carga de motores eléctricos

TABLA No 5 Consumo y ahorro de energía entre motores eléctricos

TABLA No 6 Costo en motores eléctricos

TABLA No 7 Costos de manufactura de un motor de reluctancia (simulado)

NOMENCLATURA.

MRAC **M**OTOR DE **R**ELUCTANCIA **A**CCIONADO POR **C**ONMUTACIÓN

ó SRM POR SUS SIGLAS EN INGLES "**S**WITCHED **R**ELUCTANCE **M**OTOR"

θ POSICIÓN DEL ROTOR [rad]

ω VELOCIDAD ANGULAR [rad/s]

ψ FLUJO MAGNETICO (MODELO SIMPLIFICADO) [Wb]

ϕ FLUJO MAGNETICO (MODELO GENERAL) [Wb]

N_r NUMERO DE POLOS EN EL ROTOR.

N_s NUMERO DE POLOS EN EL ESTATOR.

T PAR [N*m]

Tl PAR DE CARGA [N*m]

V VOLTAJE DE FASE [V]

β_r ARCO DEL ROTOR.[°]

β_s ARCO DEL ESTATOR. [°]

J MOMENTO DE INERCIA [Kg*m^2]

H INDUCTANCIA [H]

A CORRIENTE ELÉCTRICA [A]

W_f ENERGÍA DE CAMPO MAGNÉTICO.

W_c COENERGÍA DE CAMPO MAGNETICO.

W_m ENERGÍA MECANICA

θ_s ANGULO DE DESPLAZAMIENTO DE INDUCTANCIA ENTRE FASES [°]

θ_x ANGULO DE DESPLAZAMIENTO DE INDUCTANCIA UNO CON RESPECTO A CERO GRADOS

θ_y ANGULO DE DESPLAZAMIENTO DE INDUCTANCIA DOS CON RESPECTO A CERO GRADOS

f COEFICIENTE DE FRICCIÓN.

r.p.m. REVOLUCIONES POR MINUTO.

P POTENCIA [HP] [KW]

R RESISTENCIA DE FASE

CFE COMISION FEDERAL DE ELECTRICIDAD

PREFACIO

Este trabajo fue realizado utilizando la herramienta de programación MATLAB con simulación en SIMULINK para determinar parámetros como inductancia propia de fase, corriente de fase, y torque de fase para caracterizar a un motor de reluctancia (6 polos en estator y 4 polos en el rotor).

Con base en la teoría general y básica de máquinas eléctricas rotativas, se plantea el estudio de los motores de reluctancia accionados por conmutación, con ello se determinó las ecuaciones diferenciales generales propias del circuito eléctrico, que permiten estudiar directamente las respuestas temporales.
El presente trabajo muestra la simulación del motor de reluctancia con características lineales a partir del modelo establecido y considera el omitir algunos parámetros como es el caso de la inductancia mutua entre fases, además de considerar lineal el flujo en el entrehierro de la máquina; pero siempre tomando en cuenta los parámetros fundamentales como es el caso de la resistencia de fase, inercia, voltaje de alimentación, entre otros; que como hemos visto nos brinda aproximaciones muy buenas que esperábamos en un principio de la realización del tema.
En este caso se utilizó con el programa MATLAB ver 5.2 y SIMULINK ver 2.0, el cual en la facultad de ingeniería ha probado ser pieza fundamental para el desarrollo y análisis de sistemas dinámicos.
Los programas utilizados para la simulación se encuentran debidamente comentados para su fácil comprensión, además del diagrama de bloques de la simulación que nos brinda una idea general y sencilla de su funcionamiento.

Si bien el motivo original de este desarrollo fue el de disponer de una herramienta para fines didácticos, su potencialidad lo hace perfectamente aplicable para sistemas productivos y de diseño, donde no se justificaría el empleo de programas comerciales de mucha mayor envergadura, que recargarían considerablemente el aspecto económico del estudio del tema.

Una de las principales ventajas que presenta el motor de reluctancia, es su bajo costo de construcción, debido a su estructura simple, la cual consta de devanados solamente en el estator, además de ser una máquina eléctrica muy confiable, debido a que cada fase del motor se encuentra física, eléctrica y magnéticamente independiente. Esto nos lleva a pensar que si alguna fase del motor llegase a fallar, la máquina no dejará de funcionar (pero su rendimiento disminuiría), esto es muy importante y atractivo para sistemas que necesitan una alta confiabilidad en el proceso que efectúan.

Como se cometa en un principio, se obtuvo las respuestas temporales del motor de reluctancia conmutada, que caracterizan a dicho motor; las respuestas obtenidas están en un rango de valores reales, además fueron sometidos a diversas comparaciones con otros modelos de simulación, y el resultado fue una similitud asombrosa, esto tomando en cuenta que nosotros realizamos una simulación con un modelo lineal, y las demás simulaciones toman en cuenta una serie de parámetros mas completa y compleja.

Al tener las respuestas temporales del motor de reluctancia, pudimos caracterizar al modelo del motor simulado; con lo anterior pudimos comparar este motor con otros de tecnologías diversas, similares características y mismas dimensiones, resultando ser los motores de reluctancia accionados por conmutación una máquina eléctrica atractiva por el ahorro de energía eléctrica que presenta.
los resultados más importantes obtenidos son:

- ✓ Ahorro de energía eléctrica del 16%, basándose en consumos promedios.
- ✓ Ahorro económico en la construcción de estos motores del 27% con respecto a otras tecnologías utilizadas actualmente.

Es importante mencionar que el primer paso en el estudio de motores de reluctancia conmutada esta dado, espero que en un futuro no muy lejano, estudiantes y grupos de investigación, desarrollen temas basados en este trabajo o relacionados con este.
Sabemos que el estudio de los motores de reluctancia conmutada es muy amplio, en el área de control principalmente, y espero que este tema sea el camino para abrir un espacio en las futuras líneas de investigación.

SIMULACIÓN DINÁMICA DE UN MOTOR DE RELUCTANCIA ACCIONADO POR CONMUTACIÓN (MRAC) DE BAJO CONSUMO DE ENERGÍA ELÉCTRICA

Rosas Flores Jorge Alberto y Morales Collantes Arturo

Facultad de Ingeniería, Universidad Nacional Autónoma de México. Ciudad Universitaria. Apartado Postal 04510. Coyoacán 04510, México D. F. Tel (5) 622 31 26 ó 27, dirección de e-mail: coyantes@servidor.unam.mx, jrosas78@yahoo.com

RESUMEN.

El presente trabajo muestra la simulación del motor de reluctancia accionado por conmutación (MRAC) (6 polos en estator y 4 polos en el rotor).con características lineales; que nos ayudará a determinar el ahorro de energía que este tipo de tecnología nos brinda.

Este trabajo fue realizado utilizando la herramienta de programación MATLAB con simulación en SIMULINK

Donde los principales resultados son:

- ✓ Ahorro de energía eléctrica del 16%, basándose en consumos promedios de motores comerciales
- ✓ Ahorro económico en la construcción de estos motores del 27% con respecto a otras tecnologías utilizadas actualmente.

INTRODUCCION.

Los ingenieros destinados en el área de diseño de motores eléctricos, han estado buscando por un largo tiempo una solución a muchos problemas en su campo, que influye directamente en que las soluciones sean fundamentalmente a bajo costo, realizable, versátiles en aplicaciones, con alta confiabilidad en su uso y con bajo ruido.

La solución, que este tipo de diseñadores ha encontrado en su búsqueda de varios años, es voltear la mirada a la tecnología de motores de reluctancia accionados por conmutación (MRAC), el cual nos brinda una solución adecuada y justa a ciertas necesidades.

Los motores de reluctancia accionado por conmutación "**MRAC**" ó (*SRM*) por sus siglas en ingles "Switched Reluctance Motor" son una división de máquinas que en últimos años, han crecido de popularidad e interés, debido a la ausencia de devanados o imanes permanentes en el rotor, lo cual influye en los bajos costos y confiabilidad que estas máquinas nos brindan.

CARACTERISTICAS.

En un motor de reluctancia accionado por conmutación, únicamente existen bobinas en el estator, mientras que el rotor está hecho de una masa metálica sin ningún conductor o imán permanente.

El funcionamiento del motor de reluctancia accionado por conmutación, es muy simple al igual que su estructura, esto se basa en la generación y conmutación de campos magnéticos que se lleva a cabo en los bobinados de los polos del estator que es la parte fija de la máquina.

Si se alimentase una fase del motor con una corriente que produzca un campo magnético, que a su vez, produzca un par que tienda a alinear a los polos del rotor que se encuentren más cercanos, esto con el fin de poder hacer mínima la reluctancia entre ambos, en este caso

si una fase se encuentra alineada, por consiguiente la siguiente fase estará desalineada

Si se presenta una excitación en los bobinados del rotor secuencial entre fases, en función de la posición del rotor, se generará una producción continua de giro y par.

El sentido de giro, es determinado totalmente en el sentido de la secuencia en que es alimentado las bobinas del rotor.

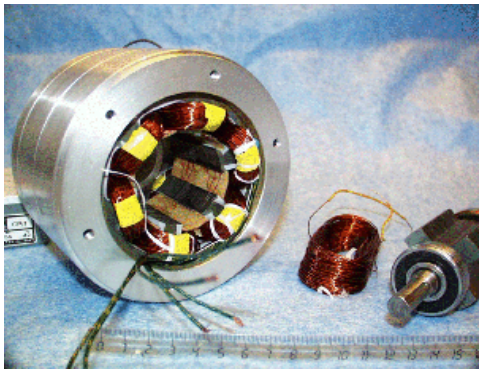

FIGURA 1. VISTA DE UN MRAC.

Cuando este tipo de tecnología es comparada con maquinas CA y CD, muestra estas ventajas:

1) Es muy barata en su construcción, además de ser muy confiable en su funcionamiento, esto debido a que cada fase está físicamente, magnética y eléctricamente independiente de las otras fases del estator de la máquina.
2) Puede alcanzar altas velocidades, consecuente a su bajo momento de inercia esto debido a que no contiene conductores o imanes en el rotor.

Mientras, el MRAC tiene algunas limitaciones:

1) La máquina debe ser alimentada siempre por conmutación y por ello no puede ser colocada o instalada en un bus de CD ó una línea de AC.
2) Debido a que este tipo de máquina es de polos salientes, presenta no linealidades magnéticas, lo cual complica el análisis y su control.

ECUACIONES ELECTROMAGNETICAS:

El voltaje instantáneo de las terminales de los devanados de una fase del MRAC, esta relacionado con el flujo producido en estos, por la ley de Faraday, como se menciona

$$V = iR_m + \frac{d\phi}{dt} \qquad (1)$$

En donde V es la terminal de voltaje, i es la corriente de fase, R_m es la resistencia del motor y ϕ es el flujo magnético del devanado.

Pero como la construcción del motor es de polos salientes (tanto el rotor como el estator), además de los efectos de saturación magnética, en general, el flujo magnético en las fases del MRAC varia en función de la posición del rotor (θ), y la corriente del motor de la ecuación 1 es complementada como sigue.

$$V = iR_m + \frac{\partial\phi}{\partial i}\frac{di}{dt} + \frac{\partial\phi}{\partial\theta}\frac{d\theta}{dt} \qquad (2)$$

donde $\frac{\partial\phi}{\partial i}$ esta definido como $L(\theta,i)$ la inductancia instantánea, $\frac{\partial\phi}{\partial\theta}$ es $K_b(\theta,i)$ que es la FEM instantánea.

ECUACION GENERAL DE PAR

La ecuación anterior (2) muestra la transferencia de energía eléctrica a campos magnéticos para el MRAC; En este punto desarrollaremos la ecuación que describe la conversión de la energía de los campos en energía mecánica.

Si nosotros multiplicamos cada lado de la ecuación (1) por la corriente eléctrica i,

obtenemos la expresión de la potencia instantánea en un MRAC.

$$Vi = i^2 R_m + i\frac{d\phi}{dt} \qquad (3)$$

La parte izquierda de la ecuación (3) representa la potencia eléctrica instantánea proporcionada por el MRAC, El primer termino en la parte derecha de la ecuación (3) representa las perdidas ohmicas en los devanados del MRAC, el siguiente termino representa la suma de la salida de la potencia mecánica del MRAC y toda la potencia es guardada en los campos magnéticos, y se puede representar así:

$$i\frac{d\phi}{dt} = \frac{dWm}{dt} + \frac{dWf}{dt} \qquad (4)$$

Donde el término $\frac{dW_m}{dt}$ es la potencia mecánica instantánea, y $\frac{dW_f}{dt}$ es la potencia instantánea, que es almacenada en los campos magnéticos. Como potencia es definida como la razón de cambio de la energía en función del tiempo.

Por lo que W_m es la energía mecánica y W_f es la energía de los campos magnéticos.

Conociendo la potencia mecánica, podremos nosotros escribir a esta como el producto de par y velocidad como sigue.

$$\frac{dWm}{dt} = T\omega = T\frac{d\theta}{dt} \qquad (5)$$

donde T, es el par, y $\omega = \frac{d\theta}{dt}$ es la velocidad rotacional del rotor o flecha.

Ahora bien, si sustituimos la ecuación número 5 en la ecuación número 4 se obtiene.

$$i\frac{d\phi}{dt} = T\frac{d\theta}{dt} + \frac{dWf}{dt} \qquad (6)$$

resolviendo la ecuación anterior (6), para obtener la ecuación de la producción de par.

$$T(\theta,\phi) = i(\theta,\phi)\frac{d\phi}{d\theta} - \frac{dWf(\theta,\phi)}{d\theta} \qquad (7)$$

MODELO UTILIZADO PARA LA SIMULACIÓN.

Los parámetros usados para la simulación basada en MATLAB-SIMULINK, fueron tomados del análisis obtenido en [1], el se describe a continuación.

$$\theta_s = 2\Pi(\frac{1}{N_r} - \frac{1}{N_s}) \qquad (8)$$

Donde N_r y N_s son el número de polos del rotor y estator respectivamente.

Un factor importante que se debe determinar es el arco del estator y el rotor, que en este caso son iguales $\beta_r=\beta_s$. Estos parámetros se pueden observar en la siguiente figura.

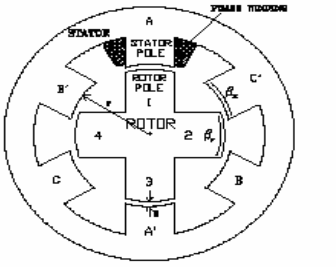

ARCOS DE ROTOR Y ESTATOR DE UN MRAC 6/4

con respecto a las figuras anteriores se obtiene la siguiente relación.

$$\theta_x = (\frac{\Pi}{N_r} - \beta_r) \qquad (9)$$

$$\theta_y = \frac{\Pi}{N_r} \qquad (10)$$

Como se indica en las anteriores figuras, el ángulo δ corresponde al desplazamiento de una fase con respecto a otra y esta determinada por:

$$\delta = 2\Pi(\frac{1}{N_r} - \frac{1}{N_s}) \qquad (11)$$

Con estos parámetros, y sabiendo que se esta haciendo un análisis en régimen lineal, la relación que el flujo tiene es:

$$\psi = L(\theta)I \qquad (12)$$

La simplificación en ecuación por linealización nos proporciona la ecuación de par siguiente:

$$T = \frac{i^2 dL}{2d\theta} \qquad (14)$$

y para poder representar las ecuaciones mecánicas del MRAC, podemos representar la siguiente igualdad.

$$J\frac{d\omega}{dt} = T - Tl - f\omega \qquad (15)$$

y

$$\frac{d\theta}{dt} = \omega \qquad (16)$$

en donde *Tl* representa el par de carga, y *f* es el coeficiente de fricción, y ω es la velocidad angular del rotor.

PARÁMETROS DEL MOTOR SIMULADO.

Los parámetros considerados para la simulación son: Números de polos del estator N_r=6, Números de polos en el rotor N_s=4; parámetros de la inductancia, Lmin=.008 [H], Lmax=.06 [H], resistencia de fase del estator, r=1.3Ω; momento de inercia, J=.003 kgm^2

ESQUEMA DE SIMULACIÓN.

A continuación se presenta el esquema general de la simulación realizada al MRAC; este esquema se refiere a la simulación en SIMULINK, con sus llamadas de programas en MATLAB. Los bloques presentados dan una perspectiva básica y general de la forma en como opera el programa.

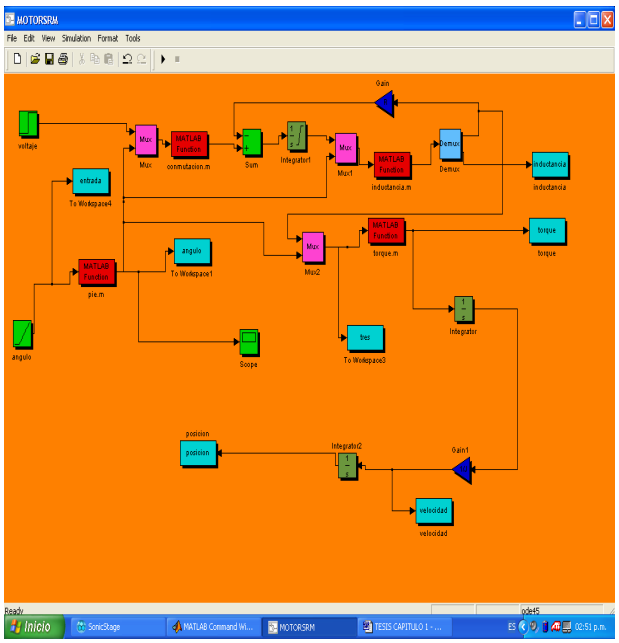

ESQUEMA DE SIMULACION SIMULINK-MATLAB

RESULTADOS DE SIMULACIÓN.

Aquí se presenta los resultados más representativos derivados de la simulación.

A. INDUCTANCIA.

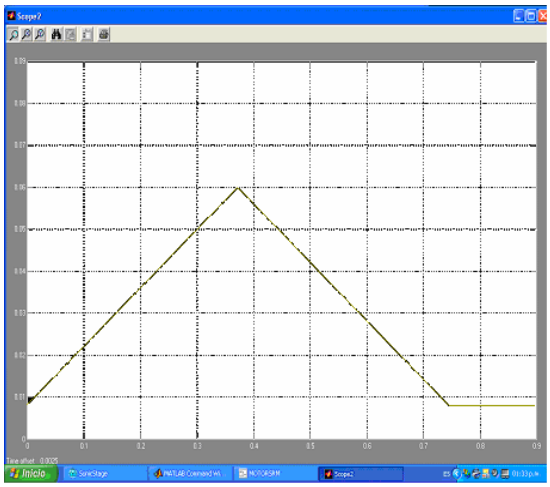

B. CORRIENTE

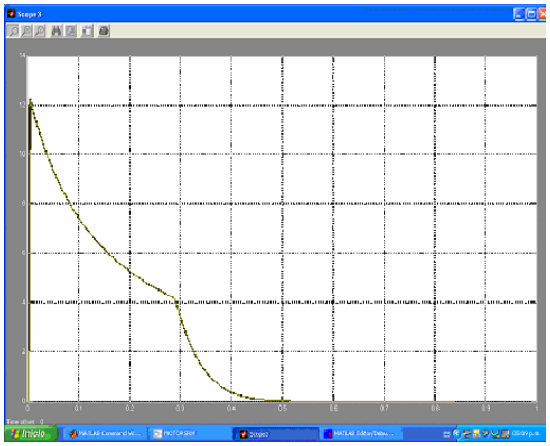

C) PAR.

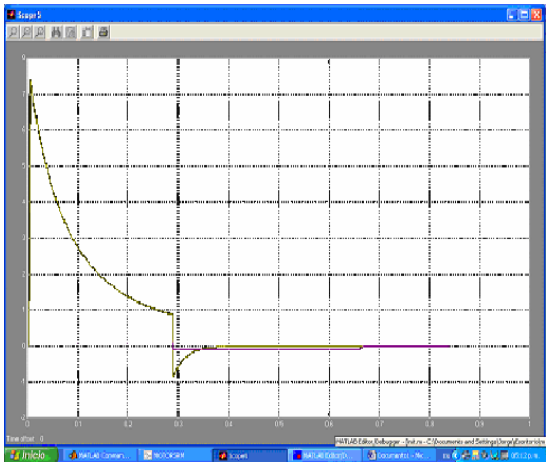

D) VELOCIDAD.

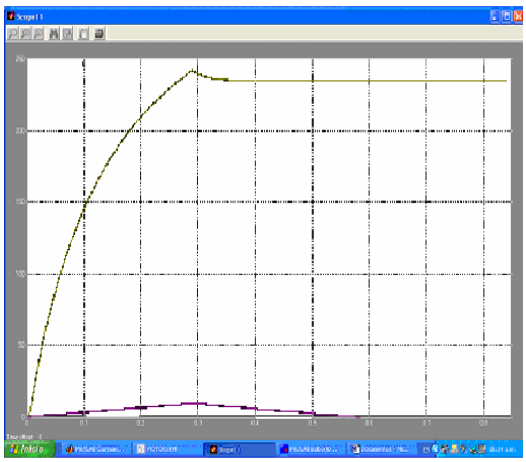

TABLA 1 CARACETRIZACIÓN DEL MRAC SIMULADO

PARAMETRO	VALOR	UNIDADES
NUMERO DE FASES EN EL ESTATOR	6	----------
NUMERO DE FASES EN EL ROTOR	4	----------
MAXIMA INDUCTANCIA	.06	[H]
MINIMA INDUCTANCIA	.008	[H]
VOLTAJE DE ALIMENTACIÓN	100	[V]
CORRIENTE DE FASE	12.1	[A]
VELOCIDAD	2197 230	[r.p.m] [rad/s]
PAR	7.4	[N.m]
MOMENTO DE INERCIA	.003	[kgm^2]
RESISTENCIA DE FASE	1.30	[Ω]
POTENCIA	2.28 1.7	[Hp] [kW]

CONSUMO DE ENERGÍA.

Un punto importante dentro del estudio de los motores eléctricos, es el poder saber el consumo de energía eléctrica que estos tienen, como se presenta más adelante, se realiza una comparación entre los motores eléctricos más comunes con respecto al MRAC simulado, como se podrá comprender, la comparación entre motores es muy difícil, esto debido a que existe una diferencia importante entre tecnologías y formas de funcionamiento, pero la idea principal de este punto es poder visualizar en forma general el comportamiento de consumo energético entre diversos equipos de similares características, en este caso se basa principalmente en la potencia de los motores.

TABLA No 2 CONSUMO Y AHORRO DE ENERGÍA ENTRE MOTORES ELÉCTRICOS

TIPO DE MOTOR	POTENCIA (FUENTE DE ALIMENTACIÓN)	TIEMPO DE UTILIZACIÓN (HORAS AL AÑO)	ENERGÍA (kW-hr)	PRECIO DEL (kW-hr) EN PESOS ($) *TARIFA 2**	CONSUMO ANUAL EN ($)	DIFERENCIA ($/AÑO)
MOTOR DE RELUCTANCIA ACCIONADO POR CONMUTACIÓN	1.21 kW	1560	1887.6	$27.60	$52,097	----------
MOTOR DE CORRIENTE CONTINUA	2.04 kW	1560	3182.4	$27.60	$87,834	$35,737
MOTOR MONOFÁSICO DE CORRIENTE ALTERNA.(valores eficaces)	1.42 Kw	1560	2223.7	$27.60	$61,376	$9,279

** obtenida de la página en internet de CFE www.cfe.gob.mx*

TABLA No 3 COSTO EN MOTORES ELÉCTRICOS

TIPO DE ALIMENTACION	*POTENCIA*	*VOLTAJE DE ALIMENTACIÓN*	*R.P.M*	*COSTO APROXIMADO DE MANUFACTURA*
CORRIENTE DIRECTA	*2 HP*	*115 [V]*	*1800*	*$489 UDS*
CORRIENTE ALTERNA (MONOFÁSICO)	*2 HP*	*127 [V]*	*1800*	*$1655*
MOTOR DE RELUCTANCIA ACCIONADO POR CONMUTACION	*2 HP**	*162[V]* EN FUENTE CONMUTADA.*	*500*	*$180 UDS**

CONCLUSIONES.

Debido a la simplicidad física de la máquina, el momento de inercia de rotor, presenta una disminución del 44% con respecto a otros motores de tecnologías convencionales de similares características y dimensiones.

Ahorro en la construcción de los motores de reluctancia accionados por conmutación (MRAC) del orden del 30% con respecto a otras tecnologías convencionales funcionando actualmente.

Ahorro en el consumo de energía eléctrica del 16% en consumos promedios con respecto a tecnologías de motores convencionales utilizados actualmente.

El ahorro de energía eléctrica anteriormente mencionado, es una señal importante para voltear la mirada a este tipo de tecnología, y brindar la oportunidad de poderse desarrollar y demostrar sus beneficios.

Como se puede observar los motores de reluctancia accionados por conmutación (MRAC) son hoy una realidad y actualmente es una opción que responde a la necesidad de ahorrar y usar eficientemente la energía eléctrica, con el fin primordial de abatir emisiones contaminantes a la atmósfera y poder prolongar la vida de los recursos no renovables.

BIBLIOGRAFÍA

[1] J.Nascimento, L. Rolim, P. Heidrich et al, "*Design and simulation aspects of a switched reluctance drive*", Proc. of 4° Brazilian Power Conference (COBEP96).

[2] P.O. Rasmussen, G. Andersen, L. Helle, J.K. Pedersen, F. Blaabjerg, "*Switched reluctance Motors drives*", IEEE Transaction on Industry Applications, 1996 (ALBORG university Denmark)

[3] Norma Oficial Mexicana NOM-001-SEDE-1999, Instalaciones Eléctricas (utilización), Diario Oficial de la Federación, 19 de abril de 1999.

JORGE ALBERTO ROSAS FLORES. Egresado de la carrera de Ingeniero Eléctrico-Electrónico de la Facultad de Ingeniería UNAM. Actualmente estudia maestría en el área de Energía en DEPFI UNAM.

ARTURO MORALES COLLANTES. Es Ing. Mecánico Electricista de la Facultad de Ingeniería UNAM, profesor titular de carrera FI UNAM en el área de Ing. Eléctrica de potencia, Actualmente es jefe del departamento de Ing. Eléctrica de Potencia de la FI UNAM.

OBJETIVO GENERAL.

Comprobar que los Motores de Reluctancia Accionados por Conmutación (MRAC) son de bajo consumo de energía eléctrica; a partir de su caracterización basada en un modelo de simulación digital.

Objetivos Particulares:

- ✓ Conocer las características físicas y matemáticas del motor de reluctancia para conocer las ventajas y desventajas que nos puede ofrecer.

- ✓ Realizar uno de los primeros estudios sobre motores de reluctancia basado en programación en MATLAB-SIMULINK.

- ✓ Conocer las respuestas temporales derivadas de la simulación dinámica basada en MATLAB-SIMULINK, como es el caso de la corriente, inductancia y torque de fase, además de la velocidad y el votaje de alimentación del motor.

- ✓ Conocer el ahorro de energía que los motores de reluctancia tienen sobre otras tecnologías de características similares de iguales dimensiones.

- ✓ Presentar en forma didáctica todos los conocimientos presentados, esto con el fin de tener una fácil comprensión por parte de la gente que consulte esta obra.
  Esta forma didáctica, será en base a un CD-ROM que contiene la programación en MATLAB y la simulación hecha en SIMULINK, además de programas hechos por investigadores dedicados al área de estudio de los motores de reluctancia; se anexan

además manuales de MATLAB-SIMULINK que ayudaran a comprender mejor lo realizado en este trabajo de tesis.

- ✓ Conocer los avances que los motores de reluctancia tiene hasta la fecha y poder saber o inferir, el impacto que estos motores nos brindarán en un tiempo no muy largo.

- ✓ Apertura y conocimiento de futuras líneas de investigación, que aporten y sirvan para formar un camino firme en el desarrollo y estudio de los motores de reluctancia

HIPOTESIS:

- ✓ Los motores de reluctancia accionados por conmutación son máquinas eléctricas de bajo consumo energético.

- ✓ Los motores de reluctancia accionados por conmutación son máquinas eléctricas que presentan una atractiva eficiencia con respecto a otras tecnologías utilizadas actualmente.

- ✓ Los motores de reluctancia accionados por conmutación presentan una sencilla forma de construcción que redunda en un bajo costo tanto constructivo como operativo.

- ✓ Esta división de máquinas eléctricas se encuentra actualmente en desarrollo en nuestro país, además de otros centros de desarrollo e investigación internacionales.

CAPITULO 1

ANTECEDENTES (MOTORES ELÉCTRICOS)

En este capítulo, haremos referencia a la ubicación que los motores de reluctancia accionados por conmutación "**MRAC**" tienen dentro de las máquinas eléctricas. En la primera sección hablaremos de conceptos básicos de motores eléctricos, como es el caso de una breve reseña histórica, clasificación y uso de los motores eléctricos, hasta poder llegar a ubicar a los *MRAC´s* dentro de las máquinas eléctricas, esto permitiendo comprender las características fundamentales que nos pueden brindar.

1.1 MOTORES ELÉCTRICOS

Los motores eléctricos efectúan la transformación de la energía eléctrica recibida de la red en energía mecánica en su eje, por intermedio de las interacciones electromagnéticas entre los devanados o los materiales magnéticos del rotor y el estator del motor.
En general el rendimiento de la transformación es muy alto comparativamente con otros dispositivos convertidores de energía. Sin embargo, hay varias razones que inducen a

prestar atención a la utilización racional de la energía en el empleo de los motores eléctricos.

Uno de ellos es el rendimiento del motor eléctrico, que esta ligado al empleo de una energía de calidad excepcional.

Otro punto es la gran difusión del uso de los motores eléctricos, entre otras razones por su alto rendimiento, economía, comodidad de empleo y limpieza, lo cual es una pieza fundamental de los procesos productivos actuales.

Como un dato muy importante se puede estimar que el 35% de la energía eléctrica se consume en los motores eléctricos.

1.2 LOS MOTORES ELÉCTRICOS EN LA HISTORIA.

Para ubicar los motores en la historia tenemos inevitablemente que remontarnos al descubrimiento y desarrollo de fenómenos magnéticos y eléctricos básicos. El fenómeno del magnetismo se conoce desde tiempos antiguos, las primeras observaciones de fenómenos magnéticos fueron hechas en la ciudad de Asia menor llamada Magnesia.

La piedra imán o magnetita, un óxido de hierro que tiene la propiedad de atraer los objetos de hierro, ya era conocida por los griegos, los romanos y los chinos. Cuando se pasa una piedra imán por un pedazo de hierro, éste adquiere a su vez la capacidad de atraer otros pedazos de hierro. Los imanes así producidos están ‘polarizados’, es decir, cada uno de ellos tiene dos partes o extremos llamados polos norte y sur. Los polos iguales se repelen, y los polos opuestos se atraen.

Tales de Mileto, seis siglos antes de Cristo, observó que una barra de ambar frotada atraía pequeñas partículas de materia.

La brújula se empezó a utilizar en Occidente como instrumento de navegación alrededor del 1300 d.C

William Gilbert publicó su libro, *De magnete* en 1600. Gilbert aplicó métodos científicos al estudio de la electricidad y el magnetismo.

Charles de Coulomb, en 1777 inventó la balanza de torsión para medir la fuerza de atracción magnética y eléctrica. Con este invento, Coulomb pudo establecer el principio, conocido ahora como ley de Coulomb, que rige la interacción entre las cargas eléctricas.

Hacia 1800 es desarrollada la llamada pila de Volta, precursora de la batería eléctrica, que producía un flujo estable de electricidad, y hace así su aparición en la historia la corriente eléctrica, uno de los fenómenos físicos que más han revolucionado al mundo.

La primera Revolución Industrial tuvo lugar en el Reino Unido a finales del siglo XVIII aproximadamente en los años posteriores a 1875, supuso una profunda transformación en la economía y sociedad británicas. Los cambios más inmediatos se produjeron en los procesos de producción: qué, cómo y dónde se producía. El trabajo se trasladó de la fabricación de productos primarios a la de bienes manufacturados y servicios. El número de productos manufacturados creció de forma espectacular gracias al aumento de la eficacia técnica. Así, la Revolución Industrial tuvo como consecuencia una mayor urbanización y, por tanto, procesos migratorios desde las zonas rurales a las zonas urbanas.

Se puede afirmar que los cambios más importantes afectaron a la organización del proceso productivo. Las fábricas aumentaron en tamaño y modificaron su estructura organizativa, es decir, se sustituyo el trabajo artesanal por producción en serie donde se utilizan maquinas (motores) para la realización de estos.

Esta etapa hace un giro total en la percepción y desarrollo de maquinas para la producción. Es aquí donde los motores eléctricos toman un camino seriamente prometedor hacia un futuro muy cercano.

Hans Christian Oersted, demostró la existencia de un campo magnético en torno a una corriente eléctrica.
En 1819 descubrió que una aguja imantada se desvía colocándose en dirección perpendicular a un conductor por el que circula una corriente eléctrica, iniciando así el estudio del electromagnetismo

André Marie Ampère En 1826 fue el primero en demostrar que dos conductores paralelos por los que circula una corriente en el mismo sentido, se atraen el uno al otro, mientras que si los sentidos de la corriente son opuestos, se repelen.

En 1831, el científico británico Michael Faraday descubrió que el movimiento de un imán en las proximidades de un cable induce en éste una corriente eléctrica; este efecto era inverso al hallado por Oersted. Así, Oersted demostró que una corriente eléctrica crea un campo magnético, mientras que Faraday demostró que puede emplearse un campo magnético para crear una corriente eléctrica

Henry experimentó y perfeccionó el electroimán, inventado en 1823 por el británico William Sturgeon. Hacia 1829 había desarrollado electroimanes con gran fuerza de sustentación y eficacia y esencialmente iguales que los utilizados más tarde en motores eléctricos. En 1831 ideó y construyó uno de los primeros motores eléctricos.

En base a lo anterior, se puede decir que el motor eléctrico, estaba listo para su desarrollo.

Otro punto muy importante en la situación histórica de los motores es la iluminación, que gracias a su crecimiento ayudo al pronto desarrollo de la tecnología de las máquinas eléctricas.

Aproximadamente a partir de 1840 fueron patentadas varias lámparas incandescentes, aunque ninguna tuvo éxito comercial hasta que el inventor estadounidense Thomas Alva Edison lanzara su lámpara de filamento de carbono en 1879

Estos dos descubrimientos: trasformar energía mecánica (donde la hubiera) en electricidad y luego, transformar en otro sitio la energía eléctrica transportada a la velocidad de arrastre de la corriente eléctrica por un cable en energía mecánica (con motores o aparatos eléctricos), fue el acontecimiento más notable en la energética de la época.

La idea de suministrarla simultáneamente y coordinadamente a un cierto número de clientes impulsó la creación de un plan para el abastecimiento desde un sistema de generación común.

George Lane-Fox en Inglaterra y Thomas Alva Edison en EE.UU. propusieron planes para el desarrollo de esta idea. De esta manera, casi simultáneamente en Londres y Nueva Cork, se pusieron en servicio en 1882 las centrales térmicas de Holborn y de la calle Peral, dando un suministro que era bastante limitado en extensión.

Aunque estos sistemas jugaron un rol importante en el comienzo del desarrollo del servicio eléctrico, pronto se hicieron evidentes las limitaciones técnicas y económicas del transporte a media y gran distancia, que para la corriente continua parecían imposibles de evitar.

Paralelamente al desarrollo comercial de la corriente continua, en 1891 Gaulard y Gibas en Inglaterra patentaron un sistema de distribución en corriente alterna. Basado en esta patente, se perfeccionó el transformador, piedra fundamental de la utilización de la corriente alterna.

Las innumerables ventajas industriales de la energía eléctrica hicieron instalar rápidamente mayores centrales eléctricas privadas, establecidas por fábricas grandes; con esto se impulsó de manera importante el uso de máquinas eléctricas que hoy en día representan una base importante en el desarrollo y bienestar del ser humano.

1.3. TIPO DE CORRIENTE DE ALIMENTACIÓN PARA LOS MOTORES ELÉCTRICOS

Es este punto trataremos las dos fuentes principales de alimentación de energía eléctrica, que son la energía eléctrica alterna, y la energía eléctrica continua.
A continuación mostramos algunos fundamentos de estas formas de energía que servirán de base para su comprensión.

1.3.1 FUNDAMENTOS DE CORRIENTE ALTERNA.

El suministro de energía eléctrica en las redes de consumidores tiene lugar mediante corriente alterna ya que los niveles de una tensión alterna pueden ser cambiados, casi sin pérdidas, en los transformadores.

Se distinguen corrientes alternas monofásicas y trifásicas. La monofásica se compone de una sola corriente alterna; la trifásica de tres corrientes alternas, separadas 120° eléctricos cada una.

En la producción de tensión por inducción, en el caso de corriente alterna, se obtiene en base a un generador síncrono, que a continuación se presenta en la figura 1.1.

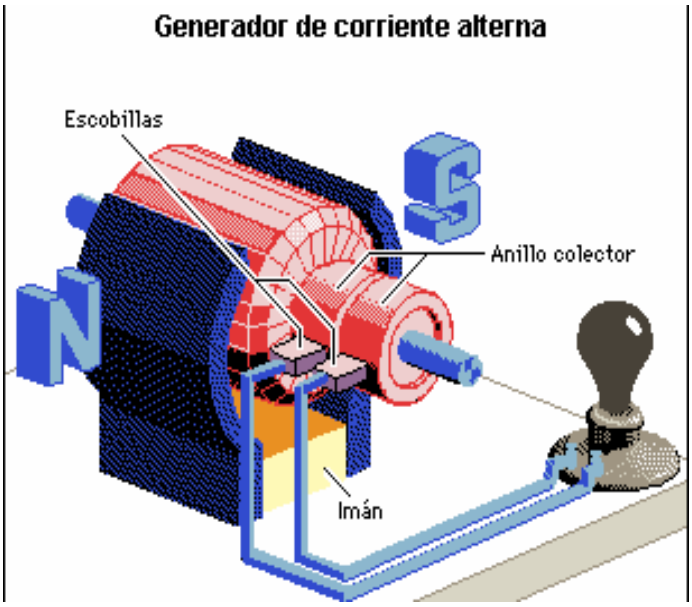

FIGURA 1.1 FUNDAMENTO DE UN GENERADOR DE CORRIENTE ALTERNA.

Obteniendose una forma de onda siguiente:

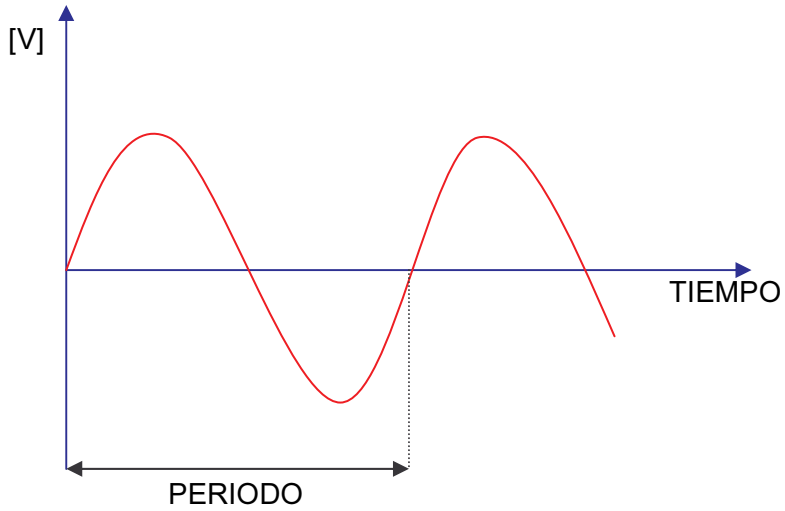

Con un giro uniforme de la espira en un campo magnético (homogéneo) aparece en ella una tensión en forma senoidal inducida, como se puede observar en la figura anterior.
En el giro uniforme de la espira, esta tensión inducida no sólo modifica su dirección sino también su magnitud. Con el movimiento giratorio se altera el flujo magnético que pasa por la espira.
Una oscilación completa se denomina periodo (T). La duración del periodo se mide en segundos.
El número de periodos por segundo se denomina frecuencia f. La unidad de frecuencia es el Hertz (símbolo Hz).
La frecuencia es tanto mayor, cuanto menor es la duración del periodo. La frecuencia es la inversa de la duración del periodo.

$$f = \frac{1}{T}$$

1.3.2 FUNDAMENTOS DE CORRIENTE CONTINUA.

El generador de corriente continua, o dínamo, es una máquina eléctrica que permite obtener en sus terminales una corriente que tiende a tener un valor constante.
En la figura 1.2 se muestra el esquema de un generador de corriente continua.

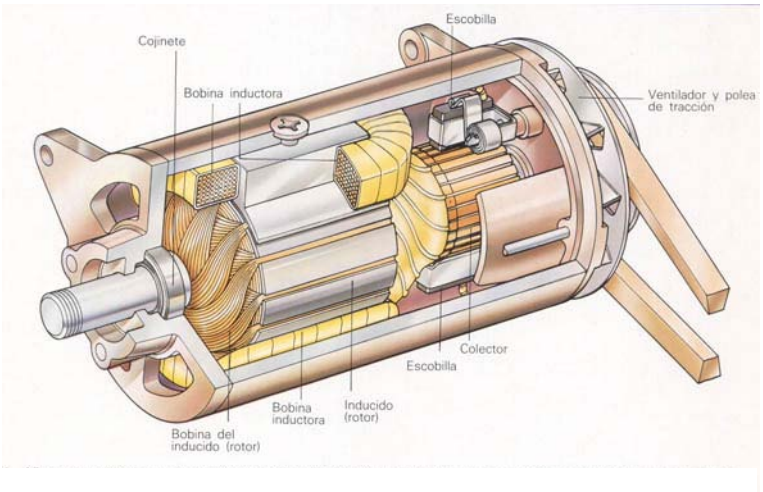

FIGURA 1.2 VISTA DE UN GENERADOR DE CORRIENTE CONTINUA.

Como se puede observar, una modificación en los anillos y escobillas del alternador de la figura 1.1 nos permite obtener un generador de corriente continua. El cambio consiste en eliminar uno de los dos anillos y seccionar en dos partes iguales el restante, cada sección debe hacer contacto con una escobilla.

De esta forma se evitan los semiciclos negativos obtenidos en el alternador y la fuerza electromotriz inducida será de corriente continua como se puede observar en la siguiente figura.

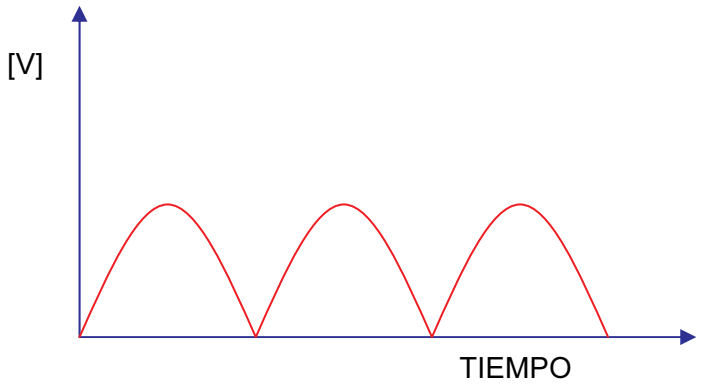

En base a estas dos principales fuentes de alimentación podremos dar una clasificación de los motores eléctricos, esto con el fin de poder ubicar a los *MRAC* dentro de las máquinas eléctricas.

1.4 CLASIFICACIÓN DE LOS MOTORES ELÉCTRICOS

La clasificación de los motores eléctricos por tipo, se plasma en el siguiente cuadro (en forma representativa en sus categorías), este se ha efectuado de acuerdo con el criterio clásico, aunque externo al motor; que es la clase de tensión o corriente principal que le alimenta.

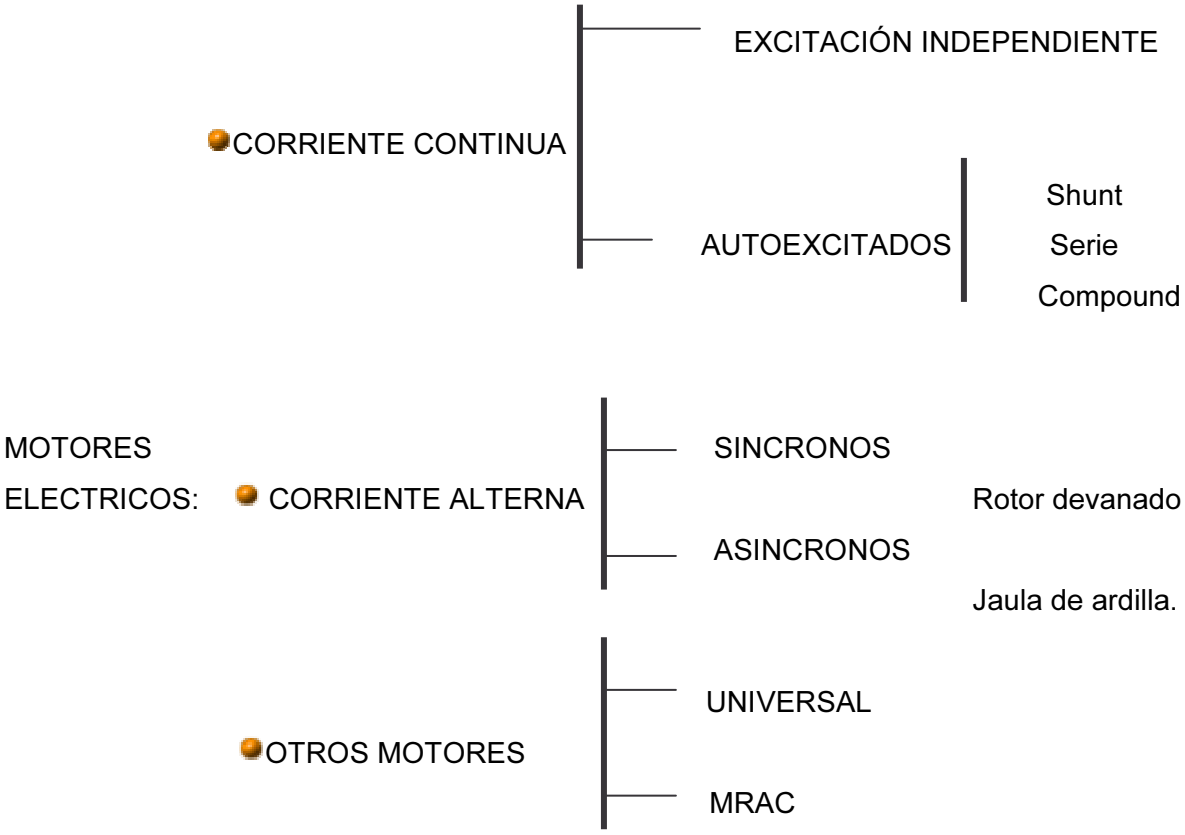

La diversidad de tipos de motores eléctricos que se hace patente en el cuadro anterior, está justificada principalmente en función de tres condiciones: el desarrollo histórico de la ciencia y la tecnología de la eléctrica-electrónica, razones económicas y finalmente la diversidad de las exigencias requeridas a los motores eléctricos, tanto a nivel de potencia como a la diferente complejidad de las aplicaciones

Los motores eléctricos son máquinas utilizadas en transformar energía eléctrica en mecánica. Son los motores utilizados en la industria, pues combinan las ventajas del uso de la energía eléctrica (bajo, costo, facilidad de transporte, limpieza y simplicidad de la puesta en marcha, etc) con una construcción relativamente simple, costo reducido y buena adaptación a los mas diversos tipos de carga.

De acuerdo a la fuente de tensión que alimente al motor, podemos realizar la siguiente clasificación:

- Motores de corriente directa (DC)
- Motores de corriente alterna (AC)
- Otros motores

A continuación se menciona en forma breve el principio de funcionamiento de cada una de las categorías descritas con anterioridad.

Motores de Corriente Directa (DC)

Se utilizan en casos en los que es de importancia el poder regular continuamente la velocidad del eje y en aquellos casos en los que se necesita de un toque de arranque elevado.

Además, utilizan en aquellos casos en los que es imprescindible utilizar corriente continua, como es el caso de trenes y automóviles eléctricos, motores para utilizar en el arranque y en los controles de automóviles, motores accionados a pilas o baterías, etc.

Para funcionar, el motor de corriente continua o directa precisa de dos circuitos eléctricos distintos: el circuito de campo magnético y el circuito de la armadura.

El campo (básicamente un imán o un electroimán) permite la transformación de energía eléctrica recibida por la armadura en energía mecánica entregada a través del eje. La energía eléctrica que recibe el campo se controla en su mayoría en la resistencia externa con la cual se regula la corriente del campo magnético. Es decir ninguna parte de la energía eléctrica recibida por el circuito del campo, es transformada en energía mecánica.

FIGURA 1.3 VISTA DE UN PEQUEÑO MOTOR DE CORRRIENTE CONTINUA.

La armadura consiste en un grupo de bobinados alojados en el rotor y en un ingenioso dispositivo denominado colector mediante el cual se recibe corriente continua desde una

fuente exterior y se convierte la correspondiente energía eléctrica en energía mecánica que se entrega a través del eje del motor.

Motores de Corriente Alterna (AC)

Bajo el título de motores de corriente alterna podemos reunir a los siguientes tipos de motor.

- Motor Síncrono
- El Motor Asíncrono o de Inducción

El Motor Síncrono

Este motor tiene la característica de que su velocidad de giro es directamente proporcional a la frecuencia de la red de corriente alterna que lo alimenta. Por ejemplo si la fuente es de 60Hz, si el motor es de dos polos, gira a 3600 RPM; si es de cuatro polos gira a 1800 RPM y así sucesivamente. Este motor o gira a la velocidad constante dada por la fuente o, si la carga es excesiva, se detiene.

El motor síncrono es utilizado en aquellos casos en que los que se desea velocidad constante. En nuestro medio sus aplicaciones son variadas y casi siempre están en relación con sistemas de regulación y control mas no con la transmisión de potencias elevadas.

A pesar de su uso reducido como motor, la maquina síncronica es la mas utilizada en la generación de energía eléctrica. Por ejemplo, en México, todas las centrales hidroeléctricas y termoeléctricas generan energía eléctrica con generadores síncronos.

FIGURA 1.4 VISTA DE UN MOTOR SINCRONO.

El Motor Asincrónico o de Inducción

Si se realizara a nivel industrial una encuesta de consumo de la energía eléctrica utilizada en alimentar motores, se vería que casi la totalidad del consumo estaría dedicado a los motores asíncronicos.

Estos motores tienen la peculiaridad de que no precisan de un campo magnético alimentado con corriente continua como en los casos del motor de corriente directa o del motor síncronico.

Una fuente de corriente alterna (trifásica o monofásica) alimenta a un estator. La corriente en las bobinas del estator induce corriente alterna en el circuito eléctrico del rotor (de manera algo similar a un transformador) y el rotor es obligado a girar.

De acuerdo a la forma de construcción del rotor, los motores asíncronicos se clasifican en:

Motor Asincrónico de Rotor Bobinado

Motor Asincrónico tipo Jaula de Ardilla

Motor Asincrónico de Rotor Bobinado

Se utiliza en aquellos casos en los que la transmisión de potencia es demasiado elevada (a partir de 200 kW) y es necesario reducir las corrientes de arranque. También se utiliza en aquellos casos en los que se desea regular la velocidad del eje.

Su característica principal es que el rotor se aloja un conjunto de bobinas que además se pueden conectar al exterior a través de anillos rozantes. Colocando resistencias variables en serie a los bobinados del rotor se consigue suavizar las corrientes de arranque. De la misma manera, gracias a un conjunto de resistencias conectadas a los bobinados del rotor, se consigue regular la velocidad del eje.

Motor Asincrónico tipo Jaula de Ardilla

Finalmente aquí llegamos al motor eléctrico por excelencia. Es el motor relativamente más barato, eficiente, compacto y de fácil construcción y mantenimiento.

FIGURA 1.5 VISTA DE UN MOTOR TIPO JAULA DE ARDILLA

Siempre que sea necesario utilizar un motor eléctrico, se debe procurar seleccionar un motor asíncronico tipo jaula de ardilla y si es trifásico mejor.

Por otro lado, la única razón para utilizar un motor monofásico tipo jaula de ardilla en lugar de uno trifásico será porque la fuente de tensión a utilizar sea también monofásica. Esto sucede en aplicaciones de baja potencia. Es poco común encontrar motores monofásicos de más de 3 [kW].

La diferencia con el motor de rotor bobinado consiste en que el rotor esta formado por un grupo de barras de aluminio o de cobre en formas similar al de una jaula de ardilla.

Otros Motores

Hemos mencionado los motores eléctricos de mayor uso en nuestro medio. Existen otros que son utilizados en casos especializados o domésticos. Entre ellos conviene destacar los siguientes:

El motor universal

El *MRAC*

Motor universal

Tiene la forma de un motor de corriente continua en conexión serie. La principal diferencia es que es diseñado para funcionar con corriente alterna. Se utiliza en los taladros, aspiradoras, licuadoras, lustradoras, etc. su eficiencia es baja (de orden del 51%), pero como se utilizan en maquinas de pequeña potencia esta ineficiencia no se considera importante.

Motor de reluctancia accionado por conmutación (MRAC)

Básicamente consiste en un motor con bobinas en el estator que al ser energizadas con corriente continua de acuerdo a una secuencia, origina el avance del eje. Estos motores son hoy en día idealizados para la utilización en sistemas directamente productivos, gracias a los avances que la electrónica de potencia nos brinda hoy en día.

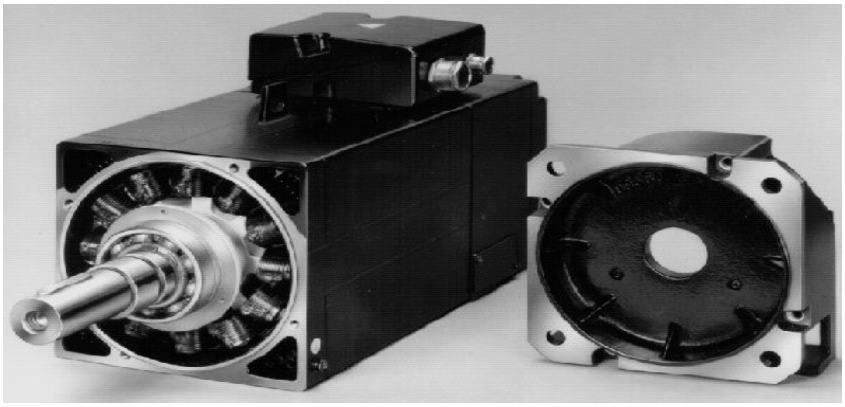

FIGURA 1.6 VISTA DE UN MOTOR DE MRAC.

1.5 USOS DE LOS MOTORES ELÉCTRICOS

El uso de motores eléctricos se lleva a cabo principalmente a nivel industrial, con base en esto, podremos referenciar los datos obtenidos en [18] que nos brinda una información esquemática, como es el caso de aplicación, potencia y tipo de motores que se utiliza para dicha actividad; esto se muestra en tabla 1 que a continuación se presenta.

TABLA No1 USOS DE LOS MOTORES ELÉCTRICOS EN LA INDUSTRIA

		CORRIENTE CONTINUA			*CORRIENTE ALTERNA MONOFASICA*	*CORRIENTE ALTERNA TRIFASICA*			
	POTENCIA	*SHUNT*	*SERIE*	*COMPOUND*		*TIPO JAULA DE ARDILLA*		*ROTOR DEVANADO*	*SÍNCRONO*
						NORMAL	*OPTIMIZADO*		
AGITADORES	.5-15 CP	X	--	--	X	X	--	X	--
MOLINOS DE HILOS	10-900 CP	X	--	X	--	--	X	X	X
MEZCLADORES	100-900 CP	--	--	--	--	X	--	--	X
BATIDORAS	100-200 CP	--	--	--	--	--	X	X	X
DESMENUZADORAS	1500 CP	--	--	--	--	--	X	X	X
COMPRESORES	200-600 CP	--	--	X	X	--	X	X	X
BANDAS TRANSPORTADORAS	3-100 CP	X	--	X	X	--	X	X	--
GRUAS Y MONTACARGAS	3-150 CP	X	X	X	--	--	--	--	--
TRITURADORAS	5-300 CP	--	--	X	--	--	--	X	X
EXTRACTORES	3-100 CP	--	--	X	--	--	X	X	--
VENTILADORES	150 CP	X	--	--	X	X	--	--	X
BOMBAS CENTRIFUGAS	1000 CP	X	--	--	X	X	--	--	X

X (valor reportados y utilizado)
--- (valor no reportado)

Son muchos los factores que deben tenerse en cuenta al elegir un motor. La solución por lo general no es única, pudiendo existir diversas opiniones respecto al cual es el motor adecuado. Sin embargo, puede resumirse que el motor apropiado es aquel que se ajusta a los requerimientos técnicos solicitados con un *costo mínimo*. Este último requisito no es factor difícil de calcular. Deben incluirse, no solo el costo de adquisición, sino también los gastos de operación. El costo de adquisición incluye la provisión de cualquiera de los equipos de alimentación y control necesarios para hacer funcionar al motor.

Los gastos de operación incluyen asimismo los gasto por la energía consumida en los circuitos de la maquina y en su control.

Los gastos de instalación también pueden ser decisivos. Por ejemplo: se necesitan cimentaciones especiales para los equipos de motores.

Algunos motores se excluyen de una aplicación determinada debido a que el ambiente de trabajo es hostil, tal como las condiciones de elevada temperatura., elevada velocidad o debido a la presencia de líquidos o ambientes corrosivos.

Por lo que hoy en día existen exigencias mayores para voltear la mirada a diferentes variedades de motores eléctricos, en este caso hablaremos de los *MRAC* que brinda sin duda alguna características especiales e importantes que como se comentará más adelante deben ser tomadas en cuenta para que en un futuro puedan ser implementados.

CAPITULO 2

LOS MRAC (PROPIEDADES)

En este capítulo se hace referencia de las propiedades que el MRAC presenta. En la primera sección se lleva a cabo una revisión de la forma de operación y características que este tipo de motor nos brinda, además de mostrar las partes constitutivas del mismo.

En la siguiente sección se muestra una revisión de estudios de simulación de los MRAC que se han realizado en diversos centros de investigación, este punto brindará la idea de el desarrollo que este tipo de máquinas han venido desarrollando desde hace tiempo.

2.1 PRINCIPIO DE OPERACIÓN DE LOS MRAC.

Los motores de Reluctancia Accionados por Conmutación MRAC ó SRM (siglas a partir de su nombre en inglés *Switched Reluctante Motor*) son una división de máquinas eléctricas que hoy en día han crecido de popularidad a su tipo de funcionamiento, para poder identificar con mayor precisión la forma en que estos motores realizan la conversión de la energía eléctrica en energía mecánica, es a partir de la clasificación siguiente.

- Máquinas que transforman la energía electromagnéticamente:

En esta categoría, el movimiento de la máquina se produce debido a la interacción de 2 campos magnéticos, uno de ellos es generado en el estator y el otro en el rotor. Cuando estos 2 campos magnéticos están acoplados mutuamente, existe un par electromagnético entre ambos, el cual tiende a llevarlos a alinearse.
En esta clasificación de máquinas, se requiere de devanados en el rotor y en el estator y además que sean excitados simultáneamente; como ejemplo de estos motores encontramos: los motores de inducción, síncronos y de C.D.
Estos motores difieren entre sí en su geometría y en como son generados los campos magnéticos actuantes, es decir, si son utilizados imanes permanentes o corrientes inducidas.

- Máquinas que transforman la energía por reluctancia variable.

Esta conversión de energía es el resultado de la reluctancia variable en el entrehierro del rotor y el estator.

Cuando un devanado del estator es energizado se produce un par reluctivo, debido a la tendencia para que el rotor se mueva de posición, de tal manera que se produzca una mínima reluctancia, en el campo magnético generado en el estator.

Esta forma de producción de energía mecánica, es análoga al par de alineamiento que se observa en dos imanes polarizados opuestamente.
El MRAC esta dentro de esta categoría de máquinas eléctricas.

Observando la clasificación anterior, el MRAC, la operación básica de funcionamiento se fundamenta en la *reluctancia*. El concepto *reluctancia* corresponde con la resistencia de flujo de campo magnético, la cual opone dicho rotor al campo electromagnético. La *reluctancia* en un circuito magnético es un equivalente a la resistencia en un circuito eléctrico.

Los MRAC, no pertenecen a las máquinas síncronas, debido que la dirección y velocidad en el giro del rotor no es igual a la rotación del flujo del estator. Es decir, el rotor gira en

dirección contraria al flujo, esto sucede si el número de polos en el rotor es menor que el número de polos en el estator.

2.2 FUNCIONAMIENTO DE LOS MRAC.

El funcionamiento del motor de reluctancia accionado por conmutación, es muy simple al igual que su estructura, esto se basa en la generación y conmutación de campos magnéticos que se lleva a cabo en los bobinados de los polos del estator que es la parte fija de la máquina.

Si se alimentase una fase del motor con una corriente que produzca un campo magnético, que a su vez, produzca un par que tienda a alinear a los polos del rotor que se encuentren más cercanos, esto con el fin de poder hacer mínima la reluctancia entre ambos, en este caso si una fase se encuentra alineada, por consiguiente la siguiente fase estará desalineada

Si se presenta una excitación en los bobinados del estator secuencial entre fases, en función de la posición del rotor, se generará una producción continua de giro y par.

El sentido de giro, es determinado totalmente en el sentido de la secuencia en que se alimenta a las bobinas del estator.

A continuación se muestra la figura *2.1* que ejemplifica lo descrito anteriormente; en este caso se muestra un MRAC 8ϕ, con una geometría de 16 polos en el estator y 12 polos en el rotor, que muestra claramente el desacoplamiento mencionado y la forma en como se alinearía el rotor en presencia del campo magnético que es conmutado en la parte estática del motor

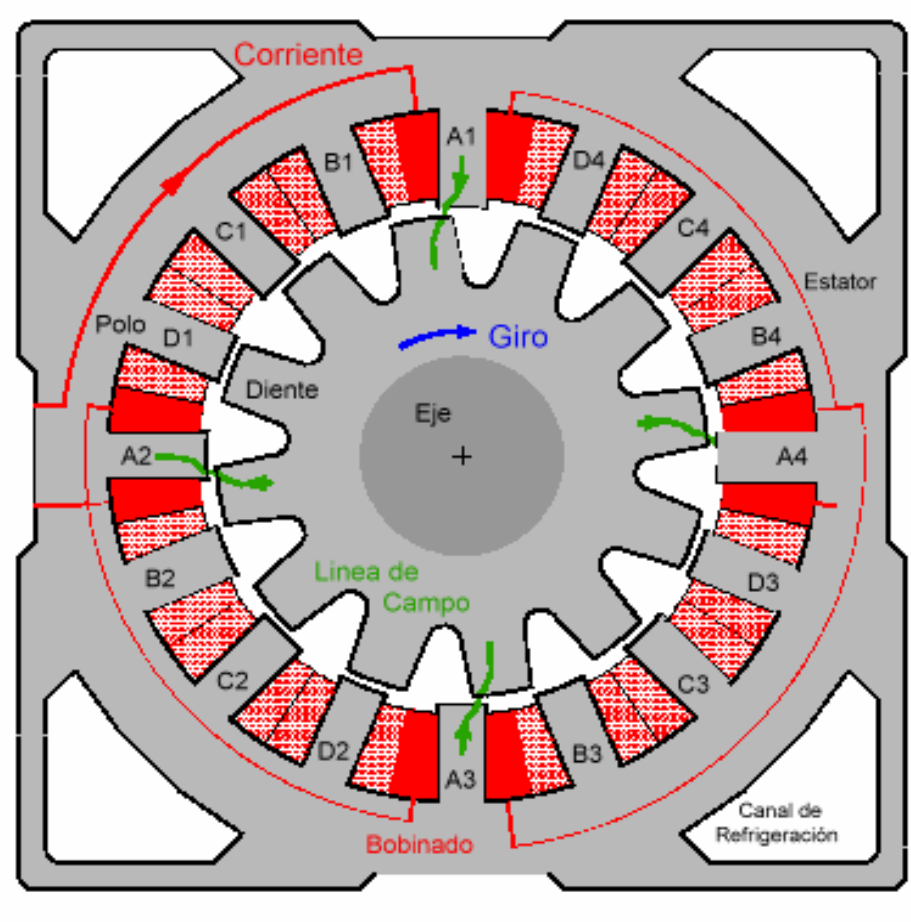

FIGURA 2.1. CORTE TRANSVERSAL DE UN MRAC

Como se mencionó anteriormente, una de las características que son primordiales de este motor, debido a su construcción y diseño, es el desacoplamiento. Cada una de las fases en el estator están desacopladas en forma física, además de eléctrica y magnética.

Estas propiedades que presenta ofrece indudablemente grandes ventajas, entre las cuales están que este tipo de máquinas puede seguir operando aún si una de sus fases es dañada, esto por supuesto afectará a su desempeño el cual no será el mismo que cuando la máquina trabajará con sus fases completas y normales, lo cual nos indica que este tipo de máquinas son muy confiables y seguras.

Un punto importante para su funcionamiento es el tipo de fuente de alimentación eléctrica para estos motores, con características muy especiales, con un principio de operación basada en la conmutación de energía eléctrica obtenida de la red de distribución.

2.3 CARACTERÍSTICAS DE LOS MRAC.

En esta sección se muestran las más importantes características que los MRAC presentan en sus diversas etapas de análisis, diseño, construcción, operación y control; tal es el caso de las curvas par-velocidad que nos brindan una visión general de la forma en como esta división de máquinas eléctricas pueden ser operadas; además de la geometría que estos motores presentan, este punto es primordial para la construcción y lógicamente el diseño de los mismos el cual dependerá fuertemente para un buen desempeño. Finalmente se presenta el concepto de la fuente de alimentación que acompaña a los MRAC, que es una pieza fundamental tanto para su diseño, operación. y control de los mismos.

2.3.1 CARACTERÍSTICAS PAR-VELOCIDAD.

La operación par-velocidad es un punto primordial de los MRAC, debido a que esta curva nos presenta una idea primordial de la forma en como trabaja este tipo de motores; esta información esta basada en el articulo [1] y la figura 2.2 representa esta característica.

Esta información esta basada en experiencias previas, las cuales conllevan a una serie de curvas o familias de curvas que se construyen en base a esta experiencia.

Como se menciona en este artículo la curva final obtenida se puede dividir en tres zonas la cuales serán explicadas posteriormente. Dentro de este articulo se menciona los siguiente “El MRAC puede ser solicitado en principio con pares de cargas de dos o tres veces superiores al par de carga nominal, en regimenes transitorios para todo el intervalo de velocidades”.

Con base en lo anterior podremos mas adelante obtener la curva del MRAC que nosotros proponemos en la simulación.

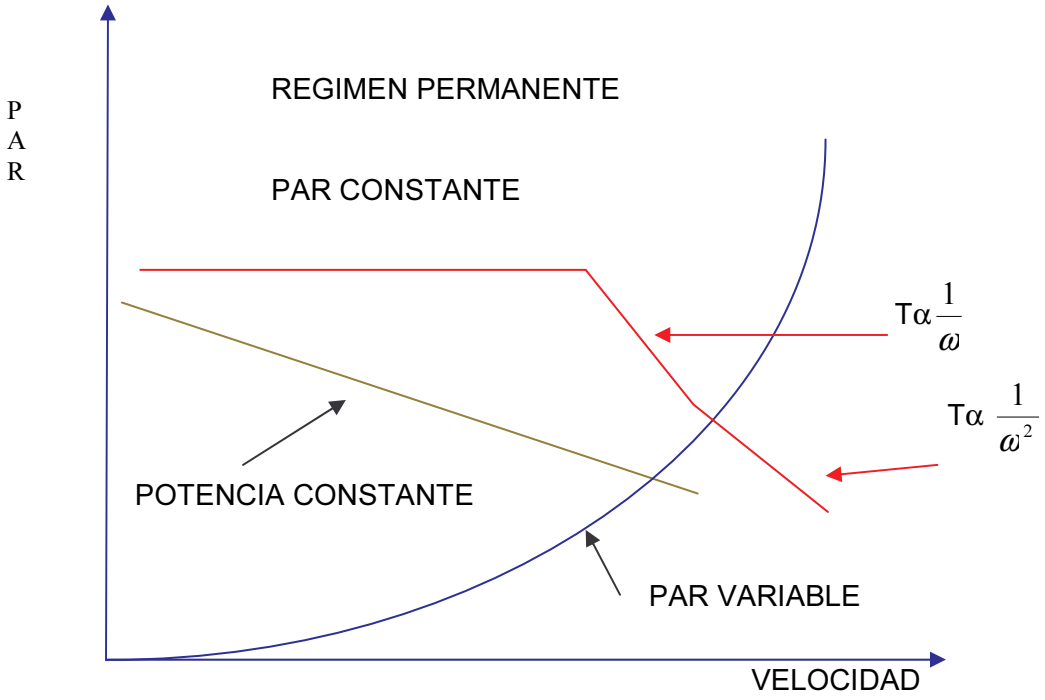

FIGURA 2.2 CURVA PAR-VELOCIDAD DEL MRAC.

2.3.2 FUENTE CONMUTADA DE ALIMENTACIÓN

La necesidad de un conmutador electrónico para llevar a cabo la alimentación de cada una de las fases también puede considerarse como una propiedad física de la máquina.

Esta necesidad es una derivación de la construcción misma de la máquina, que debido a su desacoplamiento de cada una de las fases debe ser alimentada en forma individual, no por tensiones de CD ni CA, si no por una tensión que debe ser conmutada y que depende totalmente de la posición del rotor.

El diseño del conmutador electrónico como se menciona anteriormente es una pieza fundamental para el control del MRAC ya que gran parte del buen desempeño que tenga el motor será debido a la forma en como trabaje el conmutador.

Para poder generar las señales conmutadas de estos motores es muy importante obtener la información de la posición que tiene el rotor, lo cual se puede lograr en forma física con

la implementación de un sensor de posición o en su defecto optar por una técnica de estimación del mismo como se muestra en diversos estudios [17] que su principal objetivo es de conocer el valor de posición del rotor sin necesidad de contar con algún dispositivo físico que realice esta tarea.

En la literatura científica que se revisó para este documento, hemos observado una división de trabajos que se enfocan a la conmutación en los MRAC [5], y que cada uno de ello proponen una estrategia propia para poder resolver ese problema.

En la figura 2.3 se puede apreciar uno de los esquemas electrónicos que más comúnmente son utilizados para la conmutación, en este caso se muestra una fuente conmuta para un MRAC trifásico (6 polos en el estator), como se podrá observar solo se presenta la idea principal del funcionamiento que este dispositivo tiene por fin.

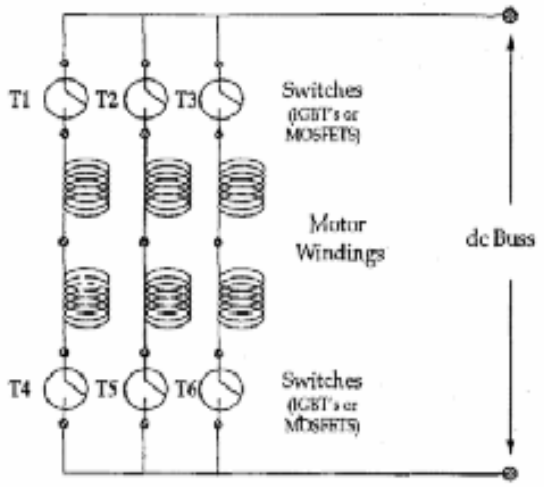

FIGURA 2.3 CONMUTADOR ELECTRÓNICO PARA UN MRAC 3ϕ

Si se observa el circuito, se puede observar que los interruptores se deben abrir y cerrar con el fin de poder obtener las curvas deseadas de corrientes del estator.

La secuencia de disparo de los interruptores es determinada propiamente por una ley de conmutación, en la revisión bibliográfica antes mencionada, se reportan estudios

detallados que han abierto un camino para el desarrollo de este tipo de componentes y leyes de conmutación.

Cabe destacar que el diseño de la fuente de conmutación es propia para cada uno de los MRAC, esto debido a que existe una gama muy amplia en geometrías de construcción de estos motores.

2.3.3 GEOMETRÍA DE LOS MRAC.

Los MRAC, son diseñados de distintas formas, en la figura 2.4 se muestra la configuración de diferentes tipos y diseños.

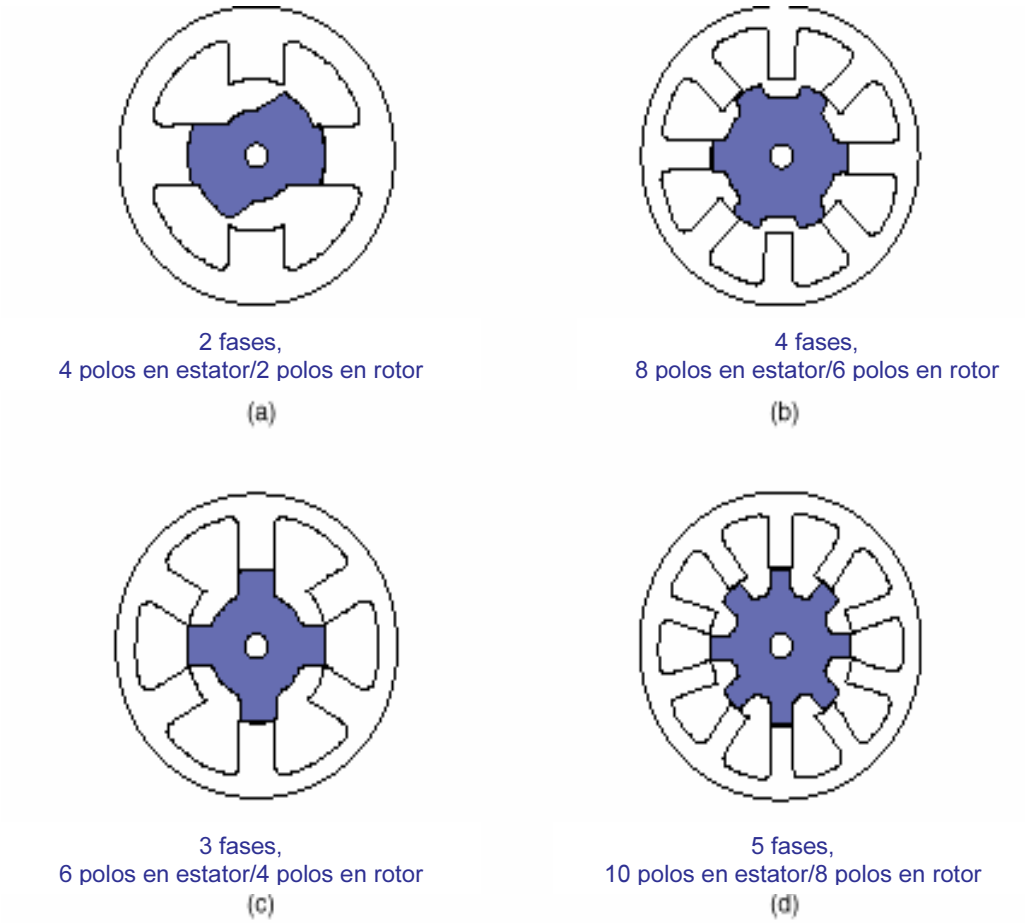

FIGURA 3.4 GEOMETRIA DE LOS MRAC

Como se muestra en la figura 2.4, se observan motores de 2 a 5 fases, los cuales son diseños que investigadores realizan para poder saber cual de todos ellos es el más optimo dependiendo de sus características propias.
Como se puede observar claramente, los polos del rotor no deben ser estrictamente la mitad de los polos del estator, lo cual nos brinda una posibilidad muy amplia de diseños.
Cabe destacar que los materiales con que se construye los MRAC son una parte sumamente importante para el buen desarrollo tecnológico de estos motores.

2.4 SECCION ESTRUCTURAL DE LOS MRAC.

Este punto es tratado y comentado en base a los estudios realizados por la compañía EMERSON MOTORS la cual en base a la experiencia en investigación ha logrado desarrollar un conjunto de recomendaciones que debemos tomar en cuenta. Estas recomendaciones están tomadas en base al articulo [1] el cual menciona a detalle lo que se escribe a continuación.

2.4.1 DEVANADOS DEL ESTATOR

El desarrollo llevado a cabo por EMERSON en base al desarrollo de fabricación de devanados para el estator de los MRAC, han conducido a concluir que estos devanados no requieren de alguna forma especial de manufactura.

En la figura 2.5 se puede observar la forma en como se encuentra los devanados de los motores.

Esta empresa reporta que como los devanados se fabrican con técnicas comunes, es posible fabricarlos muy fácilmente; un punto muy importante en los resultados reportados, conducen a un logro más para el desarrollo de los MRAC, es que como los devanados del estator, están montados sobre el polo saliente del estator, es fácilmente intercambiable, en caso de un daño del devanado. Solo habría que desmontarlo e intercambiarlo por un devanado similar de las mismas características y el problema estará solucionado.

La empresa EMERSON reporta en su estudio que ha logrado el desarrollo de montado de devanados del estator en un 85 % en base a una técnica que ellos denominan como inserción de espiras, el cual recomiendan como el método más óptimo.

Como se comento anteriormente, los MRAC no necesitan de materiales de especial manufactura para su construcción, pero la empresa EMERSON, esta desarrollando una división de construcción de MRAC con materiales magnéticos de mayor calidad que lógicamente hace aumentar el costo del motor, esta posibilidad esta en desarrollo para poder mejorar la eficiencia del motor, que es una posibilidad que se encuentra en estudio.

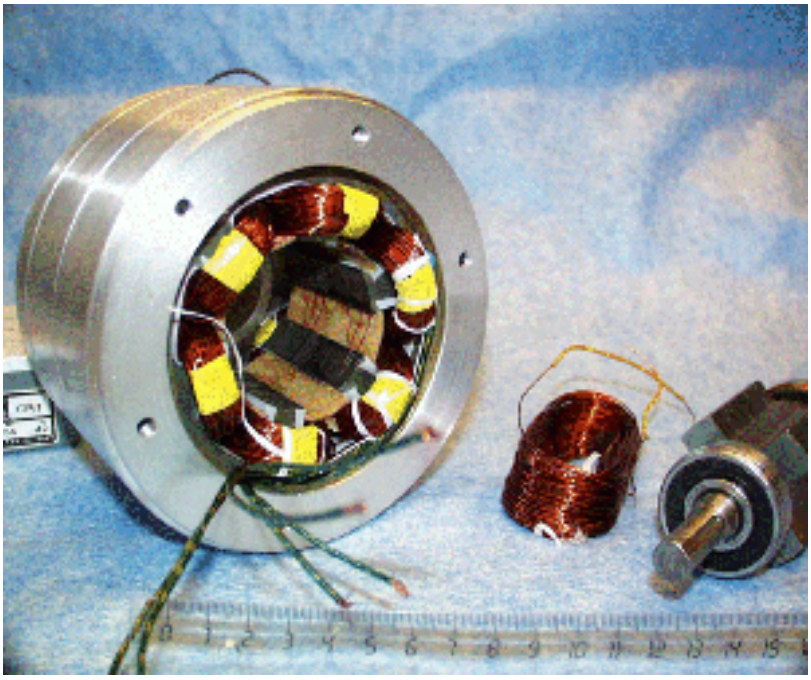

FIGURA 2.5 DEVANADOS DE LOS MRAC.

2.4.2 LAMINACION DEL ROTOR.

Para la construcción del rotor del MRAC, es lógico pensar que debe ser laminado para evitar las pérdidas por el efecto de las corrientes parásitas.
La empresa EMERSON realiza la fabricación de rotores de los MRAC, en base a técnicas de laminación semejantes a las utilizadas en los transformadores eléctricos.

Estas técnicas nos hacen pensar que la fabricación de rotores de estos motores se puede realizar con aparatos ya existentes, no con aparatos especiales, lo cual indica la sencillez de la máquina.

A continuación se muestra la figura 2.6, en la cual se puede observar la forma que tiene el rotor de estos motores.

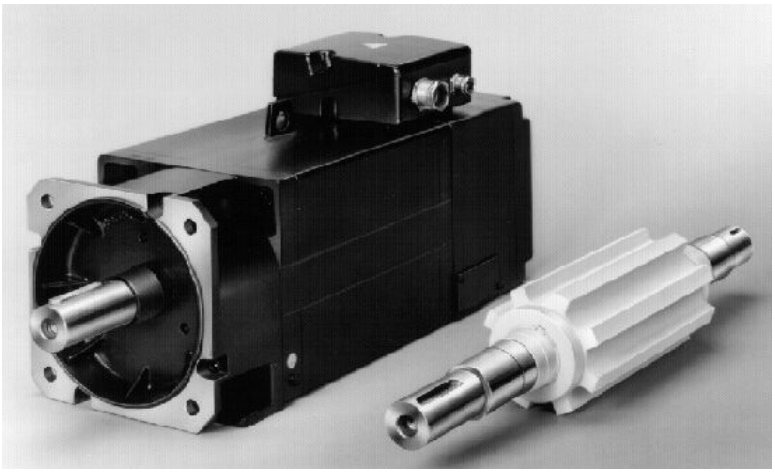

FIGURA 2.6 ROTOR DE UN MRAC.

2.4.3 ENTREHIERRO.

Los motores que se encuentran en diseño y prototipos de EMERSON, en el área de los MRAC, nos pueden reportar que durante la fabricación se presta un principal cuidado sobre las medidas de las piezas que conforman el motor, esto da pie para la medida del entrehierro formado entre los polos del rotor y el estator, es importante que se realicen con medidas que representen la menor varianza posible.

En los reportes obtenidos por EMERSON, menciona que el valor típico del entrehierro desarrollado para sus motores no debe exceder el 25% del valor nominal, dado que si esto sucediera existiría un desbalanceo físico severo que mas adelante comentaremos.

EMERSON recomienda que los valores óptimos de varianza del entrehierro sea de .004 a .008, con lo cual ellos han recomendado que el valor de .005 en su varianza para un buen desempeño del motor y así poder evitar un desbalanceo físico que a continuación comentaremos.

2.4.4 BALANCEO DEL ROTOR.

Como sabemos los devanados del estator tienen suministro eléctrico y magnético, la principal causa de desbalanceo en los motores eléctricos es la no uniformidad de distribución del rotor.
Además los cojinetes y soportes contribuyen al desbalanceo y por consecuencia a la vibración.

En la práctica el costo de balancear usualmente es bajo, pero como siempre corremos el riesgo de introducir desbalanceos por los apoyos del rotor, que pueden ser fabricados con especial cuidado y el costo no es muy elevado.

EMERSON ha estudiado a los MRAC en su comportamiento, en pruebas de laboratorio y una de las principales conclusiones que reportan, es mencionar que para motores menores de 10,000 r.p.m el efecto de desbalanceo no es muy crítico y por ello para este tipo de motores es raro que existan problemas por este motivo.

Para motores de mayor velocidad, tendríamos que analizar más detenidamente las condiciones de operación del mismo y poner mayor énfasis a las piezas que involucra el balanceo del motor.

Sobre este tema se realizan estudios sobre el ruido que los MRAC desarrollan; una muestra firme de lo comentado, esta mostrado en el siguiente programa que en su versión demo (figura 2.7 y 2.8), muestra el desarrollo de un programa que simula el ruido producido por el motor a distintas velocidades, posteriormente se muestra el diagrama utilizado para este fin.
Como se podrá observar más adelante, la forma del modelo es muy similar al desarrollado para la simulación de este trabajo.

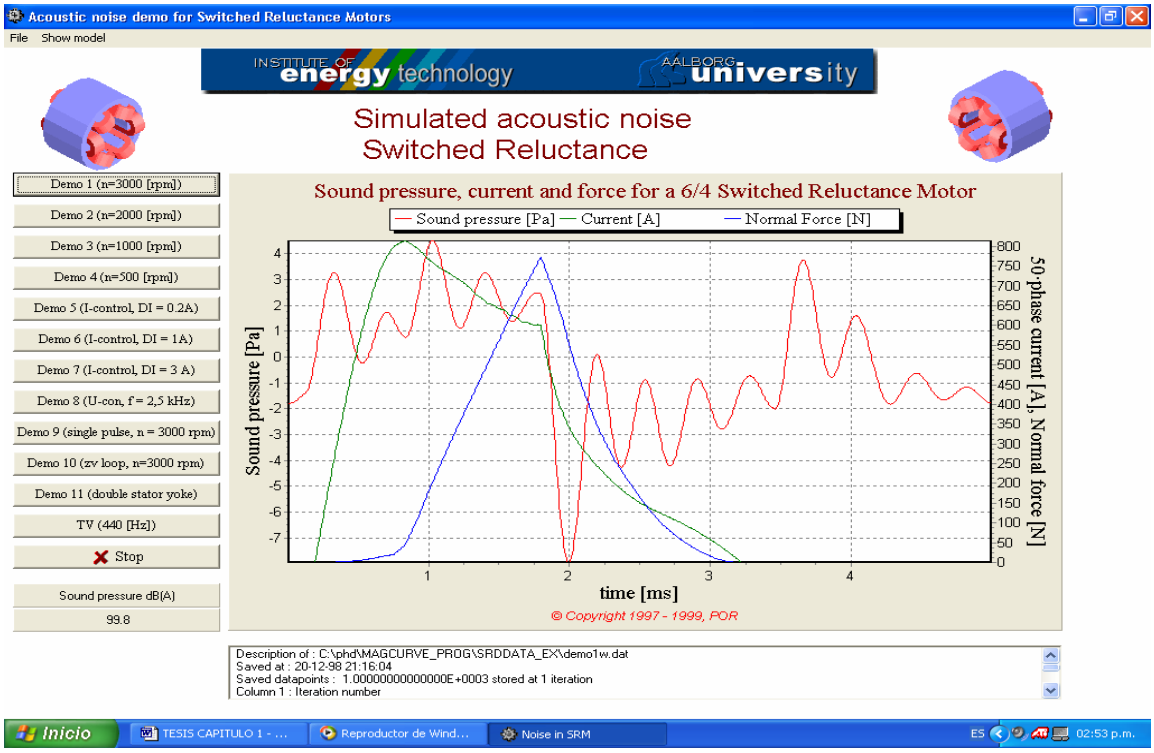

FIGURA 2.7 PROGRAMA DEMO DE ESTUDIO DE RUIDO EN LOS MRAC

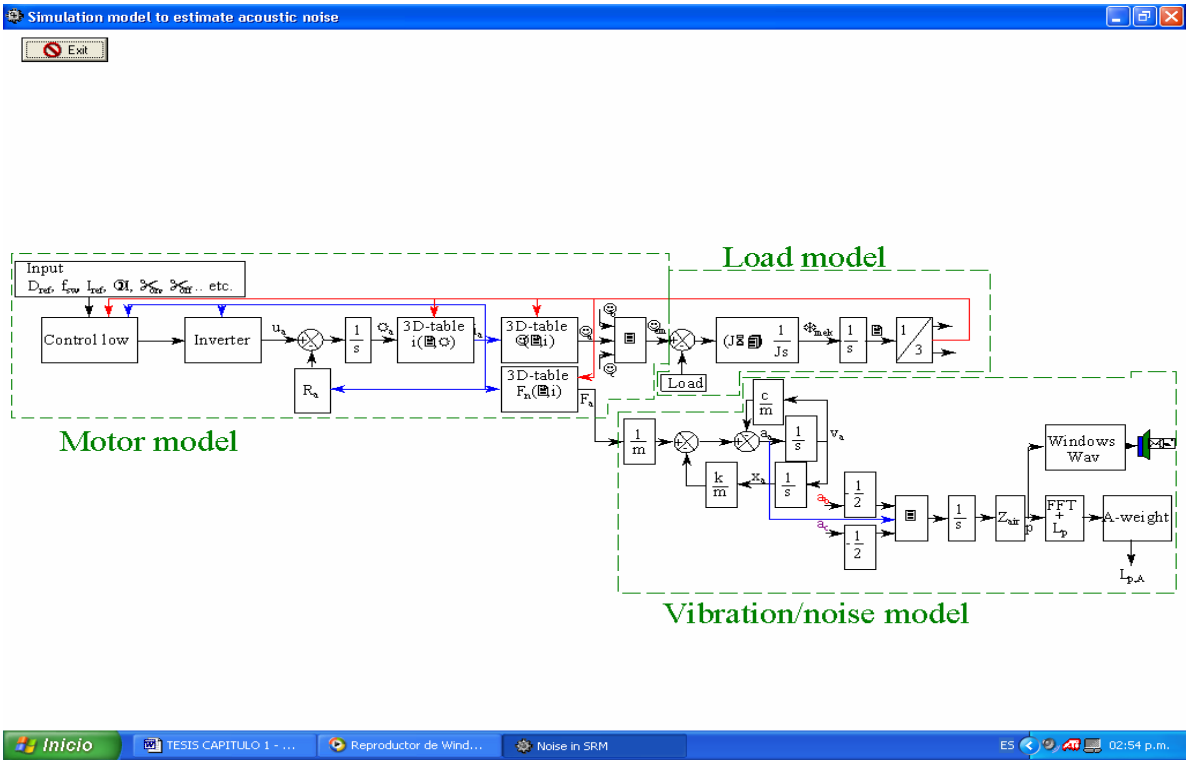

FIGURA 2.8 MODELO UTILIZADO PARA EL ESTUDIO DE RUIDO EN LOS MRAC.

Con toda esta información, podemos comentar los distintos avances que los MRAC han tenido hasta la fecha.

2.5 CONTROL EN LOS MRAC

En una revisión de la literatura utilizada para este trabajo, podemos concluir, que la limitación más común proviene de una de las características más importantes de esta máquina: la no linealidad que presenta el entrehierro en el flujo magnético que lo atraviesa, además esto aunado a que la conmutación debe ser llevada a cabo en base a la medición de la posición del rotor, hace esta tarea aun más compleja.

La mayoría de los resultados que se reportan consideran una relación lineal entre los enlaces de flujo y las corrientes de los devanados del estator en el circuito magnético, lo cual permite diseñar un modelo de control sencillo, que a postre se ha validado como un modelo confiable.

En el mismo sentido, el controlador debe diseñarse tomando en cuenta la estrategia o forma en que se realizará la conmutación, dado que el motor debe ser eléctricamente conmutado para una corriente de operación, el cual gobierna el tipo de conmutación.
Para el diseño de los controles de los MRAC, generalmente se supone una serie de factores que son:

- Las únicas variables que se encuentran disponibles par poder hacer mediciones son las corrientes del estator, la posición del rotor y la velocidad propia del motor.
- El momento de inercia es conocido
- Los parámetros del motor son completamente conocidos (resistencia, inductancia, etc.)
- Las únicas entradas de control son las tensiones conmutados que alimentan el estator.

Bajo estos parámetros se basan los grupos de trabajo para poder obtener el controlador adecuado para el MRAC.

2.6 ¿QUE OFRECEN LOS MRAC?

Los MRAC son una tecnología que tiene amplias expectativas en el área de motores eléctricos de inovación; sin duda tienen muchas características que lo hacen atractivo para poderse involucrar en distintas divisiones de estudio que actualmente son explorados por variados grupos de investigación alrededor del mundo y en especial a importantes empresas dedicadas a la comercializar motores eléctricos por varias décadas.

Para situar las características atractivas de estos motores a continuación se muestran las más importantes ventajas y algunas desventajas que los MRAC presentan.

2.6.1 VENTAJAS

La construcción de los MRAC, es una de las más sencillas. Únicamente el estator contiene devanados, los cuales son montados sobre los polos de cada fase, de tal manera que al ser conmutados, se formen polos apuestos.

El rotor no contiene ningún devanado, ni imán permanente. Este solo consiste en una masa metálica laminada montada sobre un soporte. Lo mencionado anteriormente, sobre la simplicidad en la construcción de la máquina nos lleva a observar que el costo disminuye fuertemente, como se muestra en la FIGURA 2.9.

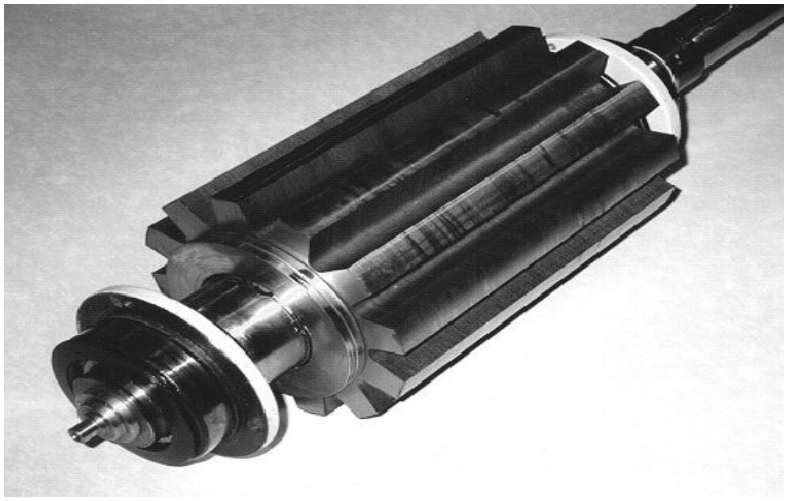

FIGURA 2.9 POLOS DEL ROTOR DE UN MRAC.

Son máquinas muy confiables dado que cada fase de la máquina es independiente tanto en forma física, eléctrica y magnética, entre fases, que hace que si una fase llegase a fallar, esto no impediría que la máquina siguiera trabajando, lo cual nos indica que esta máquina es muy confiables en cuanto a su operación y funcionamiento.

Además a la inexistencia de conductores en el rotor, este tipo de máquinas puede alcanzar velocidades considerablemente altas, aunado al tipo de conversión de energía, se puede observar que el MRAC puede generar altas potencias, comparadas con motores de las mismas dimensiones.

Otra ventaja gracias a su estructura simple, es la de poder operar continuamente en condiciones extremas, en donde la temperatura, humedad y otros agentes naturales son limitantes para la utilización de motores eléctricos.
Otra ventaja muy notoria es que el MRAC posee un momento de inercia muy pequeño, debido a la ausencia de masa en los huecos entre los dientes del motor. El rotor está compuesto únicamente por el eje en forma dentada, en base a estudios previos que investigadores realizan sobre el tema se puede observar claramente que el MRAC aventaja claramente a los motores eléctricos convencionales al punto de minimizar el momento de inercia del motor al 60% con respecto con otros motores de las mismas dimensiones.

En la figura 2.10 se muestra la figura de un MRAC 3ϕ, donde posee 6 polos en el estator y 4 polos en el rotor, que es la geometría que mayor gente en el área de estudio de estos motores recomiendan.

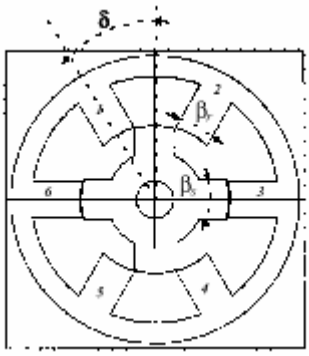

2.10. ESTRUCTURA DE UN MRAC CON 6 POLOS EN EL ESTATOR Y 4 POLOS EN EL ROTOR.

2.6.2 DESVENTAJAS.

Algunas limitaciones que produce la simplicidad mecánica de la máquina, se muestran en el análisis y el control propio de estas máquinas.

Una desventaja que se presenta en los MRAC es el hecho que para poderlos implementar en el campo productivo, no se puede alimentar directamente desde una línea de CD ni una línea de AC, debido a que debe de ser conmutado electrónicamente.

Este problema ha sido solucionado parcialmente gracias al avance en la electrónica de potencia, la cual nos brinda la posibilidad de poder controlar grandes cantidades de potencia a costos cada vez más económicos.

Otra desventaja que presenta es la que el estator y el rotor son de polos salientes, para la realización del par reluctivo, hace que esta máquina tenga características magnéticas sean fuertemente no lineales.

2.7 AVANCES TECNOLOGICOS EN LOS MRAC

Podremos mencionar que los MRAC se encuentra hoy en día en un proceso de estudio e investigación, este tipo de motores como hemos mencionado anteriormente, están ganando popularidad, debido a las características físicas propias que el motor presenta, además de poder contar hoy en día con avances en el área de la electrónica de potencia.

Esto hace a los MRAC como un fuerte candidato para ocupar un lugar en aplicaciones que así se requieran.
Hoy en día el desarrollo físico de estos motores es muy limitado, en la revisión realizada, podremos encontrar institutos que han desarrollado físicamente este tipo de motores, este es el caso de “The Elektrotechnische Instituto of the University Karlsruhe” en Alemania; que ha desarrollado un prototipo de 18.5kW a 1500 r.p.m, y es importante destacar que el modelo desarrollado es un prototipo que se encuentra actualmente en estudio; además “Institute of Energy Tecnology of The Aalborg University” en Dinamarca, tiene una división de estudios sobre MRAC con un prototipo de 550W y 2500 r.p.m.

Esta es una pequeña muestra podemos observar los grandes avances que estos motores se tienen desarrollados en forma física, es importante mencionar que existen un variado numero de personas que hoy en día están trabajando sobre investigación en esta área.

Sobre el área de controladores de los MRAC podemos encontrar a una empresa líder de componentes electrónicos como es el caso de TEXAS INSTRUMENTS, la cual ha realizado una gran serie de investigaciones hasta llegar a mostrar un circuito integrado que sirve para las funciones de control de estos motores, el modelo del circuito es el TMS320F240, cabe destacar que existen un variado grupo de investigación que desarrollan técnicas de control de los MRAC a nivel de investigación, pero nosotros tomamos como base a la empresa TEXAS, por la representatividad que ese microcircuito presenta y con el hecho que se presenta como un circuito existente y comercial.

Sobre la fabricación de los MRAC, existen una variedad de empresas de motores eléctricos que desarrollan estudios sobre estos motores. Como se ha comentado actualmente es difícil poder encontrar un MRAC en forma comercial, ya que solo se presenta como investigación y prototipos; pero hemos encontrado un sistema comercial que contiene un MRAC en su mecanismo, este es el caso de la empresa EMERSON MOTORS que brinda conjuntamente con la empresa de línea blanca MAYTAG, una lavadora de ropa, la cual es accionada por un MRAC, la lavadora se conoce con el modelo de NEPTUNE; actualmente se comercializa en U.S.A. y se espera que a finales de este año se introduzca a México.

Como se ve los MRAC se encuentran ya postrados sobre sistemas productivos, actualmente en aparatos electrodomésticos, pero esto nos hace pensar que en un futuro veremos a este tipo de máquinas eléctricas en sistemas productivos a nivel industrial diversificando así sus usos.

Al estar situados en una etapa de investigación y desarrollo; es evidente que su operación queda descrita y regida por un modelo matemático, que en la mayoría de los trabajos publicados tienen orígenes y características diferentes.

Si bien es cierto que los MRAC muestran muchas ventajas para el uso en muchas áreas; el describir su funcionamiento en operación de una forma clara y sencilla a través de modelos matemáticos, nos permitirá conocer mejor las características de respuesta y comportamiento que los MRAC nos podrá brindar bajo ciertas condiciones existentes.

A partir de lo anterior, el siguiente capitulo muestra las características del modelo general que rige al motor según la mayoría de trabajos reportados en el área.

CAPITULO 3

MODELO MATEMÁTICO DE LOS MRAC.

En este capítulo, se muestra el modelo matemático que gobierna el funcionamiento de los MRAC.

Como se ha comentado anteriormente, los MRAC son una división de máquinas eléctricas que en su construcción física presentan una gran simplicidad y economía, debido a sus propiedades y características que presenta. Esto nos hace pensar que el modelo matemático que rige a este tipo de máquinas es sencillo, por lo contrarío, su desarrollo es elaborado y debemos poner especial atención a la obtención del mismo, para tener una visión precisa del funcionamiento que los MRAC nos brindan.

En la primera parte se muestra el modelo matemático general que rigen a los MRAC, y posteriormente mostramos el modelo matemático simplificado utilizado para la simulación; el cual utilizaremos para el desarrollo de la simulación.

3.1 ¿PORQUÉ EL USO DE UN MODELO MATEMÁTICO?

En las ciencias de ingeniería, el propósito de una gran parte de la investigación es comprender las funciones de sistemas útiles para el ser humano. Con este propósito, surgen problemas relacionados con la existencia de técnicas de investigación que resultan inadecuadas por la existencia del sistema o que aún cuando pueden ser usadas su desarrollo es limitado.

También surgen obstáculos cuando existe un insuficiente conocimiento de las técnicas experimentales en uso, o con la inexistencia de ellas.

Por mucho tiempo, los modelos matemáticos fueron ignorados porque no eran visibles y parecían estar remotamente alejados de la realidad. Actualmente, se acepta que las suposiciones y apreciaciones que subyacen en el modelo teórico respecto al sistema eléctrico modelado pueden resultar similares a las que se presentan en otros modelos. Más aún, los modelos teóricos permiten rápidas modificaciones y se pueden evaluar muchas combinaciones de eventos e interrelaciones entre estructuras.

El advenimiento de las computadoras y su vertiginoso desarrollo ha impulsado el modelaje matemático y la simulación computacional (MATLAB-SIMULINK), puesto que prácticamente todo lo que puede ser concebido puede ser modelado, y además en un corto período de tiempo. Por esto, el campo del modelaje y la simulación, es actualmente una parte inseparable y por demás importante, de las ciencias de ingeniería. Sin embargo, el investigador debe tener siempre presente que el modelo matemático, a pesar de ser válido, no es exactamente igual a la realidad y no puede suplantarla.

Los modelos cubren desde conceptos e hipótesis expresados en forma gráfica o descriptiva hasta formulaciones matemáticas complejas del comportamiento dinámico de los sistemas físicos, construcciones físico-analógicas (eléctricas y/o mecánicas) y las simulaciones computacionales. Entre los objetivos de la construcción de modelos de los sistemas eléctricos están:

- Alcanzar una mejor comprensión de dichos sistemas.
- La formulación cuantitativa y cualitativa de los fenómenos y

- La predicción del comportamiento del sistema sobre la base de pocos parámetros.

La adecuada selección de suposiciones simplificadoras representa uno de los puntos más críticos del modelaje y requiere una adecuada comprensión de los fenómenos físicos para poder determinar si dichas suposiciones no distorsionan los resultados del modelaje. Como se dijo antes, la validación (comparación de los resultados obtenidos con un modelo con aquellos obtenidos con el sistema físico real, cuando se someten a las mismas entradas; si el sistema no se ha desarrollado físicamente hasta el momento, la validación se realiza en base a la comparación y discusión de resultados con otros modelos y sistemas similares) constituye la prueba decisiva para decidir sobre lo adecuado o no de un modelo.

3.1.1 REQUISITOS DE UN MODELO MATEMÁTICO

Con estas ideas en mente, un modelo debe cumplir con diversos requisitos. Entre ellos, los siguientes constituyen los más importantes:

1. Debe ser físicamente realizable y se debe construir en términos de parámetros que son significativos y medibles en el sistema físico.

2. Tiene que incluir toda la información disponible que sea pertinente, respecto al sistema físico que va a ser modelado. Aquellas suposiciones que entran en conflicto con los datos existentes deben ser evaluados y justificados con un cuidado especial.

3. Debe ser simple, porque de esa manera es mas fácil evaluar tanto su comportamiento como un todo, así como también la influencia de los componentes individuales en la diferencia que se presenta entre las salidas del modelo y del sistema físico general.

4. Es preferible, aunque no siempre posible, construir el modelo de tal forma que permita alteraciones en las suposiciones y parámetros del sistema sin un esfuerzo excesivo. El modelo debe ser más simple de manipular que el mismo sistema físico.

5. Debe servir como una guía para el investigador experimental, sugerir ciertos experimentos y excluir la necesidad de otros.

6. Debería tener poder predictivo, es decir, debe servir como fundamento para extrapolaciones, bien sea dentro del rango de los resultados observados, o también para determinar propiedades más generales del sistema real.

7. Debe ser un sustituto suficientemente válido del sistema real que permita realizar con él experimentos ficticios que se asemejen a experimentos reales; y que incluso permita realizar experimentos irrealizables en el sistema verdadero.

Con lo anterior tenemos todas las bases para poder formar un modelo matemático que describa el funcionamiento de los MRAC.

3.2 MODELO MATEMATICO GENERAL DE LOS MRAC.

El modelo general que describe el funcionamiento de los MRAC, se describe a continuación, este modelo esta basado en estudios previos realizados [5], en donde se determinan los parámetros principales que caracterizan a los MRAC, como se podrá observar, se presenta un estudio detallado de la temática utilizada para obtener las ecuaciones que describen la función y comportamiento de estos motores.

3.2.1 ECUACIONES ELECTROMAGNETICAS:

Aunque el MRAC parece tener una operación simple, requiere un estudio muy formal y completo en el área de modelado matemático.
El voltaje instantáneo de las terminales de los devanados de una fase del MRAC, esta relacionado con el flujo producido en estos, por la ley de Faraday, como se menciona

$$V = iR_m + \frac{d\phi}{dt} \qquad (1)$$

En donde V es la terminal de voltaje, i es la corriente de fase, R_m es la resistencia del motor y ϕ es el flujo magnético del devanado.

Pero como la construcción del motor es de polos salientes (tanto el rotor como el estator), además de los efectos de saturación magnética, en general, el flujo magnético en las fases del MRAC varia en función de la posición del rotor (θ), y la corriente del motor de la ecuación 1 es complementada como sigue.

$$V = iR_m + \frac{\partial \phi}{\partial i}\frac{di}{dt} + \frac{\partial \phi}{\partial \theta}\frac{d\theta}{dt} \tag{2}$$

donde $\frac{\partial \phi}{\partial i}$ esta definido como L(θ,i) la inductancia instantánea, $\frac{\partial \phi}{\partial \theta}$ es K_b (θ,i) que es la FEM instantánea.

3.2.2 ECUACION GENERAL DE PAR

La ecuación anterior (2) muestra la transferencia de energía eléctrica a campos magnéticos para el MRAC; En este punto desarrollaremos la ecuación que describe la conversión de la energía de los campos en energía mecánica.

Si nosotros multiplicamos cada lado de la ecuación (1) por la corriente eléctrica i, obtenemos la expresión de la potencia instantánea en un MRAC.

$$Vi = i^2 R_m + i\frac{d\phi}{dt} \tag{3}$$

La parte izquierda de la ecuación (3) representa la potencia eléctrica instantánea demandada por el MRAC, El primer termino en la parte derecha de la ecuación (3) representa las perdidas ohmicas en los devanados del MRAC, el siguiente termino representa la suma de la salida de la potencia mecánica del MRAC y toda la potencia es guardada en los campos magnéticos, y se puede representar así:

$$i\frac{d\phi}{dt} = \frac{dWm}{dt} + \frac{dWf}{dt} \tag{4}$$

Donde el término $\frac{dW_m}{dt}$ es la potencia mecánica instantánea, y $\frac{dW_f}{dt}$ es la potencia instantánea, que es almacenada en los campos magnéticos. Como potencia es definida como la razón de cambio de la energía en función del tiempo.
Por lo que W_m es la energía mecánica y W_f es la energía de los campos magnéticos.

Conociendo la potencia mecánica, podremos nosotros escribir a esta como el producto de par y velocidad como sigue.

$$\frac{dWm}{dt} = T\omega = T\frac{d\theta}{dt} \tag{5}$$

donde T, es el par, y $\omega = \frac{d\theta}{dt}$ es la velocidad rotacional del rotor o flecha.

Ahora bien, si sustituimos la ecuación número 5 en la ecuación número 4 se obtiene.

$$i\frac{d\phi}{dt} = T\frac{d\theta}{dt} + \frac{dWf}{dt} \tag{6}$$

resolviendo la ecuación anterior (6), para obtener la ecuación de la producción de par.

$$T(\theta,\phi) = i(\theta,\phi)\frac{d\phi}{d\theta} - \frac{dWf(\theta,\phi)}{d\theta} \tag{7}$$

y como el flujo es constante, la ecuación (7) se simplifica.

$$T = -\frac{\partial Wf}{\partial\theta} \tag{8}$$

Como se observa anteriormente, la expresión de par se expresa en función de flujo magnético; pero en ocasiones es deseable que esta expresión sea expresada en función de corrientes en vez de flujos, por ello es común que se exprese en función de co-energía, W_c en vez de energía.

Para poder comprender el concepto de co-energía, hay que analizar la figura 3.1 que representa la energía de campo magnético.

Para un constante ángulo de rotor, tenemos $\frac{d\theta}{dt} = 0$, con esta consideración, integramos la ecuación (6) y nos muestra la energía de los campos magnéticos, como se expresa en la siguiente ecuación.

$$W_f = \int_0^{\phi} i(\theta, \phi) d\phi \tag{9}$$

La interpretación gráfica se muestra a continuación.

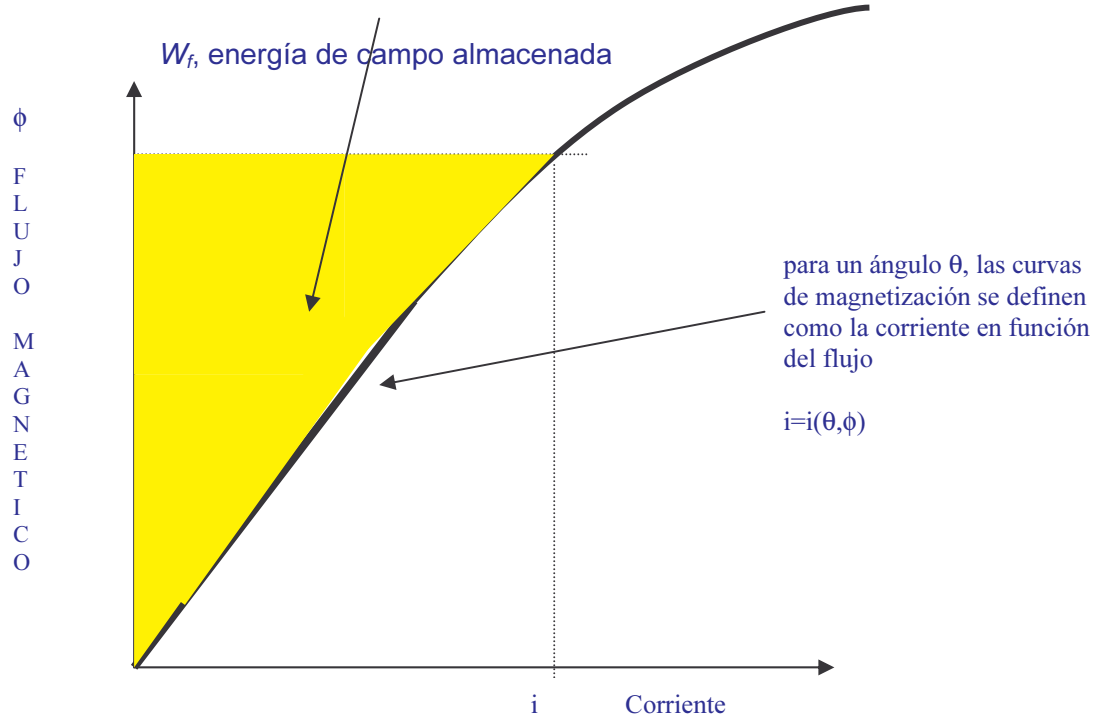

FIGURA 3.1 INTERPRETACIÓN GRAFICA DE LA ENERGÍA DE CAMPO MAGNETICO

Ahora se considera la figura 3.2 tenemos:

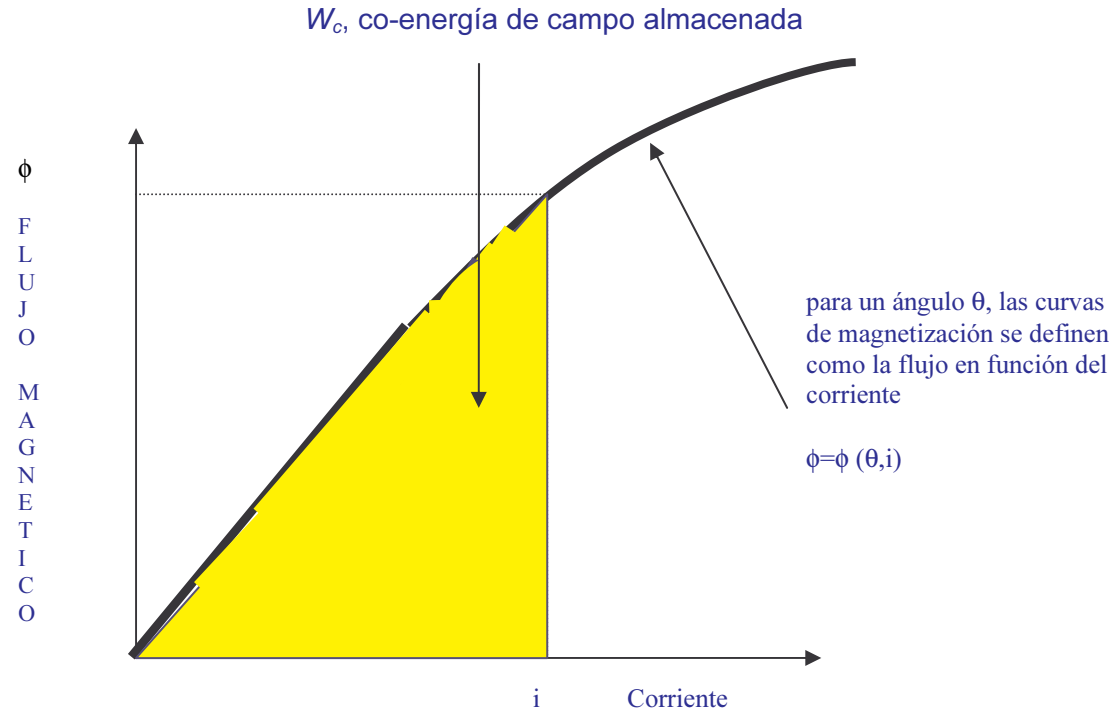

FIGURA 3.2 INTERPRETACIÓN GRAFICA DE LA CO-ENERGÍA DE CAMPO MAGNETICO.

Para un ángulo fijo θ, observamos que la curva de magnetización, el flujo es una función de la corriente, en vez de que la corriente se define como función del flujo Por lo que con el área bajo la curva se obtiene:

$$Wc = \int_0^i \phi(\theta, i)di \tag{10}$$

Esto se define como la co-energía del campo magnético.

De las figuras 3.1 y 3.2, se puede observar que el área que describe la energía y co-energía de campo, puede bien describirse con la siguiente relación.

$$Wc + Wf = i\phi \tag{11}$$

Si nosotros diferenciamos cada parte de la ecuación anterior podremos obtener.

$$dWc + dWf = \phi di + id\phi \tag{12}$$

Si resolvemos la diferencial de energía de campo en la ecuación anterior (12) y se substituye en la ecuación (7) obtendremos:

$$T = \frac{id\phi - (\phi di + id\phi - dWc(\theta, i))}{d\theta} \tag{13}$$

Para simplificar, la ecuación general de par, ecuación (13), se suele simplificar valuando para corrientes constantes.

Si diferenciamos la ecuación de co-energía se torna en términos de diferenciales parciales como sigue:

$$dWc(\theta, i) = \frac{\partial Wc}{\partial \theta} d\theta + \frac{\partial Wc}{\partial i} di \tag{14}$$

Con las ecuaciones anteriores (13) y (14), se simplifica fuertemente si se considera la corriente constante.

$$T = \frac{\partial Wc}{\partial \theta} \text{ , es si } i \text{ es constante} \tag{15}$$

3.2.3.- SIMPLIFICACION DE LA ECUACION DE PAR.

Como se puede observar anteriormente, en el desarrollo matemático se obtiene el modelo que rige al par que produce el MRAC, pero cabe resaltar que para poder hacer esta relación más sencilla podemos proponer:
La relación entre el flujo y la corriente esta dado por:

$$\phi = L(\theta) \cdot i \tag{16}$$

Como la inductancia del motor solo varia en función del ángulo del rotor. Se puede sustituir la ecuación anterior en la ecuación (10), con esto y evaluando la integral se obtiene:

$$Wc = \frac{i^2}{2} L(\theta) \tag{17}$$

Esta ecuación se puede sustituir en la ecuación (15) con lo que obtendremos una ecuación simplificada y sencilla que nos brinda el par del MRAC.

$$T = \frac{i^2 dL}{2d\theta} \tag{18}$$

3.3 MODELO UTILIZADO PARA LA SIMULACIÓN

El modelo que a continuación se muestra, esta basado en estudios realizados en [9], que se basan en hacer un estudio de los parámetros del MRAC en forma lineal; la principal característica que se presenta es hacer un análisis tomado en cuenta que los flujos magnéticos que se presentan en el entrehierro se realizan en forma lineal, no existen variaciones importantes durante el funcionamiento del motor.

3.3.1 MODELO SIMPLIFICADO DEL MRAC.

El estudio que se realizó en [9] se obtienen los parámetros necesarios que se utilizarán más adelante para la simulación.
Basándonos en la figura 3.3, que nos muestra la forma de la inductacia de cada una de las fases del MRAC, donde podremos determinar los siguientes parámetros.

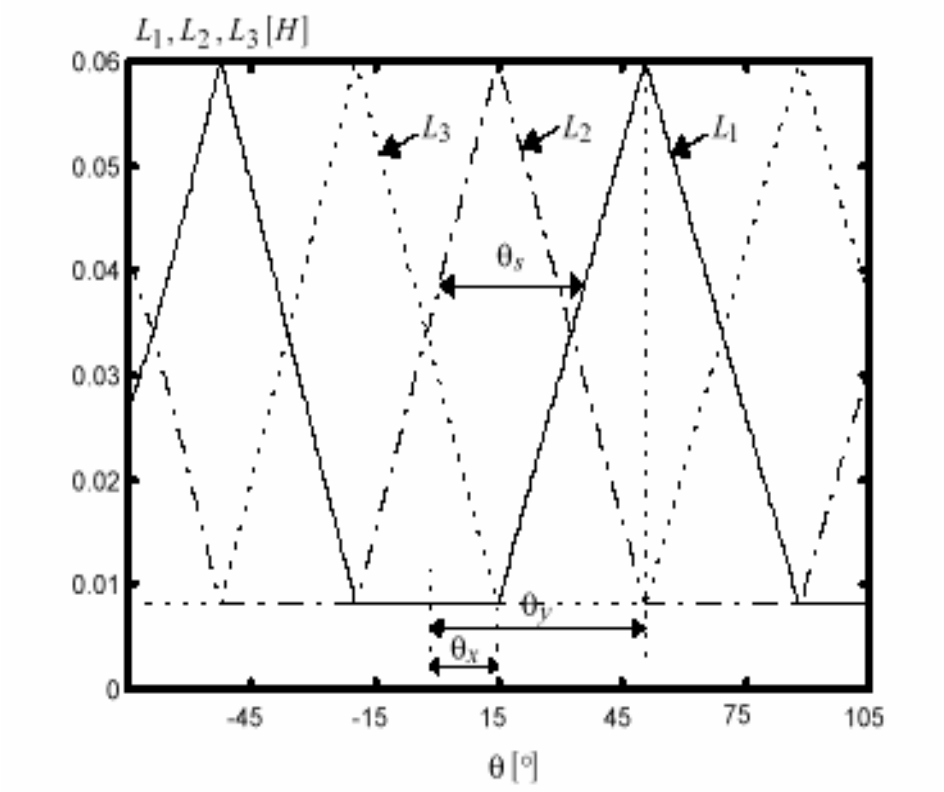

FIGURA 3.3 INDUCTANCIA DE CADA FASE DE UN MRAC 6/4

$$\theta_s = 2\Pi(\frac{1}{N_r} - \frac{1}{N_s}) \tag{19}$$

Donde N_r y N_s son el número de polos del rotor y estator respectivamente.

Un factor importante que se debe determinar es el arco del estator y el rotor, que en este caso son iguales $\beta_r=\beta_s$. Estos parámetros se pueden observar en la figura 3.4.

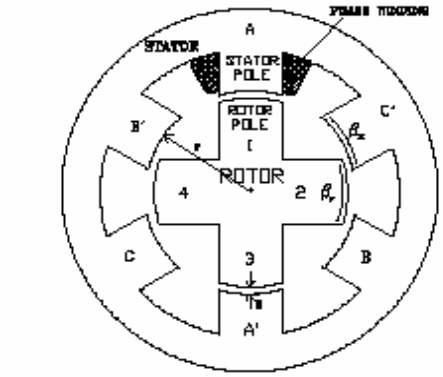

FIGURA 3.4 ARCOS DE ROTOR Y ESTATOR DE UN MRAC 6/4

con respecto a las figuras anteriores se obtiene la siguiente relación.

$$\theta_x = (\frac{\Pi}{N_r} - \beta_r) \tag{20}$$

$$\theta_y = \frac{\Pi}{N_r} \tag{21}$$

Como se indica en las anteriores figuras, el ángulo δ corresponde al desplazamiento de una fase con respecto a otra y esta determinada por:

$$\delta = 2\Pi(\frac{1}{N_r} - \frac{1}{N_s}) \tag{22}$$

Con estos parámetros, y sabiendo que se esta haciendo un análisis en régimen lineal, la relación que el flujo tiene es:

$$\psi = L(\theta)I \tag{24}$$

Que como se mencionó la co-energía esta dada por:

$$W = \frac{1}{2}L(\theta)I^2 \tag{25}$$

de donde resulta que la ecuación que representa el par es:

$$T = \frac{i^2 dL}{2d\theta} \tag{26}$$

y para poder representar las ecuaciones mecánicas del MRAC, podemos representar la siguiente igualdad.

$$J\frac{d\omega}{dt} = T - Tl - f\omega \tag{28}$$

y

$$\frac{d\theta}{dt} = \omega \tag{29}$$

en donde *Tl* representa el par de carga, y *f* es el coeficiente de fricción, y ω es la velocidad angular del rotor.

CAPITULO 4

SIMULACION DEL MRAC.

En este capítulo se mostrará la forma en que se ha realizado las simulaciones basadas en MATLAB-SIMULINK.

En la primera sección se hace mención a los fundamentos que debe llevar toda simulación que se lleva a cabo por computadora, posteriormente se hace una revisión y análisis de los trabajos que se han desarrollado en base a la simulación de los MRAC.

En la siguiente sección se hace referencia del paquete de simulación utilizado en este trabajo, que es MATLAB en su versión 5.2 y SIMULINK en su versión 2.0; se hace referencia de sus orígenes y algunas formas en como trabaja el programa, además de mencionar los alcances que el mismo nos brinda.

En la tercera parte se hace mención de la forma en como se utilizó el programa de simulación para poder desarrollar y obtener los resultados.

4.1 SIMULACION DE MOTORES ELÉCTRICOS.

Una de las más importantes y poderosas herramientas para analizar el diseño y operación de sistemas de procesos complejos, es la simulación. Aunque la solución al problema nunca es exacta, las aproximaciones que se obtienen son bastante buenas.

Por lo anterior hoy en día la simulación es una vinculación de suma importancia entre los modelos reales y los modelos que existen aún en desarrollo.

A continuación se presenta los fundamentos básicos que describen y definen a la simulación, en el área de los motores eléctricos.

4.1.1 DEFINICIÓN DE SIMULACIÓN.

Simulación es el proceso de diseñar un modelo de un sistema físico real, el cual sirve para dirigir los experimentos y desarrollos, con el propósito de entender el comportamiento del sistema y proponer varias estrategias para realizar la operación de esta.

Por sistema físico real, se refiere a la representación de un conjunto de partes o elementos propios al sistema en estudio, en este caso el término "real" se usa en el sentido de " existencia o capaz de ser puesto en existencia", esto quiere decir que el sistema no necesariamente tiene que ser real (puede ser desarrollado).

4.1.2 EL PORQUE DE LA SIMULACIÓN.

El principio racional para usar la simulación en cualquier área del conocimiento es la búsqueda del hombre por adquirir conocimientos referentes a la predicción del futuro, o la explicación lógica de un fenómeno.

El inicio del estudio de un fenómeno o sistema físico se basa en el Método Científico el cual consta de cuatro pasos:

- Observación del sistema físico en estudio.
- Formulación de hipótesis las cuales deberían explicar el comportamiento del sistema.
- Obtener una teoría que explique el comportamiento del sistema, utilizando una deducción lógica o más rigurosamente un *modelo matemático.*
- Experimentación para probar la validez de la teoría propuesta.

Pero en ocasiones es muy difícil utilizar este método en algunos sistemas particulares, entonces la *simulación* aparece como una alternativa muy *eficiente.*

4.1.3 COMPONENTES DE UNA SIMULACIÓN POR COMPUTADORA.

Antes de diseñar una simulación por computadora es decisivo tener presentes los siguientes componentes:

- Los objetivos o datos de salida del estudio de simulación que tienen la forma de un valor numérico específico.
- Los datos de entrada o valores numéricos necesarios para determinar las salidas de la simulación.

Estos pueden ser:

1. Condiciones iniciales: valores que expresan el estado del sistema al principio de una simulación.
2. Datos determinísticos: valores conocidos necesarios para calcular las salidas de la simulación.(representan la caracterización del sistema y en nuestro caso se presentan como resultado de experiencias previas)
3. Datos probabilísticos: magnitudes numéricas cuyos valores son inciertos pero necesarios para obtener las salidas de la simulación.

4.1.4 DISEÑO DE LA SIMULACIÓN POR COMPUTADORA.

- Generación de números aleatorios: se obtienen las entradas probabilísticas para el modelo generando números aleatorios de acuerdo a las distribuciones conocidas asociadas.
- Contabilidad: se diseña un método sistemático para almacenar y procesar todos los valores de entrada y para realizar los cálculos necesarios para obtener los valores de salida.
- Implementación del modelo en el computador. Hay que definir que lenguaje utilizar, para procesarlo en el computador y obtener los resultados deseados.
- Validación. A través de esta etapa es posible detallar deficiencias en la formulación del modelo a en los datos que lo alimentan.

Las formas más comunes de validar un modelo son:

1. La opinión de los expertos.
2. La exactitud con que se precisen los datos históricos.
3. La exactitud en la predicción del futuro.
4. Utilizar datos que hacen fallar al sistema real.
5. La acepción y confianza en el modelo de la persona que hará uso de los resultados obtenidos con el sistema.
6. Interpretación. Interpretar los datos que arroja la simulación y hacer uso de ellos para tomar decisiones.
7. Documentación. Hacer el manual técnico y el manual de usuario para el sistema de simulación a utilizarse.

4.1.5 VENTAJAS Y DESVENTAJAS DE LA SIMULACIÓN.

- ***Ventajas***: Podemos aplicar la simulación sino existe una formulación matemática del problema. Se aplica cuando los procedimientos matemáticos son muy complejos. Se aplica cuando no existe el elemento físicamente (aún se encuentra en un proceso de estudio). Cuando se desea hacer experimentos por un cierto periodo de tiempo par para observar el comportamiento del sistema, Cuando se requiera que el proceso sea en menos tiempo. Se aplica a la educación y el entrenamiento

- ***Desventajas***: Entre estas tenemos que: un buen modelo requiere mucho tiempo y en ocasiones muy complejo. Puede reflejar con precisión una situación del mundo real, cuando en verdad no lo hace. La simulación es imprecisa, y no se pude medir el grado de error. Generalmente los resultados son numéricos y pueden ser imprecisos por algunas cifras decimales que con el tiempo se convierten en unas cifras muy significativas al obtenerse el error.

4.2 REVISION BIBLIOGRÁFICA DE SIMULACIÓN EN LOS MRAC

El beneficio que uno tiene con el análisis y simulación de un sistema en forma integral, es importante hoy en día para la validación del mismo, además de que sirve como base para el diseño y su realización en forma experimental.

Estudios referentes a la simulación en forma dinámica de los MRAC, se han elaborado en programas como es el caso de lenguaje C y Fortran, por otra parte se han basado en estos estudios y hemos encontrado simulaciones en lenguaje ACSL (16,20), otro tipo de simulaciones se han realizado en el caso de lenguaje Delphi 2.0(15).
Por otro lado, muy poca gente estudia los MRAC, en un idioma de programación basado en lenguajes o programas como: Spice, Simulink-Matlab,Matrix,Tutsim, Vissim y Mathcad.
Se han realizado las primeras simulaciones gracias al programa de simulación Spice (7). Desgraciadamente, la técnica que se utiliza aquí no es muy apropiada, debido a que el programa Spice, se adapta sobre todo a simulaciones de circuitos eléctricos (14).

En esta ultima década, existen progresos muy importantes, en relación al ambiente de simulación de MATLAB-SIMULIK, el cual permite un desarrollo de ambientes de programación flexible dirigido a las maquinas eléctricas.

En este trabajo sobre MRAC se hace un estudio en base a la programación en MATLAB, y una simulación en SIMULIK.
La principal motivación que impulsa este trabajo, es poder mostrar la diversidad de maquinas eléctricas que se pueden utilizar para distintos campos de trabajo; esperando que alumnos del área de ingeniería se interesen por el tema para que en un tiempo corto, se pueda abrir una línea de investigación más formal sobre este tipo de motores.
Y que podamos competir directamente con los dos o tres grupos de investigación llevan la punta en inovaciones.
Se que el camino es largo y difícil, pero con buenos cimientos en el tema, la gran educación de calidad y el empeño de nosotros como estudiantes, podremos hacer investigación de muy alto nivel como el mundo de hoy en día exige.

4.3 SIMULADOR UTILIZADO EN ESTE TRABAJO (MATHLAB-SIMULINK)

El simulador empleado para este trabajo es MATLAB ver.5.2 y SIMULINK ver2.0, los cuales como se mencionó anteriormente, representa un software muy utilizado en áreas de enseñanza de ingeniería, además de mostrar una simplicidad en su estructura de programación lo cual nos brinda la ventaja de poder hacer esta simulación en una forma de fácil comprensión para el publico que consulte esta obra.

A continuación se muestra una introducción del simulador (MATLAB-SIMULINK), el cual nos ayudará a comprender los orígenes y formas en como trabaja este lenguaje de programación.

4.3.1 MATLAB

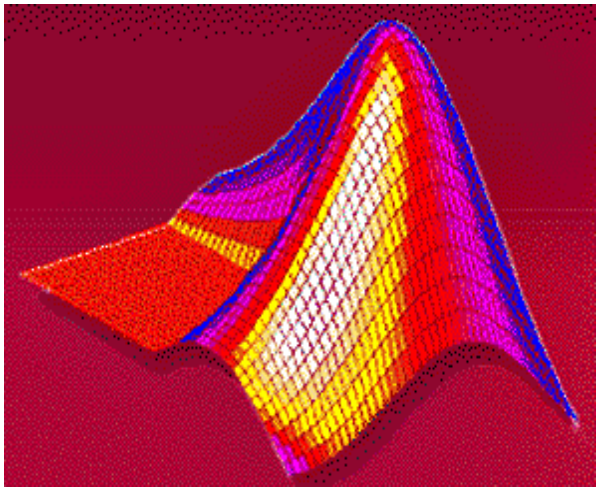

El nombre de MATLAB proviene de la contracción de los términos **MAT**rix **LAB**oratory y fue inicialmente concebido para facilitar el acceso a las librerías LINPACK y EISPACK, las cuales representan hoy en día dos de las librerías más importantes en computación y cálculo matricial.

Matlab fue originalmente desarrollado en lenguaje FORTRAN para ser usado en computadoras mainframe. Fue el resultado de los proyectos Linpack y Eispack desarrollados en el Argonne National Laboratory. Su nombre proviene de **Mat**rix **Lab**oratory. Al pasar de los años fue complementado y reimplementado en lenguaje C. Actualmente la licencia de Matlab es propiedad de MathWorks Inc .

MATLAB es un entorno de computación y desarrollo de aplicaciones totalmente integrado orientado para llevar a cabo proyectos en donde se encuentren implicados elevados cálculos matemáticos y la visualización gráfica de los mismos. MATLAB integra análisis numérico, cálculo matricial, procesamiento de señales y visualización gráfica en un entorno completo donde los problemas y sus soluciones son expresados del mismo modo en que se escribirían tradicionalmente, sin necesidad de hacer uso de la programación tradicional.

MATLAB goza en la actualidad de un alto nivel de implantación en escuelas y centros universitarios, así como en departamentos de investigación y desarrollo de muchas compañías industriales nacionales e internacionales. En entornos universitarios, por ejemplo, MATLAB se ha convertido en una herramienta básica, tanto para los profesionales e investigadores de centros docentes, como una importante herramienta para la impartición de cursos universitarios, tales como sistemas e ingeniería de control,

álgebra lineal, proceso digital de imagen, señal, etc. En el mundo industrial, MATLAB está siendo utilizado como herramienta de investigación para la resolución de complejos problemas planteados en la realización y aplicación de modelos matemáticos en ingeniería. Los usos más característicos de la herramienta los encontramos en áreas de computación y cálculo numérico tradicional, prototipaje algorítmico, teoría de control automático, estadística, análisis de series temporales para el proceso digital de señal.

MATLAB dispone también en la actualidad de un amplio abanico de programas de apoyo especializados, denominados Toolboxes, que extienden significativamente el número de funciones incorporadas en el programa principal. Estos Toolboxes cubren en la actualidad prácticamente casi todas las áreas principales en el mundo de la ingeniería y la simulación, destacando entre ellos el 'toolbox' de proceso de imágenes, señal, control robusto, estadística, análisis financiero, matemáticas simbólicas, redes neuronales, lógica difusa, identificación de sistemas, simulación de sistemas dinámicos, etc.

Además también se dispone del programa Simulink que es un entorno gráfico interactivo con el que se puede analizar, hacer su modelo y simular la dinámica de sistemas no lineales.

4.3.2 SIMULINK

Simulink es una herramienta para el modelado computacional, análisis y simulación de una amplia variedad de sistemas físicos y matemáticos, inclusive aquellos con elementos no lineales y aquellos que hacen uso de tiempos continuos y discretos. Como una extensión de Matlab, Simulink adiciona muchas características específicas a los sistemas dinámicos, mientras conserva toda la funcionalidad de propósito general de Matlab. Así Simulink no es completamente un programa separado de Matlab, sino un anexo a él. El ambiente de Matlab está siempre disponible mientras se ejecuta una simulación en Simulink.

Simulink tiene dos fases de uso: la definición del modelo y la simulación del modelo. La definición del modelo significa construir el modelo a partir de elementos básicos

construidos previamente, tal como, integradores, bloques de ganancia o servomotores. Para el análisis del modelo debe contarse con la simulación, linealización y determinar las características del modelo previamente definido.

Para simplificar la definición del modelo Simulink usa diferentes clases de ventanas llamadas ventanas de diagramas de bloques. En estas ventanas se puede crear y editar un modelo gráficamente usando el mouse. Simulink usa un ambiente gráfico lo que hace sencillo la creación de los modelos de sistemas.

Después de definir un modelo este puede ser ejecutado seleccionando una opción desde los menús de Simulink o entrando comandos desde la línea de comandos de Matlab.

Simulink puede simular cualquier sistema que pueda ser definido por ecuaciones diferenciales continuas y ecuaciones de diferencias discretas. Esto significa que se puede modelar sistemas continuos en el tiempo, discretos en el tiempo o sistemas híbridos.

Simulink usa diagramas de bloques para representar sistemas dinámicos. Mediante una interface gráfica con el usuario se pueden arrastrar los componentes desde una librería de bloques existentes y luego interconectarlos mediante conectores y alambres. La ventana principal de Simulink se activa escribiendo Simulink en la línea de comandos de Matlab, y se muestran en la figura 4.1:

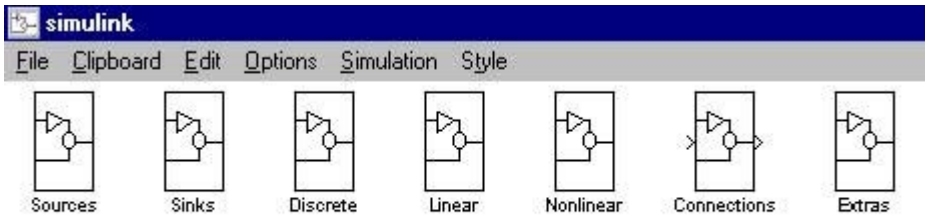

FIGURA 4.1 LIBRERIAS DE SIMULINK

4.4 SIMULACIÓN EN MATLAB – SIMULINK

Este trabajo describe una simulación basado en el ambiente de simulación MATLAB-SIMULINK, para simular un MRAC con 6 polos en el estor y 4 polos en el rotor.

Todas las simulaciones se encuentran completamente documentadas en el trabajo a través de diagramas de bloques, funciones y parámetros especiales de MATLAB para un fácil desarrollo del modelo.
Como de ha comentado anteriormente, las principales ventajas que presenta este simulador y en especial en el desarrollo del modelo del MRAC es:

- La ganancia de tiempo para el desarrollo y estudio de la simulación.
- La opción de varias técnicas de resolución numérica
- Como el programa contiene librerías especializadas, hace más sencillo integrar el estudio del motor con áreas de lógica difusa, procesamiento de señales, etc.

A continuación se muestra la forma de programación llevada a cabo para la simulación, en donde se presenta en forma desglosada.

4.4.1 PROGRAMACIÓN EN MATLAB

La programación en MATLAB, fue llevada a cabo, en base a un grupo de listados de programas, que tiene por fin desarrollar una función especial dentro de la simulación global, este grupo de programas consta de 5 partes, las cuales se mencionan a continuación.

1. principal: Este programa como su nombre lo menciona, es el alma de la simulación, dado que en el se cargan los valores característicos del motor además este programa brinda la información inicial para el desarrollo de la simulación. El nombre del programa es “inicio.m” y su desarrollo y comentarios se encuentran en los resultados obtenidos del trabajo.
2. Conmutación: Este programa permite realizar en forma correcta la conmutación que alimenta al MRAC, esto es permite determinar el momento de encendido y apagado de la fase del estator (θ_{on} y θ_{off}, lo cual sirve para controlar el funcionamiento general de motor; el listado del programa “conmutación.m”, se muestra más adelante y se encuentra detalladamente comentado para su comprensión.

3. Inductancia: determina la corriente y la inductancia de fase del MRAC, en función de la posición del rotor (θ) y del flujo de fase ψ; este programa se determina "inductancia.m" y se comenta a detalle en los resultados de simulación obtenidos.
4. par: Este programa realiza el calculo del par producido por el motor, esto con cálculos realizados en base a la posición del rotor (θ) y el valor de corriente I de las fases del estator; este programa se denomina "par.m", en los resultados se muestra y cometa el listado del programa.
5. pie: Este modulo nos ayuda a asegurar que la posición del rotor tenga una periodicidad de 2Π, y regresar a cero, para que en la simulación tenga resultados correctos, este programa se denomina "pie.m", y su listado y comentarios se encuentran en los resultados de la simulación obtenidas.

4.4.2 Simulación basada en Simulink.

La simulación basada es SIMULINK, fue llevada cabo en forma estructurada, esto con ayuda de los programas realizados previamente en MATLAB, como se comentó anteriormente SIMULINK opera en forma de bloque, lo cual hace más fácil y didáctica la solución de la simulación.
La forma de comprender la forma de operación de SIMULINK, es sencilla; esto solo con observar el diagrama de bloques utilizado para la simulación, cada bloque esta debidamente nombrado y ligado con la programación de MATLAB, además acondicionan las entradas con el fin de poder comprender y seguir tanto las entradas como salidas de cada bloque de simulación.

La forma general de solución para este trabajo, se muestra más adelante en detalle en la sección de resultados obtenidos.

CAPITULO 5

RESULTADOS DE SIMULACION.

En este capítulo mostraremos los resultados obtenidos en las simulaciones realizadas, para evaluar la caracterización del motor propuesto. Como se hace mención anteriormente, solo se trabaja con un modelo simplificado para fines prácticos. En la primera sección se hace referencia a los parámetros utilizados en el motor y al software con el que se realizo la simulación.

Posteriormente, en las siguientes secciones, se muestra los resultados obtenidos en la simulación, como es el caso de corriente, voltaje, inductancia y par de fase además de la velocidad del motor.

Cada una de estas secciones contiene los comentarios y análisis que ayudan a comprender mejor los resultados.

La siguiente parte, presenta la caracterización del motor que analizamos, mostrando algunas de las características descritas anteriormente y comparadas con motores de sus mismas dimensiones en diferentes categorías.

5.1 PARAMETROS DEL MRAC

El desempeño de la caracterización del motor MRAC fue realizado mediante simulaciones digitales. Para realizarlas, se utilizó el modelo lineal del motor con fines de simplicidad.
Los parámetros considerados para la simulación son: Números de polos del estator N_r=6, Números de polos en el rotor N_s=4; parámetros de la inductancia, Lmin=.008 [H], Lmax=.06 [H], resistencia de fase del estator, r=1.3Ω; momento de inercia, J=.003 kgm^2
Estos valores pueden en algún caso especial tomar otros valores para realizar estudios específicos.
El software de simulación que se utilizó para realizar las simulaciones fue MATLAB en su versión 5.2 y SIMULINK, en su versión 3.0. El simulador MATLAB-SIMULINK es un programa muy útil para resolver numéricamente ecuaciones diferenciales que puede ser usado para simular sistemas dinámicos que estén compuestos de varios subsistemas como a continuación se observará.

5.2 LISTADOS PARA LA SIMULACION EN MATLAB

A continuación se presenta los diferentes listados que fueron utilizados para la simulación dinámica del motor de reluctancia accionado por conmutación, como se podrá observar, cada bloque que fue utilizado, muestra sus respectivos comentarios para que sea didáctico.

5.2.1 LISTADO PARA EL PROGRAMA DE INICIO.

1. *inicio.m* Este programa en MATLAB, nos permite cargar los valores característicos del motor de reluctancia accionado por conmutación que deseamos simular, como se puede observar en los comentarios.
   A continuación se presenta el listado:

```
%%%%%%%%%%%%%%%%%%%%%%%%%%%%%%%%%%%%%%%%%%%%%%%%%%%%%%%%%%%%%%%%%%%%
%inicio.m                                                              %
%Este programa sirve para poder cargar los valores del motor "MRAC"    %
%%%%%%%%%%%%%%%%%%%%%%%%%%%%%%%%%%%%%%%%%%%%%%%%%%%%%%%%%%%%%%%%%%%%

global TETAS TETAX TETAY TETAXY TETAON TETAOFF TETAQ V AUP BUP ADOWN BDOWN
DL A B LMIN LMAX

NS=6    %Este valor nos representa el numero de polos del MRAC en el estator.
NR=4        %Este valor nos representa el numero de polos del MRAC del rotor.
P=3;        %Este valor nos representa el numero de fases de MRAC.

BETAS=30*(pi/180);
BETAR=30*(pi/180);
TETAS=(2*pi)*((1/NR)-(1/NS))
TETAX=(pi/NR)-((BETAR+BETAS)/2)
TETAY=(pi/NR)-((BETAR-BETAS)/2)
TETAZ=(BETAR-BETAS)/2
TETAXY=(TETAY+TETAZ+TETAS)
TETAON=0*(pi/180)        %Este es el ángulo en donde se comienza la conmutación.
TETAOFF=30*(pi/180)        %Este es el ángulo en donde se termina la conmutación.
TETAQ=60*(pi/180)          %Este es el ángulo en donde se encuentra totalmente desalineado
                           %el polo del rotor y el estator
TETAIN=.1*(pi/180)
V=100
R=1.30;            %Resistencia de fase
J=0.003;           %Valor de inercia


DELTAVMAX=150;
LMIN=8e-3;           %Inductancia mínima
LMAX=60e-3;           %Inductancia máxima
```

```
%%%%%%%%%%%%%%%%%%%%%%%%%%%%%%%%%%%%%%%%%%%%%%%%%%%%
%Calculos que nos serviran para obtener la inductancia en diferentes posiciones del rotor %
%%%%%%%%%%%%%%%%%%%%%%%%%%%%%%%%%%%%%%%%%%%%%%%%%%%%


G=(inv([TETAX 1;TETAY 1]))*([LMIN;LMAX]);
AUP=G(1);
BUP=G(2);
H=(inv([(TETAY+TETAZ) 1;TETAXY 1]))*([LMAX;LMIN]);
ADOWN=H(1);
BDOWN=H(2);
DL=AUP;
```

5.2.2 LISTADO PARA EL PROGRAMA DE CONMUTACIÓN.

3.- *conmutación.m* este programa de MATLAB nos permite asegurar la conmutación en el ángulo que nosotros necesitamos, en este caso se nombra un ángulo de encendido θ_{on} y el ángulo de apagado θ_{off}, los comentarios se encuentran descritos en el mismo programa que a continuación se presenta.

```
%%%%%%%%%%%%%%%%%%%%%%%%%%%%%%%%%%%%%%%%%%%%%%%%%%%%
%Este programa sirve para poder decidir en donde comienza y temina la conmutación %
%conmutacion.m %
%%%%%%%%%%%%%%%%%%%%%%%%%%%%%%%%%%%%%%%%%%%%%%%%%%%%


function Va=f(TE);  %En esta función de MATLAB se tiene la oportunidad de poder cargar
                    %el vector de entrada (voltaje y angulo)

E=TE';          %E es ahora el vector columna de entrada.
e=E(1);         %El primer termino representa la entrada de voltaje
teta=E(2);      %El segundo termino nos representa la entrada del angulo del rotor
```

```
%%%%%%%%%%%%%%%%%%%%%%%%%%%%%%%%%%%%%%%%%%%%%%%%%%%%%
%Aqui se comienza a cargar los comandos y valores generales del motor MRAC, que previamente %
%se determinaron.                                                                          %
%Las variables de TETAON y TETAOFF como se observó, fueron definidas con anterioridad  y que%
%fueron cargadas en el programa principal inicio.m el cual empezará a correr en este        %
%momento.                                                                                   %
%%%%%%%%%%%%%%%%%%%%%%%%%%%%%%%%%%%%%%%%%%%%%%%%%%%%%%

global TETAS TETAX TETAY TETAXY TETAON TETAOFF TETAQ V AUP BUP ADOWN BDOWN
DL LMIN LMAX

if ((TETAON<= teta) & (teta <=TETAOFF))
  Va=V;
end;
if ((TETAOFF<teta)&(teta<=TETAQ))
  Va=-V;
end;
if (teta>TETAQ)
  Va=0;
end;
```

5.2.3 LISTADO PARA EL PROGRAMA DE INDUCTANCIA.

4.- *inductancia.m* con este programa podemos obtener el comportamiento de la inductancia de fase del motor en función del tiempo, como se vera a detalle se especifica las entradas y salidas que brinda este programa, esto en los comentarios del mismo.
Cabe destacar que además de obtener la inductancia, otra salida que brinda el programa es la corriente que es otro parámetro que es de suma importancia en la simulación.

```
%%%%%%%%%%%%%%%%%%%%%%%%%%%%%%%%%%%%%%%%%%%%%%%%%%%%
%Este programa nos ayuda a calcular la inductancia del MRAC                    %
%inductancia.m                                                                 %
%%%%%%%%%%%%%%%%%%%%%%%%%%%%%%%%%%%%%%%%%%%%%%%%%%%%


function U=f(TE); %TE es ahora nuestro vector de entrada.

E=TE';          %E es nuestro vector columna de entrada.
flux=E(1);      %representa el flujo de entrada
teta=E(2);      %representa la posición del rotor.

%%%%%%%%%%%%%%%%%%%%%%%%%%%%%%%%%%%%%%%%%%%%%%%%%%%%
%Aquí se realizan los cálculos para la obtención de la inductancia basandose en %
%los parámetros determinados en inicio.m                                       %
%%%%%%%%%%%%%%%%%%%%%%%%%%%%%%%%%%%%%%%%%%%%%%%%%%%%

global TETAS TETAX TETAY TETAXY TETAON TETAOFF TETAQ V AUP BUP ADOWN BDOWN
DL LMIN LMAX

if((0 <= teta)&(teta <= TETAX))
U=[flux/LMIN,LMIN];        %Como se observa el primer termino representa la
                           %corriente y el segundo la inductancia.
end;

if ((TETAX < teta)&(teta <= TETAY))
  U=[flux/((AUP*teta)+BUP),((AUP*teta)+BUP)];
end;

if((TETAY < teta) & (teta <= TETAXY))
  U=[flux/((ADOWN*teta)+BDOWN),((ADOWN*teta)+BDOWN)];
end;

if(teta > TETAXY)
  U=[flux/LMIN,LMIN];
end;
```

5.2.4 LISTADO PARA EL PROGRAMA DE PAR

5.- par.m como su nombre lo menciona, en este programa podremos obtener el comportamiento del par en el tiempo, el programa se encuentra comentados para la comprensión del mismo.

```
%%%%%%%%%%%%%%%%%%%%%%%%%%%%%%%%%%%%%%%%%%%%%%%%%%%%%%%%%%%%%%%%%%%%%%%%%%%%
%Este programa sirve para obtener el par del MRAC                                %
 %par.m                                                                          %
%%%%%%%%%%%%%%%%%%%%%%%%%%%%%%%%%%%%%%%%%%%%%%%%%%%%%%%%%%%%%%%%%%%%%%%%%%%%

function T=f(TE);   %Nuevamente TE es le vector de entrada

E=TE';              %E es nuevamente el vector columna de entrada
i=E(1);             %representa la corriente
teta=E(2);           %representa la posicion del rotor

%%%%%%%%%%%%%%%%%%%%%%%%%%%%%%%%%%%%%%%%%%%%%%%%%%%%%%%%%%%%%%%%%%%%%%%%%%%%

global TETAS TETAX TETAY TETAXY TETAON TETAOFF TETAQ V AUP BUP ADOWN DL LMIN
LMAX
if((0<=teta)&(teta<=TETAX))
   T=[0,0];        %el resulta que obtenemos en el primer termino es el par

end;

if((TETAX<teta)&(teta<=TETAY))
   T=[0.5*(DL)*(i*i),DL];
end;

if((TETAY<teta)&(teta<=TETAXY))
   T=[-0.5*(DL)*(i*i),-DL];
end;

if(teta>TETAXY)
   T=[0,0];
end;
```

5.3. SIMULACIÓN EN SIMULINK

A continuación se presenta el esquema de simulación basado en SIMULINK ver 2.0, lo que se puede apreciar a primera vista, es que se trata de un sistema de bloques sistematizado, el cual brinda la idea sencilla de funcionamiento, como se observa algunos bloques son funciones que llevan implícita una función de MATLAB, en este caso se trata de la llamada de un programa o lista de programación (inicio.m,conmutación.m,inductancia.m,par.m, pie.m) los cuales son piezas fundamentales para el desarrollo de la simulación dinámica del motor de reluctancia accionado por conmutación.

Se observa claramente las rutas lógicas de simulación, con lo cual podemos seguir paso a paso el desarrollo y simulación del motor.

Además cabe resaltar que la simulación se realiza en forma monofásica, con los resultados obtenidos podremos inferir los resultados para una simulación trifásica, pero el objetivo primordial de este trabajo, es de caracterizar el motor; por lo que con la simulación monofásica nos da la solución para poder obtener los parámetros primordiales que nos ayuden a realizar nuestro objetivo.
Con este modelo de simulación monofásica obtenemos la corriente, inductancia, tensión aplicada a la fase, par, velocidad del rotor.

Cada respuesta obtenida de los parámetros obtenidos se discute en la sección de resultados y conclusiones.

La figura 5.1, representa el esquema de simulación en base al programa SIMULINK ver. 2.0, que a continuación se presenta.

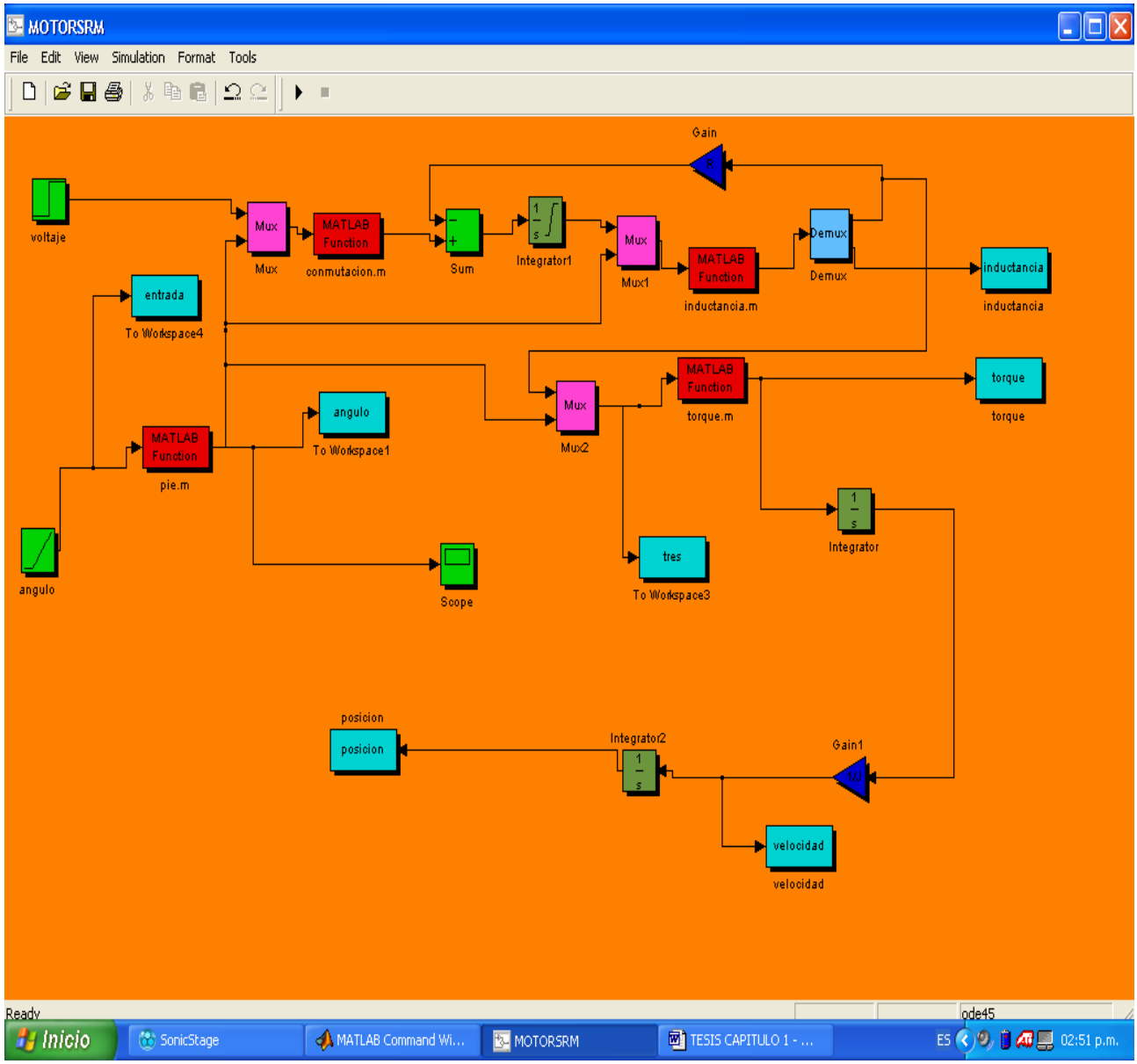

FIGURA 5.1 ESQUEMA DE SIMULACIÓN EN SIMULINK

A continuación mostramos los comentarios y anotaciones que se realizan en la simulación en SIMULINK, esto con el fin de poder comprender la forma en como trabaja el simulador. Estas anotaciones se presentan en la figura 5.2 que a continuación aparece.

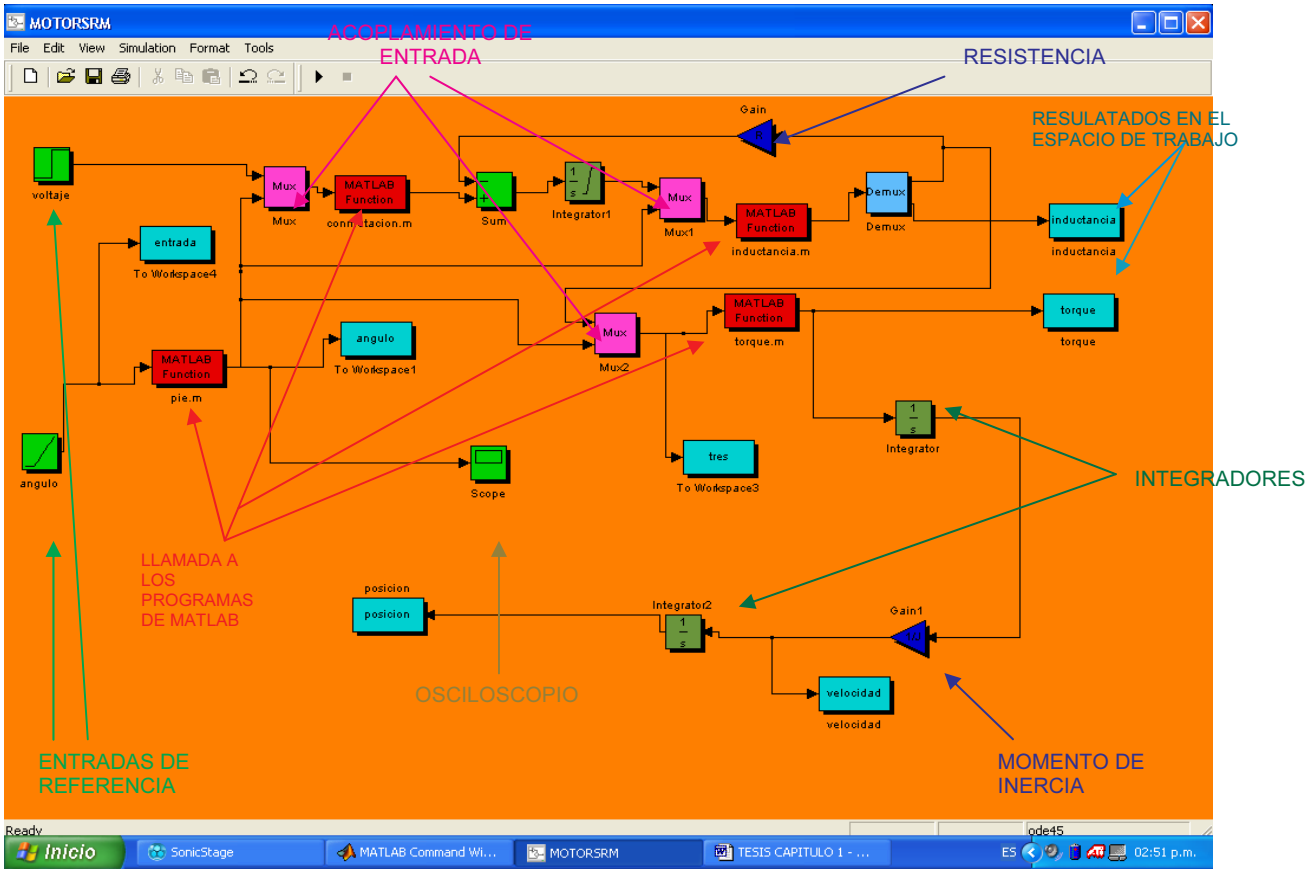

FIGURA 5.2 ESQUEMA DETALLADO DEL ESQUEMA DE SIMULACIÓN EN SIMULINK

5.4 RESULADOS DE SIMULACIÓN.

A continuación se muestra los resultados obtenidos en la simulación, se presentan gráficas como es el caso de la corriente, inductancia, tensión de alimentación, par, velocidad del motor.

Como se puede observar los resultados se presentan en tiempo real, esto es, las gráficas obtenidas son tomadas en el osciloscopio que incluye en el programa de SIMULINK.

Como se podrá observar, los resultados obtenidos en el programa SIMULINK, carecen de una flexibilidad en su presentación, esto es que la rotulación de la gráfica, ejes coordenados, diseño (forma y colores) presentan una limitación para poder presentar los resultados.

Esperamos que este programa avance en la forma de presentación de resultados, siendo más amistosa y atractiva para la gente que labora en esta área.

5.4.1 INDUCTANCIA.

La figura 5.3 que a continuación se muestra, es la curva de inductancia de fase del motor de reluctancia accionado por conmutación, que se obtuvo en la simulación, esto con los parámetros descritos anteriormente.

Como se mencionó anteriormente, los resultados obtenidos no presentan una gran diversidad en utilerías de presentación.

Cabe mencionar que en las gráficas obtenidas las unidades del eje "X" son segundos [s] y en el eje "Y" Henry [H].

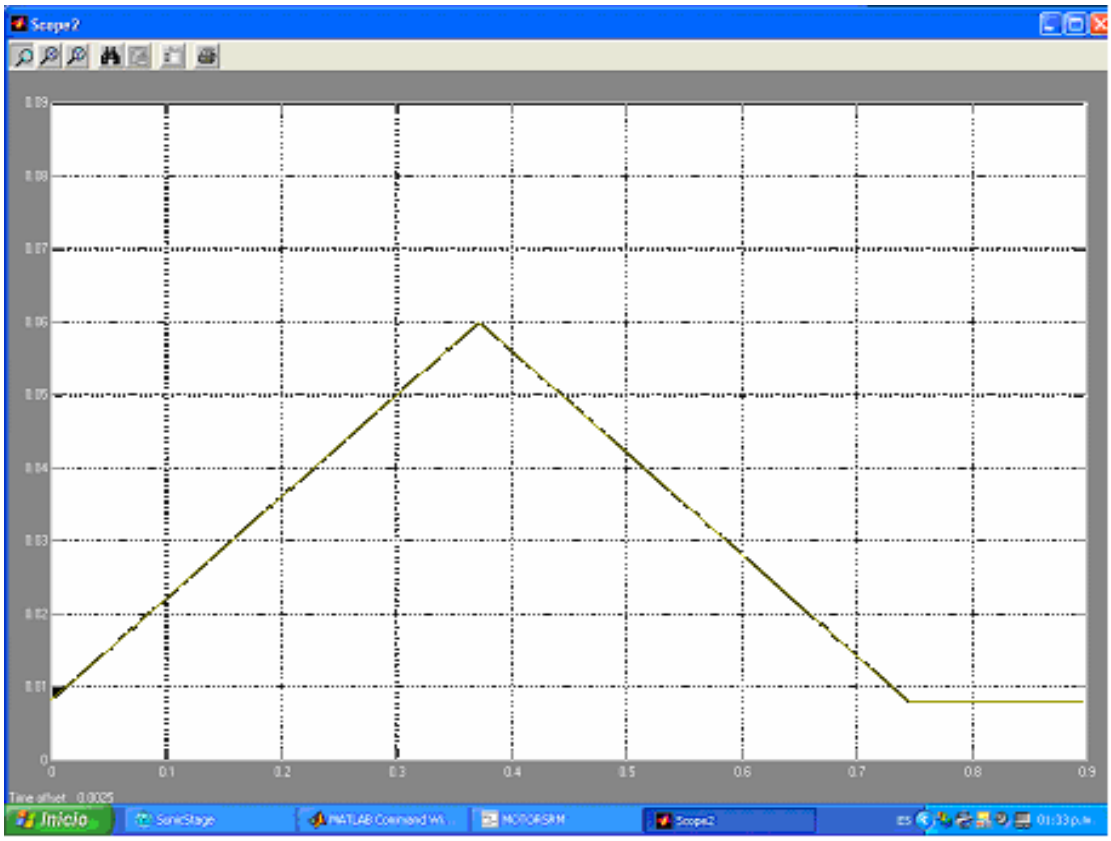

FIGURA 5.3 INDUCTANCIA DE FASE

Como podemos observar, la gráfica que obtenemos tiene valores que esperábamos (Lmin=.008 [H] y Lmax=.06 [H], esto) es que por este punto, nos brinda la idea que la gráfica obtenida contiene valores reales.

El resultado obtenido, fue debidamente comparado, con los resultados obtenidos en otras simulaciones.

Lo sorprendente, fue ver que la gráfica obtenida coincide correctamente con resultados obtenidos de otros trabajos, esto tomando en cuenta que algunas simulaciones son hechas tomando en cuenta, el modelo matemático general, que toma en cuenta todas las variables descritas.

Ante todo, es importante comprender los resultados obtenidos, esto para ser capaces de comprender la situación física del evento en estudio.

A continuación se muestra en la figura 5.4 un acercamiento de la gráfica anterior, esto para poder observar y visualizar mejor los resultados.
Como se podrá apreciar, la gráfica se puede dividir en 2 zonas de operación, que son unas de las partes más importantes de este estudio las cuales son:

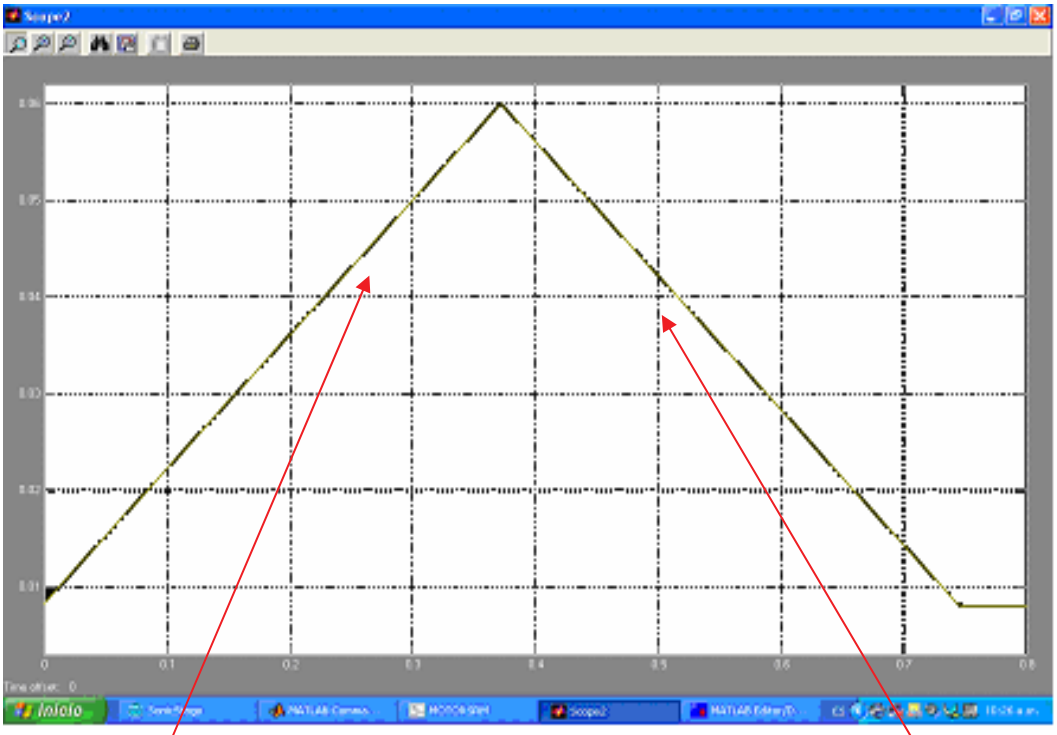

FIGURA 5.4 ACERCAMIENTO DE LA GRÁFICA 6.3

ZONA 1 ZONA 2

Como se observa en la figura 5.4, existen 2 zonas de operación, a continuación describiremos cada una de estas zonas:

- Zona 1. En esta zona se lleva a cabo el encendido del conmutador, esto para llevar a cabo la alineación del polo del rotor y estator, este proceso se podrá ver más adelante.
- Zona 2. Esta zona representa el momento en que empieza el desalineamiento de los polos del rotor y estator, una vez que el proceso de la zona 1 ha sido completado.

La figura 5.5, nos ayudará a vincular mejor la gráfica obtenida anteriormente, con la situación real del motor MRAC.

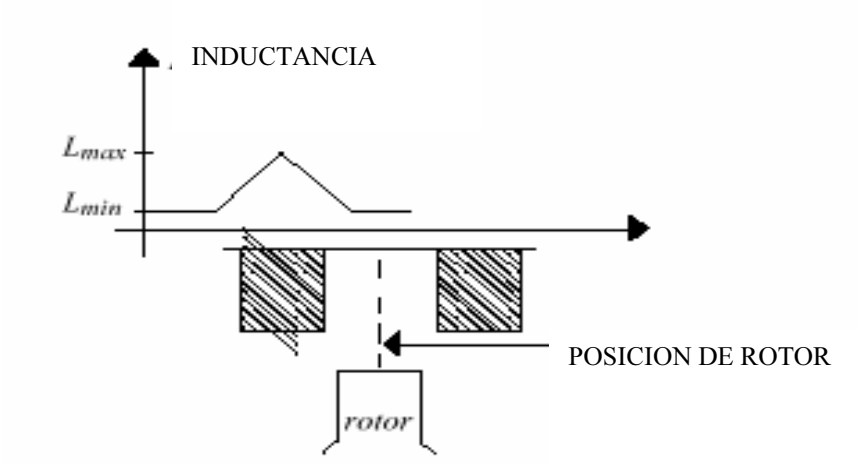

FIGURA 5.5 INDUCTANCIA EN LOS MRAC

5.4.2 TENSIÓN DE ALIMENTACION.

La figura 5.6 fue obtenida en la simulación y nos entrega la forma de la señal de tensión que se alimenta al MRAC.
Como se puede observar, la señal de tensión que proponemos, es una señal particular para el conmutador que elegimos, esto quiere decir, que para otros modelo de conmutadores la señal de pueden variar de forma o sentido de alimentación.

Antes de presentar la gráfica resultante, es impotente mencionar que en el eje "X" se maneja segundos [s] y en el eje "Y" se maneja volts [V]

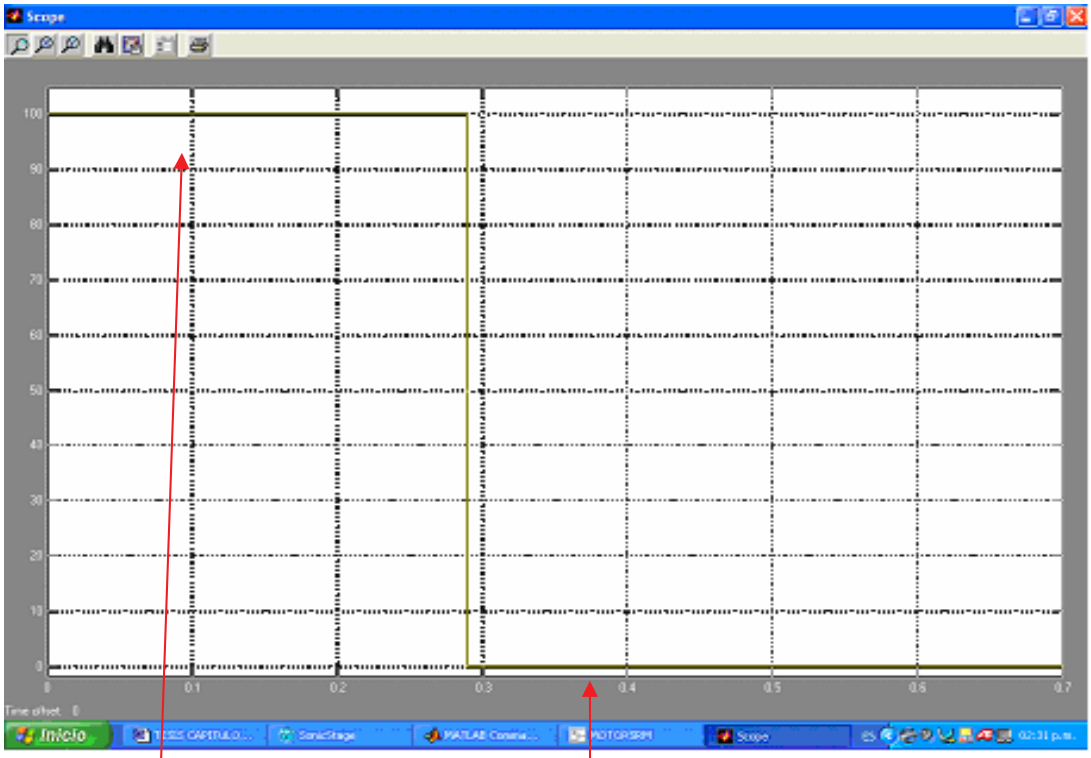

FIGURA 5.6 TENSIÓN DE ALIMENTACIÓN DEL MRAC

t=0 [s] (inicio de la conmutación) t=.29 [s] es el termino de la conmutación

Con la gráfica anterior, observamos que en el tiempo t=0, la conmutación empieza a llevarse a cabo; mientra que en el tiempo t=.29 s, la conmutación llega a su fin en esa fase.
La conmutación empieza cuando el polo del rotor y estator se encuentran desalineados, y la conmutación termina cuando el polo del rotor y estator se encuentran alineados nuevamente.

5.4.3 CORRIENTE

La corriente, es uno de los parámetros primordiales, que se buscan en la simulación.
A continuación se muestra la figura 5.7 obtenida para la corriente. Los resultados obtenidos fueron discutidos y comparados con otros resultados hechos por diversos trabajos.

Como se puede ver la forma de la onda resultante, presenta algunas alteraciones, esto debido a la forma en como el MRAC opera. La señal resultante diferencia mucho de la señal ideal que se esperaba (cuadrada).

Los ejes que la gráfica presentan tiene en el eje "X" tiempo en segundos [s] y en el eje "Y" presenta amperes [A]

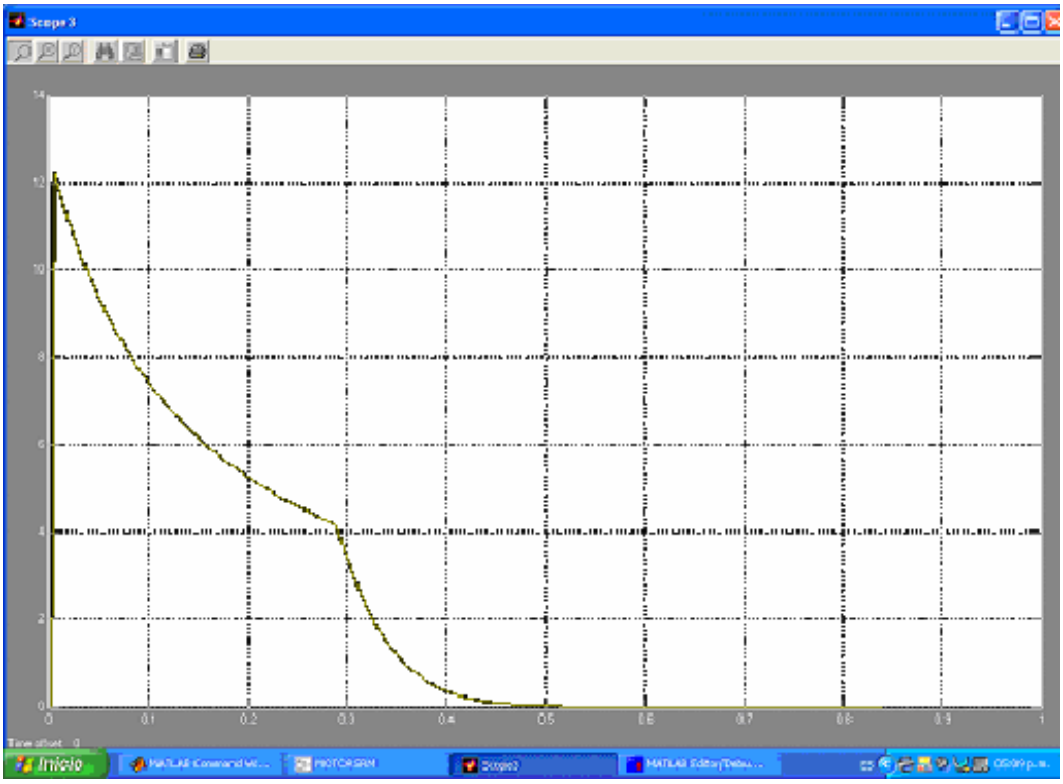

FIGURA 5.7 CORRIENTE DE FASE DEL MRAC.

La figura 5.8 que a continuación se presenta, es una acercamiento para mejor apreciación de la figura 5.7

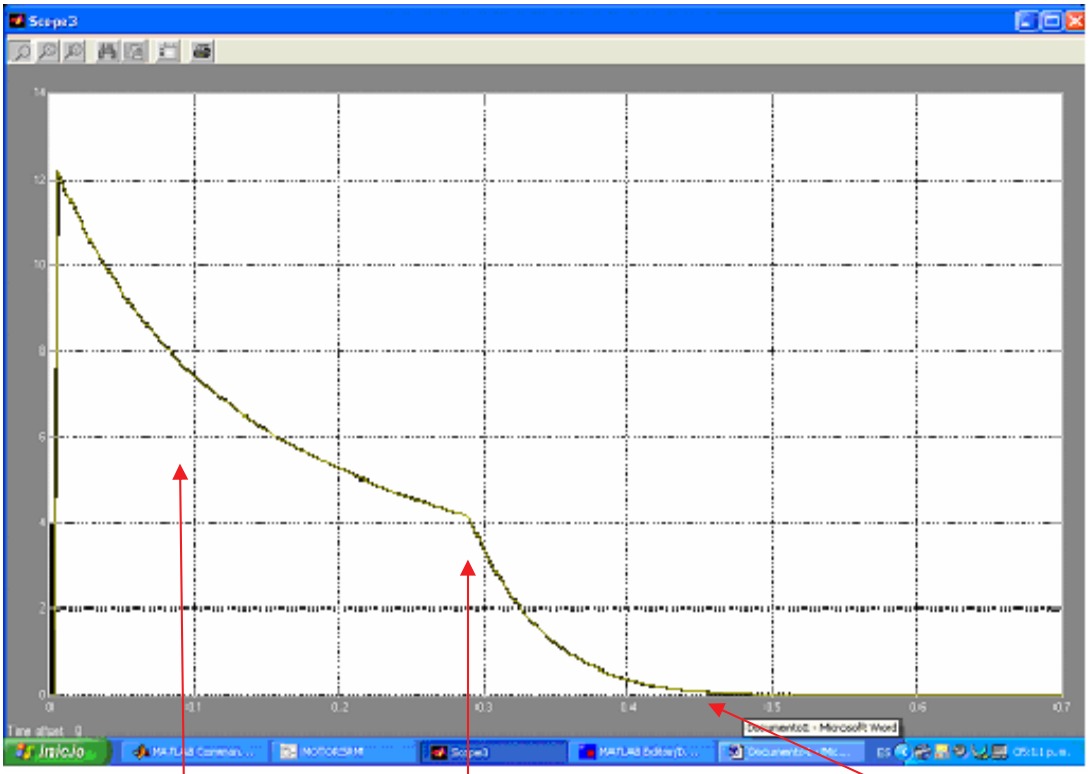

FIGURA 5.8 ACERCAMIENTO DE LA GRÁFICA 6.7

ZONA 1 ZONA 2 ZONA 3

Corriente cuando el conmutador Se encuentra encendido

Punto en donde termina la conmutación

Corriente, un tiempo después que el conmutador se apagó

Como se puede ver, la forma de la corriente obtenida, durante el funcionamiento del conmutador, presenta una forma distinta a la teórica (cuadrada). Esto influye fuertemente, en el diseño del control que se desarrolla para este tipo de motores.

Como se observa en la zona 2, se presenta el apagado del conmutador, y como esperabamos, se presenta un cambio notorio en la trayectoria de la gráfica.

En la zona 3, el conmutador se encuentra apagado, y como se observa existe un flujo de corriente aún por las espiras del rotor, que influirá fuertemente en el desarrollo del par; este punto será tratado posteriormente.

En la zona 3 es un punto de interés profundo, por el hecho de desarrollar un control que tome en cuenta esta característica particular del MRAC.

Un valor importante obtenido en la simulación, es el valor pico de la corriente que se obtiene y en este caso resulta ser de 12.1 [A], dado las características propias del motor simulado.

5.4.4 PAR

A continuación mostraremos la figura 5.9 obtenida para el par del MRAC simulado
Esta curva esta determinada por las ecuaciones de motor determinadas anteriormente y que se encuentran listadas en los programas de MATLAB.
La curva obtenida fue sometida a comparación con otros tipos de simuladores, resultando ser parecida en la forma obtenida.

Los parámetros descritos por la gráfica en el eje "X" representa tiempo [s], y en el eje "Y" se presenta Newton metro [Nm]

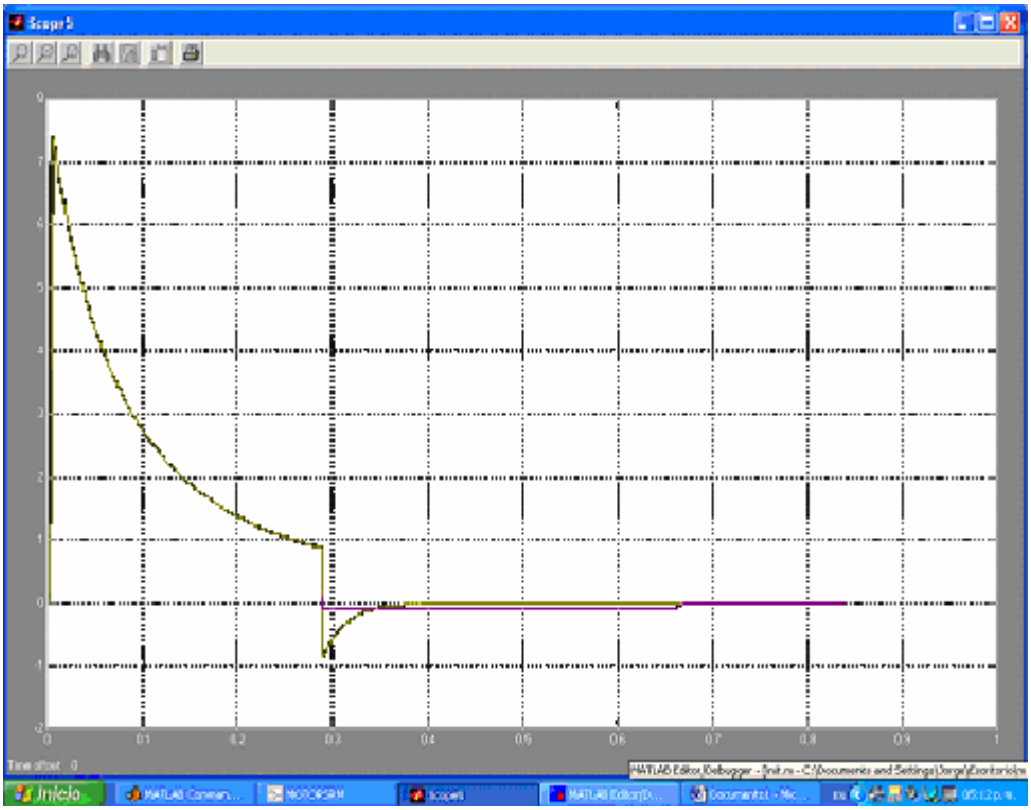

FIGURA 5.9 PAR OBTENIDO DEL MRAC

A continuación se muestra un acercamiento de la curva anterior que se puede apreciar en el figura 5.10.

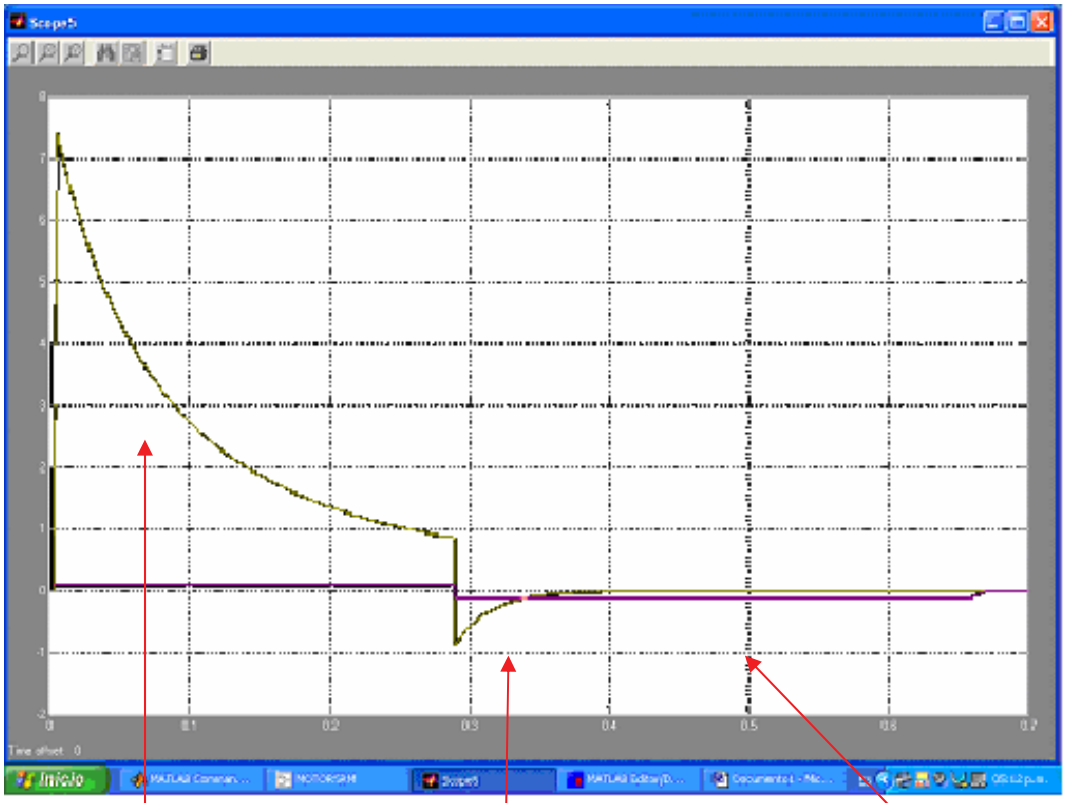

FIGURA 5.10 ACERCAMIENTO DE LA CURVA 6.9

ZONA 1 ZONA 2 ZONA 3

Entrada en funcionamiento Momento de apagado Tiempo después
Del conmutador del conmutador del apagado.

Como se puede observaren la zona 1, es el momento en que se encuentra encendido el conmutador, y la forma de onda es un poco distorsionada de la forma teórica o esperada.

En la zona 2 es el momento en que se presenta el apagado del conmutador, y tal como se esperaba, se presenta un cambio importante en la tendencia de la curva que describe el comportamiento del par.

La zona 3 es posiblemente la más importante de este punto, dado que como se puede observar, se presenta un par en sentido contrario, un tiempo después de ser apagado el conmutador, esto influye fuertemente en el desarrollo y funcionamiento del MRAC, dado que esto hace que el motor una vez apagado la fase que lo alimente, el rotor tiende a girar en sentido contrario al giro natural de funcionamiento, esto debido a la presencia de corriente en los devanados del estator, un tiempo después de ser apagado el conmutador.

Este zona es un punto de relevante importancia para ser desarrollada por el controlador, dado que este comportamiento hace que el MRAC baje su rendimiento y operación.

5.4.5 VELOCIDAD

A continuación se muestra en la figura 5.11 el resultado de la simulación para la velocidad que el MRAC presenta.

Como se podrá observar, la curva es característica del motor que se ha simulado, esto quiere decir que esta determinada en base a los datos cargados previamente.

La curva que a continuación se presenta, fue discutida y comparada en detalle con las curvas obtenida en otras simulaciones, dando como resultado valores coincidentes y semejantes, tal como se esperaba.

En el eje "X" se presenta segundos [s], y en el eje "Y" se presenta Radianes/segundo [rad/s]

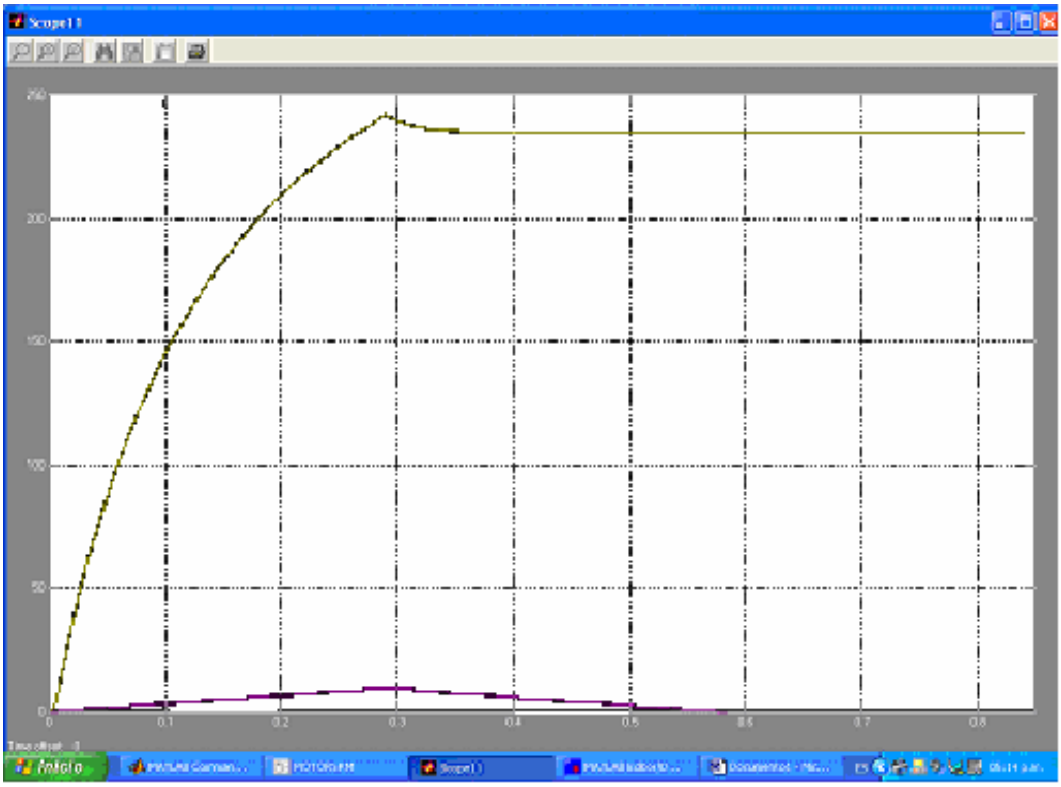

FIGURA 5.11 VELOCIDAD DEL MRAC.

A continuación se muestra en la figura 5.12 un acercamiento de la curva anterior.

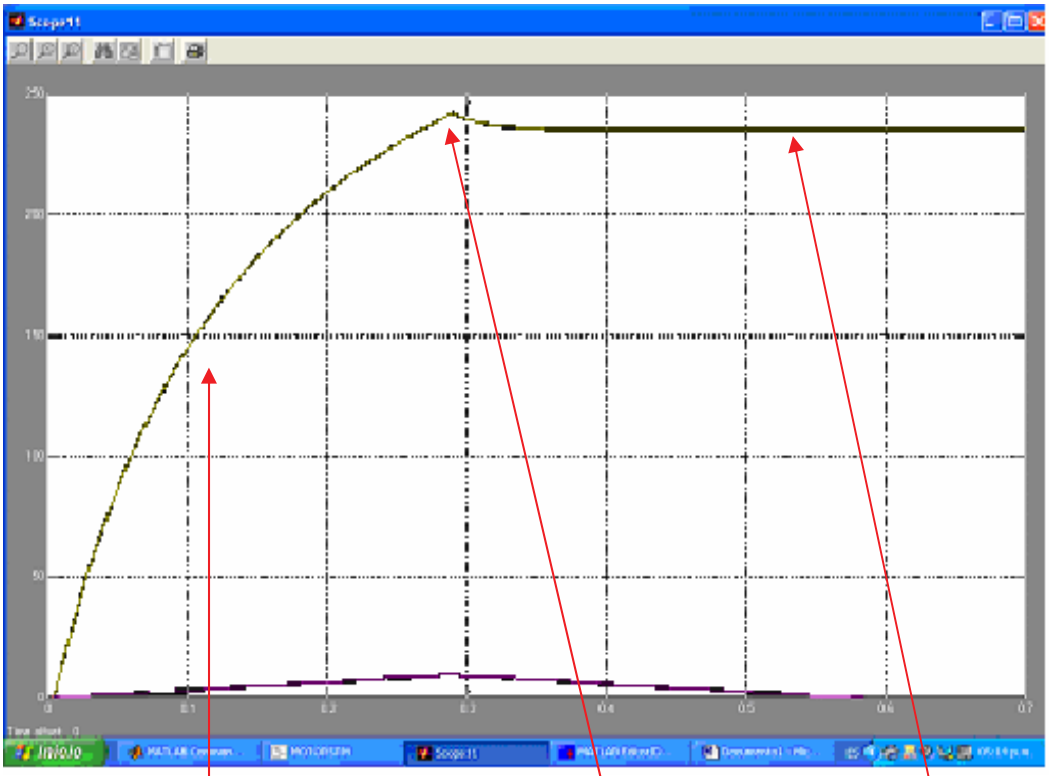

FIGURA 5.12 ACERCAMIENTO DE LA FIGURA 6.11

ZONA1	ZONA 2	ZONA 3
Se presenta el comienzo de la conmutación	Se presenta el apagado del conmutador	Un tiempo después de apagado del conmutador.

La zona 1 representa el tiempo en que el conmutador se enciende y se empieza el funcionamiento del motor, como se observa la forma en como se comporta la velocidad que desarrollo el motor en función del tiempo.

La zona 2 representa el momento en que se apaga el conmutador, y como se puede observar existe una variación en la tendencia que la curva presenta, lo más importante es observar que los efectos de la corriente influyen en el desarrollo de la velocidad del motor, esto esta mostrado en la forma en como varía la velocidad en el momento en que es apagado el conmutador (zona 2) y esto determina claramente en el desarrollo del motor.

Esta forma de comportamiento es un reflejo de lo sucedido con la corriente y par que se comentó anteriormente.

Lo más importante que se puede obtener de la curva anterior, es poder ver que el motor que se determinó con las características propuestas puede desarrollar una velocidad de 230 [rad/seg], que es un punto importante en el desarrollo de la caracterización del MRAC en estudio.

5.5 CARACTERIZACIÓN DEL MRAC

En esta sección, se realiza la caracterización del MRAC que se está estudiando, esto con ayuda de los parámetros determinados antes de la simulación, además de los resultados obtenidos de la simulación. A continuación se hace una comparación de las características que los MRAC presentan en comparación con motores de las mismas dimensiones, pero de diferentes tipos (categorías).

5.5.1 OBTENCIÓN DE LA POTENCIA DEL MRAC.

Con los valores obtenidos podremos inferir los valores característicos propios del MRAC que simulamos.
Primero obtendremos la potencia del MRAC.
Utilizaremos la formula que proporciona la potencia en el eje de cada motor.

$$P(WATT) = \tau(N.m)\omega(rad/s)$$

Con los valores obtenidos en la simulación obtenemos:

$$P(WATT) = 7.4(N.m)230(rad/s)$$

Con lo que obtenemos P= 1702 [W]

Que representa P=1.7 [kW].

También podemos representar la potencia del motor en HP (caballos de potencia), como se muestra a continuación.

Sabemos que 1HP=745.69 [W]

Con lo anterior tenemos

P=1.7 [kW]= 2.28 HP.

Con los datos anteriores podremos construir la siguiente tabla de caracterización.

TABLA No 2 CARACETRIZACIÓN DEL MRAC SIMULADO

PARAMETRO	VALOR	UNIDADES
NUMERO DE FASES EN EL ESTATOR	6	----------
NUMERO DE FASES EN EL ROTOR	4	----------
MAXIMA INDUCTANCIA	.06	[H]
MINIMA INDUCTANCIA	.008	[H]
VOLTAJE DE ALIMENTACIÓN	100	[V]
CORRIENTE DE FASE	12.1	[A]
VELOCIDAD	2197 230	[r.p.m] [rad/s]
PAR	7.4	[N.m]
MOMENTO DE INERCIA	.0013	[kgm^2]
RESISTENCIA DE FASE	1.30	[Ω]
POTENCIA	2.28 1.7	[Hp] [kW]

5.6 PEQUEÑO MOMENTO DE INERCIA. (GRAN RESPUESTA DINÁMICA)

Como se podrá observar el motor de reluctancia accionado por conmutación posee un momento de inercia pequeño, esto es debido a que el rotor esta hecho de una sola pieza metálica que tiene ausencia de masa en los huecos de los dientes del rotor.

Con lo anterior se puede observar que el rotor está hecho únicamente por el eje y un conjunto de chapas o polos salientes, (no posee ningún bobinado en esta parte).

En la siguiente tabla 3 podremos observar la comparación de momentos de inercia de distintos motores eléctricos de proporciones semejantes. En este caso hablaremos de un motor asincrono normal, un motor asincrono optimizado y nuestro motor de reluctancia accionado por conmutación.

Como se observa el motor de reluctancia accionado por conmutación aventaja claramente a sus competidores.

TABLA No 3 COMPARACION DE MOMENTOS DE INERCIA DE DISTINTOS MOTORES ELÉCTRICOS DE PROPORCIONES SEMEJANTES

	MOTOR DE RELUCTANCIA ACCIONADO POR CONMUTACIÓN	MOTOR ASINCRONO (OPTIMIZADO) MODELO (ACHA 128)	MOTOR ASINCRONO (NORMAL) MODELO (1LA4180)
MOMENTO DE INERCIA	0.0013 Kgm^2 56%	.0016 Kgm^2 ** 69%	.0023 Kgm^2 * 100%

De la tabla anterior podemos obtener una representación gráfica para poder visualizar más fácilmente lo descrito y que se presenta en la figura 5.13:

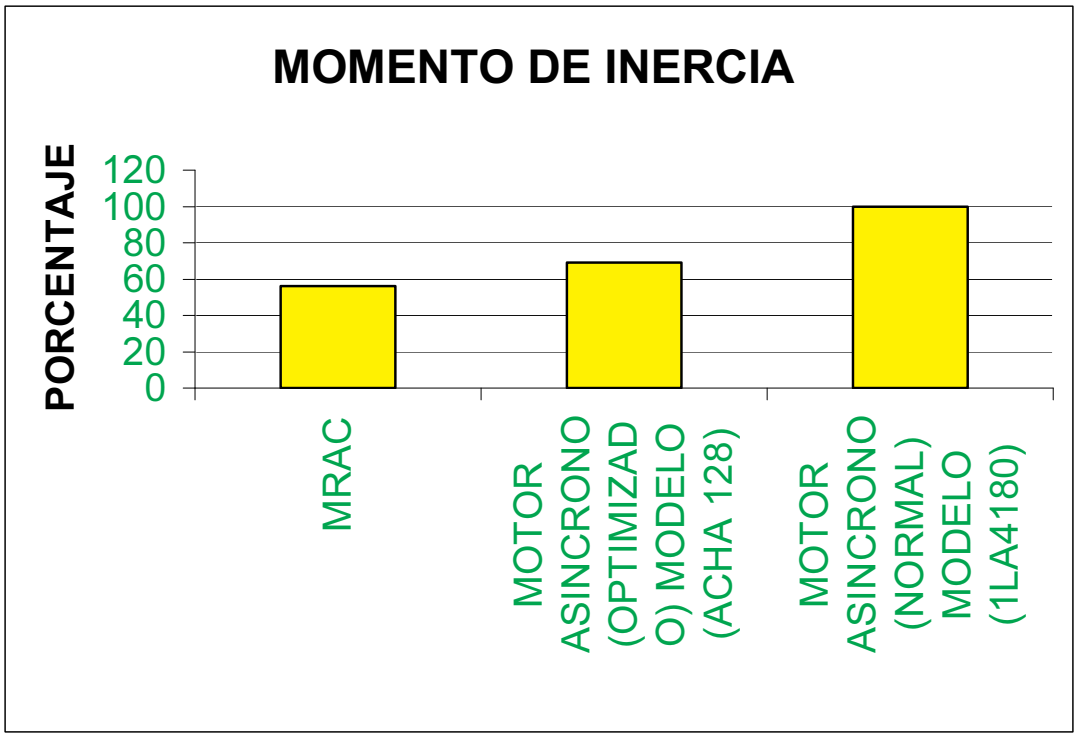

FIGURA 5.13 REPRESENTACION GRAFICA DE LOS MOMENTOS DE INERCIA

5.7 MRAC MEJOR APROVECHAMIENTO PARA BAJAS REVOLUCIONES.

En la figura 5.14 se representa el máximo par motor permitido en régimen permanente, referido respecto al momento de inercia en un intervalo de revoluciones desde 0 hasta 4200 r.p.m.

El motor de reluctancia accionado por conmutación se presenta con los parámetros inicialmente destinados para la simulación.

Si nos basamos en la curva característica par-velocidad anteriormente descrita podremos construir la curva propia del motor MRAC simulado.

Las líneas características y los valores de los motores asíncronos han sido tomados de las hojas de datos [2] y [8] proporcionados vía e-mail por grupos de investigación de los fabricantes. El volumen, dimensiones externas y el tamaño del rotor son en sus diferentes características semejantes.

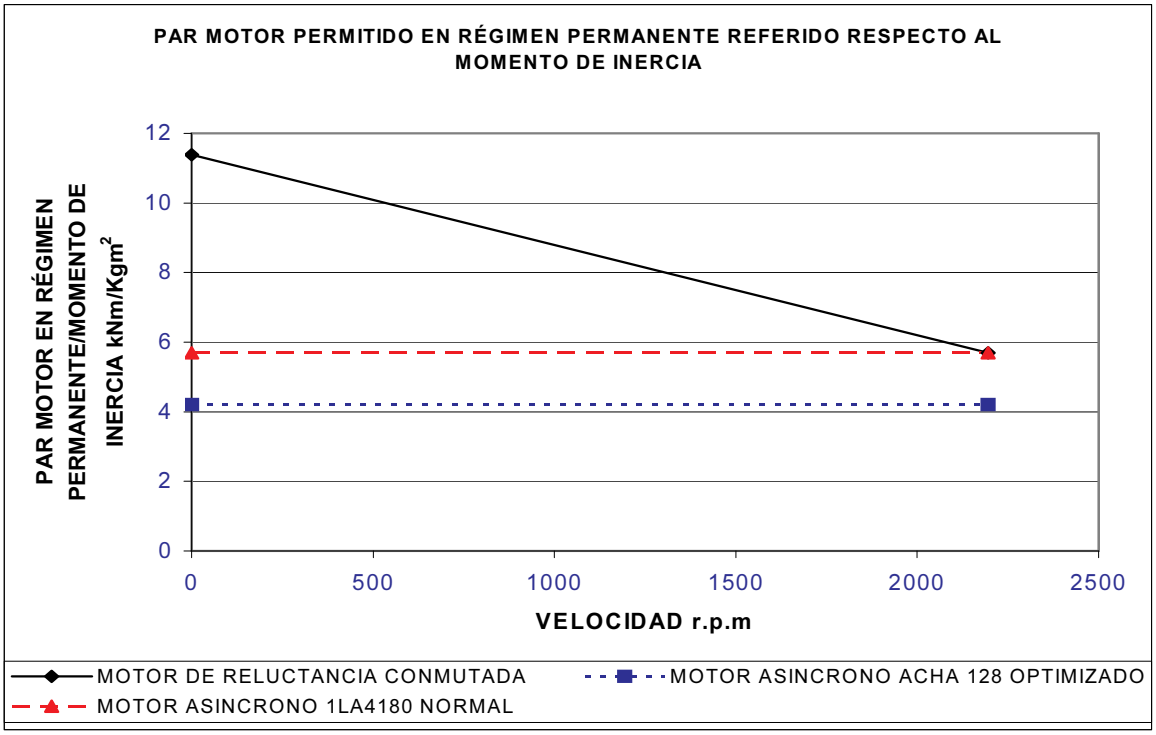

FIGURA 5.14 MÁXIMO PAR MOTOR PERMITIDO EN RÉGIMEN PERMANENTE, REFERIDO RESPECTO AL MOMENTO DE INERCIA

5.8 CONSUMO DE ENERGÍA.

Un punto importante dentro del estudio de los motores eléctricos, es el poder saber el consumo de energía eléctrica que estos tienen, como se presenta más adelante, se realiza una comparación entre los motores eléctricos más comunes con respecto al MRAC simulado, como se podrá comprender, la comparación entre motores es muy difícil, esto debido a que existe una diferencia importante entre tecnologías y formas de funcionamiento, pero la idea principal de este punto es poder visualizar en forma general el comportamiento de consumo energético entre diversos equipos de similares características, en este caso se basa principalmente en la potencia de los motores.

TABLA No 4 CORRIENTE ELÉCTRICA A PLENA CARGA DE MOTORES ELÉCTRICOS

TIPO DE MOTOR	POTENCIA [HP] [kW]	VOLTAJE DE ALIMENTACIÓN [V]	CORRIENTE [A].
MOTOR DE RELUCTANCIA ACCIONADO POR CONMUTACIÓN SIMULADO (6 POLOS EN EL ESTATOR Y 4 EN EL ROTOR)	2.28 1.7	100	12.1
MOTOR DE CORRIENTE DIRECTA.	2 1.49	120	17*
MOTOR MONOFÁSICO DE C.A	2 1.49	127	22**

*Valor obtenido de la tabla 430-147 de la Norma Oficial Mexicana NOM-001-SEDE-1999 Instalaciones Eléctricas [12]
** Valor obtenido de la tabla 430-148 de la Norma Oficial Mexicana NOM-001-SEDE-1999 Instalaciones Eléctricas[12]

A continuación se presenta una comparación en forma gráfica lo comentado anteriormente en la tabla y que se presenta en la figura 5.15.
Esto se hace con el fin de poder visualizar en forma más sencilla las ventajas que los MRAC tienen en este rubro con respecto a otros motores de características similares, el cual como se podrá observar aventaja en forma clara a su similares

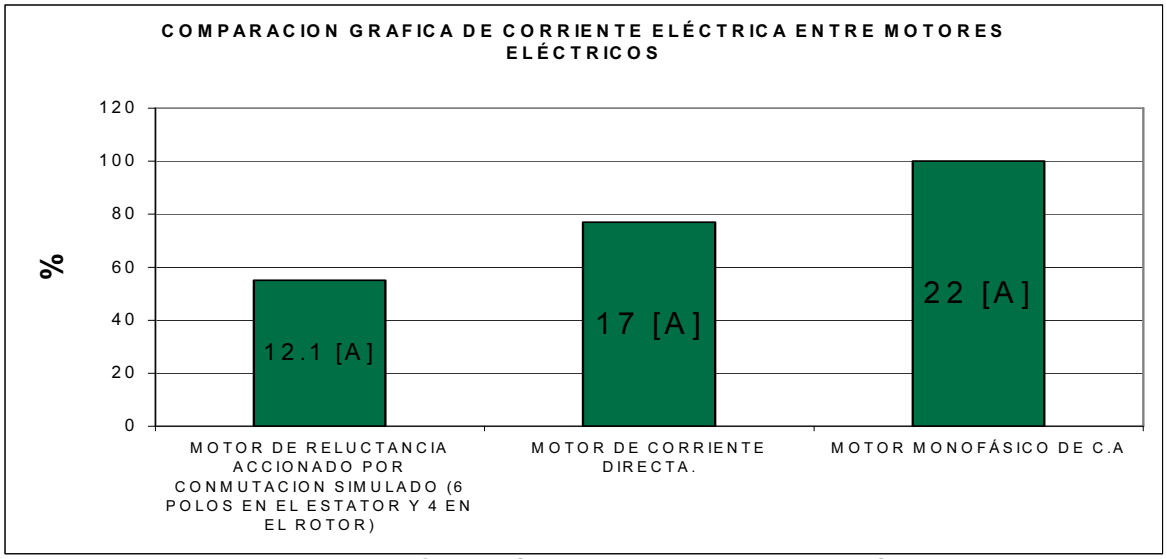

FIGURA 5.15 COMPARACIÓN GRÁFICA DE CORRIENTE ELÉCTRICO ENTRE MOTORES ELÉCTRICOS

Con la información anterior, es preciso mostrar o comparar el ahorro en $/año que estos motores pueden darnos en comparación con los motores utilizados hoy en día.

Para obtener esta comparación se utilizó las tarifas que CFE, nos brinda en sus servicios, esto en baja y media tensión.

La comparación hecha se presenta en la tabla 5 que a continuación se presenta.

TABLA No 5 CONSUMO Y AHORRO DE ENERGÍA ENTRE MOTORES ELÉCTRICOS

TIPO DE MOTOR	POTENCIA (FUENTE DE ALIMENTACIÓN)	TIEMPO DE UTILIZACIÓN (HORAS AL AÑO)	ENERGÍA (kW-hr)	PRECIO DEL (kW-hr) EN PESOS ($) ***TARIFA 2****	CONSUMO ANUAL EN ($)	DIFERENCIA ($/AÑO)
MOTOR DE RELUCTANCIA ACCIONADO POR CONMUTACIÓN	1.21 kW	1560	1887.6	$27.60	$52,097	----------
MOTOR DE CORRIENTE CONTINUA	2.04 kW	1560	3182.4	$27.60	$87,834	$35,737
MOTOR MONOFÁSICO DE CORRIENTE ALTERNA.(valores eficaces)	1.42 kW	1560	2223.7	$27.60	$61,376	$9,279

** obtenida de la página en internet de CFE www.cfe.gob.mx*

Como se observa el ahorro que se obtiene con el uso de MRAC, es significativo, cerca de $36,000/año y $10,000/año dependiendo del tipo de motor a utilizar, el cual los hace una herramienta interesante para poder ahorrar energía eléctrica.

Investigando más sobre la implementación de los MRAC en los sistemas directamente productivos, como se ha mencionado anteriormente, las lavadoras NEPTUNE de MAYTAG modelo MAH7500 , presentan un ahorro significativo de energía eléctrica, esto debido en mayor medida al motor MRAC actuante.

El ahorro que presentan es considerable, por lo anterior en los estándares para el ahorro de energía del gobierno de los Estados Unidos de América, presenta a el modelo MAH7500 como uno de los que más ahorra en su categoría.

A continuación en la figura 5.16, se presenta la hoja de especificación de ahorro de energía que se obtuvo gracias al departamento de comercialización de la empresa MAYTAG, esto vía e-mail.

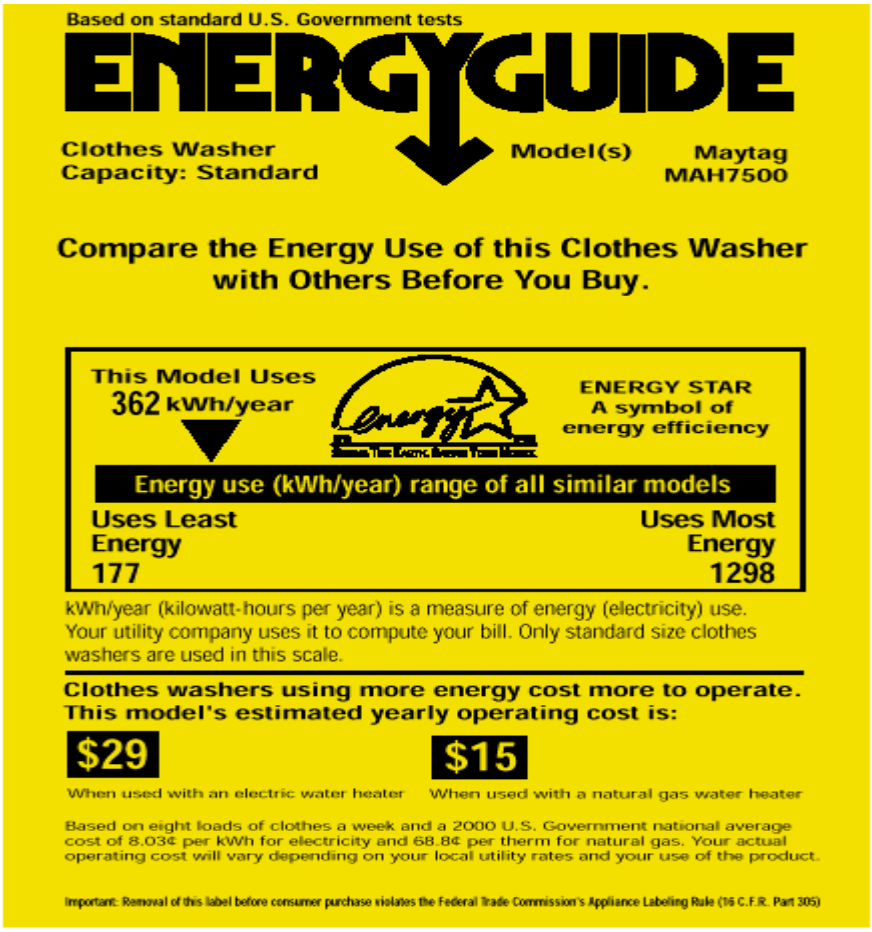

FIGURA 5.16 HOJA DE ESPECIFIOCACIÓN DE AHORRO DE ENERGÍA PARA EL MODELO MAH7500 DE MAYTAG

Como sabemos los estándares mencionados anteriormente, presentan una serie de normalizaciones a seguir, esto para el caso de el gobierno de los EUA.

Para el caso de México suponemos que la normalización debe de ser sin grandes variaciones, y esto esta representado por la NORMA Oficial Mexicana NOM-005-ENER-2000 [13], Eficiencia energética de lavadoras de ropa electrodomesticas. Límites, método de prueba y etiquetado. que se presenta como material anexo a este trabajo.

5.9 COSTOS EN LOS MOTORES ELECTRICOS.

Con la comparación anteriormente hecha, nos muestra la ventaja que los MRAC presenta con respecto a motores de similares características, esto nos lleva a pensar en lo siguiente ¿Los MRAC son igualmente económicos en su fabricación?.

En primera instancia nos brinca a la vista pensar que sí, pero con la siguiente comparación dará una respuesta convincente a la pregunta hecha.

La investigación que se realizó, se basó principalmente, en la consulta de precios de motores eléctricos monofásicos tanto de CA, como de CD, los datos obtenidos son para uso de menudeo exclusivamente, y se realizó con las principales distribuidoras de equipo y motores eléctricos y resultados obtenidos se presentan en la tabla 6

TABLA No 6 COSTO EN MOTORES ELÉCTRICOS

TIPO DE ALIMENTACION	*MARCA*	*MODELO*	*POTENCIA*	*VOLTAJE DE ALIMENTACIÓN*	*R.P.M*	*COSTO*
CORRIENTE DIRECTA	*BALDOR*	*L3605T*	*2 HP*	*115 [V]*	*1800*	*$489 UDS*
CORRIENTE ALTERNA (MONOFÁSICO)	*SIEMENS*		*2 HP*	*127 [V]*	*1800*	*$1655*
MOTOR DE RELUCTANCIA ACCIONADO POR CONMUTACION	*EMERSON*	*- - - - - DESTINADO PARA LA LAVADORA NEPTUNE DE MAYTAG (MAH 7500)*	*2 HP**	*162[V]* EN FUENTE CONMUTADA.*	*500**	*$180 UDS**

* *INFORMACIÓN PROPORCIONADA POR EL DEPARTAMENTO DE REFACCIONES DE MAYTAG EN LOS EUA.*

Como se puede observar, el costo del MRAC es menor al motor de corriente continua, pero es más caro que el motor de corriente alterna, esto nos hace pensar ¿Realmente los MRAC tiene un mayor costo?, con la información anteriormente mostrada, nos haría pensar que sí, pero hay que resaltar, que la empresa que los fabrica (EMERSON), incluye un valor agregado esto debido al desarrollo de tecnología que han desarrollado con los MRAC.
Para poder ejemplificar lo anterior, pondremos como ejemplo aparatos electrónicos actuales, tal es el caso de los televisores de pantalla plana, al principio en su introducción, los precios eran sumamente elevados para los consumidores finales, con el tiempo y la competencia los precios se han ido bajando considerablemente para su adquisición, tal es el caso de los MRAC, que se observa que el precio es elevado pero con el tiempo esperamos que el costo baje.

5.9.1 ESTIMACION DE MANUFACTURA.

Con lo descrito anteriormente, se realizó una sencilla estimación de manufactura de un MRAC de características similares al descrito en la simulación.
La investigación se llevo a cabo pensando en lugares que sirvieran para este fin, como el caso de casas de embobinados de motores eléctricos, herrería (semi especializada).
Los datos mencionados en la tabla 7, pueden representar amplias variaciones, debido al diseño y taller de fabricación.

TABLA No 7 COSTOS DE MANUFACTURA DE UN MRAC (SIMULADO)

PIEZA	MATERIAL	COSTO
CARCAZA USADA (POLOS SALIENTES)	ACERO	$250*
EMBOBINADO	COBRE	$350*
ROTOR (FABRICACIÓN)	ACERO	$400**
	SUMA	$1,000

*precio proporcionado por taller de embobinados de motores al sur de la ciudad de México

**precio proporcionado por un taller de herrería al sur de la ciudad de México.

Como se puede observar, la elaboración artesanal de un MRAC es muy económica y viable para poder empezar a desarrollar algún tipo de investigación en nuestro país.

CONCLUSIONES Y RECOMENDACIONES.

En la actualidad no se dispone de un estudio profundo en nuestro país sobre el tema de los Motores de Reluctancia accionados por Conmutación (MRAC), por lo que este trabajo de tesis aporta un estudio parcial a partir de trabajos previos, experiencias además de opiniones que investigadores y grupos corporativos internacionales especializados en el ramo nos pudieron brindar.

El estudio de los Motores de reluctancia accionado por conmutación (MRAC) que se llevo a acabo en base a una simulación digital estructurada en el lenguaje de programación Matlab y simulado con Simulink, nos brinda la información con la cual podemos concluir lo siguiente.

Debido a la simplicidad física de la máquina, el momento de inercia de rotor, presenta una disminución del 44% con respecto a otros motores de tecnologías convencionales de similares características y dimensiones.
Como se puede concluir el motor de reluctancia accionado por conmutación (MRAC) presenta un pequeño momento de inercia, esto debido a que el rotor esta hecho de una sola pieza metálica que tiene ausencia de masa en los huecos del rotor.
Esto repercutirá directamente en el costo de fabricación que es un punto de suma importancia en la selección de un motor.

Ahorro en el consumo de energía eléctrica del 16% en consumos promedios con respecto a tecnologías de motores convencionales utilizados actualmente.
El ahorro de energía eléctrica anteriormente mencionado, es una señal importante para voltear la mirada a este tipo de tecnología, y brindar la oportunidad de poderse desarrollar y demostrar sus beneficios.

Ahorro en la construcción de los motores de reluctancia accionados por conmutación (MRAC) del orden del 30% con respecto a otras tecnologías convencionales funcionando actualmente.

Con la información anterior obtenemos un panorama completo de las virtudes que los MRAC nos pueden brindar, y como se puede observar, sus beneficios son potencialmente útiles para el desarrollo y economía de cualquier proceso en donde sean requeridos.

Investigando sobre este punto, pudimos encontrar que en el sector industrial (productivo-comercial) existe actualmente el desarrollo por parte de la empresa EMERSON del (MRAC), esto en estudios e implementaciones a productos electrodomésticos, tal es el caso de la lavadora de ropa marca MAYTAG modelo MAH 7500.

Como se puede observar los motores de reluctancia accionados por conmutación (MRAC) son hoy una realidad y actualmente es una opción que responde a la necesidad de ahorrar y usar eficientemente la energía eléctrica, con el fin primordial de abatir emisiones contaminantes a la atmósfera y poder prolongar la vida de los recursos no renovables.

En la sección de recomendaciones, podremos mencionar las siguientes:

Se recomienda un estudio detallado sobre los sistemas de control que sirvan para los MRAC dado que este tema es actualmente la mayor limitante para el desarrollo de esta división de máquinas eléctricas.

Esperamos que con los resultados obtenidos en este trabajo de tesis abra la puerta para que gente o grupos de investigación de México, especialmente la

UNAM, se interesen por el estudio y desarrollo de esta naciente y prometedora tecnología.

Se recomienda la construcción física de un MRAC, para comparar los resultados del modelo físico contra los resultados obtenidos en este trabajo de tesis y así poder mejor comprender las bondades y restricciones, que esta división de máquinas eléctricas presenta.

BIBLIOGRAFÍA.

[1] Buckley George W, "Switched Reluctance Motor", Emerson Electric Co. St. Louis, Missouri,2001

[2] Catálogo "Tracción eléctrica" Siemens AG.

[3] C.R. Elliot, J.M. Stephenson et M.L. McClelland, "*Advances in switched reluctance drive systems dynamic simulation*", Proc.of EPE 19995, Vol.3

[4] Chapman, Stephen J. "Máquinas Eléctricas" McGraw Hill, Segunda Edición, Colombia 1993.

[5] DiRenzo Michael T, Texas Instruments, , "*Switched Reluctance Motor Control - Basic Operation and Example Using the TMS320F240*" SPRA420A, Febrero 2000.

[6] Dubrovsky, Hilda. "Tecnología de la electricidad", Curso latinoamericano de posgrado en economía, San Carlos de Bariloche, Argentina 1997.

[7] Franceschini G., Pirani S., Rinaldi M., Tassoni C., "*SPICE assisted simulation of controlled electric drives: an aplication to switched reluctance drives*", IEEE Transaction on Industry Applications, Vol. IA-27, No. 6. Nov/Dic 1991

[8] Hoja de datos "Motores eléctricos" en tracción eléctrica. Elbtalwerk GmbH.

[9] J.Nascimento, L. Rolim, P. Heidrich et al, "*Design and simulation aspects of a switched reluctance drive*", Proc. of 4° Brazilian Power Conference (COBEP96).

[10] MANUAL MATLAB® ver 5.2 1990 - 1999 by The MathWorks, Inc. http://www.mathworks.com

[11] MANUAL SIMULINK Dynamic System Simulation for MATLAB® ver 2.0 1990 - 1999 by The MathWorks, Inc. http://www.mathworks.com

[12] Norma Oficial Mexicana NOM-001-SEDE-1999, Instalaciones Eléctricas (utilización), Diario Oficial de la Federación, 19 de abril de 1999.

[13] NORMA Oficial Mexicana NOM-005-ENER-2000, Eficiencia energética de lavadoras de ropa electrodomésticas. Límites, método de prueba y etiquetado. Diario Oficial de la Federación el 20 de septiembre y 29 de octubre de 1999, respectivamente.

[14] O.Ichinokuta, T. Onda, M. Kimura, T. Watanabe, T. Yanada and H.J. Guo, "*Analysis of Dynamic Characteristics of Switched Reluctance Motors Based on SPICE*", IEEE Transactions on Magnetics, Vol.34, No 4.1998

[15] P.O. Rasmussen, G. Andersen, L. Helle, J.K. Pedersen, F. Blaabjerg, "*Switched reluctance Motors drives*", IEEE Transaction on Industry Applications, 1996 (ALBORG university Denmark)

[16] Skvarenina, Wasynczuk, Krause, "*Simulation of a Switched Reluctance Generator/More Electric Aircraf Power system*" , Proc, of 1996 IECEC, paper 96398

[17] Stephen J. Fedigan, Ph.D. and Charles P. Cole "A Variable-Speed Sensorless Drive System for Switched Reluctance Motors" Texas InstrumentsSPRA600 - October 1999

[18] Técnicas de Conservación Energética en la Industria, (Fundamentos y ahorro en operaciones). Ministerio de Industria y Energía, Madrid España 1999

[19] Wolff J, Spath, H. "*Switched reluctance motor with 16 stator poles and 12 rotor teeth*.". Proceeding of the 7th European Conference on Power Electronics and Applications, Vol.3 1997

[20] X. Radun, "*Switched Reluctance Stsrter/Generator Modeling Results*", Proc. of SAE Aerospace Atlantic Conference, 1995, paper 951407

APENDICE I

SIMULACIÓN DE SISTEMAS DINÁMICOS CON MATLAB Y SIMULINK

INTRODUCCION:

Matlab es al mismo tiempo un entorno y un lenguaje de programación que junto a Simulink representa una herramienta elemental para el desarrollo de una simulación dinámica. Este apendice tiene por objetivo principal introducir al modelado y simulación de sistemas dinámicos empleando Matlab.y Simulink.
Inicialmente se desarrollará la forma de trabajo de Matlab y consecuentemente la forma en como Simulink realiza su simulación.

Para el caso de Matlab, podemos fácilmente crear nuestras propias funciones y programas especiales (conocidos como archivos-M) en código Matlab. Los podemos agrupar en Toolbox: colección especializada de archivos-M para trabajar en clases particulares de problemas.
La manera más fácil de visualizar Matlab es pensar en él como en una calculadora totalmente equipada, aunque, en realidad, ofrece muchas más características y es mucho más versátil que cualquier calculadora. Matlab es una herramienta para hacer cálculos matemáticos. Es una plataforma de desarrollo de aplicaciones, donde conjuntos de herramientas inteligentes como es el caso de Simulink, nos ayuda para la resolución de problemas en áreas de aplicación específica

Entre las diversas utilidades que MATLAB presenta, se encuentran:

- ✓ Cálculo matricial y Algebra lineal.
- ✓ Polinomios e interpolación.
- ✓ Regresión.
- ✓ Ajuste de funciones.
- ✓ Ecuaciones diferenciales ordinarias.
- ✓ Integración.
- ✓ Funciones.
- ✓ Gráficos bi y tridimensionales.

MATEMATICA UTILIZADA POR MATLAB :

Aquí se muestra el entorno de trabajo con el cual Matlab opera.

VECTORES

Para crear un vector fila se utilizan corchetes dentro de los cuales los elementos deben estar separados por espacios o comas:

```
a = [1 2 3 4 5 6 9 8 7]
```

Matlab retorna:

```
a =
1 2 3 4 5 6 9 8 7
```

Nota de utilidad: si se desea que la variable creada no se muestre en pantalla, se debe ejecutar el comando con un ; final.

```
a = [1 2 3 4 5 6 9 8 7];
```

MATRICES

La creación de matrices en Matlab es similar a la de vectores (de hecho estos son un caso particular de matrices), sólo que cada fila de elementos debe separarse con un ***;*** o *return*:

```
B = [1 2 3 4; 5 6 7 8; 9 10 11 12]
B =
1   2   3   4
5   6   7   8
9 10 11 12
B = [ 1 2 3 4
5 6 7 8
9 10 11 12]
B =
1 2 3 4
5 6 7 8
9 10 11 12
```

Matlab no tiene en cuenta los espacios.

El punto y coma al final de la línea le dice a Matlab que evalúe la línea, pero que no nos diga la respuesta.

Si la sentencia es demasiado larga para que quepa en una línea, una elipsis consistente en tres puntos (**...**) seguido por **Enter** indica que la sentencia continúa en la línea siguiente.

Operaciones con matrices

MATLAB puede operar con matrices por medio de ***operadores*** y por medio de ***funciones***. Se han visto ya los operadores *suma* (+), *producto* (*) y *traspuesta* ('), así como la función *invertir* ***inv( )***.

Los operadores matriciales de MATLAB son los siguientes:

+ adición o suma

– sustracción o resta

* multiplicación

' traspuesta

^ potenciación
\ división-izquierda
/ división-derecha
.* producto elemento a elemento
./ y .\ división elemento a elemento
.^ elevar a una potencia elemento a elemento

Estos operadores se aplican también a las variables o valores escalares, aunque con algunas diferencias

Matlab ofrece las siguientes operaciones básicas para elementos escalares:

OPERACION	SIMBOLO
Suma, a+b	+
Resta, a-b	-
Multiplicación, a*b	*
División, a%b	/ o \
Potencia, a^b	^

OTRAS CARACTERISTICAS :

A.' es la transpuesta de la matriz **A**. La transpuesta compleja conjugada de la matriz **A** se escribe como **A'**.

d=eig(A) devuelve los valores propios asociados con la matriz cuadrada **A** como un vector columna.

[V,D]=eig(A) devuelve los vectores propios en la matriz **V** y los valores propios como los elementos diagonales en la matriz **D**.

[L,U]=lu(A) calcula la factorización **LU** de la matriz cuadrada **A**.

[Q,R]=qr(A) calcula la factorización **QR** de la matriz **A**.

[U,S,V]=svd(A) calcula la descomposición en valores singulares de la matriz **A**.

rank(A) devuelve el rango de la matriz **A**.

cond(A) devuelve el número de condición de la matriz **A.**

norm(A) calcula la norma de la matriz **A**. Admite el cálculo de norma-1, norma-2,

norma-F y norma.

poly(A) encuentra el polinomio característico asociado con la matriz cuadrada **A.**

polyvalm(v,A) evalúa el polinomio característico **v** usando la matriz cuadrada **A**.

EL ESPACIO DE TRABAJO DE MATLAB:

Para comprobar el valor de una variable, hay que preguntar a Matlab por ello introduciendo su nombre a continuación del indicativo de petición de orden.

Para obtener una lista de las variables usamos la orden: **who**.

Para recordar órdenes previas, usamos las teclas de cursor del teclado.

ALMACENAR Y RECUPERAR DATOS :

Matlab puede guardar y cargar datos de los archivos del computador. En el menú **File,** la opción **Save Workspace as...** guarda todas las variables actuales; y **Load Workspace...** carga variables de un espacio de trabajo guardado previamente.

ACERCA DE LAS VARIABLES :

Por defecto, Matlab almacena resultados en la variable **ans.**

Las variables son sensibles a las mayúsculas y pueden contener hasta 19 caracteres.

Deben comenzar con una letra.

Matlab tiene algunas variables especiales:

VARIABLE	VALOR
ans	Nombre por defecto de la variable usada para los resultados
pi	Razón de una circunferencia a su diámetro
eps	Número más pequeño tal que, cuando se le suma 1, crea un número en coma flotante en el computador mayor que 1
inf	Infinito
NaN	Magnitud no numérica
i y j	i = j = v-1
realmin	El número real positivo más pequeño que es utilizable
realmax	El número real positivo más grande que es utilizable

FUNCIONES MATEMATICAS COMUNES :

A continuación se muestra una tabla con las funciones matemáticas en Matlab:

FUNCIONES MATEMATICAS ESPECIALES	
abs (x)	Valor absoluto o magnitud de un número complejo
acos (x)	Inversa del coseno
acosh (x)	Inversa del coseno hiperbólico
angle (x)	Angulo de un número complejo
asin (x)	Inversa del seno
asinh (x)	Inversa del seno hiperbólico
atan (x)	Inversa de la tangente
atan2 (x,y)	Inversa de la tangente en los cuatro cuadrantes
atanh (x)	Inversa de la tangente hiperbólica
ceil (x)	Redondea hacia más infinito
conj (x)	Complejo conjugado
cos (x)	Coseno
cosh (x)	Coseno hiperbólico
exp (x)	Exponencial
fix (x)	Redondea hacia cero
floor (x)	Redondea hacia menos infinito
imag (x)	Parte imaginaria de un número complejo
log (x)	Logaritmo natural
log10 (x)	Logaritmo decimal
real (x)	Parte real de un número complejo
rem (x,y)	Resto después de la división
round (x)	Redondea hacia el entero más próximo
sign (x)	Devuelve el signo del argumento
sin (x)	Seno
sinh (x)	Seno hiperbólico
sqrt (x)	Raíz cuadrada
tan (x)	Tangente
tanh (x)	Tangente hiperbólica

Matlab sólo opera en radianes.

NUMEROS COMPLEJOS :

Matlab sigue el convenio usual, donde un número complejo se escribe como a+bi. La terminología con los dos caracteres **i** y **j** sólo funciona con números simples, no con expresiones.

Las operaciones matemáticas sobre números complejos se escriben de la misma forma que con números reales.

Las funciones **real**, **imag**, **abs** y **angle** son útiles para la conversión entre las formas polar y rectangular.

OPERACIONES RELACIONALES Y LÓGICAS :

Como entradas a todas las expresiones relacionales y lógicas, Matlab considera que cualquier número distinto de cero es verdadero, y es falso si es igual a cero.
La salida produce 1 si es verdadero, y 0 si es falso.

OPERADORES CONDICIONALES :

OPERADOR	DESCRIPCION
<	Menor que
<=	Menor que o igual a
>	Mayor que
>=	Mayor que o igual a
==	Igual a
~=	No igual a

La salida de las operaciones lógicas se pueden utilizar también en operaciones matemáticas.

OPERADORES LÓGICOS :

Los operadores lógicos proporcionan un medio de combinar o negar expresiones condicionales

OPERADOR	DESCRIPCION
&	AND
|	OR
~	NOT

GRAFICACION

Graficar en Matlab es muy sencillo y presenta una variedad de alternativas. El comando que permite “mostrar” en una figura los elementos de una variable es *plot* (o su versión tridimensional *plot3*). Un ejemplo sencillo es:

```
t=0:0.25:7;
y = sin(t);
plot(t,y)
```

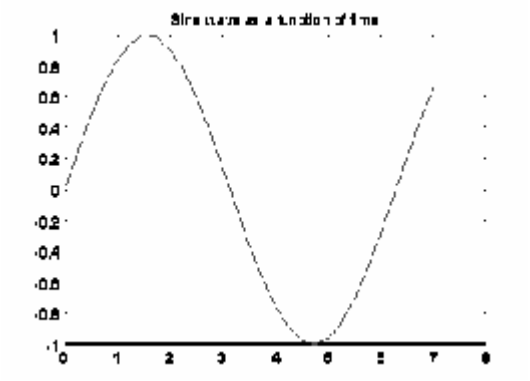

también se pueden realizar graficas polares

```
>> t=0:.01:2*pi;
>> r=sin(2*t).*cos(2*t);
>> polar(t,r)
>> title('Gráfico polar de sin(2t)cos(2t)')
```

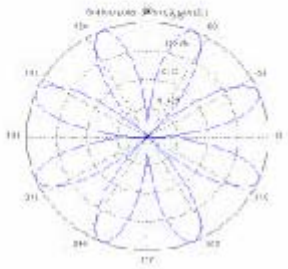

y gráficas tridimencionales como por ejemplo:

```
>> t=0:pi/50:10*pi;
>> plot3(sin(t),cos(t),t)
>> title('Hélice'),xlabel('sin(t)'),ylabel('cos(t)'),zlabel('t')
```

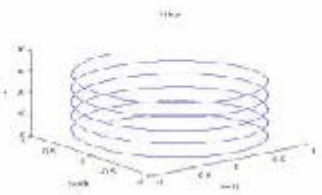

APENDICE II

ELEMENTOS BÁSICOS DE SIMULINK

La biblioteca de Simulink.

Simulink proporciona un entorno gráfico al usuario que facilita enormemente el análisis, diseño y simulación de sistemas (de control, electrónicos, etc.), al incluir una serie de rutinas que resuelven los cálculos matemáticos de fondo, junto con una sencilla interfaz para su uso.

Proporciona un entorno de uso gráfico que permite dibujar los sistemas como diagramas de bloques tal y como se haría sobre un papel.

El conjunto de componentes incluidos junto al programa Simulink, incluye bibliotecas de fuentes de señal, dispositivos de presentación de datos, sistemas lineales y no lineales, conectores y funciones matemáticas. En caso de que sea necesario, se puede crear nuevos bloques a medida del usuario.

El programa Simulink se inicia desde el boton "Simulink Library Browser" (Biblioteca de Simulink) de la ventana de comandos de Matlab, o desde la línea de comandos mediante la orden:

>>simulink

Una vez iniciado el programa, el entorno de trabajo queda dividido en tres partes.

- ✓ La ventana de comandos de Matlab (Matlab command window); desde la que se puede ejecutar cualquier comando del mismo, das valores a variables y controlar la ejecución de las simulaciones.

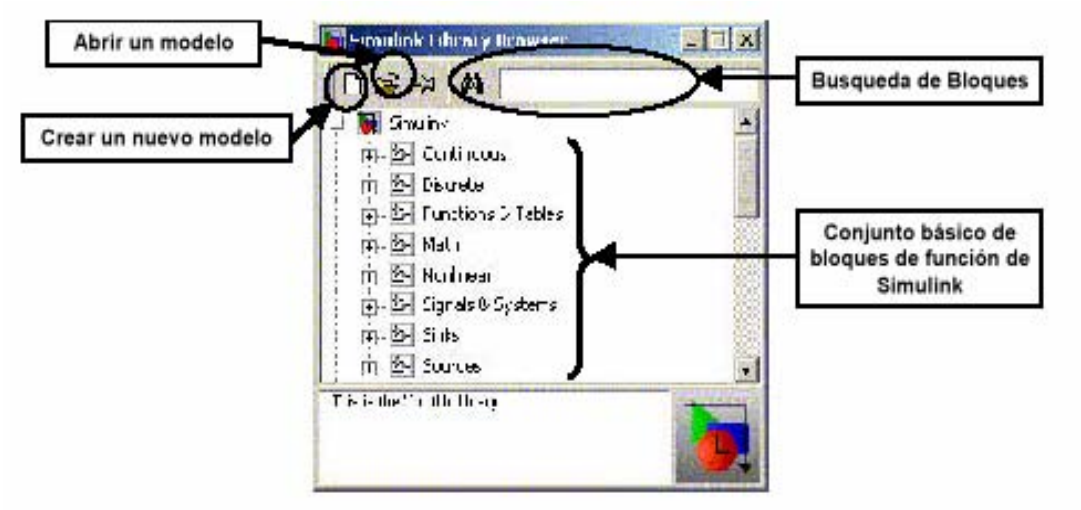

- ✓ La ventana de la biblioteca de Simulink (Simulink Library Browser); desde la que se seleccionan los componentes que se van a insertar el sistema a simular.
- ✓ La o las ventanas de los modelos: en las que se realizan dibujos de modelos y se realizan y controlan las simulaciones. Estas ventanas aparecen cuando se abre un modelo. para ello, se pueden utilizar los botones de la ventana de la librería de Simulink.

Todos los componentes básicos de Simulink, se pueden encontrar en su biblioteca de componentes. A continuación se describe los componentes básicos de la biblioteca de Simulink.

Continuous: Bloque que puede ser representado como una función continua del tiempo.

Derivative: La salida del bloque corresponde con la derivada de la entrada.

Integrator: La salida del bloque corresponde con la integral de la entrada. Los parámetrosdel bloque permiten controlar el valor inicial de la salida, así como la existencia de límites superiores e inferiores en la salida.

Transfer Fcn: Permite expresar una función de transferencia mediante su expresión en la variable compleja s. Sus parámetros son los polinomios del numerador y del denominador de la función, expresados con valores fila.

Transport Delay: La salida del bloque corresponde con la entrada del mismo retrasada una cantidad de tiempo, que se fija como parámetro en el bloque.

Zero-pole. Función de transferencia expresada en función de ganancia en régimen permanente, y la visualización de los polos y ceros del sistema.

Math: Bloques que realizan operaciones matemáticas sobre las entradas.

Abs: Calcula el valor absoluto de su entrada.

Gain: Aplica una ganancia constante a la entrada.

Math Function: Este bloque incluye la mayor parte de las funciones matemáticas típicas, con la excepción de las funciones trigonométricas.

Product: Calcula el producto escalar de sus entradas. Un parámetro del bloque permite regular el número de entradas del mismo.

Sing: Calcula el signo de la entrada +1 indica positivo, -1 negativo y 0 valor nulo.

Sum: Calcula la suma de todas las entradas, y si estas deben ser invertidas antes de la suma. Ejemplo: un valor para el parámetro "++-+" indicaría que el bloque tiene 4 entradas, y la tercera de ellas debe ser invertida antes de sumarse.

Trigonometric Fuction: En este bloque se incluyen todas las funciones trigonométricas típicas.

Nolinear: Bloque no lineal.

Dead Zone: Incluye una zona muerta en el sistema, centrada en torno a cero. El sistema no responde ante estos valores. La magnitud de la zona muerta puede ser modificada, y echa asimétrica por medio de los parámetros del sistema.

Relay: La salida pasa al estado on=1 cuando la entrada supera un valor umbral, y a un estado off=0 cuando cae por debajo del valor umbral distinto. El estado inicial es off.

Saturation. La señal de salida no sebrepasa un valor umbral, configurable con los parámetros del bloque.

Switch.: Una entrada del sistema permite escoger cual de las entradas se presenta en la salida.

Signal & Systems: Manejo de sistemas y señales.

Subsystems: Permite la realización de sistemas jerárquicos. Al abrir el subsistema, nos permite incluir en su interior, nuevos bloques constructivos, e incluso anidar nuevos subsistemas.

In1: Por defecto un subsistema no contiene entradas. Por cada entrada que se desee añadir se le debe incluir uno de estos bloques.

Out1 :Por defecto un subsistema no contiene salidas. por cada entrada que se desee añadir se le debe incluir un de estos bloques.

Mux: Permite la inclusión de un conjunto de señales en una única línea de transmisión (que transmite datos vectoriales). Parámetros número de entradas, admite tanto entradas escalares como vectoriales.

Demux; permite la descomposición de los datos puesto en forma vectorial en una línea mediante un multiplexor. Parámetros, número de de salidas.

Data store memory: define una variable del entorno de trabajo que se va ha usar como lugar de almacenamiento de datos útil par evitar tener que hacer conexiones complejas que compliquen el diagrama de bloques que se está usando.

Data Stores Read: lee el valor actual de una variable de almacenamiento, que debe estar previamente definida mediante el bloque Data Store Memory.

Data Store Write: Cambia el valor actual de una variable de almacenamiento que debe estar previamente definida mediante un bloque Data Store Memory.

Sinks: Sumideros de señales.

Display: Representa numéricamente el valor de una variable.

Scope: Representa gráficamente la evolución en el tiempo de una variable.

To Workspace: Guarda el valor de la señal de una variable del entorno de trabajo del Matlab. Se puede escoger el nombre de la misma, y limitar su tamaño.

To File: Guarda en un ficheri de tipo ".mat" los datos de la señal de entrada al bloque.

Stop Simulation: Detiene la simulación si el valor de la entrada es distinto de 0.

Sources:Fuentes de Señales

Chirp Signal. Genera una señal senoidal, modulada en frecuencia, entre un valor inicial y un valor final.

Clock: tiempo que se leva de simulación.

Constant: Proporciona una señal de valor constante.

From Workspace. Proporciona una secuencia de datos tomadas del entorno de trabajo del Matlab. La variable elegida debe contener una matriz indicando los valores de la señal, y los instantes en los que la señal toma estos valores.

From File: Proporcionan datos tomados de un fichero ".mat" en el que debe estar el valor de la variable, junto a los instantes de tiempo en que toma cada valor.

Pulse Generator: Genera una onda cuadrada, de la que se puede controlar la amplitud, el periodo y el tiempo de duty (relación entre el tiempo que la onda toma su valor máximo y el tiempo en que toma el valor mínimo).

Ramp: Genera una señal de tipo rampa.

Random Number: Genera números aleatorios distribuidos según una función normal.

Signal Generator. Simula un generador de señales electrónico, permitiendo generar ondas dientes de sierra, ondas cuadradas y senoidales.

Sine Wave: Generador de ondas senoidales.

Step: Genera una señal de tipo escalón.

Uniform Random Number: Genera números aleatorios distribuidos según una función uniforme.

Creación de un modelo.

Para simular un sistema, se deben insertar en las ventanas de simulación los distintos componentes con los que se va a construir el modelo. SE pueden seguir los siguientes pasos:

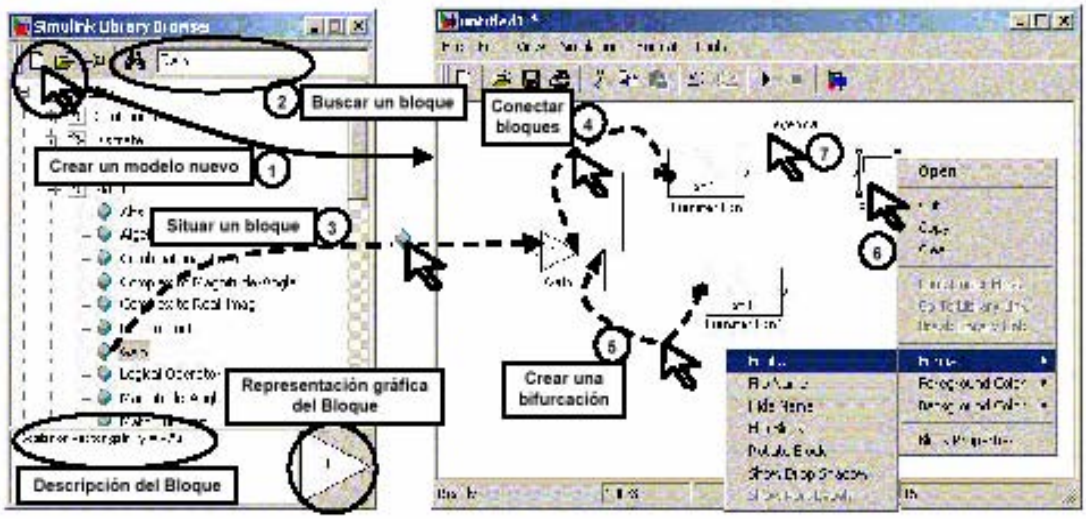

1) Crear un nuevo modelo: Para abrir una ventana de simulación se debe pulsar el botón "nuevo modelo".
2) Buscar un bloque: Se puede buscar un bloque expandiendo el árbol de la biblioteca o buscando directamente por su nombre en la ventana de búsqueda. En este caso, si hay más de un bloque que pueda corresponder a ese nombre, irán apareciendo a medida que se pulsa la tecla "enter".
3) Situar un bloque: Para situar a un bloque, se mantiene pulsado el botón izquierdo del ratón sobre el icono en forma de rombo que hay junto al nombre del bloque y se arrastra hacia la posición deseada en la ventana de simulación.
4) Conectar bloques: En cada bloque, los puntos de salida aparecen indicados mediante una flecha saliente del bloque "|>", mientras que los puertos de entrada de cada bloque se indican con una flecha entrante al mismo ">|". Se conecta la entrada de un bloque a la salida del otro, manteniendo pulsado el botón izquierdo del ratón mientras se arrastra desde el símbolo de entrada de uno de los bloques hacia el de salida de otro o viceversa.
5) Crear una bifurcación: Si se desea llevar la salida de un bloque a la entrada de mas de uno se necesita crear una bifurcación en la conexión. Para hacerlo, se arrastra con el

ratón desde la entrada del nuevo bloque a conectar hasta la línea de la conexión que se va a bifurcar.

6) Modificar los bloques: Se pueden rotar o aplicar simetrías a los bloques usados, según convenga la colocación de entradas/salidas para el esquema que se esté realizado pulsando sobre él botón derecho del ratón y utilizando los menús desplegables o mediante la opción "Formar" del menú principal ("Format/Flip Block", "Format/Rotate Block", etc.) También mediante los menús o haciendo doble click sobre el bloque, se pueden modificar sus parámetros.
7) Inserción de textos: Se puede incluir un texto aclaratorio o informativo en cualquier parte de la ventana del modelo, haciendo doble click en la zona libre y escribiendo directamente el texto.

También se pueden cambiar los nombres y posiciones de los bloques que se empleen para la simulación antes o después de conectarlos. Asimismo los enlaces de las conexiones pueden moverse o modificarse para eliminar cualquier elemento basta con seleccionarlo con un click y eliminarlo con la tecla "sup." o "delete", o utilizar algunos de los menús.

Conviene guardar ("File/Save as") periódicamente el modelo, incluso antes de terminarlo, para evitar perder el trabajo realizado.

Un ejemplo trivial incluiría la selección de dos componentes: "Simulink/Sources/SineWave" y "simulink/Links/Scope" de la ventana "Simulink Library Browser", y el arrastre de los mismos hasta la ventana de dibujo. En el caso de nuestro ejemplo básico, para conectar el generador de señales y el osciloscopio, simplemente se debe situar el ratón sobre el punto de salida del generador, pulsar el botón izquierdo, arrastrar el ratón hasta el punto de entrada del osciloscopio y soltar el botón del ratón.

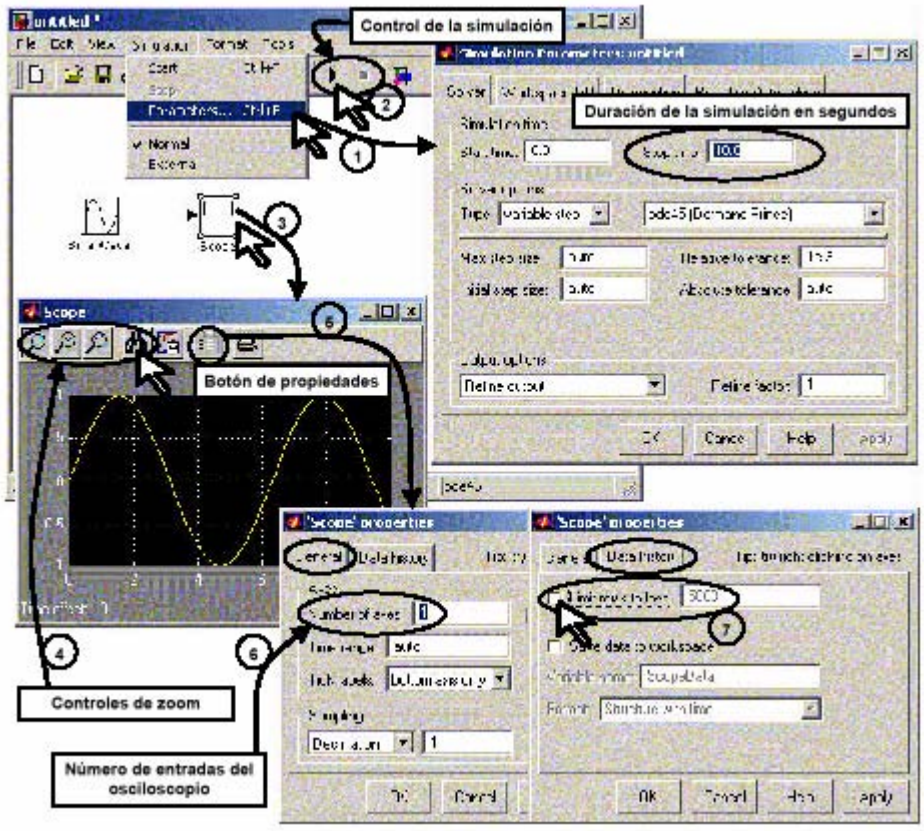

Control de la simulación y visualización de resultados.

Antes de poder ejecutar la simulación, es necesario seleccionar los parámetros apropiados para la misma (1). Desde el menú: "Simulation/Parametres", se puede desplegar un cuadro de dialogo, en el que se controlan parámetros de la simulación de entre los cuales el que se modifica más habitualmente es el tiempo final de la simulación. (Otros parámetros accesibles son el tiempo de inicio de la simulación, el método matemático que se empleará para llevarla a cabo, o las variables que se tomarán/guardarán de/en el espacio de trabajo). La simulación se puede poner en marcha o detener mediante el menú anterior o los botones de la ventana (2).

Para visualizar los resultados de la misma son muy útiles los bloques que se encuentran en el grupo "Sinks" de la biblioteca de Simulink. De entre ellos, quizá el más útil es el bloque "Scope" que simula el comportamiento de un osciloscopio. Tras realizar una

simulación se pueden ver los resultados que ha registrado haciendo un doble click sobre él (3). Para ver correctamente los resultados se utilizan los controles de zoom (4), siendo conveniente pulsar siempre tras una simulación el botón de autoescala (el de los binoculares) para ver el total de los datos registrados. los otros tres botones de zoom permiten respectivamente ampliar un área señalada con arrastre del ratón, ampliar el eje "X" de la misma manera o ampliar el eje "Y".

El bloque "Scope" tiene una serie de propiedades a las que se accede a través del botón correspondiente de la ventana "Scope" (5). Dos de las más útiles son la que permite elegir el número de entradas que se desean para el osciloscopio (6) "Number of axes" (que será también el número de gráficos que representará) y la que determina si el osciloscopio almacena todos los datos de la simulación o sólo los últimos obtenidos (7) "Limits rows to last". Respecto a este último control, es conveniente eliminar la marca "♦" del cuadrilátero blanco para que el osciloscopio mantenga todos los datos registrados durante la simulación completa.

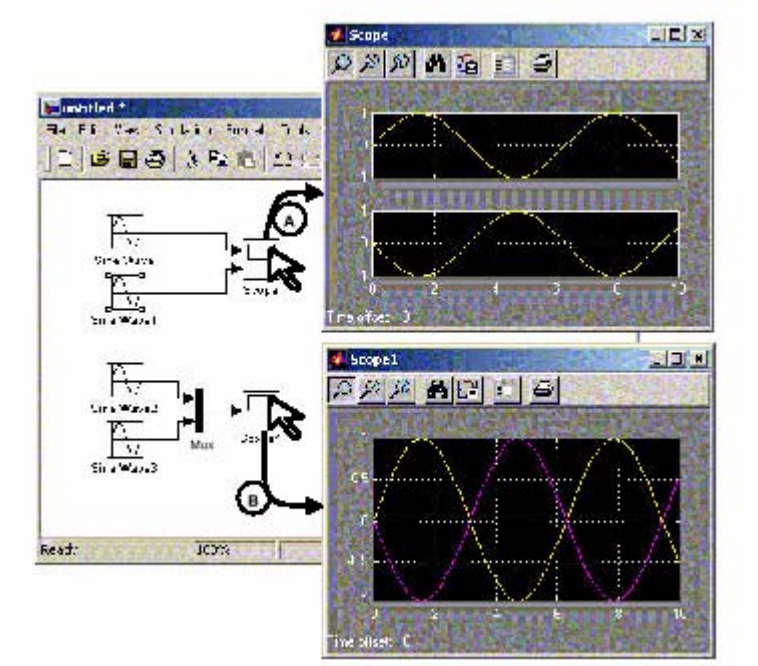

Si se desea visualizar más de una señal en un osciloscopio, existen dos posibilidades:

A) Aumentar el número de entradas del osciloscopio como se comentó anteriormente.

B) B) Utilizar un bloque "Mux" para que ambas señales aparezcan en el mismo gráfico.

Indirect rotor-position estimation techniques for switched reluctance motors - A review

Iqbal Husain
Power Electronics Laboratory
Department of Electrical Engineering
The University of Akron
Akron, OH 44325
Tel: (330)-972-8495
Fax: (330)-972-6487
e-mail: ihusain@uakron.edu

This paper gives a comprehensive review of the available indirect rotor position estimation techniques for switched reluctance motor drives. The sensing schemes are broadly classified into non-intrusive and active probing methods based on the use of an energized phase or an idle phase, respectively, for position estimation. The fundamental principles of the various methods along with their advantages and drawbacks have been discussed in detail.

I. Introduction

The various positive features of a switched reluctance motor (SRM) drive make it an attractive alternative to existing dc and ac motors in adjustable speed drives [1,2]. The SRM drives can also deliver servo-drive performance equivalent to dc brushed motors [3]. The SR motor is simple in construction and can operate at very high speeds. The simple power electronic converter requirement and the fault tolerance capability are among other specific advantages of SRM drives. However, the rotor position sensing requirements and the higher torque ripple compared to other machines are the primary disadvantages of SRM drives.

The switched reluctance machine is a doubly salient machine with unequal number of rotor and stator poles. Windings of diametrically opposite stator poles are connected in series to form one phase of the machine. The cross-section diagrams of a 3-phase, 6/4 and a 4-phase, 8/6 (# of stator poles/# of rotor poles) SRM are shown in Fig. 1. Numerous other stator and rotor pole configurations, such as single-phase 2/2, two-phase 4/2, three-phase 12/8, four-phase 16/12, five-phase 10/8 etc. are possible.

The rotor position information in SRM drives is essential in determining the switching instants for proper control of speed, torque and torque pulsations. A shaft position transducer is usually employed to determine the rotor position. In inexpensive systems the rotor position sensor is comprised of a magnetized ring with Hall effect sensors, or opto-interrupters with slotted disk that produce discrete signals with no information between the pulses. In more expensive systems, a large number of pulses per revolution can be obtained from a resolver or optical encoder. Alternatively, a large number of pulses can be obtained by phase-locking a high frequency oscillation to the

pulses of discrete position sensors. Systems with such high resolution can work well down to the zero speed. However, these sensors add complexity and cost to the system. Moreover, electromagnetic interference and temperature effects tend to reduce the reliability of the system. In order to avoid these difficulties some form of indirect position sensing scheme is desirable.

II. Methods of Indirect Position Sensing

Several indirect position-sensing methods have been patented and published for sensorless control of SRM drives. All of these methods use the instantaneous phase inductance variation information in some way to detect the rotor position indirectly. Typical flux-angle-current characteristics of an SRM is shown in Fig. 2. The magnetic material of the motor remains unsaturated for smaller values of current, and the phase inductance is given by $L(q) = \frac{l}{i}$. The core becomes saturated for higher values of current , and the constant inductance property at a particular rotor position is lost.

The methods of indirect position sensing can be broadly classified into two categories: (i) Non-intrusive methods, where position information is obtained from terminal measurements of voltages and currents and associated computations, and (ii) intrusive (or active probing) methods, where low-level, high-frequency signals are injected into an idle phase to determine the position dependent, unsaturated phase inductance characteristics.

Continuous rotor position information can be obtained from indirect position sensing schemes by a mapping of inductance, flux or current waveforms to rotor position. Alternatively, the task can be simplified in less sophisticated algorithms by threshold comparison of the indirectly measured position information to effectuate commutation. Phase advancing and retardation is possible by changing the threshold level appropriately.

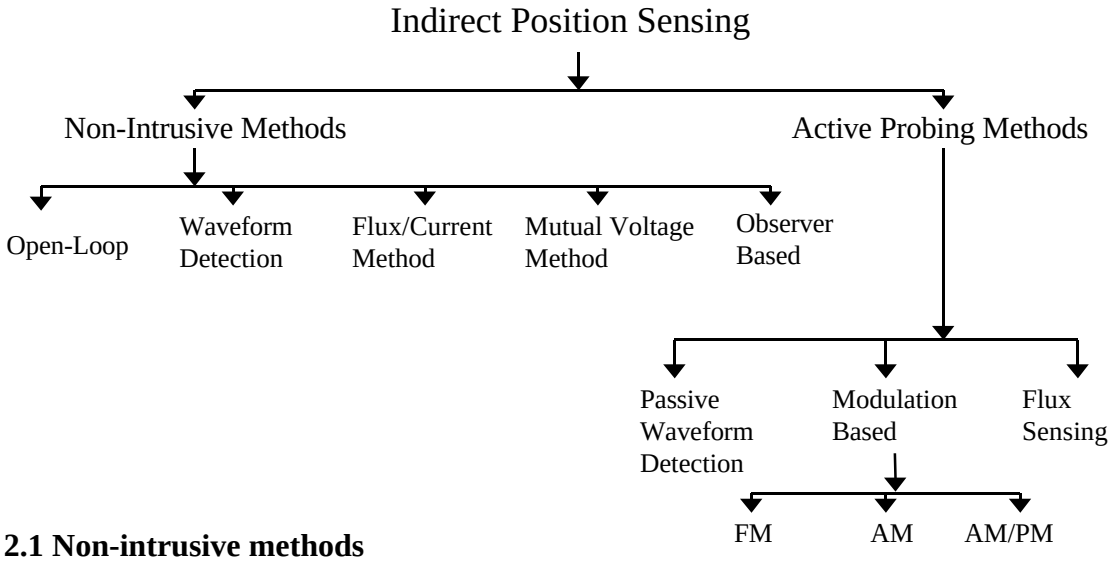

2.1 Non-intrusive methods

The non-intrusive methods rely on the machine characteristics for estimating the rotor position. The waveform detection techniques [4], model-based estimator techniques

[5,6], the flux/current method [7] and the mutual voltage method [8] are examples of methods that fall under this category. The terminal measurements of phase voltage or mutual voltage and current are used as inputs for an estimator to obtain the rotor position.

2.1.1 Waveform Detection Techniques

Acarnley et al. [4] first suggested monitoring the current waveform to detect the rotor position in stepping and switched reluctance motors, and applied this technique successfully to variable reluctance step motors. The fundamental idea behind this technique is that the rate of change of current depends on the incremental inductance, which in turn depends on the rotor position.

The phase voltage equation for an SRM, neglecting the mutual coupling effects, is

$$v_{ph} = i_{ph}R + \frac{dl}{dt} \qquad (1)$$

The rate of change of current can be derived from above as

$$\frac{di}{dt} = \frac{v_{ph} - i_{ph}R - \frac{\partial l}{\partial q}\frac{dq}{dt}}{l} \qquad (2)$$

where $l = \frac{\partial l}{\partial i}$ is the incremental inductance.

Acarnley suggested that if the back-emf and $i_{ph}R$ drop can be neglected, then l can be obtained from Eq. (2), and consequently the rotor position from l. Acarnley proposed three methods of position sensing, two of which is based on current waveform monitoring in the active phase. The methods on active phase current monitoring specifically applies to the current controlled mode of operation of an SRM when the current is increasing and decreasing at a high frequency due to chopping or PWM. The current rise and fall times can be derived from Eq. (2) as follows

$$t_{rise} = \frac{l\partial i}{v_{ph} - i_{ph}R - \frac{\partial l}{\partial q}\frac{dq}{dt}}$$

$$t_{fall} = \frac{l\partial i}{i_{ph}R + \frac{\partial l}{\partial q}\frac{dq}{dt}}$$

A simple commutation scheme could be developed based on t_{rise} or t_{fall} reaching a reference time Dt_{ref} for hysteresis type current controllers. The major problem of waveform detection techniques is the restriction to low speed applications, since otherwise the back-emf errors affect the accuracy severely. The control flexibility is also limited due to the requirement for a fixed average current during chopping. Acarnley suggested monitoring t_{rise} for maximum immunity from back-emf effects. A block diagram based on monitoring t_{rise} is given in Fig. 3.

Panda et al. [9,10,11] in later research demonstrated the detrimental effects of neglecting back-emf even at low speeds of several hundred rpm during the chopping mode. In order to compensate for the effects of back-emf, Panda modified the approach of Acarnley by adaptively changing the Dt_{ref} and the dwell angle based on operating speed. Panda also applied the method for position estimation in the single pulse mode at higher

speeds, where the initial rate of rise of current was used to find the rotor position at the beginning of each phase current pulse.

2.1.2 Model Based Estimators

Observer based state estimation provides another method of indirect position sensing for SRM. In this method, the dynamics of the motor are modeled in state space and the mathematical model is run in parallel with the real machine. The model has the same inputs as the physical machine and the difference between its outputs and the measured outputs are used to force the state estimation to converge.

In the case of SRM, terminal measurements of phase currents and voltage are sufficient to develop the observer. The phase voltage v_{ph} is the input to both the real motor and the model. The estimated output current of the machine model is compared with actual phase current and the error is used to adjust the estimator feedback gain in order to correct the trajectory of the observer. The objective is to ensure that the errors between the modeled motor and the physical motor are minimized. The position information comes out of the model as an estimated state parameter. The block diagram of the scheme is given in Fig. 4. The initial results of this method, reported by Lumsdaine et al. [5], were highly encouraging. The advantages of this method are that it does not require additional diagnostic pulse and does not have any inherent speed limitations. However, the scheme requires substantial real-time computing with a fast and powerful processor. The method needs knowledge of load parameters and an accurate machine model. Also, the estimator takes time to converge and the performance may be erratic during the convergence interval. Stability may become an issue for the overall system.

A second order sliding mode observer was used in [6] to estimate the state variables w and θ using terminal measurements of voltage and current. The estimated rotor position from the observer is used for electronic commutation of the motor. Simulation results of the closed-loop controller based on the sliding mode observer showed excellent convergence characteristics.

2.1.3 Flux/Current Methods

The unique relationship between the flux, angle and current in an SRM at any instant of time has been shown in Fig. 2. Knowing the phase current and flux, the rotor position can be estimated using a look-up table of l -*i*-*q* characteristics. The ambiguity of two rotor positions for the same values of l and i can be resolved by using the information of whether the SRM is operating in the motoring mode or regenerating mode.

Flux can be obtained using sense coils or alternatively by an open-loop integration of $(v_{ph} - i_{ph}R)$ as given below

$$l = \int (v_{ph} - i_{ph}(t)R)dt \qquad \cdots\cdots\cdots(3)$$

The current in each phase goes to zero during every cycle. Thus an initial condition of $l = 0$ can be imposed in each cycle eliminating any propagation error due to integration. The integration method is not difficult for single pulse mode of operation where $v_{ph} >> i_{ph} R$, and the effect of $i_{ph}R$ drop is insignificant. However, during chopping the repetitive transition of the applied voltage between $+V_{dc}$ and 0 or between $\pm V_{dc}$, can make the effect of $i_{ph}R$ drop significant. In addition, any change in resistance due to heating or measurement error in i_{ph} will lead to an erroneous estimation of flux and consequently to

incorrect rotor position. Therefore, the flux/current method is more suitable for high speed applications operating in the single pulse mode. One has to keep in mind that computation time becomes critical at higher speeds and the upper limit on operating speed will depend on the available processor or hardware.

The idea of flux/current method was first proposed by Hedland [12] and a similar method was later proposed by Lyons et al. [7]. The block diagram of the scheme is given in Fig. 5. In the proposed scheme, a reference rotor position q_{ref} is identified by comparing the estimated flux $\hat{l}$ with a l_{ref} obtained from stored table of l and i_{ph} for a particular q_{ref}. The transition at q_{ref} triggers a comparator which could be used to synchronize the phase excitation pulses. Lyons et al. [7] extended the work by using a multidimensional table to find l_{ref} as a function of $f(i_1,i_2,i_3,.....,i_n, q_{ref})$ to account for the mutual coupling effects of an n phase motor. The calculation network and the look-up tables can be implemented using a microcontroller or a dedicated hardware circuitry. Lyons et al. also proposed a rather complex and difficult to implement scheme using lumped parameter models. The method models all the mutual coupling effects by position dependent reluctances [13].

2.1.4 Mutual Voltage Technique

The induced voltage due to interphase coupling in phases adjacent to the active phase varies as a function of the rotor position in the SRM, particularly in the chopping or PWM mode. The variation presents another method of indirect method of indirect rotor position estimation as was presented by Husain et al. [8].

When a phase current is regulated by PWM or hysteresis control, the mutually induced voltage in an adjacent phase is given by

$$v_m = \frac{d l_m}{dt}$$

where $l_m = M(q)i \quad and \quad M(q)$ is the mutual inductance.

The voltage during the period of applied voltage can be written after simplification as

$$v_{m1} = \frac{M(q)}{L(q)}V - \frac{M(q)}{L(q)} i_{ph} \frac{dL}{dq} w - i_{ph} R_{ph} \frac{M(q)}{L(q)} + i_{ph} \frac{dM}{dq} w \qquad \cdots\cdots\cdots(4)$$

The voltage during the freewheeling period can be derived as

$$v_{m2} = -\frac{M(q)}{L(q)} i_{ph} \frac{dL}{dq} w - i_{ph} R_{ph} \frac{M(q)}{L(q)} + i_{ph} \frac{dM}{dq} w \qquad \cdots\cdots\cdots(5)$$

Any one of the adjacent phases can be studied for sensing the mutual voltage. However, for 8-6, 4-phase SRMs it is advantageous to sense the phase which is in quadrature with the energized phase. A sample and hold circuit can be used to capture any one of the mutual voltages v_{m1} and v_{m2}. The rotor position can be estimated from the calibrated conversion tables for various currents and speeds.

2.2 Active Probing Methods

In active probing methods, an idle or unexcited phase is injected with high-frequency diagnostic signals to obtain the phase inductance variation information.

Methods based on monitoring current waveforms [4,10-11, 14-17], modulation techniques [18,19] flux sensing techniques [20] are examples of methods belonging to this family. The simplicity of these methods is a definite advantage, although inherent speed limitation and generation of negative torque in the sensing phases could be a drawback in some cases.

2.2.1 Passive Detection Techniques

The passive waveform detection techniques are based on the idea that if a voltage pulse is applied to a non-conducting phase for a short duration of time Δt, the phase inductance remains unsaturated, and the current amplitude remains small; hence, speed voltage effect and phase winding resistance drop can be neglected. The method is essentially based on the third method proposed by Acarnley et al. [4]. Several researchers subsequently implemented the scheme with modifications and improvements. For low current levels, the motor phase voltage equation can be written as

$$V = iR + L(q)\frac{di}{dt} + iw\frac{dL(q)}{dq} \qquad \cdots\cdots\cdots(6)$$

If the voltage is applied for a short period of time, the equation can be approximated as

$$V = L(q)\frac{\Delta i}{\Delta t} \quad \Rightarrow \quad L(q) = V\frac{\Delta i}{\Delta t} \qquad \cdots\cdots\cdots(7)$$

Either Δi or Dt can be kept constant while the other is measured to obtain an estimated unsaturated phase inductance value. The rotor position can then be estimated from a mapping of inductance to position as follows

$$q = F^{-1}(L) \qquad \cdots\cdots\cdots(8)$$

The main limitation of the passive waveform detection technique is the inetrphase coupling effects which is particularly severe when the active phase is undergoing high frequency chopping for current regulation. Eddy currents also affect the accuracy of position sensing. Dunlop et al. first investigated the effects of mutual coupling in his implemented scheme of measuring the change in the diagnostic current over a fixed sampling period [14]. Harris et al. also used a similar technique and addressed the problems of interphase coupling and eddy current effects in detail [15].

Another drawback of injecting a diagnostic pulse from the main converter is that their magnitude could be significant, and hence can generate negative torque. Also, since the pulses are large there will be a long waiting period for the sensing pulse to decay to negligible levels before the next pulse can be applied. The rotor might move a considerable distance during that period; therefore, the resolution of sensing will decrease. Again, eddy currents in the motor prevent the phase from behaving like a linear inductor for the first few-microseconds after the diagnostic pulse is injected. One must wait these few microseconds for the effects of eddy currents to die down, and consequently, longer sensing pulses are required. All these factors limit the maximum attainable operating speed with this method of position sensing.

MacMinn et al. also later implemented the waveform detection scheme keeping *Dt* constant and measuring *Di* [16]. Mvungi et al. [17] used a look-up table to compensate for the mutual coupling effects. His method generated continuously sampled rotor position rather than detecting a threshold level for phase commutation.

2.2.2 Modulation Based Techniques

Several alternative sensorless techniques based on the modulation techniques have been developed in order to eliminate some of the drawbacks mentioned previously for passive waveform detection techniques. The fundamentals of these schemes, along with some experimental results, are given in this section.

The modulation encoding techniques of rotor position detection are based on extracting the periodically varying phase inductance in an encoded form by applying a high frequency carrier signal. The signal containing the phase inductance *L(q)* information is assumed to have a much smaller frequency of variation compared to the carrier frequency. The encoded inductance information is decoded using a suitable demodulation technique. An external resistance added in series with the phase inductance in these methods to make the scheme non-sensitive to speed voltage effects. The added resistance also makes signal measurements easier, but the associated penalty is the need for additional switches to isolate the sensing circuit from the power circuit. The block diagram of the modulation based techniques is given in Fig. 6.

FM Encoder Technique

In the frequency modulation based technique, an FM encoder generates a signal containing the inductance variation information of the SR motor [18]. A simple L-F converter which maintains a linear relationship between inductance and time period was used for the purpose. The time period, T of the FM signal can be written as,

$$T = K_1 L = \frac{1}{f} \qquad \cdots\cdots\cdots(9)$$

where K_1 is a proportionality constant and L is the phase inductance. This signal is then fed to a microcontroller to digitize the frequency count, which is essentially an encoded rotor position information.

AM/PM Encoder Technique

The phase modulation (PM) and the amplitude modulation (AM) techniques are based on the phase and amplitude variations, respectively, of the phase coil current due to the time varying inductance when a sinusoidal voltage is applied to the phase coil in series with a resistance R [19]. The current flowing through the circuit in response to the alternating voltage is a function of the circuit impedance. Since the coil inductance is varying periodically, the phase angle between the current and the applied voltage also varies in a periodic manner. Fig. 7 shows the input sinusoidal voltage and the current waveforms $i_1(t)$ and $i_2(t)$ corresponding to the minimum and maximum phase inductances, respectively. Angles f_1 and f_2 are the corresponding phase angles by which the phase current lags the input voltage.

The PM encoder technique measures the instantaneous phase angle on a continuous basis, while the AM encoder technique measures the peak current. The sinusoidal carrier voltage signal is chosen to have a frequency which is much higher than the frequency of phase inductance variation. The transient variation of the current phase or amplitude will contain information about the dynamic motor winding inductance. It can be

shown that this phase or amplitude variation is a one-to-one function of the inductance [19].

A Complete Drive System

Mathematical analysis and simulation shows that phase variation is more sensitive for lower values of inductance, while amplitude variation is more sensitive at higher inductance values [19]. This readily suggests that a combination of the two methods would result in a better sensitivity, i.e., a higher change in the decoded inductance function for the same change in the rotor angle. To achieve this better sensitivity without sacrificing simplicity, a level crossing detector can be used instead of a zero crossing detector in the PM encoder circuit to obtain the square wave representation of the phase inductance. The level crossing detector is set to a threshold value at V_T as shown in Fig. 7. The phase angle variation now corresponds to $f_3 - f_4$ for the same change in phase inductance from the aligned position to the unaligned position in Fig. 7.

An experimental prototype of a sensorless SRM drive has been developed based on the modified PM encoder technique. The block diagram of the complete SRM drive including the different controller segments is shown in Fig. 8. IGBTs are used as the power semiconductor devices and are driven by high voltage integrated circuit gate drivers IR2110. The PM encoder circuit, i.e., the sensing circuit is made of a 5KHz sine wave generator, a low pass filter and a level crossing detector. The current drive capability of the sinusoidal input voltage is improved by a power amplifier stage. A 16-bit microcontroller (Intel 80C196KR) having a clock rate of 16MHz is used to implement the control algorithm. The microcontroller is configured to take the decoded phase modulated signal and generate the gate switching signals for the three phases. The microcontroller also generates a fixed frequency PWM signal that regulates the motor phase currents.

The performance of the indirect position sensing scheme was evaluated on a 5 HP, three phase SRM with 6 stator poles and 4 rotor poles. The dc bus voltage was fixed at 40 V and the PWM switching frequency of the converter was set at 22 KHz. The results of the experiments are given in this section. Test results presented here are for the SRM running at 2500 rpm under lightly loaded conditions. The current waveform in phase B is shown in the oscillograph of Fig. 9. Note that this is an unregulated current with constant PWM duty cycle. The maximum sensing current is about 100mA and does not have any significant effect in the torque production. Each cycle of the motor phase current waveform consists of three modes. The phase coil carries the main energization current for one-third of the period, while in the previous one-third period it carries the diagnostic sensing current. The phase current is completely non-conducting for the remaining one-third portion of the cycle, as seen in Fig. 9.

2.2.3 Flux Sensing Techniques

The flux sensing method of [20] is based on applying diagnostic pulses to an idle phase and integrating the voltage across the phase to obtain the phase flux according to Eq. (3). The rotor position is then obtained from the motor flux-angle-current characteristics data. Either flux or current is kept fixed at desired levels of l_o or i_o during pulsing and the other variable is obtained as a function of the rotor position as

shown in Fig. 2. The method appears to be highly potential for position estimation at higher speeds, but an accurate knowledge of phase winding resistance is required for high resolution position estimation.

III. Conclusions

The existing indirect rotor position sensing techniques have been reviewed in this paper. It cannot be claimed that one particular method is suitable for all types of applications. The position sensing techniques depend on a number of factors, such as, the type of motor, the type of application, the type of converter used and the control strategy. The passive waveform detection techniques are well suited for low-cost, low-speed applications, but may not be suitable for high-resolution, high-performance drives. For high-resolution position sensing, computations become intensive and a signal processor becomes essential. This increases the cost of position sensing. Observer based methods and flux/current methods are examples of schemes that could be used for high-resolution position sensing. These methods are also suitable for position sensing at high-speeds, but high speed computational requirements tend to increase the cost of these type of indirect sensors even more. The need for an inexpensive indirect position sensing technique suitable for high-speed applications still exists.

References

[1] Lawrenson, P.J., Stephenson, J.M., Blenkinsop, P.T., Corda, J. and Fulton, N.N., Variable speed reluctance motors. *IEE Proc*., Vol. 127 (1980), Pt. B, No. 4, pp. 253-265.

[2] Miller, T.J.E., *Switched Reluctance Motors and their Control*, Magna Physics Publishing and Clarendon Press, 1993.

[3] Byrne, J.V., O'Dwyer, J.B. and McMullin, M.F., A high performance variable reluctance drive: A new brushless servo. *Proc. Motor-Con*, 1985, pp.147-160.

[4] Acarnley, P.P., Hill, R.J. and Hooper, C.W., Detection of rotor position in stepping and switched reluctance motors by monitoring of current waveforms. *IEEE Trans. Industrial Electronics*, Vol. IE-32 (1985), No. 3, pp. 215-222.

[5] Lumsdaine, A. and Lang, J.H., State observers for variable-reluctance motors. *IEEE Trans. Industrial Electronics*, Vol. IE-37 (1990), No. 2, pp. 133-142.

[6] Husain, I., Sodhi, S. and Ehsani, M., Sliding mode observer based control for switched reluctance motors. *IEEE-IAS Conf. Rec.* ,1994, pp. 635-643.

[7] Lyons, J.P., MacMinn, S.R. and Preston, M.A., Flux/Current methods for SRM rotor position estimation. *IEEE-IAS Conf. Rec.* ,1991, pp. 482-487.

[8] Husain, I. and Ehsani, M., Rotor position sensing in switched reluctance motor drives by measuring mutually induced voltages. *IEEE Trans. on Industry Applications*, Vol. 30 (1994), No. 3, pp. 665-672.

[9] Panda, S.K., and Amaratunga, G.A.J., Analysis of the waveform detection technique for indirect rotor position sensing of switched reluctance motor drives. *IEEE Trans. on Energy Conversion*, Vol. 6 (1991), No. 3, pp. 476-483.

[10] Panda, S.K., and Amaratunga, G.A.J., Waveform detection techniques for indirect rotor position sensing of switched reluctance motor drives, Part I Analysis and Part II Experimental Results. *IEE Proc.* Vol. 140 (1993), No. 1, pp. 80-96.
[11] Panda, S.K., and Amaratunga, G.A.J., Comparison of two techniques for closed-loop drive of VR step motors without direct rotor position sensing. *IEEE Trans. Industrial Electronics*, Vol. IE-38 (1991), No. 2, pp. 95-101.
[12] Hedland, B.G., *A method and a device for sensorless control of a reluctance motor*, International patent, WO 91/02401, 1986.
[13] Lyons, J.P., MacMinn, S.R. and Preston, M.A., *Rotor position estimator for a switched reluctance machine using a lumped parameter flux/current model*, US patent # 5107195, 1991.
[14] Dunlop, G.R. and Marvelly, J.D., Evaluation of a self-commutated switched reluctance motor. *Proc. of Int. Conf. on Electric Machines and Drives*, 1987, pp. 317-320, Adelaide, Australia.
[15] Harris, W.D. and Lang, J.H., A simple motion estimator for variable-reluctance motors. *IEEE Trans. Industry Applications*, Vol. 26 (1990), no. 2, pp. 237-243.
[16] MacMinn, S.R., Rzesos, W.J., Szczesny, P.M. and Jahns, T.M., Application of sensor integration techniques to switched reluctance motor drives. *IEEE Trans. on Industry Applications*, Vol. 28 (1992), No. 6, pp. 1339-1344.
[17] Mvungi, N.H. and Stephenson, J.M., Accurate sensorless rotor position detection in an SR motor. *EPE Conf. Proc.* 1991, Vol. I, pp. 390-393.
[18] Ehsani, M., Husain, I. and Kulkarni, A., Elimination of discrete position sensor and current sensor in switched reluctance motor drives. *IEEE Trans. on Industry Applications*, Vol. 28 (1992), No. 1, pp. 128-135.
[19] Ehsani, M., Husain, I., Mahajan, S. and Ramani, K.R. New modulation techniques for rotor position sensing in switched reluctance motors," *IEEE Trans. on Industry Applications*, Vol. 30 (1994), No. 1, pp. 85-91.
[20] Mvungi, N.H., Lahoud, M.A. and Stephenson, J.M., A new sensorless position detector for SR drives. *Fifth International Conf on Power Electronics and Variable Speed Drives*1990, pp. 249-252.

LIST OF FIGURES

Fig. 1. (a) Cross-section of SR motors: (a) 6/4, three-phase SRM, (b) 8/6, four-phase SRM.

Fig. 2. Flux-angle-current characteristics of SRM.

Fig. 3 Block diagram of Acarnely's waveform detection method.

Fig. 4 Model based estimator.

Fig. 5 Block diagram of flux/current method.

Fig. 6 Block diagram of modulation based techniques.

Fig. 7 Basic waveforms in AM and AM/PM technique.

Fig. 8 SRM drive using modified PM technique.

Fig. 9 Active phase current.

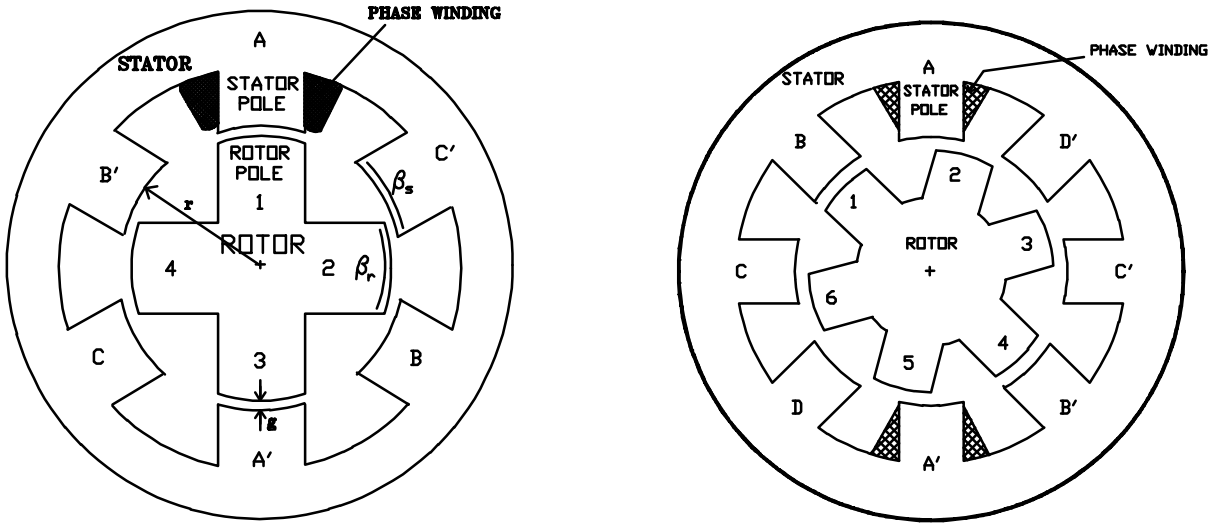

(a) (b)

Fig. 1. (a) Cross-section of SR motors: (a) 6/4, three-phase SRM, (b) 8/6, four-phase SRM.

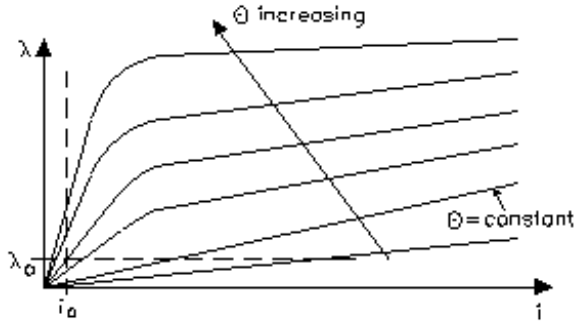

Fig. 2. Flux-angle-current characteristics of SRM.

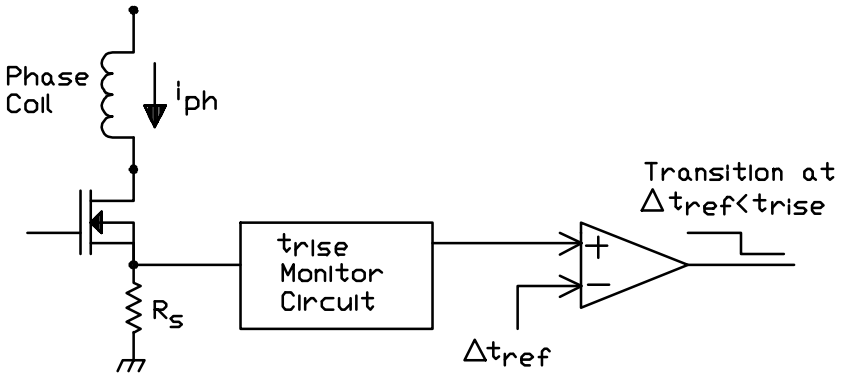

Fig. 3 Block diagram of Acarnely's waveform detection method.

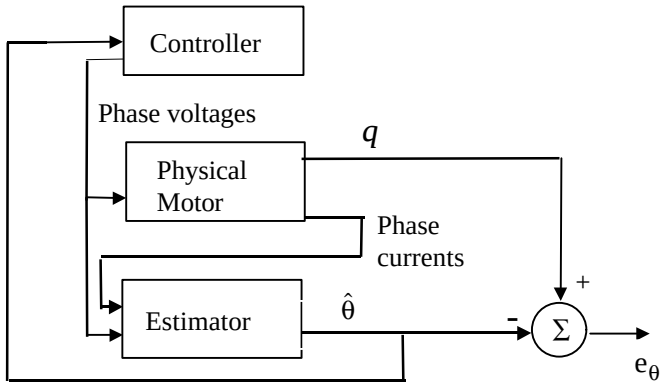

Fig. 4 Model based estimator.

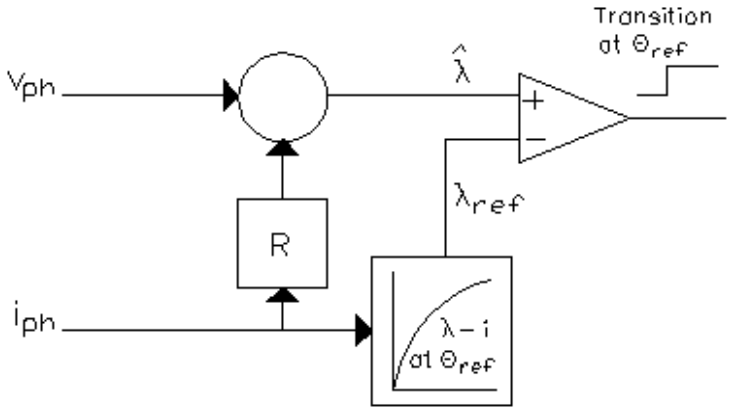

Fig. 5 Block diagram of flux/current method.

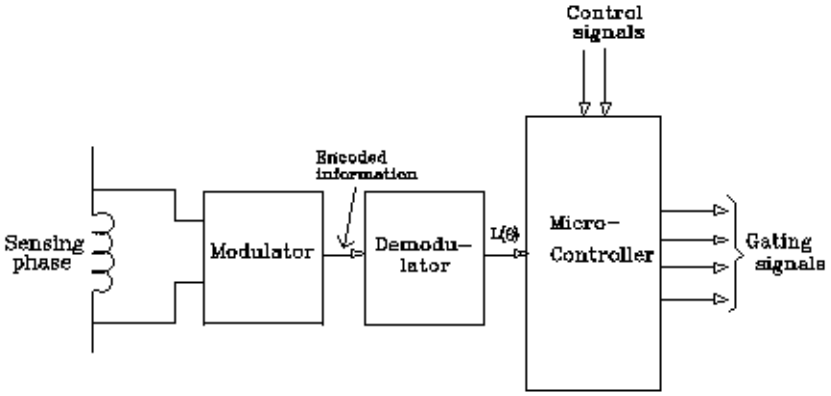

Fig. 6 Block diagram of modulation based techniques.

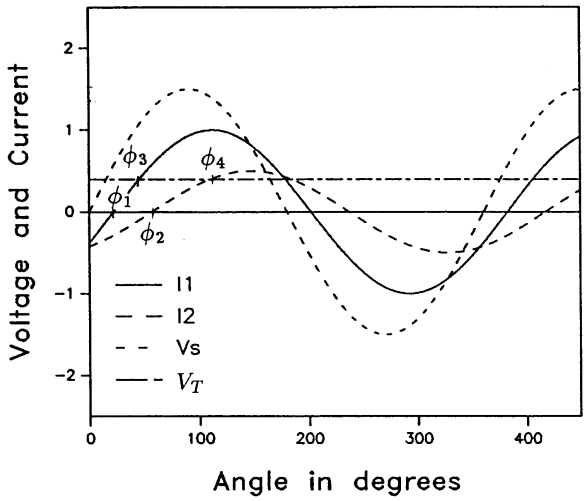

Fig. 7 Basic waveforms in AM and AM/PM technique.

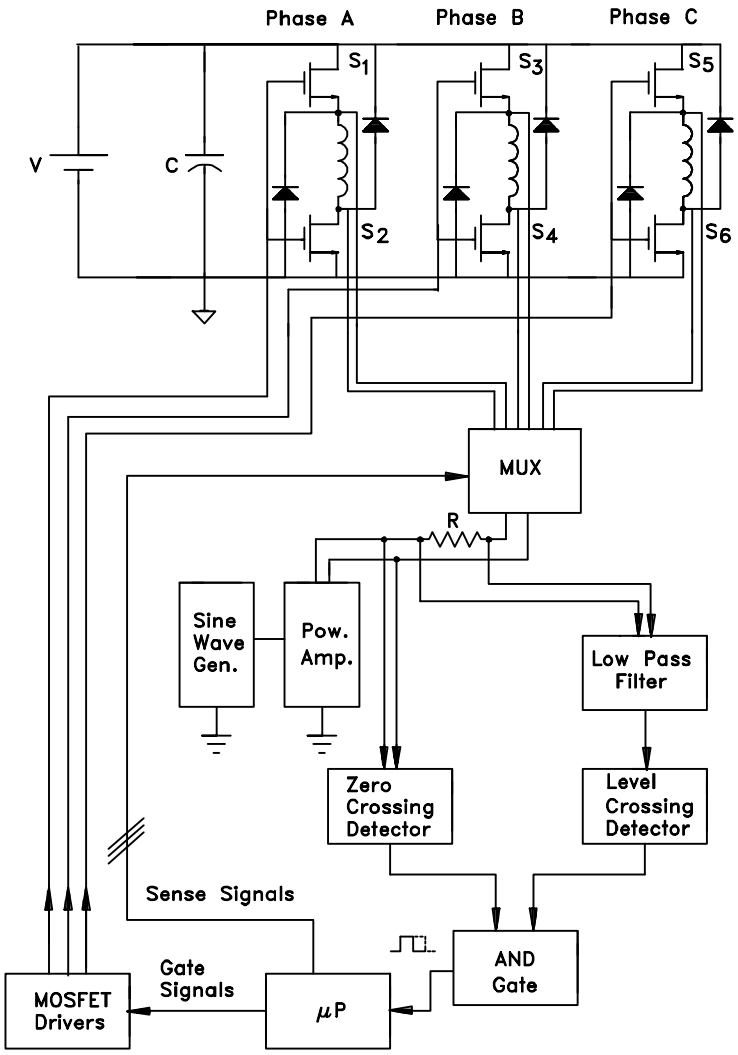

Fig. 8 SRM drive using modified PM technique

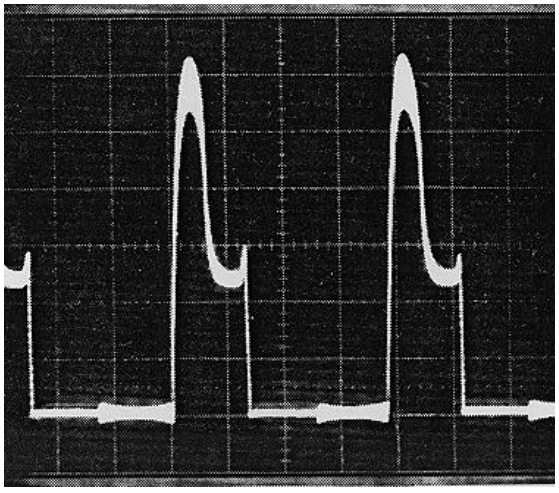

Fig. 9 Active phase current.

Trondheim

SWITCHED RELUCTANCE MOTOR WITH 16 STATOR POLES AND 12 ROTOR TEETH

J. Wolff H. Späth

Elektrotechnisches Institut, Universität Karlsruhe, Germany

Abstract: The Elektrotechnisches Institut of the University Karlsruhe has developed, optimized and manufactured a Switched Reluctance Drive with power converter and control engineering according to the latest scientific findings. The motor was constructed for the rated output of about 25 kW and for industrial applications.
The nominal speed of the test Switched Reluctance Motors is 1500 revolutions per minute. The drive works in all for quadrants and was designed for applications with highest demands for dynamics, constant torque, low noise and highest power output.

Keywords: Switched Reluctance Drive, Switched Reluctance Motor

INTRODUCTION

The Switched Reluctance Motor has already been propagated in many publications of English literature. However, these general publications do not scientifically solve the use of this motor type as variable-speed drive. Most publications treat parts of the problems only. Less attention was paid to the examination and optimization of the overall system - composed of motor, converter and control. Uncertainties regarding utilization, torque undulation, noise generation and selection of converter circuits lead to today's shadowy exixtence of this motor. Since the simple construction of the Switched Reluctance Motor promises production at low cost, the industry launched occasional enquiries and examinations regarding the Switched Reluctance Drive. Nevertheless the drive could not yet find its wide acceptance, probably due to single, technically unsolved problems.
The motivation to realize this project at the Elektrotechnisches Institut of the University of Karlsruhe is based on the unsolved technical problems, the robust construction and the favourably-priced motor.
The paper will describe important findings regarding the Switched Reluctance Drive as a whole. As an example we selected a motor with an output of 25 kW at 1500 revolutions per minute.
Different types of variable-speed electromotors, such as a.c. and d.c. motors, are widely spread with the selected technical major parameters. The Switched Reluctance Drive can therefore quickly and easily be compared with these drive types.

MOTOR DESIGN

The Elektrotechnisches Institut selected the new Switched Reluctance Motor with 16 stator poles and 12 rotor teeth. It is a 4-pase-winding machine, the 4 stator poles that are shifted by 90° to each other form one phase-winding (Figure 1).

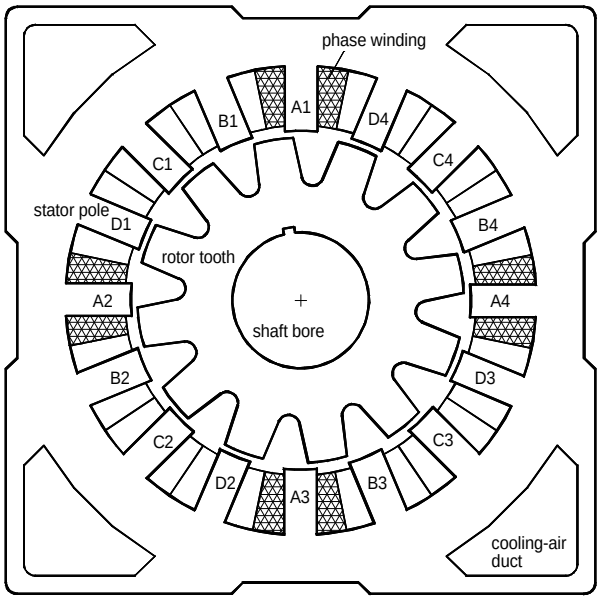

Figure 1: Schematic cross-section of the Switched Reluctance Motor

This design was proposed by author. Compared with the 3-phase Reluctance Motor, the 4-phase machine requires the same or even lower number of power semiconductors.
The four phase-winding poles split the forces up more evenly around the motor perimeter which reduces the noise. If only two opposite poles belong to one phase-winding as for example in the 4-phase-winding 8/6 reluctance motor, the forces do apply on two positions only. The 4-phase-winding 16/12 reluctance motor splits the forces up to four poles. Therefore, these are approximately only half as big as the forces of the 8/6 motor. Also, the 16/12 motor generates less noise than the 8/6 motor. These findings are proved true by comparative measurements done with a 15 kW 8/6 motor of the Oulton company.

The authors of the paper [1] compared a 6/4 motor with a 12/8 motor and showed that the utilization of the high-pole machine is better for higher torques which is due to the flux linkage and the narrow winding coils. The first causes a higher torque, the latter a lower thermal resistance from the winding to the iron. However, with a bigger number of pole/teeth the magnetic reversal frequency and iron losses increase. According to [1], a lower flux density should compensate this effect, so that iron losses of both motors range in the same size. However, the latter context does not seem to be proved true by our Switched Reluctance Motor. The iron losses increase noticeably with higher torque.

TEST DRIVE

The main components of the test drive are the Switched Reluctance Motor and the power converter. The voltage-source converter consists of mains and motor converter. The common supply for the three-phase-self-commutated mains converter is 400V/50Hz. The control electronic - including the measurement and control techniques - is superior to the power electronic. Motor and converter can be used for the four-quadrant-drive. The basic structure is shown in Figure 2.

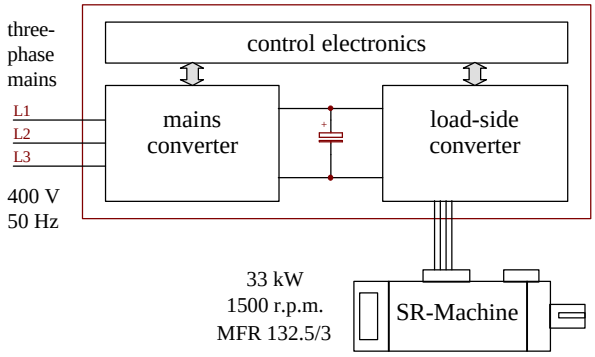

Figure 2: Basic structure of the Switched Reluctance Drive

MAINS FRIENDLINESS OF THE SWITCHED RELUCTANCE DRIVE

The mains converter is a three-phase-self-commutated IGBT-Converter. The control of the mains current has been optimized in a way that the drive, in stationary running with a power factor of about one, receives energy from or feeds energy into the 3-phase current mains. This results in a sinusoidal mains current and in conformity of the phase position between current and voltage - at long last the mains friendliness of the drive.
The mains current converter operates in all four quadrants and allows to implement highly dynamic drive solutions. For example, if the converter is used for the main drive of a group of drives, it may additionally be employed for compensating the reactive power of the auxillary drives. Figure 3 shows the current and voltage values for motor operation with 20 kW and reactive power compensation at the same time.
For reluctance drives less demanding in terms of dynamics and mains compatibility, diode bridges with smoothing and commutating reactors are used as mains current converters. The reluctance drive can also be operated with it, in most cases however, as motor only.

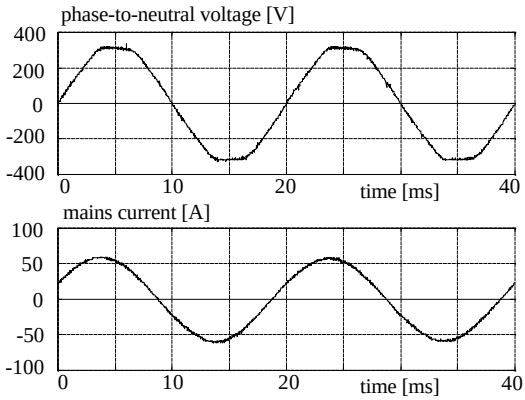

Figure 3: P_{mains} = 24,4 kW, Q_{mains} = -10 kVAr, $\cos\varphi = 0{,}925_{cap}$, P_{motor} = 20 kW, (measurement)

LOAD-SIDE CONVERTER

For the Switched Reluctance machine the output current of the converter can be limited to one direction per phase due to the unipole excitation. The rotor moves into the magnetic field when the motor is in operation. This does not depend on the direction of the magnetic flux density.
With the generator in operation, the rotor moves out of the field.
Three criteria must be complied with when selecting the converter circuit:

1. low number and low cost of power semiconductors
2. less current measurements
3. many options for influencing the phase-winding current

Criteria 3 contradicts 1 and 2. Less requirements for power electronic and measurements restrict the options for current control. When defining the converter topology, you must compromise to fulfill these demands.

If a two-quadrant chopper circuit is used for each phase and if each phase current is measured separately, many options can be used. The complete d.c link voltage U_d can be used for switching the phase-winding current on/off. The current can - for all phase-windings and at any time - be adjusted to a pre-

defined desired value. A free-wheeling of the phase-winding current is possible.

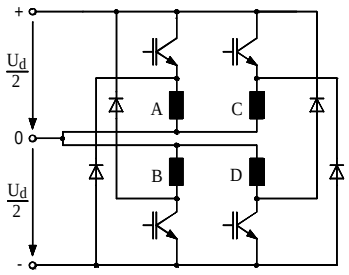

Figure 4: H-Circuit

The so-called H-Circuit [2] with connected neutral point (Figure 4) allows to control the single currents separately. This circuit only requires one power switch and one diode per phase thus operating with the lowest number of semiconductors. To profit from these benefits you must accept that there is no free-wheeling current and that only half the d.c. voltage is used. The current can only be in- or decreased with $U_d/2$. Like this, motor winding and current carrying capacity of the power semiconductors must be dimensioned for $U_d/2$. With regard to the two-quadrant chopper circuit per phase - provided that the nominal speed of the motor is the same - the number of turns per phase must be halved and the cross-section of the wire must be doubled. Additionally, power modules with doubled current carrying capacity must be selected. Two or four measurements are required to measure the phase currents. Usually, the neutral point is generated by means of a serial circuit of capacitors at the d.c. voltage source. The capacitors of both partial voltage sources must be loaded in a symmetric way. Like this, the H-Circuit can be used for all Switched Reluctance Motors with an even number of phases. It can be used for machines with two and also with four phases.
This project aims at finding a circuit which has less restrictions regarding the current control and which uses the complete d.c. link voltage with a number of power semiconductors as low as possible. We suggest the following circuit (Figure 5).

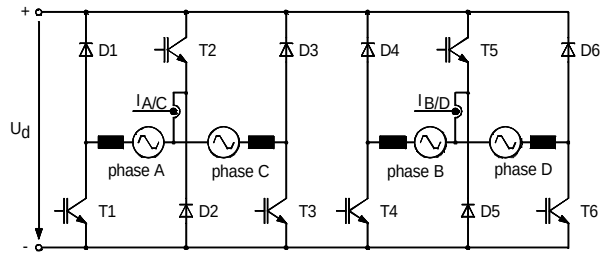

Figure 5: Circuit of the load-side converter for the 16/12 Switched Reluctance Motor

The transistors T2 and T5 supply two non-adjoining phase-windings each. When the machine turns right as motor, the phases are switched D-A-B-C-D-A. When turning right, they are switched A-D-C-B-A-D. When switching from one phase to another, current may flow in the adjoining phases. The phases A and C respectively B and D should not conduct current at the same time, since for example A generates a motoric and C a generator torque. Both torques are subtracted from each other, a not desirable status. Like this, the phases A and C respectively B and D can be supplyed with one common transistor each without further restrictions regarding the current control. The currents can be determined by one common measurement.
Only with very high output powers, the inactive phase conducts a small amount of residual current. The measurement errors resulting for the active phase are corrected in the control.
In comparison with the three-phase induction motor, the amplitudes of the phase currents are approximately 15% higher. Therefore, the power semiconductors can be selected with the size of the modules usually used in power converters of asynchronous motors.
Compared with the H-Circuit, the cost for power semiconductors from average to higher output powers are lower. The free-wheeling current can be used to lower the pulse frequency rate respectively the current ripple. Since there is no voltage neutral point this circuit can also be used for very small speeds and for standstill torques.

CURRENT AND TORQUE CONTROL

For the test drive, the torque control was optimized in switching mode for high utilization and low torque ripple with the parameters turn-on angle, current flow angle and current desired value [3].
The respective angles result from the rotor position. The turn-on angle determines the beginning of the current increase. The difference between beginning current decrease and beginning current increase is called current flow angle. The current desired value forms the amplitude of the current impulse.
Switching mode means that the power is brought to the final value after the turn-on angle and without interim pulses.
A two-step controller ist used to keep the phase-winding current on the final desired value until the current flow angle has been reached, afterwards it is switched off again without interim pulses. This method of controlling the torque can be realized easily, even without using a digital processor.
The optimal parameters of the torque control were determined off-line and were afterwards implemented in the system.
When the output power increases, the current turn-on angle is continuously pre-drawn while the turn-off angle changes insignificantly only. The current amplitude increases linearily to the torque starting at 20 Nm.
This procedure yielded a torque ripple of less than 4% in the nominal point whithout effects at the speed.

SPEED CONTROL

The control has been optimized to minimize speed variations. The speed controller is a PI-controller.

The control parameters were adjusted according to the symmetric optimum [4]. Torque and current control are united in the speed control to a delay part of first order with a small time constant. The actual speed is determined by a position encoder located at the machine. For this purpose the encoded position is differenciated and afterwards transmitted to the setpoint/actual-value comparison via a smoothing filter. Rapid changes of the desired speed must not be intruded directly into the setpoint/actual-value comparison. This requires a ramp-function generator. It transforms the jump of the desired value into a suitable ramp for the speed control. The output of the ramp-function generators increases slowly, reaches the ramp profile after a short time and drives to the end value smoothly afterwards.
This function is intruded into the setpoint/actual-value comparison as desired value. It is remarkable that the measurement value reaches the final value earlier than the output of the ramp-function generator does.

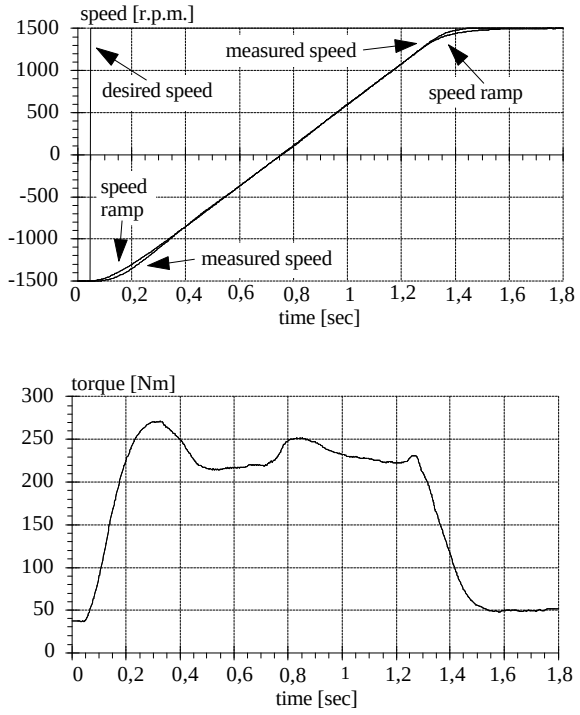

Figure 6: Speed control (measurement)
$M_{load} \cong 50$ Nm, $J_{all} = 0{,}54$ kgm^2

Figure 6 shows the reversing process from negative to positive nominal speed with a load torque of approx. 50 Nm and an accellerating torque of approx. 200 Nm. After the zero crossing of the torque, it rises a little bit, the brush friction of the d.c. machine that is coupled as working machine must be overcome.
After this desired value jump of the speed, the measured speed does not swing over.

POSITION CONTROL

Likewise, the position control of, for example, workpieces, tools, conveyor baskets etc. belongs to the applications of electric motors. The measuring result in Figure 7 proves that Switched Reluctance Motors with 16 stator poles and 12 rotor teeth are suitable position drives. After a desired value jump of 1000°, the motor performs about 2,8 turns and reaches the desired value without over-swing in one second.
An optimized position controller determines this transient response. It is superposed on the speed control circuit and has a proportional character. It can be dimensioned according to the usual adjustment regulations of other drives. The cascade structure was selected for the complete control circuit which is composed of current, torque and position control.

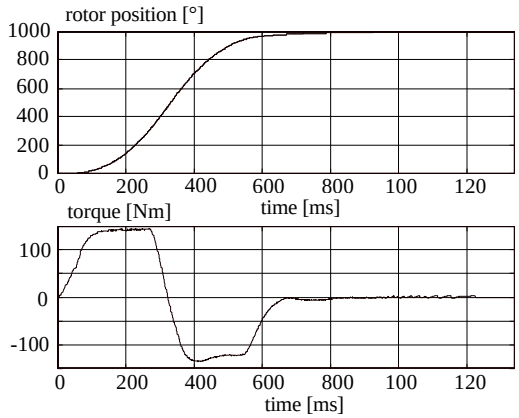

Figure 7: Position control (measurement)
$J_{all} = 0{,}54$ kgm^2

UTILIZATION

Altogehter three Switched Reluctance Motors were measured. Size and measures of these SR Motors are identical with each other. Only the quality of the used electric sheet steel and cooling method vary. Used sheet steel types include a 0,5 mm slightly alloyed respectively a 0,35 mm and highly alloyed magnetic sheet steel.
Two motors were built for continuous running duty. Cooling is obtained using an external blower, which blows air over the machine (cooling method IC416). The degree of protection is IP54. The third motor was built for continuous running duty with cooling method IC06 and protection degree of IP23. The cooling air for this motor is additionally blown through the tooth spaces of the rotor. This allows a better dissipation of the winding and rotor heat - thus increasing the maximum admissible continuous power.
The iron losses of switched reluctance motors, unlike those of asynchronous motors, make up a considerable portion of the total losses. However, the iron losses drop heavily as the speed is reduced . This effect is made use of to increase the rms currents in the pole

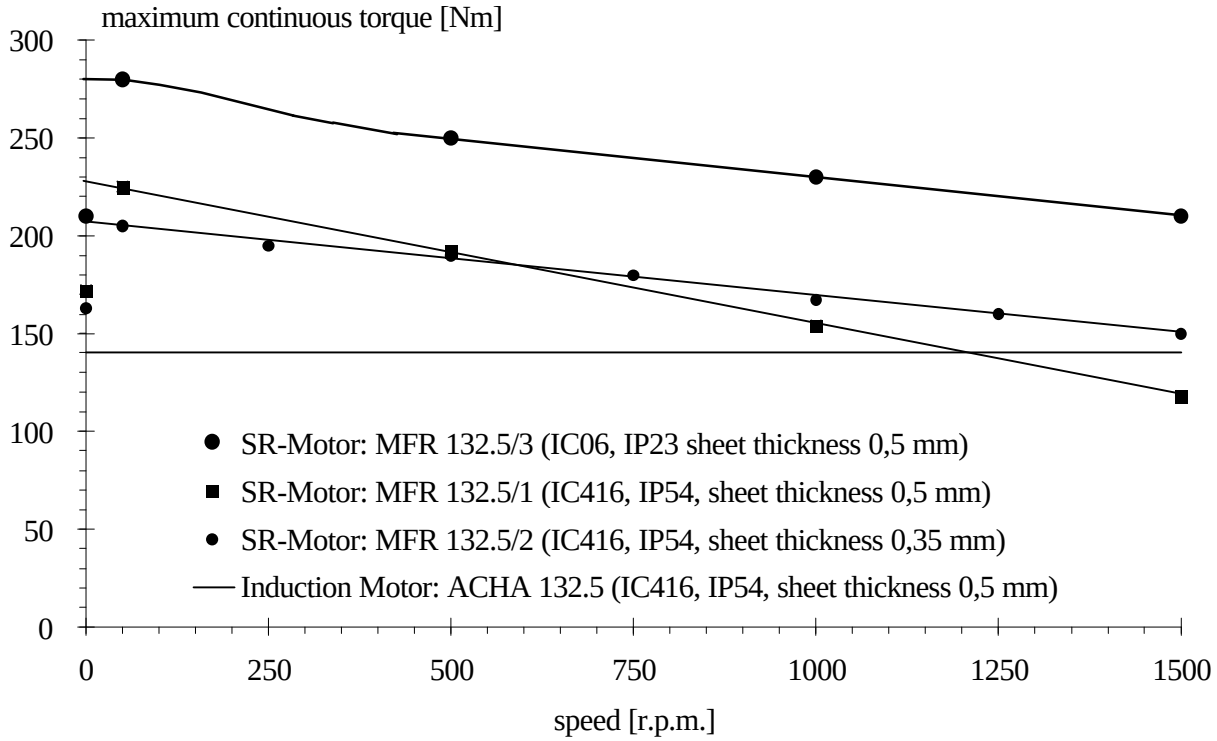

Figure 8: Maximum permissible continuous torque in the speed range from standstill to nominal speed (thermal/isolation class F, continuous running duty)

windings and obtain a high permissible continuous torque in the lower speed range. Moreover, operating the machine at low speeds results in low rotor iron losses - consequently, the rotor temperature rise remains low. In asynchronous motors, the stator and rotor winding losses make up the largest portion of total losses which remain almost constant from standstill to rated speed if the torque is assumed to be constant. This explains why asynchronous motors, when operated in continuous duty, must not be subjected to a torque higher than the nominal torque until the rated speed ist reached. Field weakening operation begins for all motor types when the rated speed is exceeded.

In Figure 8, the maximum permissible continuous torque is shown in the speed range from 0 to 1500 r.p.m. for the use of thermal and isolation class F.

For the used measurement methods with integrated temperature sensor, the temperature difference between winding and coolant temperature must not exceed 110 Kelvin.

The measurements were spot-checked with the resistance method. The measured temperatures ranged between 1 and 2 Kelvin below the maximum permissible value.

In continuous duty, the maximum permissible holding torque of the SR-Motor MFR 132.5/1 amounts to 145% of the rated torque when the motor is at rest. As soon as the rotor starts to rotate, however, all pole windings are subjected to the same thermal loads, and the continuous torque may be 190% of the rated torque at low speeds. For dynamic transient processes in the base speed range, the motors may be subjected to two to three times the rated torque.

Furthermore Figure 8 shows that using a thinner and highly alloyed magnetic sheet metal, is not always useful. Only for higher speeds the reduction of the eddy-current losses is decisive.

Below 600 r.p.m. the thicker sheet metal offers advantages: better magnetizability, higher thermal conductivity, better lamination factor and less punching works.

At nominal working point, the efficiency of the switched reluctance motor is that common for a three-phase induction motor of this performance class. In lower speed range, however, the efficiency of the reluctance motor drops insignificantly. With the motor at nominal torque, the efficiency raises to above 80% as from 400 r.p.m., and gradually increases further to approx. 90% until rated speed is reached (Figure 9).

Switched Reluctance Motors basically have a very efficient operation at partial stress.

The overall power efficiency of the test power converter is 91 % in the nominal working point.

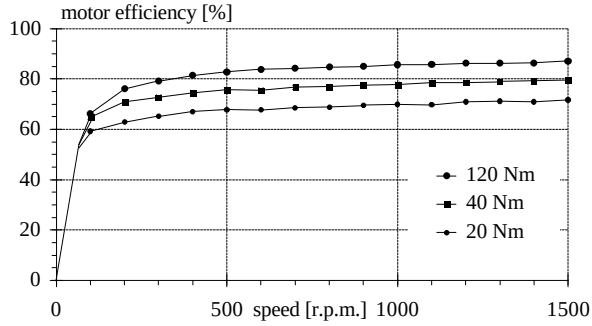

Figure 9: Efficiency of the Switched Reluctance Motor MFR 132.5/1

Table 1 compares constructive data of the Switched Reluctance Motor MFR132.5/1 and of the three-phase induction motor ACHA 132.5. Construction and function of both motors with these air gaps is not a problem. The production costs are the same.

	Switched Reluctance Machine	**Three-phase Induction Machine**
manufacturer	Elbtalwerk Heidenau GmbH	
motor type	MFR 132.5/1	ACHA 132.5
rated output power	18,5 kW	22 kW
nominal torque	118 Nm	140 Nm
nominal speed	1500 r.p.m	1500 r.p.m.
output at 1000 r.p.m	16 kW	14,7 kW
output at 500 r.p.m	10 kW	7,3 kW
moment of inertia	0,0883 kgm^2	0,105 kgm^2
lamination stack:		
quality	V 470-50A	
losses at 50 Hz and 1,5 T	4,7 W per kg	
sheet thickness	0,5 mm	
length of lamination stack	235 mm	
outside width of stator	ÿ 260 mm	
inside diameter of stator	∅ 165 mm	
width of air gap	0,3 mm	0,55 mm
shaft bore diameter	∅ 65 mm	
weigth befor punching	118,7 kg	
weight of stator stack	54,0 kg	56,1 kg
weight of rotor stack	24,2 kg	21,9 kg
windings:		
weigth of stator windings	13,3 kg copper	14,2 kg copper
copper fill factor	55,4 %	56,8 %
length of winding overhang	2 x 22 mm	2 x 70 mm
weigth of rotor winding	without winding	4,8 kg aluminium
utilization at nominal point:		
power/volume ratio	981 W/dm^3	868 W/dm^3
power/weigth ratio	202 W/kg	227 W/kg
compare conditions:		
shaft heigh	132 mm	
duty type	continuous running duty (S1)	
thermal/isolation class	F	
protection degree	IP 54	
cooling method	IC416	
cooling fan power	65 W	

Table 1: Comparision of material and utilization

ADVANTAGES - APPLICATIONS

When comparing the data listed in table 1, some advantages but also disadvantages become evident. Advantages of the three-phase induction machine are the low noise level and an already widely spread technique with high availability. The reluctance drive offers a better accelleration and production costs are lower.

The Switched Reluctance Motor ist characterized by a high operating safety after the failure of one or several motor phases. When such a failure occurs, the motor continues to run under load, and it can be accelerated or braked. However, the torque and speed fluctuations occurring are of a measurable magnitute, and the start-up of the motor is no longer ensured. Despite this drawback, the driven machine, or process under way, can be set back into safe state in many applications.

For judging the ratio power per volume respectively power per mass, the following can be assessed for 1500 r.p.m.:

The active part of the Switched Reluctance Mortor is, compared with the three-phase induction motor with the same nominal power, about 10% smaller and 10% heavier.

If the thin magnetic sheet steel is used for the SR-Motor, production costs rise, the active part of the SR Motor becomes 30% smaller and 10% lighter. (For this assess the magnetic sheet steel and the windings were considered as active part.) For a speed range of about 1500 r.p.m. the Switched Reluctance Drive can offer advantages for certain applications.

Considering the speed range below 1000 r.p.m. or the MFR 132.5/3 machine with inner ventilation, the Switched Reluctance Drive is more suitable for many applacations compared with other drive types.

At 50 r.p.m the machine with the inner ventilation can be stressed with a permanent torque of 280 Nm. The rotor heating is very low, the temperature rise of the bearing does not exceed 35 K for the overall base speed of up to 1500 r.p.m.

At 500 r.p.m., the MFR 132.5/1 machine with surface ventilation has a continuous rating of 10 kW - 37% more than the comparable three-phase induction machine.

ACKNOWLEDGEMENTS

Optimization and calculation of the Switched Reluctance Motor were made by Mr E. Vonhof at Power Electronics Dublin using a Finite Elemente Program. The motor was produced at the Elbtalwerk Heidenau GmbH. We thank the Deutsche Forschungsgemeinschaft for its financial support of this research project.

REFERENCES

[1] Lovatt, H.C.; Stephenson, J.M.: Influence of number of poles per phase in switched reluctance motors. Proc. IEE, 139, No. 4, 1992, p. 307-314

[2] Steiert, U.: Drehmomentsteuerung einer Reluktanzmaschine mit beidseitig ausgeprägten Polen und geringer Drehmomentwelligkeit. Dissertation Universität Karlsruhe, 1992

[3] Späth, H.; Wolff, J.: Der elektrische Antrieb der Zukunft? TECNICA, No. 19, 1996, p. 49-53

[4] Meyer, M.: Elektrische Antriebstechnik. Vol. 2 Springer, Berlin 1987

SIEMENS

Motores Eléctricos

Catálago General

- Motores Trifásicos
- Motores Monofásicos
- Aclaraciones Técnicas
- Variadores de Velocidad

Catálogo General de Motores Eléctricos 2000

Indice

Motores trifásicos

Horizontal estándar, tipo RGZ, eficiencia estándar 4
Servicio pesado, tipo RGZSD, eficiencia estándar 4
A prueba de explosión, tipo RGZZSD, eficiencia estándar 4

Horizontal estándar, tipo RGZE, alta eficiencia 6
Servicio pesado, tipo RGZESD, alta eficiencia 6
A prueba de explosión, tipo RGZZESD, alta eficiencia 6

Con brida C, tipo RGZ, eficiencia estándar 8
Con brida D, tipo RGZ, eficiencia estándar 8
Con brida C y espiga JM, tipo RGZ, eficiencia estándar 8

Con freno de disco, tipo RGZ, eficiencia estándar 8
De dos velocidades, tipo RGZ, eficiencia estándar 10
Verticales flecha hueca, tipo HSRGZV, eficiencia estándar 13
A prueba de goteo, NEMA 56, tipo 1RA3, eficiencia estándar 16

Datos característicos típicos de motores trifásicos eficiencia estándar 19
Datos característicos típicos de motores trifásicos de alta eficiencia 21

Dimensiones de motores con brida C 23
Dimensiones de motores con brida D 25
Dimensiones de motores de armazones NEMA, TCCVE 26

Motores monofásicos

A prueba de goteo, NEMA 56, tipo 1RF3 28
Totalmente cerrados, tipo 1LF3 33

Aclaraciones técnicas 34

Variadores de velocidad

Micro-Master básico, Micro-Master Vector, Midi-Master Vector 46

Más de un motor...
y más que un motor...
Siemens le da a Usted:

Más características de calidad, interior y exteriormente

Cada motor Siemens es una combinación de características y materiales cuidadosamente seleccionados para proporcionar un motor confiable, eficiente y durable. Cada componente es un ejemplo de excelente diseño, mano de obra calificada y valor agregado... cojinetes antifricción de alta capacidad, rotor balanceado dinámicamente bobinado de cobre, aislamiento superior.

Aseguramiento de calidad

Además de incorporar materiales de alta calidad, cada motor Siemens pasa por más de 100 distintas inspecciones de calidad antes de salir de nuestra planta. Para que sea lo suficientemente bueno para ser ofrecido a Usted.

La responsabilidad de nuestra gente ayuda a poner la confiabilidad extra en los motores Siemens.

Eficiencia en operación ahora y en el futuro cuando ésta más se necesita

Los motores Siemens están diseñados para ser resistentes en el trabajo y operan tan eficientemente que Usted estará sorprendido con su ahorro de energía. Las diferencias que Siemens le ofrece le dan más motor por su dinero y más ahorro a largo plazo.

Apoyo para elección del motor adecuado

Cuando Usted está seleccionando un motor, Siemens opina que Usted debe hablar con quien pueda apoyarle a elegir el accionamiento adecuado para el trabajo a desempeñar. Nuestros ingenieros de ventas tienen el conocimiento y experiencia para ayudarle a resolver cualquier problema de aplicación, diseño o instalación.

Motores trifásicos

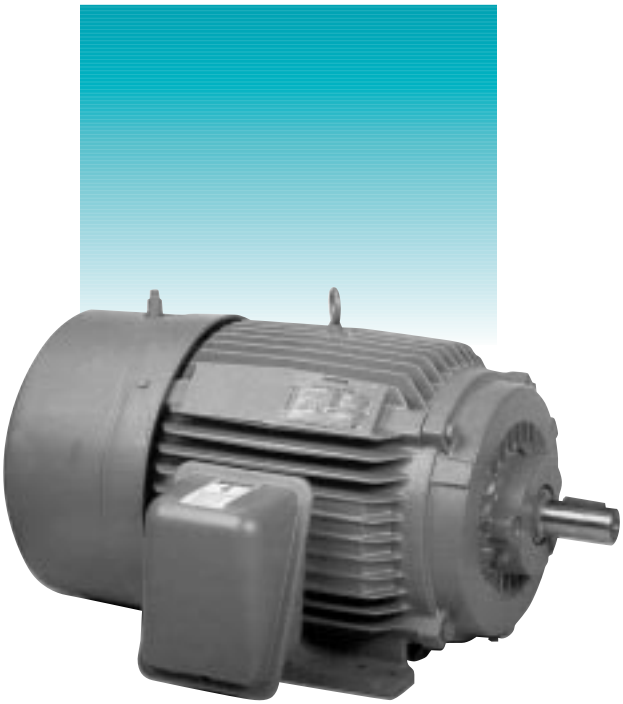

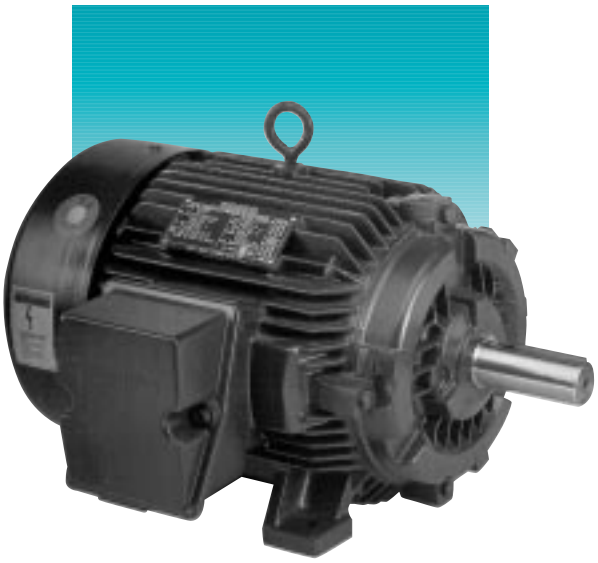

Motores trifásicos jaula de ardilla, eficiencia estándar

Construcción horizontal con patas, 60 Hz.
220-230/440-460 V, motores tipo RGZ y RGZSD de armazones 143T al 256T.
220/440 V motores tipo RGZ y RGZSD desde armazón 284T hasta 75HP.
220/440 V motores tipo RGZZSD hasta 75 HP.
440 V ó 460 V motores a partir de 100 HP.

TCCVE **Servicio pesado** **A prueba de explosión**			Tipo RGZ **TCCVE** Aisl. F - F.S. 1.15	Tipo RGZSD **Servicio pesado** Aisl. F - F.S. 1.15	Tipo RGZZSD **Prueba de Explosión** División 1 CI.1-Grupo D CI.2-Grupo F&G Aisl. B - F.S. 1.0
HP	RPM	Armazón	Cat. No.	Cat. No.	Cat. No.
0.5	900	143T	30000834	-	-
0.75	1800 1200 900	143T 143T 145T	30000815 30000826 30000900	- HSF0091 -	30001648 30001655 -
1	3600 1800 1200 900	143T 143T 145T 182T	30000804 30000857 30000890 30000948	- HSF0105 HSF0518 HSG1106	30001642 30001671 30001690 30002158
1.5	3600 1800 1200 900	143T 145T 182T 184T	30000845 30000879 30000940 30000981	HSF0119 HSF0539 HSG1113 HSG1624	30001665 30001683 30000048 30000049
2	3600 1800 1200 900	145T 145T 184T 213T	30000868 30000912 30000973 30001024	HSF0574 HSF0560 HSG1631 HSH2191	30001677 30001699 30002157 30001727
3	3600 1800 1200 900	182T 182T 213T 215T	30000923 30000932 30001013 30001071	HSG1155 HSG1134 HSH2198 HSH2758	30002153 30001705 30001722 30002176
5	3600 1800 1200 900	184T 184T 215T 254T	30000957 30000965 30001060 30001118	HSG1666 HSG1652 HSH2772 HSI3290	30002154 30002156 30001743 30001763
7.5	3600 1800 1200 900	213T 213T 254T 256T	30000991 30001002 30001106 30001165	HSH2233 HSH2219 HSI3304 HSI3808	30001711 30001716 30001760 30001777
10	3600 1800 1200 900	215T 215T 256T 284T	30001035 30001047 30001153 30005729	HSH2807 HSH2793 HSI3815 HSJ4270	30001732 30001737 30001774 -
15	3600 1800 1200 900	254T 254T 284T 286T	30001082 30001094 30007302 30007304	HSI3339 HSI3325 HSJ4277 HSJ4746	30001752 30001755 HXJ4347 -
20	3600 1800 1200 900	256T 256T 286T 324T	30001129 30001141 30007303 30007313	HSI3850 HSI3836 HSJ4753 HSK5236	30001766 30001769 HXJ4816
25	3600 1800 1200 900	284TS 284T 324T 326T	30007299 30005716 30007310 30007314	HSJ4550 HSJ4298 HSK5243 *	HXJ4592 HXJ4354 HXK5313 *

Motores trifásicos jaula de ardilla, eficiencia estándar

Construcción horizontal con patas, 60 Hz.
220-230/440-460 V, motores tipo RGZ y RGZSD de armazones 143T al 256T.
220/440 V motores tipo RGZ y RGZSD desde armazón 284T hasta 75HP.
220/440 V motores tipo RGZZSD hasta 75 HP.
440 V ó 460 V motores a partir de 100 HP.

TCCVE **Servicio pesado** **A prueba de explosión**			Tipo RGZ **TCCVE** Aisl. F - F.S. 1.15	Tipo RGZSD **Servicio pesado** Aisl. F - F.S. 1.15	Tipo RGZZSD **Prueba de Explosión** División 1 CI.1-Grupo D CI.2-Grupo F&G Aisl. B - F.S. 1.0
HP	RPM	Armazón	Cat. No.	Cat. No.	Cat. No.
30	3600 1800 1200 900	286TS 286T 326T 364T	30007300 30007301 30007311 *	HSJ5019 HSJ4767 HSK5663 *	HSJ5054 HXJ4823 HXK5712 *
40	3600 1800 1200 900	324TS 324T 364T 365T	30007306 30007308 30007320 *	HSK5467 HSK5257 HSL6041 *	HXK5502 HXK5320 HXL6090 *
50	3600 1800 1200 900	326TS 326T 365T 404T	30007307 30007309 30007321 *	HSK5845 HSK5677 HSL6398 *	HXK5887 HXK5719 HXL6440 *
60	3600 1800 1200 900	364TS 364T 404T 405T	30007315 30007317 * *	HSL6223 HSL6055 HSM6741 *	HXL6258 HXL6097 HXM6776 *
75	3600 1800 1200 900	365TS 365T 405T 444T	30007316 30007319 * *	HSL6587 HSL6405 HSM6923 *	HXL6629 HXL6447 HXM6979 *
100	3600 1800 1200 900	405TS 405T * *	* 30009067 * *	HSM7147 HSM6937 * *	HXM7182 HXM7007 * *

* Favor de consultarnos
• Armazones 284 T y mayores pueden suministrarse con espiga larga o corta: TS indica espiga corta, unicamente para acoplamiento directo.
• Todos los motores de 3600 RPM de 25HP y mayores son adecuados sólo para acoplamiento directo.
• Datos sujetos a cambio sin previo aviso.

Motores trifásicos jaula de ardilla, alta eficiencia

Construcción horizontal con patas, 60 Hz. 220/440 V.

Alta eficiencia: **TCCVE** **Servicio pesado** **A prueba de explosión**			Tipo RGZE **TCCVE** Aisl. F - F.S. 1.15	Tipo RGZESD **Servicio pesado** Aisl. F - F.S. 1.15	Tipo RGZZESD **Prueba de Explosión** División 1 CI.1-Grupo D CI.2-Grupo F&G Aisl. B - F.S. 1.0
HP	RPM	Armazón	Cat. No.	Cat. No.	Cat. No.
1	1800	143T	30000243	*	*
	1200	145T	-	*	*
	900	182T	-	*	*
1.5	3600	143T	30000236	*	*
	1800	145T	30000256	*	*
	1200	182T	-	*	*
	900	184T	-	*	*
2	3600	145T	30000249	*	*
	1800	145T	30000271	*	*
	1200	184T	-	*	*
	900	213T	-	*	*
3	3600	182T	30000279	*	*
	1800	182T	30000290	*	*
	1200	213T	-	*	*
	900	215T	-	*	*
5	3600	184T	30000318	*	*
	1800	184T	30000329	*	*
	1200	215T	-	*	*
	900	254T	-	*	*
7.5	3600	213T	30000356	*	*
	1800	213T	30000361	*	*
	1200	254T	-	*	*
	900	256T	-	*	*
10	3600	215T	30000369	*	*
	1800	215T	30000373	*	*
	1200	256T	-	*	*
	900	284T	-	*	*
15	3600	254T	30000382	*	*
	1800	254T	30000389	*	*
	1200	284T	-	*	*
	900	286T	-	*	*
20	3600	256T	30000402	*	*
	1800	256T	30000409	*	*
	1200	286T	-	*	*
	900	324T	-	*	*
25	3600	284TS	30009173	*	*
	1800	284T	30009174	*	*
	1200	324T	-	*	*
	900	326T	-	*	*
30	3600	286TS	30009175	*	*
	1800	286T	30009176	*	*
	1200	326T	*	*	*
	900	364T	*	*	*
40	3600	324TS	30009177	*	*
	1800	324T	30000581	*	*

Datos sujetos a cambio sin previo aviso.

Motores trifásicos jaula de ardilla, alta eficiencia

Construcción horizontal con patas, 60 Hz. 220/440 V.

TCCVE **Servicio pesado** **A prueba de explosión**			Tipo RGZE **TCCVE** Aisl. F - F.S. 1.15	Tipo RGZESD **Servicio pesado** Aisl. F - F.S. 1.15	Tipo RGZZESD **Prueba de Explosión** División 1 Cl.1-Grupo D Cl.2-Grupo F&G Aisl. B - F.S. 1.0
HP	RPM	Armazón	Cat. No.	Cat. No.	Cat. No.
40	1200	364T	*	*	*
	900	365T	*	*	*
50	3600	326TS	30009178	*	*
	1800	326T	30009179	*	*
	1200	365T	*	*	*
	900	404T	*	*	*
60	3600	364TS	30009180	*	*
	1800	364T	30009186	*	*
	1200	404T	*	*	*
	900	405T	*	*	*
75	3600	365TS	30009181	*	*
	1800	365T	30009187	*	*
	1200	405T	*	*	*
	900	444T	*	*	*
100	3600	405TS	30009196	*	*
	1800	405T	30009197	*	*
	1200	444T	*	*	*
	900	445T	*	*	*
125	3600	444TS	30014956	*	*
	1800	444T	30014954	*	*
	1200	445T	*	*	*
	900	447	*	*	*
150	3600	445TS	*	*	*
	1800	445T	30014953	*	*
	1200	447T	-	*	*
	900	447T	-	*	*
200	3600	447TS	*	*	*
	1800	447T	30014952	*	*
	1200	449T	-	*	*
	900	449T	-	*	*
250	3600	449TS	-	*	*
	1800	449T	-	30014955	*
	1200	449T	-	*	*
	900	S449LS	-	*	*
300	3600	449TS	-	*	*
	1800	449T	-	*	*
	1200	S449LS	-	*	*
			-	*	*
350	3600	S449SS	-	*	*
	1800	S449LS	-	*	*
	1200	S449LS	-	*	*
			-	*	*
400	3600	S449SS	-	*	*
	1800	S449LS	-	*	*

* Sobre pedido
\- No disponible
Datos sujetos a cambio sin previo aviso.

Motores trifásicos jaula de ardilla, eficiencia estándar

Construcción horizontal con patas, 60 Hz.
220-230/440-460 V, motores de armazón 143T al 256T.
220/440 V motores desde armazón 284T hasta 75HP.

Brida C **Brida D** **Espiga JM** **Con freno**		Tipo RGZ-B/C TCCVE **Con brida C** Aisl. F - F.S. 1.15		Tipo RGZ-JM TCCVE **B/C+espiga JM** Aisl. F - F.S. 1.15		Tipo RGZ-B/D TCCVE **Con brida D** Aisl. F - F.S. 1.15		Tipo RGZ-Freno TCCVE **Con freno de disco** Aisl. F - F.S. 1.15	
HP	RPM	Armazón	Cat. No.	Armazón	Cat. No.	Armazón	Cat. No.	Armazón	Cat. No.
0.5	900	143TC	*	-	-	143TD	*	143T	*
0.75	1800	143TC	30000813	-	-	143TD	*	143T	*
	1200	143TC	*	-	-	143TD	*	143T	*
	900	145TC	*	-	-	145TD	*	143T	*
1	3600	143TC	30000802	143JM	30002315	143TD	*	143T	*
	1800	143TC	30000854	143JM	30002319	143TD	*	143T	*
	1200	145TC	*	-	-	145TD	*	145T	*
	900	182TC	*	-	-	182TD	*	182T	*
	900	182TCH	*	-	-	-	-	-	-
1.5	3600	143TC	30000843	143JM	30002316	143TD	*	143T	*
	1800	143TC	30000877	143JM	30002320	145TD	*	145T	*
	1200	182TC	*			182TD	*	182T	*
	1200	182TCH	*			-	-	-	-
	900	184TC	*			184TD	*	184T	*
	900	184TCH	*			-	-	-	-
2	3600	145TC	30000866	145JM	30002317	145TD	*	145T	*
	1800	145TC	30000909	145JM	30002321	145TD	*	145T	*
	1200	184TC	*	-	-	184TD	*	184T	*
	1200	184TCH	*	-	-	-	-	-	-
	900	213TC	*	-	-	213TD	*	213T	*
3	3600	182TC	30000920 * *	182JMY	30002379 * *	182TD	*	182T	*
	3600	182TCH	30000921	182JM	30002381	-	-	-	-
	1800	182TC	30000929 * *	182JMY	30002436 * *	182TD	*	182T	*
	1800	182TCH	30000930	182JM	30002438	-	-	-	-
	1200	213TC	*	-	-	213TD	*	213T	*
	900	215TC	*	-	-	215TD	*	215T	*
5	3600	184TC	30000954 * *	184JMY	30002382 * *	184TD	*	184T	*
	3600	184TCH	30000955	184JM	30002384	-	-	-	-
	1800	184TC	30000962 * *	184JMY	30002369 * *	184TD	*	184T	*
	1800	184TCH	30000963	184JM	30002439	-	-	-	-
	1200	215TC	*	-	-	215TD	*	215T	*
	900	254TC	*	-	-	254TD	*	-	-
7.5	3600	213TC	30000989	213JM	30002464	213TD	*	213T	*
	1800	213TC	30001000	213JM	30002459	213TD	*	213T	*
	1200	254TC	*	-	-	254TD	*	-	-
	900	256TC	*	-	-	256TD	*	-	-
10	3600	215TC	30001033	215JM	30002465	215TD	*	215T	*
	1800	215TC	30001044	215JM	30002473	215TD	*	215T	*
	1200	256TC	*	-	-	256TD	*	-	-
	900	284TC	*	-	-	256TD	*	-	-

• Sobre pedido
•• Brinda C dimensión AK = 8.5 pulg.

Motores trifásicos jaula de ardilla, eficiencia estándar

Construcción horizontal con patas, 60 Hz.
220-230/440-460V, motores de armazón 143T al 256T
220/440V, motores desde armazón 284 T haste 75 HP.

Brida C **Brida D** **Espiga JM**		Tipo RGZ-B/C TCCVE **Con brida C** Aisl. F - F.S. 1.15		Tipo RGZ-JM TCCVE **B/C+espiga JM** Aisl. F - F.S. 1.15		Tpo RGZ-B/D TCCVE **Con brida D** Aisl. F - F.S. 1.15	
HP	RPM	Armazón	Cat. No.	Armazón	Cat. No.	Armazón	Cat. No.
15	3600	254 TC	30001080	254 JM	30002539	254 TD	*
	1800	254 TC	30001092	2543 JM	30002563	254 TD	*
	1200	284 TC	*	-	-	284 TD	*
	900	286 TC	*	-	-	286 TD	*
20	3600	256 TC	30001127	256 JM	30002540	256 TD	*
	1800	256 TC	30001139	256 JM	30002584	256 TD	*
	1200	286 TC	*	-	-	286 TD	*
	900	324 TC	*	-	-	324 TD	*
25	3600	284 TSC	30007344	284JM	*	284 TSD	*
	1800	284 TC	30007350	284JM	*	284 TD	*
	1200	324 TS	*	-	-	324 TD	*
	900	326TC	*	-	-	326 TD	*
30	3600	286 TSC	30007349	286JM	*	286 TSD	*
	1800	286 TC	30007351	286JM	*	286 TD	*
	1200	326 TC	*	-	-	326 TD	*
	900	364TC	*	-	-	364 TD	*
40	3600	324 TSC	*	324JM	*	324 TD	*
	1800	324 TC	*	324JM	*	324 TD	*
50	3600	326 TSC	*	326JM	*	326 TD	*
	1800	326 TC	*	326JM	*	326 TD	*

- No disponible
* Sobre pedido
Motores con brida C o D de mayor capacidad, favor consultar
Datos sujetos a cambio sin previo aviso

Motores trifásicos jaula de ardilla

Polos conmutables; un devanado, TCCVE; Aisl. F, F.S. 1.15
Construcción horizontal con patas.
Tensión hasta armazón 365T, 220V ó 440V; mayores, 440V. 60Hz.

Par variable

HP Alta vel.	HP Baja vel.	RPM	Arm.	Cat. No.
1	0.25	1800/900	143T	*
1.5	0.37	1800/900	145T	*
2	0.50	1800/900	182T	*
3	0.75	1800/900	184T	*
5	1.2	1800/900	213T	*
7.5	1.9	1800/900	215T	*
10	2.5	1800/900	254T	*
15	3.7	1800/900	256T	*
20	5	1800/900	284T	*
25	6.2	1800/900	286T	*
30	7.5	1800/900	324T	*
40	10	1800/900	326T	*
50	12	1800/900	364T	*
60	15	1800/900	365T	*
75	19	1800/900	405T	*
100	25	1800/900	444T	*
125	31	1800/900	445T	*
150	37	1800/900	447T	*
200	50	1800/900	449T	*

Par constante

HP Alta vel.	HP Baja vel.	RPM	Arm.	Cat. No.
1	0.5	1800/900	145T	*
1.5	0.75	1800/900	182T	*
2	1	1800/900	182T	*
3	1.5	1800/900	184T	*
5	2.5	1800/900	213T	*
7.5	3.7	1800/900	215T	*
10	5	1800/900	254T	*
15	7.5[1)]	1800/900	256T	*
20	10	1800/900	284T	*
25	12.5	1800/900	286T	*
30	15	1800/900	324T	*
40	20	1800/900	326T	*
50	25	1800/900	364T	*
60	30	1800/900	365T	*
75	37.5	1800/900	405T	*
100	50	1800/900	444T	*
125	62.5	1800/900	445T	*
150	75	1800/900	447T	*
200	100	1800/900	449T	*

Diagrama de conexiones; dos velocidades, un solo devanado.

Par variable

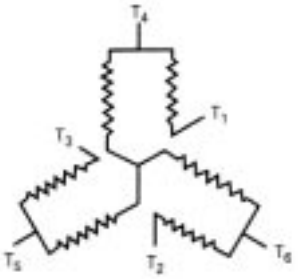

Velocidad	Línea L_1	Línea L_2	Línea L_3		Conexión
Baja	T_1	T_2	T_3	T_4 T_5 T_6 abiertas	Y
Alta	T_6	T_4	T_5	T_1 T_2 T_3 juntas	YY

Par constante

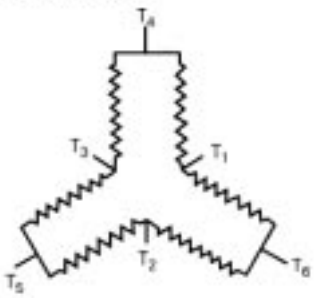

Velocidad	Línea L_1	Línea L_2	Línea L_3		Conexión
Baja	T_1	T_2	T_3	T_4 T_5 T_6 abiertas	Δ
Alta	T_6	T_4	T_5	T_1 T_2 T_3 juntas	YY

1) Aislamiento clase F, F.S. 1.0
*Fabricación sobre pedido

Motores trifásicos jaula de ardilla

Polos conmutables; dos devanados, TCCVE; Aisl. F, F.S. 1.15
Construcción horizontal con patas.
Tensión hasta armazón 365T, 220V ó 440V; mayores 440V, 60Hz.

Par variable

Alta velocidad HP	RPM	Baja velocidad HP1) 1200 RPM	900 RPM	Arm.	Cat. No.
3	1800	1.3	0.75	213T	*
5	1800	2.2	1.2	215T	*
7.5	1800	3.3	1.9	254T	*
10	1800	4.4	2.5	256T	*
15	1800	6.7	3.7	284T	*
20	1800	8.9	5	286T	*
25	1800	11	6.2	324T	*
30	1800	13	7.5	326T	*
40	1800	18	10	364T	*
50	1800	22	13	365T	*
60	1800	27	15	404T	*
75	1800	33	19	405T	*
100	1800	44	25	444T	*
125	1800	55	31	445T	*
150	1800	67	37	447T	*
200	1800	88	50	449T	*

Par constante

Alta velocidad HP	RPM	Baja velocidad HP1) 1200 RPM	900 RPM	Arm.	Cat. No.
3	1800	2	1.5	213T	*
5	1800	3.3	2.5	215T	*
7.5	1800	5[2]	3.7[2]	254T	*
10	1800	6.6[2]	5[2]	256T	*
15	1800	10[2]	7.5[2]	284T	*
20	1800	13[2]	10[2]	286T	*
25	1800	17	12.5	324T	*
30	1800	20[2]	15	326T	*
40	1800	27	20	364T	*
50	1800	33[2]	25	365T	*
60	1800	40	30	404T	*
75	1800	50[2]	37.5	405T	*
100	1800	66	50	444T	*
125	1800	84	62	445T	*
150	1800	100	75	447T	*
200	1800	133	100	449T	*

Diagrama de conexiones; dos velocidades, devanados separados.

Par variable o par constante

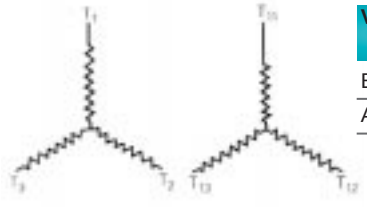

Velocidad	Línea L_1	L_2	L_3	Abierto	Conexión
Baja	T_1	T_2	T_3	T_{11} T_{12} T_{13}	Y
Alta	T_{11}	T_{12}	T_{13}	T_1 T_2 T_3	Y

Polos conmutables, conexión Dahlander, 4/2 polos, 220V ó 440V.
Construcción horizontal con patas, TCCVE, 60 Hz.

HP Baja velocidad	Alta velocidad	RPM	Armazón	Cat. No.
0.50	0.75	1800/3600	143T	*
0.75	1.0	1800/3600	143T	*
1.0	1.5	1800/3600	145T	*
1.5	2.0	1800/3600	145T	*
2	3	1800/3600	182T	*
3	5	1800/3600	184T	*
5	7.5	1800/3600	213T	*
7.5	10	1800/3600	215T	*
10	15	1800/3600	254T	*
15	20	1800/3600	256T	*

1) Sólo una de las velocidades 1200 RPM ó 900 RPM puede ser seleccionada
2) Aislamiento clase F, F.S. 1.0
*Fabricación sobre pedido

Motores trifásicos jaula de ardilla, verticales flecha hueca tipo1PM (HSRGZ)

Información General

Normas
Nuestros motores verticales flecha hueca cumplen con las normas NMX-J-75 y NEMA-MG-1-1993.

Descripción del motor
Este tipo de motores está destinado a impulsar bombas que imponen altas cargas de empuje axial descendente, como bombas de pozo profundo.

Los motores verticales flecha hueca se pueden utilizar en interior o intemperie, ya que por su diseño totalmente cerrado TCCVE, los bobinados, baleros, estator y rotor están libres de contaminación por polvo, humedad, basura y ataque de roedores, lo que garantiza un funcionamiento confiable y duradero.

Los motores están provistos con brida tipo “P” para montaje al cabezal de la bomba.

La caja de conexiones tiene espacio suficiente para realizar las conexiones de cables de una manera fácil y segura, ya que se cumple el volúmen prescrito en la norma NEMA MG-1-1987.

Aspecto eléctrico: Motor diseño NEMA “B”. El rotor es del tipo jaula de ardilla inyectado con aluminio de alta calidad.

La tensión nominal de operación es de 220/440 Volts a 60 Hz. Para motores hasta 100 HP y 440V, a partir de 125 HP

Protección
Nuestro motor vertical flecha hueca posee un trinquete, mediante el cual se evita un giro opuesto al normal del motor que pueda ocurrir por una conexión eléctrica equivocada o porque el agua que quedó en la columna de la bomba al pararse el motor, tienda a recuperar su nivel normal y esto pueda ocasionar que la flecha de la bomba se destornille.

El trinquete elimina esta posibilidad, al caer uno de los siete pernos alojados en el ventilador de algún canal de la tapa balero exterior y así detener inmediatamente el motor y evitar el peligroso sentido opuesto de giro.

Solamente personal especializado deberá realizar la instalación y acoplamiento de la bomba y motor flecha hueca.

Rodamientos
El sistema de rodamiento lo componen uno o dos baleros de contacto angular montados en el escudo (soporte de carga) y un balero guía montado en la brida. Lo anterior permite una operación suave y silenciosa.

Motores con alto empuje axial
Si no se especifica en el pedido, los motores desde 100 HP hasta 150 HP, se surten de fábrica con un rodamiento tipo 7322 BG para 3200 kg. de empuje axial, cuando el usuario necesite una carga axial mayor (hasta 5500 kg.) se instalara un rodamiento adicional del mismo tipo (7322 BG).

“PR” Protección térmica en rodamiento de carga
Los motores desde armazón 405TP (100HP) están provistos de fábrica con una protección térmica “PR” en los rodamientos de carga, el objeto de esta protección adicional en toda serie de motores es detectar cualquier anomalía durante el funcionamiento.

Mantenimiento

Está reducido a un mínimo de trabajos y costos. Para ello basta seguir las indicaciones dadas en las placas de características y lubricación del motor, sobre todo lo referente al tipo de grasa y el período de reengrase.

Motores verticales flecha hueca, tipo 1PM

Motores verticales flecha hueca 1PM
Datos técnicos

Potencia CP	No. polos	RPM en 60 Hz.	Armazón	Tipo	Cat. No.	Conex.	Aisl. clase	F.S.	Corriente nominal 220 V V	Corriente Amp. 440	Corriente de arranque en % de la corriente nominal	Par nominal en Nm	Par de arranque en % del par nominal	Par máx. en % del par nominal
15	4	1745	254TP	1PM3 254-4YK30	30004387	YY/Y	F	1.15	39	19.5	620	61	180	270
20	4	1740	256TP	1PM3 256-4YK30	30004388	YY/Y	F	1.15	50	25.0	600	82	180	230
25	4	1755	284TP	1PM6 284-4YK30	30004393	DD/D	F	1.15	64	32.0	590	101	165	210
30	4	1755	286TP	1PM6 286-4YK30	30004394	DD/D	F	1.15	77	38.5	590	122	170	215
40	4	1760	324TP	1PM6 324-4YK30	30004568	DD/D	F	1.15	99	49.5	605	162	165	225
50	4	1760	326TP	1PM6 326-4YK30	30004569	DD/D	F	1.15	124	62	600	202	160	220
60	4	1770	364TP	1PM6 364-4YK30	30004570	DD/D	F	1.15	148	74	610	241	160	225
75	4	1770	365TP	1PM6 365-4YK30	30004571	DD/D	F	1.15	182	91	620	302	165	225
100	4	1775	405TP	1PM6 405-4YK30	30004572	DD/D	F	1.15	240	20	625	401	145	220
125	4	1775	444TP	IPM0 444-4YP80	30014391	D	F	1.15	-	-	-	-	-	-
150	4	1775	445TP	IPM0 445-4YP80	30014392	D	F	1.15	-	-	-	-	-	-
200	4	1775	447TP	IPM0 447-4YP80	30014746	D	F	1.15	-	-	-	-	-	-
250	4	1775	449TP	IPM0 449-4YP80	30014747	D	F	1.15	-		-	-	-	-

1) 1N=0.1020 kgf 1Nm=0.1020 kgfm
Nota: También se pueden surtir motores con mayor número de polos en su armazón correspondiente.

Motores verticales flecha hueca, tipo 1PM

Dimensiones
Dimensiones generales en mm/pulg. del motor 1PM

Tipo	Armazón NEMA	Potencia CP 4 polos	AJØ	AKØ	BB min	BD max	BFØ	EO	CD	BV	AF	AG	AB	AC	P	BE	SH	HB	DA	Peso aprox. Kg.
1PM3	254TP	15	231.77 9.125”	209.55 8.25”	4.83 0.19”	254 10”	11.18 0.44”	115.6 4.5”	565 22.25”	223.5 8.8”	115 4.53”	681 26.8”	235 9.25”	194 7.64”	318 12.5”	16 0.63”	34.92 1.375”	163 6.4”	7 0.275”	135
1PM3	256TP	20	231.77 9.125”	209.55 8.25”	4.83 0.19”	254 10”	11.18 0.44”	115.6 4.5”	608 23.95”	243.8 9.6”	115 4.53”	724 28.5”	235 9.25”	194 7.64”	318 12.5”	16 0.63”	34.92 1.375”	183 7.2”	7 0.275”	162
1PM6	284TP	25	231.77 9.125”	209.55 8.25”	4.83 0.19”	254 10”	11.18 0.44”	144 5.7”	631 24.8”	153 6”	209 8.2”	775 30.5”	284 11.2”	233 9.2”	359 14.1”	16 0.63”	34.92 1.375”	67 2.6”	7 0.275”	200
1PM6	286TP	30	231.77 9.125”	209.55 8.25”	4.83 0.19”	254 10”	11.18 0.44”	144 5.7”	631 24.8”	153 6”	209 8.2”	775 30.5”	284 11.2”	233 9.2”	359 14.1”	16 0.63”	34.92 1.375”	67 2.6”	7 0.275”	214
1PM6	324TP	40	374.65 14.75”	342.9 13.50”	6.35 0.25”	419.1 16.5”	17.53 0.69”	105 4.1”	723 28.5”	178 7”	246 9.7”	828 32.6”	318 12.5”	259 10.2”	401 15.8”	22 0.87”	47.62 1.875”	7.8 3.1”	7 0.275”	285
1PM6	326TP	50	374.65 14.74”	342.9 13.50”	6.35 0.25”	419.1 16.5”	17.53 0.69”	105 4.1”	723 28.5”	178 7”	246 9.7”	828 32.6”	318 12.5”	259 10.2”	401 15.8”	22 0.87”	47.62 1.875”	7.8 3.1”	7 0.275”	300
1PM6	364TP	60	374.65 14.75”	342.9 13.50”	6.35 0.25”	419.1 16.5”	17.53 0.69”	116 4.6”	838 33.0”	207 8.1”	293 11.5”	293 11.5”	389 15.3”	306 12.1”	449 17.7”	23 0.91”	47.62 1.875”	31 1.2”	7 0.275”	415
1PM6	365TP	75	374.65 14.74”	342.9 13.50”	6.35 0.25”	419.1 16.5”	17.53 0.69”	116 4.6”	838 33.0”	207 8.1”	293 11.5”	293 11.5”	389 15.3”	306 12.1”	449 17.7”	23 0.91”	47.62 1.875”	31 1.2”	7 0.275”	455
1PM6	405TP	100	374.65 14.75”	342.9 13.50”	6.35 0.25”	419.1 16.5”	17.53 0.69”	161 6.3”	932 36.7”	216 8.5”	293 11.5”	293 11.5”	434 17”	351 13.9”	502 19.8”	24 0.94”	50.8 2”	40 1.6”	7 0.275”	615

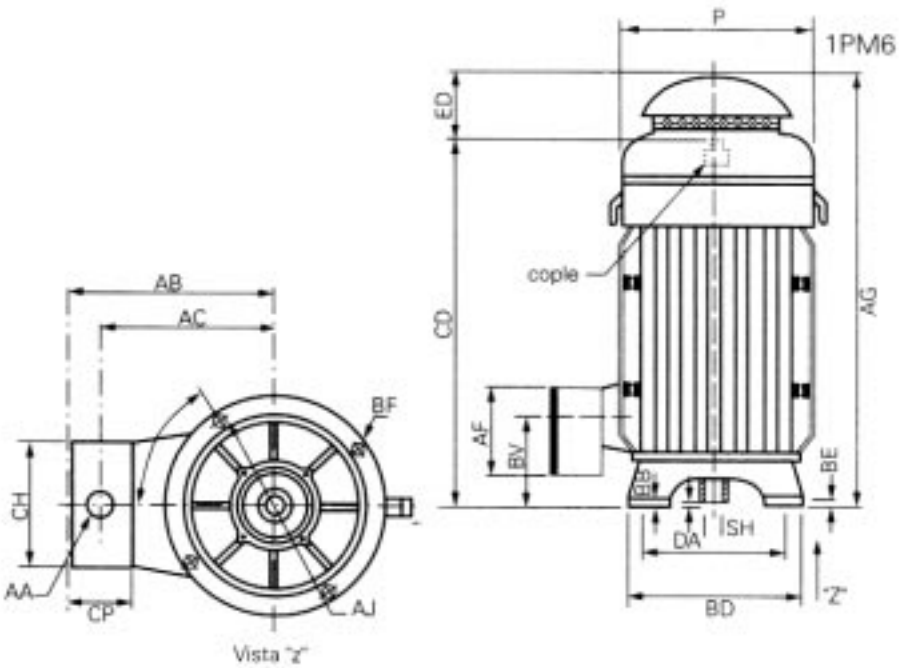

Motores verticales flecha hueca, tipo 1 PM

Dimensiones
Dimensiones generales en mm/pulg. del motor 1PM

Tipo	Armazón NEMA	Potencia CP 4 polos	Copla BZØ	A	XB	BY	Caja de conexiones CH	AAØ	CP	Empuje axial máx en kg. 1 balero lado carga	2 balero lado carga
1PM3	254TP	15	34.92 1.375”	57 2.24”	55 2.17”	10-32 NF	142 5.59”	1 1/4” -11 1/2 NPT	76 2.99”	1140	-
1PM3	256TP	20	34.92 1.375”	57 2.24”	55 2.17”	10-32 NF	142 5.59”	1 1/4” -11 1/2 NPT	76 2.99”	1140	-
1PM6	284T	25	34.92 1.375”	64 2.52”	55 2.17”	10-32 NF	174 6.8”	1 1/2” -11 1/2 NPT	93 3.7”	1600	-
1PM6	286TP	30	34.92 1.375”	64 2.52”	55 2.17”	10-32 NF	174 6.8”	1 1/2” -11 1/2 NPT	93 3.7”	1600	-
1PM6	324TP	40	44.45 1.750	73 2.87”	85 3.35”	1/4”-20 NF	200 7.9”	2”-11 1/2 NPT	112 4.4”	2100	-
1PM6	326TP	50	44.45 1.750	73 2.87”	85 3.35”	1/4”-20 NF	200 7.9”	2”-11 1/2 NPT	112 4.4”	2100	-
1PM6	364TP	60	44.45 1.750	73 2.87”	85 3.35”	1/4”-20 NF	234 9.2”	3”-8 NPT	158 6.2”	2800	-
1PM6	365TP	75	44.45 1.750	73 2.87”	85 3.35”	1/4”-20 NF	234 9.2”	3”-8 NPT	158 6.2”	2800	-
1PM6	405TP	100	53.97 2.125	73 2.87”	85 3.35	1/4”-20 NF	234 9.2”	3”-8 NPT	158 6.2”	3200	5500”

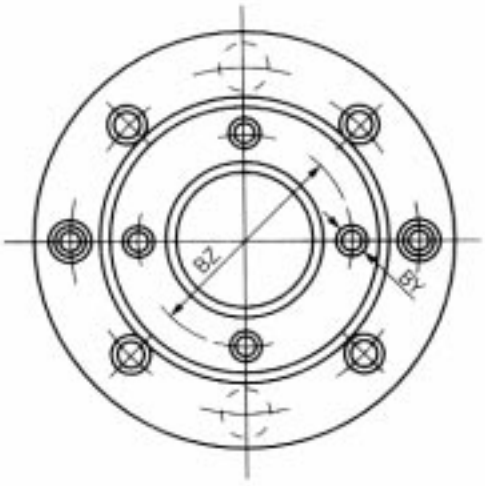

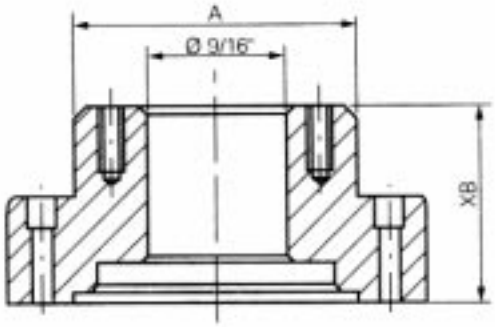

1) Opcional
* También se pueden surtir motores con mayor número de polos en su armazón correspondiente.

Motores trifásicos armazón 56

Complemento de tipos

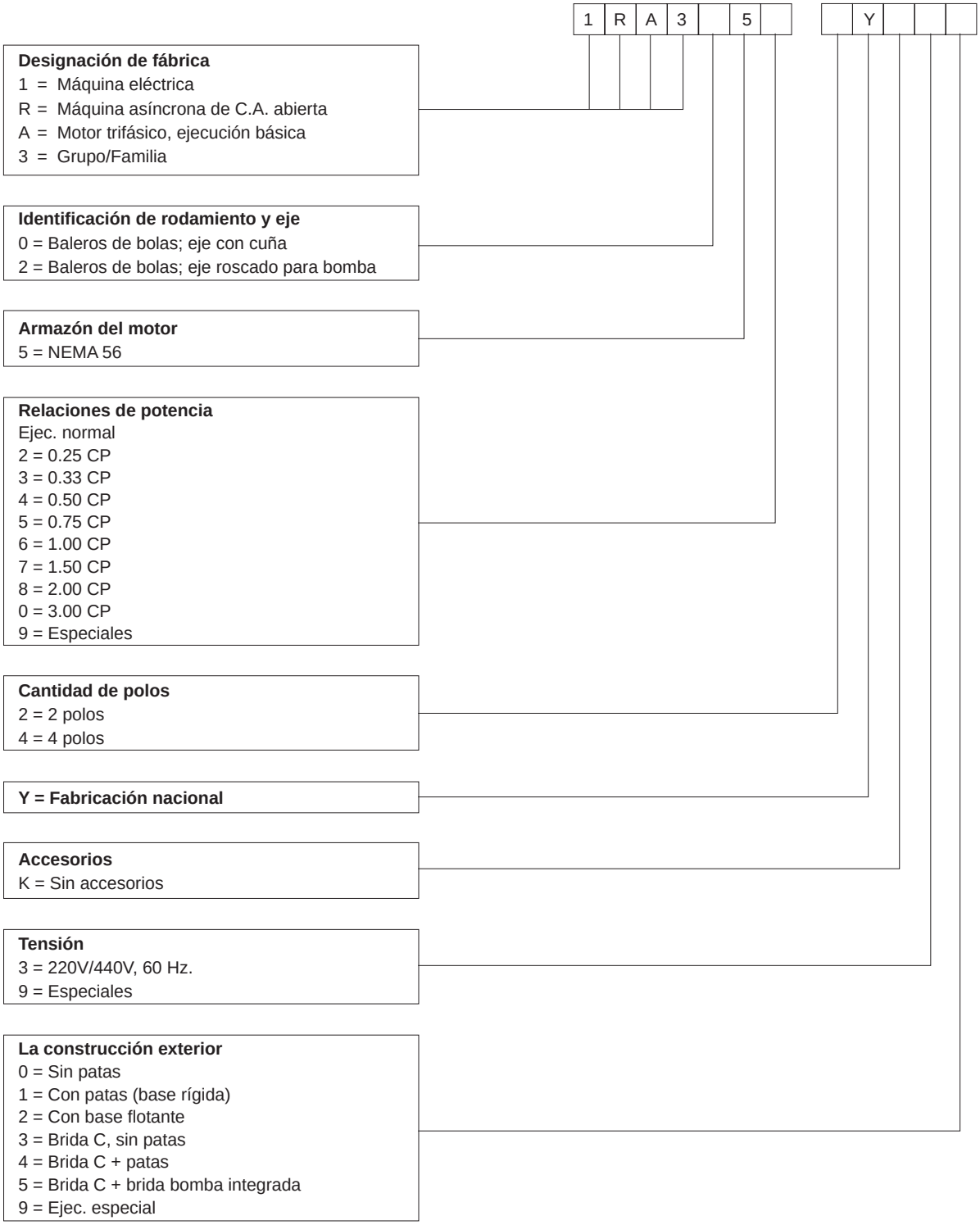

Motores trifásicos armazón 56

Tabla de selección
Motores trifásicos jaula de ardilla a prueba de goteo 220/440 V, 60 Hz, conexión YY/Y, aisl. clase B

Potencia CP	Tipo	Catálogo No.	Velocidad nominal RPM	Corriente nominal Amp 220V	440V	Corriente de arranque en % de la corriente nominal	Par nominal Nm	Par de arranque en % del par nominal	Par máx en % del par nominal	Factor de servicio	Peso neto aprox. Kg	Long. L mm
2 polos, base rígida, brida C y flecha roscada (bomba)												
0.25	1RA3 252-2YK34	30002007	3440	1.0	0.5	450	0.52	230	550	1.5	6.8	284
0.33	1RA3 253-2YK34	30002011	3425	1.4	0.7	470	0.69	250	500	1.35	7.0	284
0.50	1RA3 254-2YK34	30002015	3410	1.9	0.9	480	1.04	290	430	1.25	7.4	284
0.75	1RA3 255-2YK34	30002019	3470	2.5	1.3	540	1.54	190	420	1.25	7.9	284
1.0	1RA3 256-2YK34	30002023	3465	3.2	1.6	570	2.06	200	380	1.25	8.9	304
1.5	1RA3 257-2YK34	30002027	3470	4.4	2.2	610	3.08	225	360	1.15	11.5	326
2	1RA3 258-2YK34	30002031	3440	5.7	2.9	610	4.14	260	320	1.15	12.0	326
3	1RA3 250-2YK34	30002005	3450	8.4	4.2	650	6.19	290	300	1.15	14.9	346
2 polos, base rígida, rígida (uso general)												
0.25	1RA3 052-2YK31	30001990	3440	1.0	0.5	450	0.52	230	550	1.5	6.8	278
0.33	1RA3 053-2YK31	30001992	3425	1.4	0.7	470	0.69	250	500	1.35	7.0	278
0.50	1RA3 054-2YK31	30001994	3410	1.9	0.9	480	1.04	290	430	1.25	7.4	278
0.75	1RA3 055-2YK31	30001996	3470	2.5	1.3	540	1.54	190	420	1.25	7.9	278
1.0	1RA3 056-2YK31	30001998	3465	3.2	1.6	570	2.06	200	380	1.25	8.9	298
1.5	1RA3 057-2YK31	30000092	3470	4.4	2.2	610	3.08	225	360	1.15	11.5	320
2.0	1RA3 058-2YK31	30002002	3440	5.7	2.9	610	4.14	260	320	1.15	12.0	320
4 polos, base rígida, rígida (uso general)												
0.25	1RA3 052-4YK31	30001991	1740	1.4	0.7	360	1.02	220	340	1.35	6.3	261
0.33	1RA3 053-4YK31	30001993	1750	1.6	0.8	410	1.36	200	345	1.35	7.7	278
0.50	1RA3 054-4YK31	30001995	1730	2.1	1.1	415	2.06	195	320	1.25	7.9	278
0.75	1RA3 055-4YK31	30001997	1730	3.0	1.5	440	3.10	195	285	1.25	8.6	278
1.0	1RA3 056-4YK31	30001999	1730	4.2	2.1	570	4.1	330	400	1.15	11.0	298
1.5	1RA3 057-4YK31	30002001	1720	5.4	2.7	640	6.2	350	350	1.15	12.5	320
2.0	1RA3 058-4YK31	*	1715	7.0	3.5	640	8.3	350	360	1.15	15.6	340

* Favor de consultar

Motores trifásicos armazón 56

Tabla de selección
Motores trifásicos jaula de ardilla a prueba de goteo 220/440 V, 60 Hz, conexión YY/Y, aisl. clase B

Motor brida "C" con patas (bomba)

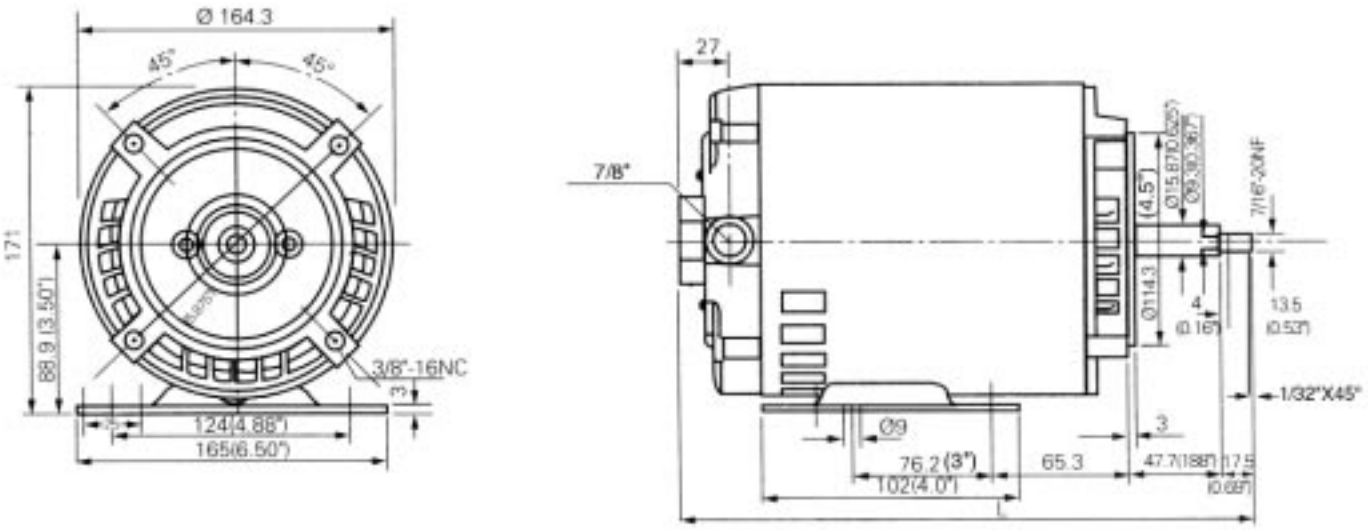

Motor para usos generales

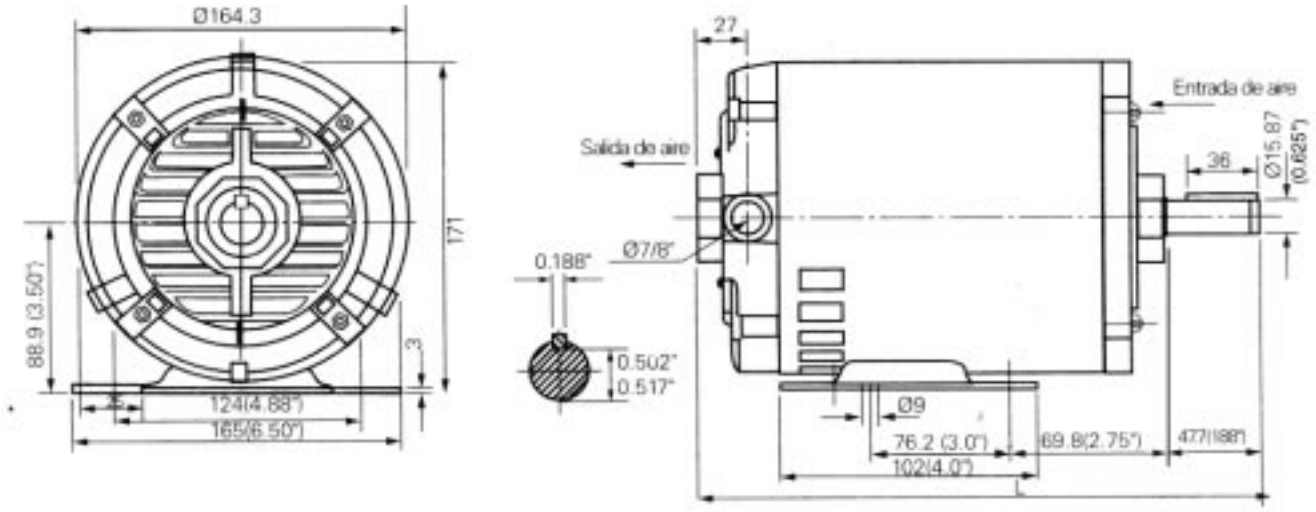

L = Ver última columna en la tabla de selección

Motores trifásicos

Datos característicos típicos
Eficiencia estándar, totalmente cerrados (TCCVE)
Tipos RGZ, RGZSD y RGZZSD
440V 60 Hz. Diseño NEMA B, 40°C ambiente

HP	RPM sincrona	RPM asincrona	Armazón	Corriente (A) en vacio	Corriente (A) plena carga	Corriente (A) arranque	Eficiencia nominal % 1/2	Eficiencia nominal % 3/4	Eficiencia nominal % plena carga	Factor de potencia 1/2	Factor de potencia 3/4	Factor de potencia plena carga	Par Nom. (Nm)	Par Rotor Bloq. %	Par Máx %	Conexión
0.5	900	845	143T		1.1	4.1	59.0	63.0	64.0	0.49	0.61	0.69	4.2	200	240	Y
0.75	1800	1740	143T		1.2	7.6	72.4	75.5	75.5	0.59	0.71	0.81	3.1	260	290	Y
0.75	1200	1155	143T		1.6	6.6	69.8	74.0	74.0	0.44	0.54	0.62	4.8	220	250	Y
0.75	900	855	145T		1.7	5.6	67.8	70.9	72.0	0.42	0.52	0.60	6.3	210	290	Y
1	3600	3455	143T		1.5	8.5	69.8	74.0	74.0	0.78	0.85	0.88	2.1	300	310	Y
1	1800	1745	143T	1.0	1.6	16	73.2	77.5	78.5	0.59	0.71	0.78	4.1	280	300	Y
1	1200	1145	145T	1.2	1.8	16	72.4	75.6	75.5	0.49	0.63	0.72	6.4	200	265	Y
1	900	855	182T	1.3	2.0	16	70.9	74.9	74.0	0.45	0.58	0.66	8.3	185	260	Y
1.5	3600	3460	143T	1.1	2.0	21	69.9	75.0	77.0	0.8	0.9	0.95	3.1	195	275	Y
1.5	1800	1730	145T	1.7	2.4	21	74.8	79.2	80.0	0.54	0.68	0.77	6.2	275	290	Y
1.5	1200	1140	182T	1.4	2.5	21	77.7	78.4	78.5	0.59	0.7	0.75	9.4	170	260	Y
1.5	900	855	184T	2.1	2.6	21	75.5	75.5	75.5	0.5	0.64	0.75	12.5	190	250	Y
2	3600	3450	145T	1.3	2.6	26	74.5	78.8	80.0	0.79	0.89	0.94	4.1	190	260	Y
2	1800	1730	145T	2.1	3.0	26	76.9	80.9	81.5	0.58	0.72	0.80	8.3	270	285	Y
2	1200	1140	184T	1.7	3.1	26	79.1	81.5	80.0	0.61	0.71	0.79	12.5	170	245	Y
2	900	865	213T	2.4	3.4	26	72.0	75.1	75.5	0.52	0.66	0.76	16.7	200	250	Y
3	3600	3485	182T	1.7	4.2	33	76.8	80.6	81.5	0.72	0.81	0.86	6.1	190	250	Y
3	1800	1725	182T	2.0	4.2	33	82.4	82.9	81.5	0.68	0.79	0.86	12.4	220	280	Y
3	1200	1160	213T	2.1	4.3	33	80.0	82.3	82.5	0.67	0.76	0.83	18.4	165	240	Y
3	900	865	215T	2.1	4.8	33	75.0	78.1	78.5	0.55	0.69	0.78	25	155	230	Y
5	3600	3475	184T	2.0	6.3	48	78.4	81.4	82.5	0.84	0.9	0.94	10.2	185	240	Y
5	1800	1715	184T	2.9	6.8	48	84.2	85.2	84.0	0.71	0.8	0.86	20.9	200	270	Y
5	1200	1155	215T	4.0	6.9	48	81.9	84.3	84.0	0.65	0.76	0.84	30.8	160	235	Y
5	900	865	254T	5.1	8.0	48	79.8	82.3	82.5	0.51	0.65	0.74	41.2	190	250	Y
7.5	3600	3500	213T	3.9	10	66	76.2	82.7	84.0	0.75	0.82	0.87	15.3	165	240	Y
7.5	1800	1745	213T	4.6	10	66	86.0	87.1	86.5	0.68	0.79	0.84	30.8	195	270	Y
7.5	1200	1170	254T	5.9	11	66	85.3	86.9	86.5	0.59	0.71	0.77	45.9	160	225	Y
7.5	900	855	256T	6.6	12	66	85.1	86.2	85.5	0.52	0.65	0.73	62.5	170	250	Y
10	3600	3490	215T	3.6	12	85	83.7	85.0	85.5	0.86	0.89	0.92	20.4	160	235	Y
10	1800	1745	215T	5.5	13	85	87.1	88.2	86.5	0.78	0.83	0.87	41.1	190	260	Y
10	1200	1165	256T	6.4	14	85	86.1	87.3	86.5	0.66	0.78	0.82	61.4	160	220	Y
10	900	875	284T	7.8	17	85	87.0	87.3	86.5	0.51	0.62	0.67	83.0	140	210	Y
15	3600	3515	254T	3.6	19	121	85.5	87.1	87.5	0.85	0.88	0.88	30.4	150	235	Y
15	1800	1755	254T	6.4	21	121	88.2	88.7	87.5	0.72	0.78	0.80	61.1	175	255	Y
15	1200	1170	284T	11.5	23	121	86.9	87.7	87.5	0.57	0.67	0.73	92	155	220	Δ
15	900	875	286T	12.5	24	121	85.1	87.3	87.5	0.53	0.64	0.7	123	160	210	Δ
20	3600	3515	256T	3.7	26	152	86.5	87.7	87.5	0.81	0.87	0.88	40.6	140	230	Y
20	1800	1750	256T	7.1	27	152	89.3	89.5	88.5	0.73	0.79	0.82	81.4	170	240	Y
20	1200	1170	286T	15	31	152	88.1	88.8	88.5	0.6	0.69	0.73	122	150	220	Δ
20	900	880	324T	15	32	152	88.2	89.0	88.5	0.58	0.63	0.68	164	130	210	Δ
25	3600	3525	284 TS	9.9	31	191	88.0	88.7	88.5	0.8	0.86	0.88	50	135	225	Δ
25	1800	1760	284 T	9.9	33	191	90.3	90.6	89.5	0.73	0.79	0.82	102	170	235	Δ
25	1200	1175	324 T	17	35	191	89.4	90.1	88.5	0.67	0.75	0.78	152	150	205	Δ
25	900	880	326 T	18	41	191	87.4	88.7	88.5	0.54	0.74	0.68	203	150	200	Δ

Datos sujetos a cambio sin previo aviso

HP	RPM sincrona	RPM asincrona	Armazón	Corriente (A) en vacio	Corriente (A) plena carga	Corriente (A) arranque	Eficiencia nominal % 1/2	Eficiencia nominal % 3/4	Eficiencia nominal % plena carga	Factor de potencia 1/2	Factor de potencia 3/4	Factor de potencia plena carga	Par Nom. (Nm)	Par Rotor Bloq.	Par Máx	Conexión
30	3600	3525	286 TS	11.5	36	228	88.7	89.5	89.5	0.8	0.86	0.87	61	135	225	Δ
30	1800	1765	286 T	11.5	38	228	90.7	91.0	90.2	0.77	0.83	0.86	122	170	235	Δ
30	1200	1175	326 T	19	42	228	90.0	90.7	89.5	0.71	0.78	0.79	182	150	210	Δ
30	900	885	364 T	25	49	228	87.3	88.7	88.5	0.53	0.63	0.68	243	150	200	Δ
40	3600	3530	324 TS	16	49	303	86.5	88.4	89.5	0.83	0.88	0.89	81	130	220	Δ
40	1800	1770	324 T	16	51	303	91.7	92.0	91.0	0.76	0.8	0.84	161	165	225	Δ
40	1200	1180	364 T	23	56	303	89.9	90.8	90.2	0.64	0.74	0.78	241	150	210	Δ
40	900	885	365 T	26	66	303	89.0	90.5	90.2	0.57	0.63	0.66	325	130	200	Δ
50	3600	3530	326 TS	19	62	380	88.4	90.2	91.0	0.83	0.87	0.87	126	130	220	Δ
50	1800	1770	326 T	20	63	380	92.3	92.7	91.7	0.78	0.84	0.85	202	165	225	Δ
50	1200	1180	365 T	28	71	380	89.7	90.5	90.2	0.64	0.74	0.78	302	150	210	Δ
50	900	880	404 T	21	72	380	92.1	92.4	91.7	0.6	0.7	0.74	404	130	220	Δ
60	3600	3530	364 TS	20	72	455	90.7	91.1	91.0	0.84	0.88	0.9	120	130	210	Δ
60	1800	1770	364 T	31	77	455	91.1	91.7	91.7	0.76	0.82	0.84	241	150	220	Δ
60	1200	1180	404 T	26	79	455	90.8	90.8	90.2	0.69	0.75	0.82	362	150	210	Δ
60	900	880	405 T	21	84	455	92.1	92.2	91.7	0.71	0.71	0.76	485	130	200	Δ
75	3600	3530	365 TS	23	89	567	91.3	91.6	91.7	0.85	0.89	0.9	150	120	210	Δ
75	1800	1770	365 T	33	92	567	91.8	91.7	91.7	0.83	0.87	0.87	301	150	210	Δ
75	1200	1180	405 T	31	94	567	92.3	92.3	91.7	0.75	0.83	0.85	453	150	210	Δ
100	3600	3550	405 TS	24	117	758	91.7	92.5	92.4	0.82	0.86	0.91	200	115	210	Δ
100	1800	1775	405 T	36	123	758	92.0	92.7	92.4	0.81	0.85	0.86	401	140	210	Δ

Datos sujetos a cambio sin previo aviso

Motores trifásicos

Datos característicos típicos
Alta eficiencia, totalmente cerrados (TCCVE)
Tipos RGZE, RGZESD, RGZZESD
440V 60 Hz. Diseño NEMA B, 40*C ambiente

HP	RPM sincrona	RPM asincrona	Armazón	Corriente (A) en vacio	Corriente (A) plena carga	Corriente (A) arranque	Letra de código	Eficiencia nominal % 1/2	Eficiencia nominal % 3/4	Eficiencia nominal % plena carga	Factor de potencia % 1/2	Factor de potencia % 3/4	Factor de potencia % plena carga	Par Nom. lb-pie	Par Rotor Bloq. %	Par Máx %	Conexión
1	3600	3490	143T	0.8	1.4	12	K	73.7	78.3	80.0	77	86	90	1.5	280	340	Y
1	1800	1745	143T	1.2	1.6	12	K	78.7	81.8	82.5	52	66	76	3.0	90	320	Y
1	1200	1140	145T	1.4	1.9	9	J	76.4	78.8	80.0	42	56	62	4.6	230	290	Y
1	900	860	182T	1.3	2.0	8	H	76.6	78.9	78.5	42	54	63	6.1	220	260	Y
1.5	3600	3485	143T	0.9	2.1	17	K	78.0	82.0	82.5	69	79	85	2.3	270	320	Y
1.5	1800	1740	145T	1.5	2.3	18	K	80.7	83.5	84.0	54	67	76	4.5	290	320	Y
1.5	1200	1160	182T	1.6	2.4	17	K	81.6	84.2	85.5	50	63	71	6.8	280	320	Y
1.5	900	855	184T	1.9	2.7	14	H	78.0	80.4	80.0	45	58	68	9.2	220	270	Y
2	3600	3495	145T	1.2	2.6	23	K	79.9	83.2	84.0	73	83	89	3.0	270	320	Y
2	1800	1735	145T	2.0	3.0	22	K	80.7	83.6	84.0	52	67	77	6.1	290	310	Y
2	1200	1160	184T	2.0	3.1	23	K	84.5	86.0	86.5	50	63	72	9.1	220	300	Y
2	900	865	213T	23	3.5	18	H	80.0	82.0	82.5	46	60	69	12	200	290	Y
3	3600	3510	182T	1.8	3.8	33	K	83.8	86.2	86.5	75	84	90	4.5	230	320	Y
3	1800	1740	182T	1.9	4.1	31	K	87.5	88.0	87.5	65	76	82	9.1	260	300	Y
3	1200	1165	213T	2.4	4.2	33	K	85.8	87.6	87.5	58	73	80	14	210	300	Y
3	900	865	215T	3.2	4.9	27	H	82.5	84.2	84.0	48	62	71	18	190	280	Y
5	3600	3490	184T	1.9	6.1	48	J	86.5	87.8	87.5	82	89	92	7.5	260	320	Y
5	1800	1730	184T	3.3	6.8	48	J	87.5	88.2	87.5	63	75	82	15	260	300	Y
5	1200	1160	215T	3.5	7.1	48	J	89.0	89.7	88.5	59	71	78	23	210	300	Y
5	900	865	254T	4.3	7.8	42	H	86.0	87.0	86.5	53	66	72	30	180	260	Y
7.5	3600	3515	213T	3.6	9.2	67	H	87.0	88.0	88.5	77	86	90	11	190	280	Y
7.5	1800	1750	213T	4.4	9.9	67	H	89.0	90.0	89.5	66	77	93	23	210	270	Y
7.5	1200	1170	254T	4.7	10	63	H	90.6	90.9	90.2	59	72	78	34	180	250	Y
7.5	900	865	256T	6.9	13	67	H	87.0	88.0	87.5	49	61	69	46	190	260	Y
10	3600	3505	215T	4.2	13	85	H	89.0	89.8	89.5	80	89	87	15	190	260	Y
10	1800	1750	215T	5.6	14	85	H	89.5	90.0	89.5	68	79	84	30	210	270	Y
10	1200	1165	256T	5.2	14	78	G	91.7	91.5	90.2	65	75	80	45	170	250	Y
10	900	875	284T	9.5	16	85	H	89.4	90.9	91.0	50	61	69	60	150	220	Δ
15	3600	3530	254T	5.2	18	121	G	88.5	90.0	90.2	84	98	92	22	190	260	Y
15	1800	1760	254T	7.6	20	121	G	91.7	92.1	91.7	68	78	82	45	190	260	Y
15	1200	1175	284T	10	21	121	G	91.0	91.7	91.0	57	71	77	67	160	270	Δ
15	900	875	286T	15	24	121	G	90.1	91.4	91.0	50	60	67	90	150	220	Δ
20	3600	3525	256T	7.7	24	152	G	88.3	89.9	90.2	82	86	90	30	180	260	Y
20	1800	1755	256T	9.5	27	152	G	92.1	92.4	91.7	67	76	80	60	190	270	Y
20	1200	1175	286T	13	27	152	G	92.1	92.4	91.7	62	73	79	89	160	250	Δ
20	900	880	324T	19	32	152	G	90.0	91.2	91.0	50	61	67	119	140	200	Δ
25	3600	3525	284TS	8.4	30	191	G	92.0	92.2	91.7	80	85	88	37	160	250	Δ
25	1800	1765	284T	14	30	191	G	93.3	93.6	93.0	72	82	87	74	220	280	Δ
25	1200	1180	324T	26	35	191	G	92.2	92.7	92.4	57	69	77	111	170	240	Δ
25	900	880	326T	23	40	191	G	89.2	90.5	90.2	50	61	68	149	150	200	Δ
30	3600	3525	286TS	9.9	36	228	G	92.0	92.2	91.7	84	89	90	45	160	250	Δ
30	1800	1765	286T	16	37	228	G	93.2	93.6	93.0	71	82	86	89	220	280	Δ
30	1200	1180	326T	20	41	228	G	92.6	92.9	92.4	58	70	78	134	170	240	Δ
30	900	885	364T	27	49	228	G	89.9	91.3	91.0	50	62	66	178	150	200	Δ

Datos sujetos a cambio sin previo aviso

Motores trifásicos

Datos característicos típicos
Eficiencia estándar, totalmente cerrados (TCCVE)
Tipos RGZE, RGZESD y RGZZESD
440V 60 Hz. Diseño NEMA B, 40*C ambiente

HP	RPM sincrona	RPM asincrona	Armazón	Corriente (A) en vacio	plena carga	arranque	Letra de código	Eficiencia nominal % 1/2	3/4	plena carga	Factor de potencia % 1/2	3/4	plena carga	Par Nom. lb-pie	Rotor Bloq. %	Máx %	Conexión
40	3600	3530	324TS	13	47	303	G	94.0	94.1	93.6	80	87	89	60	150	250	Δ
40	1800	1770	324T	16	49	303	G	94.0	94.2	93.6	77	82	76	119	190	240	Δ
40	1200	1180	364T	25	54	303	G	93.6	93.9	93.6	59	71	62	178	170	230	Δ
40	900	885	365T	38	66	303	G	90.7	92.0	91.7	49	60	65	237	150	200	Δ
50	3600	3530	326TS	16	58	380	G	94.1	94.2	93.6	82	89	91	74	150	250	Δ
50	1800	1770	326T	19	61	380	G	94.1	94.2	93.6	77	84	86	148	190	240	Δ
50	1200	1180	365T	31	69	380	G	94.0	94.2	93.6	60	71	76	223	170	230	Δ
50	900	885	404T	29	70	380	G	92.3	92.4	91.7	64	73	76	297	140	200	Δ
60	3600	3565	364TS	20	71	455	G	93.8	94.1	93.6	80	86	88	89	160	250	Δ
60	1800	1775	364T	22	74	455	G	93.9	94.1	93.6	74	82	85	178	160	240	Δ
60	1200	1185	404T	27	77	455	G	94.1	94.5	94.1	70	78	81	266	150	200	Δ
60	900	885	405T	31	82	455	G	92.3	92.4	91.7	67	76	79	356	140	200	Δ
75	3600	3565	365TS	23	89	568	G	94.3	94.5	94.1	81	86	88	111	160	260	Δ
75	1800	1775	365T	28	91	568	G	94.4	94.6	94.1	74	83	85	222	155	240	Δ
75	1200	1185	405T	36	97	568	G	85.8	94.9	94.5	68	77	80	332	150	200	Δ
75	900	885	444T	39	98	568	G	82.5	93.3	93.0	67	76	80	445	135	200	Δ
100	3600	3570	405TS	20	113	758	G	94.6	94.7	94.1	90	92	92	147	120	200	Δ
100	1800	1780	405T	31	118	758	G	95.0	95.2	94.5	80	85	87	295	160	200	Δ
100	1200	1185	444TS	40	122	758	G	94.6	94.9	94.5	75	82	85	443	140	200	Δ
100	900	885	445T	50	129	758	G	94.2	94.5	94.1	70	78	81	593	130	200	Δ
125	3600	3575	444TS	33	144	949	G	94.0	94.6	94.5	85	89	90	184	120	200	Δ
125	1800	1785	444TS	44	150	949	G	95.1	95.3	95.0	78	84	86	368	160	200	Δ
125	1200	1185	445TS	46	151	949	G	94.7	94.9	94.5	77	84	86	554	140	200	Δ
125	900	885	447T	56	159	949	G	94.1	94.2	93.6	70	79	82	742	130	200	Δ
150	3600	3575	445TS	39	171	1134	G	94.8	95.2	95.0	84	89	90	220	120	200	Δ
150	1800	1785	445TS	47	178	1134	G	95.7	96.0	95.8	80	85	86	441	150	200	Δ
150	1200	1185	447TS	47	178	1134	G	95.4	95.6	95.0	81	86	87	665	125	200	Δ
150	900	885	447T	75	194	1134	G	94.1	94.5	94.1	67	76	80	890	130	200	Δ
200	3600	3575	447TS	42	226	1516	G	94.9	95.2	95.0	88	90	91	294	120	200	Δ
200	1800	1785	447TS	63	235	1516	G	96.0	96.1	95.8	81	86	87	588	150	200	Δ
200	1200	1185	449TS	58	236	1516	G	95.4	95.5	95.0	82	86	87	886	125	200	Δ
200	900	885	449T	106	252	1516	G	94.8	94.9	94.5	71	79	82	1186	125	200	Δ
250	3600	3575	449TS	47	279	1908	G	95.3	95.6	95.4	90	92	92	368	120	200	Δ
250	1800	1785	449TS	82	294	1908	G	95.8	96.0	95.8	80	85	87	735	140	180	Δ
250	1200	1185	449TS	78	293	1908	G	95.5	95.5	95.0	82	87	88	1108	120	200	Δ
250	900	885	S449	116	317	1908	G	94.5	94.8	94.5	70	78	82	1483	105	200	Δ
300	3600	3575	449TS	71	338	2300	G	95.2	95.8	95.8	86	90	91	441	100	200	Δ
300	1800	1785	449TS	115	362	2300	G	95.0	95.5	95.4	76	83	85	882	120	200	Δ
300	1200	1185	S449	94	351	2300	G	95.5	95.5	95.0	82	87	88	1329	105	200	Δ
350	3600	3575	S449S	70	386	2666	G	95.4	95.7	95.4	90	92	93	515	80	200	Δ
350	1800	1785	S449	120	408	2666	G	95.5	95.9	95.8	79	86	88	109	100	200	Δ
350	1200	1185	S449	139	413	2666	G	95.2	95.3	95.0	77	84	87	1551	100	200	Δ
400	3600	3570	S449S	84	437	3032	G	94.2	95.6	95.4	90	93	94	588	80	200	Δ
400	1800	1785	S449	144	469	3232	G	95.7	96.0	95.8	79	85	87	1176	100	200	Δ

Datos sujetos a cambio sin previo aviso.

Motores trifásicos con brida C

Dimensiones motores 1LA3 con brida C

Armazón	BD	AJ	AK	U	AH	BA	ES	S	BF#	BF diam.
143TC	6.5	5.875	4.5	0.875	2.125	2.25	1.41	0.188	4	0.375-16 NC
145TC	6.5	5.875	4.5	0.875	2.125	2.25	1.41	0.188	4	0.375-16 NC
182TC	9	7.250	8.5	1.125	2.625	2.75	1.78	0.25	4	0.50-13 NC
184TC	9	7.250	8.5	1.125	2.625	2.75	1.78	0.25	4	0.50-13 NC
182TCH	6.5	5.875	4.5	1.125	2.625	2.75	1.78	0.25	4	0.375-16 NC
184TCH	6.5	5.875	4.5	1.125	2.625	2.75	1.78	0.25	4	0.375-16 NC
213TC	9	7.250	8.5	1.375	3.125	3.5	2.41	0.312	4	0.50-13 NC
215TC	9	7.250	8.5	1.375	3.125	3.5	2.41	0.312	4	0.50-13 NC
254TC	10	7.250	8.8	1.625	3.750	4.25	2.91	0.375	4	0.50-13 NC
256T	10	7.250	8.5	1.625	3.750	4.25	2.91	0.375	4	0.50-13 NC

1) Cuando "AJ" es mayor que "AK" la siguiente figura debe considerarse.

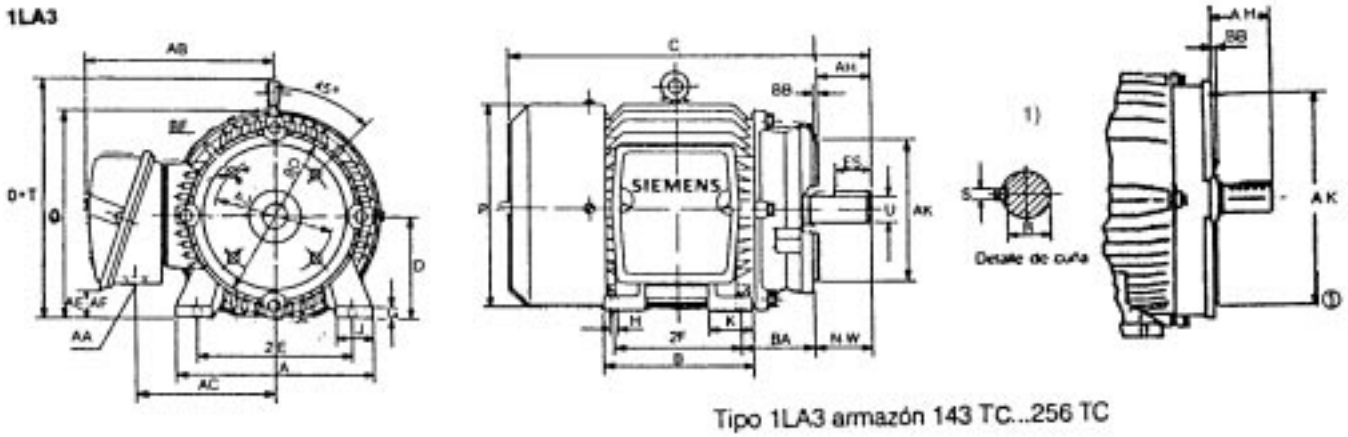

Tipo 1LA3 armazón 143 TC...256 TC

Motores trifásicos con brida C

Dimensiones

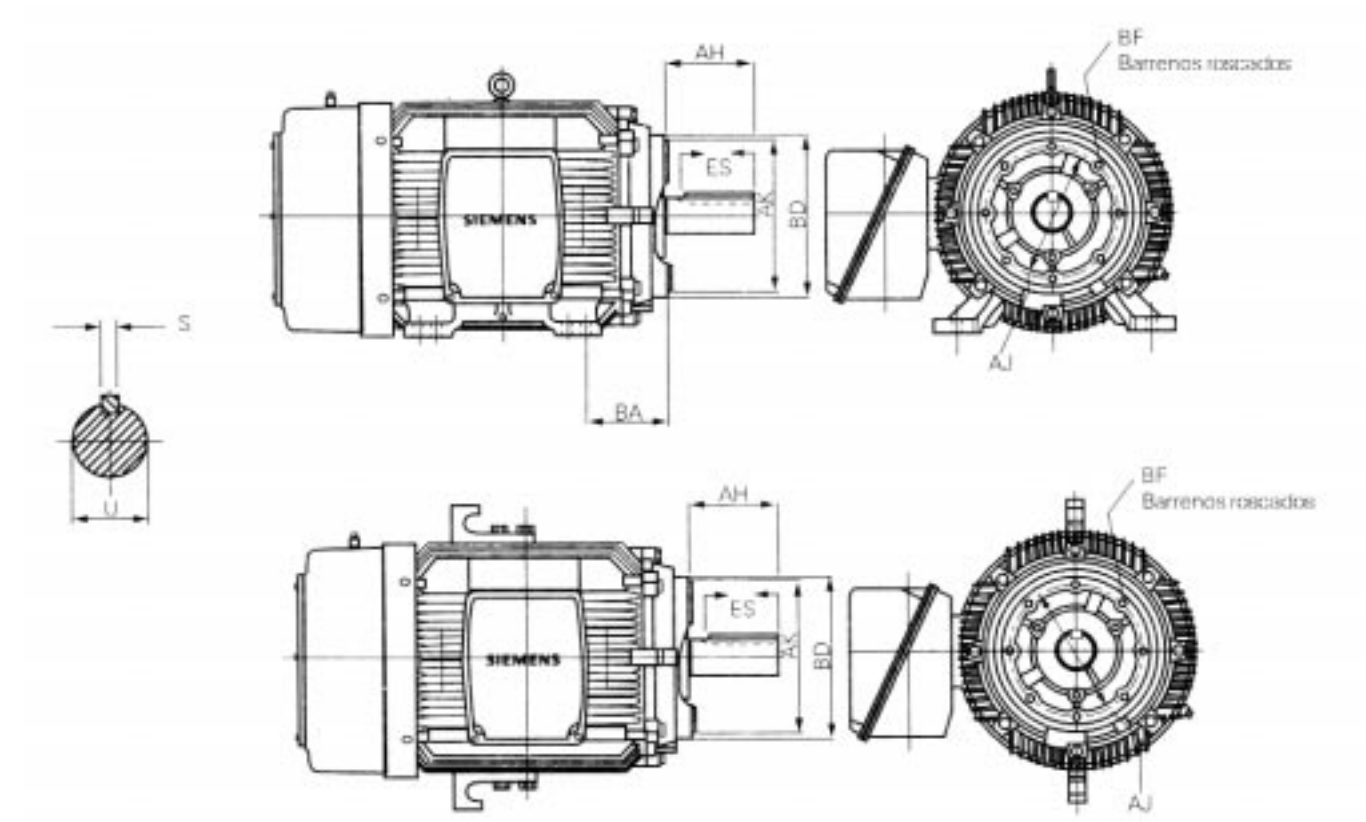

Armazón	BD	AJ	AK	U	AH	BA	ES	S	BF#	BF diam.
284/6TC	10.75	9	10.5	1.875	4.38	4.75	3.25	0.5	4	0.5-13NC
284/6TSC	10.75	9	10.5	1.625	3	4.75	1.88	0.38	4	0.5-13NC
324/6TC	12.75	11	12.5	2.125	5	5.25	3.88	0.5	4	0.625-11NC
324/6TSC	12.75	11	12.5	1.875	3.5	5.25	2	0.5	4	0.625-11NC
364/5TC	12.75	11	12.5	2.375	5.62	5.88	4.25	0.625	4	0.625-11NC
364/5TSC	12.75	11	12.5	1.875	3.5	5.88	2	0.5	4	0.625-11NC
404/5TC	13.5	11	12.5	2.875	7	6.625	5.62	0.75	4	0.625-11NC
404/5TSC	13.5	11	12.5	2.125	4	6.625	2.75	0.5	4	0.625-11NC
444/5TC	16.62	14	16	3.375	8.25	7.5	6.88	0.875	4	0.625-11NC
444/5TSC	16.62	14	16	2.375	4.5	7.5	3	0.625	4	0.625-11NC
447TC	16.62	14	16	3.375	8.25	7.5	6.88	0.875	4	0.625-11NC
447TSC	16.62	14	16	2.375	4.5	7.5	3	0.625	4	0.625-11NC
449TC	16.62	14	16	3.375	8.25	7.5	6.88	0.875	4	0.625-11NC
449TSC	16.62	14	16	2.375	4.5	7.5	3	0.625	4	0.625-11NC

Motores trifásicos con brida D

Dimensiones

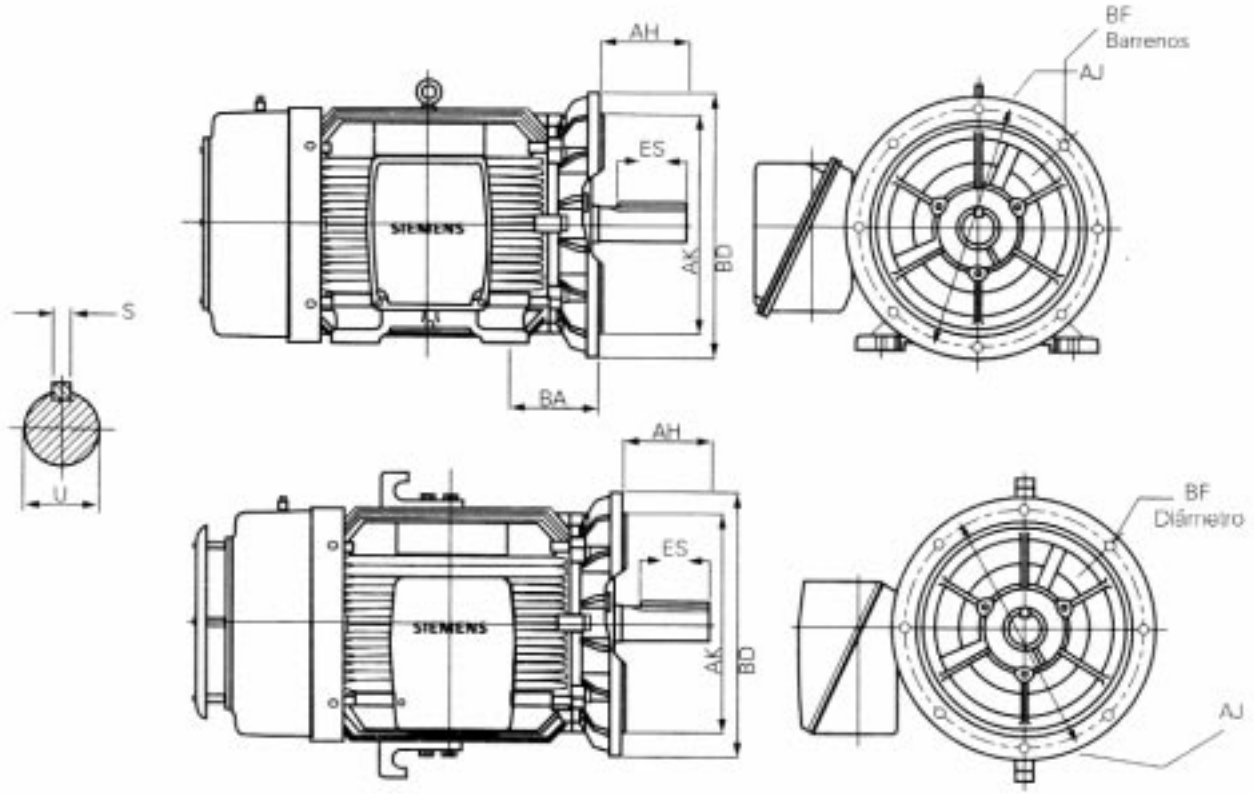

Armazón	BD	AJ	AK	U	AH	BA	ES	S	BF# •	BF DIA
143/5TD	11	10	9	.875	2.25	2.25**	1.41	.188	4	0.531
182/4TD	11	10	9	1.125	2.75	2.75**	1.78	.25	4	0.531
213/5TD	11	10	9	1.375	3.38	3.5**	2.41	.31	4	0.531
254/6TD	14	12.5	11	1.625	4	4.25**	2.91	.375	4	0.813
284/6TD	13.88	12.5	11	1.875	4.62	5.88**	3.25	.50	4	0.813
284/6TSD	13.88	12.5	11	1.625	3.25	5.88**	1.88	.375	4	0.813
324/6TD	17.88	16	14	2.125	5.25	6.25**	3.88	.50	4	0.813
324/6TSD	17.88	16	14	1.875	3.75	6.25**	2	.50	4	0.813
364/5TD	17.88	16	14	2.375	5.88	6.75**	4.25	.62	4	0.813
364/5TSD	17.88	16	14	1.875	3.75	6.75**	2	.50	4	0.813
404/5TD	21.88	20	18	2.875	7.25	7.12**	5.62	.75	8	0.813
404/5TSD	21.88	20	18	2.125	4.25	7.12**	2.75	.50	8	0.813
444/5TD	21.88	20	18	3.375	8.5	8.38**	6.88	.875	8	0.813
444/5TSD	21.88	20	18	2.375	4.75	8.38**	3	.625	8	0.813
447TD	21.88	20	18	3.375	8.5	8.38	6.88	.875	8	0.813
447TSD	21.88	20	18	2.375	4.75	8.38	3	.625	8	0.813
449TD	21.88	20	18	3.375	8.5	8.38	6.88	.875	8	0.813
449TSD	21.88	20	18	2.375	4.75	8.38	3	.625	8	0.813

** Dimension “BA” de 143TD a 445TSD difiere de dimensión NEMA
Todas las dimensiones en pulgadas.
Datos sujetos a cambio sin previo aviso.

Motores trifásicos

Dimensiones

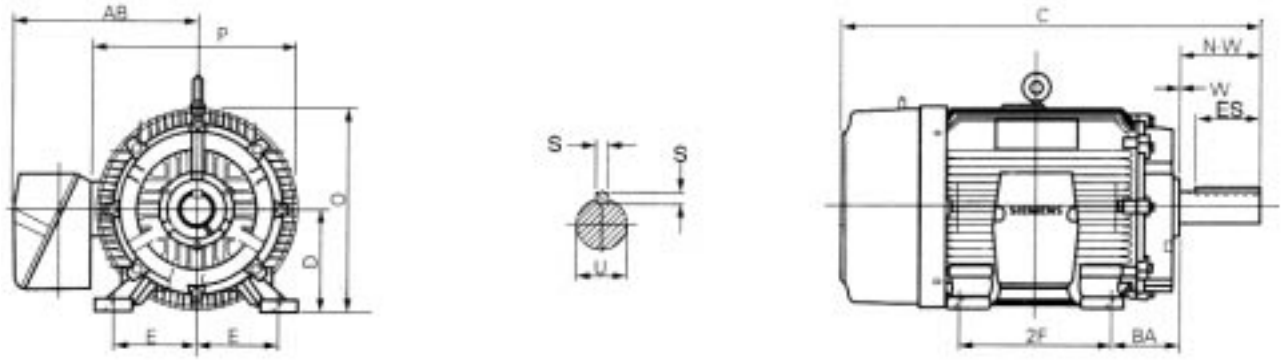

NEMA	S	S	ES	C	D	E	2F	BA	N-W	O	P	W	AB	U	Peso aprox. en lbs. RGZ	RGZZ
143T 145T	.188 .188	.188 .188	1.38 1.38	12.2 13.3	3.50 3.50	2.75 2.75	4 5	2.25 2.25	2.25 2.25	6.93 6.93	7.7 4.7	.13 .13	6.46 6.46	.875 + .0000 - .0005	45 55	65 75
182T 184T	.250 .250	.250 .250	1.75 1.75	14.2 15.2	4.50 4.50	3.75 3.75	4.50 5.50	2.75 2.75	2.75 2.75	8.86 8.86	9.7 9.7	.13 .13	7.36 7.36	1 .125 + .0000 - .0005	85 100	125 130
213T 215T	.313 .313	.313 .313	2.38 2.38	18.0 19.1	5.25 5.25	4.25 4.25	5.50 7	3.50 3.50	3.38 3.38	10.62 1062	11.2 11.2	.13 .13	9.02 9.02	1 .375 + .0000 - .0005	130 162	170 190
254T 256T	.375 .375	.375 .375	2.88 2.88	22.3 24.1	6.25 6.25	5 5	8.25 10	4.25 4.25	4 4	12.62 12.62	13.4 13.4	.13 .13	9.92 9.92	1 .625 + .000 - .001	250 295	290 360
284T 286T	.500 .500	.500 .500	3.25 3.25	28.8 28.8	7 7	5.50 5.50	9.50 11	4.75 4.75	4.63 4.63	14.19 14.19	15.5 15.5	.13 .13	12.94 12.94	1 .875 + .000 - .001	380 450	450 525
284TS 286TS	.375 .375	.375 .375	1.88 1.88	27.5 27.5	7 7	5.50 5.50	9.50 11	4.75 4.75	3.25 3.25	14.19 14.19	15.5 15.5	.13 .13	12.94 12.94	1 .625 + .000 - .001	380 450	450 525
324T 326T	.500 .500	.500 .500	3.88 3.88	32.0 32.0	8 8	6.25 6.25	10.50 12	5.25 5.25	5.25 5.25	15.94 15.94	17.1 17.1	.13 .13	15.75 15.75	2 .125 + .000 - .001	565 600	660 690
324TS 326TS	.500 .500	.500 .500	2 2	30.0 30.0	8 8	6.25 6.25	10.50 12	5.25 5.25	3.75 3.75	15.94 15.94	17.1 17.1	.13 .13	15.75 15.75	1 .875 + .000 - .001	565 600	660 690
364T 365T	.625 .625	.625 .625	4.25 4.25	34.2 34.2	9 9	7 7	11.25 12.25	5.88 5.88	5.88 5.88	17.81 17.81	18.5 18.5	.38 .38	17.69 17.69	2 .375 + .000 - .001	830 850	900 915
364TS 365TS	.500 .500	.500 .500	2 2	32.1 32.1	9 9	7 7	11.25 12.25	5.88 5.88	3.75 3.75	17.81 17.81	18.5 18.5	.38 .38	17.69 17.69	1 .875 + .000 - .001	830 850	900 915
404T 405T	.750 .750	.750 .750	5.63 5.63	39.5 39.5	10 10	8 8	12.25 13.75	6.625 6.625	7.25 7.25	19.90 19.90	19.6 19.6	.13 .13	17.50 17.50	2 .875 + .000 - .001	1100 1250	1290 1420
404TS 405TS	.500 .500	.500 .500	2.75 2.75	36.5 36.5	10 10	8 8	12.25 13.75	6.625 6.625	4.25 4.25	19.90 19.90	19.6 19.6	.13 .13	17.50 17.50	2 .125 + .000 - .001	1100 1250	1290 1420
444T 445T	.875 .875	.875 .875	6.88 6.88	45.6 45.6	11 11	9 9	14.50 16.50	7.50 7.50	8.50 8.50	21.9 21.9	21.7 21.7	.13 .13	19.94 19.94	3 .375 + .000 - .001	1620 1740	1740 1930
444TS 445TS	.625 .625	.625 .625	3 3	41.8 41.8	11 11	9 9	14.50 16.50	7.50 7.50	4.75 4.75	21.9 21.9	21.7 21.7	.13 .13	19.94 19.94	2 .375 + .000 - .001	1620 1740	1740 1930
447T 447TS	.875 .625	.875 .625	6.88 3	49.1 45.4	11 11	9 9	20 20	7.50 7.50	8.50 4.75	21.9 21.9	21.8 21.8	.13 .13	20.12 20.12	3 .375 2 .375	2000 2000	2415 2415
449T 449TS	.875 .625	.875 .625	6.88 3	54.1 50.3	11 11	9 9	25 25	7.50 7.50	8.50 4.75	21.9 21.9	21.8 21.8	.13 .13	20.12 20.12	3 .375 2 .375	2300 2300	2625 2625
S449LS S449SS	.875 .625	.875 .625	7.5 3.5	63.7 59.8	11 11	9 9	25 25	7.50 7.50	9.12 5.25	23.4 23.4	25.4 25.4	.13 .13	23.0 23.0	3 .625 2 .625	3050 3050	- -

Datos sujetos a cambio sin previo aviso.

Motores monofásicos

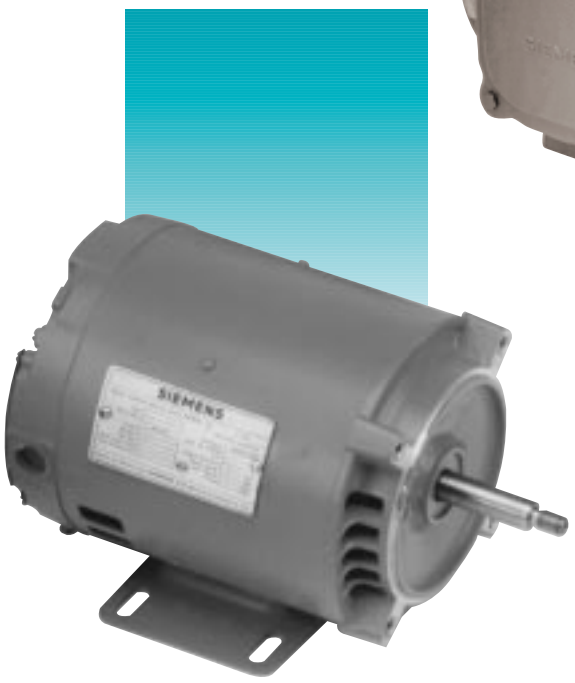

Motores monofásicos armazón 56

Complemento de tipos

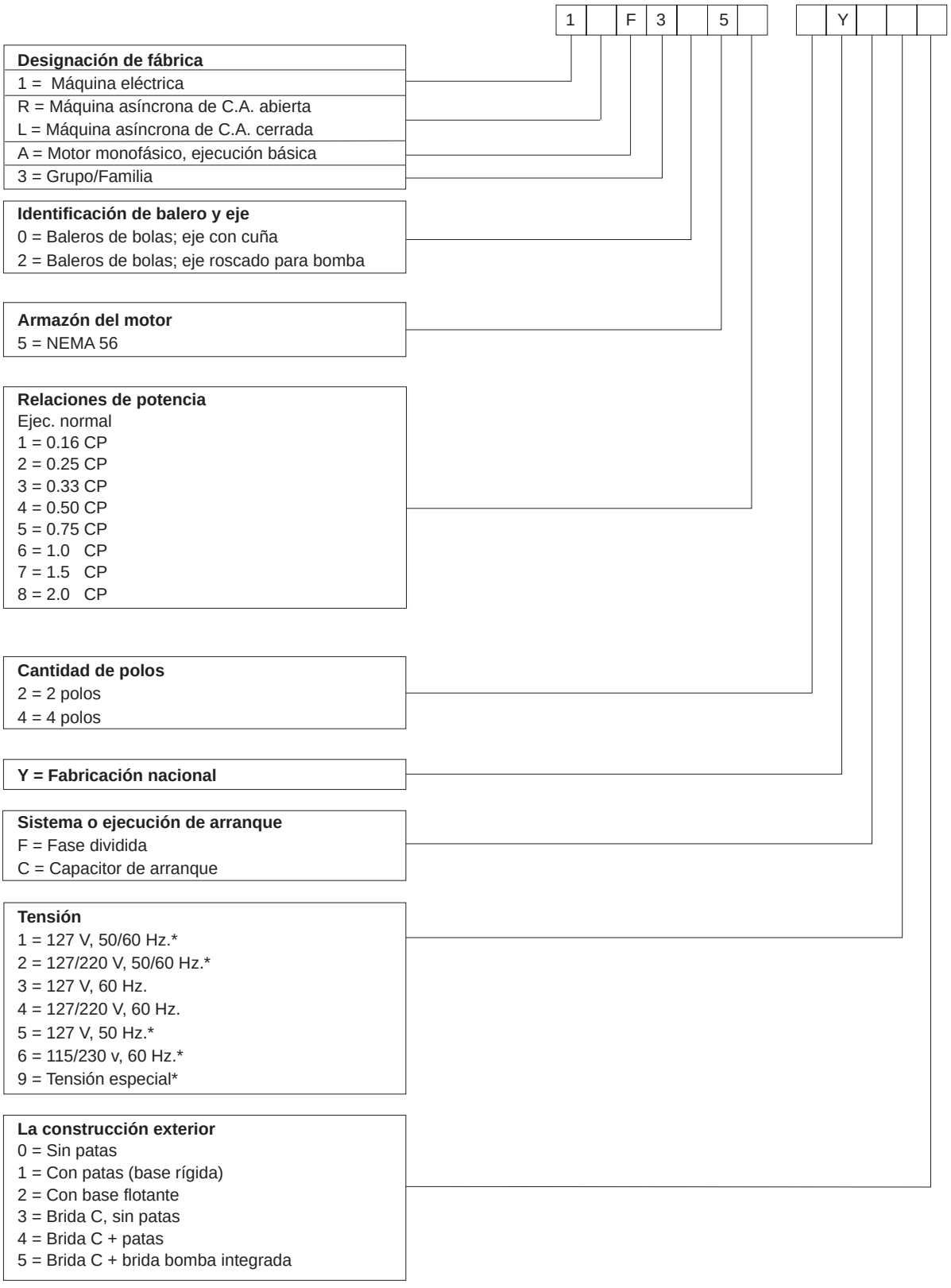

* Precios y tiempo de entrega, favor de consultarnos

Motores monofásicos armazón 56

Información general

Normas
El programa de fabricación de nuestros motores monofásicos en armazón 56 de inducción "jaula de ardilla" cumplen con lo establecido en la publicación NEMA MG-1-1993 y NMX-J-75-1985.

Datos eléctricos
Tensión y frecuencia.
Los motores pueden operarse a plena carga en redes eléctricas, en las que a frecuencia nominal la tension varia ± 10% de la nominal.

Tensiones nominales:
127 V, 60 Hz.
220V, 60 Hz.

Potencia
La potencia nominal y el factor de servicio indicados en las tablas de selección, son válidos para servicio contínuo con tensión y frecuencia nominales, una temperatura ambiente de 40°C y una altura de instalación de hasta 1000 m.s.n.m. ó 33°C a 2400 m.s.n.m.

Conexión a la red
La tablilla de conexiones es de fácil acceso y con terminales claramente identificadas. La placa de características contiene el diagrama de conexión.

Protección eléctrica
Todos los motores hasta 0.75 CP tienen un protector térmico incorporado. Los motores desde 1 CP haste 2 CP, recomendamos protegerlos mediante guardamotores.

Sistemas de arranque
Fabricamos nuestros motores para los sistemas de arranque por capacitor y arranque por fase dividida. En ambos sistemas un microinterruptor encapsulado a prueba de polvo, realiza eficientemente la desconexión del devanado de arranque.

Datos mecánicos
Tipo de montaje.
Para las diversas aplicaciones fabricamos diferentes tipos de montaje:

- Con base rígida.
- Con base flotante.
- Con base rígida, brida "C" y flecha roscada.
- Sin base, brida "C" y flecha roscada.

Sentido de giro
El sentido de giro normal del motor es el de las manecillas del reloj, viendo el motor del lado de la flecha. Para cambiar de rotación basta con intercambiar dos terminales en la tablilla de conexiones. Los motores con brida "C" y flecha roscada se proveen con rotacion fija.

Posición de montaje
Nuestros motores pueden instalarse en posición horizontal o vertical, con la flecha hacia arriba o hacia abajo.

Protección mecanica
La forma de protección de los motores monofásicos en armazón 56 corresponde a la designación: "tipo abierto a prueba de goteo y salpicaduras"

Carcasa y tapas
La carcasa es de lámina de hierro de alta calidad y las tapas de aluminio estan diseñadas para soportar alto esfuerzo mecánico y proporcionar soporte rígido al rotor.

Rodamiento
Los motores se suministran con baleros de bolas con doble sello, lubricados de por vida.

Enfriamiento
Los motores están provistos de un ventilador radial de material termoplástico, el cual enfría al motor independientemente del sentido de giro del mismo.

Pintura (color naranja)
La pintura es a base de zinc para evitar corrosión por ambientes húmedos o agresivos.

Aplicaciones de los motores monofásicos

Aplicación del motor con arranque por fase dividida, 4 polos
Están diseñados con un moderado par de arranque, para aplicaciones que no requieren alto par de arranque, tales como: extractores de aire, lavadoras y aparatos de aire acondicionado. Se pueden surtir con base rígida o con base flotante, con rodamientos de bolas. Cuando se requiere de una operación silenciosa o eliminar vibraciones, se recomienda la aplicación de un motor de fase dividida con base flotante.

Motor con arranque por capacitor, brida "C"; 2 polos
Este tipo de motor está diseñado con un moderado par de arranque y baja corriente de arranque. Las principales aplicaciones del motor con brida "C" se encuentran en las bombas centrífugas y otros equipos que requieren acoplamiento directo. Los motores se suministran con base fija o sin base y flecha roscada (sentido de rotación fijo).

Aplicaciones del motor con arranque por capacitor de 2 y 4 polos
Este tipo de motor está diseñado con un alto par de arranque y baja corriente de arranque. Para aplicaciones que requieran arranque con carga, tales como: compresores de aire, compresores de refrigerante, bombas para mover líquidos, máquinas, herramientas, etc. Se pueden surtir con base rígida o con base flotante. Por el tipo de aplicación a que estan sujetos, se suministran con rodamientos de bola, ya que están expuestos a fuertes cargas radiales, debido al empleo de bandas "V" para la transmision de las máquinas a mover.

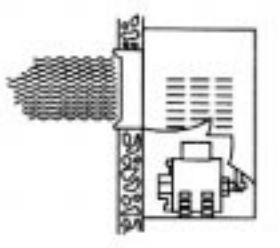

Aire acondicionado

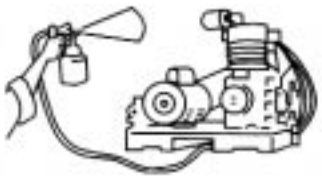

Compresores de aire

Bombas para agua

Motores monofásicos armazón 56

Tabla de selección
Motores monofásicos jaula de ardilla a prueba de goteo; aisl. clase B; **2 polos**

Potencia CP	Tipo	Catálogo No.	Peso neto kg	Velocidad nominal r.p.m.	Tensión nominal Volt	Corriente nominal A	Factor de Servicio	Corriente a F.S. A	Long. L mm
Arranque por capacitor, base rígida, con balero (uso general)									
0.25	1RF3 052-2YC41	30002034	8.3	3540/3520	127/220	7.6/3.0	2.0	8.3/3.9	254
0.33	1RF3 053-2YC41	30002043	8.4	3535/3515	127/220	8.5/3.5	2.0	9.7/4.5	254
0.50	1RF3 054-2YC41	30002051	9.7	3535/3515	127/220	9.9/4.1	1.8	12.4/6.2	271
0.75	1RF3 055-2YC41	30002059	10.5	3530/3500	127/220	12.4/5.3	1.6	14.6/7.1	271
1.0	1RF3 056-2YC41	30002064	11.9	3535/3510	127/220	15.5/6.6	1.6	18.6/9.4	291
1.5	1RF3 057-2YC41	30002069	12.8	3505/3470	127/220	18.5/9.4	1.2	20.4/10.2	291
2	1RF3 058-2YC41	30002071	15.5	3480/3460	127/220	21.6/11.0	1.15	24/12	313
Arranque por capacitor, base rígida, con balero, brida “C” y flecha roscada (bomba)									
0.25	1RF3 252-2YC34	30002074	6.7	3540	127 * *	4.5	1.8	5.4	258
0.33	1RF3 253-2YC34	30002078	7.5	3530	127 * *	5.7	1.7	6.6	270
0.50	1RF3 254-2YC34	30002082	8.5	3540	127 * *	7.5	1.6	9.0	270
0.75	1RF3 255-2YC44	30002086	10.3	3550/3530	127/220	11.6/5.0	1.6	1.35/7.0	287
1.0	1RF3 256-2YC44	30002088	11.2	3535/3515	127/220	12.3/6.0	1.4	14.5/7.5	311
1.5	1RF3 257-2YC44	30002090	13.2	3520/3500	127/220	16.6/8.4	1.2	18.2/9.7	311
2	1RF3 258-2YC44	30002092	15.5	3480/3460	127/220	21.6/11.0	1.15	24/12	320
Arranque por capacitor, sin base, con balero, brida “C” y flecha roscada (bomba)									
0.25	1RF3 252-2YC33	*	6.3	3540	127 * *	4.5	1.8	5.4	258
0.33	1RF3 253-2YC33	*	7.1	3530	127 * *	5.7	1.7	6.6	270
0.50	1RF3 254-2YC33	*	8.1	3540	127 * *	7.5	1.6	9.0	270
0.75	1RF3 255-2YC43	*	9.9	3550/3530	127/220	11.6/5.0	1.6	1.35/7.0	287
1.0	1RF3 256-2YC43	*	10.8	3535/3515	127/220	12.3/6.0	1.4	14.5/7.5	311
1.5	1RF3 257-2YC43	*	12.8	3520/3500	127/220	16.6/8.4	1.2	18.2/9.7	311
2	1RF3 258-2YC43	*	15.1	3480/3460	127/220	21.6/11.0	1.15	24/12	320

** Para doble voltaje en estas capacidades, sobre pedido
Datos sujetos a cambio sin previo aviso

Motores monofásicos armazón 56

Tabla de selección
Motores monofásicos jaula de ardilla a prueba de goteo; aisl. clase B; **4 polos**

Potencia CP	Tipo	Catálogo No.	Peso neto kg	Velocidad nominal r.p.m.	Tensión nominal volt	Corriente nominal A	Factor de servicio	Corriente F.S. A	Long. L mm
Arranque por fase dividida, base rígida, con balero									
0.25	1RF3 052-4YF31	30002040	7.9	1760	127	6.0	1.35	6.3	254
0.33	1RF3 053-4YF31	30002048	9.3	1740	127	7.0	1.35	7.5	271
0.50	1RF3 054-4YF31	30002056	9.8	1755	127	9.5	1.25	10.5	271
Arranque por capacitor, base rígida, con balero									
0.25	1RF3 052-4YC31	30002036	7.4	1760	127**	5.4	1.6	6.0	254
0.33	1RF3 053-4YC31	30002045	8.6	1755	127**	6.6	1.5	7.4	271
0.50	1RF3 054-4YC31	30002053	9.2	1745	127**	9.5	1.3	10.0	271
0.75	1RF3 055-4YC41	30002061	12.6	1735/1720	127/220	12.7/5.8	1.25	14.0/7.0	291
1.0	1RF3 056-4YC41	30002066	15.4	1745/1720	127/220	16/7.4	1.15	16.9/8.2	313
1.5 [1)]	1RF3 057-4YB41	30003716	14.3	1740/1720	127/220	13.8/7.2	1.15	15.2/8.3	313
2 [1)]	1RF3 058-4YB41	30003717	15.4	1730/1710	127/220	18.2/9.6	1.0	-	313

1) Motor con capacitores de arranque y de trabajo
** Para doble voltaje en estas capacidades, sobre pedido

Motores monofásicos armazón 56

Dimensiones generales

Estándar

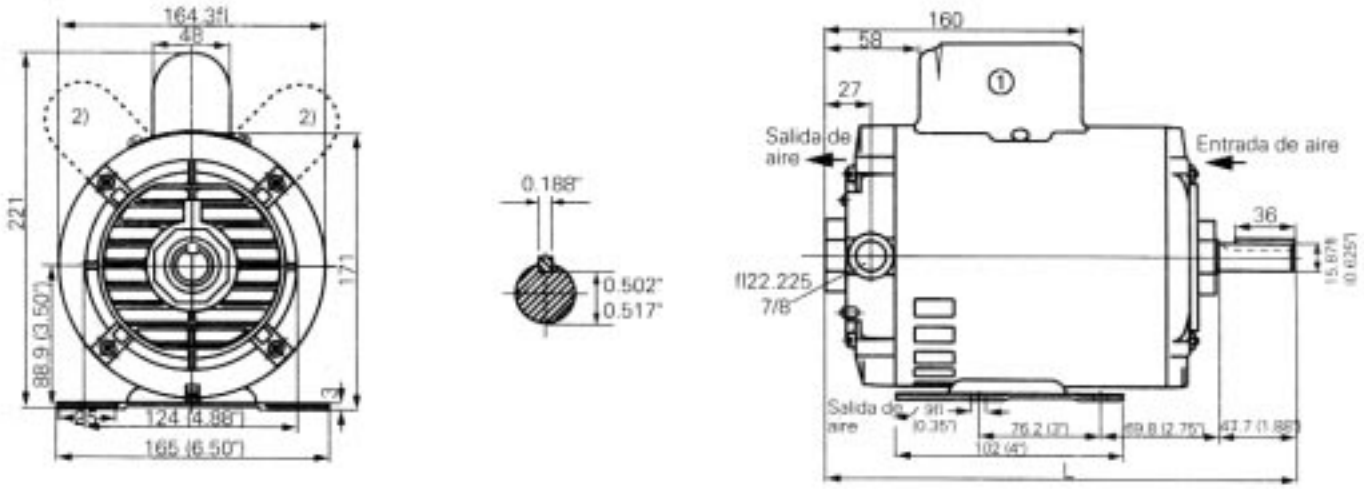

Brida C, bomba*

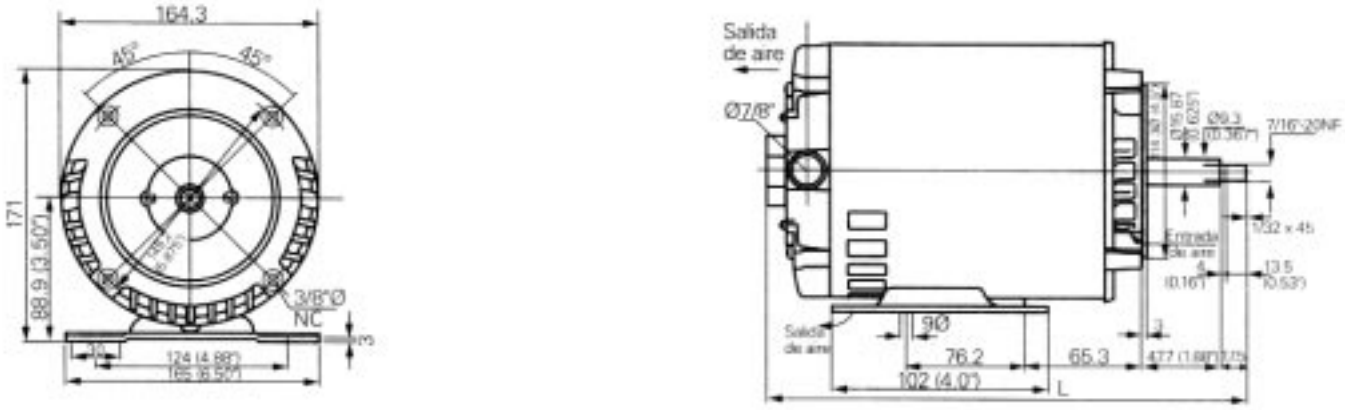

1) Motores de fase dividida, no llevan capacitor
L = Ver última columna de la tabla de selección
2) Motor de 2HP-4 Polos, con capacitores de arranque y trabajo.
* El capacitor está en el interior del escudo lado B, excepto en los motores de 2HP en los que está sobre el motor (altura 221 mm).

Motores monofásicos TCCVE

Jaula de ardilla, totalmente cerrados, aisl. clase F, F, S, 1.0

Potencia C.P.	r.p.m.	Armazón	Armazón	Catálogo No. Horizontal con patas	Catálogo No. con brida C y patas AK=4.5”	AK=8.5”	Tensión nominal V	Corriente nominal A
3	3600	182T	1LF3 182-2YK20	30002440	30000138	30000142	127/220	23.5/13.8
	1800	182T	1LF3 182-4YK20	30002444	30000139	30000143	127/220	31.2/15.2
5	3600	184T	1LF3 184-2YK40	30002441	30000140	30000144	220	21.0
	1800	184T	1LF3 184-4YK40	30002446	30000145	30000141	220	25.3

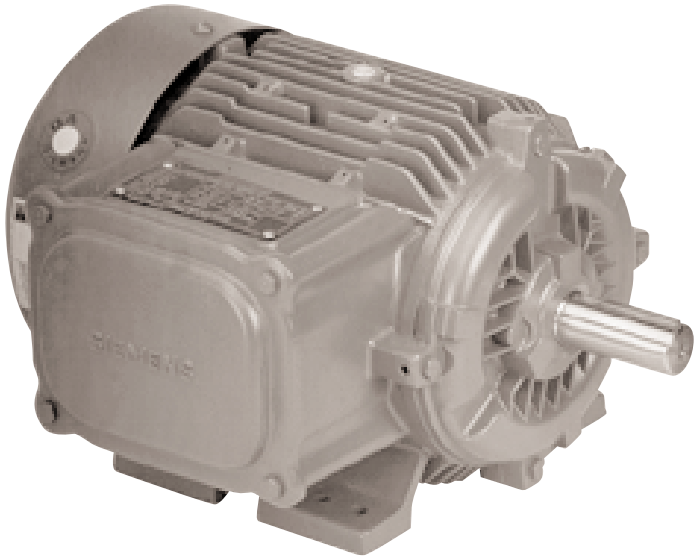

Potencia C.P.	Polos	Capacitor de arranque Bote tamaño	Mf	Volt	Ctl.	Capacitor permanente Bote tamaño	Mf	Volt	Ctl.	Dispositivo electrónico de arranque Tipo	Ctl.
3	2	7	590-708	140	30009792	5	60	250	30006238	4-7-41050-19-U01	30004766
	4	7	590-708	140	30009792	5	60	250	30006238	4-7-41050-19-U01	30004766
5	2	7	1000-1200	140	30009807	5	100	250	30004768	4-7-41080-15-N01	30004764
	4	7	1000-1200	140	30009807	5	100	250	30004768	4-7-41080-15-N01	30004764

Aclaraciones técnicas

Alta eficiencia significa rápida recuperación en su inversión

Con los motores de alta eficiencia se ha logrado hacer una conversión efectiva de la energía eléctrica a energía mecánica, lo que significa que los costos de los materiales y mano de obra requeridos para la construcción de motores de alta eficiencia se convierten en una excelente inversión.

Lo anterior se puede observar en los ejemplos siguientes, que muestran cuánto dinero se puede ahorrar y como puede recuperar rápidamente su inversión inicial con la adquisición de los motores de alta eficiencia.

Con los motores de alta eficiencia puede ahorrar dinero en su planta

$$C_T = P_I + \frac{0.746*HP*TO*R}{E}$$

donde:

C_T = Costo total de operación del motor
P_I = Precio inicial del motor
HP = Potencia del motor
TO = Tiempo de operación del motor (vida útil)
R = Tarifa de la compañia suministradora (4/kWh)
E = Eficiencia del motor

Ejemplo 1

Motor trifásico de 20 HP, 4 polos, 1800 rpm:

Motor de eficiencia estándar: E=87.5%
Precio del motor estándar: $8,336.00

Motor de alta eficiencia: E=92.4%
Precio del motor alta eficiencia $9,170.00

Para el motor estándar:

$$C_{T1} = 8336 + \frac{0.746*20*60000*1.15}{0.875} = 1,184,884.00$$

Para el motor alta eficiencia:

$$C_{T2} = 9170 + \frac{0.746*20*60000*1.15}{0.924} = 1,123,326.00$$

$$AHORRO = C_{T1} - C_{T2}$$
$$= 1,184,884 - 1,123,326 = \$\ 61,558.00$$

Con los motores de alta eficiencia puede recuperar su inversión rápidamente

$$A_A = 0.746 \times HP \times R \times TR \left[\frac{1}{E1} - \frac{1}{E2}\right]$$

donde:

A_A = Ahorro anual
HP = Potencia del motor
R = Tarifa de la compañia suministradora
TR = Tiempo de operación de trabajo al año (hr/año)
E1 = Eficiencia del motor estándar
E2 = Eficiencia del motor de alta eficiencia

Ejemplo 2

Motor trifásico de 20 HP, 4 POLOS, 1800 rpm.

Motor de eficiencia estándar: E=87.5%
Precio del motor estándar: $8,336.00

Motor de alta eficiencia: E=92.4%
Precio del motor alta eficiencia $9,170.00

Diferencia de costos = $ 834.00

$$A_A = 0.746 \times 20 \times 1.15 \times 4000 \times \left[\frac{1}{0.875} - \frac{1}{0.924}\right]$$

A_A = $ 4,159.51 ahorro anual

$$\text{Tiempo de recuperación de la inversión inicial} = \frac{\text{Dif. de costos}}{A_A}$$

$$TRI = \frac{834}{4,159.50} = 0.20 \text{ años}$$

Ventajas:

- Menor costo de operación
- Menores cargos por demanda máxima
- Menores pérdidas en vacío
- Intercambiabilidad
- Conformidad con las normas NEMA
- Empleo de equipo de control normalizado
- Mayor vida útil del aislamiento
- Mayor confiabilidad
- Mayor capacidad de sobrecarga

Aclaraciones técnicas

Motores trifásicos a prueba de explosión
Construcción, aplicación y clasificación

Construcción
Esta serie de motores trifásicos, tipo 1MJ, a prueba de explosión, son diseñados y fabricados en concordancia con las Normas Nacionales: NMX-J-283-1981: “Motores eléctricos a prueba de explosión para usarse en lugares que contengan atmósferas peligrosas clase I, grupo C,D” y NMX-J-262-1980 ”Motores eléctricos a prueba de explosión para usarse en lugares que contengan atmósferas peligrosas clase II, grupo E,F,G” listados bajo nuestro file E-120739.

Aplicación
En los procesos de manufactura, donde se generan o liberan, polvos, gases y vapores inflamables, es necesario usar motores, instalaciones, equipos y dispositivos debidamente aprobados para lugares peligrosos; ya que la concentración de los polvos, gases y vapores inflamables presentes en el aire y en atmósferas confinadas, pueden producir mezclas explosivas o encendibles.
Siemens ha desarrollado los motores a prueba de explosión, de la división I y para las clases I y II. La característica intrínseca de estos motores, es que la temperatura de cualquier superficie en operación expuesta, no exceda la temperatura de ignición de la materia presente en el área explosiva.
Nuestros motores llevan dispositivos limitadores de temperatura (tipo klixon), cuyas terminales se encuentran también en la caja de conexiones.

Clasificación de los motores Siemens a prueba de explosión

División I	Áreas con atmósfera peligrosa permanentemente.
Clase I:	Aquellos que han sido desarrollados para trabajar en atmósferas en las cuales estén o puedan estar presentes gases o vapores inflamables en el aire, en cantidades suficientes para producir mezclas explosivas o encendibles.
Grupo C: Temp. límite de partes expuestas: 180ºC. Código T3A	Para atmósferas que contienen acetaldehidos, alcoholes aleados, etileno, butaldeidos-n, monóxido de carbono, gases o vapores de equivalente código de temperatura.
Grupo D: Temp. límite de partes expuestas: 280ºC. Código T2A	Para atmósferas que contienen acetona, alcohol, bencina, benzoles, butano, gasolina, gas natural propano, o gases o vapores de equivalente código de temperatura.
Clase II:	Aquellos en los cuales existe peligro a causa de la presencia de polvo combustible.
Grupo E: Temp. límite de partes expuestas: 200ºC. Código T3	Para atmósferas que contienen polvo de metal, como aluminio, magnesio y sus aleaciones comerciales, o polvos con equivalente código de temperatura.
Grupo F: Temp. límite de partes expuestas: 200ºC. Código T3	Para atmósferas que contienen carbón negro (carbón vegetal), hulla (carbón mineral), polvo de coque o polvos con equivalente código de temperatura.
Grupo G: Temp. límite de partes expuestas: 165ºC. Código T3B	Para atmósferas que contienen harina, almidón (fécula), o polvos con equivalente código de temperatura.

Aclaraciones técnicas

Motores trifásicos a prueba de explosión
Motor a prueba de explosión seccionado

Los componentes principales han sido cuidadosamente seleccionados, los cuales están aprobadas por normas nacionales e internacionales. Se pueden resumir de acuerdo al siguiente desgloce:

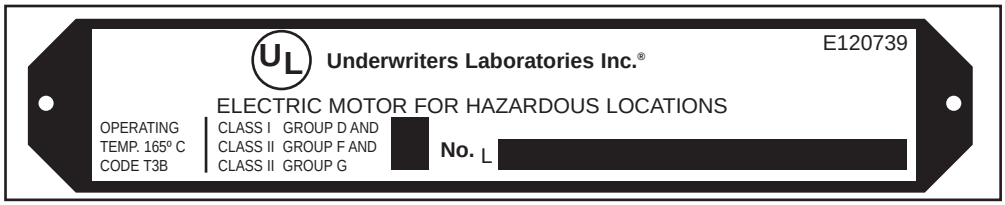

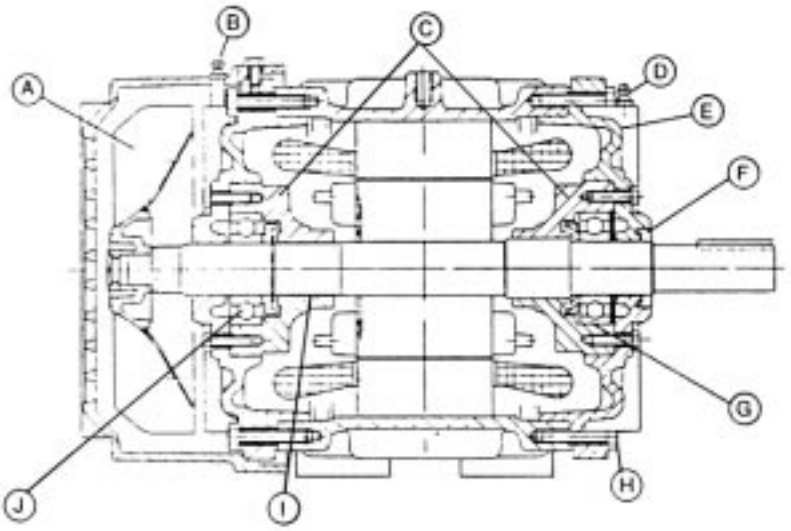

Ⓐ Ventilador plástico, conductivo antiestático.
Ⓑ Grasera lado ventilador.
Ⓒ Tapa balero interior, laberinto en ambos lados.
Ⓓ Grasera lado accionamiento.
Ⓔ Fundición gris de alta calidad.
Ⓕ Anillo exterior en bronce para motores clase I-C y clase II-E; clase I-D y clase II-F y G en neopreno.
Ⓖ Anillo laberinto interior, sólo para motores clase I-C y clase II-E (ambos lados).
Ⓗ Tornillos de alta resistencia SAE Grado 5.
Ⓘ Longitud y claro diametral restringido según Norma NMX.
Ⓙ Baleros de bolas iguales (reforzados) ambos lados, con sellos de lámina.
Ⓚ Compuesto sellador epóxico altamente resistente en ambientes corrosivos.
Ⓛ Par de apriete (torque) en los tornillos de la caja de conexión (véase tabla)*.

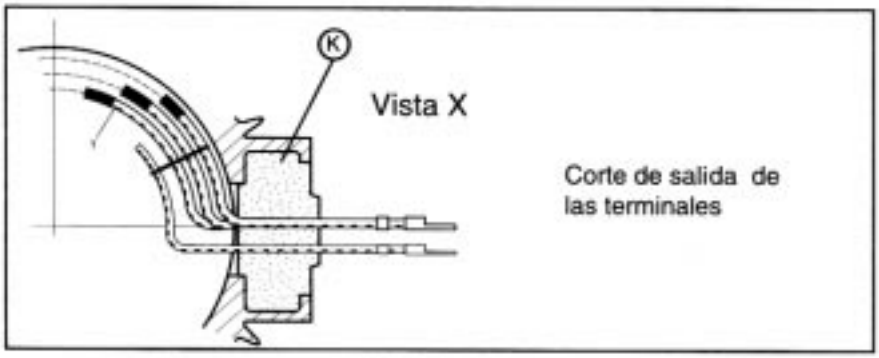

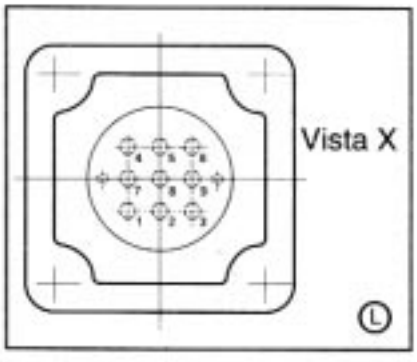

* **IMPORTANTE**

¡Nunca accione el motor si no está cerrada la tapa de la caja de conexión!

Par de apriete recomendado

Arm.	Tornillo tapa-caja	Nm*
140 180	5/16-18 NC (HEX)	22
210 250	3/8-16 NC (HEX)	38

*Nm = 0.1020 Kgfm

NOTA: Antes de apretar la tapa, limpie las superficies, aplicando después una ligera película de vaselina simple.

Aclaraciones técnicas

Motores trifásicos con freno electromagnético
Aplicación y descripción

El motor con freno tiene múltiples aplicaciones, ahí donde se precise un paro instantáneo de giro en la máquina impulsada, tales como: máquinas, herramientas, procesos de transporte (bandas de transportación), etc.
Consiste en un motor con rotor tipo jaula y un freno electromagnético.

Potencia-rpm
1.00 CP - 10 CP2 3600 rpm
0.75 CP - 10 CP4 1800 rpm
0.75 CP - 5 CP6 900 rpm
0.50 CP - 3 CP8 900 rpm

Armazones

143T a 215T

Tensión nominal del motor
220V/440 V, 60Hz

Tensión nominal de alimentación del freno
220 V CA, 60 Hz

Conexión del freno
Ver diagrama de conexiones

Funcionamiento del freno
El sistema simplificado del freno del disco (ver dibujo) es el siguiente:
El ventilador (7) transmite el par del frenado al eje (1) del motor y el ventilador (7) se fija con una cuña, pero queda libre en su movimiento axial. Al conectar el motor se energiza la bobina (4) del imán del escudo portacojinete (3) con corriente contínua (rectificación por diodos integrados).

Debido a la fuerza magnética se atrae la armadura (6) venciendo los resortes (5). Con este movimiento de la armadura (6) el ventilador queda libre de la presión y fricción de la balata (10).

El ventilador (7) y la flecha (1) pueden girar en el balero (2). La armadura (6) con la balata (10) forman una unidad. La armadura (6) se guía sobre pernos (9) montados en el escudo porta cojinetes (3).

Ajuste del par de frenado
El par de frenado máximo y el entrehierro § = 0.3 mm se ajustan en fábrica.

Si con el uso normal, pasado el tiempo, por desgaste de la balata (10) es necesario ajustar el par de frenado, existe la posibilidad de lograrlo girando el anillo roscado (8) hasta obtener un entrehierro = 0.3mm.

El par de frenado se puede disminuir a voluntad, esto se consigue retirando los resortes (5). Así retirando la mitad de los resortes, el par de frenado se reduce en un 50% aproximadamente. Los resortes que permanecen en el freno deben quedar repartidos uniformemente y el entrehierro debe ajustarse a = 0.3 mm.

Efectue estos trabajos según se indica en el instructivo que viene suministrado con cada motor 1LC3.

Protección de la bobina (4) contra sobretensiones
La bobina (4) está protegida contra sobretensiones (producidas por la desconexión en un circuito de corriente contínua) por un varistor.

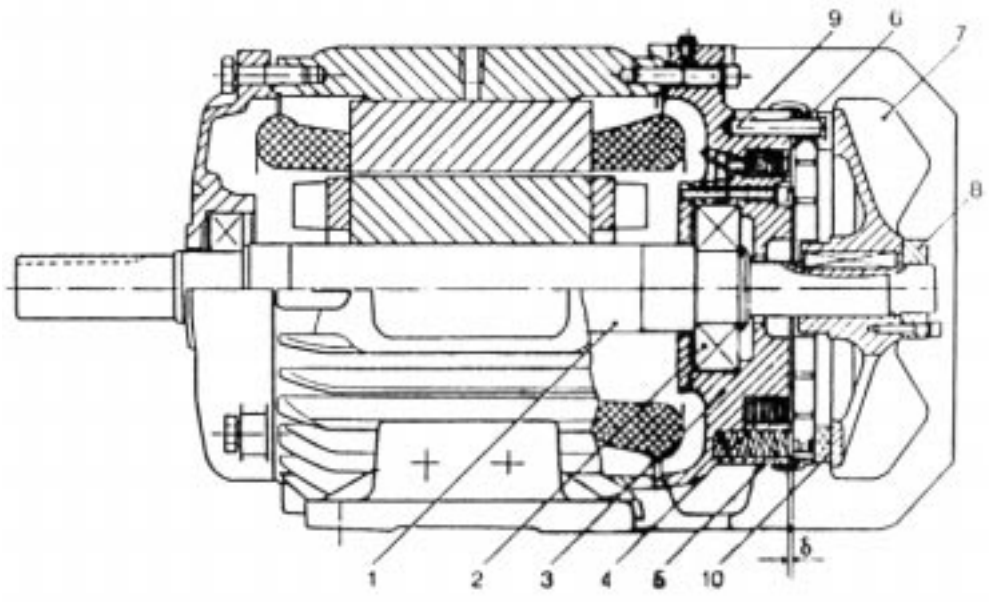

Datos técnicos de los frenos tipo 2LM1

Freno	Para motor con armazón	Freno tipo	Par de frenado NM	Potencia de consumo VA (220 VCA)	Tiempo de caida freno ms.	Tiempo de apertura ms.	Momento de inercia del freno Kgm²
A	143/5	2LM1 020-4N	20	186	230	90	0.0035
B	182/4	2LM1 050-6N	50	288	260	130	0.0080
C	213/5	2LM1 050-7N	50	288	260	130	0.0080

Aclaraciones técnicas

Motores trifásicos con freno electromagnético
Diagrama de conexión

Alimentación a motor y freno con 220 V, 3Ø, 60Hz

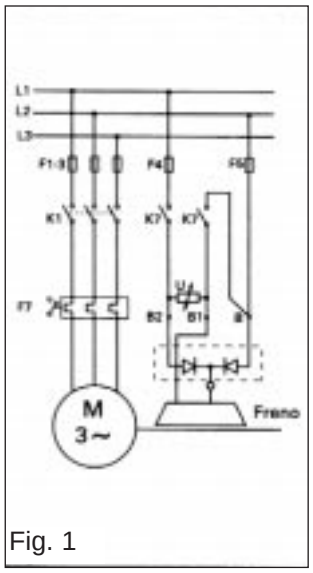

Fig. 1

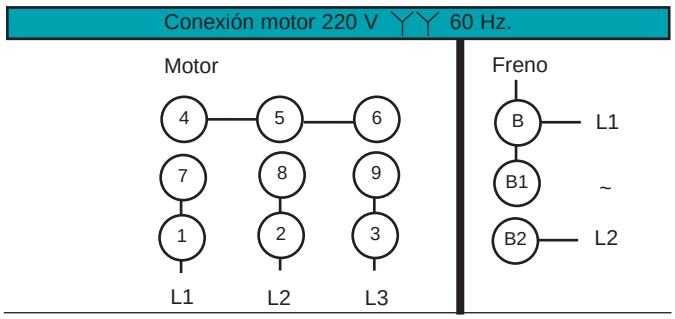

Fig. 3

Control freno y motor 1Ø, 220V, 60Hz.

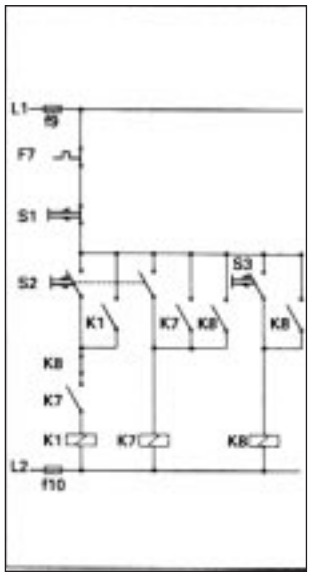

Alimentación a motor con 440V 3Ø, 60 Hz. y freno con 220V. 1Ø, 60 Hz.

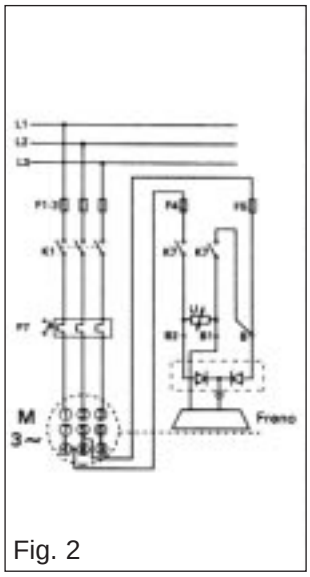

Fig. 2

Diagrama de conexión en tiempos cortos - 50 ms (fig. 1 y 2); para tiempos normales de operación (250 ms, aprox.) eliminar K7, conectando B con B1 como se muestra en la fig. 3

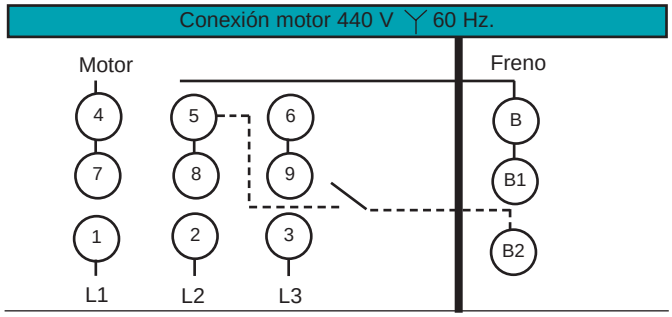

Fig. 4

Para la protección contra corto circuito de alimentación al freno (F4 y F5) y para la protección contra corto circuito del control freno y motor (F9 y F10) usar fusibles DIAZED tipo 5SB (ver catálogo de baja tensión).

Freno electromagnético de corriente continua
Los frenos electromagnéticos también pueden ser fabricados para funcionar con corriente contínua, a una tensión de 24V.
El freno deberá conectarse directamente (L+/L-), independientemente de la línea de alimentación del motor.
El tiempo normal de caída del freno es de 250 ms. aprox.

Control freno y motor, 1Ø,220 ó 440V, 60Hz.

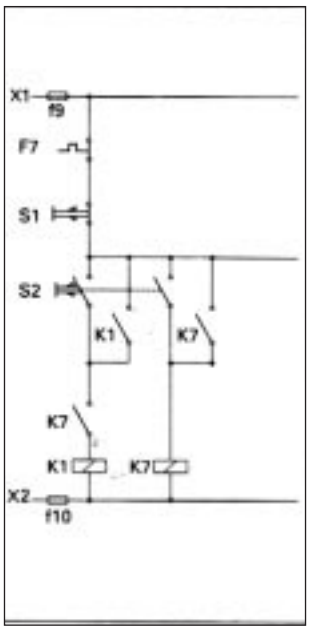

S2 Conectar freno
S1 Parar freno
S3 Despegar freno con motor parado
K1 Contactor del motor
K7 Contactor auxiliar

Aclaraciones técnicas

Motores trifásicos de baja tensión
Aclaraciones y bases de proyecto

La línea
Las redes trifásicas de baja tensión están formadas por los tres conductores activos L_1, L_2 y L_3 y pueden ejecutarse con o sin conductor neutro. Los conductores neutros están unidos al centro de la estrella del generador o del transformador correspondiente al lado de baja tensión. Dos conductores activos o uno de ellos y el neutro constituyen un sistema de corriente alterna monofásica.

Tensión de servicio
La tensión existente entre dos conductores activos (L_1, L_2, L_3) es la tensión de la línea (Tensión compuesta o tensión de la red). La tensión que hay entre un conductor activo y el neutro es la tensión simple (tensión de fase).

Se da la relación:

$U_L = 1.73 \times U$

U_L = tensión compuesta (tensión de línea)
U = tensión simple (tensión de fase)

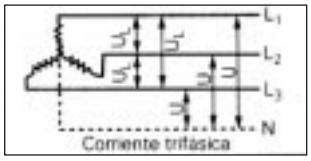

Fig. 1

Conexión de motores trifásicos
Los motores trifásico se conectan a los tres conductores L_1, L_2, L_3. La tensión nominal del motor en la conexión de servicio tiene que coincidir con la tensión compuesta de la red (tensión de servicio).

Cambio de sentido de giro de los motores trifásicos
Se consigue invertir el sentido de giro intercambiando la conexión de los conductores de alimentación.

Conexión de los motores trifásicos de polos conmutables
Los motores de polos conmutables en ejecución normal se suministran sólo para conexión directa a cualquiera de las velocidades.

El devanado se realiza en conexión dahlander para dos velocidades de rotación en relación 1:2.
Para 1800/3600 rpm, es decir, 4/2 polos ó 900/1800 rpm, es decir, 8/4 polos.

Fig. 2

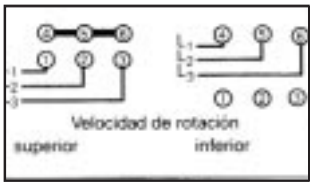

Fig. 3

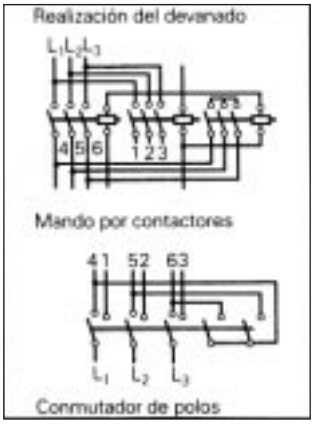

Conexiones de los motores trifásicos con jaula de ardilla
El diagrama de conexión de la figura 4 corresponde a motores 1LA3; para motores 1LA6 considerar la figura 5

Fig. 4

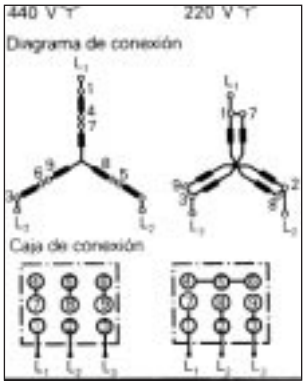

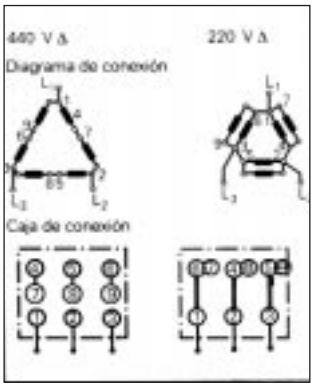

Fig. 5

Puesta a tierra y conexión del conductor de protección
Las máquinas tienen en la caja de conexiones un borne para la conexión del conductor de protección. Si se trata de máquinas de mayor potencia, para la puesta a tierra se habrá dispuesto una placa adicional en la carcasa.

Potencia nominal aparente
La red de baja tensión se alimenta directamente con un generador o por medio de un transformador conectado a su vez a la red de alta tensión. La potencia nominal del generador o del transformador medida en kVA tiene que ser, como mínimo, igual a la suma de las potencias aparentes de todos los motores que, en el caso más desfavorable, se encuentren simultáneamente en servicio.

La potencia nominal aparente es:

en los motores trifásicos

$$Ps = \frac{U \times I \times 1.73}{1000}$$

en los motores monofásicos

$$Ps = \frac{U \times I}{1000}$$

siendo:
Ps = potencia nominal aparente en kVA
U = tensión nominal en V
I = intensidad nominal en A

Caída de tensión y de frecuencia
Si se supone constante la tensión en la salida del transformador o del generador, la tensión en el motor es menor, debido a la resistencia óhmica e inductancia de las líneas intermedias. La diferencia existente entre ambas tensiones es la caída de tensión. En el caso de que el motor tenga que proporcionar la potencia nominal a la frecuencia nominal, la caída máxima de la tensión aplicada al motor durante el servicio del mismo es del 10%. La máxima variación admisible de frecuencia es del 5% de su valor nominal.

Máquina accionada

Cálculo del par motor
La potencia (kW) o el par motor de accionamiento (kgfm) y la velocidad de rotación (rpm) durante el servicio nominal de la máquina impulsada, tienen que conocerse con la mayor exactitud posible.
La potencia se expresa de la siguiente forma:

$$P[kW] = \frac{M \times n}{975} \text{ ó}$$

$$P[HP] = \frac{M \times n}{716}$$

siendo:
P = potencia en kW o HP
M = par motor en kgfm
n = velocidad de rotación en rpm

Tratándose de una carga G que describa un movimiento rectilíneo con una velocidad v, la potencia es:

$P = G \times v \quad 1 \text{ kW} = 102 \text{ kgfm/s}$

siendo:
P = potencia en kgmf/s
G = carga en kgf
v = velocidad en m/s

El par motor equivalente a una carga sometida a movimiento rectilíneo es:

$$M = 9.56 \frac{G \times v}{n}$$

Aclaraciones técnicas

siendo:
M = par motor en kgfm
G = carga en kgf
v = velocidad en m/s
n = velocidad de rotación en rpm

Conversión de potencia en kW a potencia en HP y viceversa

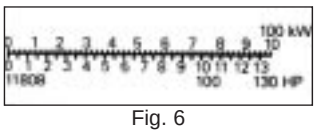

Fig. 6

Conversión de los caballos de vapor del sistema inglés:
potencia (kW) =
0.746 x potencia (HP).
potencia (HP) =
1.34 x potencia (kW).

Curva caraterística del par resistente
Para comprobar los procesos de arranque y de frenado y para seleccionar los motores con velocidades de rotación variables, se necesita conocer la curva del par resistente de la máquina impulsada (par de carga), en dependencia de la velocidad de rotación dentro de la zona a considerar. Las formas básicas representativas de los pares resistentes quedan reproducidas en la figura 7. En la figura 8 se muestran las curvas correspondientes de la potencia.

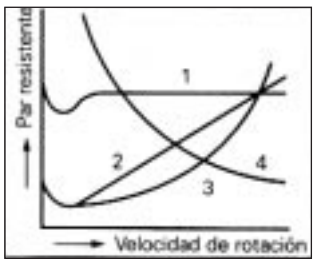

Fig. 7

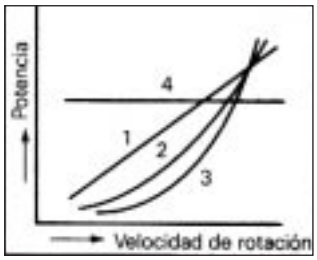

Fig. 8

1. Par resistente prácticamente constante, potencia proporcional a la velocidad de rotación. Se establece por ejemplo,en mecanismos elevadores, bombas de émbolo y compresores que impulsen venciendo una presión constante, soplantes de cápsula, laminadores, bandas transportadoras, molinos sin efecto ventilador, máquinas herramientas con fuerza de corte constante.

2. El par resistente crece proporcinalmente con la velocidad de rotación, y la potencia aumenta proporcionalmente con el cuadrado de la velocidad. Rige, por ejemplo, para calandrias.

3. El par resistente crece proporcionalmente con el cuadrado de la velocidad de rotación, y la potencia con el cubo de la velocidad de rotación. Rige para bombas centrífugas, ventiladores y soplantes centrífugos, máquinas de émbolo que alimenten una red de tuberías abiertas.

4. El par resistente decrece en proporción inversa con la velocidad de rotación, permaneciendo constante la potencia. Solamente se considerará este caso para pocesos de regulación, presentándose en los tornos y máquinas herramientas similares, máquinas bobinadoras y descortezadoras.

Si la trasmisión se ejecuta por medio de bandas o de engranajes, el par resistente se referirá a la velociadad de rotación del motor.

$$M_1 = \frac{M_2 \times n_2}{n_1}$$

siendo:

M_1 = par resistente en el eje del motor
M_2 = par resistente en el eje de la máquina
n_1 = velocidad de rotación del motor
n_2 = velocidad de rotación de la máquina

El par resistente en reposo (momento inicial de arranque) tiene que conocerse con la mayor exactitud posible.

Determinación del momento de inercia.
Además de la curva par-velocidad, para verificación de los procesos de arranque y frenado, es también nesesario conocer el momento de inercia de la máquina y del cople en kgm^2 referido a la velocidad de la flecha del motor.

Los momentos de inercia de diferentes masas giratorias montadas sobre un mismo eje pueden sumarse para obtener un momento de inercia total.

En forma similar, una masa giratoria compleja puede dividirse en secciones con momentos de inercia de cálculo sencillo, los cuales se suman subsecuentemente para obtener el momento de inercia total.

En el caso de cuerpos complejos, especialmente con máquinas completas de accionamiento, es mejor determinar el momento de inercia de la parte giratoria mediante una prueba de desaceleración.

Para un cilindro de longitud l constante y diámetro d, el momento de inercia es:

$$J = \frac{1}{8} m \cdot d^2$$

con $m = p \cdot \frac{\pi}{4} d^2 l$

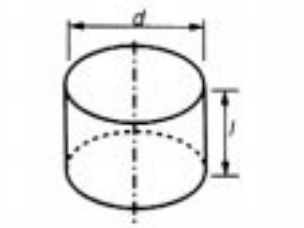

Para un cilindro hueco de longitud 1 constante y diámetros d y d_i, el momento de inercia es:

$$J = \frac{1}{8} m (d^2 + d_i^2)$$

con $m = p \cdot \frac{\pi}{4} (d^2 + d_i^2)$

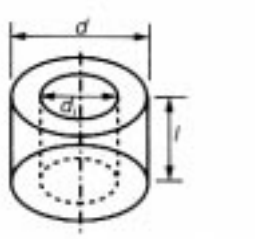

J = momento de inercia en kgm^2
m = masa en kg
p = densidad en kg/m^3
d_i = diámetro interior en m
l = longitud en m

Para referir el momento de inercia de un cuerpo giratorio de cualquier velocidad al valor específico de la velocidad del motor o para referir una masa de movimientos rectilíneo a un momento de inercia equivalente, se utilizan las siguientes ecuaciones:

J_{ad} referido a n_{mot}:

$$J_{ad}\, n_{mot} = J_{ad} \left(\frac{n_a}{n_{mot}}\right)^2$$

J total referido al eje del motor :

$$(\Sigma J)_n = J_{mot} + (J_{ad})_n$$

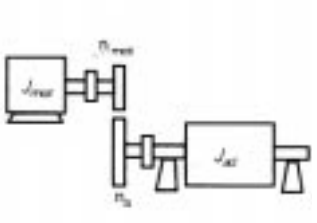

En el caso de una masa sometida a movimiento rectilíneo, tales como los accionamientos de mesas o de carros, el momento de inercia equivalente referido al eje del

Aclaraciones técnicas

motor se calcula de la siguiente forma :

$$J = \frac{m}{4\pi^2} \cdot \left(\frac{60v}{n}\right)^2$$

$$J = 912 \cdot \left(\frac{v}{n}\right)^2$$

J = momento de inercia (referido a la velocidad del motor) en kgm²
m = masa en kg
v = velocidad en m/s
n = velocidad del motor en rpm

Determinación del momento de inercia mediante prueba de desaceleración
1. Prueba de desaceleración normal:

$$J = \frac{9.55 \cdot t_b \cdot M_B}{n}$$

J = momento de inercia total, incluyendo motor, en kgm²
t_b = tiempo de desaceleración en s
M_B = par de frenado en Nm
n = diferencia de velocidades durante el tiempo t_b en rpm

J puede determinarse fácilmente cuando M_B es conocido.

2. Prueba de desaceleración con masa auxiliar conocida.

$$J = J_{aux} \frac{t_b}{t_{b\ aux} - t_b}$$

J = momento de inercia externo más inercia del motor en kgm²
J_{aux} = momento de inercia de la masa auxiliar en kgm²
t_b = tiempo de desaceleración sin J_{aux} en s
$t_{b\ aux}$ = tiempo de desaceleración con J_{aux} en s

Materiales aislantes y clases de aislamiento
En las normas, se han clasificado los sistemas de aislamiento en clases de aislamiento, habiéndose fijado para los mismos las correspondientes temperaturas exactas.

TA = temperatura del medio ambiente en ºC
STL = sobretemperatura límite (calentamiento) en grados K (valor medio)
TPM = temperatura permanente máxima en ºC (para el punto más caliente del devanado).

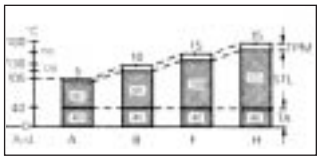

Fig. 9

Sobre temperatura límite en K

Clase de aislamiento	B	F	H
Devanados aislados	80	105	125
Anillos rozantes	80	90	100

La temperatura máxima permanentemente admisible de los diferentes materiales aislantes se compone, como queda representado en la figura anterior, de la temperatura del medio ambiente, de la sobretemperatura límite y de un suplemento de seguridad. Este último suplemento se ha introducido porque, aplicando el método de medida usual, o sea, la elevación de la resistencia del devanado, no se determina la temperatura en el punto más caliente, sino que se mide el valor medio del calentamiento. Las indicaciones de potencia de los motores están basadas en una temperatura del medio ambiente de 40 grados para todas las clases de aislamiento. Para la clase de aislamiento B, resulta por ejemplo:

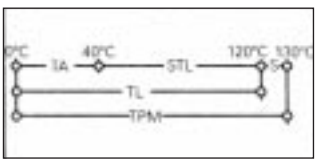

Fig. 10

TA = temperatura del medio ambiente 40°C
STL = sobretemperatura límite 80 grados
TL = temperatura límite 120°C
S = suplemento de seguridad 10 grados
TPM= temperatura permanente máxima 130 °C

Las sobretemperaturas límites de los anillos rozantes rigen para medida por termómetro, contrariamente a como sucede con las sobretemperaturas límite de los devanados.

Determinación de la potencia al variar la temperatura del medio refrigerante o la altitud de emplazamiento.
La potencia nominal de los motores indicada en los catálogos o en la placa de características rige normalmente partiendo de las siguientes condiciones:

Temperatura del medio ambiente hasta 40°C.
altura de colocación hasta 1000 msnm.

Si por razones propias del servicio o por haber diseñado los motores en conformidad con otras prescripciones diferentes se modificasen estos valores, habría que alterar en general la potencia.

Temp. ambiente °C	Capacidad admisible %	Altura s.n.m. m	Capacidad admisible %
30	107	1000	100
35	104	1500	98
40	100	2000	95
45	95	2500	91
50	90	3000	87
55	83	3500	83
60	76	4000	78

No es necesario reducir la capacidad nominal, si la temperatura ambiente baja según la tabla.

Altura s.n.m. m	Temperatura ambiente °C
1000	40
1500	38
2000	35
2500	33
3000	30
3500	28
4000	25

Temperatura de la carcasa
La temperatura de la carcasa no debe tomarse como criterio para determinar la calidad del motor, ni de base para la temperatura del local. Un motor que esté exteriormente “frío” puede representar pérdidas superiores o tener una sobretemperatura mayor en los devanados que otro motor exteriormente “caliente”. El método utilizado con frecuencia antiguamente, para determinar si el motor estaba sobrecargado o no, tocando con la mano la carcasa, es completamente inadecuado para motores eléctricos modernos. El principio constructivo de unir lo más posible el paquete del estator a la carcasa, es decir, de conseguir la mínima resistencia de paso del calor, motiva que la temperatura de la carcasa sea aproximadamente de la misma magnitud que la temperatura del devanado.

Temperatura del local
La elevación de la temperatura del local depende exclusivamente de las pérdidas y no de la temperatura de la carcasa.
Además, las máquinas accionadas frecuentemente contribuyen al calentamiento del local en mayor proporción que los motores.
En todas las máquinas elevadoras y modificadoras de materiales se transforma prácticamente la totalidad de la potencia de accionamiento. Estas cantidades de calor tienen que ser eliminadas por el aire ambiente en el local de servicio.

Pares e intensidades
El par que desarrolla un motor trifásico en su flecha presenta una magnitud muy variable entre n = 0 y n = n_s. El curso característico del par respecto a la velocidad de rotación del motor trifásico con rotor de jaula, queda representado en el diagrama.

Aclaraciones técnicas

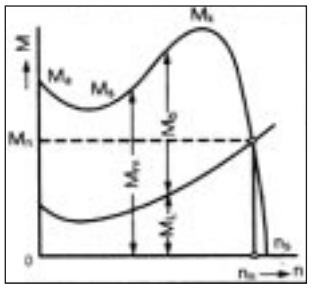

Fig. 11

siendo:
M_m = par del motor
M_L = par resistente
M_b = par de aceleración
n_n = velocidad nominal de rotación
M_a = par inicial de arranque
M_k = par máximo
M_n = par nominal
M_s = par mínimo en el arranque
n_s = velocidad de rotación de sincronismo

El margen comprendido entre M = 0 y M = M_n es el de trabajo; entre M = M_a y M = M_k queda comprendido el margen de aceleración.

El límite de la capacidad mecánica de sobrecarga está constituído por el par máximo.

Los valores correspondientes al par inicial de arranque; al par mínimo de arranque y al par máximo, así como la intensidad en el arranque para un cierto motor, pueden deducirse de los catálogos correspondientes. Según las curvas que representan funciones del par motor y de la velocidad de rotación, se pueden trazar en caso necesario, con suficiente exactitud la característica en función de la velocidad de rotación y de los pares motores. Teniendo en cuenta estas funciones, el par inicial de arranque tiene que superar en una magnitud suficiente el par resistente inicial de arranque de la máquina accionada, encontrándose durante todo el proceso de arranque el par motor por encima del par resistente, hasta llegar a alcanzar la velocidad de rotación de servicio.
Por otra parte, el momento de aceleración no debe ser excesivamente grande, puesto que, de lo contrario, los elementos de transmisión mecánica y la máquina accionada pueden sufrir daños. Un diseño NEMA superior se utilizará cuando se pretenda conseguir un par de arranque elevado.

Para conexión directa

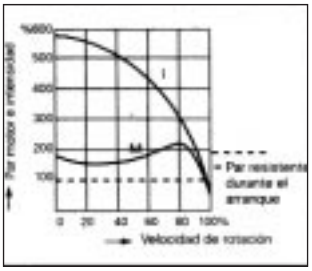

Fig. 12

La velocidad nominal de rotación del motor se diferencia de la velocidad de sincronismo en el deslizamiento nominal s_n.

$$s_n = \frac{n_s - n_n}{n_s} 100$$

siendo:
s_n = deslizamiento nominal en %
n_s = velocidad de rotación de sincronismo en rpm
n_n = velocidad de rotación nominal en rpm.

El par nominal se calcula de la siguiente forma:

$$M_n = 9.55 \times P_n \frac{1000}{n_n}$$

siendo:
M_n = par motor nominal en Nm
n_n = velocidad nominal de rotación en rpm
P_n = potencia nominal en kW

Determinación del tiempo de arranque
Partientdo del par medio de aceleración, se puede determinar aproximadamente el tiempo de duración del ciclo de arranque, desde n = 0 hasta n = n_n, de la siguiente forma

$$ta = \frac{\sum J \times n_n}{9.55 \times M_{bmi}}$$

siendo:
t_a = tiempo de arranque en s
J = momento de inercia total en kgm²
n_n = velocidad de rotación de servicio en rpm
M_{bmi} = par medio de aceleración en Nm

La figura 13 expone un método sencillo para determinar de una forma relativamente exacta el par medio de aceleración. Gráficamente se obtendrá el valor medio (por ejemplo, contando los cuadros sobre un papel milimétrico) de la característica del par motor y del par resistente.

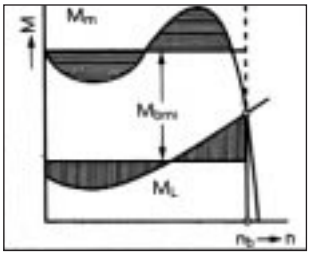

Fig. 13

M_m = par motor
M_L = par resistente
M_{bmi} = par medio de aceleración
n_b = velocidad de rotación de servicio

El momento de inercia total es igual al momento de inercia del motor más el correspondiente a la máquina impulsada y al acoplamiento o de la polea para correa (referido a la velocidad de rotación del motor). Si el tiempo de arranque así determinado fuese superior a 7 s aproximadamente tratándose de motores de 3600 rpm y a 10 s en caso de motores con velocidades de rotación inferiores, sería preciso consultar para determinar si el arranque es admisible considerando el calentamiento del motor. Igualmente, será necesario verificar el cálculo en el caso de que en pequeños intervalos se repitan los arranques. En el caso de que por ser grande el momento de impulsión y elevado el par resistente no se pueda conseguir un arranque correcto utilizando un motor con el diseño NEMA más elevado, habría que tomar un motor mayor, el cual, bajo la carga normal, resultaría mal aprovechado, o un motor trifásico con rotor de anillos rozantes y un reóstato de arranque; considerando las condiciones que para la acometida exigen las compañías distribuidoras de electricidad, es posible que resulte necesario recurrir a la clase de motor últimamente indicada. Otra de las posibilidades con que se cuenta para vencer un arranque dificil, es el empleo de embragues de fricción por fuerza centrífuga, en combinación con un motor de rotor de jaula.

Tiempos de arranque de motores con rotor de jaula que arrancan en vacío
El diagrama de la figura 14 da a conocer los tiempos aproximados de arranque en vacío (sin contar el momento de inercia adicional externo) de motores tetrapolares con rotor de jaula, provistos de refrigeración interna y de refrigeración superficial (valores medios)

a = motores con refrigeración interna APG.
b = motores con refrigeración superficial TCCVE.

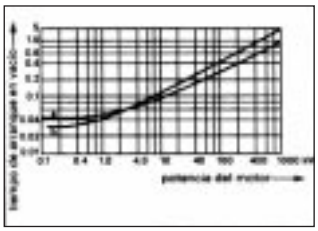

Fig. 14

Los tiempos de arranque en vacío no deben considerarse para estudiar los procesos de arranque en lo que a la solicitación térmica de los motores se refiere.

Aclaraciones técnicas

Métodos de arranque a tensión reducida de motores trifásicos con rotor de jaula

Al arrancar con un arrancador de voltaje reducido tipo autotransformador se reduce el voltaje de bornes a $E_2 = m \times E_1$. Con esto la corriente de arranque recibida por el motor es $\mathbf{I}_a^1 = m \times \mathbf{I}_a$, su par de arranque es $M_a^1 = m^2 \times M_a$ y la corriente tomada de la red es

$$\mathbf{I}_{red} = m^2 \mathbf{I}_a$$

siendo en este caso:

E_1 = Tensión nominal de la red
E_2 = Tensión en el secundario del autotransformador
m = relación de reducción de tensión del autotransformador
$\mathbf{I}_a$ = corriente de arranque del motor en arranque directo
$\mathbf{I}_a^1$ = corriente recibida por el motor en arranque a voltaje reducido
M_a = par de arranque del motor en arranque a voltaje reducido
$\mathbf{I}_{red}$ = corriente tomada de la red al arranque a voltaje reducido

Se realizará el arranque en estrella-delta de motores con rotor de jaula, cuando se exija un par motor especialmente bajo (arranque suave) o cuando se exija que las intensidades en el arranque sean reducidas.

Se requiere que el motor trifásico esté previsto para conexión en YΔ.

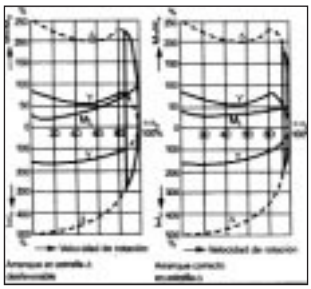

Fig. 15 Fig. 16

Frenado e inversión de marcha

Al frenar, el par de desaceleración es igual al par motor más el par resistente. Tomando un par medio de desaceleración, el tiempo de frenado de $n = n_b$ a $n = 0$ es aproximadamente:

$$t_B = \frac{J \times n_b}{9.55 \times M_{vmi}}$$

Significando:

t_B = tiempo de frenado en s
J = momento de inercia total en kgm^2
n_b = velocidad de rotación de servicio en rpm
M_{vmi} = par medio de desaceleración en Nm

La magnitud y el transcurso del par motor dependen del método de frenado que se aplique.

Existen los siguientes sistemas de frenado:

a) frenado mecánico: el motor no queda sometido a solicitación alguna. Para más detalles ver “motores con freno”.

b) Frenado por contracorriente se consigue conmutando dos fases de la acometida; al alcanzar la velocidad de rotación el valor cero, es preciso desconectar la acometida, a ser posible, de forma automática (aparato de vigilancia de frenado). El par medio de frenado del motor es generalmente mayor que el par de arranque en los motores con rotor de jaula (véase figura 17)

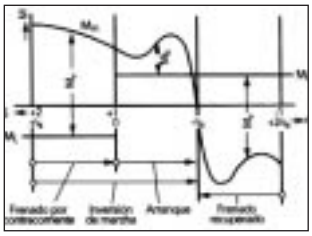

Fig. 17

Arranque, frenado e inversión con motores de rotor de jaula.
M_m = par motor
M_L = par resistente
M_b = momento de aceleración
M_v = momento de desaceleración

La generación de calor del motor equivale al doble o al triple de la correspondiente al arranque. Por este motivo, cuando los tiempos de frenado sean superiores a 3 s, habrá que consultar para determinar si es posible realizar el frenado de esta forma, considerando el calentamiento del motor. Igualmente, habrá que verificar los cálculos cuando se repitan las operaciones de frenado en intervalos reducidos.

c) Para establecer el frenado por corriente continua de motores con rotor de jaula o con rotor de anillos rozantes, es necesario desconectar de la red el estator y excitar con corriente continua a tensión reducida. La curva aproximada representativa de los pares de frenado se consigue sustituyendo, en la curva del par motor, la división del eje de las abscisas, correspondiente a la velocidad de rotación n por la velocidad de rotación de frenado $n_B = n_s - n$

Conexiones usuales para el frenado por corriente continua.

Fig. 18 Fig. 19 Fig. 20 Fig. 21
Conex.a b c d

Para una misma circulación (el mismo efecto de frenado), los factores de conversión para calcular la corriente continua en las conexiones indicadas están escalonados de la forma siguiente:

$K_a:K_b:K_c:K_d$: =1.225:1.41:2.12:2.45

La corriente continua de frenado para los motores con rotor de jaula, se calcula de la siguiente forma:

$$I_{Bg} = K \times I_A \times \sqrt{\frac{\frac{J \times n_n}{9.55 \times t_B} - M_{ext}}{f \times M_A}} \leq K \times I_A$$

siendo:

I_{Bg} = corriente continua de frenado en A
K = factor de la correspondiente conexión de frenado (por ejem. $K_a = 1.225$ para conexión a).
I_A = valor por fase de la intensidad de arranque en A
J = momento de inercia total del motor y de la máquina accionada referido al eje del motor y expresado en Kgm^2
n_n = velocidad de rotación nominal del motor en r/min.
t_B = tiempo de frenado en s (dada la solicitación térmica, se admite el valor límite $t_B \leq 10$ s)
M_{ext} = par resistente de la máquina accionada en Nm
M_A = par de arranque en Nm
f = factor f para el torque de frenado
f = 1.6 para motores hasta armazón 324

d) Frenado en hipersincronismo (recuperativo).
Esta clase de frenado resulta en los motores de polos conmutables al conmutar a baja velocidad de rotación inferior. El frenado hasta llegar al valor cero no se puede conseguir (véase figura 17). El par máximo es muy superior al que existe durante la operación de arranque. El aumento de temperatura del motor, con una relación de 1:2, resulta igual que al arrancar a la velocidad de rotación inferior.

Cuando se pasen consultas sobre los procesos de frenado y de inversión de marcha, habrá que indicar los siguientes datos:

1. Tipo de máquina accionada y empleo previsto del motor.
2. Potencia demandada y velocidad nominal de la máquina accionada.
3. Velocidad proyectada para el motor.
4. Par de carga de la máquina accionada referida a su velocidad o a la velocidad del motor.
5. Momento de inercia de la máquina accionada con

indicación de la velocidad de referencia o referido a la velocidad del motor.
6. Cantidad y tipo de los procesos de frenado o de inversión por unidad de tiempo.
7. Duración de conexión

Si se trata de motores con polos conmutables, los mencionados datos se indicarán para cada velocidad de rotación.

Regulación de la velocidad de rotación
La regulación de la velocidad de rotación se puede alcanzar de las siguientes formas: con motores de polos conmutables, motores de anillos rozantes, modificando la frecuencia de los motores de rotor de jaula, mandando en el circuito de campo o del inducido en las máquinas de corriente contínua, con máquinas trifásicas de colector y, finalmente, mediante la conexión de cascada.
La elección del método más económico se hará considerando el margen de regulación, el tiempo de duración del mismo, la característica del par resistente de la máquina accionada y la tecnología del proceso de trabajo, así como el balance energético.
El ajuste escalonado de diversas velocidades de rotación se consigue con motores de polos conmutables y rotor de jaula, operando entonces con una relación de las velocidades de rotación de 1:2, con un devanado en conexión Dahlander.

Elementos mecánicos de transmisión

Generalidades
La cuidadosa colocación de la máquina sobre una superficie exactamente plana y el buen balanceo de las piezas a montar en el extremo de la flecha son condiciones indispensables para la marcha uniforme y libre de trepidaciones. Si la máquina se atornilla sobre una base que no sea plana, quedará sujeta a tensiones internas. Consecuencia de ello son las cargas adicionales que gravitan sobre los rodamientos, lo que a su vez motiva una marcha irregular y perturbaciones en los rodamientos.

Transmisión por acoplamiento
En la mayoría de las ocasiones, la máquina motriz y la máquina accionada están directamente acopladas entre sí de forma elástica. Para adosar las máquinas formando grupos con otras de émbolo, por ejemplo, con motores diesel, se recomienda la utilización de acoplamientos especiales elásticos. Si las máquinas se acoplan entre sí, habrá que alinearlas cuidadosamente. Los ejes tienen que estar exactamente alineados y coincidir además sus centros. Casi todos los tipos de acoplamiento someten circunstancialmente los rodamientos a esfuerzos considerables si no están exactamente alineados, dando origen a una marcha irregular con emisión de ruido, deteriorándose además, en mayor o menor medida, los elementos de transmisión de acoplamiento. Esto rige asimismo para el empleo de acoplamientos elásticos. Por regla general, se utilizan acoplamientos flexibles que pueden ser rígidos al giro (por ejemplo, acoplamientos de arco dentado) o elásticos al giro. Los acoplamientos elásticos al giro forman con las masas que a través suyo se unen, un sistema capaz de oscilar con una cierta frecuencia propia. Si se originan choques periódicamente, es imprescindible observar que la frecuencia de reproducción de los choques no coincide con la frecuencia propia, puesto que en el caso de establecerse resonancia o en las proximidades de la frecuencia de resonancia, el sistema quedaría sometido a oscilaciones de una amplitud excesiva y a esfuerzos extraordinarios. Los acoplamientos más suaves reducen la frecuencia propia, elevándola los más rigidos. En casos especiales se emplean asimismo embragues que acoplan o desacoplan el eje del motor y el de la máquina, tanto en estado de reposo como durante la marcha.

Transmisión por bandas
En el caso de que el accionamiento se haga por bandas, la máquina tiene que estar montada sobre carriles tensores o sobre una base desplazable, con el fin de poder ajustar la tensión correcta de la correa y de retensarla cuando sea preciso. Si la correa se tensa demasiado, se ponen en peligro los cojinetes y el eje; por el contrario, si la tensión es demasiado baja, resbala la correa.

Dispositivos tensores para el accionamiento por bandas trapezoidales
Estos dispositivos se colocarán de manera tal que la distancia entre poleas se pueda variar, de forma que las correas se puedan colocar sin estar sometidas a tensión. Las correas se tensarán en tal medida que no tengan flecha y que no golpeen durante el servicio.

Determinación de las poleas
En la mayoría de los catálogos se hace referencia a las poleas normales. En el caso de que éstas no se pudieran utilizar, se dimensionarán las poleas de tal manera que no sobrepasen los valores admisibles de las fuerzas que actúan sobre el extremo de la flecha de la máquina eléctrica. En los accionamientos por correas, la fuerza transversal depende de la tracción de la correa y de la tensión previa de ésta. Si el accionamiento se lleva a cabo por correas planas, la dimensión debe proyectarse de tal forma que la polea no roce con la tapa portacojinetes. Con vistas al funcionamiento correcto de la transmisión, la anchura de la polea no debe ser mayor que el doble de la longitud del extremo del eje. Las dimensiones de las poleas se determinarán de acuerdo con la potencia a transmitir, la clase de polea utilizada y la relación de transmisión que se pretenda conseguir. Si fuese preciso, se consultará a la empresa suministradora de la correa. Para la polea se puede calcular aproximadamente de la siguiente forma:

$$F_T = 2 \times 10^7 \cdot \frac{P \cdot c}{nD}$$

siendo:
F_T= fuerza axial en Nm
P = potencia nominal del motor en kW
n = velocidad de rotación del motor en rpm
D = diámetro de la polea a emplear en mm
c = factor de tensión previa de la correa; este factor asciende aproximadamente a los siguientes valores:
c = 2 para correas de cuero planas, normales , con rodillo tensor
c = 2.2 para correas especiales de adhesión y correas trapezoidales

Cuando la fuerza axial calculada sea superior a la admisible y eligiendo otra correa sometida a otra tensión previa no se consigna una modificación esencial, habrá que elegir otra polea de diámetro superior. El peso de la polea se sumará a la fuerza transversal. Al elegir las poleas, habrá que observar que la calidad del material quede comprendido dentro de los límites admisibles, y que se pueda transmitir la potencia bajo una tensión previa normal de la correa. En la tabla figuran los diámetros máximos admisibles de las poleas de fundición. Para mayores diámetros habrá que emplear poleas de acero.

Aclaraciones técnicas

Velocidad de rotación rpm	Diámetro máximo admisible de las poleas de hierro fundido mm
3000	180
2500	200
2000	250
1500	355
1250	400
1000	560
750	710
600	900
500	1000

La tabla indica al mismo tiempo aquellos diámetros para los cuales la velocidad de las correas planas de cuero de calidad mediana resulta más favorable. Si se emplean correas trapezoidales, la velocidad más favorable de la correa es menor, lo que se consigue reduciendo en un 20% el diámetro. Si se utilizan correas de adhesión especiales, por ser mayor la velocidad admisible de la correa, se pueden aumentar aproximadamente en un 20% los diámetros que figuran en la tabla, debiéndose emplear, sin embargo, poleas de acero. La distancia entre ejes de las dos poleas se fijará en concordancia con las indicaciones del fabricante de correas y de poleas. En los lugares que estén expuestos a peligro de explosión, solamente podrán utilizarse correas en las que sea imposible que se originen cargas electrostáticas.

Accionamiento por engranes
Si la transmisión se realiza mediante ruedas dentadas, habrá que observar que los ejes de las máquinas sean paralelos entre sí y que sean exactamente circulares las marchas del piñon y de la corona. Los dientes del piñon no se podrán atascar en ninguna posición de la corona, puesto que, de lo contrario, se someterían los rodamientos a un trabajo inadmisible, motivándose, además, vibraciones, trepidaciones y ruidos molestos. Para comprobar el buen ajuste, se coloca entre el piñón y la corona una tira de papel del mismo ancho del piñón. Al girar, se marcan sobre la tira de papel los puntos en los que el ajuste es defectuoso. La comprobación se extenderá a todos los dientes de la corona. Según sea el resultado conseguido, se alineará cuidadosamente la máquina y se repetirá la comprobación hasta que se haya conseguido un ajuste uniforme en todos los dientes.

Montaje de los elementos de accionamiento
Los acoplamientos, las poleas para bandas, los piñones y demás elementos similares sólo se podrán montar, con cuidado y lentamente, con el dispositivo adecuado. Estos dispositivos se pueden utilizar generalmente para extraer los mencionados elementos. Los golpes deterioran los cojinetes y por tanto es imprescindible evitarlos.

MICROMASTER, MICROMASTER Vector y MIDIMASTER Vector: Los favoritos de la clase estándar

El mercado de la variación de velocidad:
Las soluciones mecánicas de variación de velocidad sobre sistemas industriales, han sido progresivamente sustituidas por controles electrónicos de última generación sobre motores eléctricos tradicionales. Éstos ofrecen soluciones mucho más simples y reducen notablemente los costos del mantenimiento. Los MICROMASTER / MIDIMASTER - sinónimos de calidad en este tipo de tecnología - han sido los precursores de esta transición.
Ahora completamos las características estándar, incluyendo de serie el control vectorial para aplicaciones que demanden un control dinámico mejor.

Tecnología de punta para todo tipo de aplicaciones
Los convertidores MICROMASTER ofrecen siempre la mejor solución en todos los aspectos: la mejor solución económica, la mejor solución tecnológica.
Pueden configurarse de manera muy simple para resolver cualquier aplicación desde cadenas de fabricación hasta seguimiento de la órbita de satélites.

Gracias a la introducción del nuevo SENSORLESS VECTOR CONTROL, los MICROMASTER Vector y MIDIMASTER Vector se convierten en la primera elección para aplicaciones del tipo elevadores, empaquetadoras o lavadoras industriales.

La misma solución para todas las aplicaciones
Toda la familia MICROMASTER; MICROMASTER Vector, MIDIMASTER Vector contiene juegos de parámetros idénticos configurables para cualquier aplicación.

En la mayoría de los casos los parámetros de fábrica son más que suficientes, pero bastan unas sencillas operaciones para configurar aplicaciones más complejas. Estas operaciones se pueden realizar bien por el panel de mandos estándar de todos los equipos, bien a través del panel opcional OPM2. Todos los convertidores de Siemens ofrecen un juego de parámetros claramente definidos, para resolver fácilmente cualquier aplicación.

con un PC estándar
- Resistencias de frenado de distintos tamaños y potencias.
- Módulos de frenado externo para unidades MIDIMASTER Vector.
- Módulo PROFIBUS para comunicaciones hasta 12 Mbaud. Software SIMOVIS bajo Windows 95/NT.
- Bobinas de salida
- Filtros tipo du/dt.

En cualquier parte del mundo
Los convertidores MICROMASTER, MICROMASTER Vector y MIDIMASTER Vector ofrecen un amplio rango de tensiones y frecuencias de alimentación, así como el mejor y más completo rango de potencias del mercado conforme a todos los estándares.

Alta fiabilidad
Los convertidores MICROMASTER, MICROMATER Vector y MIDIMASTER Vector marcan nuevas pautas en los estándares de calidad no sólo en componentes sino en fabricación, tecnología y trabajo humano.
Los convertidores están totalmente protegidos para prevenir posibles daños ocasionados por las personas o por las aplicaciones.

Sencillo de manejar
La puesta en marcha del MICROMASTER, MICROMASTER Vector, MIDIMASTER Vector se hace todavía más sencilla gracias al "autotuning" . El juego de parámetros permite el acceso a toda la funcionalidad del convertidor. Todos los convertidores ofrecen un amplio rango de características comunes desde la suavización de rampas, frecuencias fijas, rearranque automático. Con el nuevo panel OPM2 podemos incluso configurar dos juegos de parámetros diferentes del motor.

Un amplio rango de opciones
Un amplio rango de opciones adicionales se ofrecen para completar las características de los convertidores MICROMASTER, MICROMASTER Vector y MIDIMASTER Vector.
- Un nuevo panel de control externo (OPM2) como opción para MICROMASTER y MICROMASTER Vector y de serie para toda la gama MIDIMASTER Vector. Permite el control como maestro de hasta 31 convertidores distintos sobre una red de tipos RS485. Incorpora además un interface a RS232/485 para la conexión directa

MICROMASTER, MICROMASTER Vector y MIDIMASTER Vector: Fuerza gracias a la comunicación

Abierto al mundo de las comunicaciones industriales PROFIBUS-DP
Todos los convertidores de estándar de Siemens se suministran con un interface serie tipo USS. Este estándar RS485 permite que hasta 31 unidades MICROMASTER, MICROMASTER Vector, MIDIMASTER Vector y COMBIMASTER se pueden conectar sobre un bus de comunicación, con el consiguiente
ahorro en los gastos de cableado. Es posible ademas, controlar todas las unidades desde PC con nuestro software SIMOVIS.

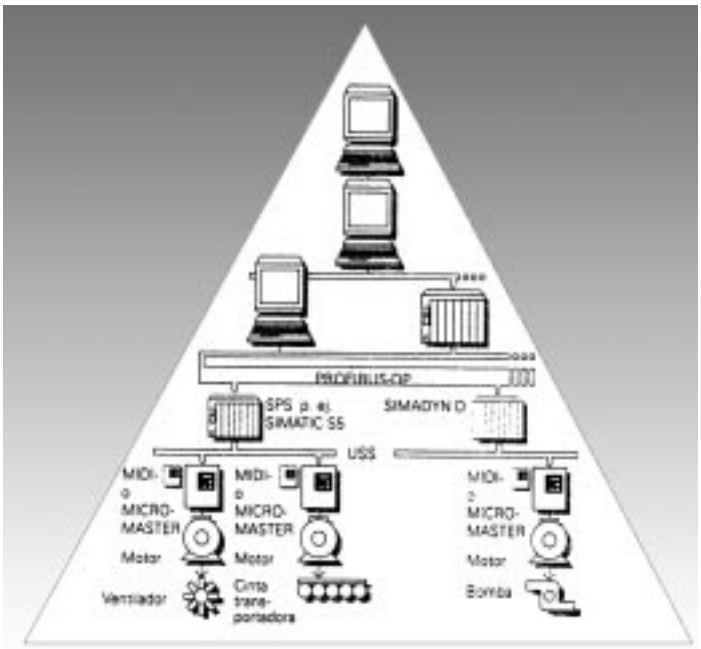

PROFIBUS-DP
Para sistemas de automatización superior, es posible incorporar sobre el frontal de los equipos la tarjeta OPMP, que permite que todos los equipos puedan ser configurados y controlados a través del PROFIBUS-DP, que se convierte día a día en el estándar universal de comunicación industrial. Este sistema ofrece comunicaciones abiertas entre sistemas para la transmisión de datos. PROFIBUS-DP es totalmente compatible con la norma DIN 19245 y funciona con velocidades de transmisión de hasta 12 Mbaud. Hasta 125 convertidores pueden ser conectados en un bus al mismo tiempo.

Compatible con Windows
El PROFIBUS-DP puede ser configurado graficamente en sistemas bajo Windows. Todos los convertidores pueden ser conectados y posicionados en el sistema con un simple click en el ratón.

PROFI PROCESS FIELD BUS

PROFIBUS

MICROMASTER; MICROMASTER Vector
MIDIMASTER Vector

Técnica con el máximo rendimiento

MICROMASTER / MICROMASTER Vector

MICRO MASTER	MICRO MASTER Vector	Potencia del motor kW	Intensidad de salida nominal A	Intensidad de salida permanente A	Intensidad de entrada (I_{m}eff) A	Anch. x Alt. x prof. mm	Peso Kg	Convertidor No. de pedido MICROMASTER	Convertidor No. de pedido MICROMASTER Vector
Monofásico/trifásico 230V± 15% (sin filtro)					1.ph/ 3ph.				
MM12/2	MMV12/2	0.12	0.75	0.8	1.8/1.1	73X147X141	0.9	6SE9210-7CA40	6SE3210-7CA40
MM25/2	MMV25/2	0.25	1.5	1.7	3.2/1.9	73X147X141	0.9	6SE9211-5CA40	6SE3211-5CA40
MM37/2	MMV37/2	0.37	2.1	2.3	4.6/2.7	73X147X141	0.9	6SE9212-1CA40	6SE3212-1CA40
MM55/2	MMV55/2	0.55	2.6	3.0	6.2/3.6	73X147X141	0.9	6SE9212-8CA40	6SE3212-8CA40
MM75/2	MMV75/2	0.75	3.5	3.9	8.2/4.7	73X147X141	0.9	6SE9213-6CA40	6SE3213-6CA40
MM110/2	MMV110/2	1.10	4.8	5.5	11/6.4	149X184X172	2.4	6SE9215-2CA40	6SE3215-2CB40
MM150/2	MMV150/2	1.50	6.6	7.4	14.4/8.3	149X184X172	2.4	6SE9216-8CA40	6SE3216-8CB40
MM220/2	MMV220/2	2.20	9.0	10.4	20.2/11.7	185X215X195	4.8	6SE9221-0CA40	6SE3221-0CC40
MM300/2	MMV300/2	3.00	11.8	13.6	28.3/16.3	185X215X195	4.8	6SE9221-3CA40	6SE3221-3CC40
MM/400/2*	MMV400/2*	4.00	15.9	17.5	21.1	185X215X195	4.8	6SE9221-8CA40	6SE3221-8CC40

Trifásico 400-500V ± 10% 400V 500V 400V 500V

MM37/3	MMV37/3	0.37	(1/2)	1.05	0.95	1.20	1.06	2.2	73X147X141	6SE9211-DA40	6SE3211-1DA40
MM55/3	MMV55/3	0.55	(3/4)	1.50	1.30	1.60	1.45	2.8	73X147X141	6SE9211-4DA40	6SE3211-4DA40
MM75/3	MMV75/3	0.75	(1.0)	2.00	1.80	2.10	1.90	3.7	73X147X141	6SE9212-0DA40	6SE3212-0DA40
MM110/3	MMV110/3	1.1	(1.5)	2.80	2.50	3.00	2.70	4.9	73X147X141	6SE9212-7DA40	6SE3212-7DA40
MM150/3	MMV150/3	1.5	(2.0)	3.70	3.30	4.00	3.60	5.9	73X147X141	6SE9214-0DA40	6SE3214-0DA40
MM220/3	MMV220/3	2.2	(3.0)	5.20	4.60	5.90	5.30	8.8	149X184X172	6SE9215-8DB40	6SE3215-8DB40
MM300/3	MMV300/3	3.0	(4.0)	6.80	6.00	7.70	6.90	11.1	149X184X172	6SE9217-3DB40	6SE3217-3DB40
MM/400/3	MMV400/3	4.0	(5.0)	9.20	8.10	10.20	9.10	13.6	185X215X195	6SE9221-0DC40	6SE3221-0DC40
MM550/3	MMV550/3	5.5	(7.5)	11.80	10.40	13.20	11.80	17.1	185X215X195	6SE9221-3DC40	6SE3221-3DC40
MM750/3	MMV750/3	7.5	(10.0)	15.80	13.90	17.00	15.20	22.1	185X215X195	6SE9221-5DC40	6SE3221-5DC40

MIDIMASTER Vector

Tipo	Tensión nominal de entrada	Intensidad nominal de salida del convertidor "constante" torque	Intensidad nominal de salida del convertidor "variable" torque	Potencia del motor				MIDIMASTER Vector IP21		
		Capacidad de sobrecarga	Intensidad permanente sin capacidad de sobrecarga	Carga de par constante (cintas trans-portadoras y hormigoneras, etc).		Carga "variable torque" (ventiladores y bombas, etc.)		No. de pedido	Dimensiones Anch. x alt. x prof. (mm)	Peso Kg
	V	A	A	kW	HP	kW	HP			
MDV 550/2		22	28	7.5	5.5	7.5	10	6SE3222-3CG40	450x275x210	11
MDV 750/2		28	42	10	7.5	11	15	6SE3223-1CG40	550x275x210	14.5
MDV 1100/2		42	-	15	11	-	-	6SE3224-2CH40	550x275x210	15.5
MDV 1500/2		54	68	20	15	18.5	25	6SE3225-4CH40	650x275x285	26.5
MDV 1850/2		68	80	25	18.5	22	30	6SE3226-8CJ40	650x275x285	27.0
MDV 2200/2		80	95	30	22	30	40	6SE3227-5CJ40	650x275x285	27.5
MDV 3000/2		104	130	40	30	37	50	6SE3231-0CK40	850x420x310	55.0
MDV 3700/2		130	154	50	37	45	60	6SE3231-3CK40	850x420x310	55.5
MDV 45002		154	-	60	45	-	-	6SE3231-5CK40	850x420x310	56.5
380-500V ± 10%, 3PH										
MDV 750/3		19 (17)*	23.5 (21)*	-	-	11	15	6SE3221-7DG40	450x275x210	11.5
MDV 1100/3		26 (21)*	30 (27)*	11	15	15	20	6SE3222-4DG40	450x275x210	12.0
MDV 1500/3		32 (27)*	37(34)*	15	20	18.5	25	6SE3223-0DH40	550x275x210	16.0
MDV 1850/3		38 (34)*	43.5 (40)*	18.5	25	22	30	6SE3223-5DH40	550x275x210	17.0
MDV 2200/3		45 (40)*	58 (52)*	22	30	30	40	6SE3224-2DJ40	650x275x285	27.5
MDV 3000/3		58 (52)*	71 (65)*	30	40	37	50	6SE3225-5DJ40	650x275x285	28.0
MDV 3700/3		72 (65)*	84(77)*	37	50	45	60	6SE3226-8DJ40	650x420x285	28.5
MDV 4500/3		84 (77)*	102(96)*	45	60	55	75	6SE3238-4DK40	850x420x310	57.0
MDV 5500/2		102 (96)*	138 (124)*	55	75	75	100	6SE3231-0DK40	850x420x310	58.5
MDV 7500/3		138 (124)*	168(156)*	75	1001	90	120	6SE3231-4DK40	850x420x310	60.0

Siemens cerca de Usted:

Sucursales:

Oficinas de Ventas México:
Poniente 122 No. 579
Col. Industrial Vallejo
02300 México, D.F.
(015) 5328-21-14 al 17
Fax 5328-20-96

Sucursal Guadalajara:
Camino a la tijera No. 1
Km. 3.5 Carretera
Guadalajara-Morelia
45640 Tlajomulco de
Zúñiga, Jal.
(013) 818-21-97
Fax 818-21-66

Sucursal Monterrey:
Carr. Miguel Alemán Km.
16.5 "C" Parque Industrial
Almacentro 66600
Apodaca, N.L.
(018) 369-36-73 al 86
Fax 369-39-12

Oficinas de ventas

Aguascalientes:
Av. de las Américas
No. 105 Desp. 102
Fracc. Las Américas
20230 Aguascalientes, Ags.
(0149) 16-44-57
Fax 16-22-48

Chihuahua:
Intermedia Bosques de
Yuridia No. 2706 Altos
Fracc. Sicomoro
31276 Chihuahua, Chih.
(0114) 16-63-97
16-22-10
Fax 37-14-75

Culiacán:
Paseo Niños Héroes 680
Oriente, Col. Centro
80000 Culiacán, Sin.
(0167) 16-08-24
16-10-27
Fax 16-08-71

Gómez Palacio:
Av. Lázaro Cárdenas y
Canatlán s/n
Parque Industrial Lagunero
35070 Gómez Palacio, Dgo.
(0117) 50-09-07
50-04-32
Fax 50-10-48

Hermosillo:
Blvd. Fco. Eusebio Kino
No. 177 Int 8 Plaza Pitic Col.
5 de Mayo
83150 Hermosillo, Son.
(0162) 15-64-06
Fax 15-63-54

León:
Blvd. Venustiano Carranza
No. 105
Col. San Miguel
37390 León, Gto.
(0147) 12-64-11 y 12
Fax 12-70-65

Puebla:
Privada Topacio 3505
Despacho 401
Col. Residencial Esmeralda
72400 Puebla, Pue.
(0122) 49-40-01
49-40-11
Fax 49-43-01

Mérida:
Calle 34 No. 392
Deptos. 1 y 2 por 39 y 37
Col. Emiliano Zapata Nte.
Plaza Lafayette
97129 Mérida, Yuc.
(0199) 44-04-39
Fax 44-03-00

Querétaro:
Km. 8 Carr. 45 Libre
Querétaro-Celaya, Fracc.
Industrial Balvanera
76920 Corregidora, Qro.
(0142) 25-05-02
Fax 25-02-91

Tijuana:
Calle Misión de Loreto
2962-101
Zona Río
22320 Tijuana, B.C.
(0166) 34-11-34 y 34-11-57
Fax 34-63-67

Veracruz:
Av. Tiburón 430-3
Edificio Alida
Fracc. Costa de Oro
94299 Boca del Río, Ver.
(0129) 22-28-44 y 49
Fax 22-28-52

Centroamérica

Costa Rica:
Siemens SA de CV
La Uruca, San José,
Costa Rica
Apartado Postal 10022-1000
S.J.
(506) 287-50-50
Fax 221-50-50

Honduras:
Relectro S. de R.L.
Plaza General San Martín
No. 436 Col. Palmira,
Apartado Postal 1098
Tegucigalpa, D.C.
(504) 32-40-62
32-40-88
Fax 32-41-11

Nicaragua:
Siemens SA
Carretera Norte Km 6
Apartado Postal 7, Managua
(505) 249-11-11
249-15-49
Fax 249-18-49

Panama:
Siemens SA
Apartado Postal 6-8682
El Dorado
(507) 287-50-50
Fax 221-50-50

Guatemala:
Siemens SA
2a Calle 676 Zona 10
Apartado Postal 1959
Ciudad de Guatemala
(502) 360-70-80
331-30-80
Fax 334-36-69
334-36-70

El Salvador:
Siemens SA
Calle Siemens No. 43
Parque Industrial Santa
Elena, Antiguo Cuscatlan
Apartado Postal 1626
San Salvador
(503) 278-33-33
Fax 278-33-34

Centros de fabricación

Fábrica Guadalajara:
Camino a la Tijera No. 1
Km. 3.5 Carretera
Guadalajara-Morelia
45640 Tlajomulco de
Zúñiga, Jal.
(013) 818-21-00
Fax 818-21-35

Fábrica de Tableros:
Km. 8 Carr. 45 Libre
Querétaro-Celaya, Fracc.
Industrial Balvanera
76920 Villa Corregidora, Qro.
(0142) 25-03-54
25-01-73
25-03-72
Fax 25-02-91

An Experimental Study on Composite Control of Switched Reluctance Motors

David G. Taylor

This paper illustrates how two-time-scale nonlinear control design techniques are applied to switched reluctance motors. The use of reduced-order feedback linearization methods leads to improved performance by reducing torque ripple. First, a nonlinear dynamic model is developed and decomposed into separate slow and fast subsystems. Second, a feedback control is designed such that, whenever the fast subsystem is at equilibrium, the dynamics of the slow subsystem are input-output equivalent to a second-order transfer function. Third, experimental results are presented from a laboratory implementation of a position control system.

Introduction

The mechanical construction features of the switched reluctance (SR) motor make it inexpensive and reliable. It operates without brushes or slip-rings and, although salient poles exist on both stator and rotor, the stator windings are concentrated on pole pairs and the rotor contains no windings or magnets. This mechanical simplicity has contributed to their recent popularity, but it is also the cause of their inherently pulsating mode of torque production [7].

Many applications require brushless motors capable of low torque ripple operation. Both the permanent-magnet synchronous motor and the induction motor are common choices for such applications. Unlike these motors, the SR motor cannot be operated with sinusoidal excitation and, consequently, has been mainly used for tasks which do not require accurate torque control. This paper describes nonlinear control methods which can significantly reduce the torque ripple of the SR motor, and demonstrates the effectiveness of these methods through a laboratory experiment. Since alternative types of motors do exist, however, it is natural to question why torque ripple reduction for the SR motor is a worthwhile goal.

Our work is motivated by four main considerations. First, construction costs for the SR motor can be much lower than for its competitors [7]. This low cost is attributed to the materials used and the relatively few manufacturing steps required. Second, high-temperature environments may not allow the use of permanent magnets, and cooling a wound rotor in such cases may not be feasible [8]. In contrast, for the SR motor most of the losses occur on the stator which is easy to cool. Third, as far as electrostatic motors are concerned, a popular design is the electromagnetic dual of the SR motor [2]. Although not yet common, these switched capacitance motors are being fabricated as micromotors on semiconductor wafers, and perhaps space-based robotic systems may benefit from the low weight of electrostatic actuators as well. Fourth, the use of electromagnetic gearing to boost torque and reduce speed is easily achieved by increasing the number of teeth stamped into SR motor laminations, in contrast to the more complex alternative of adding poles to the rotor of permanent-magnet machines [1],[5]. This property has already been used to advantage in the commercialization of the SR motor for direct-drive applications.

Despite such motivation, relatively few papers have appeared which focus on control system design for low torque ripple SR motor operation. A notable exception is [3] which employs a feedback linearization scheme. Although conceptually successful, the control technique in [3] is applied to a full-order SR motor model and, as a consequence, the control algorithm is prohibitively complex. In this paper, a design is discussed which implements the feedback linearization technique as it applies to a reduced-order SR motor model, and experimental results are provided which show to what extent the design objectives are met.

Dynamic Modeling

The most fundamental lumped-parameter characteristic of an SR motor is its flux linkage $\lambda_p=\lambda_p(\theta, i_p)$ due to current i_p in the pth stator phase, at a rotor position θ. From a specification of λ_p, several related physical quantities may be derived. We define the self-inductance of a phase by

$$L_p(\theta, i_p) = \frac{\partial \lambda_p(\theta, i_p)}{\partial i_p} \quad (1)$$

which is in agreement with the classical definition of inductance for linear magnetic circuits, but also applies when magnetic saturation is present. Ideally, there are no mutual inductances since stator phases are symmetrically wound on pole pairs. The voltage coefficient of the back-emf is given by:

$$K_p(\theta, i_p) = \frac{\partial \lambda_p(\theta, i_p)}{\partial \theta} \quad (2)$$

and the torque of electrical origin is found by differentiating the coenergy with respect to rotor position to yield

$$T_p(\theta, i_p) = \frac{\partial}{\partial \theta} \int_0^{i_p} \lambda_p(\theta, i_p)\, d i_p . \quad (3)$$

The total torque developed on the rotor is the sum of the P phase torques, that is

$$T_e(\theta, i_1, \ldots, i_P) = \sum_{p=1}^{P} T_p(\theta, i_p) . \quad (4)$$

Once these functions are known, the dynamic model can be easily established. The specific functions and coefficients used to model all these nonlinearities are discussed in the Appendix.

The phase torque T_p is a nonlinear function of both θ and i_p. Moreover, the sign of the torque produced is independent of the direction of current in the stator windings. Hence, we implicitly assume without loss of generality that $i_p \geq 0$ in all equations. A consequence of this unique torque production feature is that the electrical excitation must be applied as a sequence of pulses to the wind-

This work was partially supported by the National Science Foundation under Grants ECS-8909329 and ECS-9007778. *The author is with the School of Electrical Engineering, Georgia Institute of Technology, Atlanta, GA 30332-0250.*

0272-1708/91/0200-0031 $01.00©1991IEEE

ings, thus leading to the naturally pulsating electricaltorque.

In order to express the dynamics of a three-phase SR motor, we apply Newton's Law to the rotor and Kirchhoff's Law to the stator, yielding

$$\frac{d\theta}{dt} = \omega \tag{5}$$

$$\frac{d\omega}{dt} = J^{-1}\left(T_e(\theta, i_1, i_2, i_3) - T_m(\theta, \omega)\right) \tag{6}$$

$$\frac{di_p}{dt} = L_p^{-1}(\theta, i_p)\ (v_p - R_p i_p - K_p(\theta, i_p)\,\omega), \quad p = 1, 2, 3 \tag{7}$$

where the state variables are rotor position θ, rotor velocity ω, and stator currents i_1, i_2, i_3. The functions $T_e(\theta,i_1,i_2,i_3)$, $L_p(\theta,i_p)$, $K_p(\theta,i_p)$ are as defined above, $T_m(\theta, \omega)$ is the mechanical load torque, J is the total rotor and load inertia, R_p is the stator resistance, and v_1, v_2, v_3 denote the applied stator voltages.

To begin the two-time-scale analysis and design, it is assumed that stator voltages are applied according to

$$v_p = \gamma(u_p - i_p), \quad p = 1,2,3 \tag{8}$$

where up = up(q,w,t) is the control input for the pth phase and g is a positive design coefficient. The use of separate nested loops for feedback of electrical and mechanical variables, as indicated in (8), is common to many motor control systems. Note that although linear feedback is considered for electrical states i1, i2, i3, nonlinear feedback of mechanical states q and w will be necessary to achieve our control objective.

A decomposition of (5)-(8) into separate slow and fast subsystems [6] can be achieved by combining (7) and (8), and rewriting the electrical dynamics in the standard singular perturbation form

$$\varepsilon\frac{di_p}{dt} = L_p^{-1}(\theta, i_p) \cdot (u_p - i_p - \varepsilon\,(R_p i_p + K_p(\theta, i_p)\,\omega)) \tag{9}$$

where $\varepsilon = \gamma^{-1}$. From (9), it is clear that a two-time-scale treatment of this problem will consider the mechanical variables as "slow" and the electrical variables as "fast." The slow subsystem is obtained by formally setting $\varepsilon = 0$ in (9) and solving the resulting algebraic equation for i_p. Since $L_p(\theta,i_p)$ is strictly positive for all θ and i_p, this procedure results in the unique solution $i_p = u_p$. Using (5) and (6), the slow subsystem expressed in the t-scale is

$$\frac{d\theta}{dt} = \omega \tag{10}$$

$$\frac{d\omega}{dt} = J^{-1}(T_e(\theta,u_1,u_2,u_3) - T_m(\theta,\omega)). \tag{11}$$

In reality, u_p is only the quasi-steady-state value of i_p. The fast subsystem, which describes the dynamics of i_p away from $i_p = u_p$, is obtained by introducing a stretched time variable $\tau = t/\varepsilon$. In the τ-scale, the states of the slow subsystem (θ,ω) and inputs u_p are treated as fixed parameters and, with $\varepsilon = 0$ on the right-hand-side of (9), the fast subsystem is

$$\frac{di_p}{d\tau} = L_p^{-1}(\theta, i_p)\ (u_p - i_p), \quad p = 1, 2, 3 \tag{12}$$

An analysis of (12) easily shows that $i_p = u_p$ is its globally asymptotically stable equilibrium. For this reason, it is safe to assume that solutions of the slow subsystem (10)-(11) closely approximate the true trajectories of θ and ω from (5)-(8), for reasonably large γ. Whenever γ is not large enough, such an approximation is inaccurate and, thus, must be modified according to the integral manifold technique [6].

Control Design

Control design based on feedback linearization [4] is appealing since the resulting closed-loop dynamic behavior is linear. If performed with precision, what this approach has to offer our problem is the possibility for ripple-free torque, despite the significantly nonlinear model derived earlier. Although prior research [3] has shown that feedback linearization can be applied to the full-order model (5)-(7), we do not follow such an approach here for practical reasons. Instead, our experimental implementation of feedback linearization is designed with respect to the reduced-order model (10)-(11). Consequently, in this paper the feedback design requires only a linear dependence on the fastest states of the system, the stator currents, which can be easily implemented as an analog summing junction at the amplifier. Since position (and velocity) sensors typically feature digital outputs, no analog-to-digital converters need be used. Moreover, the only nonlinearities used for controller programming are T_e and T_m.

In view of the analysis above, we wish to remove the nonlinearity of the slow subsystem through feedback. To do so, we need to choose u_1, u_2, u_3 such that

$$T_e(\theta,u_1,u_2,u_3) = T_m(\theta,\omega) + J\alpha \cong T_e^{\,d}(\theta,\omega,\alpha). \tag{13}$$

In (13), the term $T_e^{\,d}$ is defined as the "desired" value of electrical torque, computed on the basis of mechanical variable measurements and the acceleration command a. A two-step procedure is used to solve (13). First, desired phase torques $T_p^{\,d}$ are chosen so as to sum up to the total torque required,

$$\sum_{p=1}^{3} T_p^d = T_e^d(\theta, \omega, \alpha). \tag{14}$$

Second, phase current commands u_p are chosen to exactly match phase torque requests,

$$T_p(\theta,u_p) = T_p^{\,d} \tag{15}$$

Note that if the amplifiers were to impose perfect current tracking, then $i_p \equiv u_p$ and the dynamics would be those of a double-integrator

$$\dot{\theta} = \omega. \tag{16}$$

$$\dot{\omega} = \alpha. \tag{17}$$

Note that (14) and (15) uniquely specify the reference currents u_1, u_2, u_3 during position intervals for which only one phase can produce torque of the proper polarity. However, when two phases can contribute, there exist many possible ways to satisfy (14) and (15). Hence, the sequential use of stator phases to contribute torque further requires the specification of an electronic commutator, that is, a rule for turning-off one phase while turning-on another. For the experimental work presented in the next section, the electronic commutator was chosen so that, when phase p is deemed no longer useful to develop torque of the proper sign, then $T_p^{\,d} \to 0$ at a constant rate in time.

Implementation of this strategy is complicated by the fact that even (15) cannot typically be solved for u_p in closed-form. Only when magnetic saturation is ignored, torque is proportional to the square of current as shown in the Appendix, and thus u_p can be expressed as

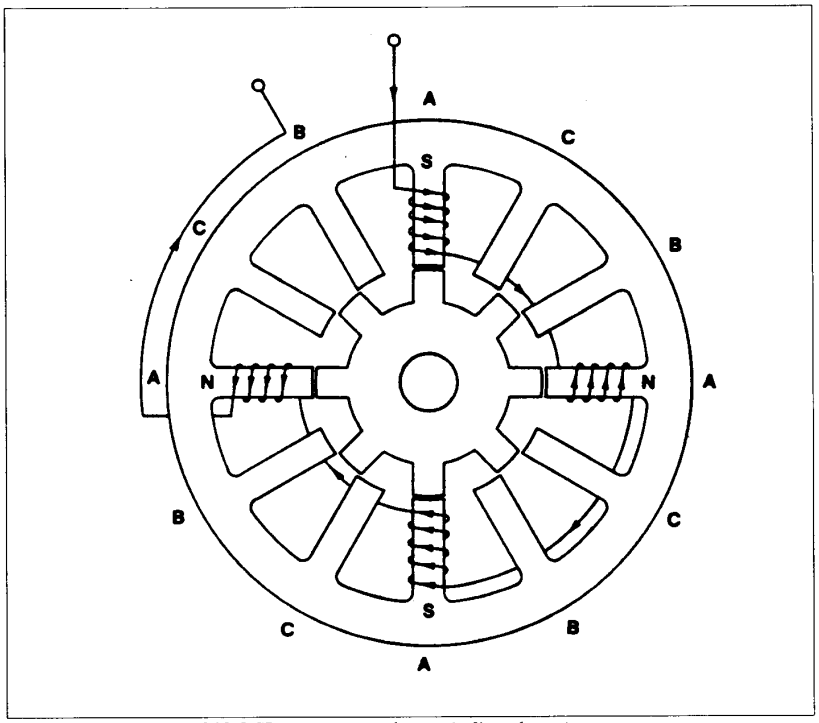

Fig. 1. Cross-section of 12/8 SR motor (one phase winding shown).

$$u_p = \left(\frac{2\,T_p^d}{N \sum_{n=2}^{\bar{n}} n\,l_n \sin\left(n\,N\,\theta - \phi_p\right)} \right)^{\frac{1}{2}} \qquad (18)$$

for values of θ at which this function is well-defined, and $u_p = 0$ otherwise.

To summarize, once the nonlinear transformation (14)-(15) has been developed, it does not ever need to be changed. Different loads are treated by modifying (13), and various control objectives can be met by designing α as necessary. For instance, a position controller for the SR motor is defined by (8) and (13)-(15), together with the PID compensator

$$\alpha = k_p e + k_i \int_0^t e\,dt + k_d \frac{de}{dt} \qquad (19)$$

where $e = r - \theta$ is the position error and r is the set-point. The linear dependence of this controller on i_p, and the possibility for neglecting nonlinearities appearing in Kirchhoff's Law, are both desirable features due to engineering considerations.

Experimental Results

A cross-section view of the 12/8 SR motor used in the experimental work is shown in Fig. 1. Since the need for reduced torque ripple is mainly present in direct-drive applications, one might suspect that our experiment would employ an SR motor with many more teeth on the stator and rotor, that is, an SR motor designed for higher torque and lower speed. However, use of the 12/8 SR motor will nevertheless suffice to demonstrate the application of nonlinear control and to reveal its benefits.

The position control system, shown in Fig. 2, consists of four main components: the motor/amplifier with position and current sensors; a nonlinear transformation which involves electrical variables; another nonlinear transformation depending only on mechanical variables; a PID position regulator loop. The SR motor frame size is 2.0 inches in diameter and 2.5 inches in length, and each of the phase windings has a resistance of 20 Ω and an average self-inductance of 45 mH. With amplifiers having gain-bandwidth products of 1.3 MHz and saturation limits of $\pm$ 45 V, it was determined that the gain $\gamma = 10$ V/mA provided excellent current tracking. Additional experimental data obtained from the same apparatus appears in [9].

The most significant control system components are the two nonlinear transformations since they achieve the feedback linearization. These transformations are actually implemented with two different sampling rates because the commutation process requires that compensation of the electrical torque nonlinearity (14)-(15) must occur faster than mechanical torque compensation (13), especially for a direct-drive SR motor. Hence, in Fig. 2 the components labeled as "fast" use digital and analog hardware whereas the "slow" components use microcomputer-based software programs. A benefit of this architecture is that new control objectives with new mechanical loads are met by

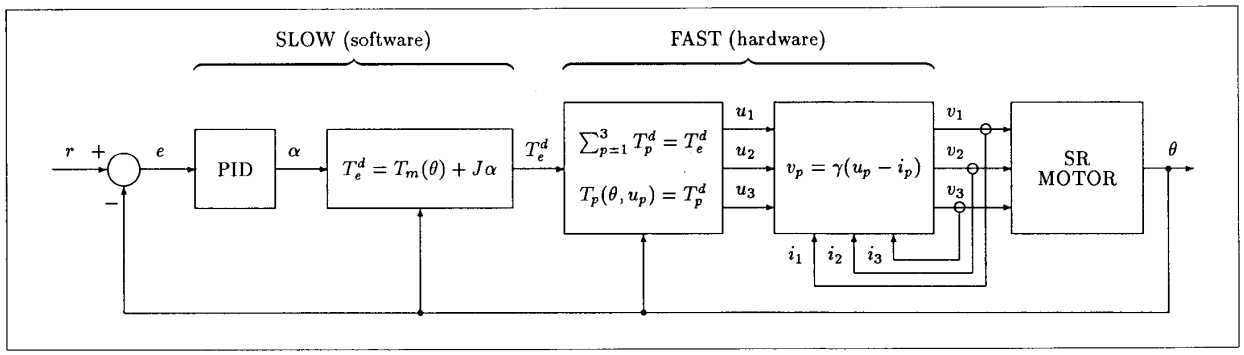

Fig. 2. Block diagram of the nonlinear control system.

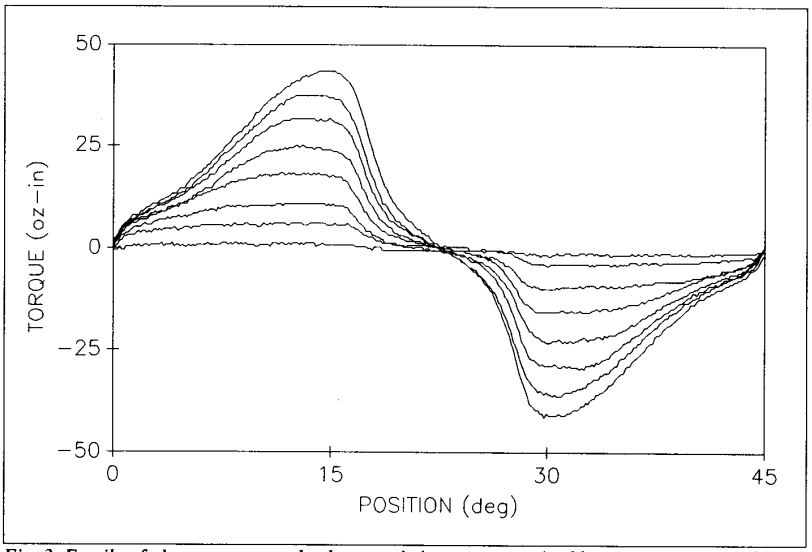

Fig. 3. Family of phase torque-angle characteristics, parameterized by current in steps of 175 mA.

simply modifying software and do not require hardware redesign.

Perhaps the most complex element of this control system design is the hardware portion of the nonlinear transformation. Its purpose is essentially to map a desired torque command into three current commands for the phase windings. An analogous process is achieved by the brush-commutator in standard DC motors, and by the DQ-transformation in sinusoidally excited brushless motors. In our case, implementation of the appropriate transformation requires knowledge of a three-dimensional nonlinear surface, called the current manifold, which is an implicit function defined by the family of phase torque-angle characteristics parameterized by phase current. This current manifold can be computed from direct measurements on the specific SR motor selected for use, then stored in a memory chip on the transformation circuit.

The procedure of programming the transformation circuit with a current manifold has been automated. A low-speed rotation of the SR motor is initiated by an external drive mechanism, and a reference command is applied to a current regulating amplifier to establish a known value of current in one stator winding. A position encoder is continuously monitored, and the output of a torque transducer is sampled each time the position value changes. Once a torque sample has been obtained for all positions of interest and stored, the current is incremented and the process is repeated. The forced rotation is slow enough to neglect torque sensor dynamics. Applied to the SR motor of Fig. 1, this scheme results in the characteristics shown in Fig. 3, where each curve corresponds to constant current in steps of 175 mA. The data must next be filtered to remove unwanted measurement noise and must also be rearranged in a different tabular format. More specifically, the independent variables must be position and torque, and the problem is to find the corresponding values of current given only the original torque data. Note that the use of this tabular representation is the only practical method of solving the transcendental torque equation in terms of current in real time. Application of a simple iterative procedure to the filtered torque data leads to the resulting current manifold shown in Fig. 4, where each curve corresponds to constant torque in steps of 1.6 oz-in. The singularities in Fig. 4 at extreme position values clearly illustrate the admissible range of commutation angles for this 15°/step SR motor. Basic operation of the transformation circuit is illustrated in Fig. 5, where its measured output is shown corresponding to a constant speed rotation at half-scale torque. The nonlinearity of these current reference waveforms has been carefully designed so as to cancell the nonlinearity of the torque function, and to eliminate torque ripple during the commutation intervals through which two phases simultaneously produce torque. The trajectories of the phase current commands change in a nontrivial way in response to variations in the magnitude and sign of desired torque.

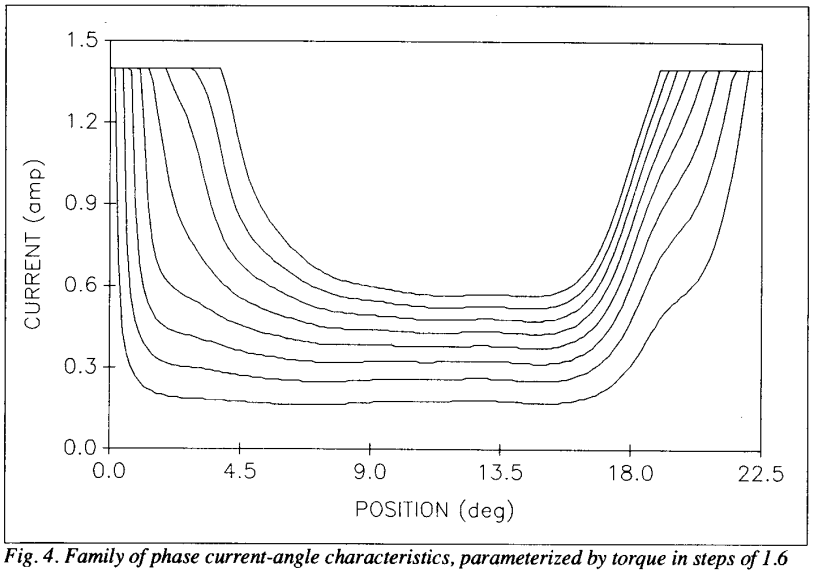

Fig. 4. Family of phase current-angle characteristics, parameterized by torque in steps of 1.6 oz-in.

Considering again the block diagram of Fig. 2, we now investigate the step responses of the system. The microcomputer is programmed with a PID algorithm (19) operating on the position error. Hence, from the viewpoint of the microcomputer-based feedback loop, the plant has one input (torque command) and one output (rotor position). The SR motor is left unloaded, except for its encoder, to keep inertial filtering from hiding the effects of torque ripple, and therefore $T_m = B\omega$. The numerical values of the total inertia and viscous friction coefficients are $J = 40 \times 10^{-6}$ Nm $\cdot$ s^2 and $B = 240 \times 10^{-6}$ Nm $\cdot$ s Since there is no nonlinear mechanical torque acting on the rotor, the mechanical nonlinearity compensation shown in Fig. 2 is unnecessary. Hence, the desired torque command is set equal to the PID compensator output, that is, $T_e{}^d = \alpha$. This dominantly

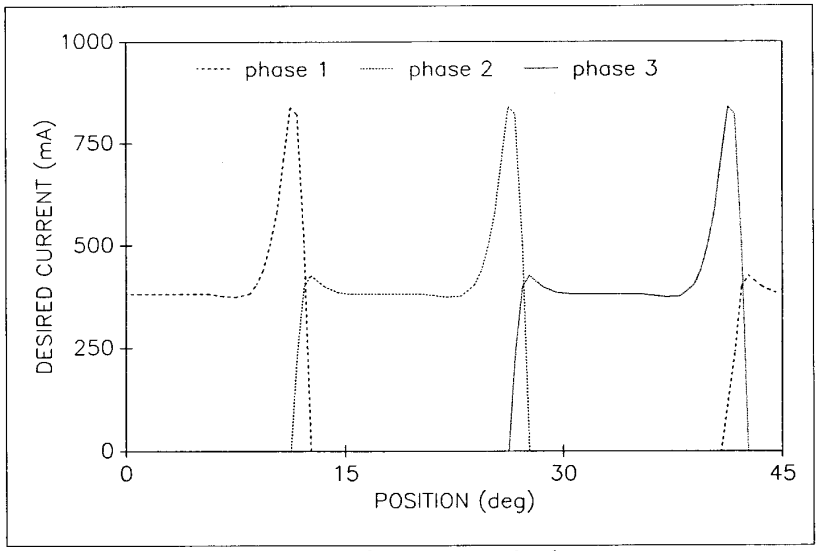

Fig. 5. Desired phase current trajectories for constant speed and constant torque.

second-order system will ideally have input-output dynamics described by the transfer function

$$\frac{\Theta(s)}{R(s)} = \frac{\omega_n^2}{s^2 + 2\zeta\omega_n s + \omega_n^2} \qquad (20)$$

where, assuming k_i is negligibly small, the damping ratio ζ and natural frequency ω_n are

$$\zeta = \frac{k_d + B}{2\sqrt{k_p J}} \qquad (21)$$

$$\omega_n = \sqrt{k_p / J} \ . \qquad (22)$$

Just as for the brush-commutated DC motor, we anticipate being able to assign a desired transient response through selection of k_p and k_d.

The goal of making the SR motor respond like a brush-commutated DC motor implies a type of operation which sounds simple, but actually is not. Such responses are not easily achieved by the SR motor because of the requisite commutations and torque sign changes. A properly selected allocation of current among the phases during commutation is crucial to avoid unwanted torque ripple. In cases where the position response requires both positive and negative torque operating modes, many traditional control schemes [7] would suffer from abrupt torque disturbances accompanying a requested change in torque sign.

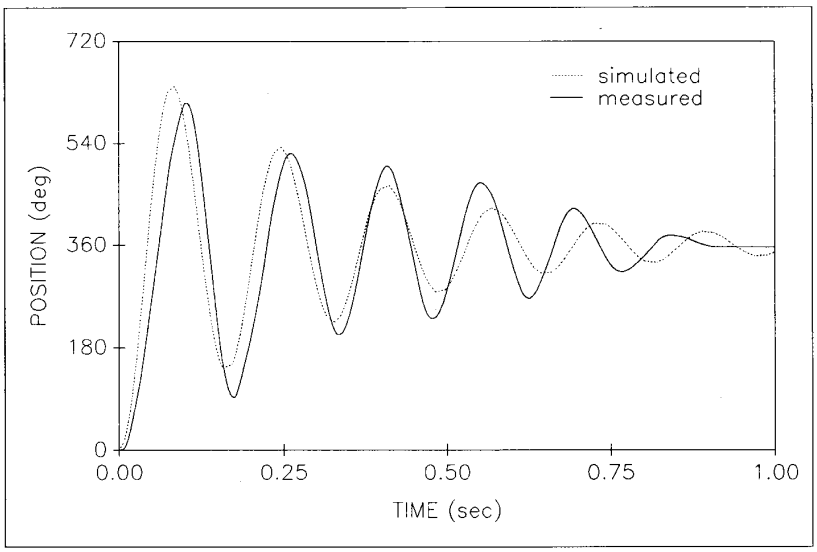

Fig. 6. Step response with $k_p = 0.06$, $k_i = 0$, $k_d = 0$.

The design principles of this control system overcome these common obstacles. In the step response tests, a step amplitude of 360° is used which requires at least 24 commutations, 15° apart. Two tests are conducted using significantly different values for ζ and ω_n. The first response is shown in Fig. 6 and corresponds to use of proportional gain only. Because of the large number of commutations and torque reversals required, this oscillatory response is a good diagnostic exercise. There are no visible indications that the commutation causes torque ripple and, furthermore, torque reversal is smoothly achieved without loss of synchronization. The second response, shown in Fig. 7, illustrates the well-tuned transient characteristics which can be achieved through adjustment of PID gains. The maximum overshoot has been dramatically reduced, and the rise time is somewhat improved as well. Again, commutation and torque reversal appear to be smoothly achieved.

In both Figs. 6 and 7, the measured step responses are compared to the simulated responses of the transfer function (20). A numerical comparison of overshoot, rise time, and settling time is provided in Tables I and II. The percent error in these specifications never exceeds 50%, and the combined average error is 23%. Hence, the transfer function (20) models the system quite well even though amplifier saturation, load friction, stator transients, and sampling effects have all been neglected. These tests indicate that, from the control viewpoint, the SR motor together with the accurately programmed transformation circuit may be treated as if they were simply a brush-commutated DC motor. The nonlinear multiple-input nature of the SR motor has been effectively removed and replaced with single-input linear dynamics.

Conclusions

This paper describes the design of a feedback control for the SR motor which incorporates both two-time-scale and feedback linearization methods. The objective of the design is to reduce the effects of torque ripple in a position control system. The merit of the approach taken is revealed through a laboratory experiment. On the basis of measured overshoot, rise time, and settling time, the prototype response is consistent with the desired linear response to within 23% error on average. The transient behavior of the SR motor can thus be adjusted over a wide range, and in a reasonably predictable fashion, by simply varying the gains

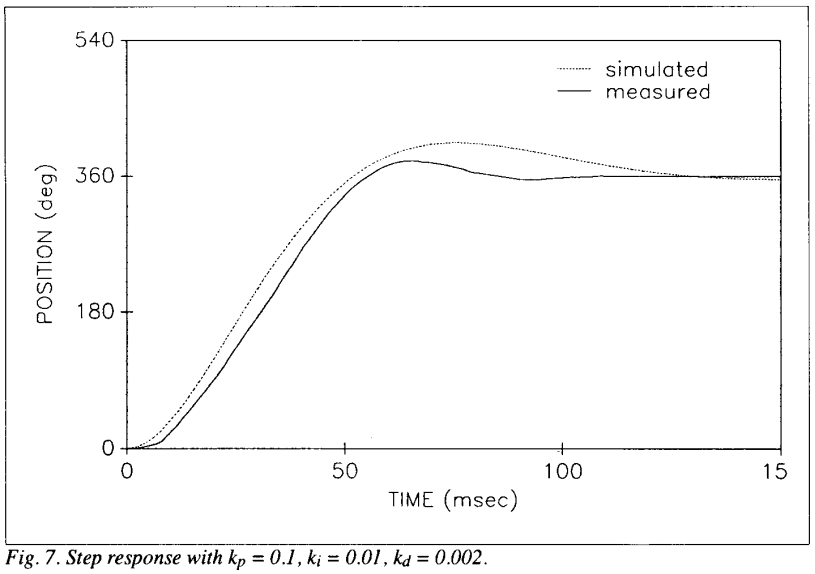

Fig. 7. Step response with $k_p = 0.1$, $k_i = 0.01$, $k_d = 0.002$.

of the outermost loop. Further transient performance enhancements are possible, at the expense of greater system complexity, and experimental work in this direction is already underway.

Appendix: Modeling Details

We consider here the torque production mechanism in more detail (see also [7],[8]). Magnetic saturation and fringing are typically significant, and their effects are modeled by introducing

Table I			
ζ = 0.08, ω_n = 38.7	Over shoot	Rise Time	Settling Time
Simulated	78%	29 ms	914 ms
Measured	70%	38 ms	800 ms
Percent Error	10%	31%	12%

a flux linkage function of the form

$$\lambda_p(\theta, i_p) = \sum_{m=1}^{\bar{m}} \sum_{n=0}^{\bar{n}} c_{mn}\, a_m^{\lambda}(i_p)\, b_n^{\lambda}(\theta) \quad (23)$$

$$a_m^{\lambda}(i_p) = 1 - e^{-mMi_p} \quad (24)$$

$$b_n^{\lambda}(\theta) = \cos(nN\theta - \phi_p) \quad (25)$$

where $N\theta$ and Mi_p are normalized values of rotor position and stator current, respectively, and where $\phi_p = (p-1)2\pi/P$. More specifically, N is the number of rotor poles and M could be, for instance, the reciprocal of rated current. Note that inductance cannot be defined in the traditional sense and, instead, the coefficients c_{mn} are selected to model the magnetic circuit characteristics. However, for small values of i_p when saturation effects may be neglected, (23) is closely approximated with $\bar{m} = 1$ by terms linearly proportional to i_p, that is

$$\lambda_p(\theta, i_p) \approx \left(l_0 - \sum_{n=}^{\bar{n}} l_n \cos(nN\theta - \phi_p)\right) i_p \quad (26)$$

where $l_0, \ldots, l_{\bar{n}}$ are inductance coefficients.

Phase torques may be computed according to

$$T_p(\theta, i_p) = \sum_{m=1}^{\bar{m}} \sum_{n=1}^{\bar{n}} c_{mn}\, a_m^{T}(i_p)\, b_n^{T}(\theta) \quad (27)$$

$$a_m^{T}(i_p) = \frac{1}{mM}\left(e^{-mMi_p} + mMi_p - 1\right) \quad (28)$$

$$b_n^{T}(\theta) = -nN\sin(nN\theta - \phi_p) \quad (29)$$

For small values of i_p, (27) reduces with $\bar{m} = 1$ to a Fourier series proportional to i_p^2 that is

$$T_p(\theta, i_p) \approx \frac{1}{2} N i_p^2 \sum_{n=1}^{\bar{n}} n\, l_n \sin(nN\theta - \phi_p). \quad (30)$$

Similar calculations would lead to models for $L_p(\theta, i_p)$ and $K_p(\theta, i_p)$ in terms of either c_{mn} or $l_0, \ldots, l_{\bar{n}}$.

Computing the coefficients c_{mn} from measured data is made systematic by formulating a least squares curve-fitting problem [9]. Of course, such a convenient numerical method can be applied here (but cannot be applied to the model in [3]) because of the linear parameterization c_{mn} imposed on the nonlinear functions.

Table II			
ζ = 0.56, ω_n = 50.0	Over shoot	Rise Time	Settling Time
Simulated	12%	' 35 ms	107 ms
Measured	6%	36 ms	71 ms
Percent Error	50%	3%	34%

References

[1] P.K. Goel and I. Cushing, "Direct-drive SR motor outperforms geared systems in robotics," *Power Conversion and Intelligent Motion Mag.*, pp. 52-55, Feb. 1989.

[2] R.T. Howe, R.S. Muller, K.J. Gabriel, and W.S.N. Trimmer, "Silicon micromechanics: Sensors and actuators on a chip," *IEEE Spectrum*, pp. 29-35, July 1990.

[3] M. Ilic-Spong, R. Marino, S.M. Peresada, and D.G. Taylor, "Feedback linearizing control of switched reluctance motors," *IEEE Trans. Auto. Control*, vol. AC-32, no. 5, pp. 371-379, 1987.

[4] A. Isidori, *Nonlinear Control Systems*, 2nd ed. New York: Springer-Verlag, 1989.

[5] D. Jones, "Current status of switched reluctance motors," *Power Conversion and Intelligent Motion Mag.*, pp. 40-42, Aug. 1989.

[6] P.V. Kokotovic, H.K. Khalil, and J. O'Reilly, *Singular Perturbation Methods in Control: Analysis and Design*. London: Academic, 1986.

[7] T.J.E. Miller, *Switched Reluctance Motor Drives*. Ventura, CA: Intertec Communications, 1988.

[8] T.J.E. Miller, *Brushless Permanent-Magnet and Reluctance Motor Drives*. New York: Oxford Univ. Press, 1989.

[9] D.G. Taylor, M.J. Woolley, and M. Ilic, "Design and implementation of a linearizing and decoupling feedback transformation for switched reluctance motors," in *Proc. 17th Symp. Incremental Motion Control Systems and Devices*, Champaign, IL, June 1988, pp. 173-184.

David G. Taylor received the B.S. degree from the University of Tennessee, Knoxville, in 1983, and the M.S. and Ph.D. degrees from the University of Illinois, Urbana, in 1985 and 1988, respectively, all in electrical engineering. During the summers from 1981 to 1983, he was employed by Oak Ridge National Laboratory and IBM Corporation where he contributed to the design of control system implementations. From 1983 to 1988, he held various fellowships and assistantships at the University of Illinois, Urbana. Since 1988, he has been an Assistant Professor in the School of Electrical Engineering, Georgia Institute of Technology, Atlanta. His research interests include nonlinear control theory and its applications to electromechanical systems.

Proceedings of the American Control Conference
Albuquerque, New Mexico June 1997
0-7803-3832-4/97/$10.00 © 1997 AACC

Switched Reluctance Motor Control Techniques

Michael T. DiRenzo, Michael K. Masten, and Charles P. Cole
Texas Instruments
Dallas, Texas 75243
direnzo@ti.com

Abstract

This paper provides a basic tutorial on SRMs, how they are controlled, and potential applications. A review of the equations governing the operation of the SRM is given and the operation of the SRM is described. Current control, commutation algorithms, and techniques for reducing torque ripple and linearizing the SRM torque response are discussed. Algorithms which allow motor operation without aid of a shaft position sensor are introduced.

1 Introduction

Electric machines can be broadly classified into two categories on the basis of how they produce torque - (1) electromagnetically or (2) by variable reluctance. In the first category, motion is produced by the interaction of the magnetic fields generated in the stator and the rotor. When two magnetic fields are mutually coupled, an *electromagnetic torque* between the two fields exists which tends to bring the fields into alignment. The vast majority of motors in commercial use today, including DC, induction, and synchronous motors operate on this principle. These motors are differentiated based on their geometries and how magnetic fields are generated in their stator and rotor; either through energized windings, through the use of permanent magnets, or through induced currents. In the second category, motion is produced as a result of the variable reluctance in the air gap between the rotor and the stator. When a stator winding is energized, a *reluctance torque* is produced by the tendency of the rotor to move to a position such that minimum reluctance is achieved in the magnetic field generated by the stator. The switched reluctance motor (SRM) falls into this class of machines. Fig. 1 shows a cross-section of an SRM which has 4 phases, 8 stator poles, and 6 rotor poles.

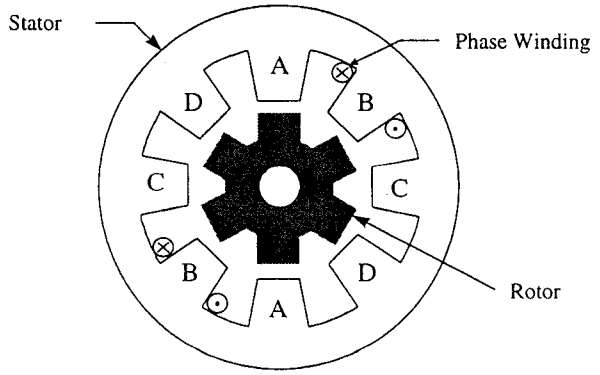

Fig. 1. Cross-section of a 4-phase, 8/6 SRM

In construction, the SRM is the simplest of all electrical machines as only the stator has windings. The rotor contains no conductors or permanent magnets; just a stack of steel laminations on a shaft. It is because of this simple mechanical construction that SRMs carry the promise of low cost, which in turn has motivated a large amount of research on SRMs in the last decade. The mechanical simplicity of the device, however, comes with some limitations. Like the brushless DC motor, SRMs can not run directly from a DC bus or an AC line, but must always be electronically commutated. Also, the saliency of the stator and rotor, necessary in order for the machine to produce reluctance torque, gives rise to strong non-linear magnetic characteristics, complicating the analysis and control of the SRM. Not surprisingly, industry acceptance of SRMs has been slow due to a combination of perceived difficulties with the SRM, the lack of established, commercially available electronics with which to operate them, and the entrenchment of traditional AC and DC machines in the marketplace. SRMs do, however, offer some advantages in addition to potential low cost. For example, they can be very reliable machines since each phase of the SRM is largely independent physically, magnetically, and electrically from the other motor phases. Also, because of the lack of conductors or magnets on the rotor, very high speeds can be achieved, relative to comparable motors.

Disadvantages often cited for the SRM; that they are difficult to control, that they require a shaft position sensor in order to operate, that they tend to be noisy, and that they have more torque ripple than other types of motors, have generally been overcome through a better understanding of motor design and the development of algorithms which can compensate for these problems.

2 Dynamic Model

The instantaneous voltage across the terminals of a single phase of an SRM winding is related to the flux linked in the winding by Faraday's law of induction,

$$v = iR + \frac{d\phi}{dt} \tag{1}$$

where, v is the terminal voltage, i is the phase current, R is the motor resistance, and ϕ is the flux linked by the winding. Because of the double salient construction of the SRM and because of magnetic saturation effects, the flux linked in an SRM varies as a function of rotor position, θ, and the motor current. Thus Eq. (1) can be rewritten as,

$$v = iR + \frac{\partial\phi}{\partial i}\frac{di}{dt} + \frac{\partial\phi}{\partial\theta}\frac{d\theta}{dt} \tag{2}$$

where $\partial\phi/\partial i$ is defined as $L(\theta,i)$, the instantaneous inductance and $\partial\phi/\partial\theta$ is $K(\theta,i)$, the instantaneous back EMF. From Fig. 2, we see that the response from voltage to current for the

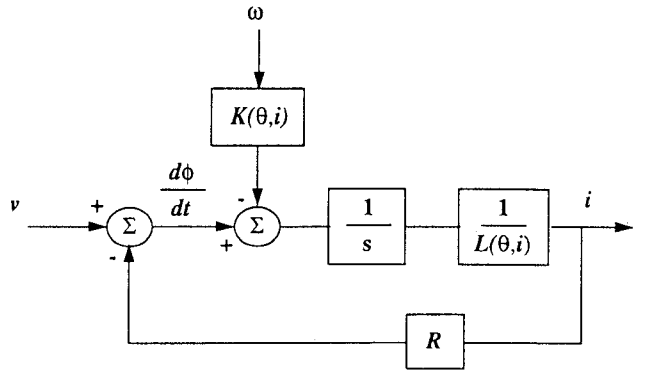

Fig. 2. Block diagram of an SRM winding

SRM can be described by a non-linear, first-order low pass filter with a variable time constant equal to $L(\theta,i)/R$. Typically, the inductance of an SRM will vary by a factor of five or six from minimum value to maximum value. The torque developed by the motor is given by

$$T = \frac{\partial W_c}{\partial \theta} \tag{3}$$

where, W_c, is the co-energy and is defined by

$$W_c = \int_0^i \phi \, di \tag{4}$$

When magnetic saturation is neglected, it can be shown that the torque equation reduces to

$$T = \frac{1}{2} i^2 \frac{dL(\theta)}{d\theta} \tag{5}$$

As described in Eqs. (3) & (5), torque produced by the SRM is a non-linear function of the rotor position and the current magnitude. The direction of torque, however, is only a function of rotor position and is independent of the current flow direction. While the rotor approaches the aligned position (inductance increasing), the torque is positive. While the rotor moves away from the aligned position (inductance decreasing) negative torque is produced. Torque curves typical of SRMs are shown in Fig. 3.

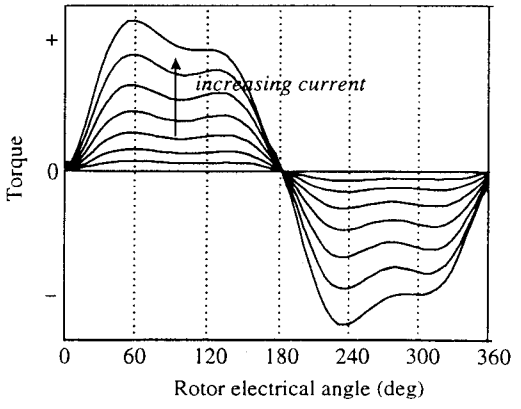

Fig. 3. Torque vs. Angle, for varied current

3 Basic Operation

The key to effective control of the SRM lies in the ability to control two parameters: *how much* current flows in the motor winding, and *when* the current flows, with respect to rotor position. Various performance levels from the SRM are achieved through the manipulation of these quantities. Although performance can be measured many ways (e.g. efficiency, torque ripple, speed regulation), generally, when current is well regulated and position information is well known, SRM performance can be maximized.

3.1 Power Electronics

The amount of current flowing through the SRM windings is regulated by switching on or off power devices such as MOSFETs or IGBTs, which connect each SRM phase to a DC bus. A popular configuration, which uses two switches and two diodes, per phase, is shown in Fig. 4. Several other configurations exist [1,2] which require fewer switches per phase, however the configuration of Fig. 4 provides the most flexibility from a control viewpoint, and maintains phase independence. A gate drive IC device, such as the IR2110, can be used to turn on and off the semiconductor switches. In the topology of Fig. 4, the low-side switch is usually held on during a commutation interval, while the top switch is used to implement the control. For efficiency, to reduce the size, and to reduce the cost of the power devices, SRMs are generally operated in a pulse-width modulation (PWM) mode to achieve the net desired voltage across the motor windings. If current control is desired, a low-ohm sense resistor or current transformer can be placed in series with the motor winding. At the end of the commutation interval, the diodes return any stored magnetic energy to the power supply.

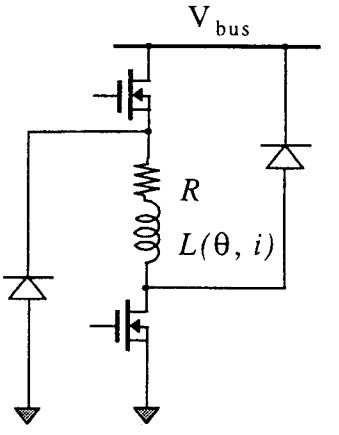

Fig. 4. Two-switch per phase SRM inverter

3.2 Current Control

The SRM can be operated in either voltage control or current control mode. Open-loop voltage control is generally less expensive, because less hardware is required for implementation. A voltage controlled SRM, however, is more sensitive to voltage ripple on the power bus and has a lower control bandwidth. When servo-type performance is desired (precise torque control), it is essential that current control be used.

Non-linear, on-off control laws with hysteresis have been widely used for SRM current control. A linear control law, has some desirable properties, but the variable time constant of the motor poses limitations. With an on-off control law, the choice of the hysteresis band controls the performance of the loop. A small band is desirable for reducing current ripple but will require faster switching frequencies of the power devices. The on-off controller, with small hysteresis band, is essentially equivalent to choosing the compensator to be a high gain. The resulting current loop thus has a high bandwidth, which is a desirable feature, especially as the

motor speed increases. This type of control also has the advantage of being very simple to implement with analog electronics. Another advantage of the on-off controller, is that it removes the complication of the variable motor time constant from the control design.

There are two clear disadvantages to this type of control. First it results in residual current ripple due to the nature of the bang-bang type of control. Secondly, the switching frequency of this approach will be variable and perhaps unknown. Switching frequency will be a function of current in the winding, the bus voltage, the choice of the hysteresis band and the variable *L/R* time constant of the motor. It is generally undesirable for the switching frequency to fall within the audible range of the human ear.

By contrast, the control law can be designed using linear system theory (a PI law, for example) provided proper consideration is given to the impact of the variable time constant in the loop. The controller output in this case corresponds to a desired duty ratio, which can be converted to on-off signals for the power switches using a fixed-frequency PWM amplifier. This method can guarantee that the PWM frequency is not audible. Although the fixed-frequency PWM method is also implemented relatively easily with analog electronics, it lends itself well to a digital implementation, using counters and compare registers. There is strong motivation, particularly in systems which already have some processing capability, for using digital current loops for motor control. A digital controller can improve system performance, through algorithms, and often lower the cost of a system by reducing the chip count or allowing for easy and quick reconfigurability.

Regardless of the nature of the control law, eventually, the motor will reach a speed where the back EMF disturbance is such that the controller will not be able to follow the command. At this speed, the power switches conduct (remain on) during the entire commutation interval. This mode of operation is often called the single-pulse mode.

3.3 Commutation

In addition to the magnitude of current, the selection of turn-on and turn-off angles, provides the control designer with two more degrees of freedom for implementing SRM control. The choice of these angles, sometimes called conduction angles or firing angles, greatly impacts the performance of the SRM. There are usually two conflicting concerns - maximizing the torque output of the motor or maximizing the efficiency of the motor. In general, efficiency is optimized by minimizing the dwell angle for a phase, and maximum torque is achieved by maximizing the dwell angle to take advantage of all potential torque output from a given phase. With the idealized current waveforms of Fig. 5, the resulting net torque from the motor is shown by the solid line. In this example, the turn-on and turn-off angles coincide with the region where maximum torque is obtained for the given amount of phase current. This commutation sequence tends to optimize efficiency. Here, a dwell angle of 120 electrical degrees is used, which is the minimum dwell angle that can be used for a three-phase SRM, without regions of zero torque.

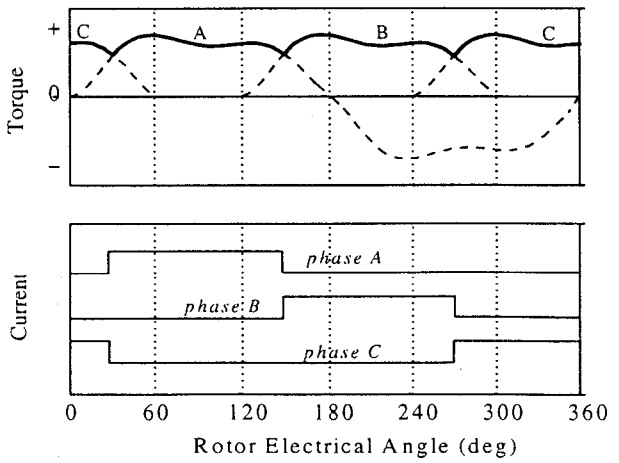

Fig. 5. Commutation of a 3-phase SRM

3.4 Varying the Conduction Angles

SRM control is often described in terms of "low-speed" and "high-speed" regimes. Low-speed operation is typically characterized by the ability to arbitrarily control the current to any desired value. With fixed firing angles, as the motor's speed increases, it becomes increasingly difficult to regulate the current because of a combination of the back EMF effects and a reduced amount of time for the commutation interval. When this occurs, the motor speed can be increased by increasing the conduction period (dwell) or by advancing the firing angles, or by a combination of both.

In Fig. 6, we see that the inductance is at a minimum just prior to the region of positive dL/dθ (i.e. positive torque region). By adjusting the turn-on and turn-off angles so that the phase commutation begins sooner, we gain the advantage of producing current in the winding while the inductance is low, and also of having additional time to reduce the current in the winding before the rotor reaches the negative torque region. Control of the firing angles can be accomplished a number of ways, and is based on the type of position feedback available and the optimization goal of the control. Becerra [3], with relatively coarse position information, proposes three modes called normal, boost, and long-dwell. The turn-on and turn-off angles for these operating modes are shown in Fig. 6. This approach provides a simple way of extending the operating range of the SRM. Normal mode tends to be the

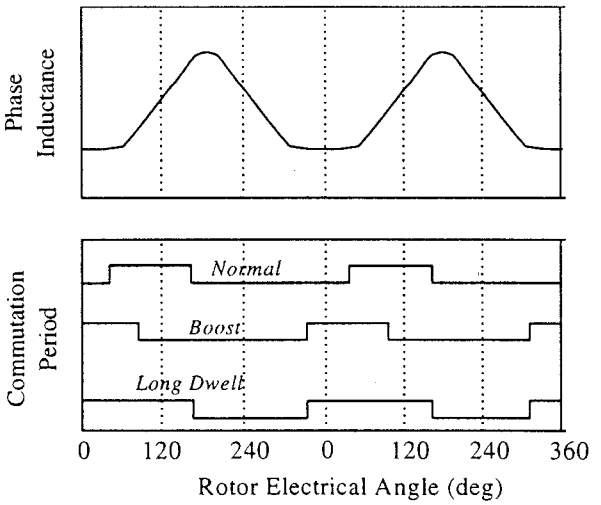

Fig. 6. Idealized SRM Inductance and Commutation modes

most efficient and best choice for low speeds. Boost can provide additional torque, as the speed of the motor increases, and long dwell can extend the torque-speed operation of the SRM even further.

When position information is more precisely known, a more sophisticated approach, for example continuously varying the turn-on and turn-off angles, can be implemented. Near turn-on, Eq. (2) can be approximated as

$$v = \frac{\partial \phi}{\partial i}\frac{di}{dt} = L_{unaligned} \cdot \frac{di}{dt} \tag{6}$$

Multiplying each side of Eq. (6) by the differential, $d\theta$, and solving for $d\theta$, gives,

$$d\theta = \frac{L_{unaligned} \cdot di}{v} \cdot \frac{d\theta}{dt} \tag{7}$$

and using first order approximations yields an equation for calculating advance angle,

$$\theta_{adv} = \frac{L_{unaligned} \cdot I_{cmd}}{V_{bus}} \cdot \omega \tag{8}$$

Alternatively, the conduction angles can be determined off-line by simulating the motor's operation over a range of conditions, while optimizing some desired parameter such as efficiency. The simulation results could then be stored in a look-up table.

3.5 Torque Ripple Reduction & Torque Linearization

A common solution to the problem of torque ripple and torque constant non-linearity in SRMs is to shape the current. The shaping techniques work by allowing phases which can simultaneously produce torque of the same direction to share the burden of providing the commanded motor torque. The sum of torques produced by each phase is equal to the desired torque. Mathematically, this can be described as

$$T_k = T_{des} \times f_s(\theta + b_k), \quad for\ k = 1,\ldots,n \tag{9}$$

where n is the number of phases, T_k is the phase torque, T_{des} is the desired total torque, and f_s is the shaping function. The same shaping function, f_s, is used for all phases of the motor, but each phase is offset by an angle, b_k, related to the geometry of the motor. The top plot of Fig. 7 depicts one possible set of shaping functions for the desired total SRM torque, indicated with the dashed line. Since torque cannot be controlled directly, the desired torque must be related to current using knowledge of the motor's torque-current-angle characteristics. If $g(\theta,T)$ is a function relating torque to current for the SRM, then the instantaneous current command for the k^{th} motor phase is given by,

$$I^k_{cmd} = g(\theta, T_k) \tag{10}$$

The impact of $g(\ )$ can be seen by comparing the idealized current waveforms of Fig. 5 to the current waveforms shown in Fig. 7.

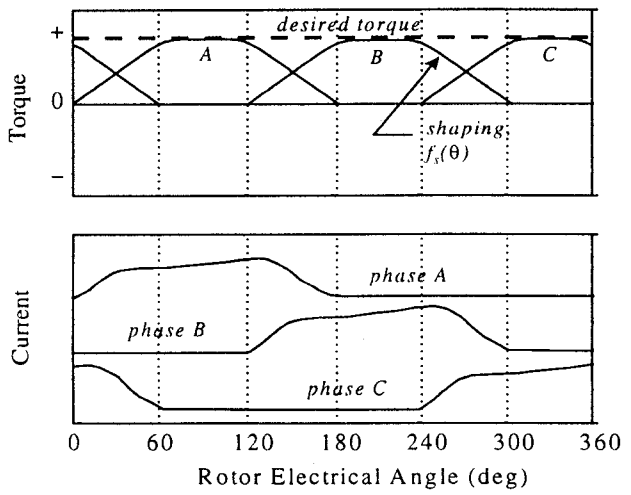

Fig. 7. Torque Linearization for SRMs

Additionally, the motor characteristics must be known accurately to achieve the best results. This can be a difficult task. Several methods [4,5] have been reported which involve an off-line computation of the current profiles, or use simplified models of the SRM [6]. In [7] a learning process is proposed, but it requires measurements from a special test rig. For some applications, the motor may operate under non-saturating conditions. In this case, Eq. (4) can be used to simplify the torque to current transformation. In [8], successful implementation of this approach has been reported.

Instantaneous torque control, via current shaping, is generally not useful for high-speed applications, because the torque ripple increases along with degraded ability to regulate the motor current.

4 Position Sensorless Commutation Approaches

SRM commutation is typically accomplished by feeding back rotor position information to a controller from a shaft angle transducer, such as an encoder or slotted disk with opto-couplers. To reduce cost, it is desirable to eliminate the shaft position sensor when possible. Various researchers have developed ways of addressing the sensor elimination problem [9]. Because of the salient nature of the SRM rotor and stator, the inductance variation is sufficiently sensitive such that the motor's inductance profile can be used to estimate rotor position. All position sensor elimination methods for SRMs exploit this relationship in some manner. Position sensorless schemes pose interesting problems for starting, low-speed operation, and high-speed operation. Low-speed techniques generally provide test signals into a phase which is normally unenergized. Conversely, high-speed techniques use the active phase current waveform.

4.1 Starting Sequences

To start the SRM, it is necessary to have some idea of the rotor position so that the appropriate phase for generating the desired torque action can be turned on. A simple solution is to arbitrarily energize one of the motor phases and wait for a short period of time. This action will align the rotor to the energized stator phase. Some applications exist, however, such as hard disk drive spindle motors, where it is important that the direction of rotation be insured at startup. For these applications, blindly turning on a phase is not acceptable, and a starting sequence similar to one described by Belanger [10] must be employed. This starting sequence relies on the fact that for small (non-saturating) currents, the SRM inductance varies as a dual-valued function of rotor position.

The starting phase is determined by applying a voltage pulse to each of the phase windings for a short period of time. The pulse must be short enough so that the phase current

remains small in magnitude, to avoid saturation. A current sensor in each phase measures the resulting current produced by the applied voltage. Because of the variable inductance characteristic of the SRM, the magnitude of the current reached in each phase, during the voltage pulse, will vary from phase to phase. By evaluating the relative magnitude of the current flow through the phase windings, sufficient information is gathered for determining the proper starting phase of the motor. Algorithms can readily be written which account for these unique relationships and can provide estimates of the rotor's position.

4.2 Low-speed Commutation Using Inactive Phase Test Pulses

In an approach described by MacMinn [11], rotor position is indirectly estimated by applying short voltage pulses to an unenergized phase. This results in a change in phase current proportional to the instantaneous value of the phase inductance. Proper commutation time is determined by

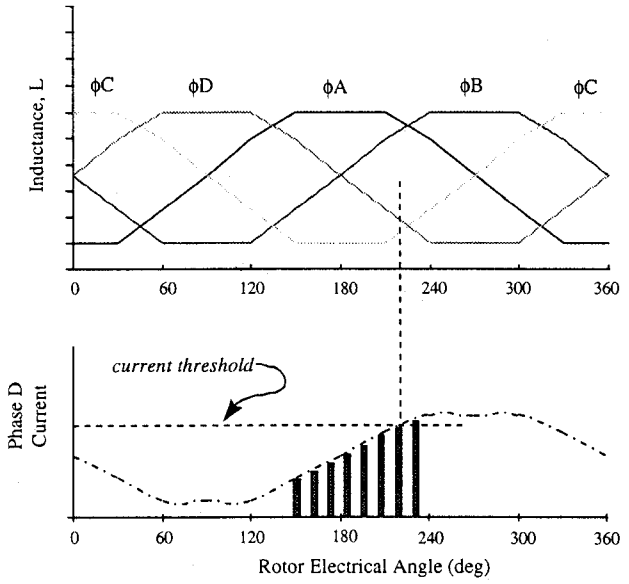

Fig. 8. Idealized Inductance Profile of a 4-phase SRM and Phase D current as a function of position, resulting from small voltage pulses

comparing the change in phase current to a threshold current, thereby synchronizing phase excitation to rotor position. This process is depicted in Fig. 8. In this example, phase D is used as a test phase in order to determine when to switch from phase B to phase C. By adjusting the threshold up or down, the commutation angle can be either retarded or advanced.

This approach has several disadvantages. Test signals are necessarily of low-amplitude to avoid negative torque production and avoid magnetic saturation. The low signal level, however, provides a challenge in implementing this technique to insure sufficient signal-to-noise ratio in the presence of mutual coupling from the excitation currents in the other phases. Also, at high speeds there is typically no unenergized phase available, and the method breaks down. This approach, as well as all approaches which make use of an inactive phase, is therefore speed limited in its application.

4.3 High Speed Commutation using an Active Phase

It is often desirable to operate the motor at higher speeds than approaches using inactive phases will allow. Lyons [12] uses a model of the SRM magnetic characteristics, mapping flux-linked to current for various rotor angles, to determine if the rotor angle is approaching, or has gone past, a known reference angle. Given knowledge of the phase voltage, phase current, and the phase resistance, phase flux can be estimated from an integral form of Faraday's law of induction.

$$\phi_{est} = \int_0^{\tau} (v - iR)dt \qquad (11)$$

With knowledge of the phase current and the flux-current map, the amount of flux that would exist at the reference

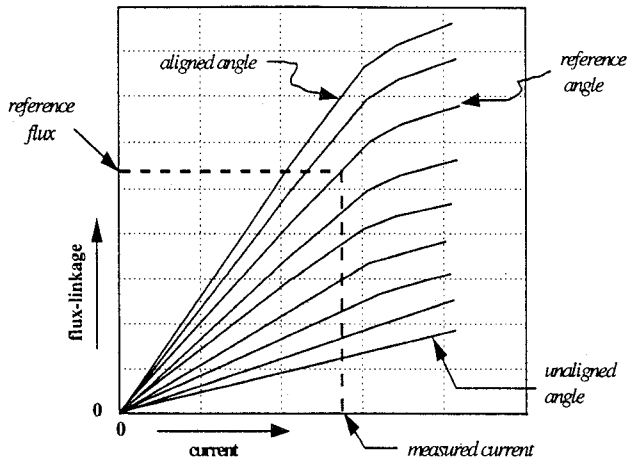

Fig. 9. Flux-current-angle relationship for an SRM

angle can also be determined, as described in Fig. 9. While the *estimated flux* is less than the *reference flux*, the actual rotor angle is farther from the aligned angle than the reference angle. Likewise, when the estimated flux equals the reference flux the rotor is at the reference angle, and when the estimated flux exceeds the reference flux the rotor is closer to alignment than the reference angle. Using this information the motor can be successfully commutated. Since this approach uses the active phase current, higher motor speeds can be achieved than with the commutation scheme of [11].

Some disadvantages to this approach are that the magnetic characteristics of the motor are not readily known and, as pointed out in [12], for small currents there is a significant reduction in sensitivity such that small current errors translate to large angle errors.

4.4 Self-Calibrating Commutation

As a practical concern, the model based approaches described above may be difficult to realize. It is possible to estimate the magnetic characteristics online, at the aligned angle with relative ease. Extending the approach of [12], this information can be used to estimate a commutation curve. By exciting any arbitrary phase with a current large enough to generate torque in excess of the starting friction of the motor,

the motor will come to the aligned position. Once at the aligned position, a calibration sequence can be cycled through where current is commanded to some set of discrete points (as shown in Fig. 10, for example) while flux-linked is estimated, via Eq. (11).

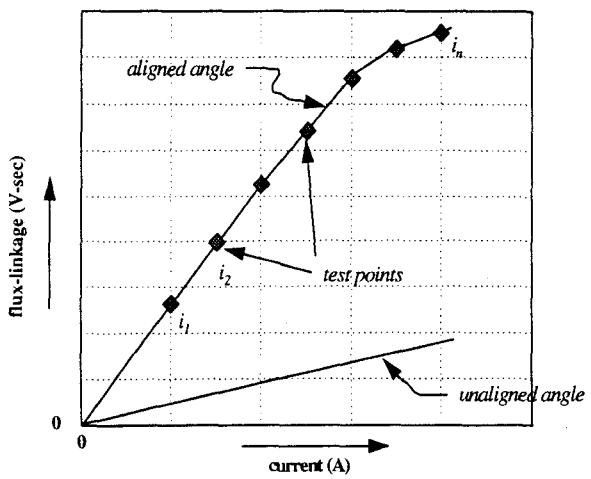

Fig. 10. Learning the flux/current relationship at the aligned angle

Upon completion of the calibration sequence, and subsequent curve fitting of the data, let $p(i)$ be a function describing the magnetic characteristics of the motor at the aligned angle,

$$f(\theta_{aligned}, i) = p(i) \qquad (12)$$

where $f(\ )$ is a function describing the flux-linkage of the SRM for all angles and current levels.

Since flux-linked increases monotonically with angle, as alignment approaches, the magnetic characteristics of the motor at some other angle, θ_r, can be defined by the expression,

$$f(\theta_r, i) = m_r(i)p(i) \qquad (13)$$

where, $0 < m_r(i) < 1 \ \forall \ i$. The problem of determining $m_r(i)$ exactly, requires costly test measurements which are undesirable. For many practical applications, however, $m_r(i)$ can be approximated by a constant, m. A velocity estimate can be obtained by counting a number of clock cycles between commutation instances, dividing the count by stroke angle of the motor, and then filtering to smooth the velocity estimate.

5 Conclusions

This paper has described the basic operation of the SRM. The torque-speed characteristics of the SRM are completely determined by the control strategy, and thus SRMs can be used for a variety of applications. Various levels of performance are achievable with SRMs, depending upon the system's processing capability, use of a shaft position sensor, and use of current sensors. High performance systems, however, generally have larger processing requirements which increases cost. Operation without the shaft position sensor is possible, but adds complexity to the controller. SRMs seem particularly well suited for applications such as fans or blowers, which demand reasonably accurate speed regulation, variable speed capability, high efficiency, and high reliability.

References

[1] S. Vukosavic and V. Stfanovic, "SRM Inverter Topologies: A Comparative Evaluation," *IEEE IAS Annual Meeting Conf. Record*, 1990.

[2] T.J.E. Miller (ed.), "Switched Reluctance Motor Drives," Intertec Communications Inc., Ventura CA, 1988.

[3] R. Becerra, M. Ehsani, and T.J.E. Miller, "Commutation of SR Motors", *IEEE Trans. Power Electronics*, vol. 8, no. 8, pp. 257-262, July 1993.

[4] D. Taylor, M. Woolley, and M. Ilic-Spong, "Design and Implementation of a Linearizing and Decoupling Feedback Transformation for Switched Reluctance Motors, " *Proc. 17th IMCSD Symposium*, Champaign, IL, pp. 173-184, 1988.

[5] D. Schramm, B. Williams, and T. Green, "Optimum Commutation-Current Profile on Torque Linearization of Switched Reluctance Motors", *Proc. ICEM, Manchester*, UK pp. 484-488, 1992.

[6] C. Rochford, R. Kavanagh, M. Egan, and J. Murphy, "Development of Smooth Torque in Switched Reluctance Motors using Self-Learning Techniques," *Proc. EPE Conf.*, vol. 6, pp.14-19, 1993.

[7] D. Reay, M. Mirkazemi-Moud, T. Green, and B. Williams, "Switched Reluctance Motor Control via Fuzzy Adaptive Systems," *IEEE Control Systems Magazine*, pp. 8-14, June 1995.

[8] I. Husain and M. Ehsani, "Torque Ripple Minimization in Switched Reluctance Motor Drives by PWM Current Control", pp. 72-77, May 1994.

[9] W.F. Ray and I.H. Al-Bahadly, "Sensorless Methods for Determining the Rotor Position of Switched Reluctance Motors," *Proc. EPE Conf.*, vol. 6, pp. 7-13, 1993.

[10] D. Belanger, U.S. Patent 5,051,680, "Simple Starting Sequence for Variable Reluctance Motors without Rotor Position Sensor," Sept. 1991.

[11] S. MacMinn, C. Stephens, and P. Szczseny, U.S. Patent 4,959,596, "Switched Reluctance Motor Drive System and Laundering Apparatus Employing Same," Sept. 1990.

[12] J. Lyons, S. MacMinn, and M. Preston, "Flux/Current Methods for SRM Rotor Position Estimation," *IEEE IAS Annual Meeting Conf. Record*, pp. 482-487, 1991.

MODEL MAH7500

THE NEW MAYTAG NEPTUNE® WASHER

USER GUIDE

TABLE OF CONTENTS

Safety Instructions 1-2
Operating Instructions 3
Control Panel 4
Controls at a Glance 5-13
Features 14-15
Care & Cleaning 16
Storing the Clothes Washer 17
Before You Call 18-19
Operating Sounds 20
Questions and Answers 21
Warranty 23
Guide de l'Utilisateur 24
Guía del Usuario 48

6 2717920 A/08/00 MCS 22003305

MAYTAG.COM
Bringing innovation home

Welcome

Welcome and congratulations on your purchase of a Maytag Neptune® washer! Your complete satisfaction is very important to us. For best results, we suggest reading this material to help acquaint you with proper operating and maintenance procedures.

Should you need assistance in the future, it is helpful to:

1) Have complete model and serial number identification of your washer. This is located on a data plate on the back of the control panel.

Date of Purchase _____
Model Number _____
Serial Number _____

2) ***IMPORTANT: Keep this guide and the sales receipt in a safe place for future reference. Proof of original purchase date is needed for warranty service.***

If you have questions, write us (include your model, serial number and phone number) or call:

Maytag Appliances Sales Company
Attn: CAIR® Center
P.O. Box 2370
Cleveland, TN 37320–2370
1-888-462-9824 USA and CANADA
1-800-688-2080 USA TTY
(for deaf, hearing impaired or speech impaired)
(Mon.–Fri., 8am–8pm Eastern Time)
http://www.maytag.com

For service and warranty information, see page 23.

NOTE: **In our continuing effort to improve the quality of our appliances, it may be necessary to make changes to the appliance without revising this guide.**

IMPORTANT SAFETY INSTRUCTIONS

read before operating your washer

⚠ **WARNING:** To reduce the risk of fire, explosion, electric shock, property damage or injury to persons when using your appliance, follow basic precautions, including the following:

1. Read all instructions before using the appliance.
2. As with any equipment using electricity and having moving parts, there are potential hazards. To use this appliance safely, the operator should become familiar with the instructions for operation of the appliance and always exercise care when using it.
3. Do not install or store this appliance where it will be exposed to the weather.
4. Install and level the clothes washer on a floor that can support the weight.
5. This appliance must be properly grounded. Never plug the appliance cord into a receptacle which is not grounded adequately and in accordance with local and national codes. See installation instructions for grounding this appliance.
6. To avoid the possibility of fire or explosion:
   a. Do not wash items that have been previously cleaned in, washed in, soaked in, or spotted with gasoline, dry-cleaning solvents, other flammable or explosive substances as they give off vapors that could ignite or explode. Hand wash and line dry any items containing these substances.

      Any material on which you have used a cleaning solvent, or which is saturated with flammable liquids or solids, should not be placed in the clothes washer until all traces of these liquids or solids and their fumes have been removed.

      These items include acetone, denatured alcohol, gasoline, kerosene, some liquid household cleaners, some spot removers, turpentine, waxes and wax removers.

   b. Do not add gasoline, dry-cleaning solvents, or other flammable or explosive substances to the wash water. These substances give off vapors that could ignite or explode.

   c. Under certain conditions, hydrogen gas may be produced in a hot water system that has not been used for 2 weeks or more. HYDROGEN GAS IS EXPLOSIVE. If the hot water system has not been used for such a period, before using a washing machine or combination washer-dryer, turn on all hot water faucets and let the water flow from each for several minutes. This will release any accumulated hydrogen gas. As the gas is flammable, do not smoke or use an open flame during this time.

Important Safety Instructions cont.

7. Do not reach into the appliance if the tumbler is moving.
8. Do not allow children to play on or in the appliance. Close supervision of children is necessary when the appliance is used near children.
9. Do not tamper with controls.
10. Do not repair or replace any part of the appliance or attempt any servicing unless specifically recommended in published user-repair instructions that you understand and have the skills to carry out.
11. Unplug power supply cord before attempting to service your clothes washer.
12. Store laundry aids and other material in a cool, dry place where children cannot reach them.
13. Do not wash or dry items that are soiled with vegetable or cooking oil. These items may contain some oil after laundering. Due to the remaining oil, the fabric may smoke or catch fire by itself.
14. Do not use chlorine bleach and ammonia or acids (such as vinegar or rust remover) in the same wash. Hazardous fumes can form.
15. Do not machine wash fiberglass materials. Small particles can stick to fabrics washed in following loads and cause skin irritation.
16. Before the appliance is removed from service or discarded, remove the door to the washing compartment.
17. Do not sit on top of the clothes washer.
18. Inlet hoses are subject to damage and deterioration over time. Check the hoses periodically for bulges, kinks, cuts, wear or leaks and replace them every five years.

Save These Instructions

Operating Instructions

*For detailed information on sorting, pretreating stains, etc., see the enclosed **Laundering Tips** booklet.*

Load the Clothes Washer

- The tub can be loaded completely full with dry unfolded clothes. However, do not pack the tub tightly.
- Overloading may reduce washing efficiency and possibly cause creasing or wrinkling of the load.
- When washing big bulky items or a couple of small items that do not fill the tub completely, such as a rug or two sweaters, a few towels should be added for improved tumbling and spin performance.
- When washing heavily soiled loads, it is very important to avoid overloading the washer to assure good cleaning results.
- To load a forgotten item, press the **Start/Pause** touchpad, add the item, close the door and press the **Start/Pause** touchpad. After a 15 to 30 second pause, the cycle will resume.

NOTE: To assure that your additional items get clean, do not wait more than five minutes after the cycle has started to add the item.

Special Note: As you use the touchscreen, if you feel you are lost, press **Back** or **Home**.

Status Display

Estimated Time Display

After pressing start, this display will show the estimated time remaining in the cycle.

Indicator Lights

Door Locked – Displays whenever the door of the clothes washer is locked. The door can be unlocked by pressing the **Start/Pause** touchpad to stop the washer.

Water Use

The amount of water used will vary with each load. The Maytag Neptune® clothes washer uses an adaptive fill valve to provide the appropriate amount of water for efficient cleaning performance and conservation of water and energy.

Control Panel

Touchscreen - An interactive display that responds with the touch of a finger.

Note: Exposure of the touch-screen to direct sunlight is not recommended.

Home - Takes you immediately to the first screen.

Off - Stops the washer and the turns off the display.

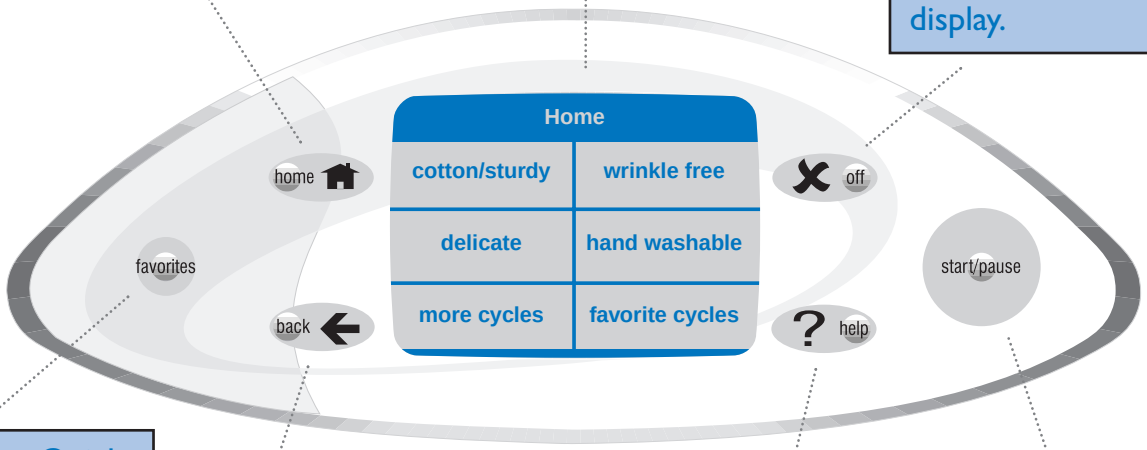

Favorites - Quick access to your named cycles.

Back - Takes you to the previous screen.

Help - Quick access to Stain Brain, Before You Call, Laundering Hints, Operating Tips, Lock Out and Select Preferences.

Start/Pause - Press this pad to start a cycle. Once started, pressing this pad will stop the washer at any point in the cycle.

Special Note: As you use the touchscreen, if you feel you are lost, press **Back** or **Home**.

Controls at a Glance

Setting a Wash Cycle

If there are no words on the touchscreen, open the door, touch any pad (except off), or touch the screen to "wake" the controls.

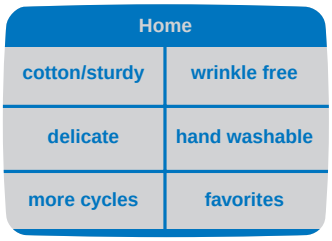

Step 1

Home Screen – Select the appropriate fabric setting.

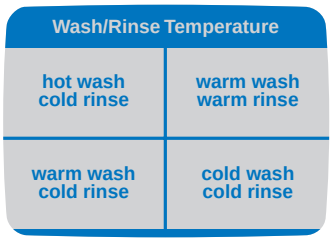

Step 2

Wash/Rinse Temps – Select the appropriate wash/rinse temperature.

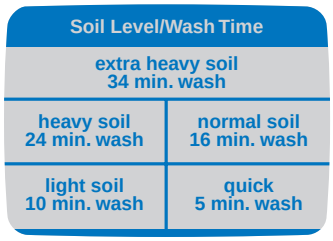

Step 3

Soil Level/Wash Time – Select the appropriate soil level/wash time.

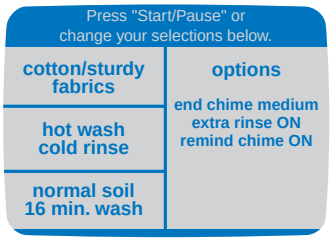

Step 4

Review Screen – This screen reviews your selections before starting the washer. You may press **Start/Pause** to begin washing or press a displayed choice to change previous selections.

Step 5

Options Screen – The option choices on the left turn the options on or off. Some option choices on the right show an additional screen with multiple choices. When the desired selections are made, touch **Continue** to see the review screen once again.

Step 6

If you are satisfied with the selections, press the **Start/Pause** pad to begin the cycle.

Special Note: As you use the touchscreen, if you feel you are lost, press **Back** or **Home**.

Favorites at a Glance

Favorites allows you to create, name and save up to 24 commonly used wash cycles.

"Blue jeans" and **"towels"** favorite cycles have been programmed for you. To change these cycles for your preferences, see Edit a Favorite on page 7.

Create a Favorite

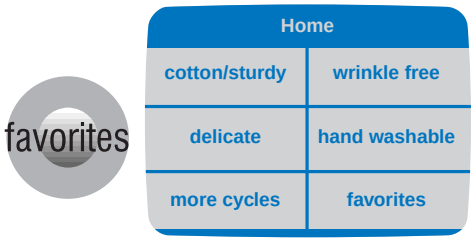

Step 1

Touch "**Favorites**" on the home screen or the **Favorites** pad.

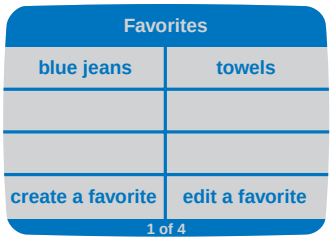

Step 2

Touch **"Create a Favorite"**.

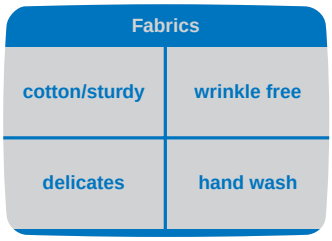

Step 3

Fabrics – Select the appropriate fabric setting.

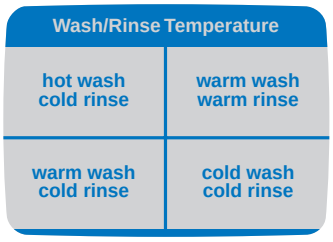

Step 4

Wash/Rinse Temps – Select the appropriate wash/rinse temperature.

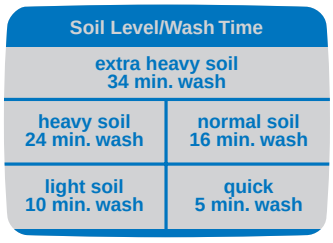

Step 5

Soil Level/Wash Time – Select the appropriate soil level/wash time.

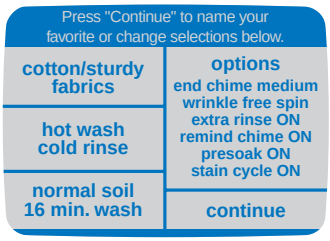

Step 6

Review Screen – This screen reviews your cycle choices, and allows you to choose Options to further customize your wash cycle. Press **"Options"** if desired, or press **"Continue"**.

Step 7

Options Screen – The option choices on the left turn the options on or off. Some option choices on the right show an additional screen with multiple choices. When the desired selections are made, touch **"Continue"** to see the review screen once again.

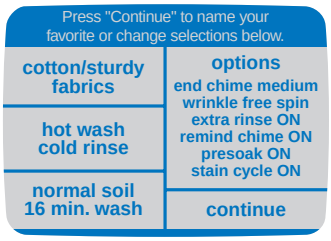

Step 8

If satisfied with your selections, press **"Continue"** to name your favorite cycle.

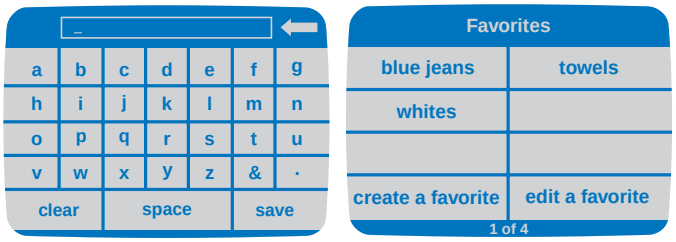

Step 9

Name A Favorite Cycle – Touch the corresponding letter and space combination to spell out your favorite cycle name, up to 12 characters. Press **"Save"**. Your new Favorite Cycle will be displayed on the Favorites page.

EDIT A FAVORITE

This allows you to change the settings of any favorite cycle.

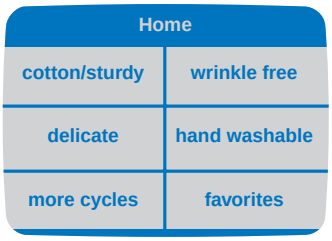

Step 1

Touch **"Favorites"** on the home screen or the **Favorites** pad.

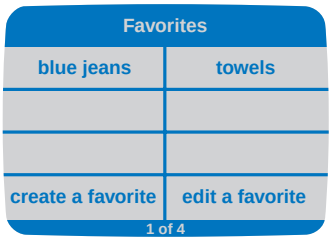

Step 2

Touch **"Edit A Favorite"** Touch the favorite cycle you want to edit.

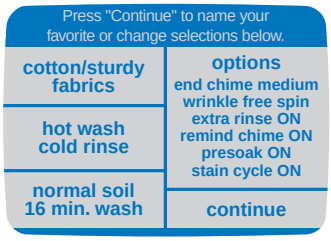

Step 3

The review screen for that specific cycle will be displayed. Make the appropriate changes by touching the area. Press **"Continue"**.

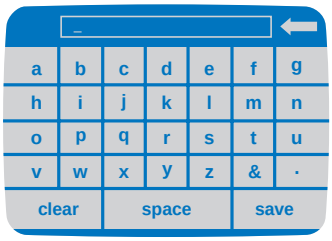

Step 4

If the current favorite cycle name still applies, touch **"Save"**. If you prefer a new name, type in the new name and touch **"Save"**.

Special Note: As you use the touchscreen, if you feel you are lost, press **Back** or **Home**.

Move a Favorite

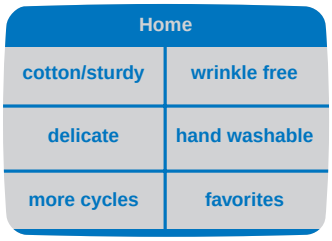

Step 1

Touch **"Favorites"** on the Home screen or the **Favorites** pad.

Step 2

Touch **"Edit a Favorite"**.

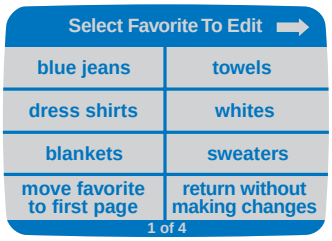

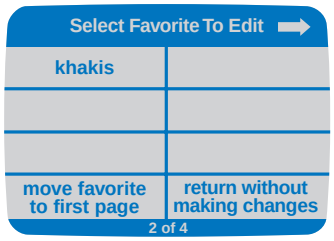

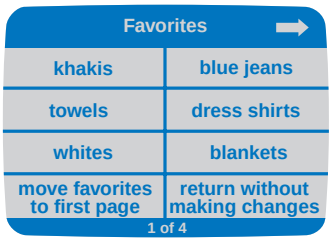

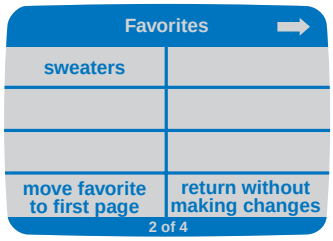

Step 3

Touch the area entitled **"Move Favorite to First Page"**. Using the arrow at the top, scroll through the pages until you get to the favorite you would like to move to the first page. Touch that favorite cycle.

Step 4

Now the favorite cycle should appear in the upper left position of the touchscreen. The other favorites cycles move back one position with the sixth favorite cycle moving to the next page.

Special Note: As you use the touchscreen, if you feel you are lost, press **Back** or **Home**.

USING HELP

The Help feature offers a variety of detailed information including the stain brain, before you call, laundry hints, operating tips, lock out feature and select preferences.

This section of the user guide will demonstrate how to easily navigate to the main areas of the topics. From there, you will easily be able to narrow your search for finding laundry information.

STAIN BRAIN

The Stain Brain provides detailed steps to treat over 50 of the most common stains. The Stain Brain also offers the user the option of all automatically setting the washer cycle for the particular stain.

Step 1

Touch the **Help** touchpad.

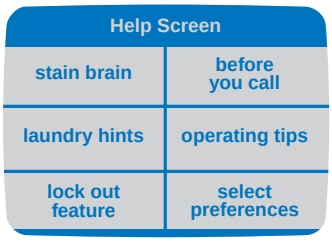

Step 2

Select **"Stain Brain"**.

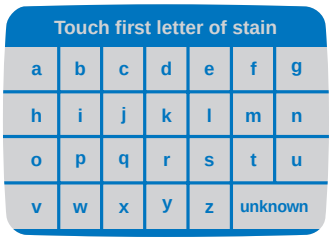

Step 3

Select the letter of the stain you want to remove.

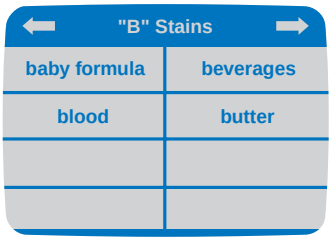

Step 4

Select the appropriate stain listing.

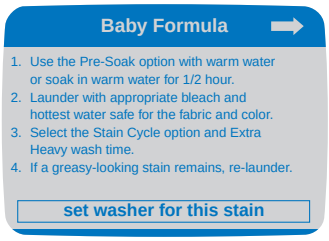

Step 5

To automatically set the washer to run the appropriate cycle for the selected stain, touch **"Set Washer For This Stain"**.

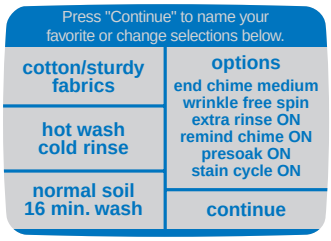

Step 6

Review Screen - This screen reviews the selections made by the Stain Brain before starting the washer. Press **Start/Pause** to begin washing, or press a displayed choice to change selections.

Note: Use the arrows at the top of the letter screen to scroll from letter to letter.

Before You Call

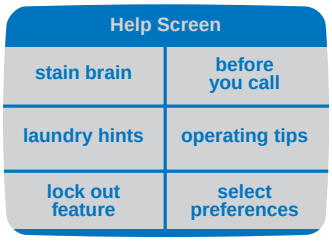

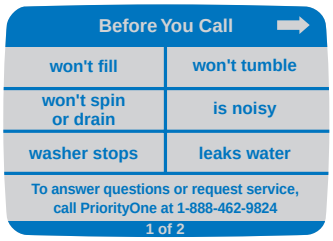

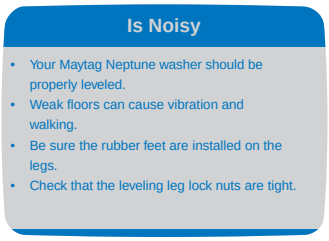

Step 1

Touch the **Help** touchpad.

Step 2

Select **"Before You Call"**.

Step 3

Here you will see headings for common trouble-shooting topics. Touch one of the displayed areas to see specific information. Touch the arrows at the top of the screen to move forward or back through the topics. For more detailed information see "Before You Call" section pg. 18-19, or call 1-888-462-9824 for further assistance.

Step 4

If you would like to see the other topics, press the **Back** touchpad to get back to the main topics.

Special Note: As you use the touchscreen, if you feel you are lost, press **Back** or **Home**.

LAUNDERING HINTS

Step 1

Touch the **Help** touchpad.

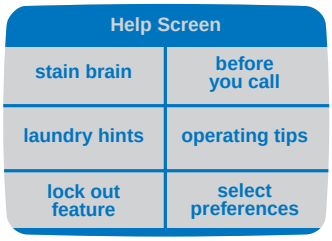

Step 2

Select **"Laundry Hints"** from the Help screen.

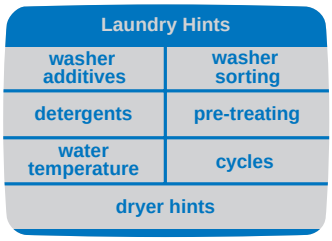

Step 3

Here you will see the available topics. Touch the topics to see specific information.

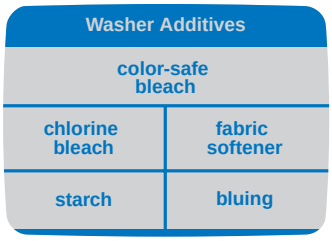

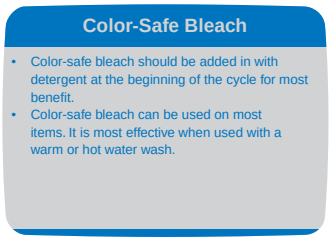

Step 4

Touch the sub-topic to see specific information.

Step 5

If you would like to see the other topics, press the **Back** touchpad to get back to the main topics.

Special Note: As you use the touchscreen, if you feel you are lost, press **Back** or **Home**.

Operating Tips

Step 1

Touch the **Help** touchpad.

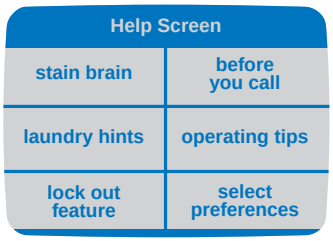

Step 2

Select **"Operating Tips"** from the Help Screen.

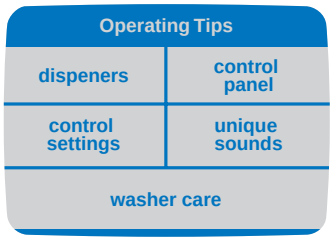

Step 3

"Operating Tips" provides information on maximizing the touchscreen controls and use of your washer.

Step 4

If you would like to see the other topics, press the **Back** touchpad to get back to the main topics.

Lock Out Feature

Step 1

Touch the **Help** touchpad.

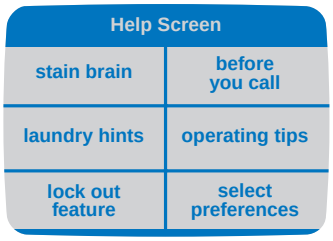

Step 2

Select **"Lock Out Feature"** from the Help Screen.

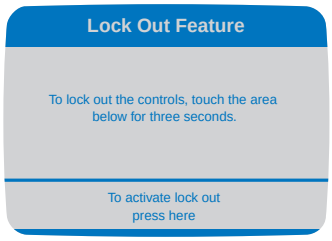

Step 3

The **"Lock Out Feature"** deactivates the touchscreen and touchpads. Use this feature for cleaning the control panel or to prevent unwanted use of the washer.

Step 4

If you would like to see the other topics, press the **Back** touchpad to get back to the main topics.

CONTROLS AT A GLANCE CONT.

SELECT PREFERENCES

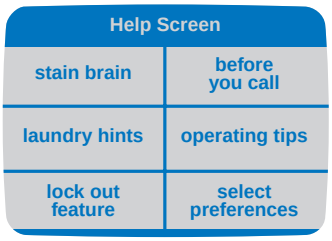

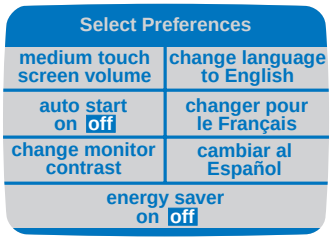

Step 1

Touch the **Help** touchpad.

Step 2

Select **"Select Preferences"**. **"Select Preferences"** allows you to select the volume of the touchscreen beeps, set the intensity of the screen display, activate the Auto Start and Energy Saver functions, and change the display language from English to French or Spanish.

TOUCHSCREEN VOLUME

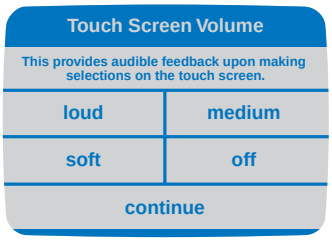

Touch **"Loud"**, **"Medium"**, **"Soft"** or **"Off"** to set the volume level of the touchscreen beeps. Touch **"Continue"** to accept the selected volume setting.

CHANGE MONITOR CONTRAST

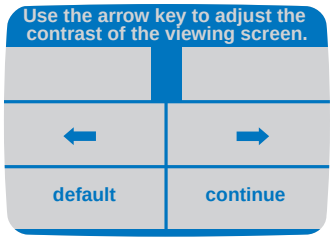

Depending on the lighting in your home and other factors, you may want to adjust the intensity of your touchscreen. Touch the arrows to lighten or darken the display. Touch **"Continue"** when finished.

CHANGE LANGUAGE

You have the ability to change the language between English, French and Spanish. You will always see the next screen in the selected language to make sure you want to change the language.

AUTO START

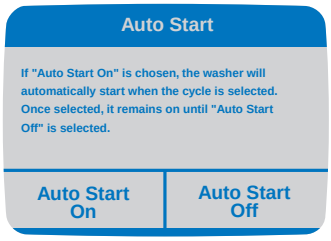

When "Auto Start on" is chosen, the washer will automatically start when the cycle is selected.

ENERGY SAVER

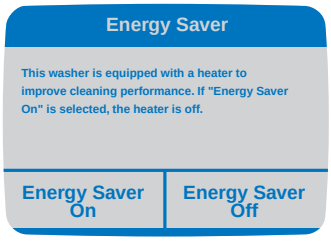

Selecting "Energy Saver on" deactivates the internal water heater. "Energy Saver off" activates internal water heating for improved cleaning performance.

Special Note: As you use the touchscreen, if you feel you are lost, press **Back** or **Home**.

FEATURES

DETERGENT

Your Maytag Neptune® washer is designed to use either high efficiency (HE) detergents or regular detergents normally used with top-loading washers.

- For best cleaning results, use a high efficiency detergent such as Tide HE or Wisk HE*. High efficiency detergents contain suds suppressors which reduce or eliminate suds. When less suds are produced, the load tumbles more efficiently and cleaning results are maximized.
- When using regular detergent formulated for top-loading washers, it is important to pay close attention to the soil level of the load, load size, and water hardness**. To avoid over-sudsing, reduce the amount of detergent used with soft water or with small or lightly soiled loads.

If using the "PRESOAK" setting, measure 1-1/2 times the amount of detergent.

* Brand names are trademarks of the respective manufacturers.

** To determine water hardness in your area, contact your local water utility or State University Extension office in your area.

AUTOMATIC DISPENSER

The automatic dispenser consists of three compartments which hold 1) liquid or granular detergent and color safe bleach, 2) liquid chlorine bleach and 3) liquid fabric softener. All laundry products can be added at once in their respective dispenser compartments. They will be dispensed at the appropriate time for most effective cleaning.

After loading the laundry additives into the dispenser, close the dispenser lid.

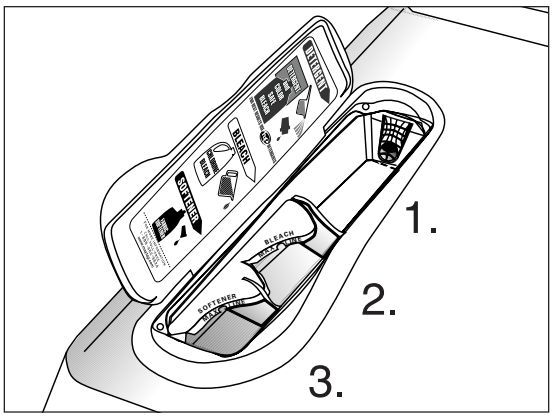

DETERGENT COMPARTMENT

1. Pour laundry detergent directly into the detergent compartment before starting the clothes washer or as the washer is filling.
2. If color-safe bleach is to be used, it should be added with detergent to the detergent compartment for best results.

- When adding color-safe bleach with detergent, it is best if both laundry products are in the same form; granular or liquid.

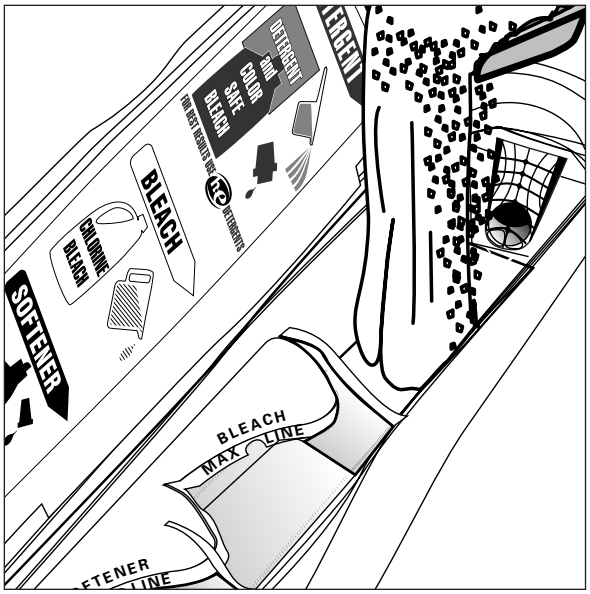

BLEACH COMPARTMENT

(Chlorine Bleach Only)

1. Add chlorine bleach to the bleach compartment DO NOT exceed the MAX FILL line. The chlorine bleach compartment will hold 3/4 of a cup.
2. Avoid splashing or over-filling the compartment. **Over-filling the compartment will release the chlorine bleach into the clothes washer too early.**
3. The washer automatically dispenses bleach into the tub when there are approximately two minutes left in the wash portion of the cycle. This maximizes the effectiveness of the bleach.
4. The dispenser automatically dilutes liquid chlorine bleach before it reaches the wash load.

NOTE:

- *Never pour undiluted liquid chlorine bleach directly onto the load or into the tub. It is a powerful chemical and can cause fabric damage, such as weakening of the fibers or color loss, if not used properly.*
- *If you prefer to use color-safe, non-chlorine bleach, add it to the detergent compartment.* ***Do not pour color-safe bleach into the bleach compartment.***

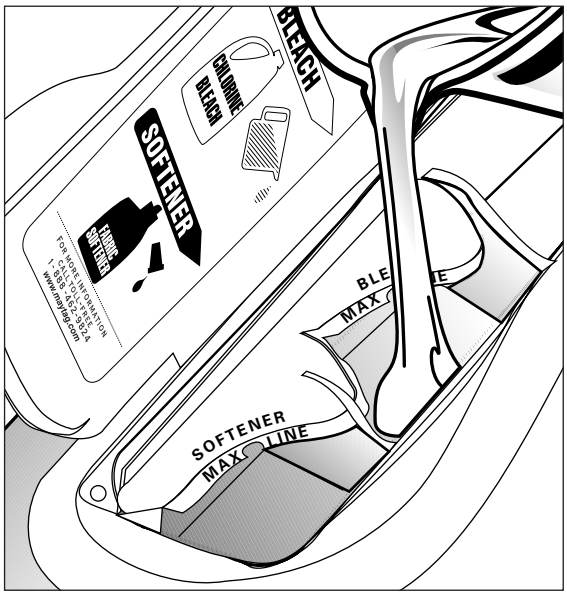

SOFTENER COMPARTMENT

1. Pour the recommended amount of liquid fabric softener into the softener compartment. For smaller loads use less than one cap full.
2. Fabric softener may be diluted with warm water until it reaches the MAX FILL line on the compartment. **Do not dilute the liquid fabric softener compartment above the MAX FILL line. If the compartment is filled above the MAX FILL line, fabric softener will enter the clothes washer too early.**
3. This compartment automatically dilutes and releases liquid fabric softener at the proper time during the rinse cycle.

NOTE:

- *Use the softener compartment only for liquid fabric softeners.*
- *Using the Downy Ball* is not recommended with this washer. It will not add fabric softener at the appropriate time. Use the dispenser on top of the washer.*

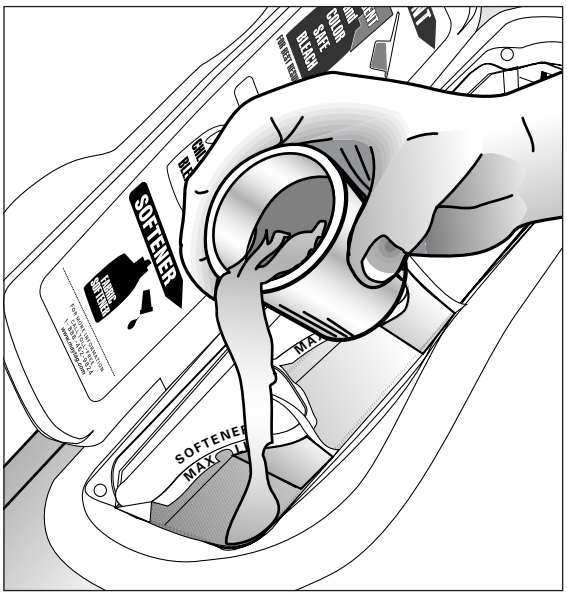

* *Brand names are trademarks of the respective manufacturers.*

Care and Cleaning

Turn off the water faucets after finishing the day's washing. This will shut off the water supply to the clothes washer and prevent the unlikely possibility of damage from escaping water.

Use a soft cloth to wipe up all detergent, bleach or other spills as they occur.

Clean the following as recommended:

Control Panel – clean with a soft, damp cloth. Do not use abrasive powders or cleaning pads. Do not spray cleaners directly on the panel.

Cabinet – clean with soap and water.

Interior – hard water deposits may be removed, if needed, using a recommended cleaner labeled clothes washer safe.

Cleaning the Dispenser

The dispenser may need to be cleaned periodically due to laundry additive build-up. For easy clean-up of the dispenser, grasp the removable two-compartment container (for bleach and softener) as shown in illustration #1. As you begin to lift the two-compartment container, tilt slightly inward, according to illustration #2 and remove from the main dispenser.

Once the two-compartment container is removed from the main dispenser, take it to a sink. Follow illustration #3 to remove the cap covering the siphon tube for the bleach and softener. Run warm water and a soft brush or cloth over the two parts to remove any excess laundry additives.

Clean the main dispenser area using water and a soft cloth. Once the main dispenser is clean, follow the illustrations in reverse order to replace the two compartment container to its original location.

NOTE: Do not use any cleaning substance but water in the main dispenser. It is possible for cleaning substances to drain into the tub. If this should happen, set the washer for a rinse and spin cycle to remove any cleaning substance from the washer before doing a load of laundry.

Step 1

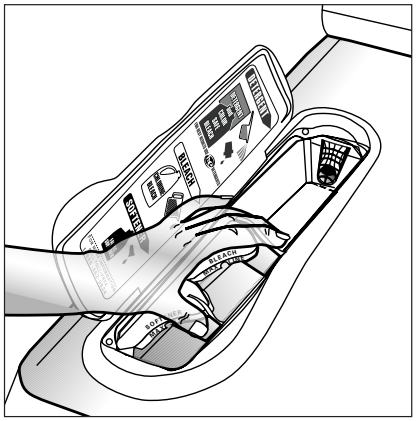

Step 2

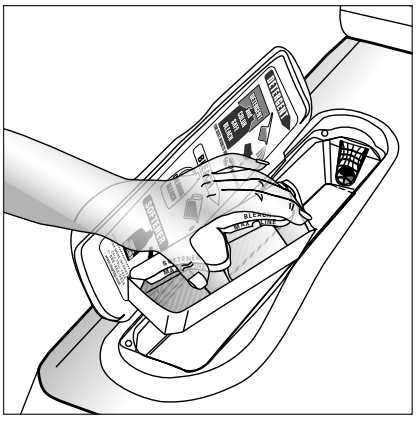

Step 3

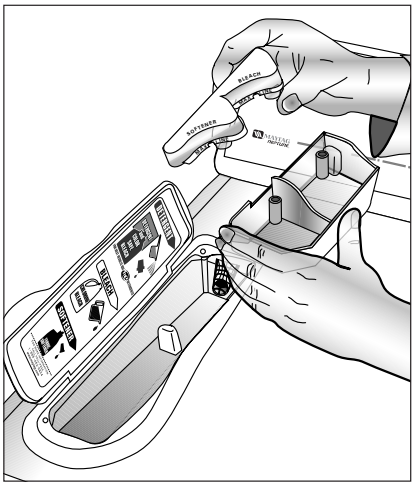

Storing the Clothes Washer

Washers can be damaged if water is not removed from hoses and internal components before storage. Prepare the washer for storage as follows:

- Select the "COTTON/STURDY" and "QUICK" setting and add one cup of bleach to the detergent dispenser without clothes in the tumbler. Run the clothes washer through a complete cycle.
- Turn the water faucets off and disconnect the inlet hoses.
- Disconnect the clothes washer from the electrical supply and leave the washer door open to let air circulate inside the tumbler.
- If the washer has been stored in below-freezing temperatures, allow time for the washer to thaw out prior to use.

For information on long-term storage or storage of your washer during extreme cold temperatures, call Maytag Customer Service toll-free at 1-888-462-9824.
U.S. customers using TTY for deaf, hearing impaired or speech impaired, call 1-800-688-2080.

Replacing Interior Light

Instructions for replacing the bulb:

1) Unplug or disconnect the clothes washer from the electrical power supply.
2) Open the door.
3) Unscrew the light bulb counter clockwise from the socket.
4) Replace the bulb with a **10 watt** candelabra base light bulb and rotate clockwise.
5) Plug in or reconnect clothes washer to the power supply.

Reversing the Clothes Washer Door

Clothes washer door swing direction can be changed using the following procedure:

1) Swing door fully open and support it while removing four hinge screws (which hold hinges to door assembly).
2) Move door to a work surface and transfer four color matched door screws to the opposite side of the door assembly.
3) Remove one screw holding top hinge to cabinet and one screw holding top hinge cover to cabinet (opposite side).
4) Remove hinge and bracket from cabinet by moving them up and down to a position where they are released.
5) Install hinge and bracket in swapped locations and drive screws to attach them securely to the cabinet.
6) Compare top hinge and top bracket to bottom hinge and bottom bracket for correct hinge assembly position.
7) Repeat procedures 4 through 6 for bottom hinge to cabinet and bottom bracket to cabinet.
8) Support door in fully open position on hinge side and drive four screws to securely attach hinges to door assembly.
9) Close door and check to see that clothes washer operates properly.

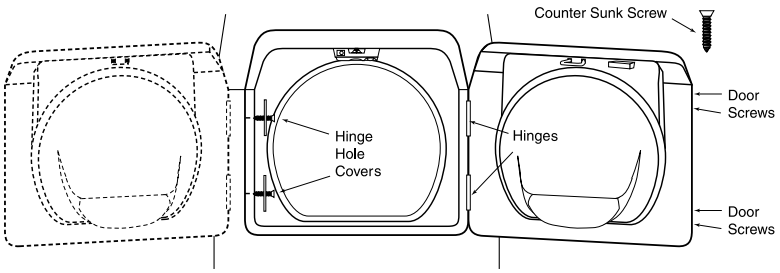

Before You Call

For problem laundry solutions (i.e. fabric damage, residue, tangling) and special laundry care procedures, see the enclosed Laundering Tips booklet.

Check these points if your Maytag Neptune® washer...

Load is Too Wet at End of Cycle	• Use Max Extract Spin Speed option. • Try using a high efficiency detergent to reduce sudsing. • Load is too small. Very small loads (one or two items) may not spin out completely.
Leaks Water	• Make sure door is firmly closed. • Make sure hose connections are tight. • Make sure end of drain hose is correctly inserted and secured to drain facility. • Avoid overloading. • Use high efficiency detergent to prevent over-sudsing.
Won't Spin or Drain	• Check fuse or reset circuit breaker. • Straighten drain hoses. Eliminate kinked hoses. If there is a drain restriction, call for service. • Close the door and push the START/PAUSE touchpad. For your safety, washer will not tumble or spin unless the door is closed. • After pressing the START/PAUSE touchpad, it will take a few moments before the clothes washer begins to spin. The door must lock before spin can be achieved. • See "Tub is Completely Full of Suds" below.
Stops	• Plug cord into live electrical outlet. • Check fuse or reset circuit breaker. • Close door and push the START/PAUSE touchpad to start the clothes washer. For your safety, washer will not tumble or spin unless door is closed. • This may be a pause or soak period in the cycle. Wait briefly and it may start. • Check screens on inlet hoses at the faucets for obstructions. Clean screens periodically.
Tub is Completely Full of Suds	• Run the clothes washer through another complete cycle using cold water. • Reduce detergent amount for that specific load size, soil level and water hardness. • Use high efficiency or low sudsing detergent specially formulated for front load washers.
Fills with the Wrong Temperature Water	• Turn both faucets on fully. • Make sure temperature selection is correct. • Make sure hoses are connected to correct faucets and inlet connections. Flush water line before filling washer. • Check the water heater. It should be set to deliver a minimum 120°F (49°C) hot water at the tap. Also check water heater capacity and recovery rate. • Disconnect hoses and clean screens. Hose filter screens may be plugged. • When warm rinse is selected, only the final rinse will be warm. The first two rinses will be cold. • While the washer is filling for cold or warm wash temperatures, both hot and cold water will go through the dispenser as the automatic temperature control feature checks incoming water temperatures. This is normal and will only happen the first time the washer is used.

Continued

Before You Call cont.

Check these points if your Maytag Neptune® washer...

Won't Fill	• Be sure the door is tightly closed. • Plug cord into a live electrical outlet (tub light should illuminate). • Check fuse or reset circuit breaker. • Open and close the door, then push the START/PAUSE touchpad. • Turn both faucets on fully. • Straighten inlet hoses. • Disconnect hoses and clean screens. Hose filter screens may be plugged. • Open and close the door, then push the START/PAUSE touchpad.
Won't Tumble	• Check fuse or reset circuit breaker. • Open and close the door and press the START/PAUSE touchpad. For your safety, the clothes washer will not tumble or spin unless the door is closed.
Door Locked Shut; Will Not Open	• Press the START/PAUSE touchpad to stop the washer. • It may take a few moments for the door lock mechanism to disengage.
Freshening Your Washer	• Open the door and wash the lower portion of the gray door seal with a solution of 1 cup chlorine bleach to 2 cups water. • Select the following control panel setting: Cotton Sturdy, Hot/Cold, Heavy soil setting. • Fill the bleach dispenser cup with liquid chlorine bleach and start the washer. • Pour an additional 1/2 cup bleach into the detergent dispenser as the washer is filling. • Allow the washer to complete the cycle. • At the end of the cycle, open the door and dry the gray door seal.
Is Noisy	• Clothes washer should be leveled properly as outlined in installation instructions. • Check the leveling leg lock nuts are tightened. • Be sure rubber feet are installed on leveling legs. • Weak floors can cause vibration and walking. • For information on normal operating sounds, see page 20.

For further assistance, call Maytag Customer Service toll-free at 1-888-4-MAYTAG (1-888-462-9824).

U.S. customers using TTY for deaf, hearing impaired or speech impaired, call 1-800-688-2080.

Operating Sounds

Normal operating sounds of your Maytag Neptune® clothes washer

High pitched sound during a spin cycle.	The motor increases speed to spin the tub to remove moisture from the load.
Flushing water sound coming from the dispenser area.	Detergent is dispensed at the start of the cycle. Bleach is dispensed during final minutes of wash. Fabric softener is dispensed during the third rinse while the washer is filling.
Sloshing or gurgling water sound when washer is off and the tub is rotated.	The sealed balance ring around the tub contains a liquid and is designed to make the washer spin smoothly.
"Whirring" or "Sloshing" sound followed by a pause, repeated throughout the wash cycle.	The tub rotates one direction followed by a pause. The tub reverses direction and pauses. This action continues throughout the cycle.
Clothes washer maintains a **slightly reduced spin speed** after achieving a higher spin speed.	After reaching the maximum spin speed, the machine may reduce spin speed slightly to create less noise and vibration.
The spin speed **slows down dramatically** when it sounds like an out-of-balance load.	The tumbler will begin to accelerate to speed, then slows back down to redistribute the load more evenly when an unbalanced load occurs.
Water is added after the washer has been tumbling for a while.	The Maytag Neptune® clothes washer uses a true adaptive fill and adds more water during the wash cycle as it is needed. **OR** Water flows through the dispenser to dilute and add bleach or fabric softener at the appropriate time. This will occur even if bleach and fabric softener are not used.
Clicking/draining sounds when washer is started.	Before the washer starts to fill, it will make a series of clicking noises to check the door lock and do a quick drain.

Questions & Answers

Q. What's the best cycle to use if I have stains on my laundry?

A. Select Cotton/Sturdy fabrics and the Heavy soil wash time. Pretreat the stains with a laundry pre-treat product. Refer to the **"Stain Brain"** under **Help** for more information on treating specific stains.

Q. How large of a load can I wash in my Maytag Neptune® washer?

A. The tub can be loaded completely full with dry, unfolded clothes. However, do not pack the tub tightly. If the load is heavily soiled it is very important not to overload the washer.

Q. At the end of the cycle my load comes out wetter than normal. What causes this?

A. During tumble and spin the washer may have had difficulty getting to a full spin speed because the load was not evenly distributed. This can occur with small loads, heavy items or a load in which too much detergent was used, causing over-sudsing. Redistribute the load in the washer, close the door and follow these steps. Touch **"More Cycles"**, **"Spin"**, and **Start Pause**.

Q. My laundry items seem to be very wrinkled at the end of the cycle. What can I do to correct the problem?

A. Wrinkling is caused by the combination of heat and pressure. Be sure wrinkle free or permanent press fabrics are washed on the Wrinkle Free cycle, and a cold rinse is used. (See pg. 5 for WASH/RINSE Temperature). DO NOT USE MAX-EXTRACT.

Q. My whites are not as white as I'd like. What can I do?

A. Wash white loads using the Cotton Sturdy fabric selection. Select the hot wash/cold rinse temperature setting and put 3/4 cup of chlorine bleach in the bleach dispenser. The bleach will be dispensed in the final minutes of the wash providing for optimal whitening. Maytag recommends a hot water wash temperature of 120-140° F (49°- 60° C).

NOTES

Clothes Washer Warranty

Full One Year Warranty

For **one (1) year** from the date of original retail purchase, any part which fails in normal home use will be repaired or replaced free of charge.

Limited Warranty

After the first year from date of original retail purchase, through the time periods listed below, the parts designated below which fail in normal home use will be repaired or replaced free of charge for the part itself, with the owner paying all other costs, including labor, mileage and transportation.

Second Year – All parts.

Third through Fifth – Electronic control.

Third through Tenth – Drive motor.

Third through Lifetime – Stainless steel inner wash basket.

Additional Limited Warranty Against Rust-Through

Should an exterior cabinet, including the top and baseframe, rust through during the one year period starting from the date of retail purchase, repair or replacement will be made free of charge. After the first, and through the tenth year, repair or replacement will be made free of charge for the part itself, with the owner paying all other costs, including labor, mileage and transportation.

Please Note: This full warranty and the limited warranty apply when the washer is located in the United States or Canada. Washers located elsewhere are covered by the limited warranty only, including parts which fail during the first two years.

The specific warranties expressed above are the ONLY warranties provided by the manufacturer. This warranty gives you specific legal rights, and you may also have other rights that vary from state to state.

To Receive Warranty Service

To locate an authorized service company in your area contact the Maytag dealer from whom your appliance was purchased; or call Maytag Appliances Sales Company, Maytag Customer Assistance at the number listed below. Should you not receive satisfactory warranty service, please call or write:

Maytag Appliances Sales Company
Attn: CAIR® Center
P.O. Box 2370
Cleveland, TN 37320-2370
U.S. or Canada (toll-free) 1-888-462-9824
U.S. customers using TTY for deaf, hearing impaired or speech impaired, call 1-800-688-2080.

When contacting Maytag Appliances Sales Company, Maytag Customer Assistance about a service problem, please include the following:

(a) Your name, address and telephone number;
(b) Model number and serial number (found on the back of the control panel) of your appliance;
(c) Name and address of your dealer and the date the appliance was purchased;
(d) A clear description of the problem you are having.
(e) Proof of purchase.

What is not covered by these warranties:

1. Conditions and damages resulting from any of the following:
   a. Improper installation, delivery, or maintenance.
   b. Any repair, modification, alteration or adjustment not authorized by the manufacturer or an authorized servicer.
   c. Misuse, abuse, accidents, or unreasonable use.
   d. Incorrect electric current, voltage or supply.
   e. Improper setting of any control.
2. Warranties are void if the original serial numbers have been removed, altered, or cannot be readily determined.
3. Light bulb
4. Products purchased for commercial or industrial use.
5. The cost of service or service call to:
   a. Correct installation errors.
   b. Instruct the user on proper use of the product.
   c. Transport the appliance to the servicer.
6. Consequential or incidental damages sustained by any person as a result of any breach of these warranties.

Some states do not allow the exclusion or limitation of consequential or incidental damages, so the above exclusion may not apply.

User's Guides, service manuals and parts catalogs are available from Maytag Appliances Sales Company, Maytag Customer Assistance.

Indirect Angle Estimation in Switched Reluctance Motor Drives Using Fuzzy Logic Based Motor Model

Nesimi Ertugrul, *Member, IEEE,* and Adrian D. Cheok, *Member, IEEE*

***Abstract*—In this paper, a novel rotor position estimation scheme is described that was developed to overcome the drawbacks of the previous sensorless techniques, which were proposed for switched reluctance (SR) motor drives. It is based on fuzzy-logic, and does not require complex mathematical models or large look up tables. The scheme was implemented by using a digital signal processor. The real-time experimental results given in this paper exhibit that the position estimation method proposed can provide accurate and continual position data over a wide range of speeds (zero/low/high), and can also function accurately at different operating conditions (chopping/single pulse mode and steady state/transient operation).**

***Index Terms*—Fuzzy logic, position sensorless operation, switched reluctance motor.**

I. Introduction

THE ACCURATE knowledge of the rotor position is required for good performance of the switched reluctance (SR) motor drive. The need for the rotor angle information in SR motors has been traditionally satisfied by the use of some form of rotor position sensor. However, in recent years, there have been extensive research activities to eliminate direct rotor position sensors, simply by indirectly determining the rotor position.

A comprehensive review of the existing indirect position detection methods in SR motors was discussed in the reference [1]. It has been shown in the reference that the indirect position determination methods can be classified into two major groups: inserting the low amplitude signals to the motor windings (major papers in this group include [2]–[4]), and monitoring the actual motor excitation waveforms (major papers in this group include [5]–[8], [28]). In [1], observations were also made about the disadvantages in the use of direct rotor position sensors.

The expected benefits of the indirect methods are: elimination of the electrical connections of sensors, reduced size, no maintenance, insusceptible to the environmental factors, and increased reliability. In addition, the expected features of the indirect methods over the other sensorless schemes should include: operating at zero speed and higher speed as in the conventional direct position sensors.

The method explained in this paper is a flux linkage based estimation method that uses a fuzzy motor model and estimation scheme to determine the position of the rotor over a wide range of practical operating conditions. As well known, motor drives are usually electrically noisy environments, and practical measurement systems are normally subject to error and inaccuracy. Therefore, a major reason for the choice of using a fuzzy logic based estimation scheme was to satisfy the requirement that the algorithm is not affected significantly by deviations and error in the input data. The use of a fuzzy motor model in the estimation algorithm provided robustness and resistance to the effects of input noise, which is demonstrated in detail in reference [9], and therefore is not discussed here.

Furthermore, it should be noted that previously developed model based schemes [10]–[12] use simplified linear motor models and involve complex mathematical computations, or require large numerical look-up tables. This makes the previous schemes practically difficult to implement due to the fact that the SR motors normally operate under magnetic saturation and thus can only be accurately described by a nonlinear model. Moreover, complex mathematical computations are disadvantageous because of the demand for a fast real-time processor, which may not be suitable for all motor drives. Other advantages and applications of fuzzy logic to electric machine drives has been extensively detailed in [13].

The reference [14] reports the preliminary structure and hardware setup of the indirect position estimator. The paper presented some initial results to prove the concept, however only off-line results were presented that were calculated from measured voltages together with current waveforms derived from simulation.

This paper develops the scheme further to take into account the issues that are related to the practical motor drive operating in real-time and with measured voltages and currents. The hardware details of the DSP based system and the modifications introduced to provide a robust practical motor drive are also explained. In the following sections of the paper, the principal sections of the method are shown, implementation details are highlighted and some typical real-time experimental results are given to demonstrate the effectiveness of the method.

II. Development of a Fuzzy Logic Based SR Motor Model

To create a fuzzy model of the motor, a training scheme is used which trains a fuzzy logic model that is based on numerical information about the SR motor. The fuzzy rule base generated in this section is used by the fuzzy reasoning mechanism to estimate the rotor position from the input values of current and flux linkage in the rotor position estimation scheme. The main

Manuscript received April 8, 1999; revised February 21, 2000. Recommended by Associate Editor J. Ojo.

N. Ertugrul is with the Department of Electrical and Electronic Engineering, University of Adelaide, Adelaide 5005, Austrailia.

A. Cheok is with the Department of Electrical and Computer Engineering, National University of Singapore, Singapore.

Publisher Item Identifier S 0885-8993(00)09797-0.

advantages of developing a fuzzy logic based model of the SR motor are as follows.

1) No complex mathematical model is required, and thus has the advantage of relatively simple mathematical calculations used for rule processing [15], and the memory requirement of the stored fuzzy model is much lower than that required by the equivalent look-up table [16]. In addition, the fuzzy motor models allow fast computation and hence provide cost effective solutions for computationally demanding algorithms in real-time systems.
2) Fuzzy models are universal approximators [17], and therefore, they can model a nonlinear continuous function of SR motor.
3) Neural networks can also be used to model the switched reluctance motor using a mathematical model free approach [18], but they often have a long learning time, and do not allow the examining of the internal structure of the model as with fuzzy logic linguistic rules [19]. Therefore, fuzzy models are favorable due to the fact that their behavior can be explained using linguistic rules, and thus, they can be easily adjusted by altering the rules [20]. Furthermore, it has been shown that the fastest possible universal computation scheme corresponds exactly to the operations in fuzzy logic methods using Max–Min computations [21], which allows faster real-time operation than is possible with an equivalent neural network model. This is an important consideration for practical SR drives.

A. Obtaining the Motor Model

To obtain a fuzzy rule based model of the test motor, the training system derives information from two main sources.

a) The static flux linkage curves of the motor, which provides important information about the electro-magnetic characteristics of the SR motor phases.
b) The dynamic real-time operating waveforms of the motor, which can include real-time operating effects, such as mutual coupling between phases, temperature variations, eddy currents, and skin effects.

Due to its suitability to practical applications (fast, simple, and accurate), *the table-look-up scheme* [15] was used for the training phase of the rotor position estimation system in order to derive a fuzzy logic based SR motor model in the form of a fuzzy rule base.

Furthermore, it should be emphasized here that the fuzzy model, which was implemented here, is not equivalent to a look up table with a linear interpolation, and has many advantages over look up tables: robustness to input noise [22], non linear model [17], much lower memory storage [16], and triggering multiple non linear rules for each numeric input (not just one rule as in a look up table).

Although the fuzzy rule generation techniques are well known, the rule generation for this specific application is briefly explained below to emphasize the practical issues.

The motor characteristics are defined as a two input (flux linkage and current)—one output (rotor angle) function. The training task involves creating a fuzzy model of this function from the training data. The training data is defined as a two-input one-output *input–output pair* (where the word "*pair*" in this term refers to the fact that there is a set of input values paired with a set of output values, and not a pair of two values). Each point of measured data presented to the training system is given as

$$(\psi^{(n)},\, i^{(n)};\, \theta^{(n)}) \tag{1}$$

where

n nth data pair;
ψ flux linkage;
i current;
θ position.

The training phase to obtain a fuzzy logic based motor model consists of the following steps.

Step A: Dividing the Input and Output Domains into Fuzzy Regions: To determine the fuzzy regions, the variable spaces of ψ(0 to 1 Wb), i(0 to 20 A), and θ(0 to 30 degrees) were divided into N_1, N_2, and N_3 regions respectively, and number of regions were chosen to be $\boldsymbol{N_1 = 39}$, $\boldsymbol{N_2 = 37}$, $\boldsymbol{N_3 = 31}$.

Note that the number of sets and all fuzzy sets were chosen to have the same shape, and thus all the membership functions were chosen to be isosceles triangular shapes, which were defined after the real-time testing of the algorithm in the real-system. This choice of sets was found to provide sufficient accuracy in this work. Although more regions would provide greater accuracy in such systems, this also leads to more memory requirement due to the greater number of fuzzy sets and rules.

Each region was then assigned to a fuzzy membership function. The maximum point of each triangle was chosen to lie at the center of the fuzzy region and is given a membership value of 1. The other two vertices were chosen to lie at the centers of the two neighboring fuzzy regions and at these two points the membership values were made zero. Each fuzzy set is denoted by a fuzzy linguistic term ranging from set SM19 to BIG19 (for Ψ'), from set SM18 to BIG18 (for I'), and from set SM15 to BIG15 (for Θ') as shown in Fig. 1. In the figure, $\mu_{\Psi'}(\psi)$ is the membership value in fuzzy set Ψ' of input flux value ψ, $\mu_{I'}(i)$ is the membership value in fuzzy set I' of input current value i, and $\Psi_{\Theta'}(\theta)$ is the membership value in fuzzy set Θ' of input angle value θ.

Step B: Generating Fuzzy Rules from Input Data of Flux, Current, and Angle: During the training phase, each input–output data pair, which consists of a crisp numerical value of measured flux linkage, current, and angle, is used to generate the fuzzy rules which model the system. To determine a fuzzy rule from each input–output data pair, the first step is to find the degree of each data value (flux, current, angle) in every membership region of its corresponding fuzzy domain. The variable is then assigned to the region with the maximum degree.

It should be mentioned here that each training data set produces a corresponding fuzzy rule, which is stored in the fuzzy rule base. However, it can be seen that with a large amount of measured training data there will normally be rules produced by different training data which are identical, and therefore the number of stored rules does not necessarily correspond to the number of training data sets. In addition there may be rules

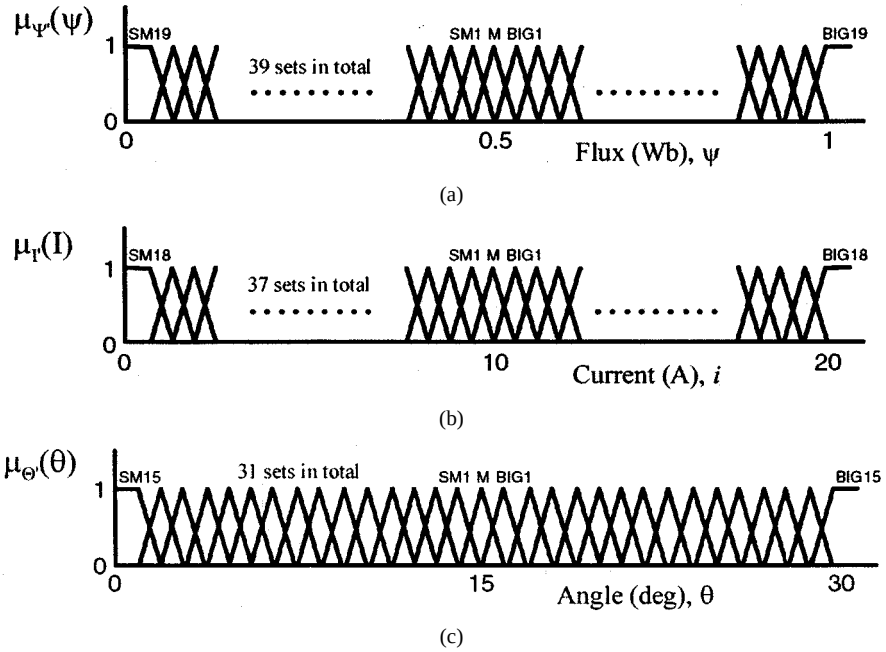

Fig. 1. Fuzzy domain regions for each variable: (a) flux Linkage, (b) current, and (c) rotor position.

generated by different data sets that are contradictory, and the method for dealing with this case is explained below.

Step C: Assigning Rule Degrees: When each new rule is generated from the input–output data pairs, a *rule degree* or *truth* is assigned to that rule, where this rule degree is defined as the degree of confidence that the rule does in fact correlate to the function relating flux linkages and current to angle. In the developed method a degree is assigned which is the *product* of the membership function degree of each variable in it's respective region. For example

"Rule): *If* i is BIG2 and Ψ is BIG5 *Then* θ is SM6"
will have a degree
"Degree (Rule) $= \mu_{\mathrm{BIG2}}(i).\mu_{\mathrm{BIG5}}(\Psi).\mu_{\mathrm{SM6}}(\theta)$"

where

$\mu_{\mathrm{BIG2}}(i)$ membership degree of current in region BIG2;
$\mu_{\mathrm{BIG5}}(\psi)$ membership degree of flux in region BIG5;
$\mu_{\mathrm{SM6}}(\theta)$ membership degree of angle in the region SM6.

The purpose of the above assignment is to choose between data sets that produce the same antecedents but different consequents. This would arise because when there is a large amount of measured data, some data pairs will produce rules that have the same antecedent but a different consequent (due to errors or noise in the measured data). This would mean that there are conflicting rules in the system, which are resolved by choosing the conflicting rule that has the highest degree. This rule is the one that is placed in the fuzzy rule base.

For example, let us consider two input–output data pairs n and m, which produced the rules

Rule (n): *If* i is BIG2 and Ψ is BIG4 *Then* θ is SM7
Rule (m): *If* i is BIG2 and Ψ is BIG4 *Then* θ is SM9.

Thus for this example, there would be two rules with the same precedent but different consequent. If the membership functions for each of the variables was as follows:

$$i)\ Data\ Set\ n\text{: } \mu_{\mathrm{BIG2}}(i^{(n)}) = 0.41,\ \mu_{\mathrm{BIG4}}(\Psi^{(n)}) = 0.73$$
$$\mu_{\mathrm{SM7}}(\theta^{(n)}) = 0.79$$
$$ii)\ Data\ Set\ m\text{: } \mu_{\mathrm{BIG2}}(i^{(m)}) = 0.92,\ \mu_{\mathrm{BIG4}}(\Psi^{(m)}) = 0.76$$
$$\mu_{\mathrm{SM9}}(\theta^{(m)}) = 0.80.$$

Then the rule n will have degree $0.41 \times 0.73 \times 0.79 = 0.236$, whilst rule m will have degree $0.92 \times 0.76 \times 0.80 = 0.559$. Therefore, only the rule with the highest degree (m) will be placed into the fuzzy rule base.

Step D: Create the Fuzzy Rule Base: As it can be seen from Step C, every training data set produces a corresponding fuzzy rule that is stored in the fuzzy rule base (except if an identical rule exists on the rule base already, or the generated rule is eliminated due to a lower degree of truth than an existing rule with the same antecedent but different consequent). Therefore, as each input-output data pair is processed, and the rules are generated, a fuzzy rule or knowledge base is in the form of a two dimensional table, which can be looked up by the fuzzy reasoning mechanism. The current and flux linkage fuzzy sets, which are the antecedents, are the axes of a two dimensional look-up table, and the stored table values are the rotor position output sets.

B. Implementation of Training Scheme

A flow-chart showing the logical flow of the training procedure software routine is given in Fig. 2 [23], which is the same for both phases of training (using the static training data and the dynamic real time training data). The training algorithm learns the motor model from the two sets of measured motor data: the static magnetization curves and the real time dynamic operation data. After training the system with all the points on the static flux linkage curves, the rule table is generated.

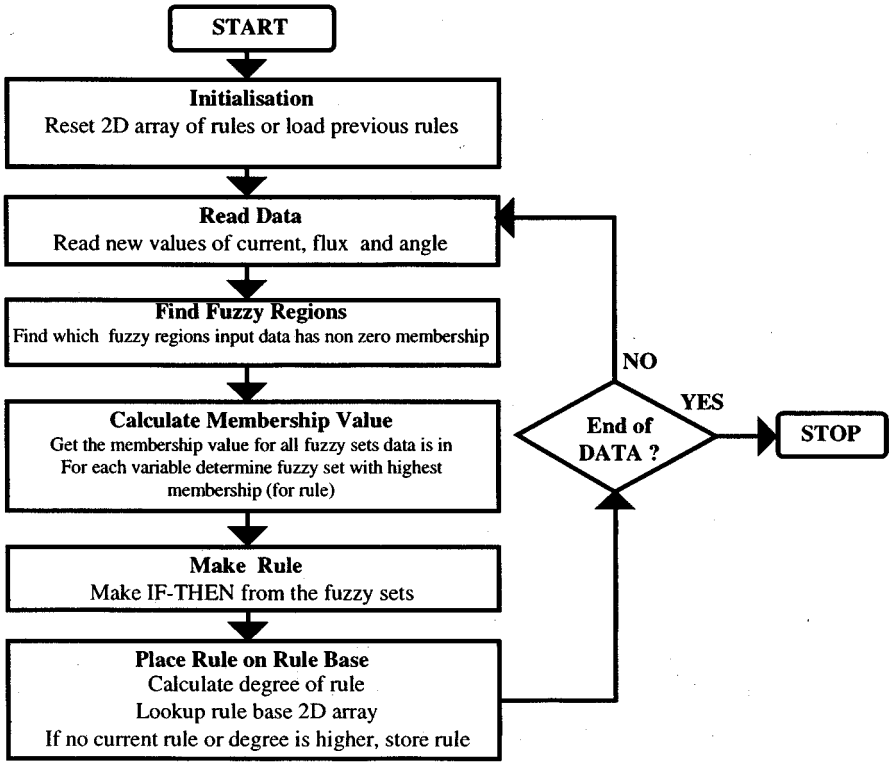

Fig. 2. Flow chart for the *training algorithm.*

It was found out that the static flux linkage curves characterize the motor to a good degree. However, the real time operating effects such as mutual inductances between phases, eddy currents, temperature effects and skin effects may be significant. It was found that there are some empty rule areas which cannot be explained by the rule table obtained as they lie in the region of flux and current in which the curves lie, and therefore, the dynamic testing requirement for the rule base determination is found to be necessary.

To determine the real time operational points of the SR motor it is important that data is measured during the real-time training phase include a wide range of operating conditions: transient and steady state speeds, step changes in load, and chopping and single pulse mode.

After the real-time running tests, the modifications made to the rule base from the static data training phase are highlighted (boxes with black background) in Fig. 3. The empty rule areas are shown by "XX" in the figure. For example, there is no rule for the inputs "Current is SMALL16 and Flux is BIG10."

It should be reported here that the amount of data that is required to be measured in the dynamic tests and used for training data cannot be exactly specified. However, it can be said that the accuracy of the model, up to a point, will increase with an increase in the data processed during the training phase. This is important because if data from a wide range of *real time* conditions is used for training, then the developed motor model will be able to predict the rotor position more accurately from the real time measurements of current and flux. Furthermore, it should be emphasize here that all the measurements in the motor are done for a single phase of the four-phase SR motor, and as a result, a single table is produced. Therefore, it can be said that the model developed here evolve an "*average model*" by using the mechanism of maximum degree of truth.

In addition to this, note that fuzzy sets are defined over a range of values, with the membership function of the fuzzy set varying for different values in the range. This means that an input data point with error or noise can still be placed, with lower membership function, in the same set as a point with no error or noise (depending on the amplitude of the error). In other words, by the use of fuzzy sets, input data that is corrupted by noise, can be accepted into the same set as clean data but with a lesser degree of truth [24]. The length of range of the membership function will determine the range of values with noise, which will be accepted as a part of the fuzzy set. Therefore by the fuzzification of the input data, small deviations in the input data do not have significant effect on the output position estimation.

III. Implementation of the Complete Rotor Angle Detection Scheme

A. Position Estimation

A block diagram of the complete position estimation algorithm is shown in Fig. 4. The position estimator essentially operates as follows: While the motor is running, the phase currents and voltages in each of the four phases are measured and the flux linkages are estimated by using trapezoidal integration (see the block A in Fig. 4) as given by

$$\psi(n+1) = \psi(n) + \Delta T \cdot [v(n) - Ri(n) + v(n-1) - Ri(n-1)]/2 \qquad \psi(0) = 0 \tag{2}$$

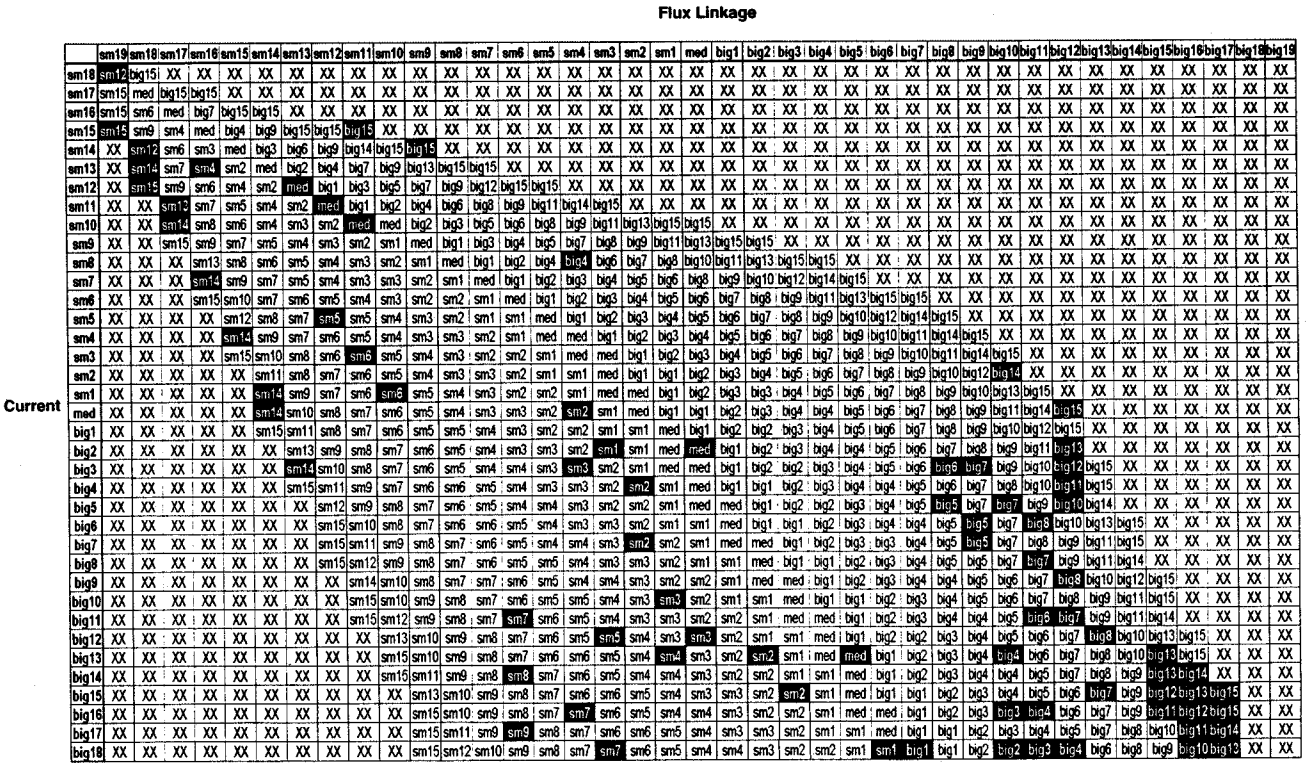

Fig. 3. Fuzzy rule bases generated after the real-time test results, **S**: small, **C**: center, **B**: big.

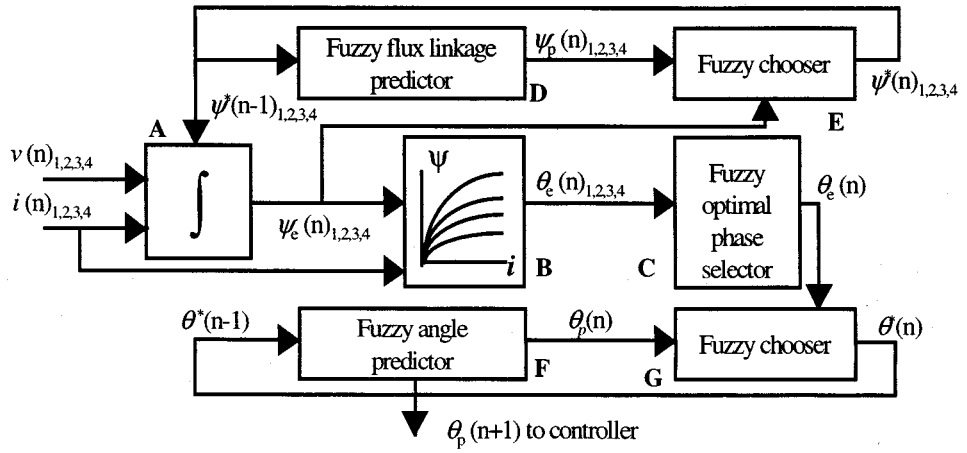

Fig. 4. Block diagram of the fuzzy logic based position estimation scheme.

where

n sample number;
ΔT sampling period;
v winding voltage;
i line current;
R winding resistor.

Note that when no current flows in a SR motor phase, the initial flux linkage value at $t = 0$ is zero. Therefore, at the end of each electrical cycle for each phase the flux linkage can be reset to zero in the integrator. Unlike the other three-phase ac motor drives, this feature of SR drive flux linkage estimation provides a means of reducing the effect of flux linkage offset error [9]. This is because the accumulation of the large errors in each phase, such as the effects of currents and voltage dc offset, measurement errors and resistance variation, will not normally continue for more than one electrical cycle.

It should also be noted here that the maximum integration error is also proportional to the highest value of the second derivative of the integrated function [23]. This means that when trapezoidal integration is applied to the flux linkage estimation, the maximum error is dependent on the second derivative of the integrated current and voltage waveforms.

It should be emphasized that, the current and voltage waveform are simple functions at high motor speeds (in the single pulse mode). However due to the commutation seen in the chopping mode, the current and voltage waveforms are more complex and nonlinear. Therefore, for the same conditions, it can be expected that the error in the integration of flux linkage in the

chopping mode may be higher than in the single pulse mode (in which the integration intervals is wider and the second derivative is lower).

In the above figure, ψ is the flux linkage, 1,2,3 and 4 represent the phase numbers, and θ is the rotor angle. n, $n-1$, and $n+1$ indicate "present," "previous" and "next step" values of the parameters respectively. The superscript, $*$ and the subscripts, $\mathbf{p}$ and $\mathbf{e}$ in the terms indicate the weighted values, the predicted values and the estimated values respectively.

In the second stage, the block B, the crisp numeric flux linkage and current values from each phase are then input to the fuzzy logic rule base (where the fuzzy motor model is located). These inputs will trigger the *If-Then* rules in the rule base, which have previously been created from the training phase. Since the crisp values of current and flux linkage will normally be members of two fuzzy sets, four rules will normally be triggered per phase measurement. Therefore, composition of multiple fuzzy rules is required, using the *Aggregation of Rules* procedure. The aggregate of the fuzzy rules triggered by the inputs of each phase will produce an output fuzzy set in the rotor position fuzzy domain. A single crisp numeric value of estimated rotor position is obtained by using defuzzification. In this paper, the Max-Product and center average defuzzification methods are chosen due to the simple calculations of these methods [15].

It should be noted here that, in practice, drive environments are electromagnetically noisy, due to the proximity of power electronic devices, which have high amplitude voltage and current switching transient waveforms, with low power computation circuits. In addition, leakage inductances and coupling capacitances, which are always finite in such systems, can lead to noise voltages being induced in measurement circuits. Therefore, the reliability and robustness of the algorithm was highly important if it is designed to operate in the practical drive. To achieve this additional performance enhancement features have been added so that the sensorless angle estimation algorithm copes better with measurement errors and inaccuracies found in real motor drives.

B. Performance Enhancement Features

Fuzzy Optimal Phase Selector: The knowledge based optimal phase selector is added (the block C in Fig. 4) to pick the most desirable phase for estimating angle in order to maximize accuracy. This sub-system is used because in the SR motor there may be more than one phase that conducts excitation current at any instant of time. For example, if three phases were conducting current at a given instant in time, this would normally consist of two phases being turned on, with one previously excited phase having a decaying current component. Therefore, any of these current carrying phases may be used for rotor position estimation. Theoretically, the same position should be output by each of the excited phase rotor position estimations. However in practice, each phase may produce a slightly different estimated angle result.

It is important to note that each phase has rotor angle regions of optimal sensing. In some rotor angle regions the rotor position estimation will be more affected by errors than at other rotor

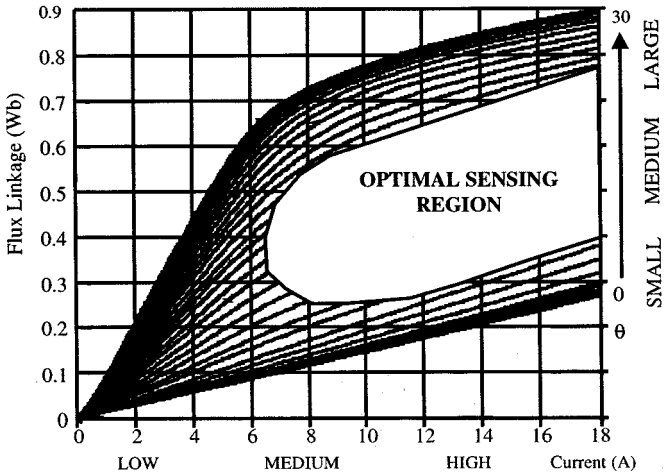

Fig. 5. Approximate optimal sensing region of the magnetization curves.

angle regions. The reason that each phase will be operating in a different phase region at any point in time is that at every physical rotor position, the rotor to stator phase angle will lie in a different region in each motor phase. Therefore, for implementation in a practical drive, the estimated rotor position from the phase in the rotor angle that lies in the optimal region should be given the most weighting. The optimal sensing region in Fig. 5 can be found from an analysis of the flux linkage curves [25].

Note also that the region shown in Fig. 5 is only approximate, as it is difficult to exactly define in an exact manner. It can generally be said from the magnetization curves, that when the angle is near the unaligned position (ie. for *small* relative angles) and the current is *low*, that the curves are very tightly bunched up. Therefore under this condition, small errors in the flux linkage estimation or current measurement will result in large errors in the position estimate. Additionally, when the angle is close to alignment (i.e., *large* relative angles) the curves are also tightly bunched up, and therefore a small error in current measurement can produce large errors in rotor angle. Therefore, the optimal sensing positions, where the best resolution is offered, is for *medium* angles between alignment and unalignment.

However, the optimal sensing region in fact does not stop or start abruptly but has a transition region, or in other words it contains smooth edges. In addition, the terms *small*, *low*, *medium*, and *large* used above to describe the regions, are linguistic terms. Furthermore it can be seen that the above descriptions in the previous paragraph describing the optimal sensing regions were in fact heuristic knowledge based rules.

Thus due to the imprecise regions, the ability to describe them using linguistic terms, and the availability of heuristic rules, a fuzzy logic rule base can be employed. Hence, to decide whether a motor phase measurement is in the optimal sensing region, a fuzzy rule based optimal phase selector (Block C) is placed after the fuzzy logic based motor model (Block B) seen in Fig. 4. The decision block encapsulates the general heuristic rules that were mentioned above, which describe the optimal sensing regions of the motor phases.

To perform the weighting of each of the position estimations from each phase, based on the heuristic rules described above, the optimal phase selector, uses a two input-single output fuzzy

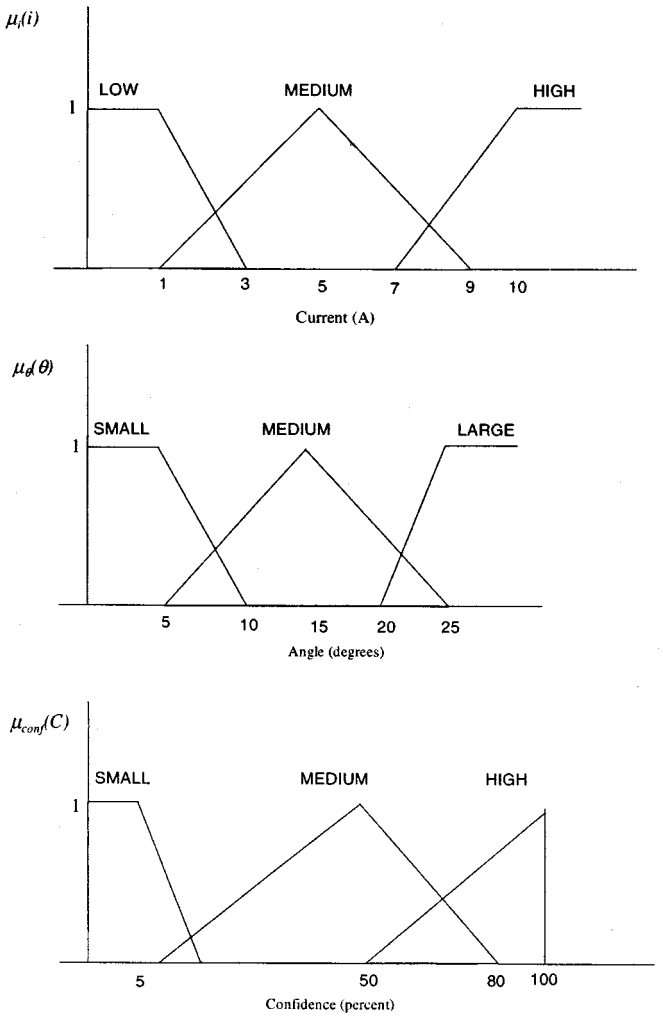

Fig. 6. Optimal phase selector domains. [$\mu_i(i)$ = fuzzy membership functions of current. $\mu_\theta(\theta)$ = fuzzy membership functions of rotor angle. $\mu_{conf}(C)$ = fuzzy membership functions of confidence.]

system. The input fuzzy domain is *current* and *angle* and the output is *confidence*. It gives a weighting or confidence value ranging from zero to 100% of each phase's rotor position estimate. The membership functions of the input and output fuzzy domains used in the optimal phase selector are shown below in Fig. 6.

A fuzzy rule base defines the linguistic rules that are used by the optimal phase selector. This is shown in the two-dimensional array of rules relating the inputs of current and angle to the output confidence value in Table I. It can be seen from the rule table that an example rule in this system is

$$\begin{aligned} &\textit{If}\ \text{current is}\ SMALL\ (\text{S})\ \text{and angle is}\ SMALL\ (\text{S}) \\ &\textit{Then}\ \text{confidence is}\ SMALL\ (\text{S}). \end{aligned} \tag{3}$$

As it was discussed above, these rules are based on heuristic knowledge about the optimal sensing regions in the flux linkage curves. The ability of fuzzy logic to model this heuristic knowledge allows a simple and easy to understand linguistic based system to be easily developed. This is achieved without the requirement of analytically defining the optimal regions of position sensing.

TABLE I
FUZZY RULE BASE FOR OPTIMAL DECISION BLOCK (S = SMALL, M = MEDIUM, L = LARGE, H = HIGH)

Current \ Angle	S	M	L
S	S	S	S
M	M	H	S
L	M	H	S

Confidence

Another advantage of using the fuzzy system is that the fuzzy linguistic rules of the optimal phase selector can remain unchanged even when a different motor is used. This is because only the definitions of the fuzzy membership functions in the input domains of current and angle are required to be changed if there is a change in the motor with different optimal phase sensing regions. For example, the membership function of *LOW* current seen in Fig. 6 could be modified to lie over a different range of the current domain. However, the fuzzy rule base does not need to be changed, and this allows the modification of the Optimal Phase Selector Block for another motor to be easily achieved.

As it was mentioned above, each of the four motor phases produces an estimated value of position, and each of them will be given a confidence weighting by the fuzzy phase selector, based on the estimated position and the phase current. This final weighted value is based on the weighting or confidence, C, of each of the rotor position estimates corresponding to which region the estimated rotor position lies in each phase. In essence, the optimal phase selector block in Fig. 4 decides the optimum phase for angle measurements, and gives this phase the greatest weighting if more than one phase is used in producing a rotor position estimate. Hence $\theta_e(n)_{1,2,3,4}$ outputs one final weighted value of $\theta_e(n)$.

To determine the final angle value $\theta_e(n)$, each estimated phase angle is multiplied by its respective confidence value found from the Optimal Phase Selector, and the total is divided by the addition of all the confidence factors. For example, if there are two phases that produce an angle estimate, then the algorithm computes the position by

$$\theta_e = \frac{\theta_1.C_1 + \theta_2.C_2}{C_1 + C_2} \tag{4}$$

where

θ_e final angle estimate;
θ_1 and θ_2 phase angle estimates of phase 1 and phase 2, respectively;
C_1 and C_2 confidence values of phase 1 and phase 2, respectively.

It should also be noted here that (4) is given only for two conducting phases. If three, or in some cases, four phases have some current (for example, trail currents, at high-speed operations), the equation should be modified to take these operating conditions into account.

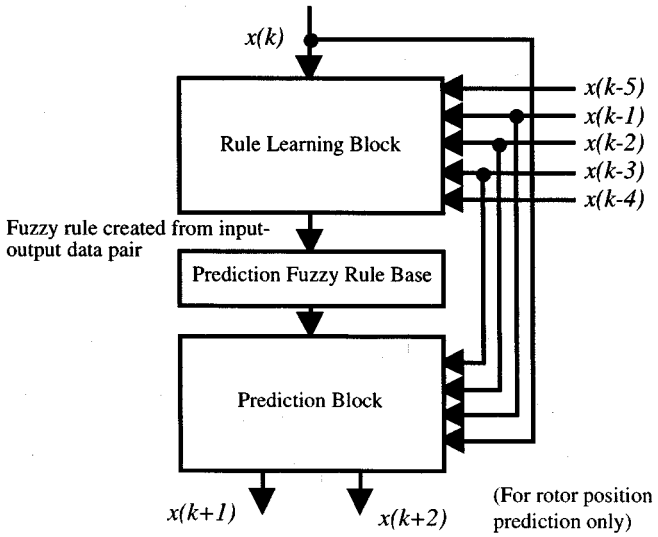

Fig. 7. Flow-chart of the prediction algorithms in the blocks D and F.

Fuzzy Flux Linkage and Angle Predictors with Fuzzy Choosers: The flux linkage and rotor angle predictors (the blocks D and F in Fig. 4) are included in the algorithm. The purpose of the predictors is to forecast future values of flux linkage and rotor position during the operation of the sensorless algorithm. The predictors are implemented using a fuzzy logic rule based system, with the rules of the fuzzy prediction system being adapted during run time.

The predictors are used to minimize errors by using a combination of the estimated and predicted rotor position and flux. To achieve this, a comparison between estimated and predicted rotor position and flux values are made during each iteration. Then some combination of these is chosen in order to lessen the effect of errors.

The problem of predicting the flux linkage and angle in future steps of time is a problem of *time series* prediction. It should be noted that in this fuzzy predictor, both learning and prediction occurs simultaneously, unlike the previously described training method. A flow-chart of the prediction algorithm is given in Fig. 7, where the values of $x(k)$ represent either flux linkage or rotor position.

When a new value of flux linkage or rotor position is estimated by the integrator or fuzzy model respectively, it is first passed into the rule learning block in Fig. 7, together with previous iteration values. For the flux linkage prediction, the rule learning block creates a new rule and modifies the rule table, from the new input–output data pair consisting of the present value $x(k)$ and the previous four values $x(k-1)$, $x(k-2)$, $x(k-3)$, and $x(k-4)$. For the fuzzy rules of the rotor predictor, however, two output predicted values, $x(k)$ and $x(k-1)$ are created from four previous inputs $x(k-2)$, $x(k-3)$, $x(k-4)$, and $x(k-5)$. For the flux prediction and the rotor position prediction, the input–output data pairs can be written, respectively, as

$$[x(k-4),\, x(k-3),\, x(k-2),\, x(k-1)],\, \rightarrow [x(k)] \quad (5)$$

$$[x(k-5),\, x(k-4),\, x(k-3),\, x(k-2)],\, \rightarrow [x(k-1),\, x(k)]. \quad (6)$$

This rule can then modify the fuzzy rule base so that the fuzzy rules which predict the next values from the previous four values is continuously adapted with each new measurement.

After the Rule Learning Block in Fig. 7, the prediction routine is executed, which estimates the next iteration value $x(k+1)$ (and $x(k+2)$ for the angle prediction), from the values of $x(k)$, $x(k-1)$, $x(k-2)$, and $x(k-3)$.

Furthermore, as shown in Fig. 4, the predicted values of rotor position $\theta_p(n)$, and flux linkage $\psi_p(n)$ are used in conjunction with the estimated values of flux linkage $\psi_e(n)$ and rotor position $\theta_e(n)$. In the ideal case, the predicted and estimated values should be exactly the same. However, due to errors the values are not equal. In this case either the predicted values or the estimated values may be used, and a decision must be made as to which value should be chosen. In this system a knowledge based, heuristic decision maker (Fuzzy Chooser) was implemented, which places a weighting on both the predicted and estimated values (the blocks E and G in Fig. 4). The decision blocks of the flux linkage and angle produce a final weighted value $\psi^*(n)$and $\theta^*(n)$ respectively.

It can be intuitively said that the confidence in predicted values will be *high* under *steady* speeds and conditions. Under transient speeds and conditions, however, confidence will be *low*. In addition, it can be said that the confidence in the predicted values will be *higher* for *low* acceleration values than for *high* acceleration values.

From the above discussion it may seem that some conventional mathematical function relating confidence in the predicted values to the actual motor acceleration can easily be defined. However some practical considerations make the use of a fuzzy system advantageous.

Firstly it can be seen from the above discussion, that high, low, and steady are linguistic terms that contain a certain amount of fuzziness. With conventional mathematical logic functions it is difficult to adequately represent heuristic knowledge directly. However, fuzzy systems can deal with situations where sharp distinctions between the boundaries of application of rules do not occur.

Furthermore, a major advantage of using a fuzzy system is that it can cope with inherent uncertainty in the input signals. In this system the input variable is acceleration, which cannot be directly measured by a mechanical sensor in this application, because the system is sensorless. Another method is to calculate acceleration from speed values. Successful techniques have been recently developed to estimate acceleration from measured speed, such as by using predictive polynomial differentiators or by model based state observation [27]. However in this case no direct measurement of position or speed is possible. If the position estimates are used instead, the errors in the estimates may be too high for calculation of acceleration.

Therefore a fuzzy system was developed to relate prediction confidence to acceleration, which only requires the acceleration feedback to be accurate enough to determine which predefined fuzzy domain the acceleration belongs to. Thus only imprecise knowledge is required about the motors acceleration.

Hence, instead of acceleration, an *acceleration factor* is used which gives an approximation of the actual acceleration. As discussed above, this approximation can be used in this application

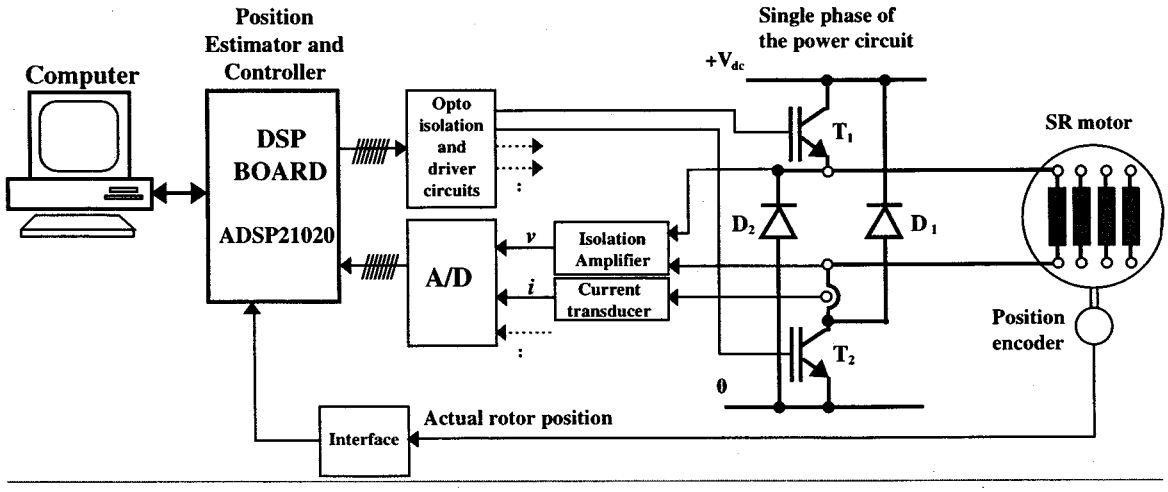

Fig. 8. SR motor drive hardware system developed.

because only the *relative* acceleration is important (e.g., *high* or *low*), and not the actual numeric value. Therefore an acceleration factor A_n is defined as

$$A_n = \frac{\theta_n - \theta_{n-k}}{k\Delta T} - \frac{\theta_{n-l} - \theta_{n-k-l}}{k\Delta T}. \tag{7}$$

Here, θ_n is the rotor angle at step n and ΔT is the time between each iteration, and k and l are constants (each chosen to be 5 in this application).

The above equation estimates the average speed over the last six iterations (i.e., over iteration n to $n-5$ where n is the last estimated position value), and compares it to a previous estimated average speed measured over $n-5$ to $n-10$). Other values of k and l may be chosen depending on the desired tradeoff between a longer sampling time of measuring the acceleration factor (which leads to less noisy values) and the delay in determining the value from the first measurement θ_{n-k-l}.

The difference of these two values provides an estimate of the relative motor speed transient magnitude. However it was found out in the practical system that, to lessens the effect of angle estimate noise on the calculation, the acceleration factor could be further modified to use the average of the previous 3 estimated acceleration factors, which is given by

$$(A_n + A_{n-1} + A_{n-2})/3. \tag{8}$$

The weighted rotor angle from the estimated and predicted value is used as an input to the rotor position predictor in Fig. 4, in order that further predictions are corrected. In addition, the flux linkage value output from the decision block is used as the next integration constant for the flux linkage integrator. In this manner, the corrected values are used to not only correct the present values of flux linkage and position, but also to correct future values of flux linkage and position. The effectiveness of the flux linkage and angle prediction with fuzzy choosers in reducing the effect of impulsive type noise commonly found in motor drives is detailed below.

IV. Issues Related to Start-Up, Initialization and Next Step Angle

In the method developed, there are some practical application points, which apply in all operations in the drive. This includes issues such as the starting procedure, the initialization of the fuzzy predictors in each test, and the use of predicted angle when the fuzzy logic based predictors do not output a predicted angle due to lack of rules in the learning period. These issues are explained below.

A. Start-Up Procedure

During the start up of the sensorless motor drive, there are two problems. Firstly, the position is not known, and therefore, the controller does not have knowledge of the required initial phase control strategy. Secondly, if only one phase is used initially, there will be two solutions to the estimate of rotor position for each flux linkage and current data pair.

In the initial starting instant, two phases of the motor are excited using a short pulse of current, to produce two sets of flux linkage and current pairs. This will produce four possible values of absolute position (two from each motor phase). Only one angle estimate of one phase will agree with one angle estimate of the other phase. This is the actual absolute rotor position. After this step is performed, the absolute value of rotor position has been found, and there will be no ambiguity in further measurements. This is because knowledge of the last rotor position, and the direction of rotation, allows the controller to decide which of the two possible angles found from a flux linkage and current pair is in fact the correct position.

B. Initialization of Fuzzy Predictors

The fuzzy predictors of flux linkage and rotor position are *initialized* at the beginning of each of the tests. Therefore, in each of the graphs that are plotted, at time $t = 0$ there are zero rules in the fuzzy prediction rule base and learning begins with the first iteration. This is performed so that every test shown in the results section has a fair comparison, regardless of whether the motor starts at $t = 0$ (as in the start up tests) or not (as in the steady-state speed tests). It should be remembered that, this

arbitrarily places a learning period at the initial stages of each test, regardless of the motor operating conditions.

In addition, when the predictors cannot make a predicted value, due to a lack of developed rules in the learning system, the output is set to zero. This signifies that no prediction can be made at that particular iteration (in addition there is a software flag output implemented in the software to differentiate between no output, and an actual predicted value of zero degrees). If no prediction can be made for the current angle and flux linkage, then it is not of high consequence. However, if no prediction can be made for the next step angle, then this creates a problem for the controller, which uses the next step for the continuous control. Therefore, a backup system is used for the prediction of the next angle value.

C. Use of Next Step Predicted Angle in Fuzzy Predictor

When the predictors can not make a prediction, the output is set to zero. However, although the fuzzy predictor of flux linkage and rotor position is only required for error minimization, the next step angle is used by the controller. Therefore, in the case when the output of the next step angle is zero, the prediction reverts to a simpler prediction scheme which is independent and running in parallel to the predicted value.

The independent next step angle prediction acts essentially as a backup, and normally is not used by the controller, except when the predictor cannot make any prediction. This independent next step angle predictor performs a linear extrapolation of the previous two iteration's angle rotor position values. The value of the predicted angle can be found from the simple relation

$$\theta_{n+1} = \theta_{n-1} + 2\frac{(\theta_n - \theta_{n-1})}{\Delta T} \tag{9}$$

where θ_{n+1}, θ_n, θ_{n-1} are the predicted angles of the next iteration step, the present iteration step, and the previous iteration step, respectively, and ΔT is the iteration period.

The predicted angle using this method is normalized to one electrical cycle (60 degrees). The new angles are used for prediction in the next iteration.

V. Hardware Details and Real-Time Test Results

To test the method described in this paper, a switched reluctance motor drive system was designed and constructed with a controller. The drive consists of several distinct sub systems as illustrated in Fig. 8: 4-phase IGBT inverter (two switch per phase type), 8/6 SR motor (4kW, 415V, 9A, 1500 rpm, four phase), the DSP board, A/D converters, and the interfaces for signal input and output (currents, voltages, position and gate signals for IGBT's).

The controller consists of a high-speed DSP chip (ADSP-21 020) with on board memory. The DSP performs the fuzzy logic based rotor position estimation in addition for providing full control of the motor via the power inverter. Inputs to the digital signal processor include the current and the voltage of each phase. To sample four phase voltages and currents simultaneously, eight A/D converters were used, and in order to provide greater digital conversion accuracy, a programmable gain amplifier was utilized to adjust the gain of the voltage signal. A shaft encoder was used to provide a reference for checking the estimated position.

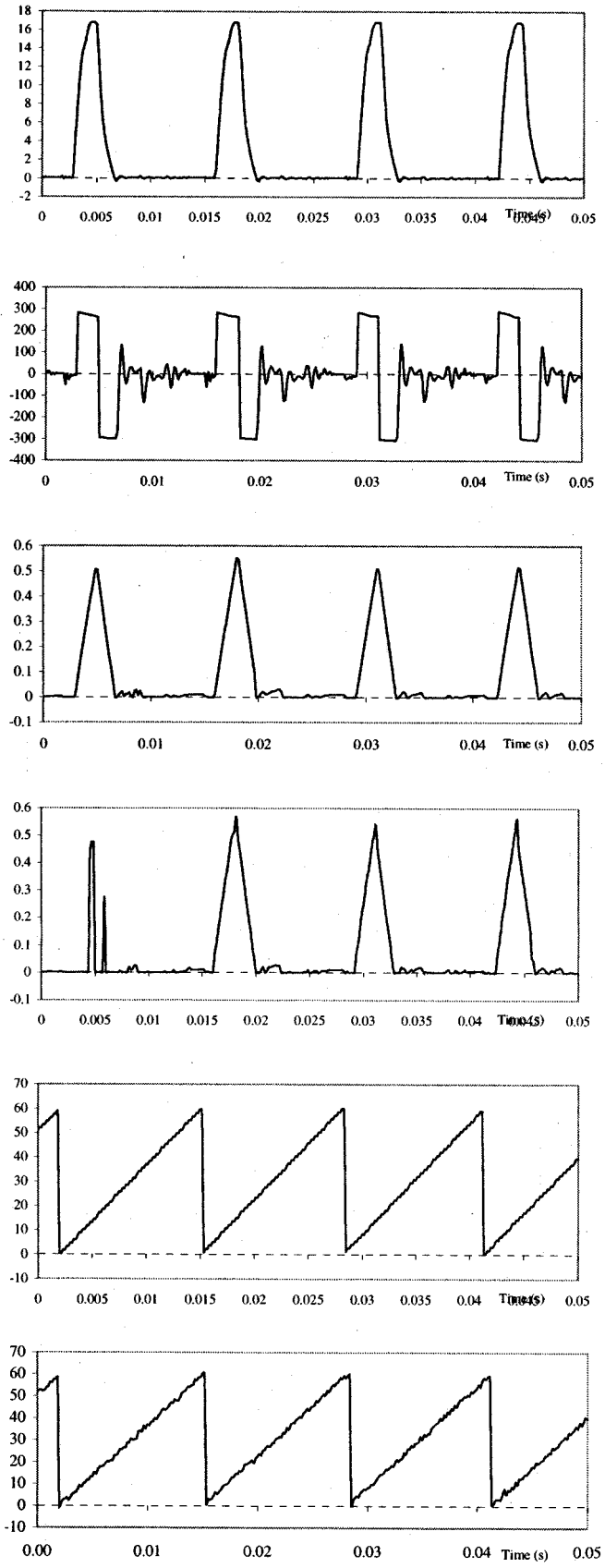

Fig. 9. Measured current, voltage, estimated flux linkage, predicted flux linkage of phase A, measured and estimated position, respectively, from the top, 810 rpm.

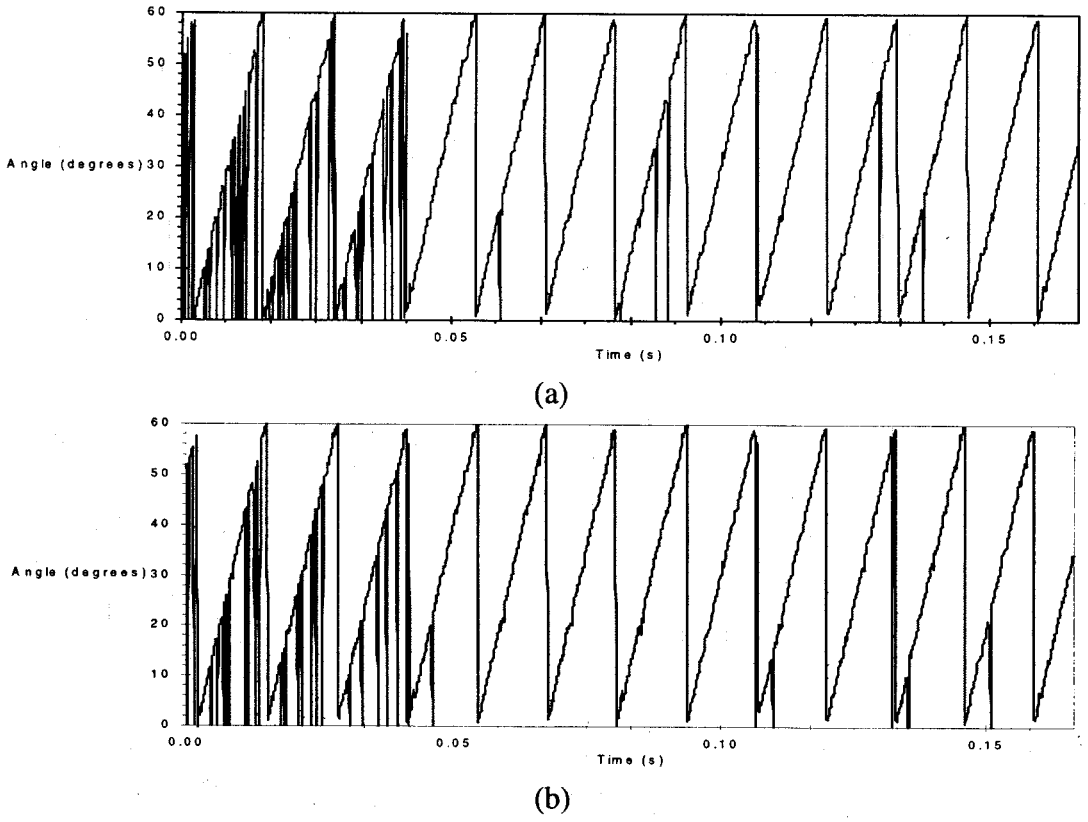

Fig. 10. Predicted and next step ahead predicted angles (in degrees).

The actual operating effects of the SR motor drive include: mutual inductance between motor phases, parameter variation of motor inductances and resistances, asymmetrical inductance variation in the motor phases, variation in the magnetization curves in each of the phases, and effects on the motor waveforms of eddy currents (which can distort the phase current, especially during current transients).

Therefore, experimental waveforms, which will be affected by all the above effects, should be used to verify the ability of the sensorless scheme to operate with a real SR motor. Using the experimental hardware, a wide range of operating modes and conditions were applied to the test motor. A few distinct operating results are presented in this paper: single pulse operation at steady-state speed, acceleration from zero speed, and zero/slow speed operation.

1) Single Pulse Mode Operation: In Fig. 9, the test results are given for the single pulse mode of the motor with a steady-state speed of 810 rpm. At high speeds, the back emf during pole overlap will become higher than the dc supply voltage. Therefore, the current does not reach the chopping mode current level (but is greater than the rated current) during the phase conduction period. Note that justification of "high" or "low" speed operation depends upon the machine details. For the motor used in this paper, low, base and high speeds correspond to the chopping mode, the changeover speed of 650 rpm and the single pulse mode, respectively.

It can also be seen in the figure that, in the single pulse mode, the current waveform is regular and the flux linkage has a simple profile, a quasitriangular wave-shape. Therefore, it was found that the fuzzy predictors of flux linkage have a short learning period with these flux linkage waveforms. This learning period was less than 200 iterations, corresponding to 46% of one revolution.

The reference position measured by the encoder had an 8-bit output, which means that 256 discrete positions per revolution can be measured, which corresponds to $256/6 \cong 43$ discrete points per electrical cycle. Therefore, in calculating the position error in the test results, the encoder measurement will normally have some quantization error, and thus not provide a very accurate reference. Nevertheless, it was taken to be the true rotor angle when comparisons were made between the estimated and the measured angle.

The predicted and next step ahead predicted angles for the test in Fig. 9 is given in Fig. 10. It was found that approximately 240 iterations were needed for the initial learning period. This was equivalent to 52% of one revolution of the rotor. In comparison with the flux linkage prediction of this test, it is seen that the learning period is slightly longer, due to the higher estimation error of position in comparison to the estimation error of flux linkage in this test.

2) Chopping Mode Transient Operation: To verify the operation of the method during transient operation, another set of experimental results is given in Fig. 11 during a transient start-up from zero speed to 346 rpm. As can be seen in the figure, the phase A motor current increases during the starting period and exceeds the rated current of 9A. However, when the motor approaches to the steady state speed of 346 rpm, the currents become significantly lower due to the decreased acceleration torque. This operation presents a more difficult problem for the position estimation due to following two main reasons.

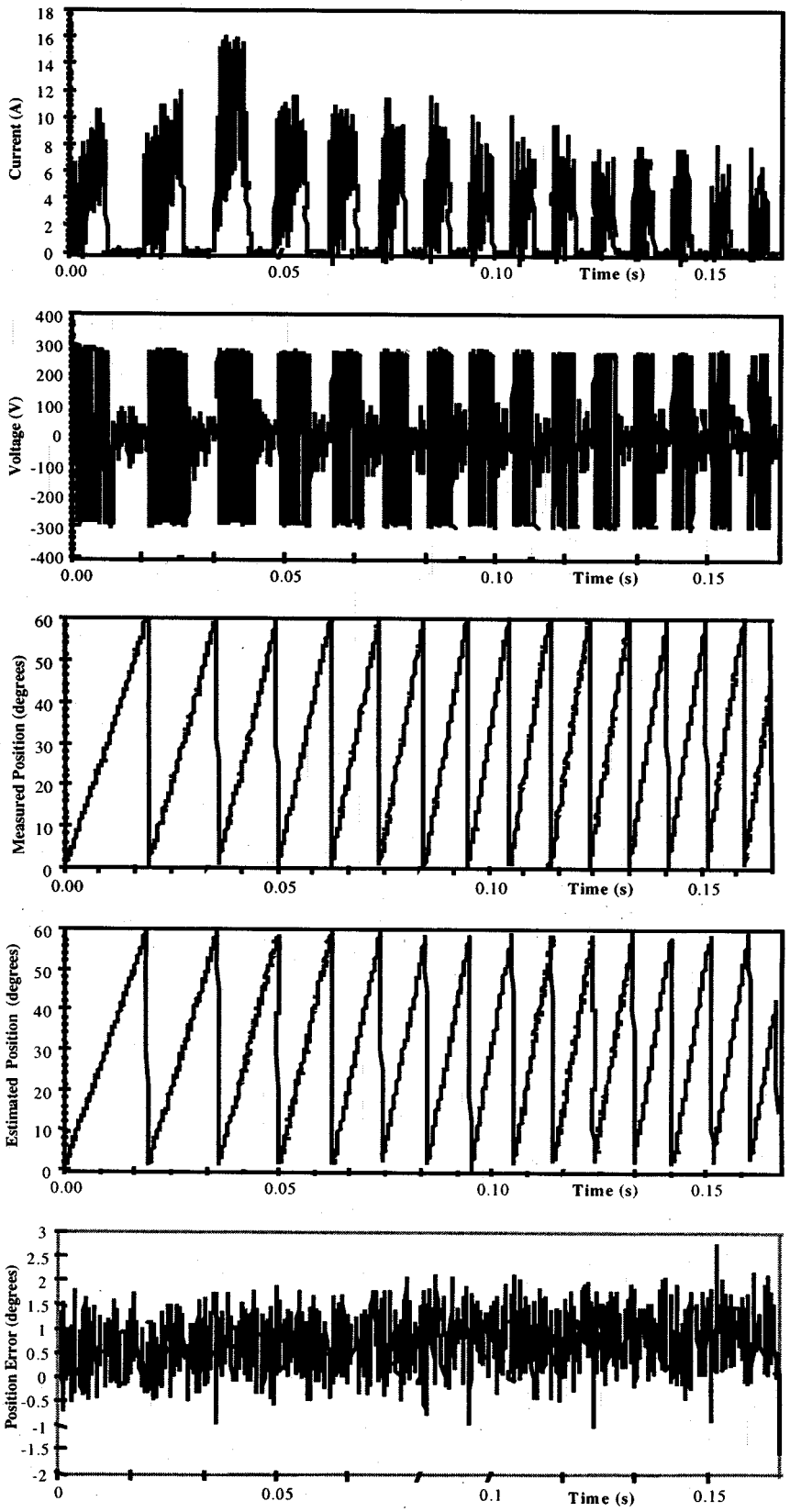

Fig. 11. Results of the transient start up with hysteresis current control: current, voltage, measured position, estimated position, and position error.

1) Not all the components of the waveforms are captured by the A/D converter at the specified constant sampling frequency of 6 kHz.

2) The predictors of flux linkage and rotor position, which are used to lessen errors in the flux linkage and position estimation, are not as effective during transient modes of

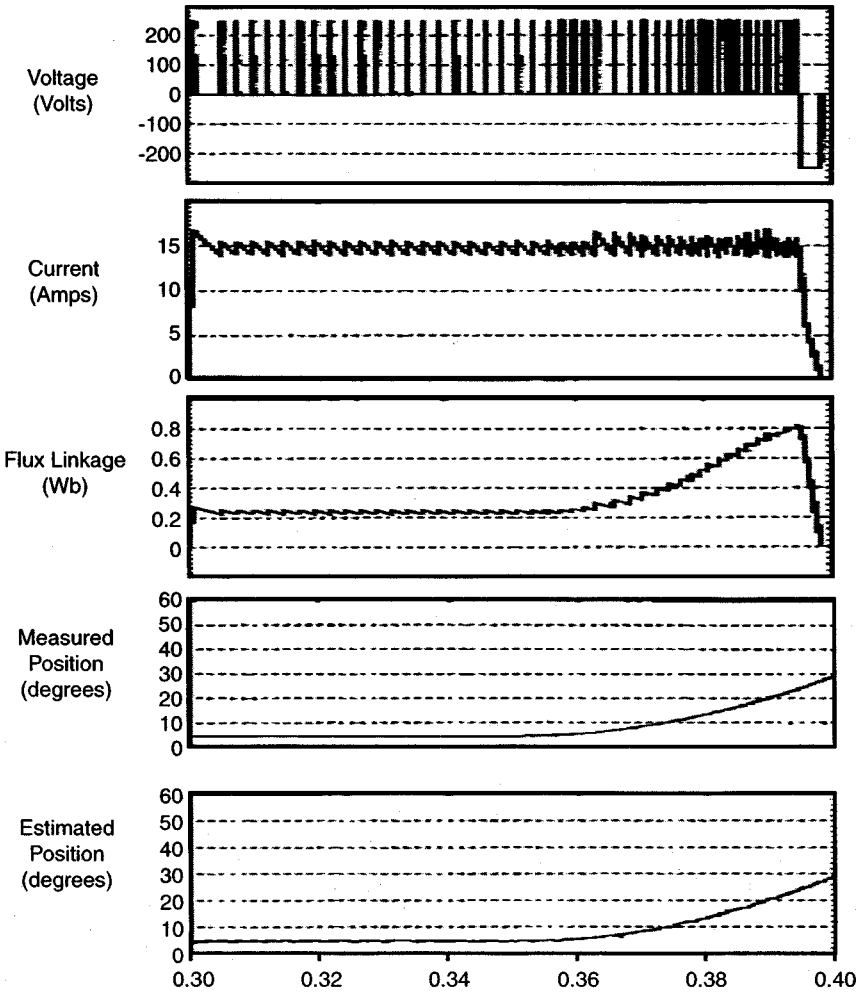

Fig. 12. Zero/low speed test.

operation as stated in Section III-A. This is because of the learning period always required when the motor waveforms vary. Therefore, the confidence in the predicted values will not be as high in the transient mode of operation.

In the transient mode of operation, the average angle error is somewhat higher. The performance has suffered due to the higher flux linkage estimation errors, and the trajectory of rotor position continuously changes in contrast to the linear variation of the previous steady-state speed tests. However, the estimated angle follows the measured position closely throughout the test.

3) Zero/Low Speed Operation: In this test the motor is initially stalled with a high inertial mechanical load that is thereafter slowly accelerated. The conditions of this test allow the sensorless position estimation algorithm to be tested for a number of important conditions. This includes zero speed operation (seen from $t = 0.3s$ to $t = 0.35s$), slow acceleration, and low speed (seen from $t = 0.35s$ onwards).

The plot of the phase current, phase voltage, phase flux linkage, as well as measured and estimated rotor position, are shown together for one motor phase in Fig. 12. At $t = 0.3s$ the rotor is stalled, and it can thus be seen that the rotor angle remains constant. However at $t = 0.35s$ the rotor is again accelerated with a low acceleration rate, and the rotor position again gradually increases.

It can be seen in the phase current waveforms of Fig. 12 that there are oscillations in the current hysteresis level even during zero and low speed. This is due to the bandwidth limitation of the hysteresis current controller. Furthermore it can be seen that the flux linkage changes when the rotor begins to accelerate from zero speed due to the change in incremental inductance with position.

The estimated angle that is seen in these results can be seen to always have some error, even though the rotor position is constant. This can be explained by the fact that the current is not constant but has variations due to the hysteresis control. This high frequency variation will not be completely captured by the A/D converters, leading to measurement errors. Furthermore noise and modeling errors that are always present will lead to the error seen in the rotor position.

A large amount of other experimental tests were performed on the motor to vigorously prove the performance and reliability of the fuzzy logic sensorless rotor position detection scheme under all conditions. Although two sets of the tests (steady state and transient) were presented above, Table II is provided to show the comparison of other distinctive test results, average of the absolute value of the position errors, maximum errors and cor-

TABLE II
SUMMARY OF TEST RESULTS ON THE ERROR ANALYSIS

OPERATION MODE	**Average of the absolute value of error** (degrees)	**Max. Error** (degrees electrical)	**Learning Period** (no of iteration)
STEADY-STATE OPERATION			
Low speed chopping mode test (command current level of 8A, ±4A hysteresis), 162 rpm, sampling frequency of 6000Hz.	0.48	1.55	~400
Mid-speed chopping mode test (command current level of 10A, ±2A hysteresis), 326 rpm, sampling frequency of 6000Hz.	0.36	2.64	<400
High-speed chopping mode test (maximum current level of 10A, ±4A hysteresis), 606 rpm, sampling frequency of 6000Hz.	0.79	2.80	~420
High-speed single pulse mode test (peak current level of 17A), 810 rpm, sampling frequency of 6000Hz.	0.52	1.92	200-250
TRANSIENT OPERATION			
Start-up from standstill to 346 rpm	0.82	2.87	
Change in load while running in chopping mode at 454 rpm	1.11	2.93	280

responding learning periods in each test [22], [23]. When the quantization error in the measured position is taken into account, the position error presented in the previous graphs and in Table II are not high. The operation of the motor has not been effected due to the small error in the position estimation. However, it should be emphasize here that the position estimation error can be reduced further if the sampling frequency and/or number of fuzzy-regions are increased. In addition to this, it should be remembered that measured reference position may also be in error.

A. Effectiveness of Fuzzy Predictors in Practical Drive Operation

The practical SR motor drive often has the problem of high amplitude impulsive type noise caused by switching or commutation of high amplitude currents in the inverter circuit. The commutated current waveforms have short rise and fall times, and thus contain significant amounts of energy at high frequencies. This radiated energy can be transmitted through parasitic stray capacitances to the control, interface, and measurement circuitry.

The characteristic feature of this generated noise is that it can have high amplitude during the switching of a power device. However, this noise is only seen during the switching instant. Therefore, the coupled noise in the control and current and voltage measurement circuits may have high amplitude, but be transient in nature. This type of high amplitude impulsive type noise is difficult to suppress efficiently [26]. However, the fuzzy predictive filters of flux linkage and angle as described above were developed to successfully lower the effect of impulsive noise for the practical operation of the sensorless position estimation scheme.

In Fig. 13, a demonstration of the fuzzy predictive filter's effectiveness is shown. Firstly, these figures show estimated flux linkage and angle derived from experimentally measured waveforms of current and voltage with the motor drive running at 670 rpm. It can be seen in the figures, that high amplitude error pulses occur in both the estimated flux linkage waveform and the estimated rotor position waveform.

In Fig. 13(a), the waveform of the flux linkage estimated from the measured current and voltages are shown, with a triangle representing each point where the flux is estimated from the current and voltage measurements. In the figure, a flux linkage waveform with high noise error can also be seen. The estimated flux linkage waveform with error is input to the flux linkage predictor instead of the actual estimated flux. It can be seen that the points with high-level noise have effectively been replaced by predicted values. It should be noted that if the predictor could not remove the erroneous value, then due to the operation of integration, all future values of the estimated flux linkage would carry this error.

Fig. 13(b), the waveforms are shown of the measured encoder angle and the estimated angle with impulsive type noise (at different test times, but with the same conditions as the flux linkage test). In the results, a triangular point shows the measured encoder positions at each sample time. In this test, the estimated angle that has been corrupted with high amplitude noise pulses is input to the angle predictor. It can be seen that the noise in the estimated angle is effectively removed in the filtered angle value. The filtered value can thus be used instead of the estimated value to reduce the effect of switching noise.

The results above have shown that when the fuzzy logic based predictive filters of flux linkage and angle are used, the high error pulses from sources such as switching noise are effectively eliminated, which leads to a more robust and stable motor drive operation.

VI. CONCLUSION

A novel fuzzy logic based rotor position detection technique is explained and implementation details are given, which provides an alternative way of measuring the rotor position in SR motor drives. The experimental tests verified that the new scheme can successfully and vigorously predict the rotor angle of the practical SR motor under the real operating conditions.

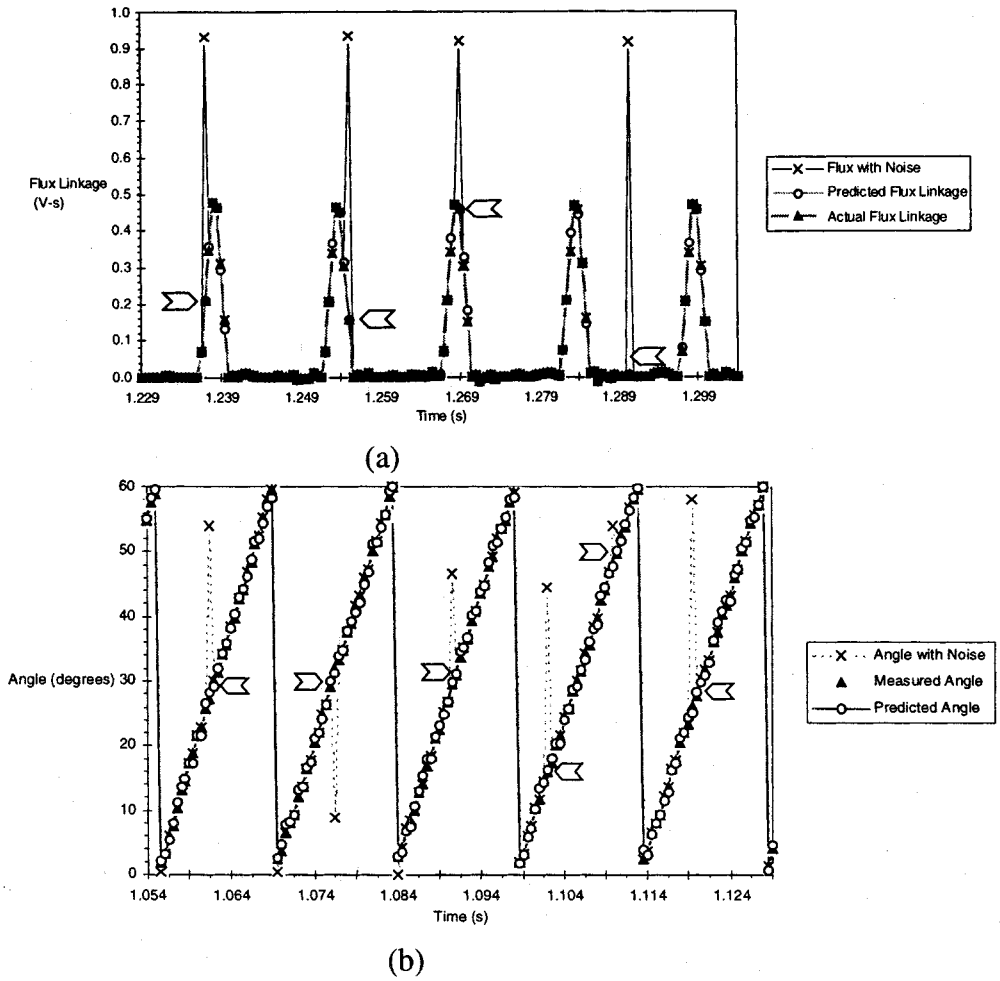

Fig. 13. Error elimination ability of fuzzy logic-based predictors: (a) flux linkage and (b) rotor position. The points with arrows highlight the iterations where the predicted value can be used instead of the estimated angle to lessen the effect of switching noise.

TABLE III
PRINCIPAL IMPROVEMENTS OF THE NEW SCHEME OVER THE MOST SOPHISTICATED METHODS TO DATE: THE MODEL BASED SCHEMES

Parameter	New Fuzzy Logic Based Scheme	Model Based Schemes
Speeds	All including stall and start-up	Not demonstrated for stall and start-up
High Robustness and Reliability	Demonstrated	Not demonstrated
Mathematical model	None required	Accurate state space model required
Includes non-linear saturation	Yes	No
Includes all real time operating effects	Yes	No
Requires test signals	No	No
Can be used under all current control conditions	Yes	No

Since there is no starting difficulty in the motor drive and no difficulty at zero speed operation, the motor drive can be operated in four-quadrants. It was shown that in general, the fuzzy logic based prediction algorithm had a fast learning period of approximately 200–250 iterations for simpler waveforms, such as the rotor angle trajectory and the flux linkage in the single pulse mode. The predictors of flux linkage and angle were also shown to be effective. The learning period became longer for highly nonlinear waveforms, such as the flux linkage in chopping mode.

The position estimator implemented in this research does not have restrictions seen in other schemes, as it can be used under

all operating speeds and conditions, including transients, standstill, and start-up. It also does not require any external testing circuitry or test signals.

The tests shown were taken with the A/D converter sampling frequency limited to 6000 Hz. This demonstrates the ability of the scheme to work with a relatively long iteration time of 166.7 μs. The average processing time of the position estimation routine is approximately 33 μs (the cycle time varies slightly according to which particular subroutines are used in the fuzzy prediction and fuzzy rule processing routines). The processing time can be further reduced by optimization of code and full assembly programming. The advantages made available by this scheme are summarized in Table III.

REFERENCES

[1] A. Cheok and N. Ertugrul, "Sensorless rotor position detection techniques in switched reluctance motor drives," in *Proc. Australasian Universities Power Eng. Conf.*, Perth, Australia, Sept. 1995, pp. 27–29.

[2] P. P. Acarnley, R. J. Hill, and C. W. Hooper, "Detection of rotor position in stepping and switched reluctance motors by monitoring of current waveforms," *IEEE Trans. Ind. Electron.*, vol. IE-32, pp. 215–222, Feb. 1985.

[3] M. Ehsani, I. Husain, and A. B. Kulkarni, "Elimination of discrete position sensor and current sensor in switched reluctance motor drives," *IEEE Trans. Ind. Applicat.*, vol. IA-28, pp. 128–135, Jan./Feb. 1992.

[4] S. K. Panda and G. A. J. Amaratunga, "Waveform detection technique for indirect rotor-position sensing of switched-reluctance motor drives—Part 1: Analysis," *Proc. Inst. Elect. Eng. B.*, vol. 141, no. 1, pp. 80–88, 1993.

[5] J. P. Lyons, S. R. MacMinn, and M. A. Preston, "Flux/current methods for SR MOTOR rotor position information," in *Proc. Conf. Rec. IEEE Ind. Applicat. Soc. Annu. Meeting*, 1991, pp. 482–487.

[6] W. F. Ray and I. H. Al-Bahadly, "A sensorless method for determining rotor position for switched reluctance motors," in *Proc. IEE 5th Int. Conf. Power Electron. Variable Speed Drives*, 1994, pp. 13–17.

[7] M. Ehsani and I. Husain, "Rotor position sensing in switched reluctance drives by measuring mutually induced voltages," in *Proc. Conf. Rec. IEEE Ind. Applicat. Soc. Annu. Meeting*, 1992, pp. 422–429.

[8] Gallegos-Lopez, P. C. Kjaer, and T. J. E. Miller, "High-grade position estimation for SRM drives using flux linkage/current correction model," *IEEE Trans. Ind. Applicat.*, vol. 35, pp. 859–869, Jul./Aug. 1999.

[9] A. Cheok and N. Ertugrul, "High robustness and reliability of a fuzzy logic based angle estimation algorithm for practical switched reluctance motor drives," in *Proc. IEEE Power Electron. Spec. Conf.*, Fukuoka, Japan, May 1998.

[10] C. Elmas and H. Zelaya-Da La Parra, "Position sensorless operation of a switched reluctance drive based on observer," in *Proc. IEEE EPE Conf.*, 1993, pp. 82–87.

[11] Lumbsdaine and J. H. Lang, "State observers for variable reluctance motors," *IEEE Trans. Ind. Electron.*, vol. 37, no. 22, pp. 133–142, 1990.

[12] Y. J. Zhan, C. C. Chan, and K.T. Chau, "A novel position and velocity observer for robust control of switched reluctance reluctance motors," *IEEE Power Electron. Spec. Conf.*, pp. 1315–1321, 1998.

[13] P. Vas, *Artificial-Intelligence-Based Electrical Machines and Drives: Application of Fuzzy, Neural, Fuzzy-Neural, and Genetic-Algorithm-Based Techniques*. New York: Oxford, 1999.

[14] A. Cheok and N. Ertugrul, "A model free fuzzy logic based rotor position sensorless switched reluctance motor drive," in *IEEE IAS Annu. Meeting*, 1996, pp. 76–83.

[15] L. X. Wang, *Adaptive Fuzzy Systems and Control: Design and Stability Analysis*. Englewood Cliffs, NJ: Prentice-Hall, 1994.

[16] G. C. D. Sousa and B. Bose, "A fuzzy set theory based control of a phase-controlled converter DC machine drive," *IEEE Trans. Ind. Applicat.*, vol. 30, pp. 34–44, Feb. 1994.

[17] J. L. Castro, "Fuzzy logic controllers are universal approximators," *IEEE Trans. Syst. Man Cybern.*, vol. 25, pp. 629–636, Apr. 1995.

[18] C. Elmas, S. Sagirogiu, I. Colak, and G. Bai, "Modeling of a nonlinear switched reluctance motor drive based on artificial neural networks," in *Proc. IEE PEVSD*, 1994, pp. 7–12.

[19] T. Frenz and D. Schroder, "Learning unknown nonlinearities using a discrete observer in combination with neural networks," in *Proc. IEEE Power Electron. Spec. Conf.*, 1995, pp. 1800–1806.

[20] S. Abe and M. Lan, "Fuzzy rules extraction directly from numerical data for function approximation," *IEEE Trans. Syst. Man Cybern.*, vol. 25, pp. 119–129, Jan. 1995.

[21] Lea and V. Kreinovich, "Intelligent control makes sense even without expert knowledge: An explanation," in *Proc. APIC'95 (Suppl. Int. J. Reliable Comput.)*, El Paso, NM, 1995.

[22] A. Cheok and N. Ertugrul, "High robustness and reliability of a fuzzy logic based angle estimation algorithm for practical switched reluctance motor drives," *IEEE Trans. Power Electron.*, to be published.

[23] A. Cheok, "A new fuzzy logic based rotor position estimation algorithm for switched reluctance motor drives," Ph.D. dissertation, Univ. Adelaide, Adelaide, Australia, Jan. 1998.

[24] G. C. Mouzouris and J. M. Mendel, "Dynamic nonsingleton fuzzy logic systems for nonlinear modeling," *IEEE Trans. Fuzzy Syst.*, vol. 5, pp. 199–208, May 1997.

[25] J. P. Lyons, S. R. MacMinn, and M. A. Preston, "Flux/current methods for SRM rotor position estimation," in *Proc. IEEE Ind. Applicat. Soc. Annu. Meeting*, 1991, pp. 482–487.

[26] Papoulis, *Probability, Random Variables, and Stochiastic Processes*. New York: McGraw-Hill, 1984.

[27] S. Väliviita and O. Vainio, "Delayless differentiation algorithm and its efficient implementation for motion control applications," in *Proc. IEEE Instrum. Meas. Technol. Conf.*, St Paul, MN, 1998, pp. 881–886.

[28] G. Gallégos-Lopez, P. C. Kjaer, and T. Miller, "A new sensorless method for switched reluctance motor drives," *IEEE Trans. Ind. Applicat.*, vol. 34, pp. 832–840, July/Aug. 1998.

Nesimi Ertugrul (M'95) received the B.Sc. (Eng). and M.Sc. degress in electrical and in electronic and communication engineering from the Istanbul Technical University, in 1985 and 1989 respectively, and received Ph.D. degree from the University of Newcastle upon Tyne, United Kingdom, in 1993.

He joined the University of Adelaide, Australia in 1994. His research topics include rotor position sensorless operation of brushless permanent magnet and switched reluctance motors, real-time control of electrical machine drives and power electronics systems, alternative energy sources, electrical vehicles, and interactive computer-based teaching/learning systems involving object-oriented programming and data acquisition. He is on the Editorial Advisory Board of the *International Journal of Engineering Education*.

Adrian D. Cheok (M'93) received the B.Eng and Ph.D. degrees from the University of Adelaide, Adelaide, Australia, in 1993 and 1998 respectively.

From 1996 to 1998, he was with Transmission and Distribution, Transportation Systems Center, Mitsubishi Electric Corporation, Amagasaki, Japan. Since 1998, he has been an Assistant Professor in the Department of Electrical Engineering, National University of Singapore, Singapore. His research interests include power electronics and motor drives, fuzzy logic and soft computing, nonlinear modeling and control, noise and EMI, embedded systems, and digital signal processing.

Elbtalwerk GmbH

Geschalteter Reluktanzmotor

Drehmomentstarker Elektromotor mit kleinem Bauvolumen

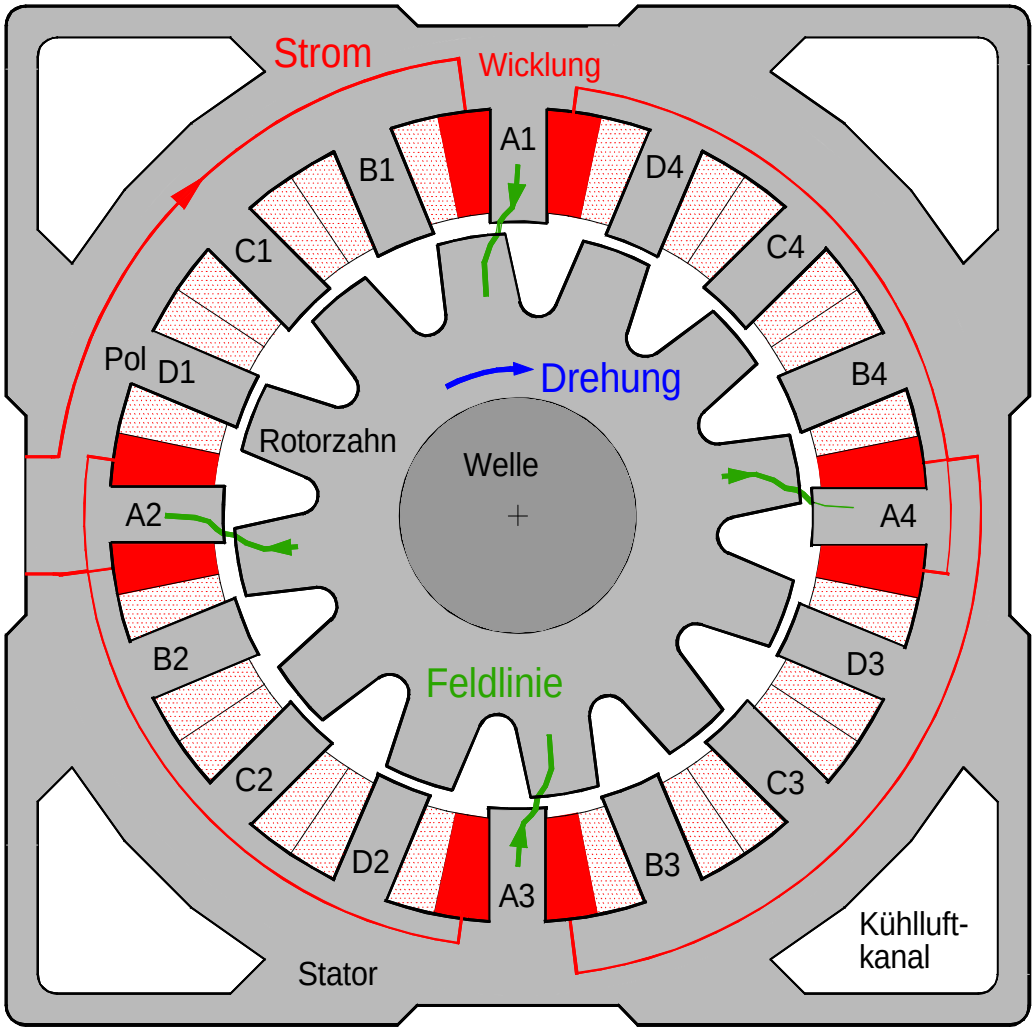

Universität Karlsruhe
Elektrotechnisches Institut

Einsatzgebiete

Der Geschaltete Reluktanzantrieb ist grundsätzlich für drehzahlveränderbare Antriebslösungen und für Positionieraufgaben geeignet. Je nach Ausführung des Umrichters ist ein Zwei-Quadranten-Betrieb oder der Vier-Quadranten-Betrieb möglich.

Im Vergleich zu anderen Antrieben zeichnet er sich durch

- überdurchschnittliches Dauerdrehmoment im Grunddrehzahlbereich
- sehr hohes Beschleunigungsvermögen
- geringe Wartung
- großes Haltemoment - auch über lange Zeiträume
- hohe Überlastbarkeit
- geringe Abmessungen
- sehr gute Notlaufeigenschaften nach Ausfall einer oder mehrerer Motorphasen
- ausgezeichneten Wirkungsgrad über einen großen Drehzahlbereich
- Robustheit
- sehr geringe Läufererwärmumg im unteren Drehzahlbereich

aus.

Für Applikationen, bei denen eine oder mehrere dieser Eigenschaften gefordert werden, lohnt der Einsatz des Geschalteten Reluktanzantriebes.

Aufgrund des ausgewählten und optimierten Querschnittes besitzt der von uns entwickelte Switched-Reluctance-Motor für alle Arbeitspunkte im unteren Drehzahlbereich eine unkritische Geräuschemission.

Höchste Drehzahlen: Der Maschinenläufer des Geschalteten Reluktanzmotors trägt weder eine Wicklung noch Permanentmagnete. Er kann deshalb mit hohen Radialkräften belastet werden und ist somit für den Betrieb bei großen Drehzahlen besonders geeignet. Aufgrund der mit der Drehzahl zunehmenden Ummagnetisierungsverluste sind für diese Anwendungen eher niederpolige Reluktanzmotoren geeignet.

Universität Karlsruhe, Elektrotechnisches Institut, Kaiserstraße 12, D-76128 Karlsruhe
Elbtalwerk GmbH, Fritz-Schreiter-Straße 31, D-01259 Dresden

Funktionsprinzip

Das Wirkungsprinzip des „Geschalteten Reluktanzmotors“, der in vielen Veröffentlichungen der englischsprachigen Literatur unter dem Namen „Switched-Reluctance-Motor“ propagiert wurde, ist denkbar einfach: Ein drehbar gelagerter Eisenstab oder auch die Eisenzähne eines Maschinenläufers richten sich in das durch einen elektrischen Strom in einem Ständerpol erzeugte Magnetfeld aus. Durch gezieltes Weiterschalten des Magnetfeldes gerät der Eisenstab oder der Motorläufer in eine drehende Bewegung. Besitzt dieser Läufer, der auch als Rotor bezeichnet wird, mehrere Zähne, so ist seine Form mit einem langgestreckten Zahnrad vergleichbar. Der Begriff „Reluktanz“ steht für den magnetischen Widerstand, den ein solcher Rotor dem elektromagnetischen Feld entgegensetzt. Erzeugung und Weiterschaltung des Magnetfeldes werden von den Polwicklungen im feststehenden Teil der Maschine und einer dem Motor vorgeschalteten Leistungselektronik übernommen. Mit der Leistungselektronik, welche als Stromrichter bzw. Frequenzumrichter bezeichnet wird, können die Drehzahl und das Drehmoment des Switched-Reluctance-Motors gezielt beeinflußt werden. Geschaltete Reluktanzmotoren lassen sich von Kleinstmotoren bis hin zu Großantrieben realisieren.

Musterantrieb

Am Elektrotechnischen Institut der Universität Karlsruhe wurden zwei Geschaltete Reluktanzantriebe mit einer Bemessungsleistung von 18,5 kW bzw. 23,5 kW bei einer Drehzahl von 1500 U/min entwickelt, optimiert und getestet. Der Umrichter ist direkt an das Drehstromnetz 400V/50Hz angeschlossen. Einige Meßergebnisse dieses Musterantriebes sollen in den nachfolgenden Abschnitten beispielhaft die Leistungsfähigkeit Geschalteter Reluktanzantriebe nachweisen. Den Auftrag über die Fertigung der Motoren übernahm das Elbtalwerk Heidenau. Auf dem Deckblatt ist die Wirkungsweise und der prinzipielle Blechschnitt des neu entwickelten Switched-Reluctance-Motors dargestellt. Dieser Motor besitzt 16 ausgeprägte Statorpole und 12 Rotorzähne.

Universität Karlsruhe, Elektrotechnisches Institut, Kaiserstraße 12, D-76128 Karlsruhe
Elbtalwerk GmbH, Fritz-Schreiter-Straße 31, D-01259 Dresden

Kleines Trägheitsmoment - große Dynamik

Aufgrund der massefreien Zahnlücken im Außenbereich des Maschinenläufers besitzt der Switched-Reluctance-Motor ein sehr kleines Trägheitsmoment. Der Rotor besteht nur aus dem Blechpaket und der Welle. Er trägt weder eine Wicklung noch Permanentmagnete. Die Tabelle 1 zeigt den Vergleich der Trägheitsmomente eines Asynchron-Normmotors, einer für hochdynamische Anforderungen optimierten Drehstrom-Asynchronmaschine und des Geschalteten Reluktanzmotors. Letzterer liegt gegenüber seinen Mitbewerbern deutlich vorn. Hinsichtlich des Bemessungspunktes, der Wärmeklasse und der Kühlung verfügen alle drei Motoren über gleichwertige technische Daten.

	Geschalteter Reluktanzmotor MFR 132.5	Asynchronmotor (optimierte Baugröße) ACHA 132.5	Asynchronmotor (Normmotor)
Trägheitsmoment	0,0883 kgm^2 59 %	0,105 kgm^2 70 %	0,150 kgm^2 100 %

Tabelle 1: Trägheitsmomente

Wesentlich bessere Ausnutzung bei kleinen Drehzahlen

Anders als bei Asynchronmotoren machen die Eisenverluste der Geschalteten Reluktanzmotoren einen erheblichen Anteil an den Gesamtverlusten aus. Mit abnehmender Drehzahl aber sinken die Eisenverluste sehr stark ab. Dieser Effekt kann zu einer Erhöhung der Effektivströme in den Polwicklungen genutzt werden und führt damit zu einem hohen zulässigen Dauer-Drehmoment im unteren Drehzahlbereich. Weiterhin entstehen im Betrieb bei kleinen Drehzahlen nur geringe Eisenverluste im Rotor - die Läufererwärmung bleibt gering. Bei Asynchronmotoren stellen die Wicklungsverluste im Stator und im Rotor den weitaus größten Anteil an den Gesamtverlusten dar. Diese bleiben mit einem festen Drehmoment vom Stillstand bis zur Bemessungsdrehzahl nahezu konstant. Somit erklärt sich, daß Asynchronmotoren im Dauerbetrieb bis zur Bemessungsdrehzahl nur mit Nenn-

Universität Karlsruhe, Elektrotechnisches Institut, Kaiserstraße 12, D-76128 Karlsruhe
Elbtalwerk GmbH, Fritz-Schreiter-Straße 31, D-01259 Dresden

moment belastet werden dürfen. Oberhalb der Nenndrehzahl beginnt für alle drei Motoren der Feldschwächbetrieb.

Im Bild 1 wurde das maximal zulässige Dauer-Drehmoment auf das Trägheitsmoment bezogen und im Drehzahlbereich von über 0 bis 1500 U/min bei Ausnutzung der Wärmeklasse F dargestellt. Bild 1 gibt Auskunft über das Beschleunigungsvermögen bzw. die Ausnutzung der Maschinen im Dauerbetrieb. Die beiden Reluktanzmotoren unterscheiden sich lediglich in der Qualität des verwendeten Elektrobleches. Im Stillstand ist für den Reluktanzmotor (Ausführung 18,5 kW) bei Dauerbetrieb ein maximales Haltemoment von 145% des Nennmomentes zulässig. Sobald aber der Reluktanzläufer dreht, werden alle Polwicklungen thermisch gleichmäßig beansprucht, und das Dauer-Drehmoment darf für kleine Drehzahlen 190% des Nennmomentes betragen. Für dynamische Übergangsvorgänge im gesamten Grunddrehzahlbereich kann den Motoren grundsätzlich das zwei- bis dreifache Bemessungsmoment abverlangt werden.

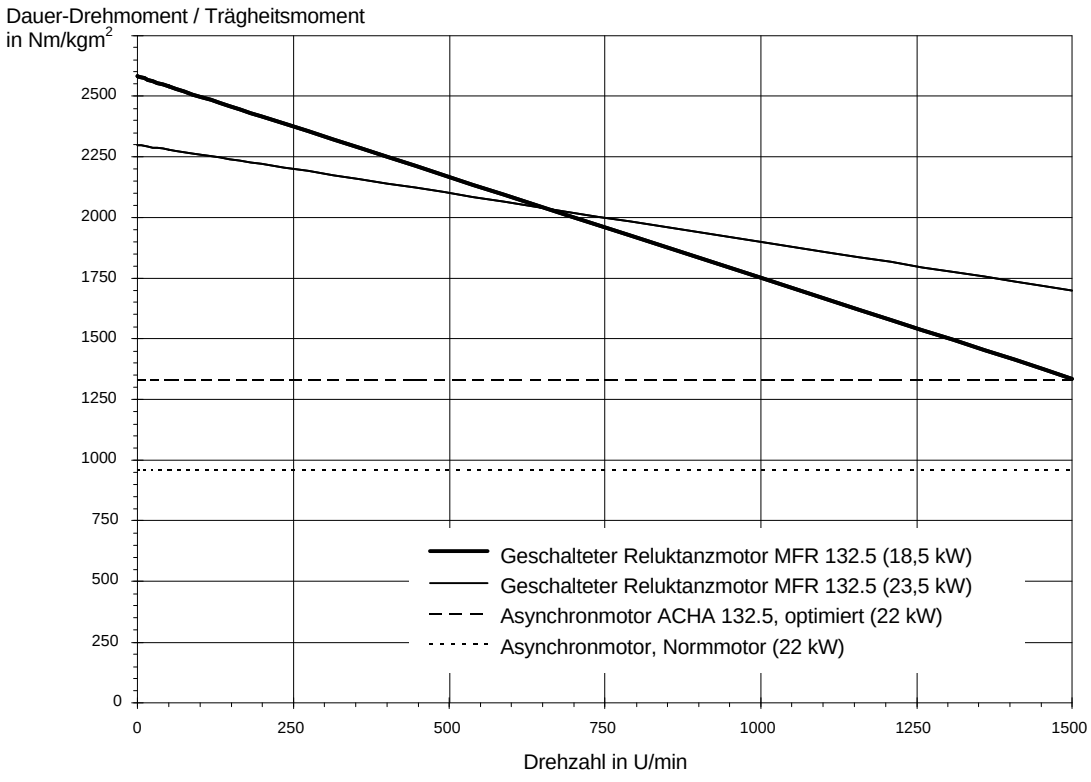

Bild 1: Zulässiges Dauer-Drehmoment bezogen auf das Trägheitsmoment bei Ausnutzung der Wärmeklasse F (Messung)

Universität Karlsruhe, Elektrotechnisches Institut, Kaiserstraße 12, D-76128 Karlsruhe
Elbtalwerk GmbH, Fritz-Schreiter-Straße 31, D-01259 Dresden

Die Kennlinien und Werte der Drehstrom-Asynchronmaschine ACHA 132.5 ist dem Datenblatt des Herstellers [1] entnommen. Bauvolumen, Baugröße, Außenabmessungen und Blechpaketlänge des optimierten Asynchronmotors ACHA 132.5 sind mit den Werten des Geschalteten Reluktanzmotors MFR 132.5 identisch.

Wesentlich besserer Wirkungsgrad unterhalb der Nenndrehzahl

Der Wirkungsgrad des Geschalteten Reluktanzmotors liegt im Nennpunkt bei einem für Drehstrommotoren dieser Leistungsklasse üblichen Wert. Allerdings fällt der Wirkungsgrad des Reluktanzmotors im unteren Drehzahlbereich nur unwesentlich ab (Bild 2). Er liegt bei Belastung mit Nennmoment bereits ab 300 U/min über 80% und steigt bis zur Nenndrehzahl allmählich auf ca. 90% an. Darin liegt ein weiterer Vorteil dieses Antriebes. Der Geschaltete Reluktanzmotor in der 23,5-kW-Ausführung erreicht im Bemessungspunkt einen Wirkungsgrad von 91,1%.

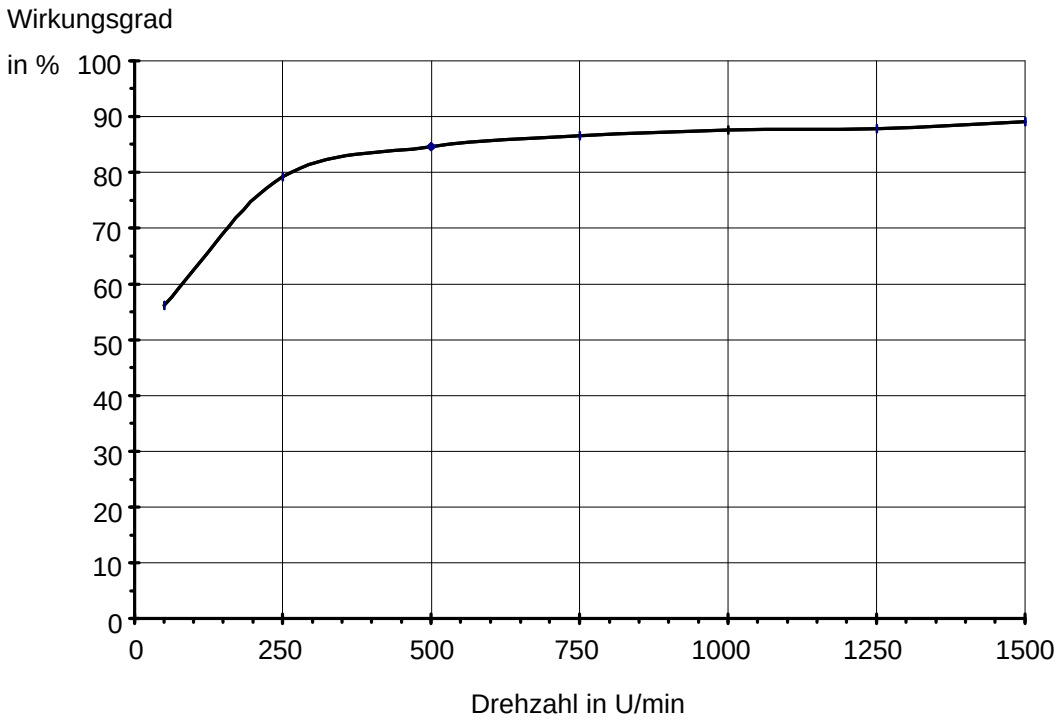

Bild 2: Wirkungsgrad bei Nennmoment und variabler Drehzahl für den Geschalteten Reluktanzmotor mit 18,5 kW (Messung)

Universität Karlsruhe, Elektrotechnisches Institut, Kaiserstraße 12, D-76128 Karlsruhe
Elbtalwerk GmbH, Fritz-Schreiter-Straße 31, D-01259 Dresden

Die Drehzahlregelung des Geschalteten Reluktanzantriebes wurde nach einem in der Antriebstechnik üblichen Verfahren entworfen und auf das Ausregeln von Drehzahlschwankungen optimiert. Ein Hochlaufgeber stellt sicher, daß bei einem Sollwertsprung der Drehzahl nahezu kein Überschwingen der Istdrehzahl auftritt. Im Bild 3 ist das Führungsverhalten bei Hochlauf auf Bemessungsdrehzahl dargestellt. Der Antrieb beschleunigt hierbei mit einem Drehmoment von ca. 170 Nm. Die Trägheit der bei dieser Messung eingesetzten Arbeitsmaschine beträgt das Fünffache des Reluktanzmotors. Damit ergibt sich die Hochlaufzeit von 630 ms.

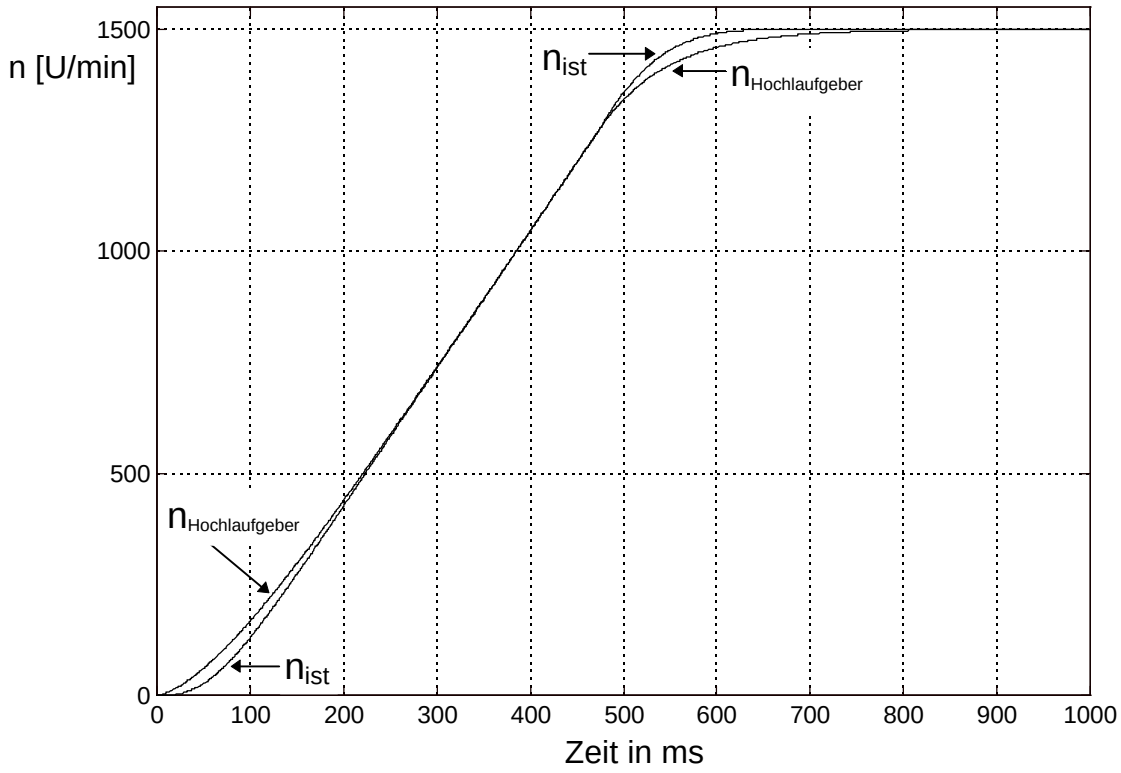

Bild 3: Hochlauf vom Stillstand auf Bemessungsdrehzahl
J_{gesamt}= 0,54 kgm^2 (Messung)

Universität Karlsruhe, Elektrotechnisches Institut, Kaiserstraße 12, D-76128 Karlsruhe
Elbtalwerk GmbH, Fritz-Schreiter-Straße 31, D-01259 Dresden

In Bild 4 ist das Störverhalten der implementierten Drehzahlregelung durch Meßergebnisse belegt. Bei einem Lastsprung von 10 Nm auf 110 Nm bleibt die Drehzahl innerhalb eines Toleranzbandes von 3%. Nach 250 ms erreicht die Drehzahl wieder ihren stationären Wert von 1000 U/min. Die Steilheit des Lastmomentenanstieges wurde durch die angekuppelte Gleichstrommaschine vorgegeben.

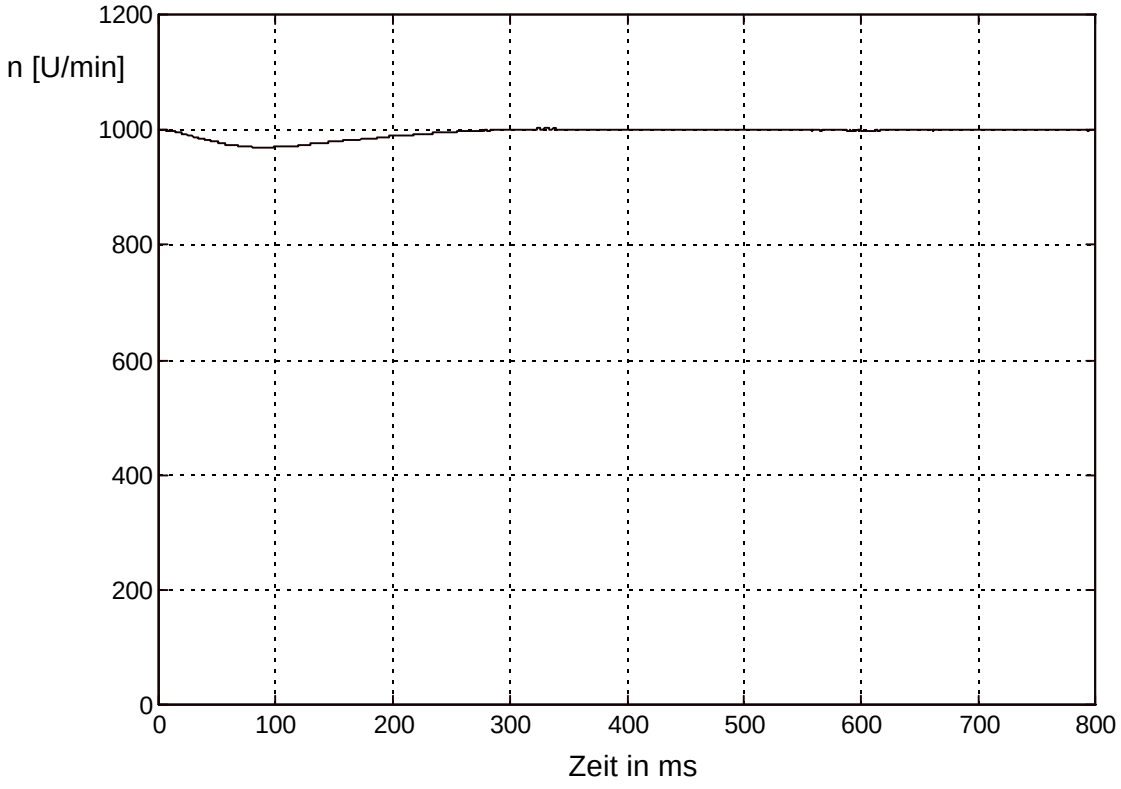

Bild 4: Drehzahlverlauf nach einem Drehmomentanstieg von 100 Nm
J_{gesamt}= 0,54 kgm^2 (Messung)

Universität Karlsruhe, Elektrotechnisches Institut, Kaiserstraße 12, D-76128 Karlsruhe
Elbtalwerk GmbH, Fritz-Schreiter-Straße 31, D-01259 Dresden

Einsatz für Positionieraufgaben

Zu den Antriebsaufgaben von Elektromotoren gehören ebenfalls die Positionierung z.B. von Werkstücken, Werkzeugen, Maschinenteilen, Förderkörben und vieles mehr. Der Geschaltete Reluktanzantrieb ist grundsätzlich auch für solche Applikationen geeignet. Das Bild 5 zeigt das Einschwingverhalten nach einem Lagesprung von 180°. Der Läufer dreht eine halbe Umdrehung weiter und erreicht nach ca. 600 ms den geforderten Sollwert. Bei vielen Positionieraufgaben, insbesondere in Werkzeugmaschinen, ist ein Überschwingen der Endposition unzulässig. Entsprechend dieser Forderung wurden die Parameter der Lageregelung gewählt.

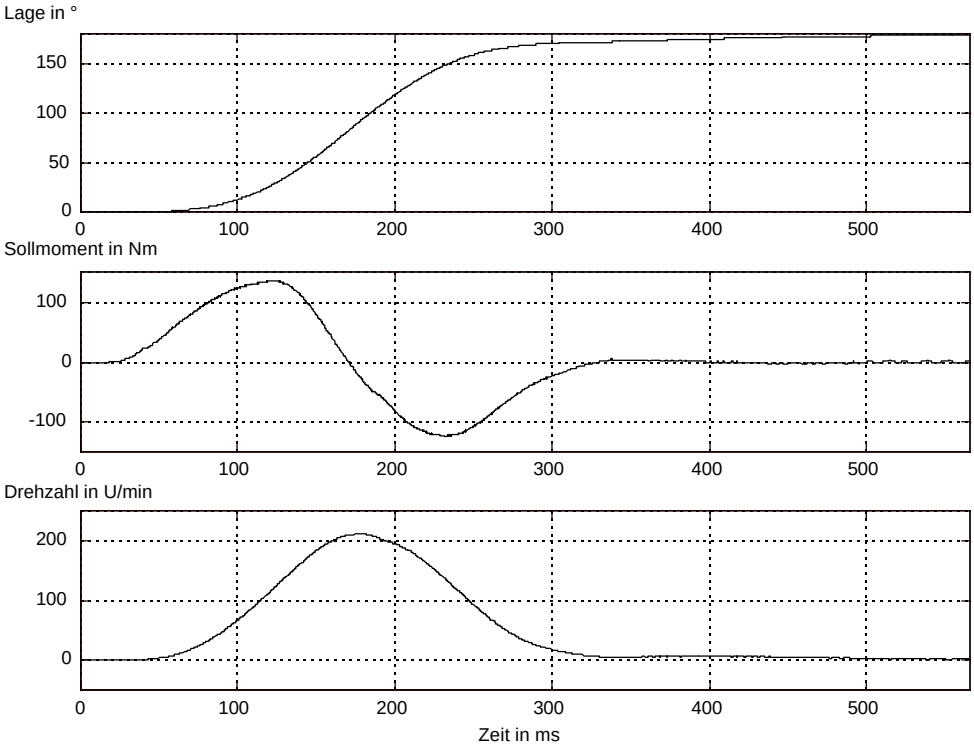

Bild 5: Positionsänderung um 180°
J_{gesamt}= 0,54 kgm^2 (Messung)

Universität Karlsruhe, Elektrotechnisches Institut, Kaiserstraße 12, D-76128 Karlsruhe
Elbtalwerk GmbH, Fritz-Schreiter-Straße 31, D-01259 Dresden

Ausgezeichnete Notlaufeigenschaften

Der Geschaltete Reluktanzantrieb zeigt eine hohe Betriebssicherheit bei Ausfall einer oder mehrerer Motorphasen. Nach Auftreten eines derartigen Fehlers läuft der Motor auch unter Last weiter, er kann beschleunigt und abgebremst werden (Bild 6). Allerdings treten meßbare Drehmoment- und Drehzahlschwankungen auf, der Anlauf des Motors ist nicht mehr gesichert. Trotzdem lassen sich somit in vielen Anwendungsfällen die Arbeitsmaschine oder der Arbeitsprozeß in einen gefahrlosen Zustand bringen.

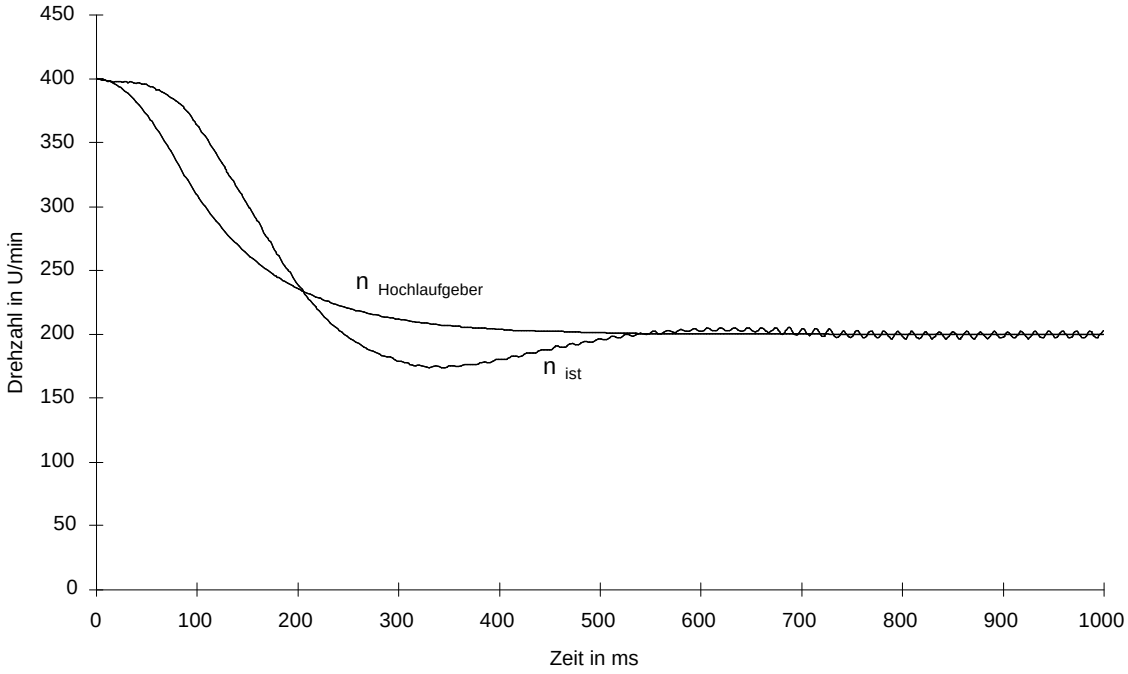

Bild 6: Drehzahländerung mit zwei defekten Motorphasen
M_{Last}= 50 Nm, J_{gesamt}= 0,54 kgm^2 (Messung)

Der Hochlaufgeber verhindert auch hier beim Bremsen der Maschine das direkte Aufschalten des Drehzahl-Sollwertsprunges auf den Soll-Istwert-Vergleich des Drehzahlreglers.

Universität Karlsruhe, Elektrotechnisches Institut, Kaiserstraße 12, D-76128 Karlsruhe
Elbtalwerk GmbH, Fritz-Schreiter-Straße 31, D-01259 Dresden

Netzfreundlichkeit des Musterantriebes

Der Netzstromrichter besteht aus einem dreiphasigen Transistor-Stromrichter. Die Regelung der Netzströme ist so optimiert, daß der Antrieb im stationären Betrieb mit einem cosφ=1 und einem Leistungsfaktor von ca. eins Energie aus dem Drehstromnetz bezieht oder einspeist. Das bedeutet einen sinusförmigen Netzstrom und die Übereinstimmung der Phasenlage zwischen Strom und Spannung - letztendlich die Netzfreundlichkeit des Antriebes. Bild 7 zeigt Spannung und Strom eines Außenleiters bei einem Lastwechsel des Reluktanzmotors von ca. 18 kW Generatorbetrieb auf 18 kW Motorbetrieb. Mit dem Einsatz dieser Netzstromrichter lassen sich der Vier-Quadranten-Betrieb und damit hochdynamische Antriebslösungen realisieren. Wird ein solcher Stromrichter z.B. für den Hauptantrieb einer Anlage eingesetzt, so kann mit ihm zusätzlich noch Blindleistung der Hilfsantriebe kompensiert werden. Für Reluktanzantriebe mit geringeren Anforderungen an Dynamik und Netzfreundlichkeit werden Diodenbrücken mit Glättungs- und Kommutierungsdrossel als Netzstromrichter eingesetzt.

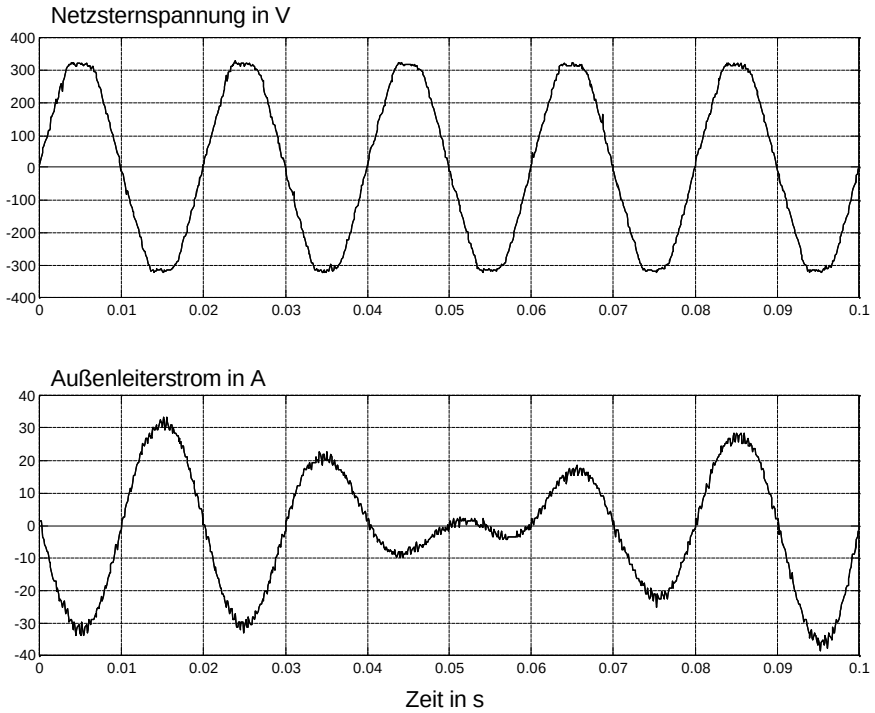

Bild 7: Netzspannung und Netzstrom bei einer Laständerung von 18 kW Generatorbetrieb auf 18 kW Motorbetrieb (Messung)

Universität Karlsruhe, Elektrotechnisches Institut, Kaiserstraße 12, D-76128 Karlsruhe
Elbtalwerk GmbH, Fritz-Schreiter-Straße 31, D-01259 Dresden

Quellenangabe:

[1] Datenblatt Drehstrom-Hauptantriebsmotoren, Elbtalwerk GmbH

Autor: J. Wolff
Universität Karlsruhe
Elektrotechnisches Institut
Kaiserstraße 12
D-76128 Karlsruhe
Bundesrepublik Deutschland

Das Elektrotechnische Institut der Universität Karlsruhe dankt der Deutschen Forschungsgemeinschaft für die Förderung des Projektes „Switched Reluctance Drive“.

Hersteller: Elbtalwerk GmbH
Fritz-Schreiter-Straße 31
D-01259 Dresden
Bundesrepublik Deutschland

Switched Reluctance Motors

George W Buckley
Emerson Electric Co.

St. Louis, Missouri

Introduction

Motor design engineers have long been searching for a solution to their drive application problems which is low cost, reliable, versatile in application, fault tolerant and quiet. The motor design which was most likely to achieve that coveted position for several years was the switched reluctance motor (SRM). However, designers found difficulty in making this type of motor quiet enough for some applications, particularly those in residential environments. Breakthroughs in noise control at Emerson and its subsidiary companies over the last two years have made that no longer an issue. Thus the SRM is now poised to win a new and powerful place in motor drive applications.

This emergence of SR technology holds all the promise of making a major impact on drive-power markets into the next century, particularly in those applications where control is a feature of the product or where high speed capability is important.

Energy Conversion in Electrical Machines

Electric motors convert energy using only one of two forms, excitation torque or reluctance torque. Most common motor forms such as either induction or synchronous motors rely on excitation torque to produce useful work. Excitation requires two windings to be present in the motor, one on the rotor and one on the stator and both must be simultaneously excited to produce torque. One winding can have induced excitation, as in the case of the induction motor or be replaced by a permanent magnet as is the case with BPM motors. The torque production mechanism in an SRM is identical to the alignment torque seen between two displaced oppositely polarized magnets.

An useful way of describing the energy conversion process in an electrical machine is via the Poynting Vector, which is:-

$$P=ExH$$

where P is the power transferred across the airgap, E is the longitudinal electric field strength and H the radial magnetic field strength. P is the vector product of E and H.

Energy transfer is thus only affected by two variables, the electrical and magnetic loadings of the machine. Because of their construction, SR motors can pack a greater stator coil density, and therefore electric loading, into the motor than can conventional induction motors, say. The electric loading is measured in Ampere-Conductors per unit periphery. Similarly, the salient pole structure of the SR motor restricts the magnetic loading in the motor. Magnetic loading is measured in magnetic flux per unit periphery. In a typical SR machine, the magnetic loading id 80% that of the induction motor while the electric loading is about 200%.

Translating this into practical terms, this implies that an SR motor can theoretically deliver about 80% x 200%, or 160% of the output of a conventional motor such as an induction motor. This has huge implications in applications where space is critical and it lowers the cost of SR motors in almost all cases a over induction motors. Similar observations can be made about brushless permanent magnet motors (BPM), though this is obviously affected by the magnet grade selected. In applications where ferrite magnets are used, which is the case for most domestic applications, the SRM will be smaller than a BPM motor of comparable power output.

Constructional Features of the Switched Reluctance Motor

As outlined above, a switched reluctance motor differs from a standard motor because forces generated by reluctance action (as against excitation action) can be many times greater than those on the current carrying conductors used in excitation torque production. The switched

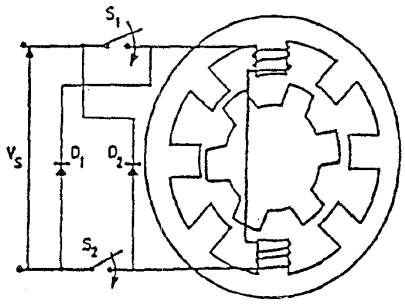

Figure 1 Basic SR Motor

reluctance drive makes these forces continuous by sequentially switching the currents on and off in pairs of opposite poles, causing the poles on the rotor to rotates continuously. Commutation is signaled by a rotor position sensor or, in some cases, by a sensorless commutation algorithm used to determine when the stator poles require energizing. The speed of the rotor is determined by the sequential switching speed of the stator poles. The output torque is determined by the magnitude and shape current passing through the stator windings. See Figure 2.

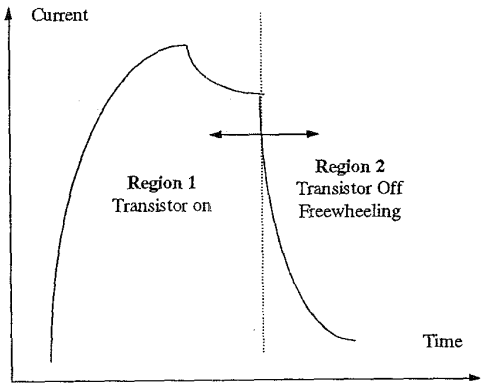

Figure 2 Current Shape in Non-regulated Mode

Controlling this commutation process requires semi-conductor switches, which means that electronic control is inherent in an SR motor rather than auxiliary to it.

The ability to control the magnitude of the current (via PWM chopping), plus control of the angular position at which currents are turned on and off, allows us to effectively program the torque profile of the motor. We can thus arrange for the motor to "mimic" any other motor type, whether dc series, vector induction, V/Hz induction etc. Some typically programed curves are shown in Figure 3 below.

Switched reluctance motors have a rotor which has

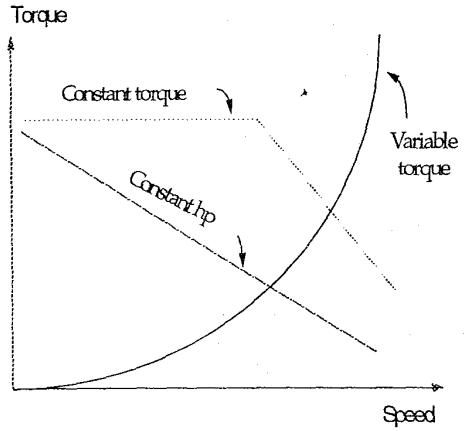

Figure 3 Typical programmable torque-speed curves for SR Motors

no magnets or windings of any kind, and it is effectively a piece of shaped laminated steel. The stator
is similar to but of more simple construction than a conventional induction motor.

The simple, rugged construction of the switched reluctance motor gives the product an extremely long life with reliable performance. As a complete system, switched reluctance motors are extremely versatile. Since the motor is singly excited, controlling the motor is very simple. By adopting different control laws for the drive, the motor can be made to have almost any torque-speed curve imaginable.

Manufacturing SR Motors

Stator Winding

The tests undertaken by Emerson have proven that no special manufacturing techniques are needed to manufacture SR motors. Stator coils can be either wound in place or inserted with conventional

winding equipment. Generally speaking, higher slot fills can be achieved with insert methods than gun winding. Emerson has achieved slot fills up to 85% on SR motors using insert winding. This makes better use of the magnetic material and makes for a more cost effective motor. It also allows existing equipment to be used.

Lamination Punching

Conventional presses and press beds are being used with a roughly seven stage lam progression. Progressive rotation is being used during stacking to eliminate the effects of crowning and hence loose

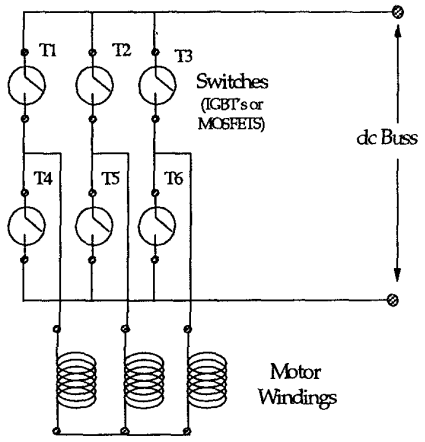

Figure 4 Conventional Inverter Bridge

stacks.

Assembly and Airgap Control

Because SR motors have no rotor windings no rotor equalizing currents can flow. Motor folklore suggest that tight airgap control is therefore vital to avoid unbalanced magnetic pull (UMP), excessive bearing loading and rotor pullover. In reality, this problem is by no means as large as the folklore would have us believe.

The energization times cover periods when the rotor and stator poles are not completely aligned, so the effective airgap for magnetization purposes is actually longer than the motor's "mechanical" airgap. Consequently, UMP is smaller than might be anticipated. Moreover, equalizing currents can still flow in the stator, so proper connection combinations in the winding can reduce UMP further.

Typical small induction fhp motors manufactured by Emerson have airgaps with variances in the band 0.004 to 0.008. Typically this does not exceed 25% of the nominal airgaps. In SR motors, we have found it possible to consistently achieve 0.005, so the issue of UMP is essentially a non-event.

Rotor Balancing

Assuming the winding(s) have electrical and magnetic symmetry, the principal cause of unbalance in electric motors is the non-uniform weight distribution introduced by the rotor windings. Bearings and couplings also contribute to unbalance and consequential vibration. Since SR motors have no windings, the main source of uneven weight distribution has been eliminated.

In practice the cost of balancing is usually very small and there is always a risk of introducing unbalance in the couplings and bearings so the economic value of eliminating balancing is quite small. However, tests show that on machines running up to about 10,000 rpm, the naturally even weight distribution in the rotor is good. Consequently, balancing is rarely needed.

Electronic Drive

As outlined above, the SR motor is simpler, with no rotor windings, less complex stator windings, and in many cases, no need for balancing. It is also intrinsically reliable both in the motor and in the electronic drive.

The switched reluctance motor circuit design permits the use of cheaper, smaller, and often fewer electronic switches and simpler fault protection. BPM motors are typically of three phase design and will normally use a six transistor inverter bridge arrangement. See Figure 4.

The sequence of switching on the bridge is with T1, T5 & T6 ON to feed the phase winding A. Sequentially, T2, T4 & T6 are turned ON to feed phase winding B. T3, T4 & T5 are turned ON to feed phase C. A fault (say a switch failing short) in any one of the switches can short circuit the dc buss. Practical circuits need to recognize this and add high speed sensing of inverter currents and

shut down of switches to prevent catastrophic failures.

In switched reluctance motor switching drives, the circuit is intrinsically much more reliable. See Figure 5. Even if a switch fails short, the result is non damaging. Fault currents from short circuits of switches are limited because the switches are in series with the phase windings not just across the dc buss as they are with induction motors or BPM.

Circuit boards are being manufactured by Emerson in mixed mode, part IMS and part conventional PCB, usually FR4. Signal and logic level on FR4, power stages on IMS. Most parts are in surface mount technologies.

This presentation explains how Emerson and its partners, who are in the process of developing numerous product solutions using this technology, will transform the rotating electrical machines industry with more efficient, more reliable and better cost turnkey solutions.

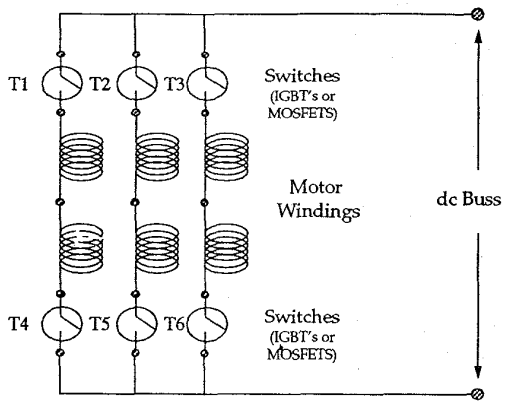

Figure 5 Switched Reluctance Drive

SENSORLESS SPEED CONTROL OF A SWITCHED RELUCTANCE MOTOR FOR INDUSTRIAL APPLICATIONS

J. Wolff R. Rahner H. Späth
Elektrotechnisches Institut, Universität Karlsruhe
Kaiserstraße 12, 76128 Karlsruhe, Germany
Email: wolfju@eti.etec.uni-karlsruhe.de

Abstract: *The Elektrotechnische Institut of the University Karlsruhe has developed, optimised and manufactured a Switched Reluctance Drive with power converters and control engineering according to the latest scientific findings. The motor has been constructed for the rated output power of 18,5kW at 1500r.p.m. for industrial applications. The common supply for the voltage-source converter is 3x400V/50Hz. For this application the authors have developed a method to estimate the rotor position and the speed without a rotor position encoder. This method calculates the position of the rotor by using the flux linkage and the phase currents of the motor.*

Keywords: *OPTIM,* Switched Reluctance Motor, Sensorless Speed Control, Estimation of Rotor Position

1. Introduction

The sensorless speed control and the estimation of the rotor position have already been treated in several publications. The authors of these publications preferrably used smaller motors or high-speed drives for their tests. (e.g. [Brö] 2Nm/1200r.p.m., [Lyo] 34Nm/25.000r.p.m.)
Differing from these publications, this paper will discuss the sensorless speed control of a motor with a relatively high rated torque of 118 Nm. Furthermore, the strength of this Switched Reluctance Motor must be seen in a speed range below 1000r.p.m. Within this range, its efficiency and its dynamic is very high [Wo1].
This paper treats the operation of a high torque SR-drive for low-speed applications without a rotor position encoder.
The results of this test do not provide a complete solution for the sensorless speed control but they can be seen as basic idea and as stimulation for following further tests. The selection of the method, its restrictions and possibilities will be discussed here.

2. Motor design

The Elektrotechnische Institut selected the Switched Reluctance Motor with 16 stator poles and 12 rotor teeth. It is a 4-phase-winding machine, the 4 stator poles that are shifted by 90° to each other form one phase-winding (Figure 1).

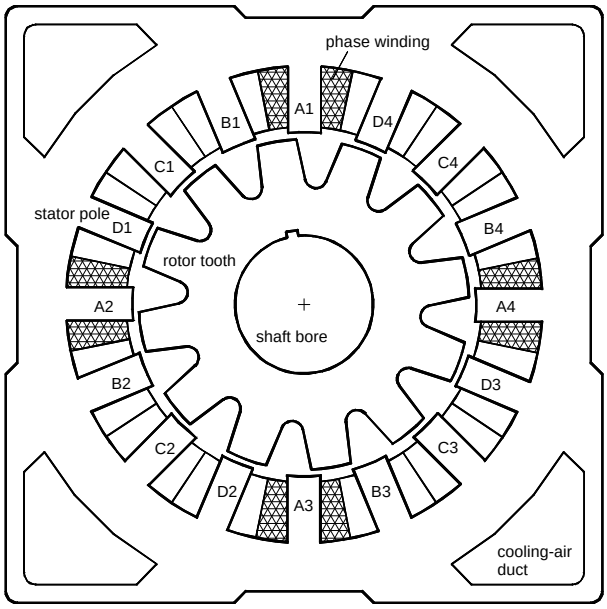

Figure 1: Schematic cross-section of the Switched Reluctance Motor

3. Voltage-source converter

The voltage-source converter consists of a mains and a motor converter. The common supply for the three-phase-self-commutated mains converter is 400V/50Hz. The d.c. link voltage U_d is constantly set to 750V. Figure 2 shows the circuit of the load-side converter.

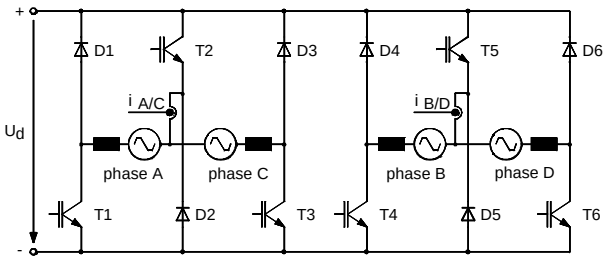

Figure 2: Circuit of the load-side converter

The phases A and C respectively B and D should not conduct current at the same time, since for example A generates a motor- and C a generator-torque. Both torques are subtracted from each other, a not desirable status. Therefore, the phases A and C respectively B and D can be supplied with one common transistor without further restrictions regarding the current control. The currents can be determined by one common measurement.

4. Flux-current method

The procedure for the sensorless estimation of rotor position and speed must be suitable for the test drive with 18,5kW, 118Nm and 1500r.p.m. It definitely has to use the non-linear model of the Switched Reluctance Motor. A very good overview of sensorless methods for determining the rotor position of switched reluctance motors is given in [Ray]. For the test drive, we selected the flux-current method.

Before being produced the 16/12 Switched Reluctance Motor was optimised and calculated with a finite element method (Figure 3).

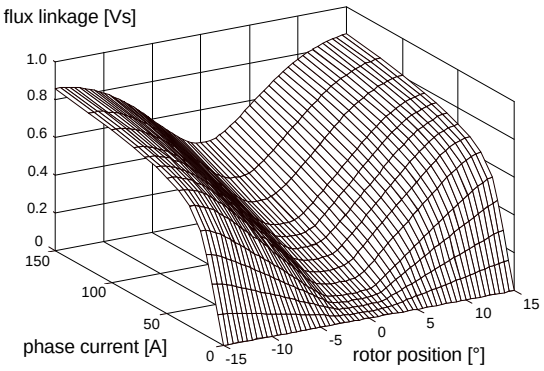

Figure 3: Characteristic of flux linkage depending on current and rotor angle (calculation)

Figure 3 shows the flux linkage for a rotor position between -15° and 15°. The value +/- 15° is the aligned position. Stator pole and rotor tooth are in line, 0° is the unaligned position. At this position, there is a gap between the teeth opposite to the stator pole. The motor has 12 rotor teeth and so this characteristic feature is repeated for the observed stator pole respectively for the observed phase 12 times per rotation. Furthermore, the reference field is symmetrical between 0° to 15° and 0° to -15°. One rotor rotation corresponds to 360°.
With the known phase current and flux linkage, the rotor position can be read out of this characteristic. This is the basic idea of the flux-current method.
The successful use of this method basically depends on the accuracy of the calculated characteristic. Since the flux linkage had not been measured for the test motor a comparison is not possible.
However, the torque depending on the rotor position and phase current was calculated for the torque control by means of this characteristic. The following equations were used:

$$W^* = \int_0^i y \; di \qquad \text{(eq. 1)}$$

$$m = \frac{d \; W^*}{d \; j} \qquad \text{(eq. 2)}$$

Figure 4 illustrates the very good correspondence between calculation and actual measurement results.

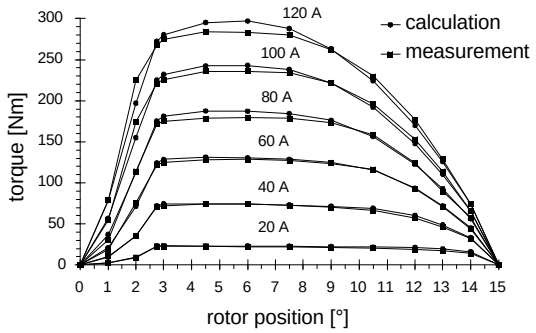

Figure 4: Torque depending on rotor position with phase current as parameter (comparison of measurement and calculation)

The various torque testings were performed using a locked rotor with the phase current as parameter. The rotor position was varied. Since the measured torque corresponded very well to the torque calculated by means of the flux linkage, we assumed that the characteristic of the calculated flux linkage would also correspond to the actual values and would therefore be suitable for the flux-current method.

In order to be able to read the rotor position out of the characteristic (figure 3), the flux-linkage needs to be defined.
The electrical part of the SRM can be described by the voltage equation of the machine:

$$u = R \cdot i + \frac{d \, y \, (i, j)}{d \, t} \qquad \text{(eq. 3)}$$

In this equation u means the phase voltage, R the coil resistance and ψ the flux linkage.

To calculate the mechanical rotor position, the current and the flux linkage must be given. It is not difficult to define the current since we can use the measurement of the normal motor-control. It is, however, much more complicated to define the present flux linkage in the machine. We calculate the flux by eq. 4, a special form of the voltage-equation.

$$y = \int (u - R \cdot i)\, dt \qquad \text{(eq. 4)}$$

This algorithm has been realised by a small analogue-circuitry, in discrete technology (Figure 5). Main component of this hardware application is the integrator which can be controlled and reset with the help of a finite state machine.

The gate switch impulses (T1 to T6) for the power transistors constitute the inputs for the circuit. These impulses are generated by the current controllers realised by means of analogue circuits.

The current controllers are two-step controllers, Further inputs are the current measurement values $i_{A/C}$ and $i_{B/D}$.

The three-phase-self-commutated mains converter sets the d.c. link voltage in steady operation to constant 750V. Even during a higher load change and transient reactions this voltage remains within a tolerance band of 730V to 770V [Wo2]. This allows to use the gate switch impulses of the transistors to determine the phase voltage u. Due to the circuit of the load-side converter the phase voltage can be -750V (i>0), 0V or +750V.

The phase voltage is determined by means of a logic using the levels of the gate switch impulses. If the d.c. link voltage is not stable, the actual measurement value would additionally have to be considered in this logic.

In the next step, the ohmic voltage drop above the phase resistance is deducted from the phase voltage. It is calculated by multiplying the measured current value with the phase resistance. The phase resistance is 110mΩ given a winding temperature of 20°C. With a continuous running duty in the rated point, it increases to approximately 155mΩ. The amplitude of the phase current is approximately 60A at the rated torque. Like this, the amplitude of the ohmic voltage drop is between 6V and 9,3V. Compared to the phase voltage, this value is very small and could therefore possibly be neglected. Since the calculation of the ohmic voltage drop could easily be realised, it was taken into consideration. The following integrator integrates this voltage difference up to the flux linkage. The value of the flux linkage and also the value of the phase current are transmitted via A/D converters to the digital signal processor for further processing.

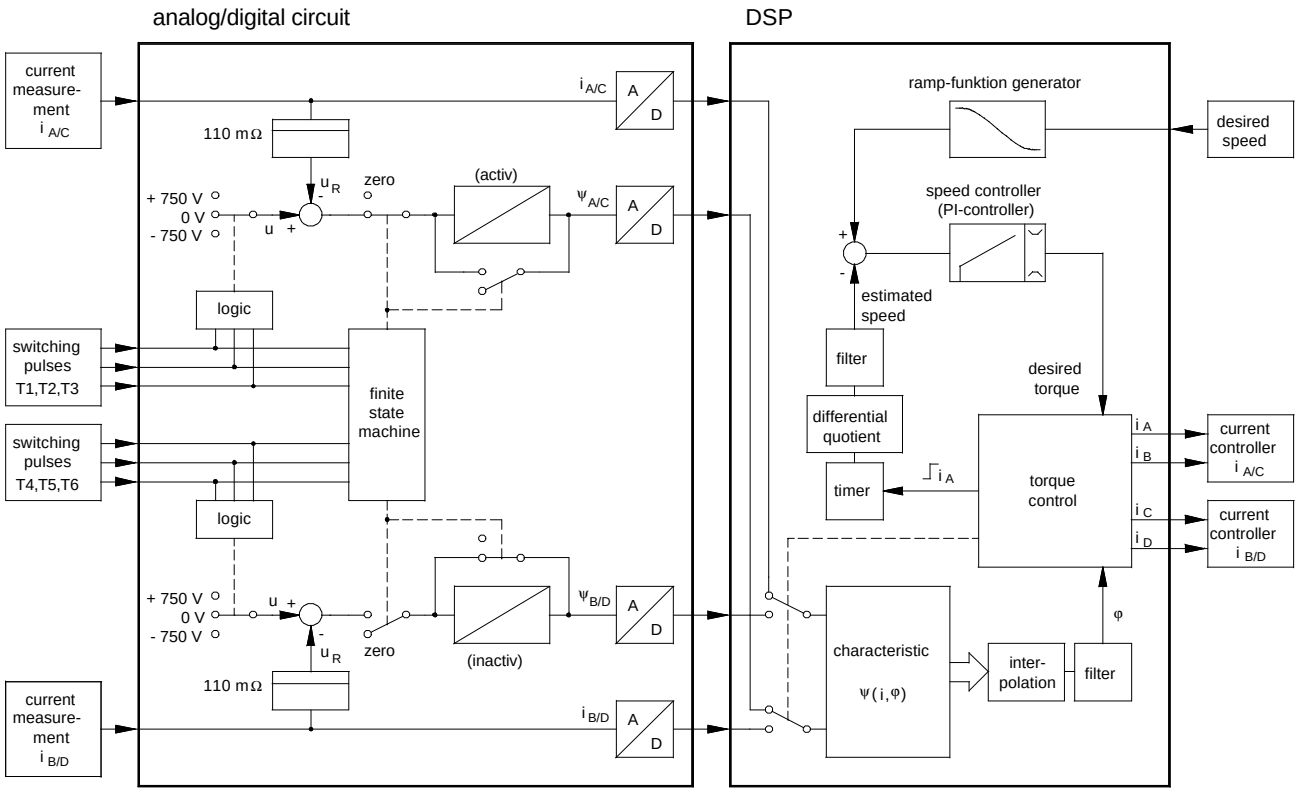

Figure 5: Realisation and implementation of the flux-current method

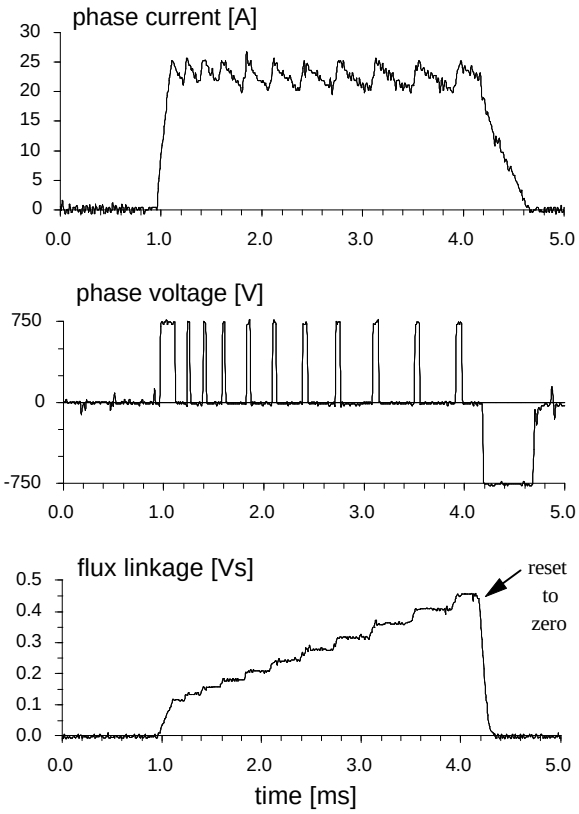

Figure 6: Phase current, phase voltage and flux-linkage at 30Nm and 400r.p.m. (measurement)

For calculating the flux linkage only two integrators are needed for four motor phases. Similar to only one current measurement needed for 2 phases, the flux linkage of 2 phases can be calculated with one integrator. The integrator interval for one phase begins with the rising edge of the phase current and ends with the current rising edge of the next phase. During one integration interval the rotor turns by 7,5°. A finite state machine determines the beginning and the end of the integration intervals from the switch impulses. At the end of an interval the output of the integrators is set back to zero by an electronic switch. It remains zero until a new integration interval begins.

A part of the characteristic according to figure 3 for the rotor position from 0° to 15° was saved to the memory of the DSP (Digital Signal Processor). Due to the symmetry already described this is sufficient for defining the angle. We used TMS320C40 from Texas Instruments as DSP. The sampling time is 120 µs. In the beginning of each detection cycle the analogue current controllers receive the new aim values. Afterwards the actual measurement values of the phase currents and the values of the flux-linkage are read in. For the value of the flux linkage and the respective measurement value of the current, the required pairs of interpolation points are read out of the characteristic in the DSP memory. This is used to define the rotor angle by means of an interpolation.

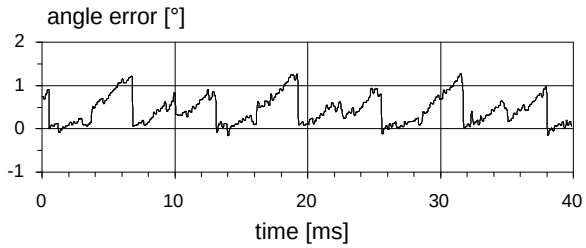

Figure 7: Difference between estimated and original rotorposition at 30Nm and 400r.p.m. (measurement)

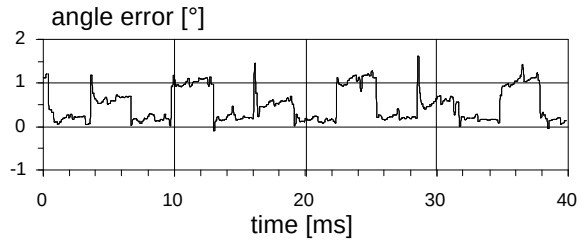

Figure 8: Difference between estimated and original rotorposition at 120Nm and 400r.p.m. (measurement)

As an example, figures 7 and 8 illustrate the error of the angle estimation for two operation points of the switched reluctance motor. The error is the difference between the estimated rotor position and the values measured by a rotor position encoder. It ranges between 0,5° and 1,5° (mechanical angle). The evident jumps allow to allocate the error values to the single integration intervals. An integration interval corresponds to a rotor rotation of approximately 7,5°. At a speed of 400r.p.m. the rotor rotates by 7,5° in 3,12ms.

5. Iron loss

With higher speeds the angle error increased noticeably towards the end of the 7,5° interval. The estimated angle is smaller than the actual rotor position. According to the model shown in figure 9 the measured phase current is devided into two currents.

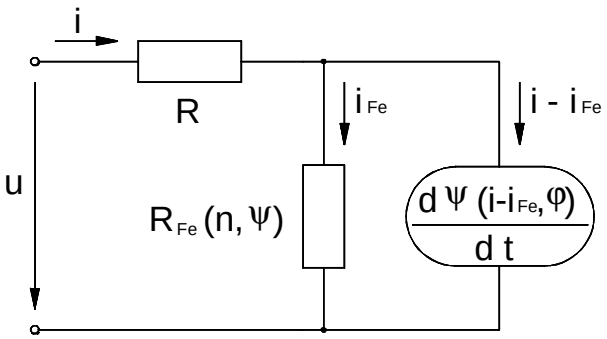

Figure 9: Substitutional block diagram of a phase under consideration of iron losses

The first partial current i_{Fe} covers the iron losses of the switched reluctance machine. It flows via the resistance R_{Fe}. Only the second partial current $i-i_{Fe}$

influences the flux linkage value as magnetising current. According to the characteristic in figure 3 the flux linkage is only known with dependency on the magnetising current and the rotor angle. Therefore, the measured phase current must be reduced by i_{Fe} for reading the rotor position out of the reference field. For the test drive, i_{Fe} was calculated using equation 5:

$$i_{Fe} = const. \cdot n \cdot y^{2} \cdot i \qquad \text{(eq. 5)}$$

This estimation allowed to expand the sensorless speed control to a speed of 1.200r.p.m. The constant was determined in an experimental way.
In figures 7 and 8 the correction according to equation 5 was already taken into consideration.

6. Angle filter

Despite the good results for the estimation of the rotor position, single values can vary strongly from the actual position. There are ranges within the characteristic of the flux-linkage where smaller changes of the current or flux cause a bigger change of the rotor position. Within these ranges, already smaller measurement inaccuracies cause a relatively big error in the estimation of the rotor position. Experiments have shown that the estimation within an angle ranging from -3° to -7° respectively from 3° to 7° operates very reliably. For the remaining range the estimated angle should undergo a plausibility check. Due to the inertia moment of the motor, the speed remains almost constant during a sampling time of 120µs. If the angle of the actual sampling instant which is estimated from the flux linkage deviates from the previous detection step in inadmissable size, the new angle is calculated by the previous angle and product of speed and sampling time.
Within the torque control the estimated angle is required for defining the switch-on / switch-off times for the phase currents. Torque and speed control of the Switched Reluctance Drives are described in [Wo1]. They have also been implemented on the DSP.

7. Speed estimation

It is necessary to determine the actual speed value for the speed control. This is done by means of the timewise change of the estimated angle. A timer in the DSP determines the time period needed for at rotor revolution of 30°. Within the angle interval of 30° (π/6) each of the 4 phases is activated once. Beginning and ending of a phase are defined by the beginning current increase in phase A. The moving average value above three of such angle intervals is the actual speed for the comparison of actual and aim values of the speed controller (eq. 6).

$$n = \frac{1}{2p} \cdot \frac{1}{3} \sum_{k=1}^{3} \frac{p/6}{\Delta t(k-3)} \qquad \text{(eq. 6)}$$

The differential quotient of angle change

$$n = \frac{1}{2p} \frac{\Delta j}{T_A} \qquad \text{(eq. 7)}$$

and detection period did - even with afterwards filtering not provide a useable result. For this difference quotient the fluctuations of the angle estimation are to strong.

8. Dynamic running

In addition to the stationary running a dynamic running must also be possible. After a load change the speed control should quickly reset the actual speed to the aim value. Furthermore the actual speed should quickly follow after a change of the aim value. Within stationary running aim and actual value must correspond to each other.
Figure 10 shows a load jump from 20Nm to 120Nm at 500r.p.m., produced by a DC-motor, which is coupled to the Switched Reluctance Motor. The dynamic of the sensorless speed control is, in this case, relatively good. After approximately 400ms the actual speed reaches the aim value again. The use of single speed measurement with a rotor position encoder did not provide better results [Spä].

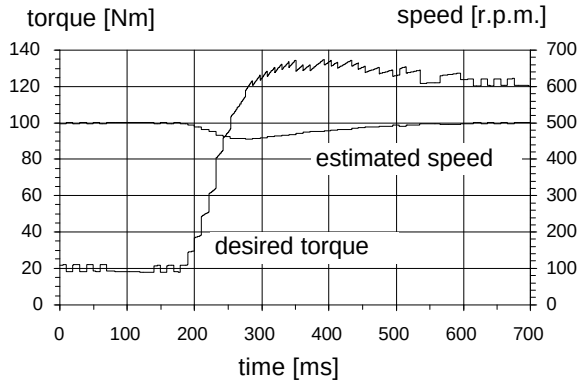

Figure 10: Load jump from 20Nm to 120Nm at 500r.p.m. sensorless, J_{all} = 0,54kgm^2 (measurment)

Figure 11 shows the speed course after a jump of the aim value form 400r.p.m. to 1000r.p.m. The sensorless speed control needs a relatively long period for these interim processes.
A ramp function generator restricts the aim value jumps to an admissible ramp before aim and actual values are compared. When the slope of this ramp increases noticeably the motor will pull out of synchronism.

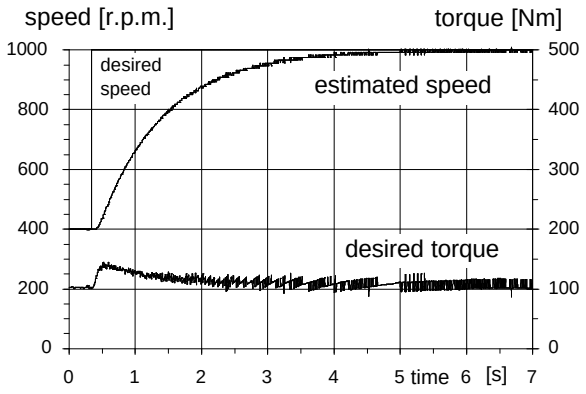

Figure 11: Speed jump from 400r.p.m. to 1000r.p.m. at a load of about 100Nm sensorless, J_{all} = 0,54kgm^2 (measurment)

In stationary running the correspondence of aim and actual values is widely safeguarded (figures 10, 11).
The reason for the unsteady running of the estimated speed and also of the desired torque must be seen in the speed calculation. Only after a rotation of 30° a new speed value is calculated. During these angle intervals, the value of the estimated speed remains constant.

9. Conclusion

The flux-current method allowed to realise the sensorless speed control within a speed range of 200r.p.m. to 1200r.p.m. up to 150Nm for the test drive. The sensorless control allows load jumps and variable speeds.
Given the characteristic of the flux linkage, this procedure can easily be realised.
The operation below 200r.p.m would either call for an improved voltage integration or for a different method. A speed higher than 1200r.p.m. requires a more accurate estimation of the iron loss.
The filtering of the estimated values has to be seen as a basic problem.

10. Acknowledgements

Optimisation and calculation of the Switched Reluctance Motor were made by Mr E. Vonhof at Power Electronics Dublin using a Finite Elemente Program. We thank the Deutsche Forschungs-gemeinschaft for its financial support of this research project.

Symbols

i	phase current
i_{Fe}	current for the iron losses
i_A	current of the phase A (A/B/C/D phase quantities)
J	moment of inertia
m	phase torque
n	motor speed
R	winding resistance
R_{Fe}	resistance for the iron losses
t	time
T_A	sampling time
u	phase voltage
U_d	d.c. link voltage
W*	coenergy
φ	rotor position (mechanical angle)
ψ	flux linkage

converter features

typ	IGBT double-way converter (laboratory converter)
supply connection	3x400V, 50Hz
max. mains load	40kW
mains power factor	≅ 1
d.c. link voltage	750V

motor features

typ	MFR 132.5
manufacturer	Elbtalwerk Heidenau GmbH
rated output	18,5kW
rated torque	118Nm
rated speed	1500r.p.m.
duty type	continuous running (S1)
thermal class	F
shaft heigh	132mm
moment of inertia	0,0883kgm^2

11. References

[Brö] Brösse, A.; Henneberger, G.: Sensorless Control of a Switched Reluctance Motor Using a Kalman Filter. Proceedings of the 7th European Conference on Power Electronics and Applications, Vol. 4, p. 561-566, Trondheim 1997

[Lyo] Lyons, J.P.; MacMinn, S.R.; Preston, M.A.: Flux/Current Methods For SRM Rotor Position Estimation. IEEE IAS Conf., p. 482-487, 1991

[Wo1] Wolff, J.; Späth, H.: Switched Reluctance Motor with 16 stator poles and 12 rotor teeth. Proceedings of the 7th European Conference on Power Electronics and Applications, Vol. 3, p. 558-563, Trondheim 1997

[Ray] Ray, W.F.; Al-Bahadly, I.H.: Sensorless Methods for Determining the Rotor Position of Switched Reluctance Motors. Proceedings of the EPE, p. 7-12, Brighton 1993

[Ste] Steiert, U.: Drehmomentsteuerung einer Reluktanzmaschine mit beidseitig ausgeprägten Polen und geringer Drehmomentwelligkeit. Dissertation Universität Karlsruhe, 1992

[Wo2] Wolff, J.; Bauer, G.; Simon, O.: Netzfreundlicher Anschluß elektrischer Antriebe an das Drehstromnetz durch verbesserte Regelung. atp (1997) No. 11, p. 44-51

[Spä] Späth, H.; Wolff, J.: Der elektrische Antrieb der Zukunft? TECHNIKA (1996) No. 19, p. 49-53

Switched Reluctance Motor Control – Basic Operation and Example Using the TMS320F240

Michael T. DiRenzo *Digital Signal Processing Solutions*

ABSTRACT

This report describes the basic operation of switched reluctance motors (SRMs) and demonstrates how a TMS320F240 DSP-based SRM drive from Texas Instruments (TI™) can be used to achieve a wide variety of control objectives.

The first part of the report offers a detailed review of the operation and characteristics of SRMs. The advantages and disadvantages of this type of motor are cited.

The second part of the report provides an example application of a four-quadrant, variable speed SRM drive system using a shaft position sensor. The example has complete hardware and software details for developing an SRM drive system using the TMS320F240. The SRM operation is described, along with the theoretical basis for designing the various control algorithms. The example can be used as a baseline design which can be easily modified to accommodate a specific application.

This report contains material previously released in the Texas Instruments application report *Developing an SRM Drive System Using the TMS320F240 (*literature number SPRA420*)*, and has been updated for inclusion in the Application Design Kit (ADK) for switched reluctance motors.

Contents

1 Introduction 2
2 Motor Characteristics 3
2.1 Torque-Speed Characteristics 4
2.2 Electromagnetic Equations 5
2.3 General Torque Equation 6
2.4 Simplified Torque Equation 8
3 Control 9
4 Example – SRM Drive with Position Feedback 12
4.1 Hardware Description 12
4.1.1 SRM Characteristics 12
4.1.2 Control Hardware 12
4.1.3 Position Sensor 12
4.1.4 Power Electronics Hardware 14
4.2 Software Description 16
4.2.1 Program Structure 17
4.2.2 Initialization Routines 20

4.2.3 Current Controller 21
4.2.4 Position Estimation 23
4.2.5 Velocity Estimation 24
4.2.6 Commutation 27
4.2.7 Velocity Controller 29
5 References 32
Appendix A Software Listings for a TMS320F240-Based SRM Drive With Position Sensor . . . 34

List of Figures

Figure 1. Various SRM Geometries 4
Figure 2. SRM Torque-Speed Characteristics 5
Figure 3. Graphical Interpretation of Magnetic Field Energy 7
Figure 4. Graphical Interpretation of Magnetic Field Co-Energy 7
Figure 5. Basic Operation of a Current-Controlled SRM – Motoring at Low Speed 9
Figure 6. Commutation of a 3-Phase SRM 10
Figure 7. Single-Pulse Mode – Motoring, High Speed 11
Figure 8. SRM Shaft Position Sensor 13
Figure 9. Opto-Coupler Output Signals vs. Rotor Angle 13
Figure 10. Opto-Coupler Connections to the TMS320F240 EVM 14
Figure 11. Two-Switch Per Phase Inverter 15
Figure 12. Schematic Diagram of SRM Inverter Using the IR2110 and Connections to the EVM 16
Figure 13. Block Diagram of the SRM Controller 17
Figure 14. TMS320F240 SRM Control Program Structure 17
Figure 15. Processor Timeline Showing Typical Loading and Execution of SRM Control Algorithms 18
Figure 16. Initialization Flowchart 20
Figure 17. Approximate SRM Current Loop Model 21
Figure 18. Frequency Response Plots for the SRM Current Loop at the Unaligned Position (Squares) and at the Aligned Position (Circles) 22
Figure 19. State Transition Diagram for the SRM Position Pickoff 23
Figure 20. Simplified Block Diagram of SRM Velocity Loop Using PI Control 30
Figure 21. Open-Loop Frequency Response of the SRM Velocity Loop at Several Motor Speeds, for a = 0.73 rad/s 31

List of Tables

Table 1. SRM Parameters 12
Table 2. Benchmark Data for the Various SRM Drive Software Modules 19

1 Introduction

Electric machines can be broadly classified into two categories on the basis of how they produce torque – electromagnetically or by variable reluctance.

In the first category, motion is produced by the interaction of two magnetic fields, one generated by the stator and the other by the rotor. Two magnetic fields, mutually coupled, produce an electromagnetic torque tending to bring the fields into alignment. The same phenomenon causes opposite poles of bar magnets to attract and like poles to repel. The vast majority of motors in commercial use today operate on this principle. These motors, which include DC and induction motors, are differentiated based on their geometries and how the magnetic fields are generated. Some of the familiar ways of generating these fields are through energized windings, with permanent magnets, and through induced electrical currents.

In the second category, motion is produced as a result of the variable reluctance in the air gap between the rotor and the stator. When a stator winding is energized, producing a single magnetic field, reluctance torque is produced by the tendency of the rotor to move to its minimum reluctance position. This phenomenon is analogous to the force that attracts iron or steel to permanent magnets. In those cases, reluctance is minimized when the magnet and metal come into physical contact. *As far as motors that operate on this principle, the switched reluctance motor (SRM) falls into this class of machines.*

In construction, the SRM is the simplest of all electrical machines. Only the stator has windings. The rotor contains no conductors or permanent magnets. It consists simply of steel laminations stacked onto a shaft. It is because of this simple mechanical construction that SRMs carry the promise of low cost, which in turn has motivated a large amount of research on SRMs in the last decade. *The mechanical simplicity of the device, however, comes with some limitations. Like the brushless DC motor, SRMs can not run directly from a DC bus or an AC line, but must always be electronically commutated. Also, the saliency of the stator and rotor, necessary for the machine to produce reluctance torque, causes strong non-linear magnetic characteristics, complicating the analysis and control of the SRM. Not surprisingly, industry acceptance of SRMs has been slow. This is due to a combination of perceived difficulties with the SRM, the lack of commercially available electronics with which to operate them, and the entrenchment of traditional AC and DC machines in the marketplace.* SRMs *do, however,* offer some advantages along with potential low cost. For example, they can be very reliable machines since each phase of the SRM is largely independent physically, magnetically, and electrically from the other motor phases. Also, because of the lack of conductors or magnets on the rotor, very high speeds can be achieved, relative to comparable motors.

Disadvantages often cited for the SRM; that they are difficult to control, that they require a shaft position sensor to operate, they tend to be noisy, and they have more torque ripple than other types of motors; have generally been overcome through a better understanding of SRM mechanical design and the development of algorithms that can compensate for these problems.

2 Motor Characteristics

The basic operating principle of the SRM is quite simple; as current is passed through one of the stator windings, torque is generated by the tendency of the rotor to align with the excited stator pole. The direction of torque generated is a function of the rotor position with respect to the energized phase, and is independent of the direction of current flow through the phase winding. Continuous torque can be produced by intelligently synchronizing each phase's excitation with the rotor position.

By varying the number of phases, the number of stator poles, and the number of rotor poles, many different SRM geometries can be realized. A few examples are shown in Figure 1.

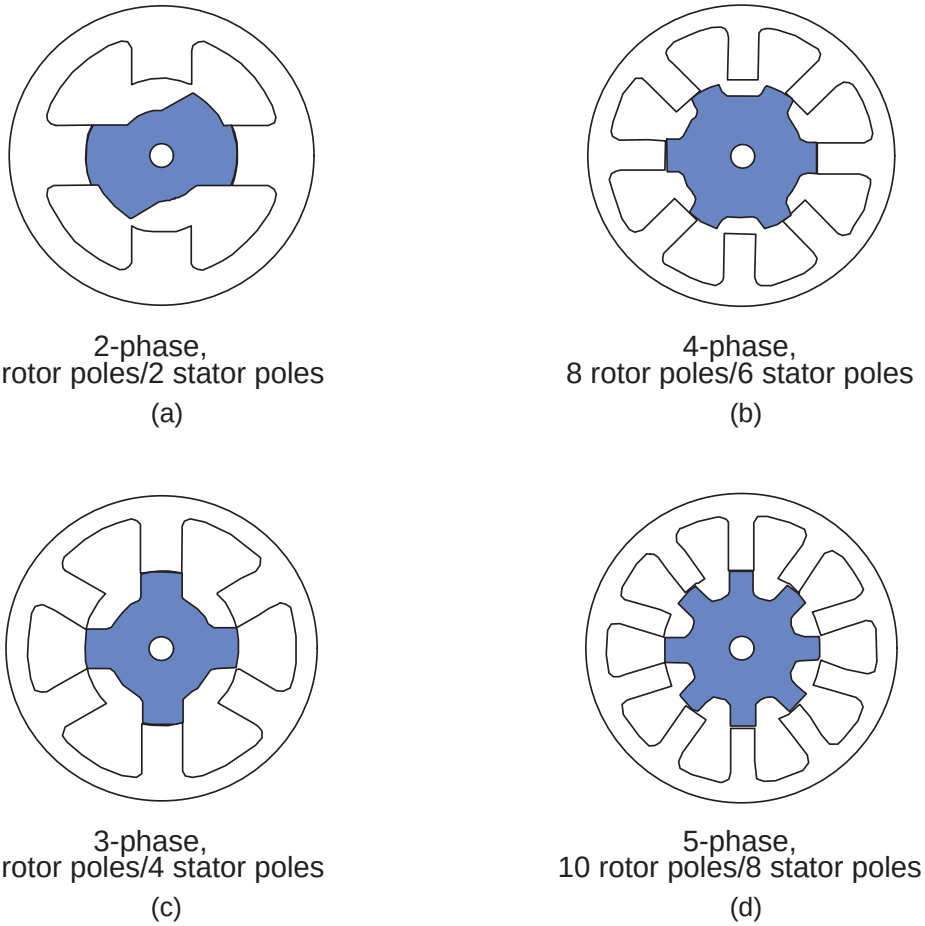

Figure 1. Various SRM Geometries

Note that although true of these examples, the number of phases is not necessarily equal to half the number of rotor poles.

Generally, increasing the number of SRM phases reduces the torque ripple, but at the expense of requiring more electronics with which to operate the SRM. At least two phases are required to guarantee starting, and at least three phases are required to insure the starting direction. The number of rotor poles and stator poles must also differ to insure starting.

2.1 Torque-Speed Characteristics

The torque-speed operating point of an SRM is essentially programmable, and determined almost entirely by the control. This is one of the features that makes the SRM an attractive solution. The envelope of operating possibilities, of course, is limited by physical constraints such as the supply voltage and the allowable temperature rise of the motor under increasing load. In general, this envelope is described by Figure 2.

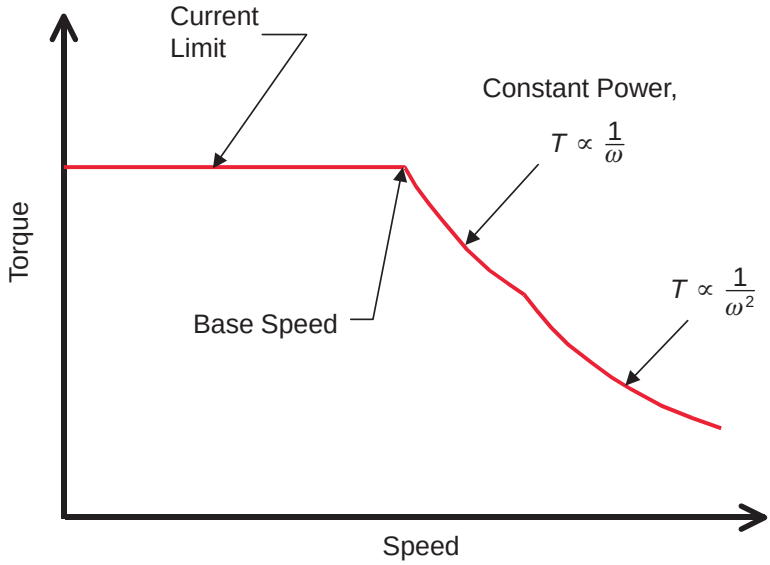

Figure 2. SRM Torque-Speed Characteristics

Like other motors, torque is limited by maximum allowed current, and speed by the available bus voltage. With increasing shaft speed, a current limit region persists until the rotor reaches a speed where the back-EMF of the motor is such that, given the DC bus voltage limitation we can get no more current in the winding—thus no more torque from the motor. At this point, called the base speed, and beyond, the shaft output power remains constant, and at it's maximum. At still higher speeds, the back-EMF increases and the shaft output power begins to drop. This region is characterized by the product of torque and the square of speed remaining constant.

2.2 Electromagnetic Equations

Although SR motor operation appears simple, an accurate analysis of the motor's behavior requires a formal, and relatively complex, mathematical approach. The instantaneous voltage across the terminals of a single phase of an SR motor winding is related to the flux linked in the winding by Faraday's law,

$$v = iR_m + \frac{d\phi}{dt} \tag{1}$$

where, v is the terminal voltage, i is the phase current, R_m is the motor resistance, and ϕ is the flux linked by the winding. Because of the double salient construction of the SR motor (both the rotor and the stator have salient poles) and because of magnetic saturation effects, in general, the flux linked in an SRM phase varies as a function of rotor position, θ, and the motor current. Thus, Equation (1) can be expanded as

$$v = iR_m + \frac{\partial\phi}{\partial i}\frac{di}{dt} + \frac{\partial\phi}{\partial\theta}\frac{d\theta}{dt} \tag{2}$$

where, $\frac{\partial\phi}{\partial i}$ is defined as $L(\theta, i)$, the instantaneous inductance, $\frac{\partial\phi}{\partial\theta}$ is $K_b(\theta, i)$, the instantaneous back EMF.

2.3 General Torque Equation

Equation (2) governs the transfer of electrical energy to the SRM's magnetic field. In this section, the equations which describe the conversion of the field's energy into mechanical energy are developed. Multiplying each side of Equation (1) by the electrical current, *i*, gives an expression for the instantaneous power in an SRM,

$$vi = i^2 R_m + i\,\frac{d\phi}{dt} \tag{3}$$

The left-hand side of Equation (3) represents the instantaneous electrical power delivered to the SRM. The first term in the right-hand side (RHS) of Equation (3) represents the ohmic losses in the SRM winding. If power is to be conserved, then the second term in the RHS of Equation (3) must represent the sum of the mechanical power output of the SRM and any power stored in the magnetic field. Thus,

$$i\,\frac{d\phi}{dt} = \frac{dW_m}{dt} + \frac{dW_f}{dt} \tag{4}$$

where, $\frac{dW_m}{dt}$ is the instantaneous mechanical power, and $\frac{dW_f}{dt}$ is the instantaneous power, which is stored in the magnetic field. Because power, by it's own definition, is the time rate of change of energy, W_m is the mechanical energy and W_f is the magnetic field energy.

It is well known that mechanical power can be written as the product of torque and speed,

$$\frac{dW_m}{dt} = T\omega = T\frac{d\theta}{dt} \tag{5}$$

where, T is torque, and $\omega = \frac{d\theta}{dt}$ is the rotational velocity of the shaft.

Substitution of Equation (5) into Equation (4) gives,

$$i\,\frac{d\phi}{dt} = T\,\frac{d\theta}{dt} + \frac{dW_f}{dt} \tag{6}$$

and solving Equation (6) for torque yields the equation,

$$T(\theta,\phi) = i(\theta,\phi)\,\frac{d\phi}{d\theta} - \frac{dW_f(\theta,\phi)}{d\theta} \tag{7}$$

and for constant flux, Equation (7) simplifies to,

$$T = -\frac{\partial W_f}{\partial\theta} \tag{8}$$

Since it is often desirable to express torque in terms of current rather than flux, it is common to express torque in terms of co-energy, W_c, instead of energy. To introduce the concept of co-energy, first consider a graphical interpretation of field energy. For constant shaft angle, $\frac{d\theta}{dt} = 0$, integration of Equation (6) shows that the magnetic field energy can be given by the equation,

$$W_f = \int_0^{\phi} i(\theta,\phi)\,d\phi \tag{9}$$

and graphically by the shaded area in Figure 3.

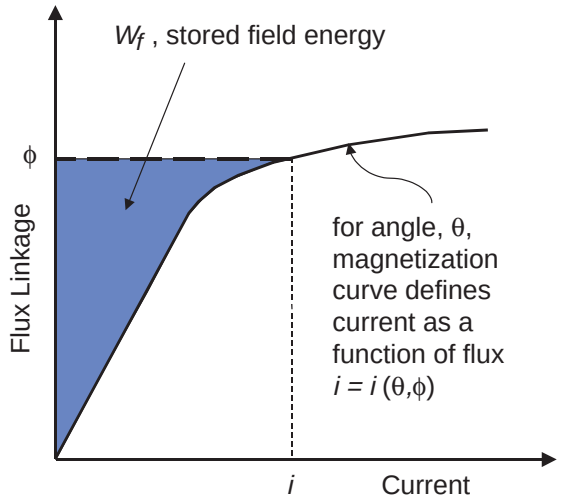

Figure 3. Graphical Interpretation of Magnetic Field Energy

Now, consider Figure 4.

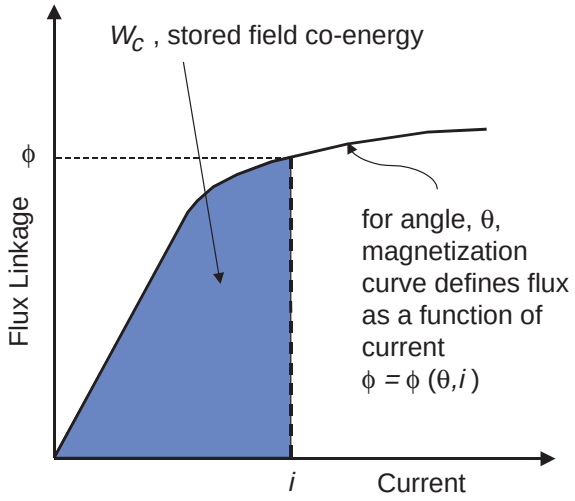

Figure 4. Graphical Interpretation of Magnetic Field Co-Energy

For the fixed angle, θ, let the magnetization curve define flux as a function of current, instead of current defined as a function of flux. The shaded area below the curve,

$$W_c = \int_0^i \phi(\theta, i)\, di \tag{10}$$

is defined as the magnetic field co-energy.

From Figure 3 and Figure 4, we see that the area defining the field energy and co-energy can be described by the relation,

$$W_c + W_f = i\phi \tag{11}$$

Differentiating both sides of Equation (11) yields

$$dW_c + dW_f = \phi di + id\phi \tag{12}$$

Solving for the differential field energy in Equation (12) and substituting back into Equation (7) gives,

$$T = \frac{id\phi - \left(\phi di + id\phi - dW_c(\theta, i)\right)}{d\theta} \tag{13}$$

For simplification, the general torque equation, Equation (13), is usually simplified for values of constant current. The differential co-energy can be written in terms of its partial derivatives as,

$$dW_c(\theta, i) = \frac{\partial W_c}{\partial \theta}\, d\theta + \frac{\partial W_c}{\partial i}\, di \tag{14}$$

From Equation (13) and Equation (14), it is fairly easy to show that under constant current,

$$T = \frac{\partial W_c}{\partial \theta}, \quad i \text{ constant} \tag{15}$$

2.4 Simplified Torque Equation

Often, SRM analysis proceeds under the assumption that, magnetically, the motor remains unsaturated during operation. This assumption can be useful for “first cut” control designs or performance predictions. When magnetic saturation is neglected, the relationship from flux to current is given by,

$$\phi = L(\theta) \cdot i \tag{16}$$

and the motor inductance varies only as a function of rotor angle. Substituting Equation (16) into Equation (10) and evaluating the integral yields,

$$W_c = \frac{i^2}{2} L(\theta) \tag{17}$$

and then substituting Equation (17) into Equation (15) gives the familiar simplified relationship for SRM torque,

$$T = \frac{i^2}{2}\frac{dL}{d\theta} \tag{18}$$

3 Control

SRM drives are controlled by synchronizing the energization of the motor phases with the rotor position. Figure 5 illustrates the basic strategy.

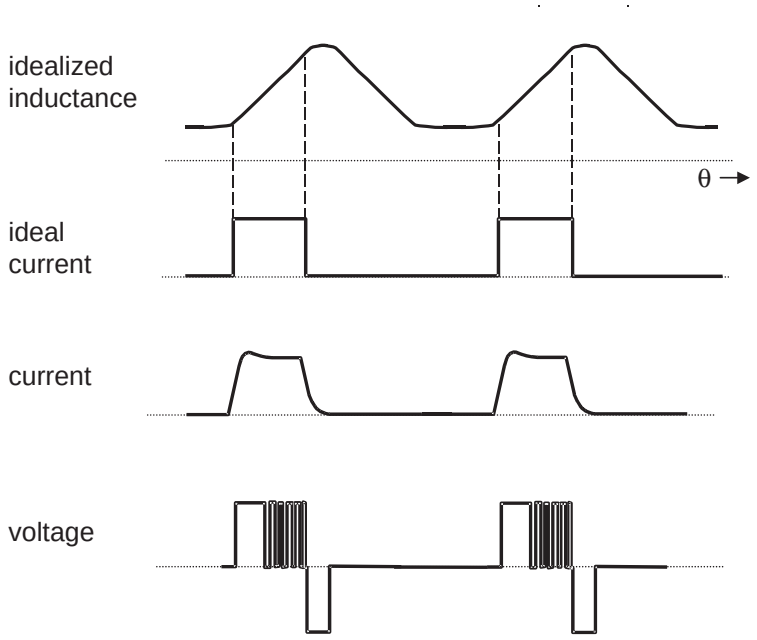

Figure 5. Basic Operation of a Current-Controlled SRM – Motoring at Low Speed

As Equation (18) suggests, positive (or motoring) torque is produced when the motor inductance is rising as the shaft angle is increasing, $\frac{dL}{d\theta} > 0$.

Thus, the desired operation is to have current in the SRM winding during this period of time. Similarly, a negative (or braking) torque is produced by supplying the SRM winding with current while $\frac{dL}{d\theta} < 0$.

The exact choice of the turn-on and turn-off angles and the magnitude of the phase current, determine the ultimate performance of the SRM. The design of commutation angles, sometimes called firing angles, usually involves the resolution of two conflicting concerns – maximizing the torque output of the motor or maximizing the efficiency of the motor. In general, efficiency is optimized by minimizing the dwell angle (the dwell angle is the angle traversed while the phase conducts), and maximum torque is achieved by maximizing the dwell angle to take advantage of all potential torque output from a given phase.

A simple and effective commutation scheme is depicted in Figure 6.

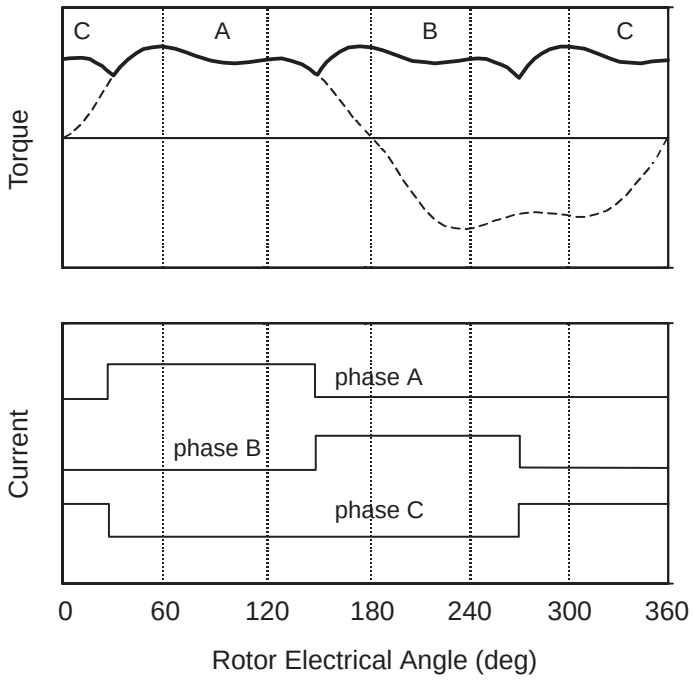

Figure 6. Commutation of a 3-Phase SRM

In the top plot of Figure 6, the dashed line shows the torque that would be generated by phase A, should constant current flow through the phase winding during an entire electrical cycle of the SRM. With the idealized current waveforms of the figure, the resulting net torque from the motor is shown by the solid line. The turn-on and turn-off angles coincide with the region where maximum torque is obtained for the given amount of phase current.

This commutation sequence tends to optimize efficiency. Here, a dwell angle of 120 electrical degrees is used, which is the minimum dwell angle that can be used for a three-phase SRM, without regions of zero torque.

Of interest to note from Figure 6 is that constant current results in non-constant torque. As might be expected, schemes have been proposed by Husain and Ehsani[1], Ilic-Spong, *et al*[2], and Kjaer, *et al*[3] that attempt to linearize SRM output torque by shaping and controlling the phase currents through some non-linear function that depends upon the motor characteristics. This application, although not covered in this report, is well suited for DSP implementation.

Figure 6 illustrates the effect that the choice of commutation angles can have upon the SRM performance. Equally important is the magnitude of the current that flows in the winding. Commonly, the phase current is sensed and controlled in a closed-loop manner, and as seen in the voltage curve of Figure 5, the control is typically implemented using PWM techniques.

1 I. Husain and M. Ehsani, " Torque Ripple Minimization in Switched Reluctance Motor Drives by PWM Current Control," *Proc. APEC'94*, 1994, pp. 72–77.
2 M. Ilic-Spong, T. J. E. Miller, S. R. MacMinn, and J. S. Thorp, "Instantaneous Torque Control of Electric Motor Drives," *IEEE Trans. Power Electronics*, Vol. 2, pp. 55–61, Jan. 1987.
3 P. C. Kjaer, J. Gribble, and T. J. E. Miller, "High-grade Control of Switched Reluctance Machines," *IEEE Trans. Industry Electronics*, Vol. 33, pp. 1585–1593, Nov. 1997.

SRM control is often described in terms of ”low-speed” and ”high-speed” regimes. Low-speed operation is typically characterized by the ability to arbitrarily control the current to any desired value. Figure 5 illustrates waveforms typical of low-speed SRM operation. As the motor’s speed increases, it becomes increasingly difficult to regulate the current because of a combination of the back EMF effects and a reduced amount of time for the commutation interval. Eventually a speed is reached where the phase conducts (remains on) during the entire commutation interval. This mode of operation, depicted by Figure 7, is called the single-pulse mode.

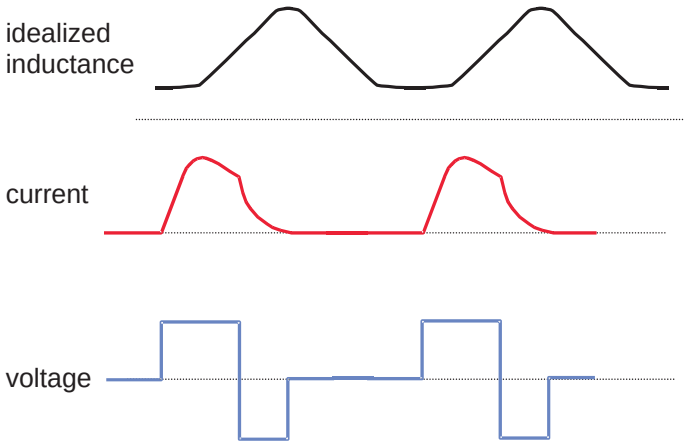

Figure 7. Single-Pulse Mode – Motoring, High Speed

When this occurs, the motor speed can be increased by increasing the conduction period (a greater dwell angle) or by advancing the firing angles, or by a combination of both. By adjusting the turn-on and turn-off angles so that the phase commutation begins sooner, we gain the advantage of producing current in the winding while the inductance is low, and also of having additional time to reduce the current in the winding before the rotor reaches the negative torque region. Control of the firing angles can be accomplished a number of ways, and is based on the type of position feedback available and the optimization goal of the control, as discussed in publications by Becerra, *et al*,[4] and Miller.[5] When position information is more precisely known, a more sophisticated approach can be used. One approach is to continuously vary the turn-on angle with a fixed dwell.

Near turn-on, Equation (2) can be approximated as

$$v = \frac{\partial \phi}{\partial i}\frac{di}{dt} = L_u \cdot \frac{di}{dt} \tag{19}$$

4 R. Becerra, M. Ehsani, and T. J. E. Miller, “Commutation of SR Motors,” *IEEE Trans. Power Electronics*, Vol. 8, July 1993, pp. 257–262.

5 T. J. E. Miller, “Switched Reluctance Motors and Their Control,” Magna Physics Publishing, Hillsboro, OH, and Oxford, 1993.

Multiplying each side of Equation (19) by the differential, $d\theta$, and solving for $d\theta$, gives,

$$d\theta = \frac{L_u \cdot di}{v} \cdot \frac{d\theta}{dt} \tag{20}$$

and using first order approximations yields an equation for calculating advance angle,

$$\theta_{adv} = \frac{L_u \cdot i_{cmd}}{V_{bus}} \cdot \omega \tag{21}$$

where i_{cmd} is the desired phase current and V_{bus} is the DC bus voltage.

4 Example – SRM Drive with Position Feedback

This section describes an example application of an SRM drive with position feedback. The SRM is a 3-phase 12/8 machine that is speed and current controlled.

4.1 Hardware Description

4.1.1 SRM Characteristics

The characteristics of the SRM used in this application report are given by Table 1.

Table 1. SRM Parameters

number of phases, m	3
number of stator poles, N_S	12
number of rotor poles, N_R	8
nominal phase resistance, R_m	8.1 Ω
nominal aligned inductance, L_a	240 mH
nominal unaligned inductance, L_u	60 mH
phase current (max)	4 A
DC bus voltage, V_{bus}	170 VDC

4.1.2 Control Hardware

The control hardware used in this application report is the TMS320F240 evaluation module (EVM).

4.1.3 Position Sensor

Shaft position information is provided using an 8-slot, slotted disk connected to the rotor shaft and three opto-couplers mounted to the stator housing as shown in Figure 8.

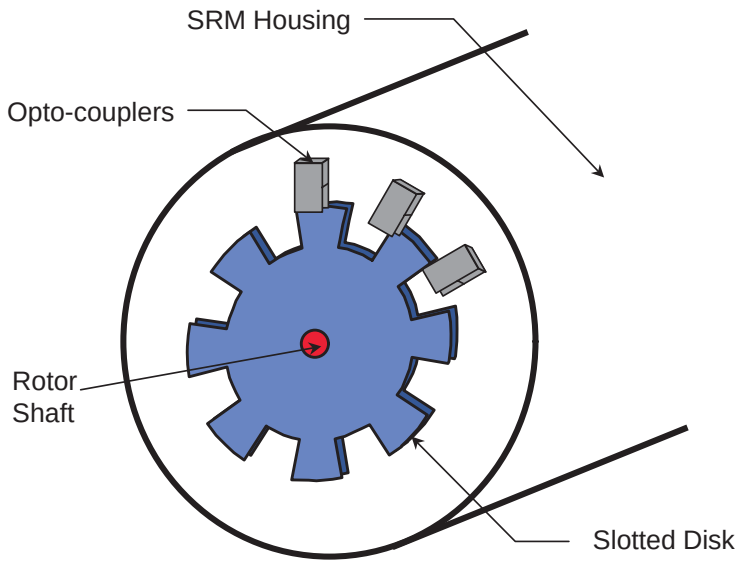

Figure 8. SRM Shaft Position Sensor

The opto-couplers are nominally located 30° apart from each other along the circumference of the disk. This configuration and geometry produces the output waveforms shown in Figure 9.

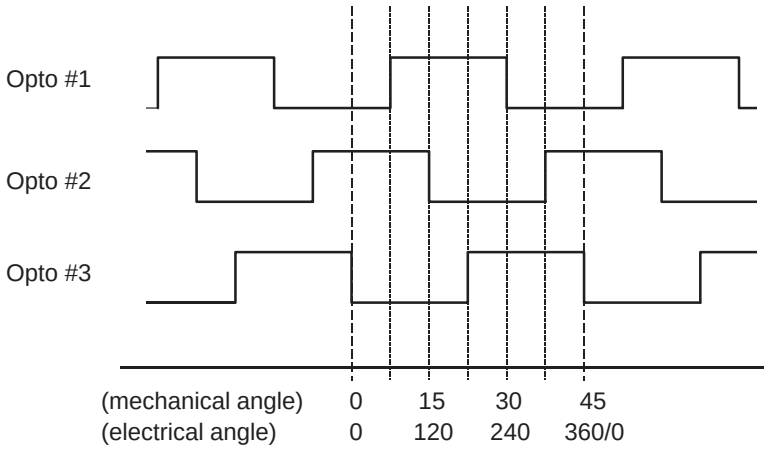

Figure 9. Opto-Coupler Output Signals vs. Rotor Angle

This configuration generates an opto-coupler edge for every 7.5° of mechanical rotation. For every 45° of mechanical rotation the signal pattern repeats, corresponding to one electrical cycle of the SRM, of which there are 8 per shaft revolution.

In this report both mechanical angle and electrical angle are referenced. Mechanical angle is useful when considering velocity control of the SRM, and electrical angle is convenient when considering commutation. Electrical angle is related to mechanical angle by the number of rotor poles, N_R. In Figure 9, the angles are arbitrarily defined with respect to some convenient point. Here, 180° electrical is defined as *the aligned position for phase A of the motor*. This is easily verified by energizing phase A and then monitoring the opto-coupler output waveforms on an oscilloscope to observe that the rotor is at the point where opto-coupler #3 switches state, while opto-coupler #2 is low and opto-coupler #1 is high. For a 3-phase SRM, phases B and C are related to the position of phase A by adding 120 and 240 electrical degrees, respectively.

A fundamentally identical position sensor can be implemented by replacing the opto-couplers with Hall-effect sensors and embedding permanent magnets within the teeth of the slotted disk. The opto-couplers are connected to the F240 EVM as shown in Figure 10.

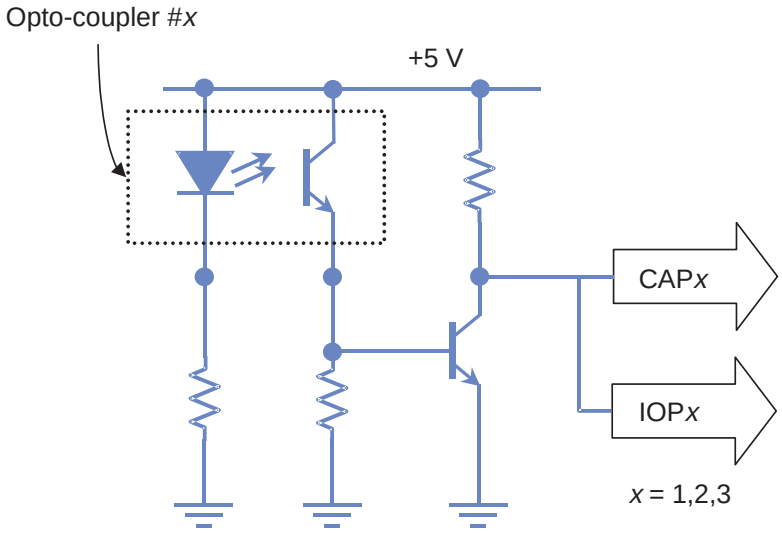

Figure 10. Opto-Coupler Connections to the TMS320F240 EVM

Here, each opto-coupler output is connected to both a capture input and a digital I/O input. As will be explained in further detail below, the capture inputs are used once the motor is running, and the digital I/O inputs are used for estimating initial rotor position and for starting the SRM.

4.1.4 Power Electronics Hardware

The amount of current flowing through the SRM windings is regulated by switching on or off power devices, such as MOSFETs or IGBTs, which connect each SRM phase to a DC bus. The power inverter topology is an important issue in SRM control because it largely dictates how the motor can be controlled.

There are numerous options available, and invariably the decision will come down to trading off the cost of the driver components against having enough control capability (independent control of phases, current feedback, etc.) built into the driver. A popular configuration, and the one used in this application report, uses 2 switches and 2 diodes per phase. This topology is depicted in Figure 11.

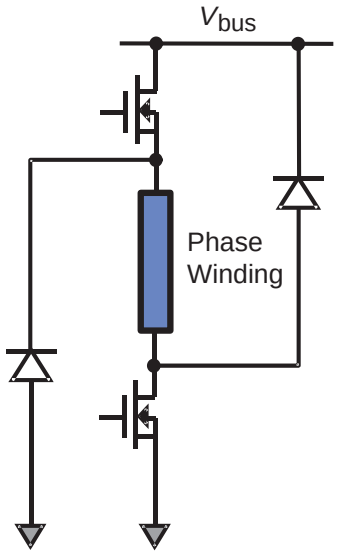

Figure 11. Two-Switch Per Phase Inverter

Publications by Vukosavic and Stfanovic[6] and Miller[7] offer several other configurations that require fewer switches per phase, although with some penalty on control flexibility and maintaining phase independence. A gate drive IC device, such as the IR2110, is used to turn on and off the semiconductor switches. In the topology of Figure 11, the low-side switch is usually held on during a commutation interval, while the top switch is used to implement the control. For independent current control of each phase, a low-ohm sense resistor is placed between the source of the low-side n-channel power MOSFET and ground.

A schematic diagram of the inverter used in this application report, including the gate drive circuit and the connections to the EVM, is given in Figure 12.

6 S. Vukosavic and V. Stfanovic, “SRM Inverter Topologies: A Comparative Evaluation,” *IEEE IAS Annual Meeting Conf. Record*, 1990.

7 T. J. E. Miller (ed.), “Switched Reluctance Motor Drives,” Intertec Communications Inc., Ventura CA, 1988.

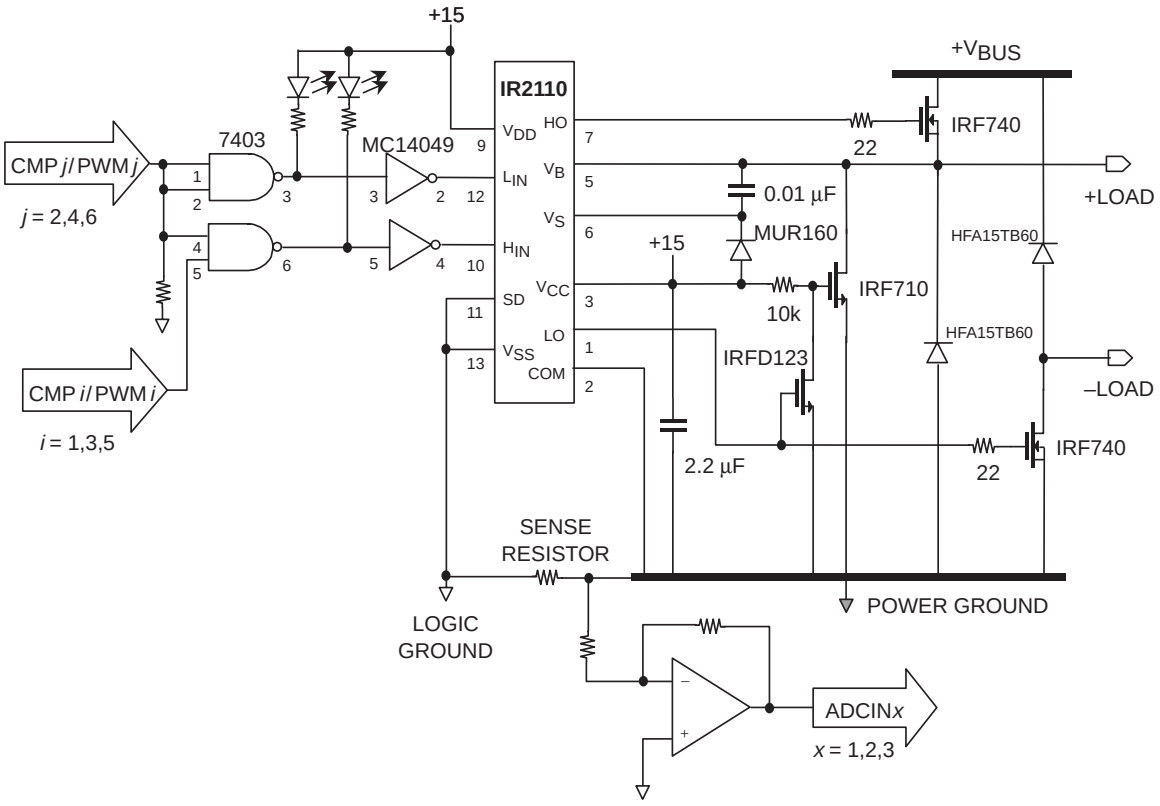

Figure 12. Schematic Diagram of SRM Inverter Using the IR2110 and Connections to the EVM

The diagram shows the components used for a single phase. Each phase uses two IRF740 n-channel power MOSFETs for the switching elements in the output stage. The IRF740 is rated at 400 VDC, 10 A. The drain to source on resistance of these devices is 0.55 Ω. The free-wheeling diodes used in the power stage are HFA15TB60s, fast recovery diodes. The HFA15TB60 has a reverse recovery time of 60 ns, and is rated at 600 VDC, 15 A. Logic is implemented at the input to the gate drive IC such that the top power MOSFET can be turned on only when the bottom MOSFET is also on. The reasons for this limitation, and other circuit details, are discussed more thoroughly in a publication by Clemente and Dubhashi.[8]

4.2 Software Description

The software described in this application report is written in C and is designed for operating a 3-phase 12/8 SRM in closed loop current control and closed loop speed control. A block diagram of the algorithms implemented is given in Figure 13.

8 S. Clemente and A. Dubhashi, “HV Floating MOS-Gate Driver IC,” *International Rectifier Application Note AN-978A*, International Rectifier, El Segundo, CA, 1990.

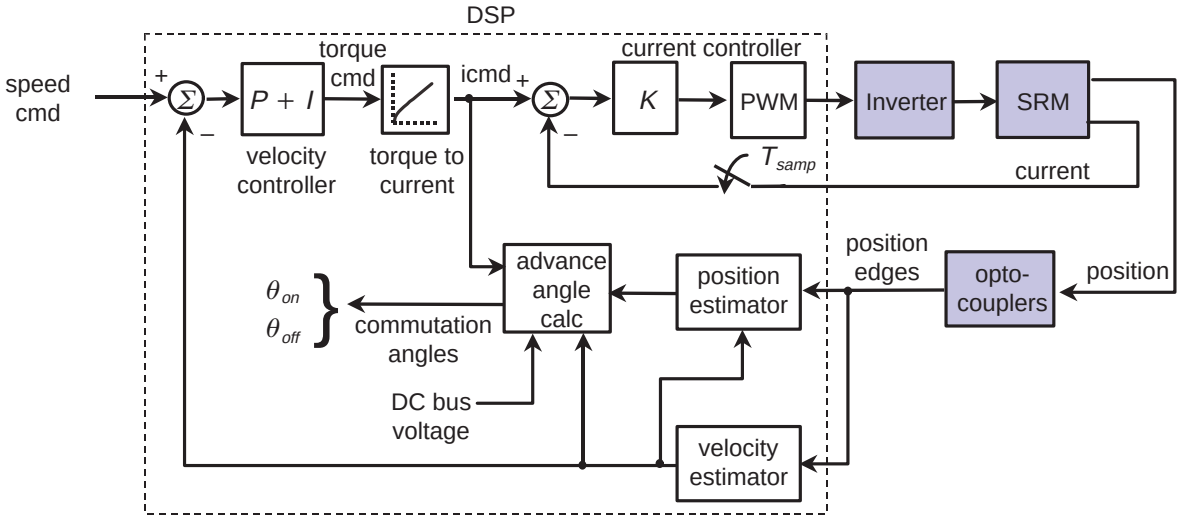

Figure 13. Block Diagram of the SRM Controller

Velocity is estimated by monitoring the elapsed time between opto-coupler edges, which are a known distance apart. A velocity compensation algorithm determines the torque required to bring the motor velocity to the commanded value.

A commutation algorithm converts the torque command into a set of phase current commands, and the current in each phase is individually regulated using a fixed-frequency PWM scheme. Further details on each of the algorithms are provided in subsequent sections of this report.

4.2.1 Program Structure

Figure 14 shows the structure of the SRM control software for the TMS320F240 DSP.

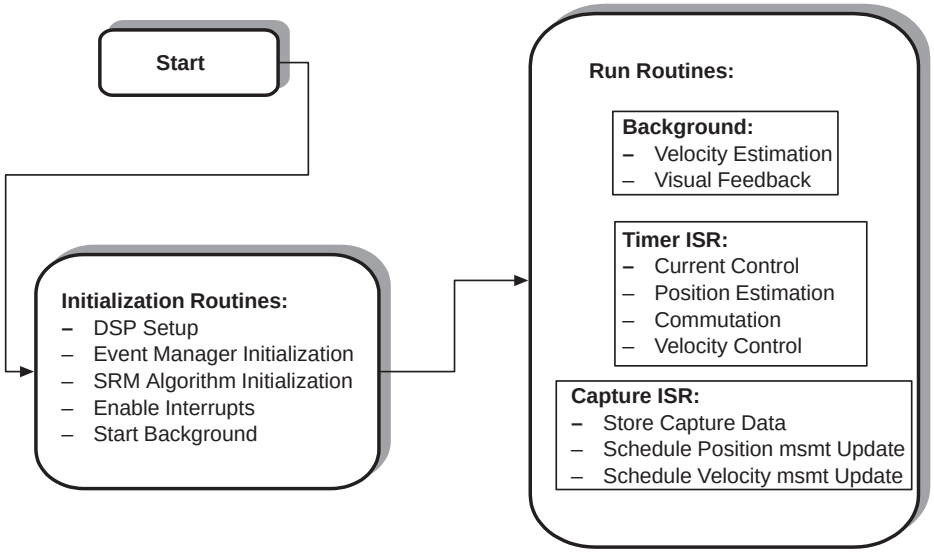

Figure 14. TMS320F240 SRM Control Program Structure

At the highest level, the software consists of initialization routines and run routines. Upon completion of the necessary initialization, the background task is started. The background is simply an infinite loop, although when required, lower priority processing including velocity estimation and a visual feedback routine is executed. The velocity estimation involves double-precision division arithmetic, thus it is executed in background mode so that the timeline is not violated. This algorithm is initiated in the capture interrupt service routine. The visual feedback function simply toggles an LED on the EVM board to provide a signal to the user that the code is running.

All of the time critical motor control processing is done via interrupt service routines. The timer ISR is executed at each occurrence of the maskable CPU interrupt INT3. This interrupt corresponds to the event manager group B interrupts, of which we enable only the timer #3 period interrupt, TPINT3. The frequency, *F*, at which this routine is executed is specified by loading the timer 3 period register with the desired value. The SRM control algorithms which are implemented during the timer ISR are the current control, shaft position estimation, commutation, and velocity control. As illustrated in Figure 15, only the current control and shaft position estimation are executed at the frequency, *F*.

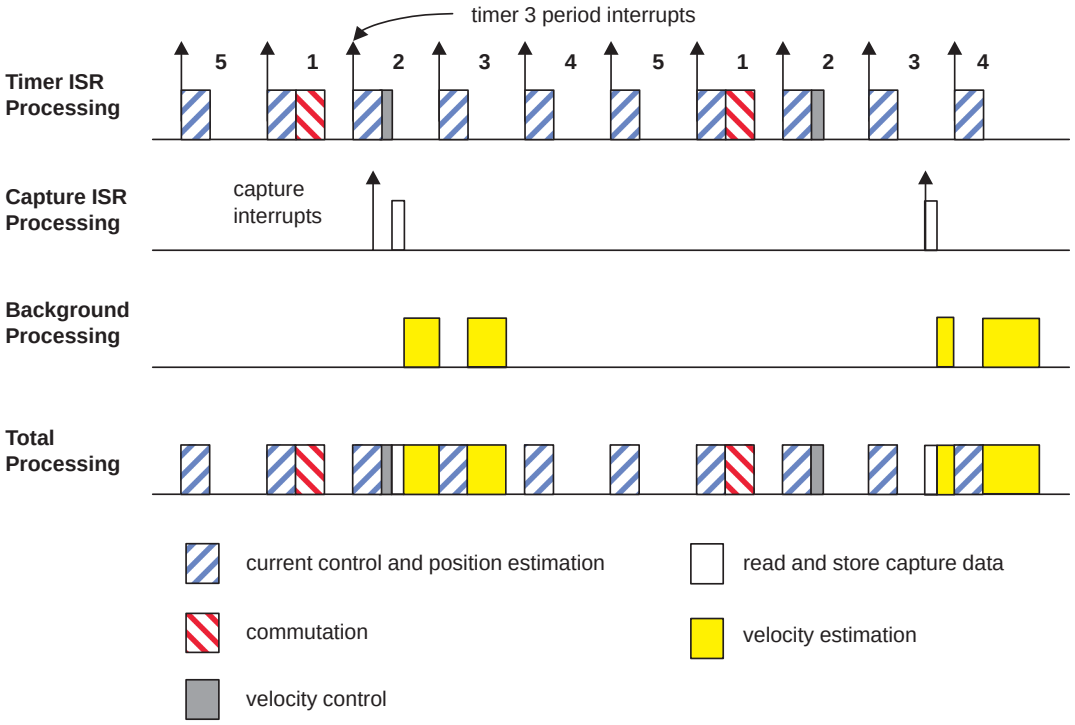

Figure 15. Processor Timeline Showing Typical Loading and Execution of SRM Control Algorithms

Because of their lower bandwidth requirements, velocity control and commutation are performed at a frequency of *F*/5. Considering the timer ISR as being sliced into fifths with a pattern repeating every five slices, commutation is run only in the first slice and the velocity loop only in the second. Current control and position estimation are performed in each slice.

The capture interrupt service routine is executed at each occurrence of the maskable CPU interrupt INT4. This CPU interrupt corresponds to the event manager group C interrupts, of which we enable the three capture event interrupts, CAPINT1–3. This ISR executes asynchronously to the timers on board the DSP and the frequency of execution is dependent on the SRM shaft speed according to the equation,

$$\text{capture ISR frequency (Hz)} = \text{shaft speed (rpm)} \times \frac{360\ \text{(deg)}}{\text{(rev)}} \times \frac{1}{7.5\ \text{(deg)}} \times \frac{1\ \text{(min)}}{60\ \text{(sec)}} \qquad (22)$$

The capture ISR is used to determine which capture interrupt has occurred, read the appropriate capture FIFO register, and then store the data. Although no algorithm is explicitly executed in this ISR, flags are set which initiate velocity and position estimation actions. As described above, the velocity estimate update calculation is performed in the background. The position estimation algorithm, which executes during the timer ISR, is notified that a new position measurement has been received.

Table 2 summarizes the processing requirements for each of the major software functions for the SRM controller.

Table 2. Benchmark Data for the Various SRM Drive Software Modules

S/W Block	Module	Number of Cycles	Execution Time @ 50 ns	Execution Frequency	Relative Time @ 5 kHz
Velocity Estimation	Background	3620	181.0 µs	800 Hz†	29.0 µs
Visual Feedback	Background	60	3.0 µs	2 Hz	0.0 µs
Current Control	Timer ISR	948	47.4 µs	5000 Hz	47.4 µs
Position Estimation	Timer ISR	258	12.9 µs	5000 Hz	12.9 µs
Commutation	Timer ISR	1296	64.8 µs	1000 Hz	13.0 µs
Velocity Control	Timer ISR	444	22.2 µs	1000 Hz	4.4 µs
Misc. Overhead	Timer ISR	140	7.0 µs	5000 Hz	7.0 µs
Capture ISR	Capture ISR	500	25.0 µs	800 Hz†	4.0 µs
C Context Switch	RTS.LIB	120	6.0 µs	5800 Hz	7.0 µs
Total					124.7 µs

† at a shaft speed of 1000 rpm

The data in Table 2 shows that when the timer ISR frequency, *F*, is chosen as 5 kHz, that the overall processor loading is equal to

$$\text{processor loading} = \frac{124.7\ \mu\text{s}}{200.0\ \mu\text{s}} = 62.4\%\ , \qquad (23)$$

when running the DSP at a 20 MHz clock frequency. The code size is 2456 words and 167 words are required for variable/data storage. Thus, the total memory requirement is less than 3K words. Complete code listings are given in Appendix A.

It should be noted that this benchmark data was taken with the program and data memory located off chip, as can be seen in the link.cmd file located in the appendix. A 2× to 3× improvement in execution can be achieved by moving the .bss and .stack sections of the firmware to the on-chip B0/B1 area of the DSP and by moving the .text section of the firmware to the flash memory.

4.2.2 Initialization Routines

A flowchart describing the initialization routines is given in Figure 16.

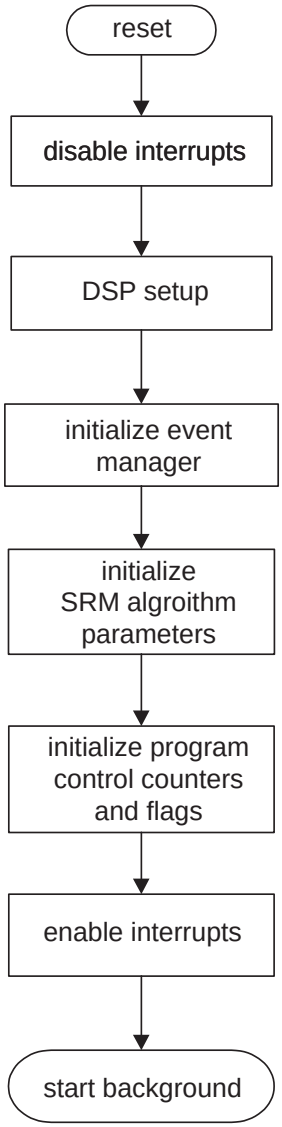

Figure 16. Initialization Flowchart

The DSP is configured so that the watchdog timer is disabled. The TMS320F240 EVM has a 10 MHz crystal, which is used in conjunction with the PLL module of the DSP to yield a 20 MHz CPUCLK.

The event manager initialization configures the timer units, the capture units, the compare units, and the A/D converters. Also, the CAP1–CAP4 and IOPB0–IOPB3 pins, whose functions are software programmable, are configured to operate as capture pins and digital output pins, respectively.

Each of the timers are programmed to operate in the continuous up count mode. Timer #1 provides the timebase for the fixed-frequency PWM control of the phase current. Timer #2 provides the timebase for the capture events, and timer #3 is used to provide a CPU interrupt at a fixed rate. The compare units are configured to the PWM mode, where PWMs 1,3, and 5 (used for switching the high-side power MOSFET) are configured as active high.

The SRM algorithm initialization defines the parameters of the position estimation state machine and sets the initial conditions of the motor, for example, setting the shaft velocity estimate to zero. Also, during this routine, the logic states of the opto-couplers are read from the digital I/O pins, and this information used to estimate the rotor position.

Upon initializing several flags and counters which are used for program flow control, the infinite loop background routine is called, and the normal operation of controlling the SRM drive begins.

See the comments in the code listings found in Appendix A for further information on the program initialization.

4.2.3 Current Controller

Current is regulated by fixed-frequency PWM signals with varying duty cycles. The TMS320F240 accomplishes this using compare units and output logic circuits. The compare units are programmed for PWM mode, to use timer #1 as a time base. The desired output logic polarity is controlled by the ACTR register. The PWM frequency is specified by loading the period register of timer #1, T1PER, with a value, *P*, defined by,

$$P = \frac{\text{CPUCLK frequency}}{\text{PWM frequency}} - 1 \qquad (24)$$

For the F240, the CPUCLK frequency is 20 MHz. The percentage duty cycle for the x^{th} phase is controlled by loading the appropriate compare register, CMPR*x*, with an appropriate value between 0 and *P* (0 = 0%, *P*/2 = 50%, *P* = 100%). A PWM frequency of 20 kHz is used. The value is significantly higher than the bandwidth of the current loop and also at a frequency which is inaudible.

The percentage duty cycle command is calculated by the current loop compensation algorithm, which is designed using linear analysis. The analysis begins with an approximate model of the current loop, given by Figure 17.

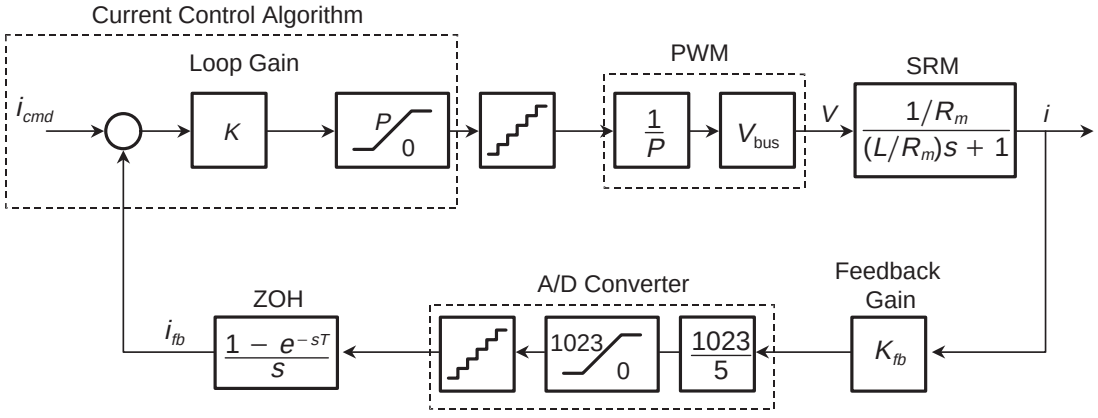

Figure 17. Approximate SRM Current Loop Model

Using the SRM data of Table 2, and with $P = 999$, $K_{fb} = 1.17$ V/A, the open-loop frequency response, $G(\omega)$, of the SRM current loop, from i_{cmd} to i_{fb}, is given in Figure 18 for values of phase inductance at both the aligned rotor position ($L = L_a$) and the unaligned rotor position ($L = L_u$).

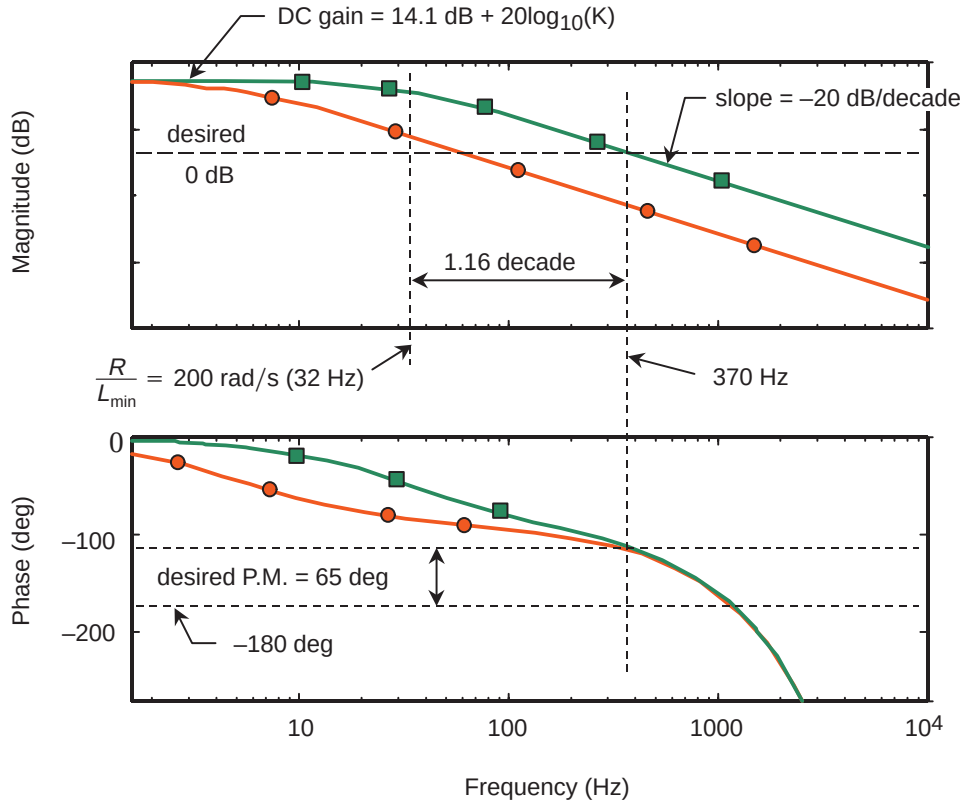

Figure 18. Frequency Response Plots for the SRM Current Loop at the Unaligned Position (Squares) and at the Aligned Position (Circles)

Because of the digital implementation of the current loop, additional phase loss, beyond the 90° due to the motor pole, is contributed by the sample and hold process and the processing delay inherent in the loop. These dynamics essentially limit the current loop bandwidth to an open loop crossover frequency near 370 Hz. The time delay due to the zero-order hold (ZOH) is equal to ½ of the sampling period, in this case ½ of 200 µsec, or 100 µsec. Since the phase loss at any frequency, ω, due to a pure time delay, τ, is given by the expression,

$$\theta_{\text{loss}} = \omega\tau \tag{25}$$

using Equation (25), we calculate that the phase loss due to the ZOH sampling at 370 Hz is equal to

$$\theta_{\text{loss}} = 2\pi \times 370 \times \left(100 \times 10^{-6}\right) = 0.232 \text{ rad} = 13.3^{\text{o}} \tag{26}$$

Assuming that the processing delay is equal to 50% of a loop cycle, or another 100 µsec, then the net effect of digital implementation yields about 26° of phase loss at 370 Hz. When combined with the 90° due to the motor pole, the phase loss through the loop is approximately 116°, at 370 Hz. If the loop gain, K, is chosen such that the 0 dB point of the open-loop magnitude occurs at 370 Hz, then the resulting phase margin in the loop will be about 64°. This amount of phase margin provides a very stable loop design. The DC gain of the loop is given by,

$$\frac{K \cdot V_{bus} \cdot K_{fb} \cdot 1023}{P \cdot 5 \cdot R} = 5.092\,K \tag{27}$$

which, when written in decibels, is equal to,

$$\text{DC gain} = 14.1\ \text{dB} + 20\log_{10}(K) \tag{28}$$

For frequencies where $\omega > (R/L)$, the magnitude of the loop response is equal to,

$$|G(\omega)| = 14.1\ \text{dB} + 20\log_{10}(K) - 2 \times \left(\frac{\omega}{R/L}\right) \tag{29}$$

In Equation (29), letting $L = L_U$ provides the most conservative choice, resulting in a stable design for all rotor positions. Setting the left-hand side of Equation (29) to 0 dB while $\omega = 2\pi(370)$ rad/s, and solving for K, yields the value of K which ensures the desired open-loop crossover point for the current loop. In this case $K = 2.8$.

Often, a PI controller is used. In this example adding an integrator to the control law will not make much difference in the loop performance, except only at very low speeds, because the integrator action must be slower than the motor pole to stabilize the loop. In this example using a 3-phase, 12/8 SRM, the motor pole is located near 32 Hz. The SRM operating speed required to produce the equivalent of 32 Hz commands to the SRM current loops is 240 rpm. Thus, in this case, only at operating speeds lower than 240 rpm would any integrator action be helpful.

The current loop gain is set using the ILOOP_GAIN constant in the file CONSTANT.H. For this value, Q3 scaling is used, thus setting ILOOP_GAIN = 22 results in $K = 2.75$, which is sufficiently close to the desired value of 2.8, for this application.

4.2.4 Position Estimation

Recall that Figure 9 showed six possible combinations of the opto-coupler output states per electrical cycle of the SRM. The transitions of the outputs define specific angles. This information can readily be described by a state machine, such as Figure 19.

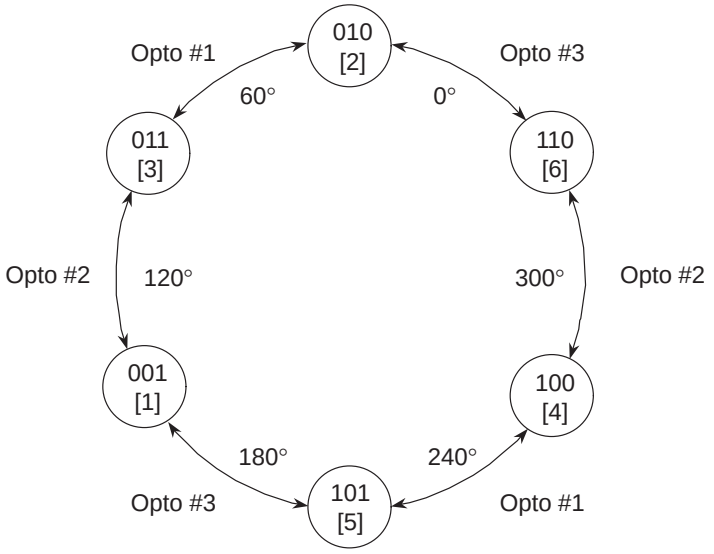

Figure 19. State Transition Diagram for the SRM Position Pickoff

The state, [ ], is defined by '*zyx*', where *z* is the logic state of opto-coupler #3, *y* of opto-coupler #2, and *x* is the state of opto-coupler #1.

Position measurements are made by using this state machine and identifying which opto-coupler transition occurs, using the DSP's capture units.

The opto-couplers and slotted disk provide position measurements at six discrete points per electrical cycle of the SRM. Many commutation schemes, however, require continuous position information to optimize performance. Thus, to provide a position estimate between measurements, the equation,

$$\hat{\theta}(k) = \hat{\theta}(k-1) + \hat{\omega}_f(\bar{k}) \times \frac{1}{f_s} \tag{30}$$

is used, where f_S is the estimation update rate and $\bar{k}$ represents the time of the most recent capture edge. Equation (30) is implemented, using double precision arithmetic, as follows:

```
long dp;   /* delta–position in mechanical angle */
int speed;
int temp;

if (anSRM–>wEst_10xrpm > 0) {
       dp = anSRM–>wEst_10xrpm * K_POSITION_EST + anSRM–>dp_remainder;
       anSRM–>dp_remainder = dp & 0xffff;
       temp = (int) (dp >> 16);
       anSRM–>position = anSRM–>position + (temp * NR);
}
else {
       speed = –anSRM–>wEst_10xrpm;
       dp = speed * K_POSITION_EST + anSRM–>dp_remainder;
       anSRM–>dp_remainder = dp & 0xffff;
       temp = (int) (dp >> 16);
       anSRM–>position = anSRM–>position – (temp * NR);

}
```

The constant K_POSITION_EST (Q16), compensates for units (shaft velocity is available in the software as `SRM.wEst_10xrpm` with units of rpm × 10) and is calculated according to the equation,

$$\text{K\_POSITION\_EST} = \frac{1}{10}(\text{rpm} \times 10) \times \frac{1\ (\text{sec})}{f_s} \times \frac{1\ (\text{min})}{60\ (\text{sec})} \times \frac{360^o}{(\text{rev})} \times \frac{65535}{360^o} \times 2^{16} \tag{31}$$

for, f_S = 5 kHz, K_POSITION_EST = 1432.

During startup, the digital I/O ports determine the state of the rotor and initial position is estimated in the mid-range of the state. For example, a reading of [100], (consistent with Figure 19) yields an initial position estimate of 270 electrical degrees. The capture units provide subsequent measurements, by recognizing the edges, or state transitions.

4.2.5 Velocity Estimation

The three opto-coupler outputs produce an edge every 7.5° of mechanical rotation, and each opto-coupler produces an edge every 22.5° mechanical. At each edge, velocity is calculated according to the equation,

$$\hat{\omega} = \frac{\Delta\theta}{\Delta t} = \frac{60 \cdot \Delta\theta \cdot f_{clk}}{N} \tag{32}$$

where, $\hat{\omega}$ is the velocity estimate (rpm)

$\Delta\theta$ is the distance between opto-coupler edges (rev)

Δt is the time between edges (min)

N is the number of clock counts between edges

f_{clk} is the clock frequency (Hz)

The time between edges is determined from the capture units. The capture units are programmed via the CAPCON register to use timer #2 as a time base, and to trigger on both rising and falling edges. Timer #2 is programmed to count at 1.25 MHz via the T2CON. Although we trade-off resolution in measuring Δt, a clock frequency of 1.25 MHz is chosen, versus a maximum of 20 MHz, so that the 16-bit registers containing the count do not overflow except at very low speeds. Using a 1.25 MHz clock, the counter overflows only at shaft speeds less than 71.5 rpm, considered very low for our application. So that we can operate (although degraded) at speeds lower than about 100 rpm, Δt in Equation (32) is determined by a software counter of the number of 5 kHz timer interrupts that occur between opto-coupler edges.

It can be shown that when instantaneous velocity is estimated by Equation (32) that the quantization of a velocity estimate is given by

$$Q = \frac{d\hat{\omega}}{dN} = \frac{\omega^2}{60 \cdot \Delta\theta \cdot f_{clk}} \tag{33}$$

and, Q is the quantization of velocity (rpm). In our design, $\Delta\theta$ = 1/16 revolution (22.5° mechanical) and f_{clk} = 1.25 MHz. Thus, at 1200 rpm, the quantization is 0.31 rpm.

Various filtering can be applied to Equation (32) for smoothing the velocity estimate, depending upon the application. What has proven useful is a combination of FIR and IIR filtering of the form:

$$\hat{\omega}_f(\bar{k}) = \alpha \cdot \hat{\omega}_f(\bar{k} - 1) + (1 - \alpha) \cdot \sum_{j=(\bar{k}-5)}^{\bar{k}} \hat{\omega}(j) \tag{34}$$

The FIR filter portion of Equation (34) uses six (from $\bar{k} - 5$ to $\bar{k}$) instantaneous velocity estimates. Because there are six opto-coupler edges per electrical cycle, once per cycle estimation errors are removed.

The FIR filtering and the determination of the instantaneous velocity estimate is calculated using double precision as follows:

```
DWORD a1,a2,a3,a4,a5,a6;
DWORD sum_cnt;
int  inst_velocity;

/*-------------------------------------------*/
/*  Obtain instantaneous velocity estimate   */
/*-------------------------------------------*/
if (mode == 1) {/* use timer #2 as time base */

   /*-----------------------------------------------------*/
   /* FIR filter for removing once per electrical cycle */
   /* effects                                             */
   /*-----------------------------------------------------*/
   a1 = (DWORD) anSRM->capture_delta[0][0];
   a2 = (DWORD) anSRM->capture_delta[0][1];
   a3 = (DWORD) anSRM->capture_delta[1][0];
   a4 = (DWORD) anSRM->capture_delta[1][1];
   a5 = (DWORD) anSRM->capture_delta[2][0];
   a6 = (DWORD) anSRM->capture_delta[2][1];
   sum_cnt = a1+a2+a3+a4+a5+a6;

   /*-----------------------------------------------------*/
   /* apply "velocity = delta_theta/delta_time" algorithm  */
   /*-----------------------------------------------------*/
   sum_cnt = K1_VELOCITY_EST/sum_cnt;
   inst_velocity = ((int) sum_cnt) * anSRM->shaft_direction;
}

else {      /* else, use timer ISR count as time base */

   /*-----------------------------------------------------*/
   /* apply "velocity = delta_theta/delta_time" algorithm  */
   /*-----------------------------------------------------*/
   sum_cnt = K2_VELOCITY_EST/anSRM->delta_count;
   inst_velocity = ((int) sum_cnt) * anSRM->shaft_direction;
}
```

Here, K1_VELOCITY_EST and K2_VELOCITY_EST are constants which incorporate $\Delta\theta$ and units so that the instantaneous velocity estimate has units of (rpm $\times$ 10). The constants are calculated using,

$$\text{K1\_VELOCITY\_EST} = 6 \times 22.5\ (\text{deg}) \times \frac{1.25\text{e}6\ (\text{cnts})}{(\text{sec})} \times \frac{1\ (\text{rev})}{360\ (\text{deg})} \times \frac{60\ (\text{sec})}{(\text{min})} \times 10 \qquad (35)$$

$$\text{K2\_VELOCITY\_EST} = 1 \times 7.5\ (\text{deg}) \times \frac{5000\ (\text{cnts})}{(\text{sec})} \times \frac{1\ (\text{rev})}{360\ (\text{deg})} \times \frac{60\ (\text{sec})}{(\text{min})} \times 10$$

The IIR filtering is implemented as:

```
long filt_velocity;

/*-----------------------------------------------------*/
/*  IIR filter for smoothing velocity estimate       */
/*-----------------------------------------------------*/
filt_velocity = (ALPHA * anSRM->wEst_10xrpm)
+ (ONE_MINUS_ALPHA * inst_velocity);
anSRM->wEst_10xrpm = (int) (filt_velocity >> 3);
```

The filter coefficient, α, is chosen equal to 0.875, [ALPHA = 7 (Q3)]. Let α approach zero for a higher bandwidth velocity estimate (less smoothing, more noise) and let α approach one for more smoothing, less noise, and lower bandwidth.

4.2.6 Commutation

The commutation strategy ultimately determines the performance of the SRM. Torque-speed range, machine efficiency, torque ripple, and acoustic noise all depend, to some extent, on the commutation algorithm. Design of the commutation algorithm must consider requirements in each of these areas, while trading off cost issues such as the algorithm complexity and the availability or accuracy of various sensors. For a current controlled SRM, commutation can be described as the transformation of the desired net motor torque into a set of desired phase currents. This is described mathematically by the equation,

$$i^{j}_{cmd} = g_j(\cdot) \times T_{cmd} \tag{36}$$

and $j = 1,...,m$ and m is the total number of motor phases. In general, $g(\ )$, is a non-linear function of shaft angle θ, shaft speed ω, the desired torque command T_{cmd}, the DC bus voltage V_{bus}, and the motor instantaneous inductance, L. The most simple choice for $g(\ )$ is given by

$$g(\theta) = \begin{cases} 1, & \theta_{ON} \le \theta < (\theta_{ON} + \delta\theta) \\ 0, & \text{otherwise} \end{cases} \tag{37}$$

where the dwell angle, $\delta\theta$, must be at least equal to $360°/m$ (electrical), to avoid regions of zero torque production. An example of commutation described by Equation (37) is illustrated by Figure 6. The turn-on angle, θ_{ON}, is typically a few degrees beyond the unaligned position of a phase. Equation (37) is useful for only single-quadrant operation. For four quadrant operation, Equation (37) must be modified, for example,

$$g(\theta, T_{cmd}) = \begin{cases} 1, & \left[\theta_{ON} \le \theta < (\theta_{ON} + \delta\theta)\right] \& T_{cmd} > 0 \\ 1, & \left[(\theta_{ON} + \pi) \le \theta < (\theta_{ON} + \pi + \delta\theta)\right] \& T_{cmd} < 0 \\ 0, & \text{otherwise} \end{cases} \tag{38}$$

where the conduction angles are offset by 180° electrical (π radians) when negative torque is desired. This allows a phase to conduct during the region where $\frac{dL}{d\theta} < 0$. An even more flexible approach, which results in a wider operating range for the SRM, allows the turn-on and dwell angles to vary. For example, Equation (38) is extended to allow θ_{ON} and $\delta\theta$, to be functions of velocity, desired torque, and the DC bus voltage.

Often, for minimizing torque ripple, the commutation is designed such that two phases conduct simultaneously and share the job of producing the desired SRM torque. In this case, Equation (38) is further extended to a function of the form,

$$g(\theta, T_{cmd}) = \begin{cases} \rho(\theta), & \left[\theta_{ON} \le \theta < (\theta_{ON} + \delta\theta)\right] \,\&\, T_{cmd} > 0 \\ \rho(\theta), & \left[\begin{array}{l}(\theta_{ON} + \pi) \le \theta \\ \theta < (\theta_{ON} + \pi + \delta\theta)\end{array}\right] \,\&\, T_{cmd} < 0 \\ 0, & \text{otherwise} \end{cases} \tag{39}$$

where $\rho(\theta)$ is the sharing function. Sharing functions are not implemented in this application report, however, further information on the choice of sharing functions can be found in a publication by Kjaer, *et al.* [9] Essentially commutation schemes of the form in Equation (39) use knowledge of the motor characteristics to design a non-linear function, $\rho(\theta)$, that produces a linear output torque.

In this example, the commutation coefficients, $g(\ )$, were calculated using Equation (38), where $\theta_{ON} = \pi/6 + \theta_{adv}$ (radians), $\delta\theta = \pi/3$ (radians), and the advance angle, θ_{adv}, is given by Equation (21). This yields a single-quadrant, fixed-dwell, variable turn-on commutation algorithm. This algorithm is implemented as follows:

```
int phase;
WORD electricalAngle;
WORD angle;
int channel;
long advance;

/*----------------------------*/
/* Advance angle calculation */
/*----------------------------*/
advance = (anSRM->wEst_10xrpm * anSRM->desiredTorque);
advance = advance >> 9;

/*-----------------------------------------------------------*/
/* Offset for advance angle negative torque, if required */
/*-----------------------------------------------------------*/
if (anSRM->desiredTorque > 0) {
       electricalAngle = anSRM->position + (int) advance;
}
else {
       electricalAngle = anSRM->position + PI_16 - (int) advance;
}
```

9 P. C. Kjaer, J. Gribble, and T. J. E. Miller, pp. 1585–1593.

```
for (phase=0; phase< NUMBER_OF_PHASES; phase++) {

       /*------------------------------*/
       /* 120 degree offsets for phase */
       /*------------------------------*/
       angle = electricalAngle – phase * TWOPIBYTHREE_16;
       /*--------------------------------------------------------*/
       /* turn phase on, if between desired angles and switch       */
       /* the mux on the A/D to measure the desired     */
       /* phase current                                 */
       /*--------------------------------------------------------*/
       if ( (angle >= (PIBYSIX_16)) && (angle < (FIVEPIBYSIX_16)) ) {
       anSRM–>active[phase] = 1;
       channel = anSRM–>a2d_chan[phase];
       switch_mux(channel,channel+8);
       }
       else {
       anSRM–>active[phase] = 0;
       }
       }
}
```

As seen in the code above, the advance angle calculation (which yields an advance angle in units of bits, 65535 bits = 360 electrical degrees) is computed according to the equation,

$$\theta_{adv}\,(\text{bits}) = \frac{i_{cmd}\,(\text{bits}) \times \hat{\omega}(\text{rpm} \times 10)}{K}, \quad K = 2^9 = 512 \tag{40}$$

From Equation (21) and Equation (40), we can show that the calculation for K which includes L_{min}, V_{dc}, and accounts for units is given by

$$\frac{1}{K} = L_u\,(\text{H}) \times \frac{1}{V_{\text{bus}}\,(\text{V})} \times \frac{(\text{rpm} \times 10)}{10} \times \frac{1\ (\text{A})}{239.4\ (\text{bits})} \times \frac{1\ (\text{min})}{60\ (\text{sec})} \times \frac{360^{o}\ (\text{m})}{(\text{rev})} \times \frac{8^{o}\ (\text{e})}{1^{o}\ (\text{m})} \times \frac{65535\ (\text{bits})}{360^{o}\ (\text{e})} \tag{41}$$

With L_u and V_{bus} given by Table 1, K = 776.25. However, the value of 512 was used because dividing by multiples of 2 is readily accomplished using simple shift instructions. For our application, this simplification provided satisfactory results.

4.2.7 Velocity Controller

Speed is regulated in a closed-loop manner by comparing the desired shaft velocity to the estimated shaft velocity and then compensating the error. We use a PI (proportional plus integral) control action for the velocity loop compensation, so that the steady-state velocity error is zero. The PI coefficients are determined using linear analysis.

Figure 20 shows a simplified model of the velocity loop, where the coefficient, γ, having units of (rad/s)/A, is a non-linear quantity, including the shaft/load inertia and the instantaneous torque constant of the SRM.

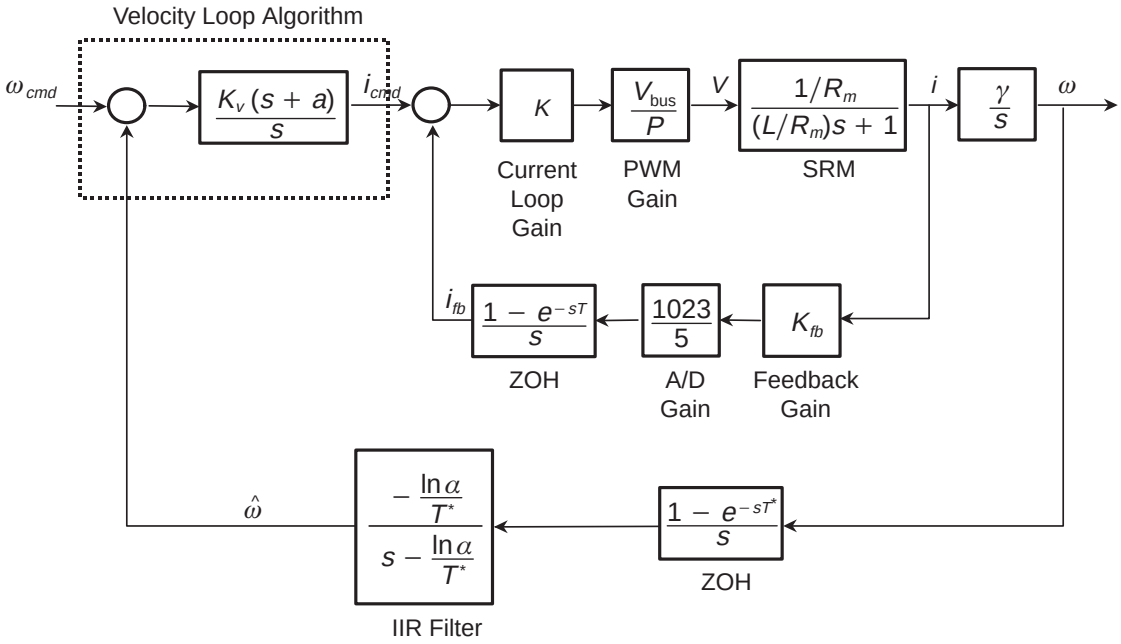

Figure 20. Simplified Block Diagram of SRM Velocity Loop Using PI Control

In the figure, K_V controls the loop gain and '*a*' is the radian frequency of the PI zero.

The non-linearity in γ is due to the non-linear torque/current relationship of the SRM where for non-saturating conditions is given by Equation (18) and, in general, by Equation (15). Thus, the open-loop gain of the velocity loop will vary, approximately, as current squared. This variation can be significant over the operating range of the SRM. From 4 A to 1 A, for example, the gain variation is 16, or 24 dB. Depending on the application, this gain variation may need to be compensated, with a square root law, for example, to stabilize the loop. In this example, the loop compensation was design with sufficient margin, at the expense of dynamic response, so that this variation can be ignored. The IIR filter used for smoothing the velocity estimate, has a *z*-transform given by,

$$H(z) = \frac{(1-\alpha)z}{z-\alpha} \tag{42}$$

and is modeled in the Laplace domain as shown in Figure 20.

Another interesting feature of this speed loop is that although the velocity loop update rate is a fixed-frequency of 1 kHz, the feedback (provided by the opto-coupler edges) occurs at a variable rate which is a function of rotor speed and given by,

$$f_{samp}\,(\text{Hz}) = 0.8 \times (\text{speed in rpm}) = \frac{1}{T^*} \tag{43}$$

This behavior generates a variable time delay in the velocity loop, due to the zero-order hold, and also makes the dynamics of the IIR filter time-varying.

Using the information in Table 1 and Figure 20, it is possible to obtain the open-loop frequency response, $\frac{\hat{\omega}}{\omega_{cmd}}$ (see Figure 21) for the velocity loop, independent of γ.

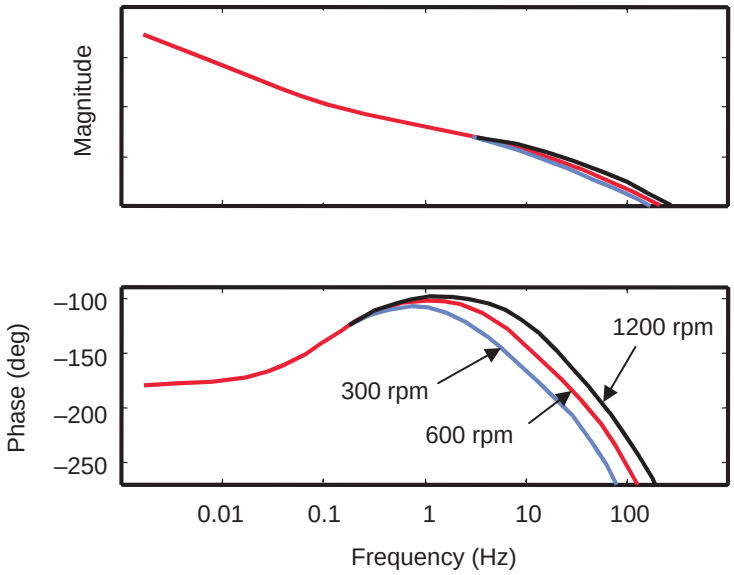

Figure 21. Open-Loop Frequency Response of the SRM Velocity Loop at Several Motor Speeds, for *a* = 0.73 rad/s

The phase loss due to the variable time delay as a function of rotor speed is apparent.

The absolute magnitude as a function of frequency is unknown; however, the shape of the magnitude and the phase are correct. From Figure 21, clearly the desired open-loop crossover frequency is in the 1–4 Hz range for this particular loop. By moving the PI zero, *a*, beyond 0.73 rad/s, the bandwidth can be extended, while trading off stability margins. If the load inertia and motor torque constant information are known (i.e., γ known), then K_V can be determined analytically; otherwise, the velocity loop gain is set experimentally.

The PI algorithm is implemented as:

```
/*------------------------------*/
/* calculate error signal      */
/*------------------------------*/
speed_error = anSRM->wDes_10xrpm - anSRM->wEst_10xrpm;

/*------------------------------*/
/* integrate error*/
/*------------------------------*/
anSRM->integral_speed_error = anSRM->integral_speed_error +
(long)speed_error;

/*------------------------------*/
/* apply integrator limit      */
/*------------------------------*/
if (anSRM->integral_speed_error > INTEGRAL_LIMIT) {
      anSRM->integral_speed_error = INTEGRAL_LIMIT;
}
if (anSRM->integral_speed_error < -INTEGRAL_LIMIT) {
      anSRM->integral_speed_error = -INTEGRAL_LIMIT;
}

/*------------------------------*/
/* PI filter*/
/*------------------------------*/
integral_error = (int) ((KI*anSRM->integral_speed_error) >> 13);
anSRM->desiredTorque = ((KP*speed_error) >> 1) + integral_error;
```

This implements a PI compensator, with integrator limits, of the form,

$$K_P + \frac{K_I}{s} = \frac{K_V(s+z)}{s} \Rightarrow \begin{cases} K_p = K_V \\ K_I = K_V \times z \end{cases} \tag{44}$$

Through experimentation, it was determined that $K_V = 0.5$, provided satisfactory performance. In the software implementation of the integrator, the multiplication by Δt is not performed. Thus, this factor is carried implicitly in K_I. For $z = 0.73$ rad/s and $\Delta t = 1/1000$ sec, $K_I = 0.365$. This is approximately implemented by setting KI = 3 (scaled Q13 $\times$ 1000) in the file CONSTANT.H.

The integrator limit value is calculated such that the condition is, $\frac{\text{KI} \times \text{INTEGRAL\_LIMIT}}{2^{12}} \leq 1000.$

5 References

Anderson, B. and J. Moore, *Optimal Filtering*, Prentice-Hall Publishing, Englewood Cliffs, NJ, 1979.

Becerra, R., M. Ehsani, and T. J. E. Miller, “Commutation of SR Motors,” *IEEE Trans. Power Electronics*, Vol. 8, pp. 257–262, July 1993.

Clemente, S. and A. Dubhashi, “HV Floating MOS-Gate Driver IC,” *International Rectifier application note AN–978A*, International Rectifier, El Segundo, CA, 1990.

Husain, I. and M. Ehsani, ” Torque Ripple Minimization in Switched Reluctance Motor Drives by PWM Current Control,” *Proc. APEC’94*, 1994.

Ilic–Spong, M., T. J. E. Miller, S. R. MacMinn, and J. S. Thorp, “Instantaneous Torque Control of Electric Motor Drives,” *IEEE Trans. Power Electronics*, Vol. 2, Jan. 1987.

Kjaer, P. C., J. Gribble, and T. J. E. Miller, “High-Grade Control of Switched Reluctance Machines,” *IEEE Trans. Industry Electronics*, vol. 33, Nov. 1997.

Lewis, F. *Applied Optimal Control & Estimation*, Prentice Hall Publishing, Englewood Cliffs, NJ, 1992.

Lyons, J., S. MacMinn, and M. Preston, “Flux/Current Methods for SRM Rotor Position Estimation,” *IEEE IAS Annual Meeting Conf. Record,* 1991.

Miller , T. J. E. (ed.), “Switched Reluctance Motor Drives,” Intertec Communications Inc., Ventura, CA, 1988.

Miller, T. J. E., “Switched Reluctance Motors and Their Control,” Magna Physics Publishing, Hillsboro, OH, and Oxford, 1993.

Ray, W. F. and I. H. Al-Bahadly, “Sensorless Methods for Determining the Rotor Position of Switched Reluctance Motors,” *Proc. EPE Conf.*, Vol. 6, 1993.

Vukosavic, S. and V. Stfanovic, “SRM Inverter Topologies: A Comparative Evaluation,” *IEEE IAS Annual Meeting Conf. Record*, 1990.

Appendix A Software Listings for a TMS320F240-Based SRM Drive With Position Sensor

This appendix contains the software to implement an SRM drive using a slotted disk type position sensor for a TMS320F240 DSP.

File	Major Modules	Description
TYPEDEFS.H		header file – data type definitions
C240.H		header file – C240 register definitions
CONSTANT.H		header file – SRM constant defintions
SRM.H		header file – SRM variable declarations
MAIN.C	main( )	supervisory program
	c_int3( )	timer ISR
	c_int4( )	capture ISR
SRM.C	Time_Update_Position( )	time update algorithm for position estimation
	Msmt_Update_Position( )	measurement update algorithm for position estimation
	Msmt_Update_Velocity( )	velocity estimation algorithm
	Commutation_Algorithm( )	SRM fixed-dwell, variable turn-on commutation algorithm
	velocityController( )	shaft velocity loop compensation algorithm
	currentController( )	phase current loop compensation algorithm
EVMGR.C		modules for event manager initialization and operating the event manager peripherials
VECTORS.ASM		interrupt vectors
LINK.CMD		linker command file

```
/*********************************************************
*   File: TYPEDEFS.H                                     *
*   TMS320x240 Test Bed Code                             *
*   Texas Instruments, Inc.                              *
*   Copyright (c) 1996 Texas Instruments Inc.            *
*   11/05/96   Version 1.0                               *
*   Jeff Crankshaw                                       *
*********************************************************/
#ifndef TYPEDEFS_H
#define TYPEDEFS_H

#define FALSE 0
#define TRUE  1

typedef unsigned int   WORD;          /* 16-bit data */
typedef unsigned long  DWORD;         /* 32-bit data */
typedef volatile WORD * PORT;

#define STR(x) #x

#define OUTMAC(address,data)  \
 asm("        LDPK    _"STR(data));  \
 asm("        OUT     _"STR(data) "," STR(address))

#define INMAC(address,data)   \
 asm("        LDPK    _"STR(data));  \
 asm("        IN      _"STR(data) "," STR(address))

#define Int_Read(addr)         * (int *) (addr)
#define Int_Write(addr,data)   * (int *) (addr) = (data)

#endif  /* _TYPEDEFS */



/*********************************************************
*   File: C240.H                                         *
*   TMS320x240 Test Bed Code                             *
*   Texas Instruments, Inc.                              *
*   Copyright (c) 1996 Texas Instruments Inc.            *
*   11/05/96   Version 1.0                               *
*   Jeff Crankshaw                                       *
*                                                        *
*   TMS320C240 Peripheral Register Addresses             *
*                                                        *
*********************************************************/
#ifndef c240_h
#define c240_h

#include "typedefs.h"

/*-----------------------------------------------------------*/
/* definitions of I/O space macros                           */
/*-----------------------------------------------------------*/
#define STR(x) #x

#define OUTMAC(address,data)  \
 asm("        LDPK    _"STR(data));  \
 asm("        OUT     _"STR(data) "," STR(address))

#define INMAC(address,data)   \
 asm("        LDPK    _"STR(data));  \
 asm("        IN      _"STR(data) "," STR(address))

#define LED_LOC 000ch  /* F240 EVM I/O space location for LEDs */
```

```
/*-----------------------------------------------------------*/
/* definitions of CPU core registers                         */
/*-----------------------------------------------------------*/
#define IMR_REG        (( PORT )0x0004 )
#define IFR_REG        (( PORT )0x0006 )

/*-----------------------------------------------------------*/
/* External Memory Interface Registers                       */
/*-----------------------------------------------------------*/
#define WSGR        0x0ffff
/* Wait State Generator Register                             */

/*-----------------------------------------------------------*/
/* System Module Registers                                   */
/*-----------------------------------------------------------*/
#define SYSCR         (( PORT )0x07018)      /* System Module Control Register */
#define SYSSR         (( PORT )0x0701A)      /* System Module Status Register */
#define SYSIVR        (( PORT )0x0701E)      /* System Interrupt Vector Register */
#define XINT1_CR      (( PORT )0x07070)      /* Int1 (type A) Control reg */
#define NMI_CR        (( PORT )0x07072)      /* Non maskable Int (type A) Control reg */
#define XINT2_CR      (( PORT )0x07078)      /* Int2 (type C) Control reg */
#define XINT3_CR      (( PORT )0x0707A)      /* Int3 (type C) Control reg */
#define PDPINT_CR     (( PORT )0x0742C)      /* Power Drive Protection Int cntl reg */

/* System Interrupt Vector Register – Address offsets */
#define PHANTOM_INT_VECTOR    0x00
#define NMI_INT_VECTOR        0x02
#define XINT1_INT_VECTOR      0x01
#define XINT2_INT_VECTOR      0x11
#define XINT3_INT_VECTOR      0x1f
#define SPI_INT_VECTOR        0x05
#define SCI_RX_INT_VECTOR     0x06
#define SCI_TX_INT_VECTOR     0x07
#define RTI_INT_VECTOR        0x10
#define PDP_INT_VECTOR        0x20
#define EV_CMP1_INT_VECTOR    0x21
#define EV_CMP2_INT_VECTOR    0x22
#define EV_CMP3_INT_VECTOR    0x23
#define EV_SCMP1_INT_VECTOR   0x24
#define EV_SCMP2_INT_VECTOR   0x25
#define EV_SCMP3_INT_VECTOR   0x26
#define EV_T1PER_INT_VECTOR   0x27
#define EV_T1CMP_INT_VECTOR   0x28
#define EV_T1UF_INT_VECTOR    0x29
#define EV_T1OF_INT_VECTOR    0x2a
#define EV_T2PER_INT_VECTOR   0x2b
#define EV_T2CMP_INT_VECTOR   0x2c
#define EV_T2UF_INT_VECTOR    0x2d
#define EV_T2OF_INT_VECTOR    0x2e
#define EV_T3PER_INT_VECTOR   0x2f
#define EV_T3CMP_INT_VECTOR   0x30
#define EV_T3UF_INT_VECTOR    0x31
#define EV_T3OF_INT_VECTOR    0x32
#define EV_CAP1_INT_VECTOR    0x33
#define EV_CAP2_INT_VECTOR    0x34
#define EV_CAP3_INT_VECTOR    0x35
#define EV_CAP4_INT_VECTOR    0x36
#define AC2_INT_VECTOR        0x04
```

```
/*-------------------------------------------------------------*/
/* Digital I/O  Registers                                      */
/*-------------------------------------------------------------*/
#define OCRA          (( PORT )0x07090)     /* Output Control Reg A */
#define OCRB          (( PORT )0x07092)     /* Output Control Reg B */
#define PADATDIR      (( PORT )0x07098)     /* I/O port A Data & Direction reg. */
#define PBDATDIR      (( PORT )0x0709A)     /* I/O port B Data & Direction reg. */
#define PCDATDIR      (( PORT )0x0709C)     /* I/O port C Data & Direction reg. */


/*-------------------------------------------------------------------------*/
/* Watch-Dog(WD) / Real Time Int(RTI) / Phase Lock Loop(PLL) Registers     */
/*-------------------------------------------------------------------------*/
#define RTICNTR       (( PORT )0x07021)     /* RTI Counter reg */
#define WDTCNTR       (( PORT )0x07023)     /* WD Counter reg  */
#define WDTKEY        (( PORT )0x07025)     /* WD Key reg */
#define RTICR         (( PORT )0x07027)     /* RTI Control reg */
#define WDCR          (( PORT )0x07029)     /* WD Control reg */
#define CKCR0         (( PORT )0x0702B)     /* PLL control reg 1 */
#define CKCR1         (( PORT )0x0702D)     /* PLL control reg 2 */

/*-------------------------------------------------------------*/
/* Analog-to-Digital Converter(ADC) registers                  */
/*-------------------------------------------------------------*/
#define ADCTRL1       (( PORT )0x07032)     /* ADC Control & Status reg */
#define ADCTRL2       (( PORT )0x07034)     /* ADC Configuration reg */
#define ADCFIFO1      (( PORT )0x07036)     /* ADC Channel 1 Result Data */
#define ADCFIFO2      (( PORT )0x07038)     /* ADC Channel 2 Result Data */

/*-------------------------------------------------------------*/
/* Serial Peripheral Interface (SPI) Registers                 */
/*-------------------------------------------------------------*/
#define SPICCR        (( PORT )0x07040)       /* SPI Config Control Reg */
#define SPICTL        (( PORT )0x07041)       /* SPI Operation Control Reg */
#define SPISTS        (( PORT )0x07042)       /* SPI Status Reg */
#define SPIBRR        (( PORT )0x07044)       /* SPI Baud rate control reg */
#define SPIEMU        (( PORT )0x07046)       /* SPI Emulation buffer reg */
#define SPIBUF        (( PORT )0x07047)       /* SPI Serial Input buffer reg */
#define SPIDAT        (( PORT )0x07049)       /* SPI Serial Data reg */
#define SPIPC1        (( PORT )0x0704D)       /* SPI Port control reg1 */
#define SPIPC2        (( PORT )0x0704E)       /* SPI Port control reg2 */
#define SPIPRI        (( PORT )0x0704F)       /* SPI Priority control reg */

/*-------------------------------------------------------------*/
/* Serial Communications Interface (SCI) Registers            */
/*-------------------------------------------------------------*/
#define SCICCR        (( PORT )0x07050)       /* SCI Comms Control Reg */
#define SCICTL1       (( PORT )0x07051)       /* SCI Control Reg 1 */
#define SCIHBAUD      (( PORT )0x07052)       /* SCI Baud rate control */
#define SCILBAUD      (( PORT )0x07053)       /* SCI Baud rate control */
#define SCICTL2       (( PORT )0x07054)       /* SCI Control Reg 2 */
#define SCIRXST       (( PORT )0x07055)       /* SCI Receive status reg */
#define SCIRXEMU      (( PORT )0x07056)       /* SCI EMU data buffer */
#define SCIRXBUF      (( PORT )0x07057)       /* SCI Receive data buffer */
#define SCITXBUF      (( PORT )0x07059)       /* SCI Transmit data buffer */
#define SCIPC1        (( PORT )0x0705D)       /* SCI Port control reg1 */
#define SCIPC2        (( PORT )0x0705E)       /* SCI Port control reg2 */
#define SCIPRI        (( PORT )0x0705F)       /* SCI Priority control reg */
```

```
/*-------------------------------------------------------*/
/* Event Manager (EV) Registers                          */
/*-------------------------------------------------------*/
#define GPTCON        (( PORT )0x07400)     /* General Timer Controls */
#define T1CNT         (( PORT )0x07401)     /* T1 Counter Register */
#define T1CMP         (( PORT )0x07402)     /* T1 Compare Register */
#define T1PER         (( PORT )0x07403)     /* T1 Period Register */
#define T1CON         (( PORT )0x07404)     /* T1 Control Register */
#define T2CNT         (( PORT )0x07405)     /* T2 Counter Register */
#define T2CMP         (( PORT )0x07406)     /* T2 Compare Register */
#define T2PER         (( PORT )0x07407)     /* T2 Period Register */
#define T2CON         (( PORT )0x07408)     /* T2 Control Register */
#define T3CNT         (( PORT )0x07409)     /* T3 Counter Register */
#define T3CMP         (( PORT )0x0740a)     /* T3 Compare Register */
#define T3PER         (( PORT )0x0740b)     /* T3 Period Register */
#define T3CON         (( PORT )0x0740c)     /* T3 Control Register */
#define COMCON        (( PORT )0x07411)     /* Compare Unit Control */
#define ACTR          (( PORT )0x07413)     /* Full Compare Unit Output Action Ctrl */
#define SACTR         (( PORT )0x07414)     /* Simple Comp Unit Output Action Ctrl */
#define DBTCON        (( PORT )0x07415)     /* Dead Band Timer Control */
#define CMPR1         (( PORT )0x07417)     /* Full Compare Channel 1 Threshold */
#define CMPR2         (( PORT )0x07418)     /* Full Compare Channel 2 Threshold */
#define CMPR3         (( PORT )0x07419)     /* Full Compare Channel 3 Threshold */
#define SCMPR1        (( PORT )0x0741a)     /* Simple Comp Channel 1 Threshold */
#define SCMPR2        (( PORT )0x0741b)     /* Simple Comp Channel 2 Threshold */
#define SCMPR3        (( PORT )0x0741c)     /* Simple Comp Channel 3 Threshold */
#define CAPCON        (( PORT )0x07420)     /* Capture Unit Control */
#define CAPFIFO       (( PORT )0x07422)     /* FIFO1–4 Status Register */
#define FIFO1         (( PORT )0x07423)     /* Capture Channel 1 FIFO Top */
#define FIFO2         (( PORT )0x07424)     /* Capture Channel 2 FIFO Top */
#define FIFO3         (( PORT )0x07425)     /* Capture Channel 3 FIFO Top */
#define FIFO4         (( PORT )0x07426)     /* Capture Channel 4 FIFO Top */
#define IMRA          (( PORT )0x0742c)     /* Group A Interrupt Mask Register */
#define IMRB          (( PORT )0x0742d)     /* Group B Interrupt Mask Register */
#define IMRC          (( PORT )0x0742e)     /* Group C Interrupt Mask Register */
#define IFRA          (( PORT )0x0742f)     /* Group A Interrupt Flag Register */
#define IFRB          (( PORT )0x07430)     /* Group B Interrupt Flag Register */
#define IFRC          (( PORT )0x07431)     /* Group C Interrupt Flag Register */
#define IVRA          (( PORT )0x07432)     /* Group A Int. Vector Offset Register */
#define IVRB          (( PORT )0x07433)     /* Group B Int. Vector Offset Register */
#define IVRC          (( PORT )0x07434)     /* Group C Int. Vector Offset Register */

#endif


/*++++++++++++++++++++++++++++++++++++++++++++++++++++++++++++++++*/
/*                                                                */
/*File:               CONSTANT.H                                  */
/*Target Processor:   TMS320F240                                  */
/*Compiler Version:                                               */
/*Assembler Version:                                              */
/*Created:            10/1/97                                     */
/*                                                                */
/*----------------------------------------------------------------*/
/*  Constants for the SRM control algorithms                      */
/*++++++++++++++++++++++++++++++++++++++++++++++++++++++++++++++++*/
```

```
/*-----------------------------------------------*/
/* clock frequencies and time related constants */
/*-----------------------------------------------*/
#define PWM_FREQ              20000          /* PWM frequency (Hz)         */
#define SYSCLK_FREQ           20000000       /* DSP clock frequency (Hz)   */
#define CPU_INT_FREQ          5000           /* timer ISR frequency (Hz)   */
#define ONE_HALF_SECOND       (CPU_INT_FREQ/2)

/*-----------------------------------*/
/* current loop algorithm constants  */
/*-----------------------------------*/
#define ILOOP_GAIN            22             /* current loop gain:                */
                                             /*     (Q3: gain = 2.75)             */
#define ILIMIT                1023           /* current limit: (1023 bits =       */
                                             /*   5 V x 0.855 A/V = 4.273 A)      */
#define MAXIMUM_DUTYRATIO     999            /* limit on the PWM duty cycle:      */
                                             /*   100 % =                         */
                                             /*   (SYSCLK_FREQ/PWM_FREQ – 1)      */

/*-------------------------------------------*/
/* velocity loop algorithm constants         */
/*-------------------------------------------*/
#define INTEGRAL_LIMIT        2793472        /* integrator limit                  */
#define KI                    3              /* (Q13*1000): Ki = 0.366            */
#define KP                    1              /* Q1: Kp = 0.5                      */


/*-----------------------------------------------------------*/
/* position & velocity estimation algorithm constants       */
/*-----------------------------------------------------------*/
#define K_POSITION_EST        1432
#define K1_VELOCITY_EST       281250000
#define K2_VELOCITY_EST       62500
#define ALPHA                 7              /* Q3: alpha = 0.875                 */
#define ONE_MINUS_ALPHA       1              /* Q3: 1–alpha = 0.125               */

/*-------------------------------------------*/
/* motor geometry related                    */
/*-------------------------------------------*/
#define NR                    8              /* number of rotor poles             */
#define NUMBER_OF_PHASES      3

/*-------------------------------------------------*/
/* Electrical Angles: 2*pi (rad) = 65535            */
/*-------------------------------------------------*/
#define PIBYSIX_16            5461
#define PIBYFOUR_16           8192
#define PIBYTHREE_16          10923
#define TWOPIBYTHREE_16       21845
#define THREEPIBYFOUR_16      24576
#define FIVEPIBYSIX_16        27307
#define PI_16                 32768
#define FOURPIBYTHREE_16      43690
#define FIVEPIBYTHREE_16      54613
#define TWOPI_16              65535

/*++++++++++++++++++++++++++++++++++++++++++++++++++++++++++++++++++*/
/*                                                                  */
/*File:               SRM.H                                        */
/*Target Processor:   TMS320F240                                   */
/*Compiler Version:                                                */
/*Assembler Version:                                               */
/*Created:            10/1/97                                      */
/*                                                                 */
/*------------------------------------------------------------------*/
/*  Variable declarations for the SRM control algorithm            */
/*++++++++++++++++++++++++++++++++++++++++++++++++++++++++++++++++++*/

#include ”constant.h”
```

```
#include ”typedefs.h”

/*------------------------------------------------------------*/
/* position estimation state machine data structure         */
/*------------------------------------------------------------*/
typedef struct {
  int   state;
  WORD  position;
  int   direction;
} state_machine;

/*-------------------------------------------------------------------------------------*/
/* SRM variables data structure:                                                       */
/*-------------------------------------------------------------------------------------*/
/*a2d_chan[i]  –> sets which A/D pin is used for the ith phase current
/*desiredTorque       –> torque command (output of velocity loop)
/*integral_speed_error –> velocity loop integrator for PI compensator
/*iDes[i]             –> current command for the ith phase
/*capture_edge[i]     –> timer #2 count value at the occurence of
/*             the most recent ith capture
/*capture_delta[i][2] –> change in the timer #2 count value between
/*             the occurences of the ith capture events.  The two most
/*             recent events are stored.
/*delta_count  –> change in the software counter of the timer ISR
/*             between occurences of any capture event.
/*wEst_10xrpm  –> shaft velocity estimate (units of rpm*10)
/*      wDes_10xrpm    –> desired shaft velocity (units of rpm*10)
/*      active[i]      –> flag indicating whether the ith phase is ON (1 = on)
/*      iFB[i]         –> current feedback measurement for the ith phase
/*      dutyRatio[i]   –> commanded % duty ratio for the high–side FET of
/*             the ith phase
/*position     –> shaft position estimate (electrical degrees)
/*             scaled: 2*pi (rad) = 65535 bits
/*position_state      –> position state of the SRM (defined by opto–couplers)
/*shaft_direction     –> direction which the shaft is rotating.
/*trans_lut[7][4]     –> the position state machine
/*position_initial_guess[7] –> initial position guess, based on state
/*dp_remainder –> 16–bit remainder used in the position estimation alg
/*last_capture –> the most recent capture to occur
/*-------------------------------------------------------------------------------------*/
typedef struct  {
  int          a2d_chan[NUMBER_OF_PHASES];
  int          desiredTorque;
  long         integral_speed_error;
  WORD         iDes[NUMBER_OF_PHASES];
  WORD                capture_edge[NUMBER_OF_PHASES];
  WORD                capture_delta[NUMBER_OF_PHASES][2];
  WORD         delta_count;
  int                 wEst_10xrpm;
  int          wDes_10xrpm;
  int          active[NUMBER_OF_PHASES];
  WORD         iFB[NUMBER_OF_PHASES];
  int          dutyRatio[NUMBER_OF_PHASES];
  WORD         position;
  int          position_state;
  int          shaft_direction;
  state_machine       trans_lut[7][4];
  WORD         position_initial_guess[7];
  long         dp_remainder;
  int          last_capture;
} anSRM_struct;
```

```
/*-----------------------------------------------------------------*/
/*PROTOTYPE DEFINITIONS                                            */
/*-----------------------------------------------------------------*/
void eventmgr_init();
void initializeSRM(anSRM_struct *anSRM);
void Commutation_Algorithm(  anSRM_struct *anSRM);
void Time_Update_Position(anSRM_struct *anSRM);
void velocityController(  anSRM_struct *anSRM);
void currentController(  anSRM_struct *anSRM);
void computePositionAndVelocity(anSRM_struct *anSRM);
void Msmt_Update_Velocity(anSRM_struct *anSRM, int mode);
void Msmt_Update_Position(anSRM_struct *anSRM);
void switch_lowside(int phaseactive);
void switch_mux(int adc1, int adc2);
void disable_interrupts();
void dsp_setup();
void initialize_counters_and_flags();
void enable_interrupts();
void start_background();
void check_for_stall();


/*++++++++++++++++++++++++++++++++++++++++++++++++++++++++++++++++++
/*
/*File:               MAIN.C
/*Target Processor:   TMS320F240
/*Compiler Version:   6.6
/*Assembler Version:  6.6
/*Created:            10/31/97
/*
/*++++++++++++++++++++++++++++++++++++++++++++++++++++++++++++++++++
/* This file is the main program for the control of an SRM drive with a
/*position sensor
/*++++++++++++++++++++++++++++++++++++++++++++++++++++++++++++++++++*/

/*-----------------------------------------------------------------*/
/*INCLUDE FILES                                                    */
/*-----------------------------------------------------------------*/
#include ”c240.h”
#include ”srm.h”

/*---------------------------------------------------------*/
/*GLOBAL VARIABLE DECLARATIONS                              */
/*---------------------------------------------------------*/
int  count;
int  slice;
int  old_count;
int  Update_Velocity;
int  Toggle_LED;
int  Msmt_Update;
anSRM_struct SRM;
int  LEDvalue;

/*---------------------------------------------------------*/
/*MAIN PROGRAM                                              */
/*---------------------------------------------------------*/

void main() {

  disable_interrupts();
  dsp_setup();
  initializeSRM(&SRM);
  eventmgr_init();
  initialize_counters_and_flags();
  enable_interrupts();

  start_background();

}
```

```
/*+++++++++++++++++++++++++++++++++++++++++++++++++++++++++++++++ */
/*BACKGROUND TASKS                                                */
/*---------------------------------------------------------------- */
/*Upon completion of the required initialization, the main
/*program starts the background task.  The background is
/*simply an infinite loop.  Time critical motor control
/*processing is done via interrupt service routines and lower
/*priority processing is done in the background, when they
/*are needed.  Two background operations are defined:
/*
/*1) Update_Velocity – when a capture interrupt occurs,
/*      the ISR stores the capture data and then intiates
/*      this task.  The velocity update is done in
/*      background, because it is doing a floating point
/*      division.
/*2) Toggle_LED – this task toggles an LED on the EVM to
/*      provide visual feedback to the user that the code
/*      is running.  This task is initiated at a fixed
/*      rate set by the ONE_HALF_SECOND value.
/*
/*+++++++++++++++++++++++++++++++++++++++++++++++++++++++++++++++ */
void start_background()
{

  while (1)

  {
      /*-----------------------*/
      /* Velocity update task */
      /*-----------------------*/
      if (Update_Velocity) {
        if (Update_Velocity == 1) {   /* use capture data    */
                                      /*    as time base     */
           Msmt_Update_Velocity(&SRM,1);
        }
        else {    /* else shaft is rotating too slowly, capture
                  /* data may be in error by overflow.
                  /* use count of timer ISR's between captures
                  /* as time base.   */
           Msmt_Update_Velocity(&SRM,2);
        }
        Update_Velocity = 0;
      }

      /*-----------------------*/
      /* Visual feedback task  */
      /*-----------------------*/
      if (Toggle_LED) {

        LEDvalue = –LEDvalue;
        if (LEDvalue == 1) {
               asm("   OUT  1, 000ch");
        }
        else {
               asm("   OUT  0, 000ch");
        }
        Toggle_LED = 0;
        SRM.wDes_10xrpm = 6000;       /* motor speed command units = (rpm x 10)    */
                                      /*    just hard–coded here, but setup        */
                                      /*    another background task to allow       */
                                      /*    command from an external input         */
      }

  }  /* infinite loop */

}
/*+++++++++++++++++++++++++++++++++++++++++++++++++++++++++++++++++*/
/*TIMER ISR                                                        */
/*-----------------------------------------------------------------*/
```

```
/*
/*This interrupt service routine is executed at each
/*occurence of the maskable CPU interrupt INT3.  This CPU
/*interrupt corresponds to the event manager group B interrupts,
/*of which we enable only the timer #3 period interrupt, TPINT3.
/*The frequency, F, at which this routine is executed is specified
/*using the CPU_INT_FREQ parameter.
/*
/*The SRM control algorithms which are implemented during the
/*timer ISR are:
/*
/*      1.  Current control (frequency = F)
/*      2.  Rotor position estimation (frequency = F)
/*      3.  Commutation (frequency = F/5)
/*      4.  Velocity control (frequency = F/5)
/*
/*Additionally, time can be measured (coarsely) by counting
/*the number of executions of this ISR, which runs at a
/*known fixed rate.  This measure of time is used for several
/*reasons, including:
/*
/*- For precaution against over-current, a simple
/*test is made to determine if the rotor has stalled.
/*
/*- Also, the visual feedback task is initiated if the correct
/*amount of time has elapsed.
/*
/*+++++++++++++++++++++++++++++++++++++++++++++++++++++++++++++++++++++++*/
void c_int3()
{

  *IFR_REG = 0x0004;                /* clear interrupt flags             */
  *IFRB = 0xff;

  currentController(&SRM);          /* current loop algorithm            */

  if (Msmt_Update) {                /* position estimation               */
     Msmt_Update_Position(&SRM);    /*      if recent capture edge       */
     Msmt_Update = 0;               /*      use this information         */
  }
  else {                            /*      else, propagate pos est      */
     Time_Update_Position(&SRM);    /*      using algorithm              */
  }

  check_for_stall();

  count = count + 1;                /* increment count                   */
  slice = slice + 1;                /* increment slicer                  */

  if (slice == 1) {
     Commutation_Algorithm(&SRM);   /* do commutation in the 1st         */
  }                                 /*      slice.                       */
  else if (slice == 2) {            /* velocity loop algorithm in        */
     velocityController(&SRM);      /*      the 2nd                      */
  }
  else if (slice == 5) {
     slice = 0;                     /* reset slicer                      */
  }

  if (count == ONE_HALF_SECOND) {   /* set flag for toggling the         */
     Toggle_LED = 1;                /*      EVM LED, if time             */
     count = 0;
  }

}

/*+++++++++++++++++++++++++++++++++++++++++++++++++++++++++++++++++++++++ */
/*CAPTURE ISR                                                            */
/*---------------------------------------------------------------------- */
```

```
/*
/*This interrupt service routine is executed at each
/*occurence of the maskable CPU interrupt INT4.  This CPU
/*interrupt corresponds to the event manager group C interrupts,
/*of which we enable the three capture event interrupts,
/*CAPINT1–3.  This ISR executes asynchronously and the
/*frequency of execution is dependent on the shaft speed
/*of the SRM.
/*
/*The ISR performs the following processing:
/*
/*      clear interrupt flags;
/*      determine which capture has occured;
/*      read the appropriate capture FIFO register;
/*      store capture data;
/*      set flag for position update using measurement;
/*      set flag for initiating velocity estimate
/*             update in background;
/*      return;
/*
/*+++++++++++++++++++++++++++++++++++++++++++++++++++++++++++++++++*/
void c_int4()
{
  int groupc_flags;
  int capture;
  int n;
  int delta_count;
  WORD edge_time;

  *IFR_REG = 0x0008;          /* clear CPU interrupt flag   */

  /*-------------------------------------------------------*/
  /* determine which capture interrupt occured and read    */
  /*    the appropriate FIFO                               */
  /*-------------------------------------------------------*/
  groupc_flags = *IFRC;              /* read event manger interrupt */
                                     /*      flag register          */

  if (groupc_flags & 0x1){           /* capture #1                  */
     *IFRC = 0xf9;                   /*      clear flag register    */
     capture = 1;                    /*                             */
     edge_time = read_fifo(capture); /*      read FIFO              */
  }
  else if (groupc_flags & 0x2) {     /* capture #2                  */
     *IFRC = 0xfa;
     capture = 2;
     edge_time = read_fifo(capture);
  }
  else if (groupc_flags & 0x4) {     /* capture #3                  */
     *IFRC = 0xfc;
     capture = 3;
     edge_time = read_fifo(capture);
  }
  else {                             /* not a valid capture         */
     *IFRC = 0xff;
     capture = 0;
  }

  /*-------------------------------------------------------------*/
  /* if a valid capture occured, store capture data and set flags  */
  /*    foor position and velocity estimate updates.  The most     */
  /*    recent two time intervals between edges is saved           */
  /*    to allow for some filtering of the velocity estimate.      */
  /*    The number of timer ISR's which occur between capture      */
  /*    interrupts is also checked.  When this time exceeds a      */
  /*    certain value, then the capture data could be in error     */
  /*    by an overflow, so the lower resolution delta–time         */
  /*    associated with the ISR count is used in the velocity      */
  /*    estimate calculation.                                      */
```

```
  /*-------------------------------------------------------------*/
  if (capture > 0) {

     SRM.last_capture = capture;     /* save capture data          */
     n = capture-1;
     SRM.capture_delta[n][1] = SRM.capture_delta[n][0];
     SRM.capture_delta[n][0] = edge_time - SRM.capture_edge[n];
     SRM.capture_edge[n] = edge_time;

     Msmt_Update = 1;                /* position update flag       */

     /*-------------------------------------------------------------*/
     /* Set flags & select time base for use with velocity update */
     /*-------------------------------------------------------------*/
     delta_count = count - old_count;
     old_count = count;
     if (delta_count < 0) delta_count = delta_count + ONE_HALF_SECOND;

     if (delta_count > 100) {        /* low shaft speed use        */
                                     /*      ISR counter           */
       SRM.delta_count = delta_count;
       Update_Velocity = 2;
     }

     else {                          /* else, shaft speed ok       */
                                     /*      use 1.25MHz clk       */
       SRM.delta_count = delta_count;
       Update_Velocity = 1;
     }
  }

}

/*+++++++++++++++++++++++++++++++++++++++++++++++++++++++++++++++++*/
/*UTILITY SUBROUTINES                                              */
/*+++++++++++++++++++++++++++++++++++++++++++++++++++++++++++++++++*/


/*****************************************************************/
void disable_interrupts()
{
  asm(" SETC    INTM");
}


*****************************************************************/
void dsp_setup() {

  int temp;

  /*-------------------------*/
  /* Disable watchdog timer */
  /*-------------------------*/
  temp = *WDCR;
  temp = temp | 0x68;
  *WDCR = temp;
```

```
  /*--------------------------------------*/
  /* initialize PLL module (10 MHz XTAL1) */
  /*--------------------------------------*/
  *CKCR1 = 0xb1;              /* 20MHz CPUCLK = 10MHz crystal      */
                              /*       and 2x PLL mult ratio       */
  *CKCR0 = 0xc3;              /* low-power mode 0,                 */
                              /*      ACLK enabled,                */
                              /*      PLL enabled,                 */
                              /*      SYSCLK=CPUCLK/2              */
  *SYSCR = 0x40c0;

}

/*************************************************************************/
void initialize_counters_and_flags() {

  count = 0;                  /* current timer ISR count    */
  slice = 0;                  /* ISR slice count            */
  old_count = 0;              /* timer ISR count at last    */
                              /*      capture edge          */
  Toggle_LED = 0;             /* flag for visual feedback   */
                              /*      background task       */
  LEDvalue = 1;               /* current LED value          */
  Update_Velocity = 0;        /* flag for velocity update   */
                              /*      background task       */
  Msmt_Update = 0;            /* flag for mode of position  */
                              /*      estimate update       */

}

/*************************************************************************/
void enable_interrupts() {

  *IFR_REG = 0xffff;          /* Clear pending interrupts   */
  *IFRA = 0xffff;
  *IFRB = 0xffff;
  *IFRC = 0xffff;
  *IMR_REG = 0x000c;          /* Enable CPU Interrupts:     */
                              /*      INT4 & INT3           */
  *IMRA = 0x0000;             /* Disable all event manager  */
                              /*      Group A interrupts    */
  *IMRB = 0x0010;             /* Enable timer 3 period      */
                              /*      interrupt             */
  *IMRC = 0x0007;             /* Enable CAP1-CAP3 interrupts*/
  asm(" CLRC    INTM");       /* Global interrupt enable    */

}

/*************************************************************************/
void check_for_stall()
{
  int delta_count;

  /*-------------------------------------------------------------*/
  /*  The SRM is assumed to have stalled if the number of timer  */
  /*   ISR's which are executed exceeds 1000.  At F = 5 kHz      */
  /*   this corresponds to roughly 6 rpm.  If this condition     */
  /*   is detected, the opto-coupler levels are read and the     */
  /*   rotor position is re-initialized                          */
  /*-------------------------------------------------------------*/
  delta_count = count - old_count;
  if (delta_count < 0) delta_count = delta_count + ONE_HALF_SECOND;
  if (delta_count > 1000) {
     SRM.wEst_10xrpm = 0;
     SRM.position_state = *PBDATDIR & 0x7;
     SRM.position = SRM.position_initial_guess[SRM.position_state];
  }
```

```
}

/*++++++++++++++++++++++++++++++++++++++++++++++++++++++++++++++++++++++++*/
/*      File:                  SRM.C                                      */
/*Target Processor:    TMS320F240                                         */
/*Compiler Version:    6.6                                                */
/*Assembler Version:   6.6                                                */
/*Created:             10/31/97                                           */
/*------------------------------------------------------------------------*/
/*  This file contains the algorithms for control of anSRM using          */
/*a position sensor.  The position sensor consists of a slotted           */
/*disk and opto-couplers.                                                 */
/*++++++++++++++++++++++++++++++++++++++++++++++++++++++++++++++++++++++++*/

/*------------------------------------------------------------------------*/
/*INCLUDE FILES                                                           */
/*------------------------------------------------------------------------*/
#include "srm.h"
#include "c240.h"


/*++++++++++++++++++++++++++++++++++++++++++++++++++++++++++++++++++++++++*/
/*TIME UPDATE OF THE ROTOR POSITION ESTIMATE                              */
/*------------------------------------------------------------------------*/
/*  Between the capture events, which provide a shaft position            */
/*measurement, position is estimated according to the equation            */
/*                                                                        */
/*      theta(k) = theta(k-1) + w * delta_t;                              */
/*                                                                        */
/*where        theta = the position measurement (electrical angle)       */
/*      w = the current shaft velocity estimate                           */
/*      delta_t = the execution frequency of the algorithm                */
/*                                                                        */
/*The arithmetic is performed using double precision.                     */
/*                                                                        */
/*input:       old position (where 2^16 = 2*pi radians)                   */
/*      w (units of rpm * 10)                                             */
/*      K (constant incorporate delta_t and units)                        */
/*                                                                        */
/*output:      new position (where 2^16 = 2*pi radians)                   */
/*                                                                        */
/*pseudo-code: dp = w * K;                                                */
/*             position = position + (dp * NR)                            */
/*                                                                        */
/*++++++++++++++++++++++++++++++++++++++++++++++++++++++++++++++++++++++++*/
void Time_Update_Position(anSRM_struct *anSRM)
{


   long dp;    /* delta-position in mechanical angle */
   int speed;
   int temp;

   if (anSRM->wEst_10xrpm > 0) {
        dp = anSRM->wEst_10xrpm * K_POSITION_EST + anSRM->dp_remainder;
        anSRM->dp_remainder = dp & 0xffff;
  temp = (int) (dp >> 16);
        anSRM->position = anSRM->position + (temp * NR);
   }
   else {
  speed = -anSRM->wEst_10xrpm;
  dp = speed * K_POSITION_EST + anSRM->dp_remainder;
        anSRM->dp_remainder = dp & 0xffff;
  temp = (int) (dp >> 16);
        anSRM->position = anSRM->position - (temp * NR);
   }

} /* end Time_Update_Position */
```

```
/*++++++++++++++++++++++++++++++++++++++++++++++++++++++++++++++++++++++++*/
/*MEASUREMENT UPDATE OF THE ROTOR POSITION ESTIMATE                       */
/*-----------------------------------------------------------------------*/
/* At a capture interrupt, the rotor is at 1 of 6 positions.             */
/* In between interrupts, the pickoff will be at 1 of six states,        */
/* defined by the opto-couplers.  The states are defined by [zyx]        */
/* where:      z = output of opto-coupler #3                             */
/*      y = output of opto-coupler #2                                    */
/*      x = output of opto-coupler #1                                    */
/*                                                                       */
/*State 2: 010                                                           */
/*State 3: 011                                                           */
/*State 1: 001                                                           */
/*State 5: 101                                                           */
/*State 4: 100                                                           */
/*State 6: 110                                                           */
/*                                                                       */
/*++++++++++++++++++++++++++++++++++++++++++++++++++++++++++++++++++++++++*/
void Msmt_Update_Position(anSRM_struct *anSRM)
{

   int old_state, new_state;
   int cap;

   /*-------------------------------------------------------------------*/
   /* Based on capture and current state, get new state from the        */
   /*   state-machine look-up table                                     */
   /*-------------------------------------------------------------------*/
   cap = anSRM->last_capture;
   old_state = anSRM->position_state;
   new_state = anSRM->trans_lut[old_state][cap].state;

   /*---------------------------------------------------*/
   /* If transition is valid, update position and state  */
   /*---------------------------------------------------*/
   if (new_state != 0) { /* valid transition, update data */

  anSRM->position = anSRM->trans_lut[old_state][cap].position;
  anSRM->shaft_direction = anSRM->trans_lut[old_state][cap].direction;
  anSRM->position_state = new_state;
   }

   else { /* else, not a valid transition, use opto-coupler */
    /*  level & re-initialize position estimate             */

  anSRM->position_state = *PBDATDIR & 0x7;

   }

}
```

```
/*+++++++++++++++++++++++++++++++++++++++++++++++++++++++++++++++++++++++  */
/*VELOCITY ESTIMATION ALGORITHM                                           */
/*-------------------------------------------------------------------- */
/* This algorithm estimates the SRM shaft velocity.  It is executed*/
/*after each capture interrupt is received.  If the shaft is       */
/*moving fast enough, this routine is called with mode = 1 and     */
/*the capture data is used.  Otherwise, the # of timer ISRs        */
/*which are executed between capture events is used in the         */
/*velocity calculation.                                            */
/*                                                                 */
/*Velocity is calculated according to the equation:                */
/*                                                                 */
/*      w = delta_theta / delta_t                                  */
/*                                                                 */
/*where delta_theta is known:                                      */
/*                      (7.5 mech deg between each capture)        */
/*                     (22.5 mech deg between the same capture)    */
/*and delta_t is the measured number of clock cycles.              */
/*                                                                 */
/*The algorithm is implemented in double precision and is of       */
/*the form:                                                        */
/*             w = Kx_VELOCITY_EST/count                           */
/*                                                                 */
/*where the constant Kx_VELOCITY_ESTIMATE (x=1,2) incorporates     */
/*delta_theta and other units so that                              */
/*w has units of (rpm * 10).                                       */
/*                                                                 */
/*+++++++++++++++++++++++++++++++++++++++++++++++++++++++++++++++++++++++ */
void Msmt_Update_Velocity(anSRM_struct *anSRM, int mode)
{
   DWORD a1,a2,a3,a4,a5,a6;
   DWORD sum_cnt;
   int  inst_velocity;
   long filt_velocity;

   /*-------------------------------------------------*/
   /*  Obtain instantaneous velocity estimate       */
   /*-------------------------------------------------*/
   if (mode == 1) {    /* use timer #2 as time base  */

  /*-------------------------------------------------------------*/
  /*  FIR filter for removing once per electrical cycle effects */
  /*-------------------------------------------------------------*/
       a1 = (DWORD) anSRM->capture_delta[0][0];
       a2 = (DWORD) anSRM->capture_delta[0][1];
       a3 = (DWORD) anSRM->capture_delta[1][0];
       a4 = (DWORD) anSRM->capture_delta[1][1];
       a5 = (DWORD) anSRM->capture_delta[2][0];
       a6 = (DWORD) anSRM->capture_delta[2][1];
  sum_cnt = a1+a2+a3+a4+a5+a6;

  /*-------------------------------------------------*/
  /* apply velocity = delta_theta/delta_time algorithm */
  /*-------------------------------------------------*/
  sum_cnt = K1_VELOCITY_EST/sum_cnt;
  inst_velocity = ((int) sum_cnt) * anSRM->shaft_direction;
   }

   else {      /* else, use timer ISR count as time base */

  /*-------------------------------------------------*/
  /* apply velocity = delta_theta/delta_time algorithm */
  /*-------------------------------------------------*/
  sum_cnt = K2_VELOCITY_EST/anSRM->delta_count;
       inst_velocity = ((int) sum_cnt) * anSRM->shaft_direction;
   }

   /*-------------------------------------------------*/
   /*  IIR filter for smoothing velocity estimate   */
   /*-------------------------------------------------*/
```

```
   filt_velocity = (ALPHA * anSRM->wEst_10xrpm)
                + (ONE_MINUS_ALPHA * inst_velocity);
   anSRM->wEst_10xrpm = (int) (filt_velocity >> 3);

} /* end, velocity estimation */


/*++++++++++++++++++++++++++++++++++++++++++++++++++++++++++++++++++++++++++ */
/*COMMUTATION ALGORITHM                                                     */
/*-------------------------------------------------------------------------- */
/* A four quadrant commutation algorithm, using a fixed-dwell angle         */
/*      of 120 electrical degrees and a variable turn on angle.  With       */
/*a fixed dwell of 120 electrical degrees, only a single phase              */
/*is active at any one time.  The advance angle is calculated as            */
/*a function of speed and desired current.                                  */
/*++++++++++++++++++++++++++++++++++++++++++++++++++++++++++++++++++++++++++ */
void Commutation_Algorithm(anSRM_struct *anSRM)
{
   int phase;
   WORD electricalAngle;
   WORD angle;
   int channel;
   long advance;
   int whats_active;
   int desiredCurrent;
   int temp;

   /*---------------------------*/
   /* Advance angle calculation */
   /*---------------------------*/
   advance = (anSRM->wEst_10xrpm * anSRM->desiredTorque);
   advance = advance >> 9;

   /*-----------------------------------------------------------*/
   /* Offset for advance angle negative torque, if required */
   /*-----------------------------------------------------------*/
   if (anSRM->desiredTorque > 0) {
  electricalAngle = anSRM->position + (int) advance;
  desiredCurrent = anSRM->desiredTorque;
   }
   else {
  electricalAngle = anSRM->position + PI_16 - (int) advance;
  desiredCurrent = -anSRM->desiredTorque;
   }

   /*---------------------------------*/
   /* for each phase do ...           */
   /*---------------------------------*/
   whats_active = 0x0;
   for (phase=0; phase< NUMBER_OF_PHASES; phase++) {

  /*-------------------------------*/
  /* 120 degree offsets for phase */
  /*-------------------------------*/
  angle = electricalAngle - phase * TWOPIBYTHREE_16;

  /*-------------------------------------------------------------*/
  /* turn phase on, if between desired angles and switch       */
  /*    the mux on the A/D to measure the desired              */
  /*    phase current                                          */
  /*-------------------------------------------------------------*/
  if ( (angle >= (PIBYSIX_16)) && (angle < (FIVEPIBYSIX_16)) ) {
     anSRM->active[phase] = 1;
     temp = 0x1 << phase;
     channel = anSRM->a2d_chan[phase];
     switch_mux(channel,channel+8);
     anSRM->iDes[phase] = desiredCurrent;
     if (anSRM->iDes[phase] > ILIMIT) anSRM->iDes[phase] = ILIMIT;
  }
  else {
```

```
      anSRM->active[phase] = 0;
      temp = 0;
      anSRM->iDes[phase] = 0;
   }
   whats_active = whats_active | temp;

    }

    /*-------------------------------------*/
    /* switch low-side FETs, as required  */
    /*-------------------------------------*/
    switch_lowside(whats_active);

}


/*+++++++++++++++++++++++++++++++++++++++++++++++++++++++++++++++++++++++++++ */
/*VELOCITY CONTROL LOOP ALGORITHM                                             */
/*-------------------------------------------------------------------------- */
/*  The algorithm implements a PI compensator for the velocity              */
/*control of the SRM.  The PI filter limits the integrator         */
/*to prevent windup                                                 */
/*                                                                          */
/*+++++++++++++++++++++++++++++++++++++++++++++++++++++++++++++++++++++++++++ */
void velocityController(anSRM_struct *anSRM)
{


   int speed_error;
   int integral_error;

   /*-------------------------------*/
   /* calculate error signal       */
   /*-------------------------------*/
   speed_error = anSRM->wDes_10xrpm - anSRM->wEst_10xrpm;

   /*-------------------------------*/
   /* integrate error              */
   /*-------------------------------*/
   anSRM->integral_speed_error = anSRM->integral_speed_error + (long)speed_error;

   /*-------------------------------*/
   /* apply integrator limit       */
   /*-------------------------------*/
   if (anSRM->integral_speed_error > INTEGRAL_LIMIT) {
        anSRM->integral_speed_error = INTEGRAL_LIMIT;
   }
   if (anSRM->integral_speed_error < -INTEGRAL_LIMIT) {
        anSRM->integral_speed_error = -INTEGRAL_LIMIT;
   }

   /*-------------------------------*/
   /* PI filter                    */
   /*-------------------------------*/
   integral_error = (int) ((KI*anSRM->integral_speed_error) >> 13);
   anSRM->desiredTorque = ((KP*speed_error) >> 1) + integral_error;


}   /* end  velocityController */
```

```
/*------------------------------------------------------ */
/*CURRENT CONTROL LOOP ALGORITHM                         */
/*+++++++++++++++++++++++++++++++++++++++++++++++++++++++ */
void currentController(anSRM_struct *anSRM) {

   int phase;
   int ierr;

   for (phase=0; phase < NUMBER_OF_PHASES; phase++) {


  /*-----------------------------------------------*/
  /* for each active phase do ...                  */
  /*-----------------------------------------------*/
  if (anSRM->active[phase] > 0) {

     /*--------------------*/
     /* read A/D converter */
     /*--------------------*/
     anSRM->iFB[phase] = read_a2d(1);

     /*---------------------------*/
     /* calculate error signal       */
     /*---------------------------*/
     ierr = anSRM->iDes[phase] - anSRM->iFB[phase];

     /*---------------------------*/
     /* current loop compensation */
     /*---------------------------*/
          anSRM->dutyRatio[phase] = ILOOP_GAIN * ierr;
     anSRM->dutyRatio[phase] = (anSRM->dutyRatio[phase] >> 3);

     /*------------------*/
     /* limit duty ratio */
     /*------------------*/
     if (anSRM->dutyRatio[phase] < 0) {
               anSRM->dutyRatio[phase] = 0;
     }
     if (anSRM->dutyRatio[phase] > MAXIMUM_DUTYRATIO) {
               anSRM->dutyRatio[phase] = MAXIMUM_DUTYRATIO;
     }

  }

  /*-----------------------------------------------*/
  /* else, phase is not active                     */
  /*-----------------------------------------------*/
  else {
     anSRM->iFB[phase] = 0;
     anSRM->dutyRatio[phase] = 0;
  }

   } /* end for loop */

   /*--------------------------------------*/
   /* output PWM signals to high-side FET's */
   /*--------------------------------------*/
   *CMPR1 = anSRM->dutyRatio[0];
   *CMPR2 = anSRM->dutyRatio[1];
   *CMPR3 = anSRM->dutyRatio[2];

} /* end currentController */


/*------------------------------------------------------------- */
/*SRM ALGORITHM INITIALIZATION                                  */
/*------------------------------------------------------------- */
void initializeSRM(anSRM_struct *anSRM)
{

   int i,j;
```

```
 /*-------------------------------------------------------*/
 /* define mux positions for current feedback of each phase */
 /*-------------------------------------------------------*/
 anSRM->a2d_chan[0] = 1;    /* phase A current on pin ADCIN1 */
 anSRM->a2d_chan[1] = 2;    /* phase B current on pin ADCIN2 */
 anSRM->a2d_chan[2] = 3;    /* phase C current on pin ADCIN3 */

 /*-------------------------------------------------------------*/
 /* Define position estimation state machine.                   */
 /*                                                             */
 /*   Given current state, i, and capture event, j, with        */
 /*   every transition (capture event), 3 parameters are defined: */
 /*          1. trans_lut[i][j].state = the new state           */
 /*          2. trans_lut[i][j].position = the shaft position   */
 /*          3. trans_lut[i][j].direction = the shaft direction  */
 /*-------------------------------------------------------------*/

/*-----------------------------------------------------*/
/* fill table with zeros.  zeros will define illegal */
/*   transitions                                       */
/*-----------------------------------------------------*/
     for (i=0; i<7; i++) {
     for (j=0; j<4; j++) {
            anSRM->trans_lut[i][j].state = 0;
            anSRM->trans_lut[i][j].position = 0;
            anSRM->trans_lut[i][j].direction = 0;
     }
     }

/*------------------------------*/
/* 'new-state' definitions  */
/*------------------------------*/
     anSRM->trans_lut[1][2].state = 3;
     anSRM->trans_lut[1][3].state = 5;
     anSRM->trans_lut[2][1].state = 3;
     anSRM->trans_lut[2][3].state = 6;
     anSRM->trans_lut[3][1].state = 2;
     anSRM->trans_lut[3][2].state = 1;
     anSRM->trans_lut[4][1].state = 5;
     anSRM->trans_lut[4][2].state = 6;
     anSRM->trans_lut[5][1].state = 4;
     anSRM->trans_lut[5][3].state = 1;
     anSRM->trans_lut[6][2].state = 4;
     anSRM->trans_lut[6][3].state = 2;

/*--------------------------------------*/
/* 'shaft direction' definitions   */
/*--------------------------------------*/
     anSRM->trans_lut[1][2].direction = -1;
     anSRM->trans_lut[1][3].direction = 1;
     anSRM->trans_lut[2][1].direction = 1;
     anSRM->trans_lut[2][3].direction = -1;
     anSRM->trans_lut[3][1].direction = -1;
     anSRM->trans_lut[3][2].direction = 1;
     anSRM->trans_lut[4][1].direction = -1;
     anSRM->trans_lut[4][2].direction = 1;
     anSRM->trans_lut[5][1].direction = 1;
     anSRM->trans_lut[5][3].direction = -1;
     anSRM->trans_lut[6][2].direction = -1;
     anSRM->trans_lut[6][3].direction = 1;
```

```
  /*--------------------------------------*/
  /* 'shaft position' definitions         */
  /*--------------------------------------*/
       anSRM->trans_lut[1][2].position = TWOPIBYTHREE_16;
  anSRM->trans_lut[1][3].position = PI_16;
       anSRM->trans_lut[2][1].position = PIBYTHREE_16;
       anSRM->trans_lut[2][3].position = 0;
       anSRM->trans_lut[3][1].position = PIBYTHREE_16;
       anSRM->trans_lut[3][2].position = TWOPIBYTHREE_16;
       anSRM->trans_lut[4][1].position = FOURPIBYTHREE_16;
       anSRM->trans_lut[4][2].position = FIVEPIBYTHREE_16;
       anSRM->trans_lut[5][1].position = FOURPIBYTHREE_16;
       anSRM->trans_lut[5][3].position = PI_16;
       anSRM->trans_lut[6][2].position = FIVEPIBYTHREE_16;
       anSRM->trans_lut[6][3].position = 0;


   /*-------------------------------------------------------------------- */
   /*  define initial guesses for each state.  The initial position       */
   /*  is assumed at the midpoint of each state                           */
   /*-------------------------------------------------------------------- */
   anSRM->position_initial_guess[1] = TWOPIBYTHREE_16 + PIBYSIX_16;
   anSRM->position_initial_guess[2] = PIBYSIX_16;
   anSRM->position_initial_guess[3] = PIBYTHREE_16 + PIBYSIX_16;
   anSRM->position_initial_guess[4] = FOURPIBYTHREE_16 + PIBYSIX_16;
   anSRM->position_initial_guess[5] = PI_16 + PIBYSIX_16;
   anSRM->position_initial_guess[6] = FIVEPIBYTHREE_16 + PIBYSIX_16;


   /*-----------------------------------------------------*/
   /* read opto-couplers and get initial position estimate */
   /*-----------------------------------------------------*/
   anSRM->position_state = *PBDATDIR & 0x7;
   anSRM->position = anSRM->position_initial_guess[anSRM->position_state];


   /*-------------------------*/
   /* set initial conditions  */
   /*-------------------------*/
   for(i = 0; i < NUMBER_OF_PHASES; i++) {
  anSRM->iDes[i] = 0;
       anSRM->active[i] = 0;
       anSRM->iFB[i] = 0;
  anSRM->capture_delta[i][0] = 65535;
  anSRM->capture_delta[i][1] = 65535;
   }

   anSRM->wEst_10xrpm = 0;
   anSRM->shaft_direction = 0;
   anSRM->dp_remainder = 0;
   anSRM->integral_speed_error = 0;
   anSRM->wDes_10xrpm = 0;

}

/*++++++++++++++++++++++++++++++++++++++++++++++++++++++++++++++++++++++
/*
/*File:               EVMGR.C
/*Target Processor:   TMS320F240
/*Compiler Version:   6.6
/*Assembler Version:  6.6
/*Created:            10/31/97
/*
/*++++++++++++++++++++++++++++++++++++++++++++++++++++++++++++++++++++++
/* This file contains the routines for initializing and using the event
/* manager peripherials.
/*++++++++++++++++++++++++++++++++++++++++++++++++++++++++++++++++++++++*/

/*--------------------------------------------------------------- */
```

```
/*INCLUDE FILES                                                    */
/*-----------------------------------------------------------------*/
#include "c240.h"
#include "constant.h"


/*+++++++++++++++++++++++++++++++++++++++++++++++++++++++++++++++++*/
/*EVENT MANAGER INITIALIZATION                                     */
/*+++++++++++++++++++++++++++++++++++++++++++++++++++++++++++++++++*/
/* Through appropriate programming of the event manager control
/*registers, this routine sets up the event manager so that:
/*
/*all timers run in the continuous up count mode
/*timer 1 provides the desired PWM frequency timebase
/*timer 2 counts at 1/16 of the CPUCLK and is used as the time
/*      base for capture events.  Prescaling prevents overflow
/*      except at only low shaft speeds.
/*timer 3 provides the CPU interrupt
/*A/D conversions are synchronized with timer 3 period occurences
/*compare units are configured to the PWM mode
/*PWMs 1,3, and 5 (used for high-side switching) are active low
/*PWMs 2,4, and 6 (used for low-side switching) are forced hi/low
/*sets up shared pins as capture inputs and digital inputs for
/*      interface with the opto-couplers
/*initiates continuous A/D conversions.
/*
/*-------------------------------------------------------------------*/
/*   GPTCON Initialization parameters
/*                                          GPTCON = 0x1055
/*
/*                                          xxx1 0000 0101 0101
/*                                          ___---__---_-- __--
/*                                           |  | |  | | |  | |
/* (15-13)     Read-only status bits ---------|  | |  | | |  | |
/* (12-11)     Start A/D on timer 3 period ------| |  | | |  | |
/* (10-9)      No timer 2 event starts A/D --------|  | | |  | |
/* (8-7)       No timer 1 event starts A/D -----------| | |  | |
/* (6)         Enable timer compares ------------------| |  | |
/* (5-4)       Timer 3 active low -------------------------|  | |
/* (3-2)       Timer 2 active low ----------------------------| |
/* (1-0)       Timer 1 active low ----------------------------|
/*


/*-------------------------------------------------------------------*/
/*   T3CON Initialization parameters
/*                                          T3CON = 0x9040
/*
/*                                          1001 0000 0100 0000
/*                                          __----___ -_-- __-_
/*                                          |  |    |  || | | ||
/* (15-14)     Stop on suspend --------------|  |    |  || | | ||
/* (13-11)     Continuous up-count mode --------|    |  || | | ||
/* (10-8)      Clock prescaler = 1 ------------------|  || | | ||
/* (7)         Use own TENABLE bit --------------------|| | | ||
/* (6)         Enable timer  ---------------------------| | | ||
/* (5-4)       Use internal clock source ------------------| | ||
/* (3-2)       Reload at zero -----------------------------| ||
/* (1)         disable timer compare ------------------------||
/* (0)         Use own period register ----------------------|
/*
/*-------------------------------------------------------------------*/
/*   T2CON Initialization parameters
/*                                          T2CON = 0x9440
/*
/*                                          1001 0100 0100 0000
/*                                          __----___ -_-- __-_
/*                                          |  |    |  || | | ||
```

```
/* (15–14)     Stop on suspend --------------|  |   |  || | | ||
/* (13–11)     Continuous up–count mode --------|   |  || | | ||
/* (10–8)      Clock prescaler = 1/16 --------------|  || | | ||
/* (7)         Use own TENABLE bit ---------------------|| | | ||
/* (6)         Enable timer  ---------------------------| | | ||
/* (5–4)       Use internal clock source ----------------| | ||
/* (3–2)       Reload at zero -------------------------------| ||
/* (1)         disable timer compare -------------------------||
/* (0)         Use own period register ------------------------|
/*
/*-----------------------------------------------------------------------*/
/*   T1CON Initialization parameters
/*                                          T1CON = 0x9040
/*
/*                                          1001 0000 x100 0000
/*                                          __----___ -_-- __-_
/*                                          |  |   |  || | | ||
/* (15–14)     Stop on suspend --------------|  |   |  || | | ||
/* (13–11)     Continuous up–count mode --------|   |  || | | ||
/* (10–8)      Clock prescaler = 1 ----------------|  || | | ||
/* (7)         Reserved on timer 1 ---------------------|| | | ||
/* (6)         Enable timer  ---------------------------| | | ||
/* (5–4)       Use internal clock source ----------------| | ||
/* (3–2)       Reload at zero -------------------------------| ||
/* (1)         Disable timer compare -------------------------||
/* (0)         Use own period register ------------------------|
/*
/*-----------------------------------------------------------------------*/
/*   COMCON Initialization parameters
/*
/*                                          COMCON = 0x8207
/*
/*                                          1000 0010 xxxx x111
/*                                          _--_ --_- -__---_-_
/*                                          | || | || | | | |||
/* (15)        Enable compares --------------| || | || | | | |||
/* (14–13)     Reload compare at 0 ------------|| | || | | | |||
/* (12)        Disable Space Vector PWM --------| | || | | | |||
/* (11–10)     Reload ACTR at 0 -------------------| || | | | |||
/* (9)         Enable full compare output pins -----|| | | | |||
/* (8)         Hi–Z simple compare output pins ------| | | | |||
/* (7)         Simple compare time base ---------------| | | |||
/* (6–5)       Simple compare reload ----------------------| | |||
/* (4–3)       Simple compare SACTR reload ----------------| |||
/* (2)         Compare #3 to PWM mode ------------------------|||
/* (1)         Compare #2 to PWM mode -------------------------||
/* (0)         Compare #1 to PWM mode --------------------------|
/*
/*-----------------------------------------------------------------------*/
/*   ACTR Initialization parameters
/*                                          ACTR = 0x0111
/*
/*                                          xxxx 0001 0001 0001
/*                                          ____ --__ --__ --__
/*                                           |   |  | |  | |  |
/* (15–12)     Space vector PWM related ------|   |  | |  | |  |
/* (11–10)     PWM6 = Force Low -------------------|  | |  | |  |
/* (9–8)       PWM5 = Active Low ----------------------| |  | |  |
/* (7–6)       PWM4 = Force Low ------------------------|  | |  |
/* (5–4)       PWM3 = Active Low  -------------------------| |  |
/* (3–2)       PWM2 = Force Low ---------------------------|  |
/* (1–0)       PWM1 = Active Low -------------------------------|
/*
/*-----------------------------------------------------------------------*/
/*   ADCTRL1 Initialization parameters
/*                                          ADCTRL1 = 0x2c00
/*
/*                                          0010 110x 0000 0000
```

```
/*                                          _-_- _-_- _--- ___-
/*                                         |||| |||| | |   | |
/* (15)        Suspend – Soft ---------------|||| |||| | |   | |
/* (14)        Suspend – Free ----------------||| |||| | |   | |
/* (13)        Start A/D Conversions ----------|| |||| | |   | |
/* (12)        Disable Channel 1 ---------------| |||| | |   | |
/* (11)        Enable Channel 2 -------------------|||| | |   | |
/* (10)        Continuous conversion  -------------||| | |   | |
/* (9)         Disable interrupt  -------------------|| | |   | |
/* (8)         ADC Interrupt flag --------------------| | |   | |
/* (7)         Conversion status ----------------------| |   | |
/* (6-4)       ADC1 mux select --------------------------|   | |
/* (3-1)       ADC2 mux select ------------------------------| |
/* (0)         Start conversion bit --------------------------|
/*
/*+++++++++++++++++++++++++++++++++++++++++++++++++++++++++++++++++++*/
void eventmgr_init() {

  WORD iperiod;

  /*-------------------------------------------------------*/
  /* Initialize GP timer 3 to provide desired CPU interrupt */
  /*-------------------------------------------------------*/
  iperiod = (SYSCLK_FREQ/CPU_INT_FREQ) - 1;

  *GPTCON = 0x1055;   /* Setup general-purpose control reg         */
  *T3PER = iperiod;   /* Load timer #2 period register             */
  *T3CON = 0x9040;    /* Initialize timer #3 control register      */

  /*-------------------------------------------------------*/
  /* Initialize GP timer 1 to provide a 20 kHz time base for */
  /*         fixed frequency PWM generation                 */
  /*-------------------------------------------------------*/
  iperiod = (SYSCLK_FREQ/PWM_FREQ) - 1;

  *T1PER = iperiod;   /* Load timer #1 period                      */
  *T1CON = 0x9040;    /* Initialize timer #1 control register      */

  /*-------------------------------------------------------------*/
  /* Initialize GP timer 2 to provide time base for clocking   */
  /*   capture events                                           */
  /*-------------------------------------------------------------*/
  *T2PER = 0xffff;    /* Load timer #2 period                      */
  *T2CON = 0x9440;    /* Initialize timer #2 control register      */

  /*--------------------------------------*/
  /* Setup Compare units for PWM outputs */
  /*--------------------------------------*/
  *ACTR = 0x0111;     /* Initialize action on output pins */
  *DBTCON = 0x0;      /* Disable deadband */
  *CMPR1 = 0x0;       /* Clear period registers */
  *CMPR2 = 0x0;
  *CMPR3 = 0x0;
  *COMCON = 0x0207;   /* Setup COMCON w/o enable */
  *COMCON = 0x8207;   /* Setup COMCON and enable */

  /*-------------------*/
  /* Setup shared pins */
  /* ------------------*/
  *OCRA = 0x0;        /* pins IOPB0-IOPB7 & IOPA0-IOPA3 to I/O pins */
  *OCRB = 0xf1;       /* pins are: ADSOC, XF, /BIO, CAP1-CAP4 */
  *PBDATDIR = 0xf0f0; /* inputs IOPB0-IOPB3 */
                      /* outputs IOPB4-IOPB7, set high */

  /*----------------------*/
  /* Setup capture units */
  /*----------------------*/
  *CAPCON = 0x0;      /* reset capture control register */
  *CAPFIFO = 0xff;    /* Clear FIFO's */
  *CAPCON = 0xb0fc;   /* enable #1-3, use Timer2, both edges */
```

```
  /*----------------------*/
  /* Setup A/D converter */
  /*----------------------*/
  *ADCTRL1 = 0x2c00;  /* Initialize A/D control register */
  *ADCTRL2 = 0x0403;  /* Clear FIFO's, Pre-scaler = 4 */

}


/*************************************************************/
/*SWITCH A/D INPUT CHANNEL                                   */
/*-----------------------------------------------------------*/
/* Each A/D converter unit has an 8:1 input multiplexer which
/* must be selected to the desired channel, prior to sampling.
/* The channel is selected by manipulating bits
/* of the ADCTRL1 control register
/*
/* inputs:     adc1 = desired input channel for A/D #1
/*                    range:  0-7
/*             adc2 = desired input channel for A/D #2
/*                    range:  8-15
/*outputs:     none
/*
/*+++++++++++++++++++++++++++++++++++++++++++++++++++++++++++ */
void switch_mux(int adc1, int adc2)
{

  WORD ctrl_word;

  ctrl_word = 0x2c00;                       /* mask channel select bits */
  ctrl_word = ctrl_word | (adc1 << 4);      /* set ADC1 channel bits */
  ctrl_word = ctrl_word | ((adc2-8) << 1);  /* set ADC2 channel bits */
  *ADCTRL1 = ctrl_word;
  *ADCTRL2 = 0x0403;
}


/*********************************************************** */
/*READ A/D FIFO REGISTER                                     */
/*---------------------------------------------------------- */
/* This routine is used to read the sampled A/D data from the
/*appropriate FIFO.  The 10-bit A/D data is stored in the
/*FIFO in bits 15-6.  A right shift of 6, limits the data
/*to the range 0-1023.
/*
/*inputs:             a2d_chan = which FIFO to read
/*                    range: 1-2
/*outputs:     inval = A/D data
/*                    range: 0-1023
/*                           0 VDC = 0 bits
/*                           5 VDC = 1023 bits
/*+++++++++++++++++++++++++++++++++++++++++++++++++++++++++++ */
WORD read_a2d(int a2d_chan)
{

  WORD inval;

  if (a2d_chan == 1) {
     inval = (*ADCFIFO1 >> 6) & 0x03ff;
  }
  else if (a2d_chan == 2) {
     inval = (*ADCFIFO2 >> 6) & 0x03ff;
  }

  return inval;
}


/*************************************************************/
/*SWITCH LOW-SIDE MOSFETS                                    */
```

```
/*-------------------------------------------------------- */
/* The state of the low-side power MOSFETS is controlled by the
/*level on the PWM2, PWM4, and PWM6 output pins, for phases
/*A, B, and C, respectively.  Active high logic is used,
/*but since the low-side switches are used for commutation
/*instead of PWM control, we just use the force-low or
/*force-high action options.
/*
/*inputs:             phaseactive = bits 0,1, and 2 control
/*                    the state of the PWM2, PWM4, and
/*                    PWM6 output pins, respectively.
/*
/*             (ex. phaseactive = 0x5 will force PWM2 &
/*                    PWM6 high, PWM4 low )
/*outputs:     none
/*
/*+++++++++++++++++++++++++++++++++++++++++++++++++++++++++ */
void switch_lowside(int phaseactive)
{

  WORD action;

  /*-------------------------------------------------------*/
  /* load action register and mask PWM2, PWM4, and PWM6 */
  /*   to force low                                        */
  /*-------------------------------------------------------*/
  action = *ACTR;
  action = action & 0xf333;

  /*---------------------------------------*/
  /* Force hi PWM2 if phase0 (A) is active */
  /*---------------------------------------*/
  if (phaseactive & 0x1) {
     action = action | 0x000c;
  }

  /*---------------------------------------*/
  /* Force hi PWM4 if phase1 (B) is active */
  /*---------------------------------------*/
  if (phaseactive & 0x2) {
     action = action | 0x00c0;
  }

  /*---------------------------------------*/
  /* Force hi PWM6 if phase2 (C) is active */
  /*---------------------------------------*/
  if (phaseactive & 0x4) {
     action = action | 0x0c00;
  }

  /*-----------------------------------*/
  /* Write new word to action register */
  /*-----------------------------------*/
  *ACTR = action;

}
```

```
/*********************************************************** */
/*READ CAPTURE FIFO REGISTERS                                 */
/*---------------------------------------------------------- */
/* This routine is used to read the data from the capture FIFO
/*registers.
/*
/*inputs:             capture = which FIFO to read?
/*                    range = 1–3
/*outputs             fifo_data =
/*                    range = 0–65535
/*
/*+++++++++++++++++++++++++++++++++++++++++++++++++++++++++++ */
WORD read_fifo(int capture)
{
  WORD fifo_data;
  int fifo_status;


  if (capture == 1) {
     do {
        fifo_data = *FIFO1;          /* read value */
        fifo_status = *CAPFIFO & 0x0300;     /* read status register, mask bits */
     } while (fifo_status != 0);
        }
  else if (capture == 2) {
     do {
        fifo_data = *FIFO2;          /* read value */
        fifo_status = *CAPFIFO & 0x0c00;     /* read status register, mask bits */
     } while (fifo_status != 0);
  }
  else if (capture == 3) {
     do {
        fifo_data = *FIFO3;          /* read value */
        fifo_status = *CAPFIFO & 0x3000;     /* read status register, mask bits */
     } while (fifo_status !=0);
  }
  else {
     fifo_data = 0xffff;                    /* error, not a valid capture */
  }

  return fifo_data;
}



*+++++++++++++++++++++++++++++++++++++++++++++++++++++++++++++*
*                                                             *
* File:              VECTORS.ASM                              *
* Target Processor:  TMS320F240                               *
* Assembler Version: 6.6                                      *
* Created:           10/31/97                                 *
*                                                             *
*-------------------------------------------------------------*
*   This file contains the interrupt vectors                  *
*************************************************************


    .length 58
    .option T
    .option X

********************************************************* *
*   ILLEGAL INTERRUPT ROUTINE                              *
********************************************************* *;
    .text
    .def         _int_0

_int_0:   B      _int_0           ; ILLEGAL INTERRUPT SPIN
```

```
*********************************************************** *
*   INTERRUPT VECTORS                                       *
*********************************************************** *
    .sect      "VECTOR"
        .ref   _c_int0
    .ref       _c_int3
  .ref  _c_int4

        B      _c_int0        ; RESET
    B   _int_0          ; INT1
    B   _int_0          ; INT2
    B   _c_int3         ; INT3
    B   _c_int4         ; INT4
    B   _int_0          ; INT5
    B   _int_0          ; INT6
    B   _int_0          ; Reserved
    B   _int_0          ;
    B   _int_0          ;
    B   _int_0          ;
    B   _int_0          ;
    B   _int_0          ;
    B   _int_0          ;
    B   _int_0          ;
    B   _int_0          ;
    B   _int_0          ;
    B   _int_0          ; TRAP
    B   _int_0          ; NMI
    B   _int_0          ;
    B   _int_0          ;
    B   _int_0          ;

    .end


/* Linker command file for TMS320F240 EVM */

vectors.obj
evmgr.obj
srm.obj

-c              /* use ROM autoinitialization model */
-m  main.map
-o  main.out
-l  c:\2xxtools\rts2xx.lib

MEMORY
{
    PAGE 0:    VECTORS:  origin = 0x0000 length = 0x0040    /* EMIF    */
    PAGE 0:    CODE:     origin = 0x0040 length = 0x1FC0    /* EMIF    */
    PAGE 1:    MMRS:     origin = 0x0000 length = 0x0060    /* MMRS    */
               B2:       origin = 0x0060 length = 0x0020    /* DARAM   */
       B0:       origin = 0x0100 length = 0x0100    /* DARAM   */
       B1:       origin = 0x0300 length = 0x0100    /* DARAM   */
       DATA:     origin = 0xa000 length = 0x2000    /* EMIF    */

}

SECTIONS
{
    .VECTOR  > VECTORS PAGE 0
    .text    > CODE    PAGE 0
    .cinit   > CODE    PAGE 0
    .switch  > CODE    PAGE 0
    .mmrs    > MMRS    PAGE 1    /* Memory Mapped Registers */
    .data    > DATA    PAGE 1
    .bss     > DATA    PAGE 1
    .const   > DATA    PAGE 1
    .stack   > DATA    PAGE 1
    .sysmem  > DATA    PAGE 1
```

IMPORTANT NOTICE

Texas Instruments and its subsidiaries (TI) reserve the right to make changes to their products or to discontinue any product or service without notice, and advise customers to obtain the latest version of relevant information to verify, before placing orders, that information being relied on is current and complete. All products are sold subject to the terms and conditions of sale supplied at the time of order acknowledgement, including those pertaining to warranty, patent infringement, and limitation of liability.

TI warrants performance of its semiconductor products to the specifications applicable at the time of sale in accordance with TI's standard warranty. Testing and other quality control techniques are utilized to the extent TI deems necessary to support this warranty. Specific testing of all parameters of each device is not necessarily performed, except those mandated by government requirements.

CERTAIN APPLICATIONS USING SEMICONDUCTOR PRODUCTS MAY INVOLVE POTENTIAL RISKS OF DEATH, PERSONAL INJURY, OR SEVERE PROPERTY OR ENVIRONMENTAL DAMAGE ("CRITICAL APPLICATIONS"). TI SEMICONDUCTOR PRODUCTS ARE NOT DESIGNED, AUTHORIZED, OR WARRANTED TO BE SUITABLE FOR USE IN LIFE-SUPPORT DEVICES OR SYSTEMS OR OTHER CRITICAL APPLICATIONS. INCLUSION OF TI PRODUCTS IN SUCH APPLICATIONS IS UNDERSTOOD TO BE FULLY AT THE CUSTOMER'S RISK.

In order to minimize risks associated with the customer's applications, adequate design and operating safeguards must be provided by the customer to minimize inherent or procedural hazards.

TI assumes no liability for applications assistance or customer product design. TI does not warrant or represent that any license, either express or implied, is granted under any patent right, copyright, mask work right, or other intellectual property right of TI covering or relating to any combination, machine, or process in which such semiconductor products or services might be or are used. TI's publication of information regarding any third party's products or services does not constitute TI's approval, warranty or endorsement thereof.

Application Report
SPRA600 - October 1999

A Variable-Speed Sensorless Drive System for Switched Reluctance Motors

Stephen J. Fedigan, Ph.D. and Charles P. Cole *DSPS Research and Development Center*

ABSTRACT

With the advent of high-speed digital signal processors (DSPs) specialized for motion control applications, it has become possible to control motors without mechanical (speed or position) sensors. This is achieved by algorithms that estimate the desired quantities in real time, based on the electrical signals in the motor windings. Benefits include cost savings and improved reliability due to reduced component count. This application report presents a low-cost, sensorless drive system for a switched reluctance motor (SRM) based on the Texas Instruments TMS320F243 DSP. Detailed descriptions of the hardware configuration, the sensorless commutation algorithm, its implementation details, and procedures for measuring motor parameters should enable readers to rapidly duplicate and customize a sensorless SRM drive system to meet their specific application.

Contents

1 Hardware to Demonstrate Sensorless Control of the Switched Reluctance Motor Using the Texas Instruments TMS320F243 DSP 4
1.1 Demonstration Goals 4
1.2 Hardware Description 4
1.2.1 Switched Reluctance Motor Characteristics 5
1.2.2 Digital Motor Controller 6
1.2.3 TMS320F243 Evaluation Module 7
1.2.4 Magtrol Dynamometer 7
1.2.5 Dynamometer Controller 8
1.3 Operational Procedures 8
1.4 Sensorless SRM Performance 10
2 Control Software for a Sensorless SRM Drive System 11
2.1 Overview of the Sensorless SRM Control Software 11
2.2 Sensorless Commutation and Velocity-Update Algorithm 13
2.2.1 Flux Estimator 14
2.2.2 Flux Estimator Implementation 15
2.2.3 Flux Reference Generator 16
2.2.4 Lockout Window 16
2.2.5 Velocity Estimator 18
2.2.6 Stall Detector 19
2.2.7 Low-Speed Operating Mode (<400 RPM) 19
2.2.8 Commutation and Velocity-Update Algorithm Summary 20
2.3 Velocity Loop 22
2.3.1 Motor Start-up Under Load 22
2.4 Current Control Loop 23
2.5 Ramp Controller 24
2.6 Serial Comms 26
3 Calibration for a Sensorless SRM Drive System 27
3.1 Stator Flux Estimation 27
3.2 Measuring the Voltage “Loss” Function 28
3.3 Generating a Voltage “Loss” Look-up Table 29
3.4 Measuring the Voltage “Loss” Data 29
3.5 Flux Measurement Method 30
3.5.1 Flux Measurement Hardware 31
3.5.2 Demo SRM Flux Measurements 32
3.5.3 Look-up Table Generation Method 33
References 34

List of Figures

Figure 1. Interconnection Diagram for SRM Demo Hardware 5
Figure 2. SRM Power Driver Topology 6
Figure 3. Software Block and Timing Diagrams 12
Figure 4. Graph of Flux Estimate and Flux Threshold vs. Time 14
Figure 5. SRM Power Driver Topology 15
Figure 6. Flux Estimator Code 16
Figure 7. Flux Estimate and Threshold at 2500 RPM Under Full Load 17
Figure 8. Illustration of Sensorless Commutation Algorithm With Lockout Window 18
Figure 9. Low-Speed Operating Mode With a Second Flux Threshold for an Additional Velocity Update 19
Figure 10. Commutation and Velocity-Update Flow Diagram 21
Figure 11. Block Diagram of the Velocity Control Loop 22
Figure 12. Instantaneous Velocity Estimate and Velocity Loop Output During Start-up 23
Figure 13. Block Diagram of the Current Control Loop 23
Figure 14. State Transition Diagram for the Ramp Controller 25
Figure 15. Flow Chart for Voltage “Loss” Measurement Program 28
Figure 16. Voltage “Loss” vs. Current for the Emerson Electric SRM and the Spectrum Digital Motor Control Board 30
Figure 17. SRM Magnetization Curves 31
Figure 18. Analog Flux Measurement Circuit 32
Figure 19. Flux Linkage Curves for Demo Platform SRM 33

List of Tables

Table 1. Performance Parameters of the Demo SRM Drive System 4
Table 2. Switched Reluctance Motor Characteristics 5
Table 3. Description of Commands 9
Table 4. Sensorless SRM Performance Summary 10
Table 5. Execution Times of Foreground Activity 13
Table 6. Serial Communications Module Commands 26

1 Hardware to Demonstrate Sensorless Control of the Switched Reluctance Motor Using the Texas Instruments TMS320F243 DSP

This section describes the hardware used to demonstrate the sensorless control of a typical switched reluctance motor (SRM) drive using the Texas Instruments TMS320F243 digital signal processor (DSP). Research completed in March of 1998 and documented in the Application Report titled “Developing an SRM Drive System Using the TMS320F240” (literature number SPRA420) led to a baseline software algorithm for conventional operation of the SRM drive using a shaft position sensor. Follow-on research completed in August of 1999 extended the performance range of a specific SRM without a shaft position sensor using a sensorless control algorithm. Detailed information on the sensorless software control algorithm can be found in Section 2. Hardware used in this follow-on research was the 3-phase, 12/8 stator-pole-configured SRM manufactured by Emerson Electric Company, and the digital motor controller board designed and manufactured by Spectrum Digital Incorporated (www.spectrumdigital.com), which utilizes the Texas Instruments TMS320F243 DSP. The hardware and software algorithm as described are intended to be used primarily for potential customer demonstrations and to serve as examples of extended performance sensorless control of SRM drive systems.

1.1 Demonstration Goals

The basic goals of this research work were to build upon the baseline software algorithm as described in the application report referenced above and to extend the performance range of the SRM drive using sensorless control. Performance parameters (listed in Table 1) of the SRM drive were set to cover a wide range of potential customer applications such as white goods (washing machine), compressor pumps, and blower fan applications.

Table 1. Performance Parameters of the Demo SRM Drive System

Speed range	150 to 4500 rpm
Load torque	no load to 48 oz-in
Speed regulation	10% over full speed/torque range

In addition to these basic requirements, other goals were to successfully start the SRM from standstill under a full load torque of 48 oz-in.

1.2 Hardware Description

Hardware used for this demonstration is described in the following sections. A diagram of the interconnections between the various hardware elements that make up this SRM demonstration platform is shown in Figure 1.

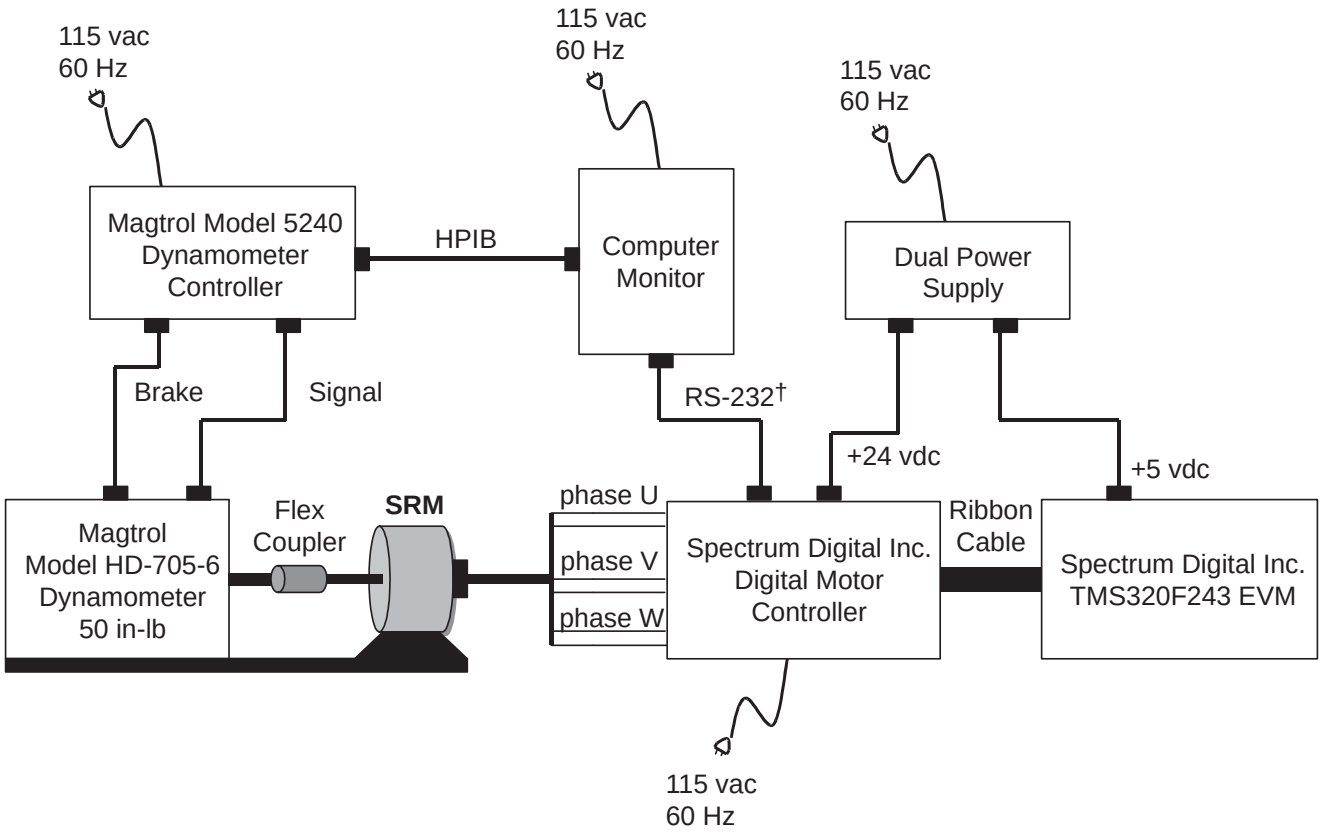

Figure 1. Interconnection Diagram for SRM Demo Hardware

1.2.1 Switched Reluctance Motor Characteristics

The characteristics of the switched reluctance motor are shown in Table 2.

Table 2. Switched Reluctance Motor‡ Characteristics

Number of phases	3
Number of stator poles	12
Number of rotor poles	8
Phase resistance	2.5 ohms
Aligned inductance	52 mH
Unaligned inductance	9.5 mH
Phase current (max)	4 amps

‡ Manufactured by Emerson Electric Company for the Maytag™ Neptune™ Auto Washer.

Maytag and Neptune are trademarks of Maytag Corporation.

† TIA/EIA Standard 232-F – October 1997, Interface Between Data Terminal Equipment and Data Circuit-Terminating Equipment Employing Serial Binary Data Interchange.

1.2.2 Digital Motor Controller

The board is designed and manufactured by Spectrum Digital Incorporated and utilizes the Texas Instruments TMS320F243 DSP. This controller board has an ac-to-dc converter that generates a full-wave-rectified and -filtered 162-volt dc from an ac supply input of 115 vac at 50/60 Hz. With placement of on-board jumpers, the board can be configured in a voltage doubler mode to generate 320 volts dc if the intended motor application requires the higher voltage. It also has a three-phase power inverter powered from the 162-volt dc bus. This power inverter can be configured, with proper placement of jumpers, to drive typical three-phase ac induction motors, three-phase brushless dc motors, or three-phase SRMs. In the SRM configuration, the power driver uses the popular and standard two-switches-per-phase topology as shown in Figure 2.

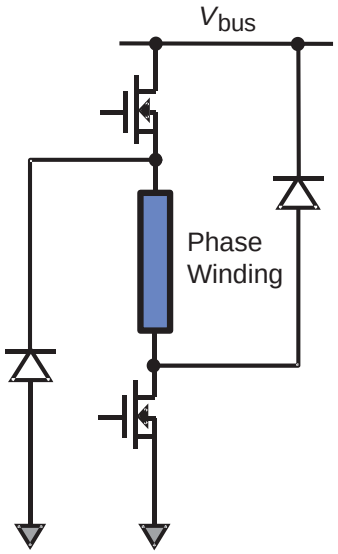

Figure 2. SRM Power Driver Topology

Current-sensing resistors are included in each low-side power driver leg with variable gain buffer amplifiers to output current feedback samples in each phase winding of the motor. In this example application of the SRM drive system, the gain of these buffer amplifiers has been set to give a current-sensing scale factor of 1.0 amp/volt. On-board low-voltage power supplies of +5 volts dc and +15 volts dc are also included so that this board can operate independently from 115 volts ac at 50/60 Hz.

Other features of this controller board are current-sensing resistors on the bus to enable power factor correction capability. This feature is not used in this example application. Some minor modifications to the board have been made for this example application and include removal of the R5 (0.03 ohm) bus current-sensing resistor. Current-sensing resistors R2, R3, and R4 have also been changed from 0.04 ohm to 0.2 ohm to adjust the current feedback scale factor and reduce electrical noise sensitivity. A serial communications interface (RS-232) port is also provided on the board and is used in this example application to introduce input set speed commands so that the motor speed can be changed on the fly while the motor is running.

1.2.3 TMS320F243 Evaluation Module

This evaluation module (EVM), based upon the Texas Instruments TMS320F243 digital signal processor, is designed and manufactured by Spectrum Digital Incorporated. It is an excellent platform to develop and run software on the ’F24x family of processors and was used extensively in the development and testing of the software algorithm for the sensorless control of the SRM drive system in this demonstration hardware. Key features of the TMS320F243 EVM are:

- 544 words of on-chip data memory
- 28K words of onboard memory
- on-chip FLASH memory
- on-chip UART
- MP7680 four-channel digital-to-analog converter
- 5-volt-only operation

(For additional information, see the Technical Reference on this TMS320F243 EVM published by Spectrum Digital Incorporated in 1998.)

To operate the demonstration as described in the operational procedures section, the sensorless control software must be embedded in the TMS320F243 DSP. (For details on embedding the software in FLASH, please refer to the *TMS320F20x/F24x DSP Embedded Flash Memory Technical Reference*, literature number SPRU282.)

1.2.4 Magtrol Dynamometer

The dynamometer used to control load torque on the SRM in this demonstration hardware platform is manufactured by Magtrol Incorporated. It is a load cell dynamometer (model 705-6) that features a hysteresis brake for precise torque loading up to a maximum of 50.0 in-lb of torque and has a maximum speed capability of 10,000 RPM. Power rating for the model 705-6 dynamometer is 300 watts continuous and 1400 watts for less than five minutes. To achieve the best accuracy capability of 0.25%, attention must be given to the calibration of the unit for zero offset and scale factor as specified in the user’s manual. The motor shaft is attached to the dynamometer through a precision aligned flexible coupling that has been custom modified for this demonstration platform. Alignment of the motor shaft through the flexible coupling is critical to prevent vibration and mechanical induced noise at higher operation speeds above 2500 RPM. This type of flexible couplers can be obtained through Magtrol Incorporated.

1.2.5 Dynamometer Controller

Control of the dynamometer is provided by a Magtrol model 5240 controller that is a speed-controlled power supply, designed to interface with any type of IBM-compatible computer using an IEEE-488† general-purpose interface bus (GPIB) instrument controller. The model 5240 controller can be used to control any Magtrol Load Cell Dynamometer. In addition, it can be set to return torque-speed data to the computer when used with appropriate computer software. In this demonstration hardware, testing of the SRM performance was accomplished with an automatic-motor-testing software (M-TEST, version 2.03) provided by Magtrol.

1.3 Operational Procedures

To operate the demonstration, a serial communications link must be established between the ’F243 and the host PC by using a standard RS-232 through-pin serial cable. This cable is attached to the DB9 connector on the Spectrum Digital board and the COM port on the PC.

WARNING:

Do not use the DB9 connector on the EVM board. This connector is not isolated, and ignoring this warning could result in hardware damage, injury, or even death.

Commands can be issued through a terminal program such as a Hyperterm, which is included in the Windows™ operating system. To properly configure Hyperterm, the connection speed must be set at 19,200 baud, with 7 data bits, odd parity, and 1 stop bit, and all flow control must be disabled.

With the connection established, the demonstration rig can be turned on, using the following procedure:

1. Power up the PC, load controller, and dynamometer brake.
2. Run the terminal program and the Magtrol M-TEST software.
3. Turn on the dual power supply.
4. Plug in the bus supply line on the Spectrum Digital board.

Once power has been applied to all of the components, the terminal program can be used to issue the ‘turn on’ command, which is ‘>t’ followed by a carriage return. When the EVM receives the ‘turn on’ command, the ’F243 injects an alignment current into phase 2. After the shaft has settled at the aligned position, the ’F243 begins commutating the motor, causing it to spool up in the counterclockwise direction to its initial target speed of 1000 RPM. At this point, the ’F243 is ready to receive new commands, which are summarized in Table 3.

Windows is a registered trademark of Microsoft Corporation.
† ANSI/IEEE Standard 488.1 – 1987, IEEE Standard Digital Interface for Programmable Instrumentation.

Table 3. Description of Commands

Command†	Description
>t	Turn on drive system
>sxxxx	Set new target speed (in RPM) (0150 ≤ xxxx ≤ 4500)
>b	Brake motor and reverse direction
>a	Agitate the motor
>c	Cut off the drive system

† Each command must be followed by a carriage return.

These commands can set new target speeds, reverse the motor direction, agitate, or cut off the motor. If the speed command (‘>s’, followed by a four-digit number between 0150 and 4500) is issued, the motor will ramp up or down at 100 RPM/sec to the new requested target speed, provided it is between 0150 and 4500 RPM. If a speed is requested above the top speed of 4500 RPM, the new target speed will be set to 4500 RPM. Likewise, if the requested target speed is below 150 RPM, the new target will be set to 150 RPM. After the ramp is completed, the software will wait for a settling period of several seconds, and then wait to receive the next speed command.

If the next command is a brake command (‘>b’), the software will apply passive braking, which is accomplished by injecting a constant current into phase 2. After the motor slows down and aligns with phase 2, it will start up in the opposite direction, spool up to the initial target speed of 1000 RPM, and then continue ramping up or down to its former speed. The agitate command is quite similar to the brake command. When it is issued, the motor simulates the agitation action of a washing machine, i.e., it repeatedly brakes, aligns, reverses direction, and spools up to 1000 RPM. After repeating this sequence ten times, the software exits the agitation mode, and waits for a new command.

To turn off the motor, the user can either turn off the bus power or can issue the ‘cut off’ command (‘>c’), which de-energizes all of the motor phases and spinlocks the processor. Once this command is issued, the user can restart the system by following the procedure outlined above. (For further details concerning the ramp controller and serial communications, please refer to Section 2.)

Note: Commands issued while the motor is ramping and settling at a new target speed will be ignored.

1.4 Sensorless SRM Performance

Table 4 summarizes the performance of the SRM drive system.

Table 4. Sensorless SRM Performance Summary

Parameter	Value/Units
Speed range	150 – 4500 rpm
Load torque	48 oz-in
Speed regulation	< 8%
– low-speed	< 8%
– mid-range	< 1%
– hi-speed	< 2%
Start-up load torque	48.0 oz-in

For operating speeds between 1000 and 3500 RPM, regulation is tighter than 1%, within the design load of 48.0 oz-in. For higher speeds, regulation is more challenging and grows to 3% at the top speed of 4500 RPM. This happens because the speed measurement resolution decreases as the speed squared, due to sample rate effects. At the low end, speed regulation is affected by the reduced frequency of speed updates. This update rate is tied to the shaft speed, and these updates occur less and less frequently as the speed is decreased. To achieve the 10% performance specification below 400 RPM, the controller enters a special low-speed operating mode, which doubles the update rate and in turn preserves the bandwidth of the velocity loop. This keeps the regulation error below 8% at 150 RPM. (For further details concerning the low-speed operating mode, please refer to Section 2.) With the help of an open-loop start-up procedure, the motor can also be started reliably under a full load of 48.0 oz-in. This is valuable in pump and compressor applications, where the load is constant throughout the entire operating speed range.

2 Control Software for a Sensorless SRM Drive System

This section describes the control software for a sensorless SRM drive system using the TMS320F243 DSP. The drive system is intended for demonstration purposes and is composed of a TMS320F243 evaluation module (EVM); a digital motor controller board available from Spectrum Digital Incorporated; a 3-phase, 12/8 stator-pole-configured 0.40-HP SRM manufactured by Emerson Electric Company; and a Magtrol 50.0 lb-ft dynamometer and load controller. (For further details concerning the hardware and performance specifications for this drive system, refer to Section 1.)

The control software features a flux-based sensorless algorithm for 3-phase SRMs operating on 170 V of bus voltage and up to 4.0 A of phase current. The algorithm is capable of two quadrant speed control between 150 and 4500 RPM, with better than 8% speed regulation (<1% between 1000 and 3500 RPM), and reliable start-up under a design load of 48.0 oz-in. An RS-232 serial link permits users to issue commands from a host PC to turn on, cut off, and change motor speed and the direction of rotation on the fly. This software can be launched via the EVM's JTAG port using a XDS510PP™ emulator board inline with a SPI 110 optoisolator or the software can be directly embedded in the EVM's FLASH memory. (For further details on FLASH programming, refer to the *TMS320F20x/F24x DSP Embedded FLASH Memory Technical Reference*, literature number SPRU282.)

2.1 Overview of the Sensorless SRM Control Software

The software for the sensorless drive system is written primarily in C, with the exception of a few assembly language subroutines for high-speed computations. The code fits into the TMS320F243's 8K of FLASH program memory and the DSP's internal RAM blocks, and requires no external memory. It consumes about 6K of program memory and 300 words of data memory. To execute the code on a TMS320C242 DSP controller, the program storage requirements can be reduced to less than 4K by replacing the look-up tables used by the commutation algorithm with polynomial interpolating functions.

As shown in Figure 3, the software is composed of five key modules: an algorithm for sensorless commutation, an outer loop for velocity control, an inner loop for current control, a serial command processor, and a ramp controller. The first three of these modules execute in the foreground. They are called from a timer interrupt service routine (ISR), which is fired every 66.7 μsec (15.0 kHz) by a free-running onboard timer. As shown in the timing diagram of Figure 3, the commutation controller and current control loop execute every interrupt cycle (at 15.0 kHz), while the velocity loop only executes every sixth interrupt cycle (at 2.5 kHz).

XDS510PP is a trademark of Texas Instruments Incorporated.

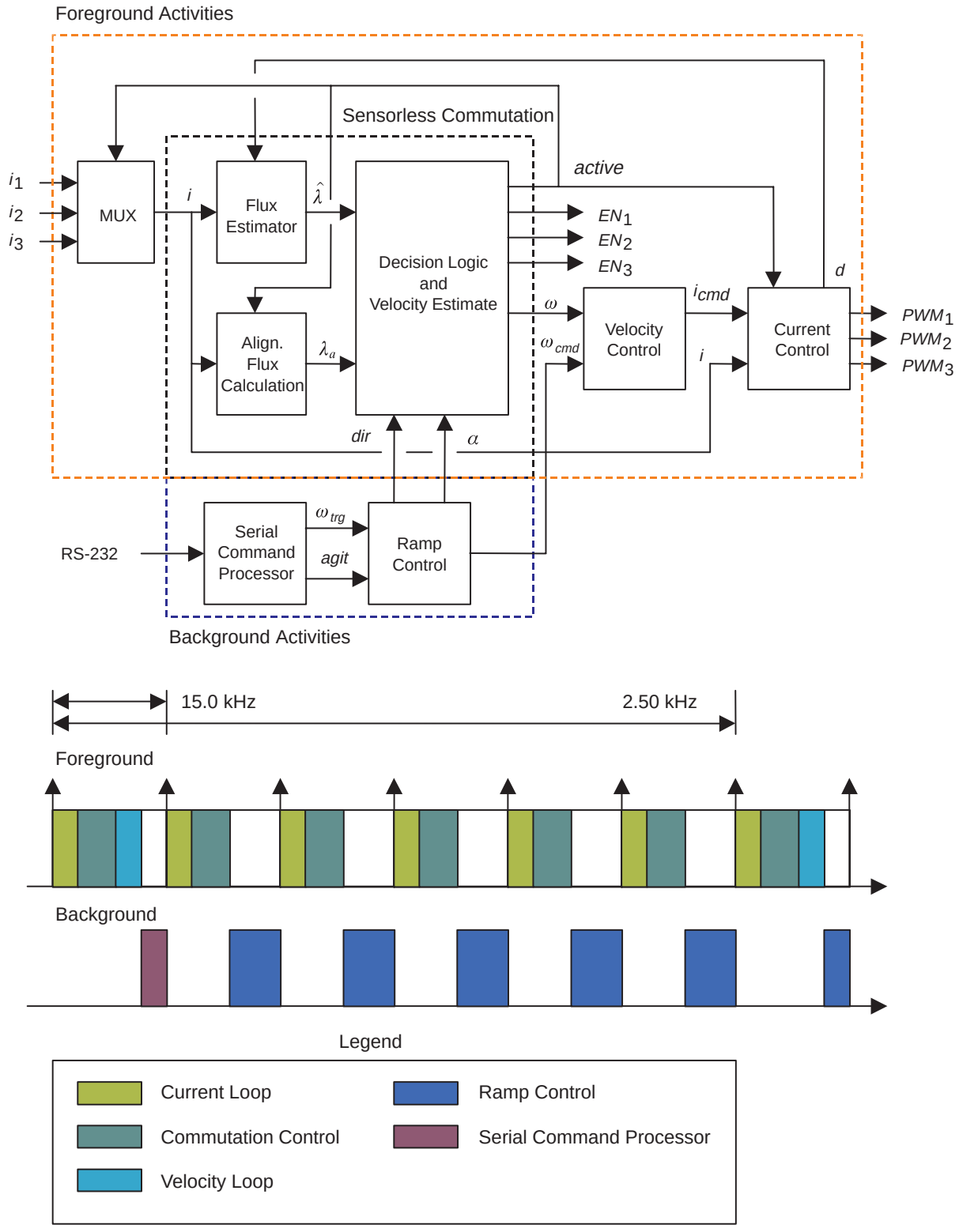

Figure 3. Software Block and Timing Diagrams

The execution time of each foreground activity shown in the software block diagram is listed in Table 5.

Table 5. Execution Times of Foreground Activity

Activity	Execution Time (μsec)
Flux Estimator	8.3
Sensorless Commutation	15.5 to 34.8
Current Control Loop	10.6
Velocity Control Loop	11.3

Note that execution time of the sensorless commutation algorithm varies. If the motor needs to switch phases and perform a velocity update, the run time will be 34.8 μsec; otherwise, the run time will be 15.5 μsec.

Overall, execution time of the ISR varies from 34.4 μsec to 53.2 μsec, depending on which activities must execute. On average, the interrupt service routine utilizes 55% of the processing time, leaving the remaining 45% for the background loop, which includes a serial command processor and ramp speed controller.

2.2 Sensorless Commutation and Velocity-Update Algorithm

At the core of the sensorless algorithm is the commutation controller, which contains a flux estimator, flux reference generator, and decision logic. Ideally, the decision logic should commutate the motor when the rotor and stator poles are nearly in alignment. For this particular algorithm [1], the flux in the active phase winding is compared with a reference flux, which is a scaled version of the flux at the aligned pole position. The decision logic commutates the motor when the flux linkage exceeds the switching or reference flux. To be precise, the motor is commutated when:

$$\hat{\lambda} > \alpha_c \lambda_a \tag{1}$$

where $\hat{\lambda}$ is an estimate of flux in the active phase winding; α_c is a scalar between 0 and 1, which is analogous to a conduction angle; and λ_a is the flux at the aligned rotor position. This commutation condition is shown graphically in Figure 4.

As indicated by condition (1), properly timed commutation depends on an accurate estimate of the flux in the active phase winding, a knowledge of the magnetization curve at the aligned rotor position, and a carefully selected firing angle.

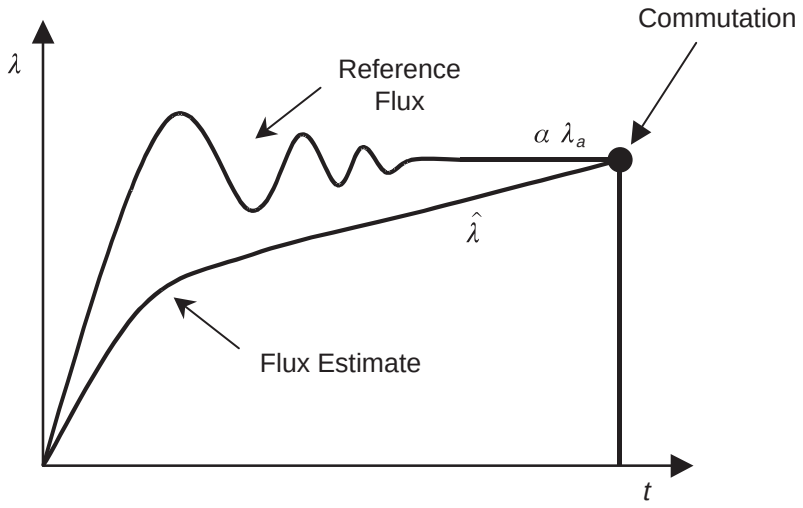

Figure 4. Graph of Flux Estimate and Flux Threshold vs. Time

2.2.1 Flux Estimator

As shown in the software block diagram of Figure 3, the quantity $\hat{\lambda}$ is generated by the flux estimator block, which calculates flux based on the pulse width modulation (PWM) duty cycle and the current in the active phase winding. Its principle of operation is the same as a “classical” flux estimator, which uses the update law

$$\lambda_{n+1} = \lambda_n + \underbrace{v_n - i_n\, r_w}_{v_{EMF}} \tag{2}$$

to integrate the back EMF in the active phase winding. In Equation (2), v_n is the motor terminal voltage, i_n is the coil current, and r_w is the winding resistance. However, unlike this classical flux estimator, which requires terminal voltage *and* coil current measurements, this modified estimator only relies on current measurements. Instead of measuring the terminal voltage, it is approximated using the formula

$$v_n \approx V_{\text{bus}}\, d_n - v_{\text{trans}}\,(i_n) - v_{\text{diode}}\,(i_n) \tag{3}$$

which takes into account the voltage drops across the active devices in the power inverter, whose topology is shown in Figure 5. In Equation (3), V_{bus} is the bus voltage; d_n, the duty cycle; v_{trans}, the voltage drop across the power transistor; and v_{diode}, the diode voltage drop. Notice that Equation (3) assumes that the bus voltage is a stiff source, and that the $v - i$ curves of the power devices are known. Substituting Equation (3) into the original formula, the new update law becomes

$$\lambda_{n+1} = \lambda_n + \underbrace{V_{\text{bus}}\, d_n - v_{\text{trans}}\,(i_n) - v_{\text{diode}}\,(i_n) - i_n\, r_w}_{v_{EMF}} \tag{4}$$

For simplicity, the drops across the power transistor, diode, and winding resistor are combined into a single term, called the loss voltage, permitting Equation (4) to be written as

$$\lambda_{n+1} = \lambda_n + \underbrace{V_{\text{bus}}\, d_n - v_{\text{loss}}\,(i_n)}_{v_{EMF}}, \quad \text{where} \quad v_{\text{loss}}\,(i_n) \equiv v_{\text{trans}}\,(i_n) + v_{\text{diode}}\,(i_n) + i_n r_w \tag{5}$$

With the “loss” voltage tabulated as a function of current, the update is performed in the software with two additions, a scalar multiplication, and a single look-up operation. (For more information on how to construct the voltage loss table, please refer to Section 3.)

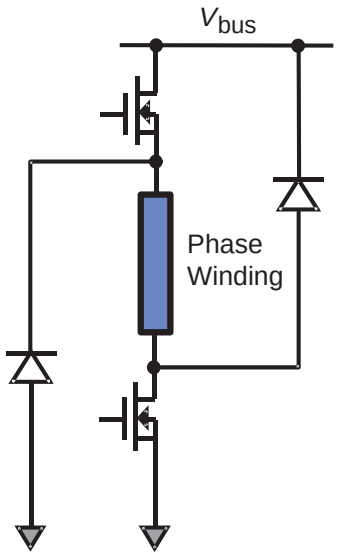

Figure 5. SRM Power Driver Topology

2.2.2 Flux Estimator Implementation

The subroutine `update_flux_estimate()` updates the flux estimate based on the duty cycle applied to the PWM generator and the current measured in the active phase winding. As shown in Figure 6, the code implements Equation (5) in a straightforward manner, with the exception of the look-up operation. To perform the look-up operation, an index into the 256-point table is generated by shifting i_n, a 10-bit unsigned integer, two places to the right. The address of the desired table element is formed by adding this index to the table’s base address, and the table is accessed by invoking the assembly language subroutine `long_table_read()`. This subroutine reads the desired table element from FLASH program memory using a table-read operation (`TLBR`) and returns the value in a desired data memory address. After completing the table read, both terms in Equation (5) are added to the previous flux estimate to form the new one, and the update is stored in the SRM data structure. This update is a scaled version of actual flux linkage in the winding. To convert it to physical units of V-sec, multiply by the following scale factor:

$$\hat{\lambda} = \frac{\texttt{anSRM -> fluxEstimate}}{1000 \times 15000} \tag{6}$$

In Equation (6), the factor of 1000 reflects the fact that the actual volts have been scaled by the maximum duty cycle count of 1000, and the factor of 15,000 reflects the fact that the time-step of 66.7 μsec has been omitted from the integration.

```
void update_flux_estimate(anSRM_struct *anSRM)
{
      int phase;
      long temp1, temp2;
      long dflux;

      phase = anSRM–>Active;

      /*-----------------------------------------------*/
      /* update flux linkage estimate                  */
      /*-----------------------------------------------*/
      temp1 = (VBUS * anSRM–>dutyRatio[phase]);
      long_table_read(VoltTable+(anSRM–>iFB[phase]>>2),&temp2);
      dflux = (temp1–temp2);

      anSRM–>fluxEstimate[phase] = anSRM–>fluxEstimate[phase] + dflux;

      if (anSRM–>fluxEstimate[phase] < 0 ) {
            anSRM–>fluxEstimate[phase] = 0;
      }
}
```

Figure 6. Flux Estimator Code

2.2.3 Flux Reference Generator

To check the commutation condition, the decision logic must compare the flux estimate against a reference flux λ_c, which is the product of a conduction angle α_c and the flux at the aligned rotor position λ_a. The conduction angle α_c is established by the ramp controller, which varies α_c as a function of operating speed to maximize the motor's efficiency. The quantity λ_a, is returned by the subroutine `get_alignedFlux ()`. This routine looks up what the flux would be at the aligned rotor position, given the current i_η and the active phase winding. As in Section 2.2.2, the `long_table_read()` subroutine must be invoked to retrieve the desired table element from FLASH memory.

2.2.4 Lockout Window

The decision logic which has been described to this point will time the commutations properly if the motor has been well characterized and if a *low-noise* current measurement is available. However, under certain operating conditions, noise levels in the current signal will rise, and this may trip the decision logic at the wrong moment. While the integral action of the flux estimator naturally filters out noise, the flux threshold is more sensitive, since it depends only on the *instantaneous* current. At low current levels, present at the beginning of the commutation cycle, the noise may be sufficient to suddenly drop the switching threshold, and accidentally trip the commutation logic. This problem is particularly apparent at high load torques and manifests itself in the form of motor speed oscillations, which are shown in Figure 7.

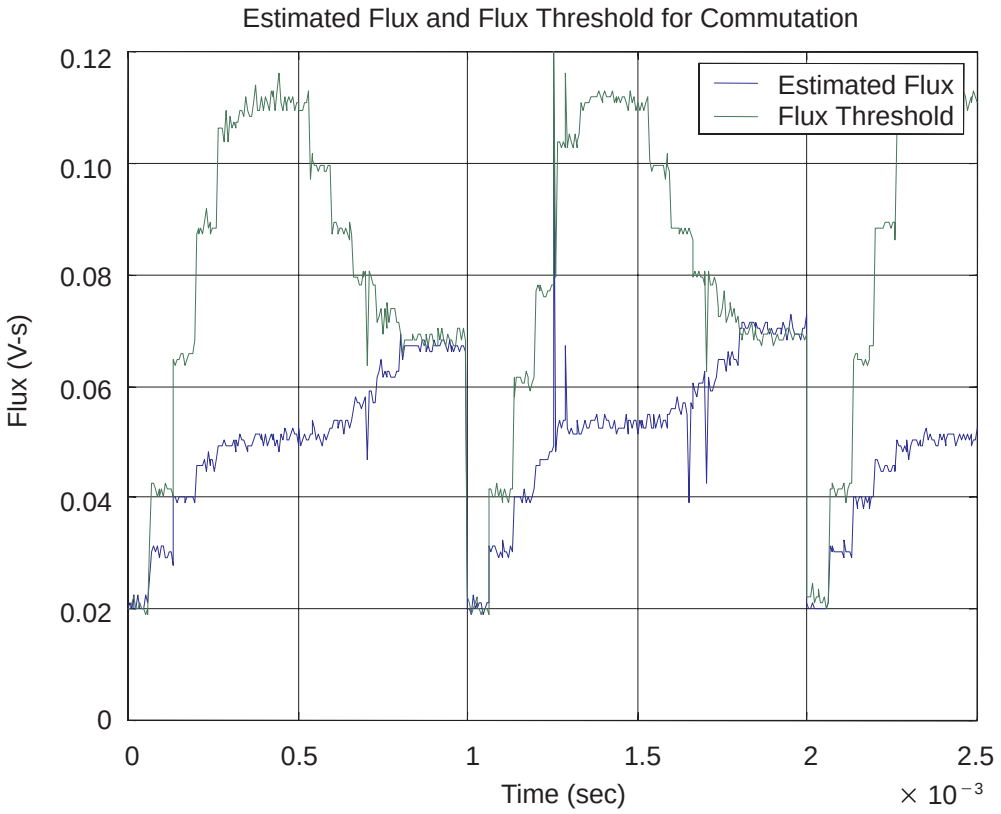

Figure 7. Flux Estimate and Threshold at 2500 RPM Under Full Load. The flux threshold comes perilously close to tripping the commutation logic at the beginning of the commutation cycle.

By enforcing a lockout window, depicted in Figure 8, which prohibits commutation for three sample periods (200 µsec at 15.0 kHz) at the beginning of the commutation cycle, current noise is unable to prematurely trip the commutation logic. While improving the noise rejection of the commutation algorithm, this lockout interval does impose an upper limit on the motor's commutation rate, which in turn, limits the motor's maximum speed to 12,500 RPM.

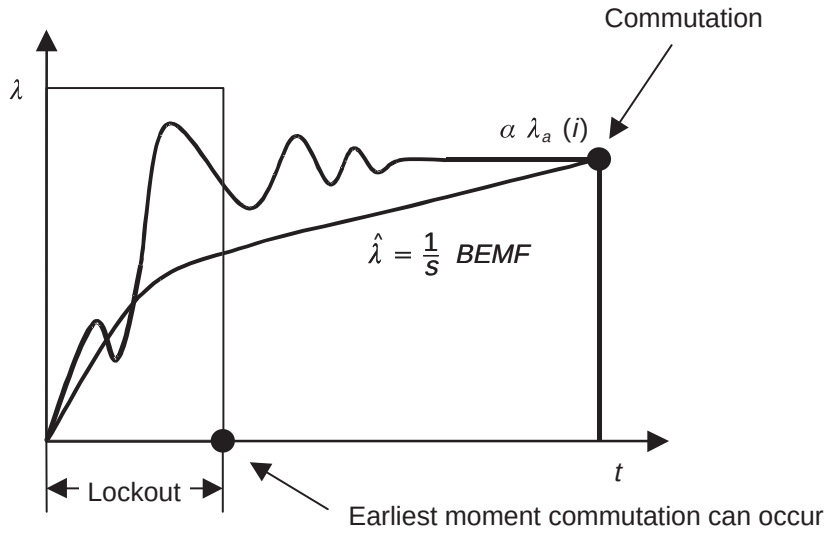

Figure 8. Illustration of Sensorless Commutation Algorithm With Lockout Window

2.2.5 Velocity Estimator

To estimate shaft velocity, a software timer counts the number of sample periods between successive commutations. When a commutation occurs, the instantaneous velocity is evaluated in RPM using the formula

$$\hat{\omega}_{INST} = K_{conv}\left(\frac{\Delta\theta}{\Delta t}\right) = K_{conv}\, f_s \left(\frac{\Delta\theta}{N}\right) = \frac{37,500}{N} \tag{7}$$

where N is the sample count, K_{conv} converts rads/sec to RPM, and f_S is the sampling frequency of 15.0 kHz. Since Equation (7) involves a reciprocal calculation, this formula is implemented as an assembly language function. This function performs the reciprocal operation using 16 back-to-back conditional subtract instructions (SUBC). As a result, the entire operation only requires 2.0 μsec.

After the instantaneous velocity is calculated, the estimate is processed by a first-order infinite impulse response (IIR) filter of the form

$$\hat{\omega}_{FILT_{n+1}} = \beta\hat{\omega}_{FILT_n} + (1 - \beta)\ \hat{\omega}_{INST} \tag{8}$$

where β is a number close to 1.0 before it is passed on the velocity loop. This additional filtering deliberately reduces the velocity loop bandwidth to prevent the velocity loop from acting on noisy estimates. This filter block also improves operation at high speeds where the instantaneous velocity can vary significantly from estimate to estimate due to the small number of samples in a commutation period. By providing the velocity loop with a velocity measurement “averaged” over many commutation periods, speed oscillations are avoided.

2.2.6 Stall Detector

If the instantaneous shaft velocity drops below 60 RPM after the motor startup has completed, a stall detector in the decision logic will engage. After the logic detects a stalled condition, it calls a subroutine which immediately cuts off the motor. This routine sets all PWM generator duty cycles to zero, switches off the lowside power transistors, zeroes out all of the desired currents, illuminates all LEDs on the EVM board, and goes into an infinite loop. A processor reset is required to restart the system. This safety feature prevents the motor from overheating if the shaft suddenly becomes locked in place.

2.2.7 Low-Speed Operating Mode (<400 RPM)

As the shaft speed is lowered, velocity updates arrive with decreasing frequency, and the bandwidth of the velocity loop suffers. If the motor is suddenly loaded at a low operating speed (<400 RPM), the integrator in the velocity loop may not respond before the shaft velocity dips low enough to trigger the stall detector. To help improve loop bandwidth under these conditions, at speeds below 400 RPM, the commutation algorithm enters a special low-speed operating mode. In this mode, the velocity-update rate is doubled, by estimating the velocity twice every commutation cycle. As shown in Figure 9, this is done by adding a second flux threshold, which triggers *only* a velocity update.

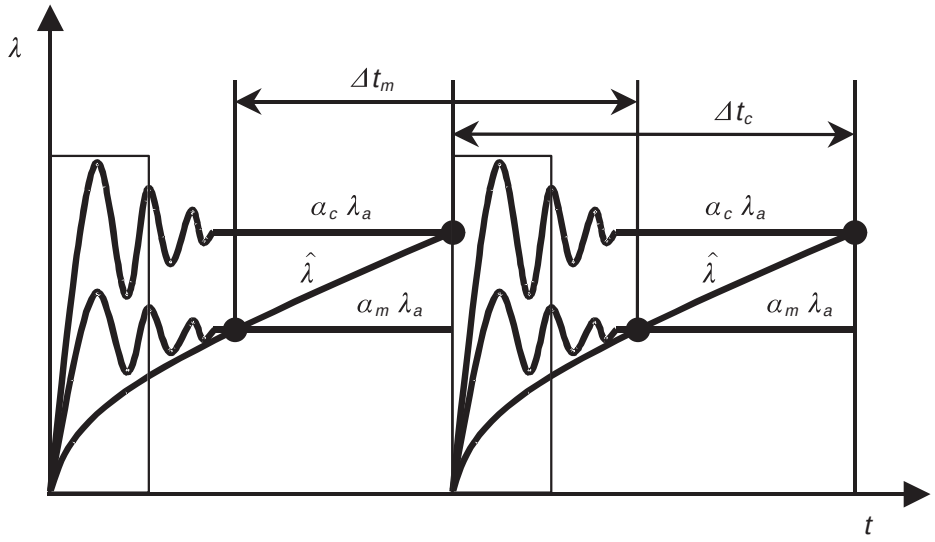

Figure 9. Low-Speed Operating Mode With a Second Flux Threshold for an Additional Velocity Update

As before, this threshold is a scaled version of the aligned rotor flux. Due to the sawtooth shape of the flux waveform, by setting $\alpha_m = \alpha_c / 2$, the new velocity update will occur approximately midway through the commutation. To implement the midway velocity update, a second counter is used to keep track of the number of samples between successive crossings. These overlapping measurement intervals permit the update rate to be doubled, and using this approach, it has been possible to extend the lower speed range from 300 RPM to 150 RPM. As in the commutation, a lockout interval is enforced to prevent current noise from accidentally triggering a velocity update at an unintended moment.

2.2.8 Commutation and Velocity-Update Algorithm Summary

The flowchart in Figure 10 summarizes the entire commutation and velocity-update algorithm. After the algorithm commutates the motor, it resets the flux estimator, the lockout sample counter, and the second velocity counter. Every sample period, the ISR calls the sensorless commutation routine, which increments both velocity counters. If the lockout counter is non-zero, it is decremented just before exiting the subroutine. However, if the lockout counter has expired, a commutation can occur, and further tests are performed. If low-speed mode is enabled (<400 RPM) and the first velocity update has not occurred, the flux estimate is compared against the first threshold. If the estimate has crossed the threshold, a new instantaneous velocity is calculated using the value in the first update counter, and a flag is set to indicate that the first update has occurred. This flag is important, because if it is not used, then the velocity update will occur every time the ISR is invoked until the commutation cycle ends, each time with a velocity estimate of 12,500 RPM! Following the first threshold crossing, the algorithm will check the flux estimate against the second flux threshold. When the second threshold is crossed, the velocity is updated using the second counter, and the motor is commutated.

When the motor is commutated, the current request for the active winding is zeroed, and the software advances to the next active phase, based on the direction of rotation. Next, the velocity loop's output is assigned to the current request for the next active winding. While this assignment will be made the next time the velocity loop is executed, it may take up to six sample periods for this to happen. While a variable delay of one to six sample periods is acceptable at low operating speeds, this causes problems at high speeds where there is a much smaller number of samples in a commutation cycle. Finally, the A/D MUX is switched to the next channel, and the lowside insulated gate bipolar transistor (IGBT) is turned on for the next phase winding and the lowside IGBT in the previous phase is turned off.

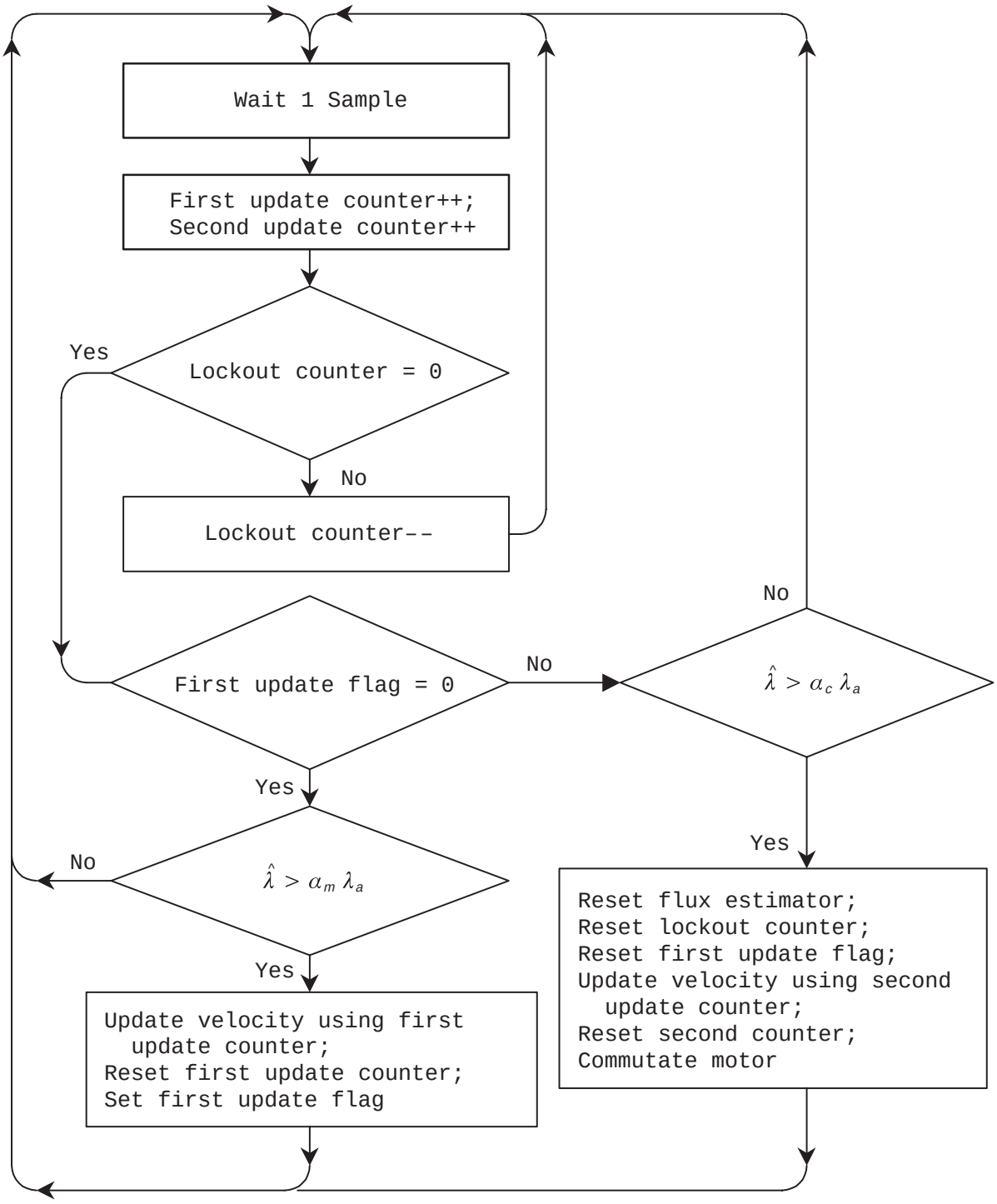

Figure 10. Commutation and Velocity-Update Flow Diagram

2.3 Velocity Loop

The velocity loop, which executes at a frequency of 2.50 kHz, employs a discretized proportional-integral (PI) control law to control motor shaft speed. The proportional term in the control law damps out speed oscillations and the integral term drives the DC speed errors to zero. As shown in the block diagram of Figure 11, for safety reasons, a windup limit of 6.25 A in the positive direction and the same in the negative direction is imposed on the integrator. In addition, an upper and a lower current command limit are placed on the output of the velocity loop. The upper limit is imposed for safety reasons and varies with operating speed; the lower positive limit ensures that there is sufficient amount of current to make commutation decisions.

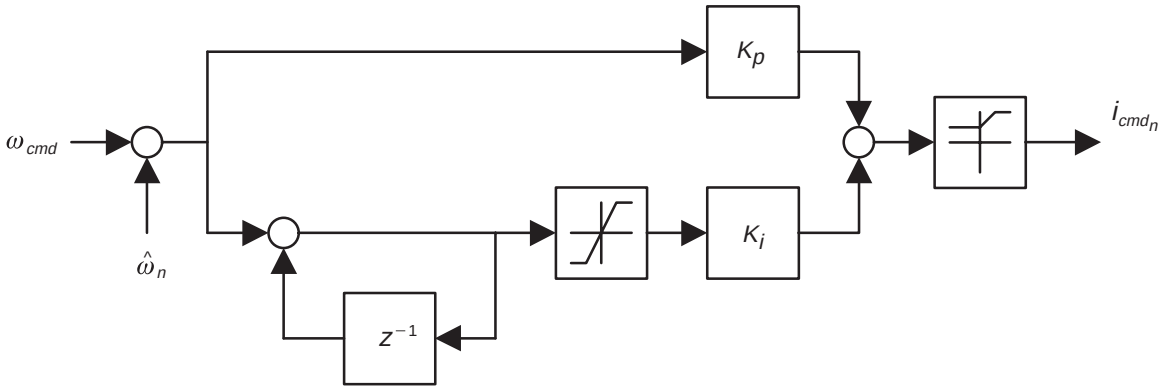

Figure 11. Block Diagram of the Velocity Control Loop

2.3.1 Motor Start-up Under Load

When the motor is started under load, the software counters that gauge the time between commutations can roll over, corrupting the speed estimates, and causing the velocity loop to command an improper amount of current. When this happens, the motor may experience start-up hesitation, may start up in the wrong direction, or may even stall altogether. To solve this problem, the integrator in the velocity loop is given a large initial value, which exceeds the current command limit. This causes the initial velocity estimates to be neglected and a large amount of torque to be applied to the motor. In effect, the velocity controller runs open-loop. When the velocity estimates start to exceed the initial target velocity of 1000 RPM, the integrator begins “unwinding” at a rate that depends on the difference between the estimated and desired velocity. As the integrator output decreases, eventually the velocity loop output falls below the current command limit, and the velocity controller resumes closed-loop operation and regulates the speed to 1000 RPM.

This initial integrator value should be sufficient to start the motor up reliably under full load, but should be no larger than necessary. A oversized value will cause too much velocity overshoot, perhaps more than the application can tolerate, whereas an undersized value may not start the motor up reliably. In the code, an initial integrator value has been chosen which is sufficient to start the motor up reliably under a load of 48.0 oz-in. The start-up procedure which has been described is shown in Figure 12, which graphs the estimated velocity and the command current versus time for a no-load condition.

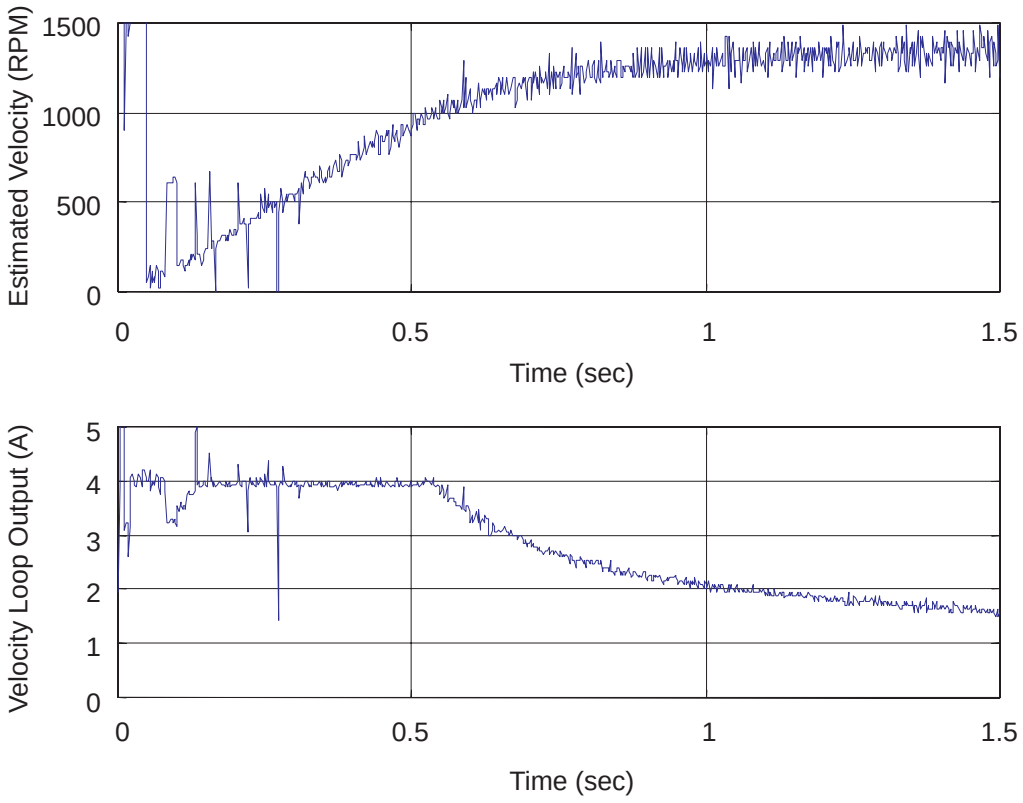

Figure 12. Instantaneous Velocity Estimate and Velocity Loop Output During Start-up

In Figure 12, it is evident that the velocity is overestimated immediately following start-up. This causes a momentary drop in the integrator output from saturation, but the integrator winds up again, the velocity controller saturates for approximately the first 0.50 seconds. Shortly after reaching the initial target velocity, the integrator unwinds enough to bring the velocity controller out of saturation, and the system resumes closed-loop operation. The velocity loop overshoots about 30% under no-load conditions, but under the design load of 48.0 oz-in, the overshoot is less than 10%.

2.4 Current Control Loop

The current control loop, illustrated in Figure 13, which executes at the sampling frequency of 15.0 kHz, employs a proportional control law to realize the current requests which arrive from the velocity loop.

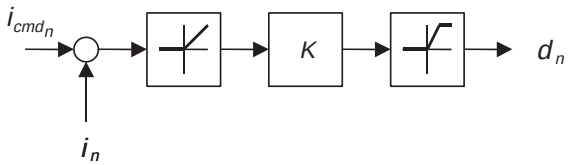

Figure 13. Block Diagram of the Current Control Loop

Every sample period, the current controller reads the latest current sample and calculates the current error, which is the difference between the measured and requested current. For positive errors, the controller calculates a duty cycle to the active PWM channel in proportion to the error. This calculated duty cycle becomes the applied one, provided that the calculated value is below the current command limit. Otherwise, the assigned duty cycle is the saturation limit. This saturation limit is set to 50% for start-up, but is relaxed to 90% after the motor reaches its steady-state operating speed. A 100% duty cycle is never permitted, because the drivers need time to refresh. For negative errors, the duty cycle is set to zero; this soft-chops the channel, and the current decays until the error once again becomes positive.

2.5 Ramp Controller

The ramp controller receives speed and direction commands from the serial comms module and applies the necessary sequence of commands to the commutation controller, velocity loop, and current loop to achieve the new target speed and direction. It runs in the background as a software-state machine. After the motor has settled to a new target speed and direction, the ramp controller enters its wait state. In this state, it continually checks with the serial command processor to see if a new command has arrived across the RS-232 link.

If a new target speed arrives, the ramp controller shifts into its ramp state, as shown in the state transition diagram of Figure 14. Depending upon whether the new target speed is above or below the current operating speed, the ramp controller will either increment or decrement the current command speed by 1 RPM. As the command speed is increased or decreased, the conduction angle is adjusted for efficient torque production and the current command limit is also adjusted. If the command speed falls below 400 RPM, the low-speed operating mode is activated, which doubles the velocity-update rate. A real-time delay is also inserted, to ensure specific ramp-up and ramp-down rates of 100 RPM/sec or 50 RPM/sec, respectively. The ramp controller remains in this state until the command speed has reached the target speed. When this happens, the controller resets the settle counter and transitions into the settle state. The purpose of this state is to allow any speed transients to die down before accepting any new target speeds from the serial command processor. The controller remains in the settle state until the counter expires, which happens after approximately two seconds. When the counter expires, the controller returns to the wait state, and awaits a new target speed.

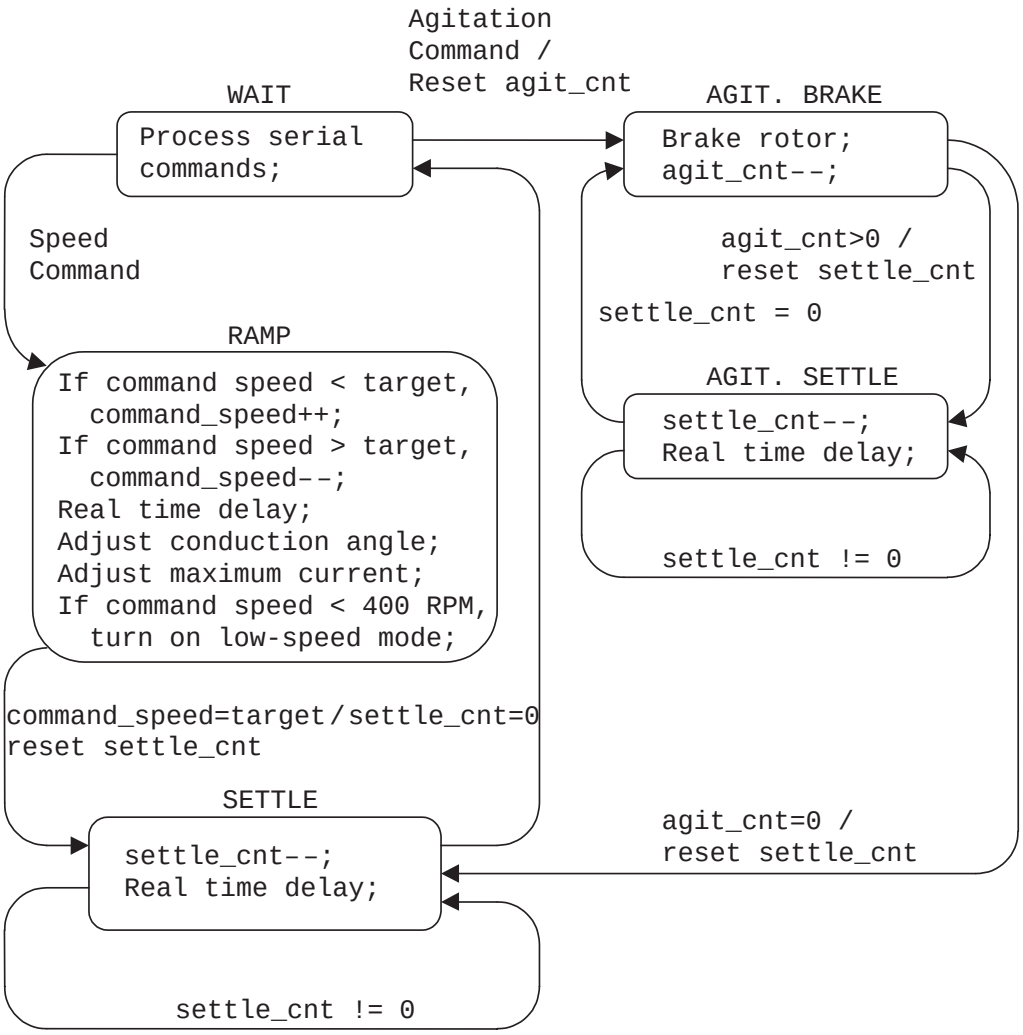

Figure 14. State Transition Diagram for the Ramp Controller

If the controller receives an agitation command, it resets its agitation counter before moving into the agitation brake state. Once there, a braking routine is called, disables the velocity loop and commutation controller. To passively brake the motor, phase 2 of 2 is energized with a constant current command of 3.0 A. The software delays four seconds while the motor brakes and the shaft aligns. Next, the phase is de-energized, the motor data structure, various counters and flags are re-initialized, and a new target speed of 1000 RPM is established and the commutation direction is reversed. To restart the motor, phase 0 or 1 is energized, depending on the direction of rotation, the A/D MUX is switched to the appropriate channel, and the commutation and velocity loops are re-enabled. Once the motor has started in the opposite direction, the agitation counter is decremented, the settle counter is reset, and the ramp controller enters the agitation settle state. It remains in this state for about 20 seconds, which allows the motor to settle to its 1000-RPM target speed. After the settle counter expires, the processor repeats until the agitation counter reaches zero, at which point, the controller transitions to the settle state, and eventually to the wait state, ready to accept a new serial command.

2.6 Serial Comms

The serial communications module receives and processes character command strings which are sent by users across the RS-232 link from the host computer. The serial communications interface (SCI) on the ’F24X is configured to run at 19,200 baud with 7 data bits, 1 stop bit, and odd parity. The communications module has five commands in its command set, which are summarized in Table 6.

Table 6. Serial Communications Module Commands

Command†	Description
>t	Turn on drive system
>sxxxx	Set new target speed (in RPM) (0150 ≤ xxxx ≤ 4500)
>b	Brake motor and reverse direction
>a	Agitate the motor
>c	Cut off the drive system

† Each command must be followed by a carriage return.

These commands are used to turn on the drive system, set a new target speed, reverse motor direction, agitate the motor, and cut off the drive. Note that all commands start with a ‘>’ lead-in character, followed by a command character, and must end with a carriage return, which is not shown in the command column. The speed command ‘s’ character is followed by four digits and a carriage return to indicate a new target speed.

The command processor is implemented as a software-state machine, and is invoked only when the ramp controller is in the wait state. (The exception to this is the ‘turn on’ command, which must be issued to initiate the motor start-up sequence.) Commands which are issued at other times, such as when the ramp controller is ramping the motor to a new target speed, are ignored. When the command processor is called, it checks to see if a character is waiting in the SCI receive buffer. If a character has arrived, that character is processed; otherwise, the routine promptly exits and returns control to the ramp controller. The action which is taken depends on the newly received character and the current state of the command processor.

In its default lead-in state, the command processor waits for a lead-in character. Once a lead-in character is received, the processor transitions to the command state. In this state, it waits for a valid command character. If the ‘turn on’ command ‘t’ is received, the command processor waits for a carriage return, and then sets the ‘turn on’ flag. This begins the motor startup sequence. If the speed command character ‘s’ is received, the processor waits for four digits, converts these four characters to a number, and then waits for a carriage return. At this point, the processor checks to see if the target speed is within bounds. If not, the processor limits the upper speed to 4500 RPM and the lower speed to 150 RPM. Next, the processor notifies the ramp controller that a new target speed has arrived by setting a flag and then returns to the lead-in state. If the agitation command ‘a’ is received, the agitation counter is reset, the ramp controller is placed in the agitation brake state (starting the agitation motion sequence), and the processor returns to the lead-in state. If the reverse command ‘b’ is received, the processor goes through passive breaking and alignment, starts the motor in the opposite direction, places the ramp controller in the ramp state to bring the motor up to its previous speed. This is the same sequence as a single agitation. If the ‘cut off’ command ‘c’ is received, the processor disables all interrupts, cuts off the motor in the same manner as the stall detector, and returns to the lead-in state.

3 Calibration for a Sensorless SRM Drive System

The sensorless algorithm presented in Section 2 depends on an accurate estimation of flux in the active phase winding. To enhance estimation accuracy, this algorithm includes the voltage drops across the power devices, which must be obtained as a function of current. The first part of Section 3 describes a technique for measuring the combined voltage drop across the power devices and the winding resistance as a function of current using the existing demonstration hardware. Besides an accurate flux estimate, the algorithm requires a knowledge of the magnetization curve at the aligned rotor position. The second part of Section 3 documents an analog flux-measuring circuit used to obtain the aligned magnetization curve to a high degree of accuracy. With this procedure, users can adapt the sensorless algorithm for SRMs with different electrical properties.

3.1 Stator Flux Estimation

Besides a knowledge of the magnetization curves at the aligned rotor position, an accurate flux estimate must be developed by the motor-control software to successfully commutate the motor. To estimate the flux linkage, the back EMF of the active phase winding is integrated, using the update law:

$$\lambda_{n+1} = \lambda_n + \underbrace{v_n - i_n\, r_w}_{v_{EMF}} \tag{9}$$

In Equation (9), v_n is the motor terminal voltage, i_n is the coil current, and r_w is winding resistance. To reduce the cost of the motor drive system, the terminal voltage is not measured explicitly. Instead, it is approximated, using the formula

$$v_n \approx V_{\text{bus}}\; d_n - v_{\text{trans}}\;(i_n) - v_{\text{diode}}\;(i_n) \tag{10}$$

where V_{bus} is the bus voltage; d_n, the duty cycle; v_{trans}, the voltage drop across the power transistor; and v_{diode}, the diode voltage drop. Notice that Equation (10) assumes that the bus voltage is a stiff source, and that the $v - i$ curves of the power devices are known. Substituting Equation (10) into the original formula, the new update law becomes

$$\lambda_{n+1} = \lambda_n + \underbrace{V_{\text{bus}}\; d_n - v_{\text{trans}}\;(i_n) - v_{\text{diode}}\;(i_n) - i_n\, r_w}_{v_{EMF}} \tag{11}$$

For simplicity, the drops across the power transistor, diode, and winding resistor are combined into a single term, called the loss voltage, permitting Equation (11) to be written as

$$\lambda_{n+1} = \lambda_n + \underbrace{V_{\text{bus}}\; d_n - v_{\text{loss}}\;(i_n)}_{v_{EMF}}\quad,\quad \text{where}\quad v_{\text{loss}}\;(i_n) \equiv v_{\text{trans}}\;(i_n) + v_{\text{diode}}\;(i_n) + i_n r_w \tag{12}$$

In Equation (12), the update is performed in the software with two additions, a scalar multiplication, and a single look-up operation.

3.2 Measuring the Voltage “Loss” Function

To implement Equation (12), the “loss” voltage is measured as a function of current and a look-up table is constructed. This is accomplished by applying a fixed duty cycle PWM waveform to the motor winding. After the transients die down, the flux on the left- and right-hand side of Equation (12) will be equal, and can be cancelled out, leaving the steady-state equation:

$$v_{loss}\ (i_n) = V_{bus}\ d_n \tag{13}$$

A simple program, whose flow diagram is shown in Figure 15, can be written on the ’F243 automate data collection for the look-up table construction. The program begins by setting up the PWM generator and clearing the index counter. At the start of the program loop, the compare register is assigned the index value, which generates a fixed PWM duty cycle corresponding to $d_n = n/n_{max}$, where n_{max} is the counter value that corresponds to a 100% duty cycle. For a ’F243 running at 20.0 MHz with a carrier frequency of 20.0 kHz, n_{max} = 1000. After applying the fixed duty cycle, the program waits for several seconds until the current reaches a steady-state value. When this happens, the current-voltage pair is recorded in an array. Next, the index is advanced, and if the new index value is less than n_{final}, the process is repeated.

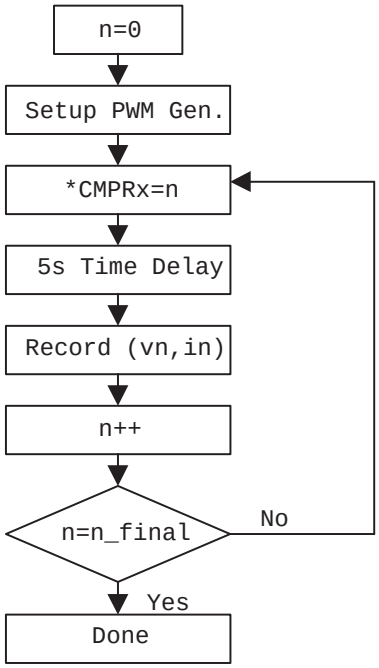

Figure 15. Flow Chart for Voltage “Loss” Measurement Program

To avoid blowing fuses that are located on the digital motor controller board or damaging components, n_{final} must be carefully chosen. To calculate an approximate value for n_{final}, calculate the “loss” voltage at the maximum current, using the formula:

$$v_{loss}\ (i_{max}) = v_{diode}\ (i_{max}) + v_{trans}\ (i_{max}) + i_{max}\ r_w \tag{14}$$

From this, calculate the duty cycle needed to generate this “loss” voltage:

$$n_{final} = \left\{ \frac{v_{loss}(i_{max})}{V_{bus}} \right\} n_{max} \tag{15}$$

Using an i_{max} = 4.0 A, a diode drop of 0.70 V, and a voltage drop of 1.1 V across the IGBT, a winding resistance of 2.5 ohms, a typical bus voltage of 170.0 V, and an n_{max} = 1000, $n_{final} \approx 70$.

3.3 Generating a Voltage “Loss” Look-up Table

After the voltage-current data is recorded in the array, it is exported via the XDS510™ to the PC, the data is fitted with a polynomial curve, with voltage as a function of current. To simplify calculation of the table index, the function is evaluated at the current points

$$i_n = i_{max} \left(\frac{n}{256} \right) \forall\ n = 0 \ldots 255 \tag{16}$$

Using these points, an index into the 256-point look-up table can be rapidly calculated by right-shifting the 10-bit current measurement over two places.

3.4 Measuring the Voltage “Loss” Data

Figure 16 shows a loss table constructed exactly in the manner described in the preceding section. This figure contains two curves, which compare the total v_{loss} against purely ohmic losses. At low currents, the voltage drops across the diode and the transistor dominate; whereas, at higher currents, this drop becomes almost a constant 1.8 volts, and the ohmic losses dominate. As the figure shows, accounting for the active components significantly improves the accuracy of the flux estimator, particularly at low currents, where the voltage losses are due primarily to the high dynamic impedance of the diode and the transistor. By including the power devices, motor commutation is improved considerably under no-load and light-loading conditions, resulting in more accurate speed regulation.

XDS510 is a trademark of Texas Instruments Incorporated.

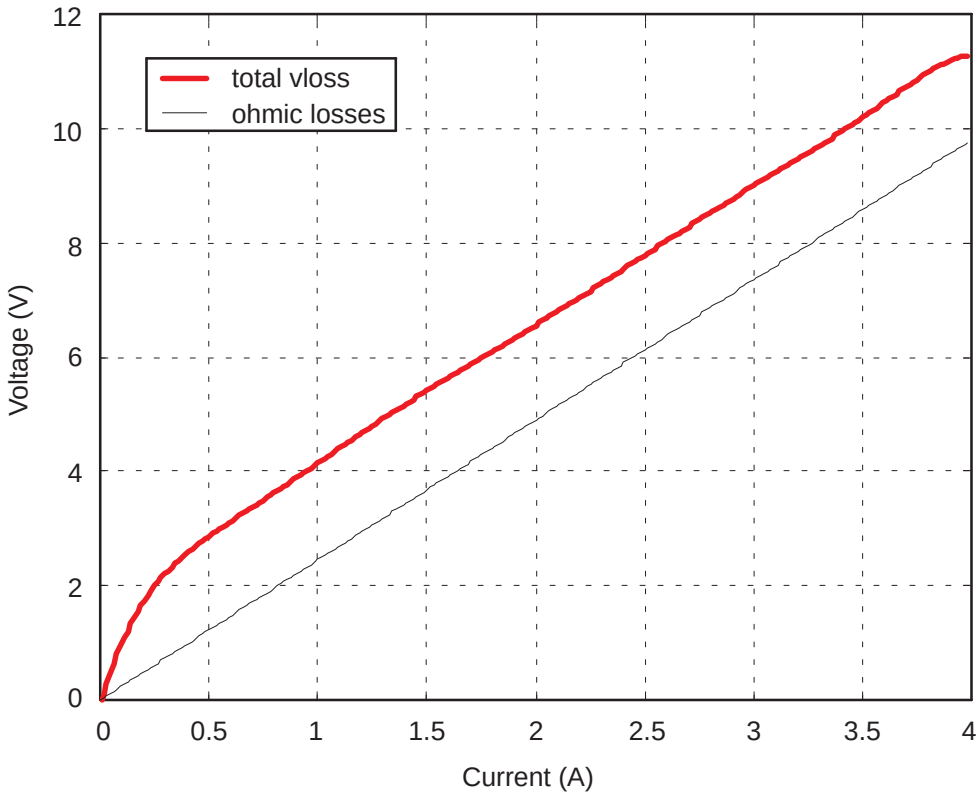

Figure 16. Voltage "Loss" vs. Current for the Emerson Electric SRM and the Spectrum Digital Motor Control Board

3.5 Flux Measurement Method

In most sensorless commutation methods, it is very desirable to have a full set of SRM magnetization curves (as in Figure 17) showing typical flux linkage (V-sec) versus phase current (amps) over the full angular range from unaligned to fully aligned rotor position. These flux linkage measurements require a precision angle indexer to hold the SRM shaft while making the measurement of flux linkage versus current flowing through the motor phase winding. This SRM magnetic model is then used along with an estimate of the flux linked by a phase to determine rotor position. The commutation algorithm used in the SRM demonstration platform only requires the flux linkage characteristic at the aligned rotor angle. Since injecting a DC current into the phase winding causes the rotor poles to align with the stator, no special alignment hardware is required. After the rotor shaft settles into alignment with the stator, flux data is then taken at this aligned rotor position using the flux measurement hardware as described in Section 3.5.1.

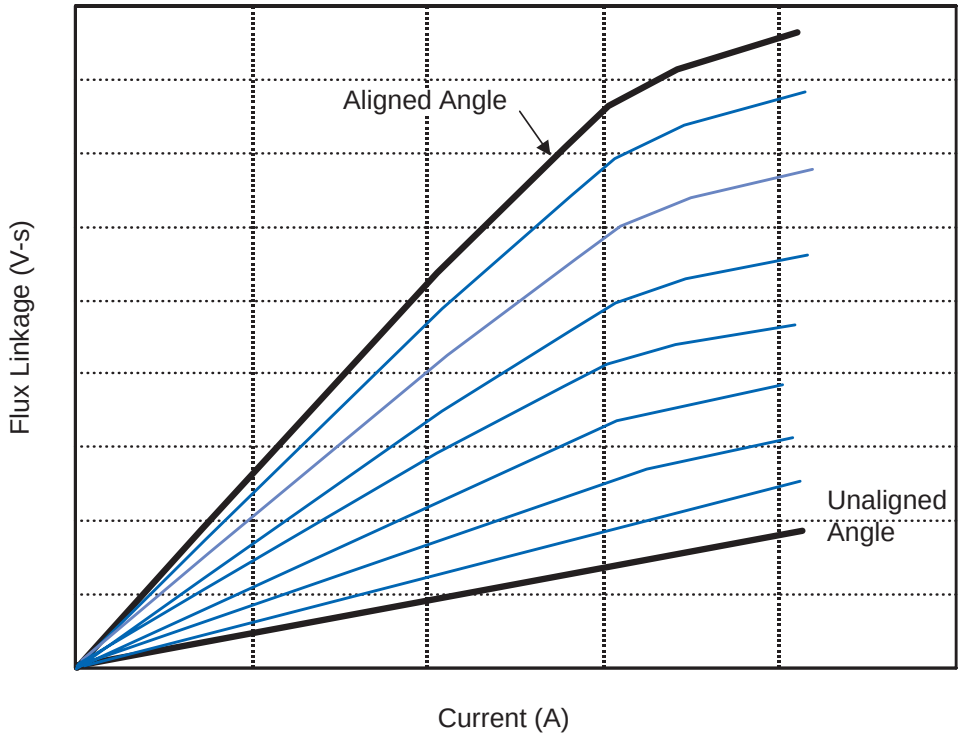

Figure 17. SRM Magnetization Curves

3.5.1 Flux Measurement Hardware

Figure 18 shows the schematic of the analog flux measurement hardware used to collect magnetic data for the SRM used in the demonstration platform. In the SRM, flux linkage in each phase of the motor can be calculated from the basic equation $\hat{\lambda} = \int (V - iR)\ dt$, relating flux linkage $\left(\hat{\lambda}\right)$ to voltage across the phase winding and current flow through the winding. Referring to the schematic, the semiconductor switch (Q1) controls the current through the SRM phase winding and is driven by a pulse generator at the gate drive input with a pulse width that is adjusted to allow the current to reach a steady-state level. For the SRM used in this demonstration platform with an electrical time constant of 20 msec, the pulse width of the gate drive should be set to approximately 100 msec.

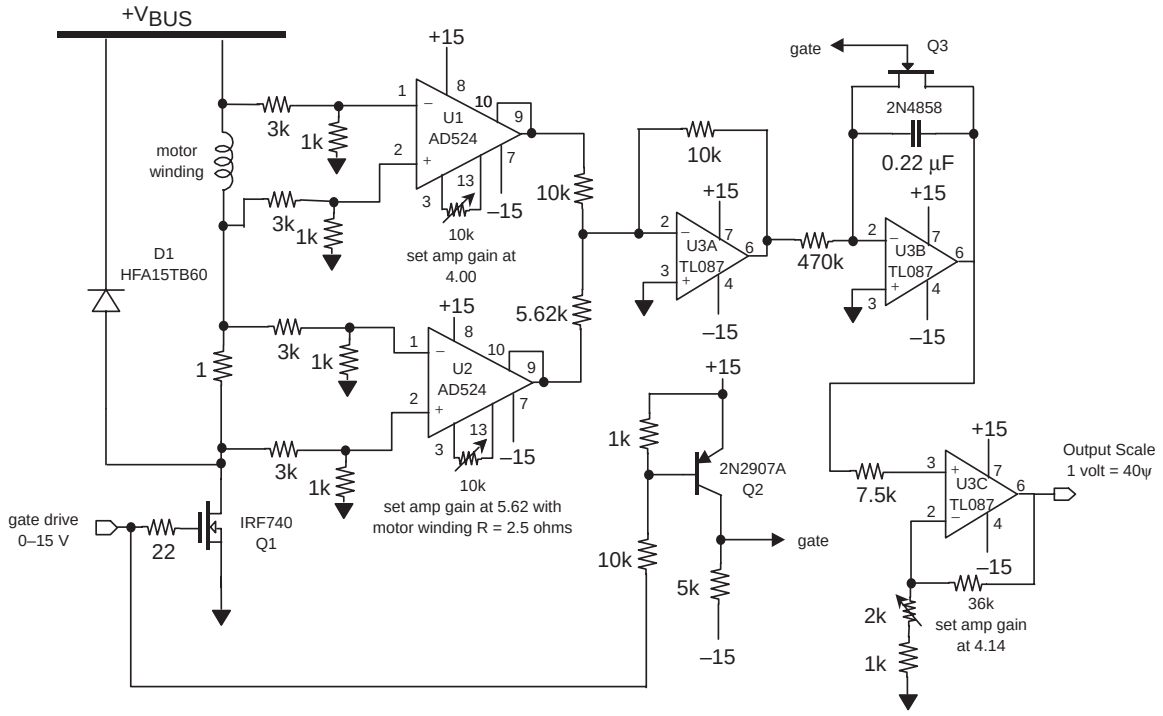

Figure 18. Analog Flux Measurement Circuit

The voltage level at $+V_{bus}$ should be adjusted for the maximum current desired for the flux measurement. Due to limitations in the measurement circuitry, the $+V_{bus}$ should never be set greater than about +40 volts dc. Differential instrumentation op amps (U1 and U2) measure the voltage across the phase winding and the current flow through the winding with a current-sensing resistor of 1 ohm. The summation amplifier (U3A) subtracts the ir_W drop from the voltage across the winding to $v - ir_W$ form and the result is then integrated in the reset integrator (U3B) to form the flux measurement $\left(\hat{\lambda}\right)$. Gains shown in the schematic have been set to give reasonable values within the dynamic range of the circuitry for the SRM used in this demonstration platform. Other SRMs may require different scaling to give correct results of flux measurement.

3.5.2 Demo SRM Flux Measurements

Magnetization flux data was collected on the SRM used in the demonstration platform from low current levels to a maximum current of 4 amps. Figure 19 shows this flux linkage data over this current range at the aligned rotor position. Note that the curve is very linear to the maximum current level of 4 amps, indicating no magnetic saturation at these current levels. Also, the slope of the curve as measured is the inductance of the SRM at the aligned position and indicates an inductance of about 52 mH. Flux linkage data from measurements of all three phases of the SRM are shown and indicate excellent balance between the phase windings for this particular SRM.

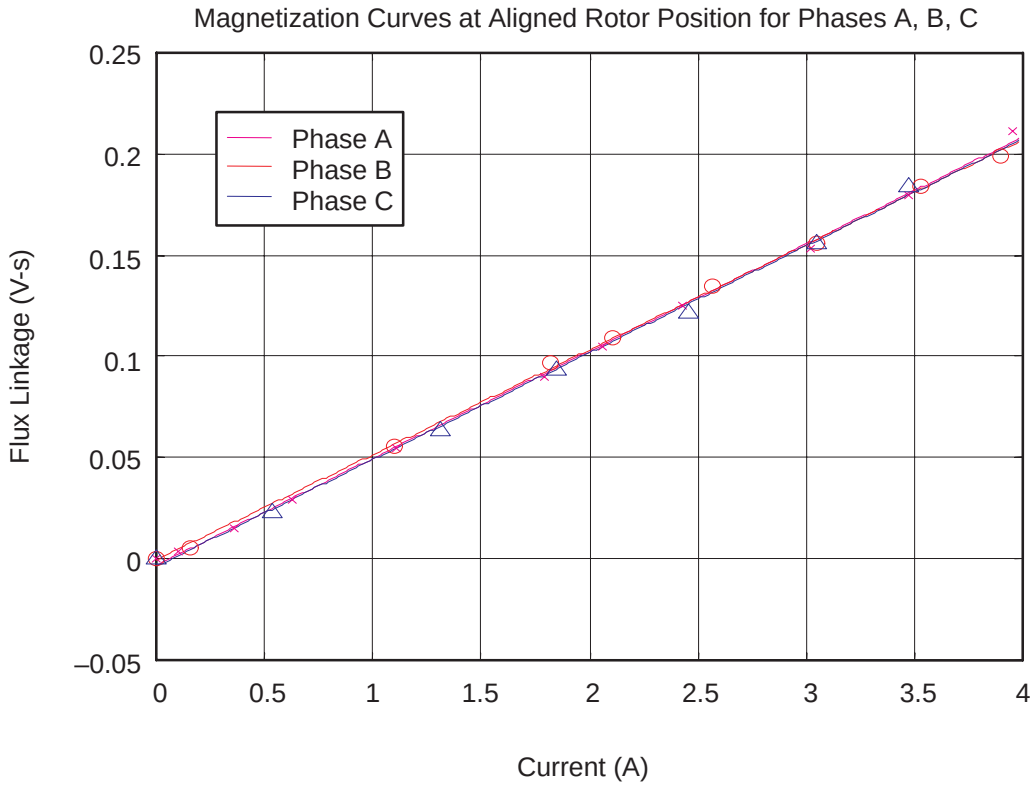

Figure 19. Flux Linkage Curves for Demo Platform SRM

3.5.3 Look-up Table Generation Method

To generate a look-up table from the raw magnetization data, a polynomial curve fit is performed on the data. For the motor used in the demostration, the magnetization curve is very linear up to the maximum operating current of 4.0 A, and a first-order curve accurately fits the data. However, other motors may have magnetization curves which are nonlinear, and a higher-order polynomial may be needed to capture the “knee” of the curve. After the fitting, the function is evaluated at the currents

$$i_n = i_{\max}\left(\frac{n}{256}\right) \;\forall\; n = 0 \ldots 255 \tag{17}$$

These points are chosen to allow an index into the 256-point look-up table to be calculated by right-shifting the 10-bit current measurement over two places. After generating the look-up table, it is multiplied by the scaling factor $n_{\max} f_S$ (maximum duty cycle count times the sampling frequency) to make it compatible with the scaling of the flux estimator. The reasons for this particular flux scaling are discussed in Section 2.

References

1. Lyons, J., S. MacMinn, and M. Preston. “Flux/Current Methods for SRM Rotor Position Estimation.” IEEE IAS Meeting Conf. Record, 1991.

IMPORTANT NOTICE

Texas Instruments and its subsidiaries (TI) reserve the right to make changes to their products or to discontinue any product or service without notice, and advise customers to obtain the latest version of relevant information to verify, before placing orders, that information being relied on is current and complete. All products are sold subject to the terms and conditions of sale supplied at the time of order acknowledgement, including those pertaining to warranty, patent infringement, and limitation of liability.

TI warrants performance of its semiconductor products to the specifications applicable at the time of sale in accordance with TI's standard warranty. Testing and other quality control techniques are utilized to the extent TI deems necessary to support this warranty. Specific testing of all parameters of each device is not necessarily performed, except those mandated by government requirements.

CERTAIN APPLICATIONS USING SEMICONDUCTOR PRODUCTS MAY INVOLVE POTENTIAL RISKS OF DEATH, PERSONAL INJURY, OR SEVERE PROPERTY OR ENVIRONMENTAL DAMAGE ("CRITICAL APPLICATIONS"). TI SEMICONDUCTOR PRODUCTS ARE NOT DESIGNED, AUTHORIZED, OR WARRANTED TO BE SUITABLE FOR USE IN LIFE-SUPPORT DEVICES OR SYSTEMS OR OTHER CRITICAL APPLICATIONS. INCLUSION OF TI PRODUCTS IN SUCH APPLICATIONS IS UNDERSTOOD TO BE FULLY AT THE CUSTOMER'S RISK.

In order to minimize risks associated with the customer's applications, adequate design and operating safeguards must be provided by the customer to minimize inherent or procedural hazards.

TI assumes no liability for applications assistance or customer product design. TI does not warrant or represent that any license, either express or implied, is granted under any patent right, copyright, mask work right, or other intellectual property right of TI covering or relating to any combination, machine, or process in which such semiconductor products or services might be or are used. TI's publication of information regarding any third party's products or services does not constitute TI's approval, warranty or endorsement thereof.

Based on standard U.S. Government tests

ENERGYGUIDE

Clothes Washer
Capacity: Standard

Model(s) **Maytag MLE2000A**

Compare the Energy Use of this Clothes Washer with Others Before You Buy.

This Model Uses
314 kWh/year

ENERGY STAR
EPA DOE
SAVING THE EARTH. SAVING YOUR MONEY.

ENERGY STAR
A symbol of energy efficiency

Energy use (kWh/year) range of all similar models

Uses Least Energy	Uses Most Energy
177	1298

kWh/year (kilowatt-hours per year) is a measure of energy (electricity) use. Your utility company uses it to compute your bill. Only standard size clothes washers are used in this scale.

Clothes washers using more energy cost more to operate. This model's estimated yearly operating cost is:

$25	$11
When used with an electric water heater	When used with a natural gas water heater

Based on eight loads of clothes a week and a 2000 U.S. Government national average cost of 8.03¢ per kWh for electricity and 68.8¢ per therm for natural gas. Your actual operating cost will vary depending on your local utility rates and your use of the product.

Important: Removal of this label before consumer purchase violates the Federal Trade Commission's Appliance Labeling Rule (16 C.F.R. Part 305)

Based on standard U.S. Government tests

ENERGYGUIDE

Clothes Washer
Capacity: Standard

Model(s) **Maytag MAH7500**

Compare the Energy Use of this Clothes Washer with Others Before You Buy.

This Model Uses
362 kWh/year

ENERGY STAR
A symbol of energy efficiency

Energy use (kWh/year) range of all similar models

Uses Least Energy	Uses Most Energy
177	1298

kWh/year (kilowatt-hours per year) is a measure of energy (electricity) use. Your utility company uses it to compute your bill. Only standard size clothes washers are used in this scale.

Clothes washers using more energy cost more to operate. This model's estimated yearly operating cost is:

$29	$15
When used with an electric water heater	When used with a natural gas water heater

Based on eight loads of clothes a week and a 2000 U.S. Government national average cost of 8.03¢ per kWh for electricity and 68.8¢ per therm for natural gas. Your actual operating cost will vary depending on your local utility rates and your use of the product.

Important: Removal of this label before consumer purchase violates the Federal Trade Commission's Appliance Labeling Rule (16 C.F.R. Part 305)

Based on standard U.S. Government tests

ENERGYGUIDE

Clothes Washer
Capacity: Standard

Model(s) **Maytag MAH6500**

Compare the Energy Use of this Clothes Washer with Others Before You Buy.

This Model Uses
388 kWh/year

EPA DOE
SAVING THE EARTH. SAVING YOUR MONEY.

ENERGY STAR
A symbol of energy efficiency

Energy use (kWh/year) range of all similar models

Uses Least Energy	Uses Most Energy
177	1298

kWh/year (kilowatt-hours per year) is a measure of energy (electricity) use. Your utility company uses it to compute your bill. Only standard size clothes washers are used in this scale.

Clothes washers using more energy cost more to operate. This model's estimated yearly operating cost is:

$31	$17
When used with an electric water heater	When used with a natural gas water heater

Based on eight loads of clothes a week and a 2000 U.S. Government national average cost of 8.03¢ per kWh for electricity and 68.8¢ per therm for natural gas. Your actual operating cost will vary depending on your local utility rates and your use of the product.

Important: Removal of this label before consumer purchase violates the Federal Trade Commission's Appliance Labeling Rule (16 C.F.R. Part 305)